UC Davis
Dissertations

Title

Investigation into Aging Mechanisms and Performance of Rubber-Modified Asphalt Binder and Mix

Permalink

Author

Liang, Yanlong

Publication Date

2021

Investigation into Aging Mechanisms and Performance of Rubber-Modified Asphalt Binder and Mix

By

YANLONG LIANG
DISSERTATION

Submitted in partial satisfaction of the requirements for the degree of

DOCTOR OF PHILOSOPHY

in

Civil and Environmental Engineering

in the

OFFICE OF GRADUATE STUDIES

of the

UNIVERSITY OF CALIFORNIA

DAVIS

Approved:

_____
John T. Harvey, Chair

_____
David Jones

_____
Adam J.T. Hand

Committee in Charge

2021

i

Yanlong Liang
Ph.D. Dissertation, January 2021
Advisor: Dr. John T. Harvey
Civil and Environmental Engineering
University of California, Davis

Investigation into Aging Mechanisms and Performance of Rubber-Modified Asphalt Binder and Mix

ABSTRACT

Crumb rubber modifier (CRM) produced from waste tires has been used in pavement engineering for more than half a century. This recycling methodology improves sustainable development because of environmental benefits of recycling scrap tires and because of improved performance of pavement materials when the recycled tire rubber is used as modifier in asphalt binders. This application improves both rutting and cracking resistance of asphalt pavement when an appropriate design is followed.

Adding the CRM to asphalt binders leads to modification of binder properties, including rheological properties and aging resistance. This modification alters pavement performance in-service. Previous studies found that rubber-modified binders had better aging resistance than their base binders. However, the mechanism of rubber modification on aging resistance was not well understood. This study aimed to explore this mechanism for rubber-modified binders. This study also evaluated the performance-related properties of dense-graded asphalt mixes using smaller quantities of CRM than are used in current applications, and their expected performance in different structural applications.

A literature survey regarding aging of rubber-modified binders revealed the following knowledge and technology gaps that were addressed in this study: 1) tracking chemical and rheological changes attributed to rubber modifiers and oxidative aging; 2) modeling viscosities of aged rubber-

modified binders from chemical components; 3) investigating oxidative aging in hot mix asphalt; 4) performance evaluation of rubber-modified materials.

Previous studies often used Fourier transform infrared spectroscopy (FTIR) to measure the chemical components in asphalt binders. The accepted aging indicators are carbonyl and sulfoxide components. This study applied FTIR to track chemical changes in 15 rubber-modified binders from four suppliers.

The results showed that the carbonyl component continuously increased in the rubber-modified binder throughout the oxidative aging process simulated by rolling thin film oven (RTFO)-aging and pressure aging vessel (PAV)-aging. In contrast, the sulfoxide component mainly developed during the early aging stage (RTFO-aging). The CRM did not contain any carbonyl components before and after long-term laboratory-aging simulated by PAV-aging, and it did not show significant sulfoxide changes after PAV-aging. Considering that the carbonyl and sulfoxide components are the main aging products developed during oxidative aging of base asphalt binders, the FTIR results indicated that the CRM aged differently to the oxidative aging of the asphalt binder. Adding rubber might decrease the aging products in rubber-modified binders because part of the base binder was replaced by digested rubber particles. In other words, the rubber could dilute the aging products in the rubber-modified binder.

The comparison between FTIR measured component indices and calculated component indices based on the dilution hypothesis indicated that the rubber dilution effect could explain the carbonyl component changes for binders without extender oils in unaged and PAV-aged conditions. During RTFO-aging, chemical interactions occurred in the rubber-modified binder at elevated

temperatures (>160˚C). This interaction significantly changed the carbonyl components in the rubber-modified binder beyond those that could be explained by the dilution effect alone.

The extender oil contained carbonyl and sulfoxide components, and these two components increased in the extender oil after RTFO- and PAV-aging. When extender oil was used, chemical interactions occurred in the rubber-modified binders in the unaged condition and after RTFO-aging and PAV-aging that changed the measured carbonyl component values considerably. The carbonyl component changes were beyond the reductions that could be explained by dilution. The FTIR measurement also indicated that the dilution could not explain the sulfoxide component changes for rubber-modified binders (with and without extender oils) in the unaged, RTFO-aged, and PAV-aged conditions.

Although the carbonyl and sulfoxide components also increased with aging in rubber-modified binders as they did in the conventional unmodified binders, the rates of increase of these aging products in the rubber-modified binders were lower than their base binders.

The butadiene component was generally used to track the presence of crumb rubber modifier in asphalt binders. The butadiene area index was measured in the rubber used in this study, but not in most base asphalt binders or the extender oil. This study found that butadiene components showed a strong correlation to rubber content for rubber-modified binders containing between five to 35 percent rubber by weight of the binder.

The rheological properties of rubber-modified binders were measured to evaluate age-hardening effects. When rubber particles are between 250 microns and 2.36 mm in size, the current Superpave (SUperior PERforming asphalt PAVEments) performance-grading (PG) system might not necessarily provide an accurate measurement of the performance properties of the rubber-modified

binder. Previous researchers studied the modification of PG test methods to accommodate binders with rubber particles greater than 250 microns in size. Those previous studies proposed modified PG tests for obtaining the high and low PG for rubber-modified binders.

This dissertation study further refined the modified PG test methods to allow measurement at various test temperatures (high PG tested at temperatures exceeding 58°C, and intermediate PG tested between 16°C and 50°C. This dissertation validated the refined PG test methods using three unmodified binders, two styrene-butadiene-styrene (SBS) modified binders and two terminal-blended rubber-modified binders. This refined test method was used to characterize the performance of rubber-modified binder with rubber particles up to 2.36 mm under different aging conditions.

Glover et al. proposed a dual-rate aging model to describe the correlation between binder chemical changes and physical changes from oxidative aging. Their model divides oxidative aging into short- and long-term aging phases. In the long-term aging stage, the age-hardening rate is defined as a binder specific constant value called "hardening susceptibility (HS)". It correlates the increase in carbonyl area (CA) index to the increment of low shear viscosity (viscosity at 60°C, 1.59E-05 Hz [0.0001 radians/second]).

This study developed a generic hardening susceptibility (GHS) model to predict viscosity beyond the low shear viscosity region. This model defines the linear correlation between logarithmic viscosity beyond the low shear viscosity region and the CA index. The slope of this correlation is the GHS.

The GHS model was calibrated and validated for seven unmodified binders, two SBS modified binders, three reclaimed asphalt pavement (RAP) binders, and eight rubber-modified binders. The

GHS model was found to be capable of predicting age-hardening after long-term aging of rubber-modified binders containing between five and 20 percent rubber and maximum rubber particle sizes up to 2.36 mm.

The extension of the age-hardening model improved the understanding of oxidative aging mechanisms in binders. This GHS model also provided a reasonable prediction of age-hardening of the binder in two types of asphalt mixes (conventional dense-graded mix and gap-graded rubberized mix) after long-term laboratory-aging. Measured properties of extracted binders from laboratory-aged mixes could be fitted in the GHS model.

The mix aging protocol used in this study followed the long-term loose mix aging protocol proposed in the National Cooperative Highway Research Program (NCHRP)-871 report. The loose mix aging protocol maximizes the mix exposure to oxygen, which decreases the aging gradient observed in the conventional specimen aging protocol. This study found that the long-term aged loose mixes could be compacted into fatigue beams at the target air-void content. The loose mix aging protocol showed similar variabilities in binder contents, mix stiffnesses, and fatigue test results among different aging durations compared to those in the compacted specimen aging protocol. The long-term aged loose mixes showed that oxidative aging increased mix stiffness, while it decreased fatigue life at higher strain levels (>300 mircostrain) and increased fatigue life at lower strains in a controlled-strain flexural beam fatigue test.

Aged binders extracted and recovered from these two mixes showed increases in carbonyl components and viscosities. The GHS model provided reasonable estimates of the viscosity changes in the recovered binder. The model showed that binder viscosity could be used to predict the corresponding mix stiffness. A log-linear correlation between CA index and beam fatigue life

(Nf) at a single strain was proposed for these two laboratory-aged mixes with the ln (Nf)-CA mode $(N_f = \beta e^{\alpha(CA)})$. In the ln (Nf)-CA model, parameters alpha and beta were dependent on the mix properties. This model quantitatively defined the aging influence on the mix fatigue performance. Further investigation of this model at different strains and for different mixes is warranted for the evaluation of aging effects in mechanistic-empirical (ME) design.

There is a growing interest in using crumb rubber modifier in hot mix asphalt because of its environmental benefits, potential life cycle cost benefits, and widespread availability compared with commonly used polymers such as SBS. The most common mix types for using the crumb rubber modifier are gap-graded and open-graded mixes. These mixes contain sufficient voids in the aggregate structure to accommodate swelled rubber particles.

In 2015, the California Department of Transportation expressed interest in studying additional asphalt mix applications to increase the use of crumb rubber modifier produced from scrap tires that may otherwise end up as landfill. Following this motivation, a study was completed in this dissertation to investigate the use of relatively small amounts of crumb rubber modifier in dense-graded mixes and the use of these mixes in different pavement structures. Small amounts are defined as five to ten percent rubber by weight of the binder or approximately 0.25 to 0.50 percent rubber by weight of the aggregate. These materials were collectively labeled "PG+X" materials, meaning that the modified binders needed to meet California Superpave PG binder specifications with X amount of CRM.

Four proposed approaches for PG+X materials were studies as part of this thesis:

1. Approach-1: Addition of five to ten percent rubber particles smaller than 250 microns, not resulting in a change to the PG of the base binder, achieved by blending softer base binders and/or polymers to meet this PG.

2. Approach-2: Addition of five to ten percent rubber particles smaller than 2.36 mm, with allowable changes to the PG of the base binder, and produced using a field-blending process.

3. Approach-3: Adding 0.25 to 0.50 percent rubber by weight of the aggregate directly into the mix using a dry-process.

4. Approach-4: Addition of five to ten percent rubber with particles smaller than 250 microns, with allowable changes to the PG of the base binder, and produced using a field-blending process.

This study of PG+X materials investigated 14 options for using small amounts of CRM in asphalt binder and ten options for using small amounts of CRM in dense-graded mixes. Laboratory test results revealed that PG+X binders showed equal or better performance compared to their base binders, including rutting resistance and low temperature cracking resistance.

The Approach-1, Approach-2, and Approach-4 PG+X binders were found to be suitable for use in dense-graded mixes. Mixes with binders containing rubber particles smaller than 250 microns met volumetric design criteria at the same binder content as the control base binder. Other mixes with larger rubber particles up to 2.36 mm) in the binder required higher optimum binder contents than the control mix to meet volumetric criteria. Mixes with dry-process rubber containing 0.25 to 0.50 percent coarse rubber (smaller than 2.36 mm) by weight of the aggregate also needed higher optimum binder contents than the control mix to accommodate the rubber.

Beam flexural modulus tests showed that PG+X mixes containing wet-process binders with rubber particles smaller than 250 microns (Approach-1 and Approach-4) had higher stiffnesses at high temperatures than the control mixes produced with the base binder, but only a marginal stiffness difference at intermediate temperatures. These PG+X mixes had better moisture resistance and rutting resistance than the control mixes and longer fatigue lives at strain levels below 400 microstrain in the flexural bending fatigue test. The PG+X mixes with five percent rubber showed a higher anti-cracking index than the base binder mixes in the uniaxial thermal stress and strain test used to evaluate low-temperature cracking performance.

The Approach-2 PG+X mixes containing wet-process binders with rubber particles smaller than 2.36 mm showed higher stiffnesses, better moisture, and rutting resistance than the control mix. The fatigue results for the Approach-2 PG+X mixes were inconsistent across range of strains, with the control mix performance generally falling between the five percent rubber content mix (longer fatigue life than the control) and the ten percent rubber content mix (shorter fatigue life than the control).

The Approach-3 mixes with dry-process rubber showed poorer rutting and thermal cracking resistance than the control mix, but better fatigue performance at strains higher than 600 microstrain. Based on these results, caution should be taken regarding the use of dry-process rubber.

These laboratory tests only revealed material performance under a specific set of controlled test conditions, but field conditions could be more complicated given that the combined impacts of environmental and traffic loading lead to a wide range of stresses and strains.

To predict the field response, laboratory test results were used as inputs for ME simulation. The purpose of the ME simulations was to evaluate the performance of PG+X mix layers under various combinations of pavement structure, traffic, and environmental conditions. The simulations compared the PG+X mixes to conventional asphalt mix in the same simulation cases. Although most PG+X mixes performed better than conventional mixes in laboratory tests, simulation results indicated that field performance in different pavement structures varied on a case-by-case basis, depending on the scenario. The appropriate application of PG+X mixes should be determined by a comprehensive analysis of mix properties, pavement structure, traffic, and climate for each potential project-level application.

In a total of 50 conditions (each simulation condition represents a typical pavement structure, climate, and traffic conditions in California) simulated for PG+X mixes with wet-process binders, at least one type of PG+X mix had better performance than their control mixes in 36 cases. The Approach-1 and Approach-4 PG+X mixes with ten percent rubber performed best in a thin overlay structure in the inland valley, north coast, and high desert California climates. On the other hand, the mix with five percent rubber performed best in a high desert climate for Approach-2 PG+X mixes. The five percent rubber dosage was also the optimum usage in the thick pavement structure in the inland valley, north coast, and desert climates for Approach-1 and Approach-4 PG+X mixes. A total of 20 conditions were simulated for the Approach-3 PG+X mixes with dry-process rubber and their control mixes. The mixes with maximum rubber particles smaller than 2.36 mm generally performed equal to or worse than the control mix in the 20 simulations where they were applied.

The finding from this dissertation indicates that laboratory stiffness and fatigue tests at one specific temperature and strain condition might not necessarily represent overall field performance. Material properties, pavement structure, climate conditions, traffic, and the interaction among

these factors all influence field performance. Therefore, a complete series of laboratory tests and field performance simulations based on ME principles are recommended to be conducted in any pavement design.

In summary, this study analyzed the oxidative aging process of asphalt binders and mixes. This study also evaluated rubber-modified binder and mix performance, with the goal of optimizing the application technology to meet various traffic and environmental requirements. Contributions to knowledge from this study include the following:

- Crumb rubber modifier ages differently to the asphalt binder. Adding rubber into the binder decreases the aging components (carbonyl and sulfoxide components) in rubber-modified binders after laboratory-aging.

- The viscosity of long-term aged binders at a given temperature and loading frequency can be predicted using the generic hardening susceptibility (GHS) model developed in this study.

- The GHS model can also predict the binder viscosity in the laboratory-aged mix, and the model predicted binder viscosity can be used to estimate the mix stiffness.

- The carbonyl component in the extracted binder can be used to predict the corresponding mix fatigue life at a single test strain.

- Using a small amount of CRM in dense-graded mixes (PG+X) by wet-process generally provides satisfactory laboratory results, including moisture resistance, rutting resistance, fatigue resistance, and low-temperature cracking resistance. Caution should be used for mixes with dry-process rubber.

- Mechanistic-empirical (ME) simulation shows that PG+X mixes produced with wet-process binders generally provide equal or better performance than the conventional

control mixes. ME simulation should be used to select an appropriate mix based on the pavement structure, climate, and traffic conditions of a given project.

ACKNOWLEDGEMENTS

It has been a long journey to complete this doctoral study. I would like to express my deepest appreciation to the people that have supported me in this endeavor.

I have been blessed to grow up in a happy family. My father and mother taught me to be an honest and kind man. They have stood by my side in every step of my life. I am also blessed to meet my wife in school. Her love keeps me strong to face the challenges in these years. Without their encouragement and support, I could not have achieved these accomplishments.

I sincerely express thanks to my advisor, John Harvey, for his guidance, inspiration, caring, and support for my study and life in Davis. I want to thank David Jones for his conscientiousness and patience to guide me through this academic work at Davis. I also want to express my gratitude to my dissertation committee member, Adam Hand, for his guidance in completing this dissertation.

I truly appreciate the support received from the University of California Pavement Research Center. Special thanks go to Ronzong Wu, Jeffery Buscheck, Irwin Guada, and Angel Matoes for their great intellectual comments and physical support through my research. I also want to express thanks to the engineers, technicians, and administrators who assisted my study, including Julian Brotschi, Jessica Cisneros, Anai Cazares-Ramirez, Mark Troxler, Mark Hannum, and David Miller. It was also a pleasure for me to grow together with my current and former fellows in the laboratory, Shawn Hung, Arash Saboori, Stephanus Louw, Ashkan Saboori, Julio Paniagua, Fabian Paniagua, Liya Jiao, Sampat Kedarisetty, and Christina Pang. Long live the memories for the days we were working together and had fun together.

I also want to acknowledge Hui Li, Mohamad Alavi, Bernhard Hofko, Mohamed Elkashef, and Hashim Rizvi for their help in my study.

TABLE OF CONTENTS

LIST OF FIGURES

LIST OF TABLES

1 INTRODUCTION

1.1 Background

In the United States, more than 94 percent of pavement surfaces are paved with hot mix asphalt (HMA) *(1,2)*. These pavements are subjected to various challenges caused by repeated traffic loadings and daily/seasonal weather fluctuations. The interaction between the pavement, the loading, and the environmental conditions requires a durable asphalt mix that can provide a smooth riding surface and a reliable structural capability. To this end, three performance standards are generally required: 1) asphalt mixes should not have excessive permanent deformation under heavy traffic loadings; 2) asphalt mixes should not crack under stresses caused by material contractions or expansions under daily or seasonally temperature fluctuation; 3) asphalt mixes should not crack during fatigue under repeated traffic loading/unloading cycles within its design life. A durable asphalt pavement layer satisfies these performance criteria throughout its service life.

HMA is generally produced in a mixing plant by blending mineral aggregates and asphalt binder at an elevated temperature, which usually exceeds 140°C *(2)*. Aggregates include dust, sand, gravel, and crushed stone. The aggregate itself generally accounts for 91 to 96 percent of the total weight of HMA *(2)*. The aggregates need to be sufficiently mechanically and chemically durable to withstand the damage caused by traffic loading and the environment. Pavement engineers ensure the durability of the aggregate by using high-quality mineral sources and applying appropriate manufacturing processes. High-quality aggregate is less likely to experience chemical reactions and durability problems within the mix.

Asphalt binder is extracted from crude oil during refining. Asphalt binder is a composite mixture of organic molecules that can be grouped into four types: saturate, aromatic, resin, and asphaltene *(3)*. These groups have molecular weights ranging from several hundred to a few thousand Dalton (standard molecular weight unit, which is numerically equivalent to 1 gram/mol). Unlike the aggregate, asphalt binder is not stable over time. It is highly reactive to oxygen. This reaction generates additional polar molecules, resulting in stiffening of the binder. This phenomenon is called "oxidative aging" *(1)*.

Aged asphalt binder loses the capacity of relaxing stress and becomes vulnerable to fracture. The oxidative aging process also causes the asphalt mix to be susceptible to fracture and fatigue damage. Aged asphalt binder loses cohesion to the aggregate, resulting in raveling under traffic and moisture-related damage when exposed to water. Binder sources, mix properties, and environmental conditions all influence the oxidative aging process *(4,5)*.

Recent research results suggest that adding rubber into asphalt binder appears to slow down the oxidative aging process *(1,4,5)*. Although the anti-aging mechanism of rubber modifier was not fully understood, it was generally accepted that rubber-modified binders experienced less age-hardening than unmodified base binders *(6)*.

Adding rubber into asphalt also improves binder performance *(7-9)*. Rubberized HMA (RHMA) can be paved in a thin pavement surface layer (30 mm to 60 mm thick) *(8,9)*. The rubber-modified binder provides sufficient shear strength to resist rutting at high in-service temperatures. In most California inland regions, pavement surface temperatures exceed 60°C during summer. These high temperatures soften the asphalt and can lead to deformation under heavy traffic. Digested rubber particles improve the resistance to repeated traffic loading/unloading cycles. Reduction in

reflective cracking is also achieved at intermediate in-service temperatures, which generally range from 10°C to 40°C as an average surface layer temperature in California *(1,8)*.

Rubber modifiers can be divided into two types according to the material source. One is natural rubber modifier produced from rubber trees, and the other is crumb rubber modifier (CRM) manufactured from scrap tires. Using rubber in pavement activities provides an approach to reduce landfilling waste tires. From this perspective, RHMA has considerable environmental benefits *(5,9)*. Otherwise specified, the item-rubber used in the following sections to the end of this dissertation refers to crumb rubber modifier.

The Federal Highway Administration (FHWA) Recycled Materials Policy was established in 2002. This policy states that recycled materials should be considered in the material selection phase. This promotes recycling technologies and develops new opportunities for recycled materials *(10)*.

The Recycled Materials Policy motivates the use of rubber in pavement engineering. Departments of Transportation (DOTs) in many states have studied RHMA applications, including but not limited to Arkansas, Arizona, California, Florida, Georgia, Kansas, Louisiana, Michigan, Mississippi, New Jersey, Texas, and Wisconsin *(7,11,12)*. According to the U.S. Environmental Protection Agency, California and Arizona were the leaders in rubber utilization in 2016, followed by Florida. Approximately 12 million tires are recycled and used in paving applications annually across these states in 2016 *(13)*.

California faces the challenge of diverting more than 40 million scrap tires from disposal annually *(11)*. The California Department of Resources, Recycling, and Recovery (CalRecycle) is responsible for developing new implementation approaches for waste tires. Thirty-three million of

these tires (81 percent) were diverted from landfills through various alternatives, including reuse, retreading, recycling, and combustion. In 2018, 8.8 million scrap tires were recycled to be used in paving applications in California, which showed a 29 percent increase compared to the year 2017 *(14)*.

The California Department of Transportation (Caltrans) is actively interested in studying RHMA, given the environmental considerations of reducing landfilling of scrap tires. The rubber used in RHMA in California contains 75 ± 2 percent scrap tire rubber (typically obtained from waste car and pickup tires), 25 ± 2 percent high natural rubber (typically obtained from waste truck tires), maximum 0.01 percent wire, maximum 0.05 percent fabric, and maximum 3 percent calcium carbonate or talc *(12)*.

In 2005, the California Legislature passed, and the Governor signed AB 338, which requires Caltrans to use a specific percentage of crumb rubber per metric ton of the total amount of asphalt paving materials used. Specifically, as of 2013, Caltrans was required to use, on an annual average, 5.2 kg (11.58 lb) of crumb rubber per metric ton of asphalt paving materials in the state highway system. This equates to 35 percent of the total paving asphalt placed per year *(15)*. Figure 1.1 presents the objective and actual utilization of tires in asphalt by Caltrans between 2000 and 2017.
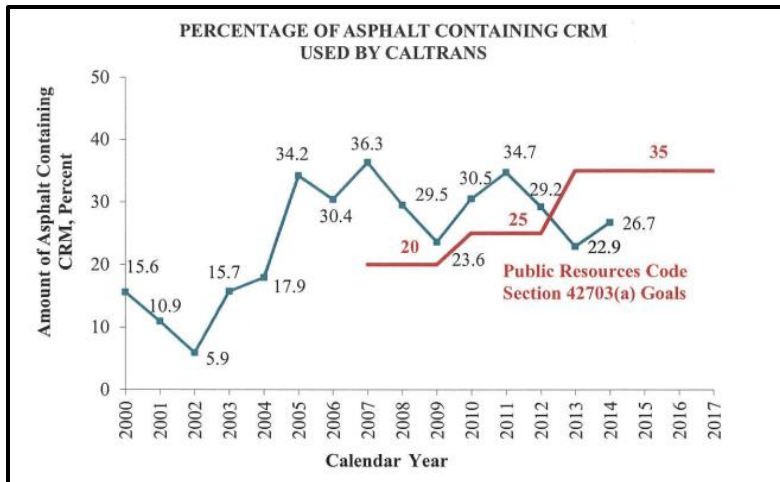
Figure 1.1: CRM application by Caltrans *(15)***, the blue line is the utilization data, and the red line is the target of AB338.**

Caltrans has adjusted its mission statement to include sustainability and to have the goal of sustainability and stewardship, to preserve and enhance California's resources and assets *(16)*. As part of this mission, in 2015, Caltrans considered new approaches for using more recycled tire rubber to reduce the landfill disposal of scrap tires. This initiated the "PG+X" project, which aimed to investigate using small amounts of rubber in dense-graded mixes *(17)*. This increased interest in the rubber application was the primary motivation of this study.

1.2   Problem Statement

Two issues have been identified in using the rubber modifier in pavement engineering. One is that the aging mechanism of rubber-modified binder is not fully understood. Lack of understanding of the aging mechanism makes it difficult to develop performance-related specifications and to apply mechanistic-empirical (ME) pavement design procedures for RHMA. Secondly, the performance of rubber-modified material in different mix types and pavement structures has not been thoroughly evaluated.

5

Several aging models have been developed to describe the chemical-physical properties after aging *(18- 20)*. None of them were developed specifically for rubber-modified asphalt. Consequently, predicting oxidative aging in rubber-modified asphalt is not precise using these aging models. Without a substantial evaluation of oxidative aging, caution should be given to the mechanical analysis of rubber-modified mixes in the long-term service phase.

Issues are also identified for precisely measuring the performance-related properties of rubber-modified binders, especially those containing large rubber particles (smaller than 2.36 mm [passing the #8 sieve]) *(2)*. Testing conventional binders follows the Superpave binder specification developed during the Strategic Highway Research Program (SHRP) in the early 1990s. Conventional binders are those containing particulates smaller than 250 microns (passing the #60 sieve) *(21)*. The procedure is not appropriate for testing rubber-modified binders containing rubber particle sizes larger than this size. These unanswered questions cause specification, quality control, and quality assurance issues.

RHMA performance in various pavement structures also requires investigation. Previous research studies have mainly focused on using RHMA in thin surface pavement layers (less than 60 mm thick) since the primary target of the current usage of RHMA is to reduce the reflective cracking from sublayers *(7-9)*. The usual structure in the thin RHMA surface layer is either gap-graded (RHMA-G) or open-graded (RHMA-O). These mix types have discontinuous gradations that provide voids between aggregates to accommodate large, swelled rubber particles, and in the case of RHMA-O mixes, to also drain water. The rubber-modified binder contents (base binder plus rubber together) are higher than the binder content in dense-graded mixes, resulting in a thicker stress-absorption film that alleviates reflective cracking issues. However, gap-and open-graded mix layers typically have lower structural capacity than dense-graded mixes of the same thickness.

6

Findings on the performance of using rubber-modified mixes in thicker layers are inconclusive *(9,22)*. In recent years, traffic volumes have increased significantly, requiring thicker pavement layers. Using multiple lifts of rubber-modified mixes is an interesting topic requiring further investigation. This new demand promotes the study of using PG+X mixes in different pavement structures. It is also environmentally beneficial to use PG+X mixes in different pavement layers to consume more waste tires than current approaches (RHMA-G and RHMA-O).

1.3   Study Goal and Scope

The goal of this dissertation is to study the above issues. It aims to improve the understanding of the oxidative aging progression and its impact on asphalt performance. This study will also evaluate PG+X mix performance. A recommendation for using this new rubber-modified mix (PG+X) will be drawn based on the results of this study.

The first task was to investigate the aging mechanism in more detail than that documented in the literature, with a focus on the effect of the rubber on anti-aging potential. This improved understanding of oxidative aging was then used to modify, calibrate, and verify aging models for rubber-modified binders. Additionally, the effect of oxidative aging on mix performance (stiffness and fatigue performance) was investigated.

Rheology test of rubber-modified binder was also investigated in this study. The Superpave performance-grading system developed in previous studies was adapted for use with a rubber-modified binder with large, incompletely digested rubber particles. The refined performance-grading system was used to evaluate the properties of rubber-modified binder subjected to various aging conditions. A series of laboratory tests were also conducted on PG+X mixes to investigate performance. Finally, laboratory test results were used as inputs for mechanistic-empirical

7

simulation to evaluate PG+X mixes under various combinations of pavement structures, traffic, and environmental conditions.

In summary, this study aims to evaluate the oxidative aging progress and the binder and mix performance, with the goal of optimizing the application technology to meet various traffic and environmental requirements. Based on a better understanding of these mechanisms, it is anticipated that CRM utilization will increase.

2 LITERATURE REVIEW

2.1 Rubberized Asphalt Binder and Mix

2.1.1 History of Crumb Rubber Application in Asphalt Pavement

As early as the 1930s, natural rubber was blended with asphalt binder for paving activities to improve engineering performance *(23)*. In the mid-1960s, recycled rubber from waste tires was added to asphalt binder by Charles H. McDonald *(24)*, who blended up to 20 percent of recycled rubber with conventional asphalt binder at approximately 200°C for ten to 90 minutes, together with some additional solvents to achieve workability. The end product was a hot, jellied mix that could be applied to seal cracks or repair distressed pavement surfaces *(24)*. After years of development, rubber-modified asphalt became a widely used material in asphalt pavement.

Asphalt rubber (AR) binder and terminal-blend rubber (TR) binder are the most widely used traditional rubber-modified binders *(25)*. AR binder produced from a field-blending approach is a highly viscous material. It is obtained by blending rubber particles and base binders at an elevated temperature (>180˚C) with a high agitation speed for a sufficient time to allow rubber swelling. The swelled rubber absorbs light fractions from the base binder, resulting in rubber swelling. Although most rubber particles are swelled, some can still be physically observed in the binder. Therefore, the digestion of rubber particles in the binder phase is incomplete for AR binders *(12,26)*. The American Society for Testing and Materials (ASTM) defines AR binder as containing at least 15 percent rubber by weight of the binder *(27)*. Certain limitations are specified for impurities (fibers and metal particles) and moisture content. This definition is not based on any limiting technical factors.

The Arizona DOT has been successfully using AR binder based on guidance from McDonald's since the 1960s. Decades of monitoring showed that RHMA reduced reflective cracking, increased rutting resistance, and decreased traffic noise. Using RHMA instead of the conventional HMA could cut the maintenance cost by $666 per lane mile per year in the late-1990s *(7)*.

Caltrans began to use rubber in chip seals from the 1970s and built the first-trial section with RHMA around 1980. Caltrans specifies the rubber amount in the AR binder to be 18 to 22 percent *(25)*. The maximum particle size must be smaller than 2.36 mm (pass the #8 sieve), with requirements for impurities (fibers and metal particles) and moisture content *(25)*. It also requires adding two to four percent extender oil by weight of the binder. The extender oil is an aromatic oil that improves workability and promotes swelling of the rubber particles. The mixing/blending temperature and times for AR binder production are typically at 190°C to 220°C for more than 45 minutes following the guidance *(21)*.

In California, traditional applications of AR binders include chip seals, stress absorbing membrane interlayers, and gap- and open-graded rubberized hot mix asphalt (RHMA-G and RHMA-O). Field observations indicate that rubberized chip seals significantly prolong the service life and improve the reflective cracking resistance of the existing pavement surface. RHMA-O provides better surface friction and better durability than conventional open-graded HMA *(25)*. RHMA-G can be highly cost-effective when paved in thin surface layers (less than 60 mm thick). It can provide a 50 percent thickness reduction compared to conventional HMA layers when used over existing cracked asphalt pavement.

University of California Pavement Research Center (UCPRC) conducted a study of RHMA-G using accelerated pavement test in the late-1990s. Laboratory test results further validated the

reduction in the overlay thickness *(9)*. Other studies also reported that newly paved RHMA-G and RHMA-O could reduce traffic noise by 1.0 dBA and 1.9 dBA than the conventional HMA. The lower pavement surface macrotexture achieved noise reduction. After ten years of service, the benefit of traffic noise reduction was still noticeable *(28,29)*, which was attributed primarily to the slow aging nature of the binder.

Terminal-blended (TR) binder is produced using a different process to the AR binder. It is known as a "terminal-blended binder" owing to the production technology, as this modified binder is mostly manufactured at asphalt plant terminals. The rubber used in TR binders is relatively small, typically smaller than 600 microns (passing the #30 sieve), with five to 15 percent dosage by weight of the binder *(25)*. Unlike the field-blending method, the terminal-blending approach does not require agitation force. Rubber particles can be self-digested in asphalt binders at elevated temperatures (i.e.,>200°C) after several hours of swelling, credited to the relatively small particle sizes. These digested fine rubber particles alleviate particle settling and inhomogeneity issues *(30-32)*. Lately, many DOTs are increasingly interested in the application of TR binders as an alternative to styrene-butadiene-styrene (SBS)-modified binders.

Florida DOT has been actively paving rubber-modified HMA since the late 1990s. They allow up to five percent of rubber with particles smaller than 300 microns (passing the #50 sieve) in dense-graded mixes and up to 12 percent of rubber with particles smaller than 600 microns (passing the #30 sieve) in open-graded mixes. These rubber particles are preblended with asphalt binders. They are not treated as a substitution of the fine portion of the aggregates. Long-term pavement performance monitoring revealed that the rubber-modified mixes exhibited a better friction index, better rutting resistance, and better durability than conventional HMA *(8)*.

In 2015, the Florida DOT updated its rubberized asphalt specification to require a minimum of 17 percent rubber by weight of the binder to produce a PG 76-22 binder. This rubber-modified binder met all Superpave PG criteria except for solubility *(30)*. Solubility measures the homogeneity of a modified binder. Settling of rubber particles might lead to separation during transport or storage. However, this separation does not necessarily lead to unsatisfactory performance in service. Laboratory and accelerated pavement tests showed that this PG 76-22 binder provided equivalent rutting and cracking resistance to PG 76-22 SBS binder in the dense-graded mix *(31)*.

The Louisiana DOT permits the addition of about nine percent rubber into PG 64-22 binder to produce a PG 76-22 rubber-modified binder by the terminal-blend approach. There are no solubility requirements for this modified binder. Laboratory and accelerated pavement test results indicated that mixes produced with the PG 76-22 rubber-modified binder provided satisfactory performance compared to control mixes produced with a PG 76-22 SBS-modified binder when assessed using the criteria listed in the American Association of State Highway and Transportation Officials (AASHTO) M 320 specification *(30,32)*.

Besides using the wet-process rubber-modified binder in the mix, rubber can also be directly added into asphalt mix without pre-blending with the asphalt binder. This application is called "dry-process". The rubber particles used in a mix with dry-process rubber can range from fine sizes to coarse sizes (600 microns to 2.36 mm [passing the #30 sieve to #8 sieve]). In the dry-process approach, generally, up to three percent rubber by weight of the aggregate is mixed with aggregates in the blending drum *(25)*. The rubber particles are considered a partial proportion of the aggregates. After sufficient heating and mixing, the batched dry materials are blended with the hot binder to produce a mix with dry-process rubber.

The production process for the mix with dry-process rubber is relatively simple compared to the wet process. The amount of rubber is small compared to the amount of aggregate, and blending is typically undertaken on feed belts and in the drying and/or mixing drum. Researchers were aware of potential issues for using this mix. Mixes with dry-process rubber sometimes have undesirable mix performance and/or performance variability within the project. Rubber swelling can cause laboratory specimens to expand when they are extruded from molds, which can affect density, air-void content, and stone-to-stone contact. These factors can all influence test results and overall mix performance *(33-35)*.

In summary, federal and state agencies, research institutes, and industries have studied rubber-modified asphalt in relatively thin pavement surface layers (30 mm to 60 mm) since the 1960s. Some general findings from comprehensive literature reviews include the following *(7-9,25,31-36)*:

1. Mixes containing wet-process binders used in a thin surface layer provide better in-service performance than conventional unmodified HMA, including rutting, thermal cracking, and fatigue cracking resistance.

2. The initial construction cost of RHMA is higher than conventional HMA for the same layer thickness because of the slightly higher asphalt binder content and the higher production costs of producing the rubber-modified binder. RHMA also requires higher mixing and paving temperatures, which consumes more energy. A recent Caltrans study showed that the initial cost for RHMA was only 9.1 percent more expensive than conventional HMA in the construction *(16)*. These increased costs per mass or volume of the mix are typically offset by performance improvement. Using RHMA permits a thinner layer over cracked existing pavement that reduces the overall aggregate and binder consumption.

3. The settlement of rubber particles in the binder during transport and storage can influence performance and performance variability in a project. Caltrans flexible pavement maintenance specification limits a maximum of two-hour duration that RHMA can be stored in the silo.

Wet-process binder performance is affected by four primary factors: blending/reaction condition, rubber content, rubber type, and rubber gradation *(37)*. The following sections summarize a review of recent research on these four factors.

2.1.2   *Effect of Blending Temperature and Duration*

The primary activities that occur during the blending/digestion phase are swelling and degradation. The separation of these two activities is dependent on time and temperature. Generally, swelling dominates the rubber-binder interaction at relatively low temperatures (i.e., 160°C to 220°C), while degradation mostly controls the interaction at relatively high blending temperature (i.e.,>240°C) *(38)*.

Swelling is the process of rubber particles absorbing lighter components from the binder and swelling two to three times their original volume. Rubber swelling reduces the free space between rubber particles and the base binder, resulting in a gel-like matrix that stiffens the binder. The viscosity of the rubber-modified binder is, therefore, higher than the base binder *(23,39)*.

Degradation is the process of rubber particles dispersing in the asphalt binder after extended periods at temperatures typically over 220°C. The degradation can be subdivided into depolymerization and devulcanization. Depolymerization converts the polymer (macromolecules) into component monomers (small molecules). Devulcanization converts large molecules into a

mixture of monomers and creates cross-link chemical bonds *(40)*. It is the reverse process of vulcanization, which is used to harden synthetic rubber during the tire producing process.

Depolymerization and devulcanization are not significantly different from each other. Both of them break chemical bonds within the rubber-binder matrix, resulting in a gradual reduction in the viscosity *(23,40)*. A binder containing a high molecular weight and a high content of polar compounds tends to depolymerize. In contrast, binders with low molecular weight and more aromatic compounds tend to devulcanize *(41)*.

In the Superpave PG system, binder properties are characterized by two rheological parameters: complex modulus (G*) and phase angle (δ). These two parameters change during the blending progress. At lower blending temperatures (i.e., 160°C), the G* value of rubber-modified binders increases, while δ value decreases along with time. Rubber swelling dominates this blending phase at this relatively low blending temperature. Degradation starts when the temperature increases to 200°C. During this temperature increase, G* value increases slowly, and δ value continues to decrease. At an intermediate blending temperature (i.e., 200°C), the G* value trends from increasing to decreasing, indicating that the blending progress transitions from swelling to degrading *(38)*. When the temperature is exceptionally high (>240°C), degradation starts to overwhelm swelling. Under these conditions, G* value reduces and δ value increases, indicating that degradation starts to dominate at this point *(42)*.

Figure 2.1 presents the change of viscosity, rubber particle attribute changes, and rubber-binder matrix along with blending time. Zanzotto and Kennepohl *(40)* found that although the rubber-modified binder always showed different performance from the base binder, increasing temperature from 200°C to 280°C leads to a partial modification loss that reduces the difference

in performance, including the creep stiffness at -20°C, elastic recovery at 20°C, and viscosity at 60°C.
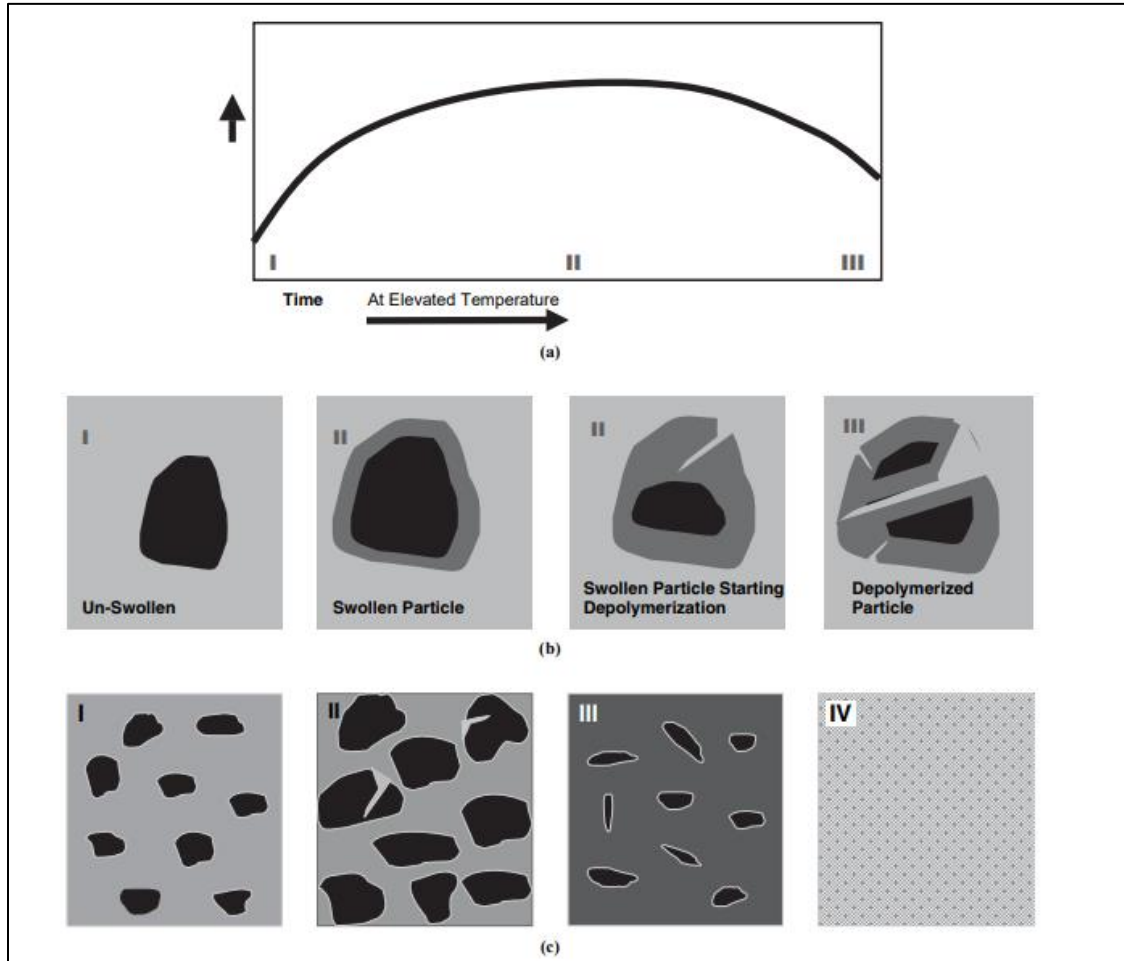
Figure 2.1: Progression of rubber-binder interaction at an elevated temperature: (a) viscosity change over time, (b) rubber particle size over time, (c) binder matrix over time *(42)*.

To understand the blending duration effect, researchers evaluated rubber digestion at a particular blending temperature of 177°C. Different rubber particle sizes ranging from 180 microns (passing the #80 sieve) to 1.40 mm (passing the #12 sieve) were studied. Lee *(43)* studied the large molecular size (LMS) of rubber using gel-permeation chromatography. Observations indicated that the LMS increased after blending. Although the LMS increased continuously over eight hours, no further complex modulus changes were observed after the first hour of blending. Xiao et al.

(44) weighted rubber particles after soaking in the asphalt binder. The result indicated that the rubber mass continued decreasing over a 24-hour blending period, but the rubber particle size reduction occurred primarily during the first three hours.

Large molecule groups can be developed throughout the blending process within the rubber-modified binder as smaller particles combine into long cross-linked chains. The degree of rubber modification can be controlled by precisely controlling the blending temperature and duration *(43)*.

In this study, the blending process was carefully controlled to ensure material quality. The quality control system followed CalRecycle recommendations *(45)*, including blending the rubber with the binder for at least 30-minute and at least 190°C.

2.1.3   Effect of Rubber Content

Rubber content is the primary factor influencing the rheological properties (i.e., complex modulus, phase angle, viscosity) of rubber-modified binders. Kök and Çolak *(46)* concluded that as little as three percent rubber could noticeably change binder rheological properties. In general, adding rubber increases binder viscosity and decreases binder phase angle. Rubber-modified binder shows an increased stiffness, better elastic recovery, lower penetration, and lower creep stiffness than the base binder *(46-57)*.

For rubber content increasing from zero to 22 percent, the binder PG, determined by $G^*/\sin(\delta)$ and viscosity, increases with increasing rubber content at high in-service temperatures (>40°C) *(47-55)*. The corresponding mix stiffness (Marshall stiffness, simple uniaxial creep stiffness) and flow number in a repeated loading test also increase with increasing rubber content. This translates to improved rutting resistance *(46,56)*.

At intermediate in-service temperatures (10°C to 40°C), the intermediate PG determined by $G^* \times \sin(\delta)$ value decreases with increasing rubber content *(50)*. RHMA has a longer fatigue life than conventional HMA in controlled-strain flexural beam fatigue tests *(50,51)*, which are typically conducted in the intermediate temperature range. Mixes produced with eight percent rubber by weight of the binder have about 50 percent higher initial stiffness and resist about five times more load cycles before failure than the control mix made with the base binder. In the same mix aggregate structure, eight percent rubber provides equal fatigue resistance to four percent SBS polymer *(46)*.

At low in-service temperature (≤0°C), adding the rubber results in a reduction in creep stiffness compared to the base binder. Although the m-value is controlled by the base binder rather than rubber, increasing the rubber content leads to a lower creep stiffness. This reduced creep stiffness reduces stresses under thermal contraction *(47,50,53,55,57)*, thereby alleviating thermal cracking at low temperatures.

Based on the above discussion, it is clear that increasing rubber content can improve rheological properties and mix performance to a point. Statistical results show no noticeable rheological property increase when rubber content is over 20 percent by weight of the binder *(53)*. This is because the rubber swelling is incomplete for rubber-modified binders with a high rubber content (over 20 percent). Rubber swelling is the process that rubber particles absorb light components from the base binder *(54)*. Once these light components are consumed, adding more rubber particles will have little effect on the rheological properties *(55)*.

One consequence of high rubber contents (over the general 20 percent dosage) is the notable increase in binder viscosity. This causes potential workability issues that require a high

temperature for mixing and compacting *(52,56,58)*. Wet-process rubber-modified binder (both AR and TR) generally requires mixing the rubber-modified binder with aggregates at elevated temperatures of 170°C to 200°C. These temperatures are about 20°C to 40°C higher than conventional HMA mix-production temperatures *(56)*. Consequently, RHMA production processes consume more energy. The compaction temperature of RHMA is also higher than conventional HMA, which can affect transportation and paving operations. This becomes a severe problem when the asphalt plant is away from the construction location or paving RHMA in the winter session. Lower than optimal mix temperature leads to poor compaction in the field that can result in early pavement distresses *(59,60)*.

Another consequence of high rubber content is that incompletely digested rubber particles cause stability issues when settlement occurs after long-distance transportation *(48,55)*. Settlement is the physical separation between the heavier rubber and lighter asphalt binder, which further reduces the homogeneity of the rubber-modified binder. Navarro et al. *(48)* found that the storage stability decreased with increasing rubber content, and it reached the worst when the rubber content was around 15 percent *(55)*. The binder stability would then recover when rubber content continued growing. Satisfactory storage stability was observed in a rubber-modified binder containing 40 percent rubber due to the high bulk viscosity that restricted the settlement of rubber particles. However, this high rubber content (40 percent rubber by weight of the binder) was over the normal rubber usage (20 percent by weight of the binder), and it has not been authorized to be used in California by the year 2020.

In summary, the rubber content should be adjusted according to project requirements and operating conditions. Sebaaly et al. *(57)* suggested that the optimum rubber content was dependent on binder source and rubber particle size.

For avoiding extremely high operation temperature and stability issues, the application of PG+X binder (five and ten percent rubber) potentially has less of the negative effects discussed above compared to conventional rubber-modified binders containing 15 percent and more rubber particles by weight of the binder.

2.1.4 *Effect of Rubber Production Methods*

Crumb rubber modifiers are produced by crushing at either ambient or cryogenic temperatures. Figure 2.2 illustrates these two grinding processes *(61)*, which are as follows:

1. Ambient-temperature grinding process: scrap tires are fed into shredders at or over the ambient-temperature (20°C to 40°C), and no cooling system is used to embrittle the rubber. This process typically provides rubber particles containing a rough and porous texture with a large surface area.

2. Cryogenic grinding process: scrap tires are cooled to temperatures below the glass transition temperature (i.e., <-62°C) using liquid nitrogen. At this low temperature, rubber can be crushed so that it shatters into small particles. Cryogenic processes require less energy and fewer machines compared to ambient-temperature grinding processes. Rubber particles manufactured by the cryogenic grinding process have a shiny, smooth surface.
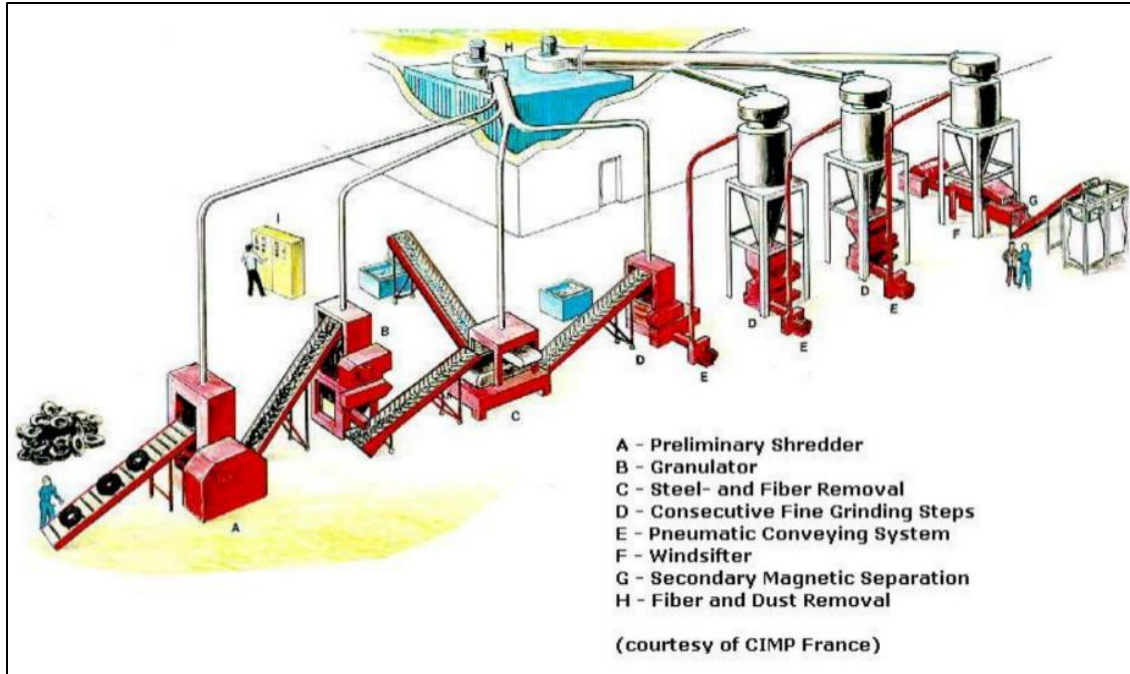
a: Ambient-temperature grinding process
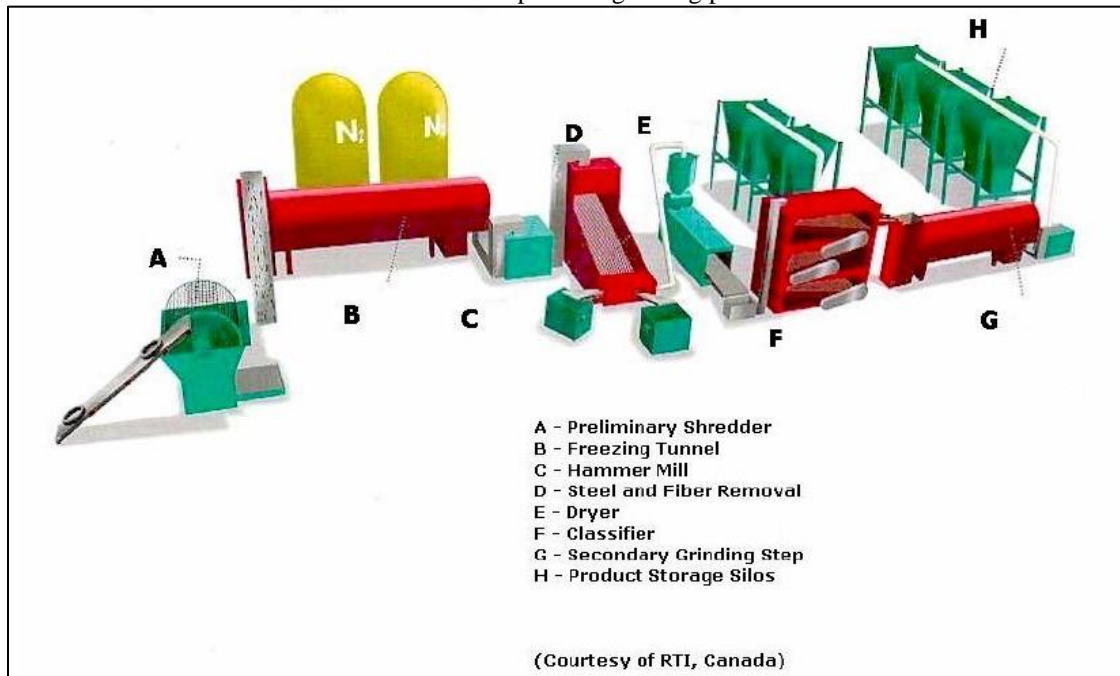
b: Cryogenic grinding process
Figure 2.2: Procedure for manufacturing the crumb rubber from scrap tires *(61)*.

Bahia and Davies *(47)* found that both ambient-temperature and cryogenically ground rubber (particles smaller than 600 microns) continued swelling in the binder at 160°C after 23 hours.

Thieves et al. *(41)* further investigated rubber swelling using a scanning electron microscope (SEM). They observed that the ambient-temperature ground rubber swelled faster than the cryogenic one. Both of them were fully digested in the binder after 90 minutes of blending at 180°C.

Theoretically, crumb rubber produced using the ambient temperature grinding process should perform better than cryogenically produced rubbers in terms of modification. Ambient-temperature ground rubber is porous and rough-textured, which enhances the swelling progress. Many studies *(41,49,62)* have found that ambient-temperature ground rubber had better modifications of binder rheological properties (higher complex moduli, lower phase angle) than fractured cryogenically ground rubber did. The former led to a more homogenous product.

Figure 2.3 shows the difference between these two types of rubber in the microstructure. The surface area of rubber particles produced at ambient temperatures is twice that of the particles produced cryogenically, implying an improved rubber-binder interaction for the former *(62)*. Researchers analyzed these rubber particles using gel permeation chromatography, which revealed that the ambient-temperature grinding process produces rougher edges because of the tearing action. In contrast, the cryogenically processed particles exhibited a flat structure due to the freezing and fracturing process *(63)*.

Shatanawi et al. *(63)* found that at the same rubber content, ambient-temperature ground rubber led to a better modification than the cryogenically ground rubber. The larger surface area in ambient-temperature ground rubber improves the rubber digestion by enabling a stronger chemical bond between the rubber and the binder phase. Compared to the cryogenically ground rubber, binders produced with the ambient-temperature ground rubber have a higher viscosity, higher

G*/sin(δ) values at high temperatures, lower G*$\times$sin(δ) value at intermediate temperatures, and lower creep stiffness at low temperatures *(52,64)*. Rubber-modified binders produced with ambient-temperature ground rubbers also have better storage stability *(63)*.
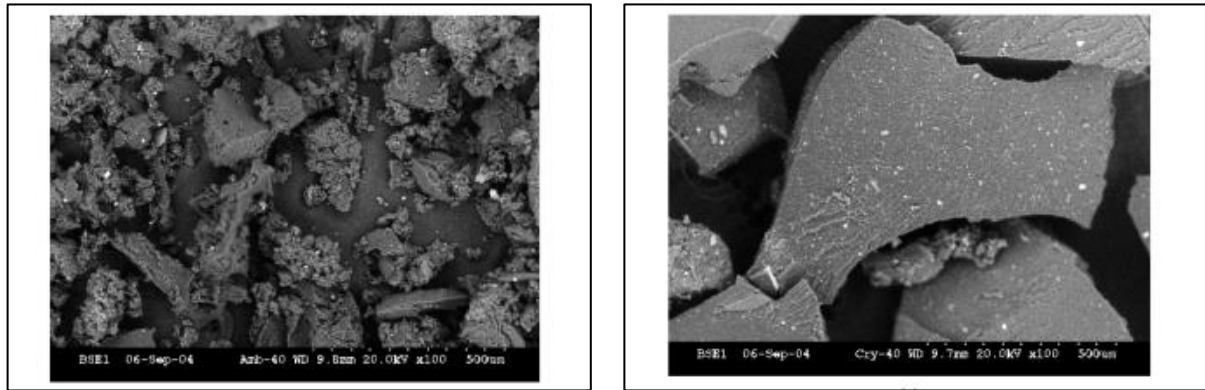
a): Ambient-temperature ground rubber   b): Cryogenically ground rubber
Figure 2.3: SEM images of ambient-temperature ground and cryogenically ground rubber *(41)*.

The literature review *(2-25)* revealed that most states used ambient-temperature ground rubber. In California, Caltrans only allows the cryogenic process for the initial breakdown of the tire to remove steel and fibers. The crumb rubber must be produced by ambient-temperature grinding to achieve the desired rough and porous texture. Therefore, this study exclusively evaluated the ambient-temperature ground rubber in asphalt binders and mixes.

2.1.5   Effect of Rubber Gradation

Crumb rubber modifiers can be fabricated into different gradations, ranging from less than 75 microns up to 2.36 mm (passing the #200 sieve up to #8 sieve). However, no standardization clarifies the boundary between fine and coarse rubber. In this study, rubber gradations specified for TR binder with particles smaller than 250 microns are defined as fine rubber, while the specifications typically used for field-blended binders are referred to as coarse rubber. From a performance perspective, fine rubber is preferred over coarse rubber for the following reasons.

1. The fine rubber particles are easier to digest, which accelerates the blending process. Due to the greater surface area, fine rubber absorbs light oils more efficiently. The relatively larger particle surface of fine rubber particles benefits rubber modification *(65,66)*. A rubber-modified binder produced with fine particles exhibits a higher complex viscosity and a lower phase angle at high in-service temperatures (i.e., 60°C) and a lower creep stiffness at low-temperatures than binders produced with coarse rubber *(4,53)*. Mixes produced with rubber-modified binders containing fine particles also provide better rutting resistance *(67)*.

2. The finer rubber with a larger particle surface improves the storage stability of the modified binder. Binders modified with fine rubbers are more viscous and more stable than those produced with the same content of coarse rubber. Figure 2.4 presents evidence for this conclusion *(39)*. This figure contains a fluorescence figure of rubber digestion of four-particle sizes in two base binders. In both binders, the finer rubber particles appear to have digested more effectively than the coarser particles. Rubber particles can be observed in the figure when particle sizes are 420 microns and 250 microns. In comparison, it is harder to detect rubber particles when the size drops down to 150 microns *(38)*.
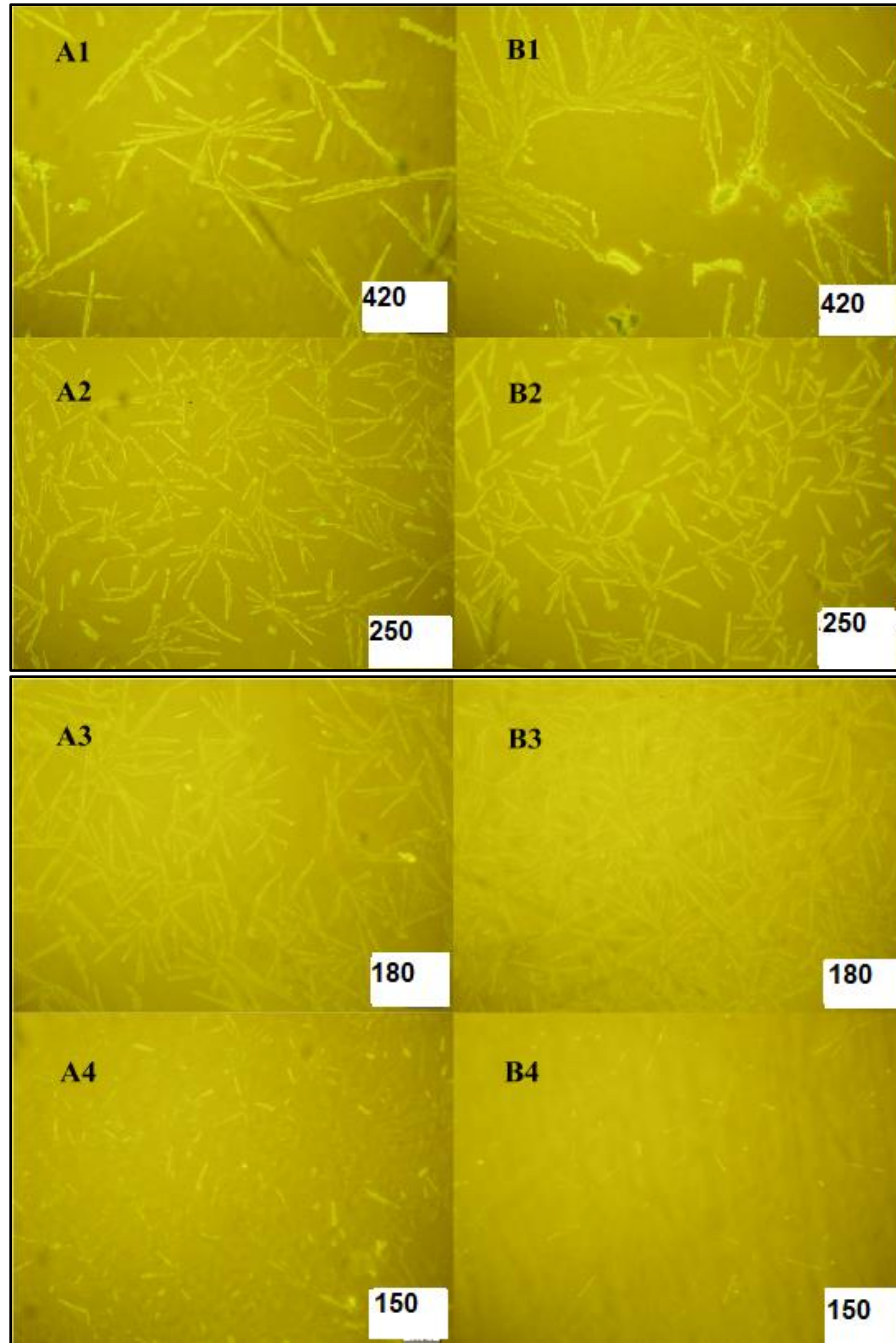
Figure 2.4: Fluorescence microscopy for two rubber-modified binders (A and B) with the rubber particle size of (1) 420 microns, (2) 250 microns, (3) 180 microns, (4) 150 microns *(39).*

In summary, the rubber particle surface area increases as particle size decreases. Smaller particles digest into the base binder more effectively than larger particles, resulting in a shorter blending time. The efficient interaction between fine rubber particles and the binder creates a more

homogenous product with better storage stability and in-service performance. Further studies are needed regarding the effect of rubber gradation on fatigue performance where conflicting observations were found in the literature *(50,53,67)*. Grinding rubber into finer particles is expensive. Therefore, optimum rubber gradations should be selected based on careful consideration of performance requirements and project budgets.

2.1.6   Rheological Measurement of Rubber-Modified Binder

Producing RHMA is conducted at elevated mixing and paving temperatures, typically 20°C to 40°C higher than the production temperatures for conventional HMA *(56)*. Consequently, the laboratory test of rubber-modified binders appears to require a modification of the current accelerated aging protocols to better reflect production temperatures in the field. The laboratory short-term oven-aging protocol needs to be modified to simulate the RHMA production process in an asphalt plant.

As mentioned in Section 2.1.2, the rubber-binder interactions in rubber-modified binders are complex, which leads to challenges in quantitative evaluation. The change in physical properties can indicate the degree of rubber modification, which also controls the rubber-modified binder performance. It is generally accepted that the evaluation criteria for rubber-modified binders should be dependent on physical parameters rather than chemical ones *(68)*.

The Superpave PG system is widely used to evaluate asphalt binder properties. It is appropriate for testing rubber-modified binders containing rubber particle sizes smaller than 250 microns (passing the #60 sieve), such as TR binders *(30)*. However, it may yield incorrect results when evaluating rubber-modified binders containing coarser rubber particles larger than 500 microns, such as AR binders *(70)*.

The following reasons mostly cause this incorrect measurement: first, the proximity of large rubber particles to the test plate can decrease the measuring accuracy. However, the current Superpave PG system *(30,74)* uses a parallel plate geometry with 1-mm or 2-mm gaps depending on the testing temperatures. Therefore, it is appropriate for determining the rheological properties of unmodified and TR binders since the particles are smaller than 250 microns (i.e., the gap size is greater than four times the size of the rubber particles). However, the system is not appropriate for AR binders because the rubber gradations used in them have particles that are larger than 500 microns, up to 2.36 mm. Investigation of the rheological measurement of these rubber-modified binders is warranted.

Second, according to the representative volume element (RVE) theory, the smallest sample volume size for the measurement to yield a value representative of the whole property is recommended to be three to four times the maximum individual particle size *(71-73)*. This theory is the generally accepted criteria for property evaluation.

Consequently, modification of the current Superpave PG system is necessary for evaluating rubber-modified binders containing coarse rubber particles. Researchers *(75,76)* proposed some potential modifications using concentric cylinder geometry, which was validated for PG testing at high temperatures (>58°C). This promising finding inspired the investigation of this geometry in a broader temperature range, including intermediate temperatures around 20°C, which are the usual temperatures for analyzing the fatigue performance. In this study, refinement of the modified PG system was conducted in preparation for evaluating PG+X binders.

2.1.7   Application of Rubber-Modified Binder in Hot Mix Asphalt

RHMA is commonly used in three aggregate gradations: dense-gradation, gap-gradation, and open-gradation. The performance of dense-graded rubberized hot mix asphalt (RHMA-D) depends on the elastic rubber recovery and mix stiffness. The structural capacity of RHMA-D is comparable with an SBS modified dense-graded mix *(45,77,78)*. RHMA-D appears to be only suitable for binders produced with fine rubber particles (i.e., TR binder). Xiao et al., Zhu et al., and Dong et al. *(45,77,78)* found that voids in the dense-graded mix might not be large or numerous enough to accommodate the large incompletely digested rubber particles, which influences compaction, and in turn, influences rutting and moisture resistance.

Gap-graded rubberized hot mix asphalt (RHMA-G) is the most widely used RHMA type in California. The gap-graded structure provides sufficient space in the aggregate (VMA) for accommodating the incompletely digested, coarse rubber particles. Hence, the minimum VMA requirement for RHMA-G is increased to 18 percent, compared to the 13 to 16 percent VMA range in a conventional dense-graded HMA *(2)*.

RHMA-G also requires higher binder content than dense-graded mix because the rubber is pre-blended with the binder. Therefore, the binder content in RHMA-G is the sum of rubber content and binder content together. The combination of rubber and binder provides a thick film covering the aggregates, which reduces the low temperature susceptibility of the mix. RHMA-G can potentially better withstand thermal cracking than the conventional dense-graded HMA *(53)*. In a thin surface layer (30 mm to 60 mm), RHMA-G usually has a long service life with better resistance to fatigue cracking and reflective cracking than the conventional dense-graded HMA *(79)*.

Open-graded rubberized hot mix asphalt (RHMA-O) is widely used as a surface layer to provide a quieter and more durable riding surface than HMA-O. The open-graded mixes generally require larger voids and consume more binders than dense-graded mixes. RHMA-O and RHMA-G have similar field performance, including better moisture damage resistance and rutting resistance than conventional dense-graded HMA *(80-82)*.

The literature review showed that RHMA had been widely studied. However, previous studies mostly investigated the use of RHMA in thin surface layers (typically 60 mm). When well designed, using RHMA in a thick layer is promising. This potential application of using rubber-modified mixes in different layer thicknesses with incorporating the rubber in additional ways fills in the study objective of the PG+X project.

2.2   Aging Mechanism of Asphalt Binder and Mix

Irreversible volatilization, steric hardening, oxidation, and reversible thixotropy are four identified asphalt aging processes *(83)*. The first three processes are irreversible, and they can stiffen the binder significantly. The reversible thixotropic hardening stiffens the binder by forming binder particles into a lattice structure, which is not a stable aging product. Thixotropic is recoverable when materials are exposed to heat and agitation *(84)*. Therefore, thixotropic hardening provides minor contributions to asphalt aging compared to the other three processes for in-service asphalt pavement.

Volatilization and steric hardening mostly occur during mix production and paving operations. Volatilization is defined as the loss of light binder compounds through evaporation at elevated temperatures (typically exceeds 110°C). Steric hardening, on the other hand, is a progressive polymerization process in which small molecules combine into large molecule-groups *(85)*. These

two processes are mostly observed in the early stages of aging (i.e., during the paving operation and the first few months after placement on the road).

The essential aging process is oxidation, which occurs throughout the life of asphalt materials. It is defined as binder compounds reacting with oxygen, creating large oxidative molecular groups. Oxidation is generally recognized as the primary aging process for in-service asphalt mix, with volatilization, steric hardening, and thixotropy aging having minor contributions to long-term aging *(85)*. Accessing oxidation or oxidative aging is the primary focus of this study.

Binder chemistry can also affect the rate of oxidative aging. Asphalt binder is a thermoplastic compound containing chemical elements of carbon, sulfur, and hydrogen, together with relatively small amounts of nitrogen, vanadium, nickel, and manganese *(86)*. Scholars usually divide the organic binder constituents into two groups: maltenes and asphaltenes. The chemical elements are the same in these two groups, but the molecular group size and structure are not. The mass weight of maltene is lower than that of asphaltene in any binder.

Maltenes can subdivide into saturates, aromatics, and resins according to the molecular weight in increasing order. Saturates consist of nonpolar materials, including linear, branched, and cyclic saturated hydrocarbons. Aromatics contain multiple aromatic rings. Resins contain relatively more polar substituents than aromatics. These polar substituents also exist in asphaltenes. The distinction between resin and asphaltene is solubility. The former can be dissolved in heptane or pentane, while asphaltene substituent is not *(87)*.

Asphaltenes have the highest polarity and the highest molecular weight compared to other molecular groups in asphalt binders. Asphaltenes and maltenes can be assembled in a colloidal structure to model the properties and performance of asphalt binders. Asphaltene forms the core,

covered by resins and aromatics, which are dispersed in saturates, as shown in Figure 2.5 *(88)*. Asphaltenes and resins generally control the binder stiffness and strength. In contrast, aromatics and saturates dominate viscous and plasticizing properties *(89)*. Therefore, the rheological properties of asphalt binder depend on the properties of these four individual fractions and their proportions that are all influenced by the aging process.
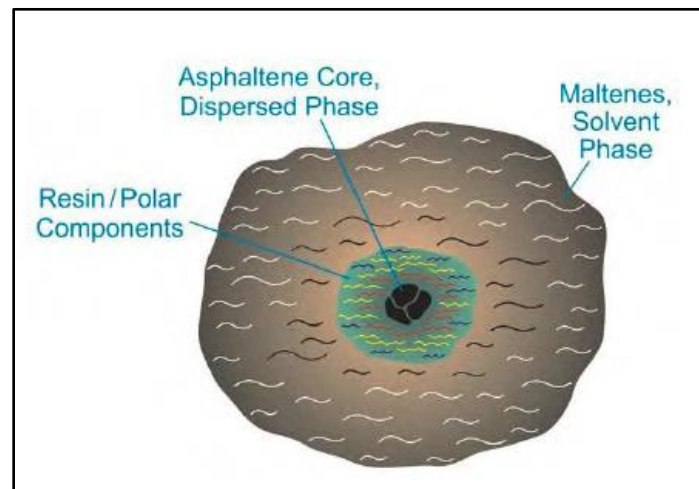
Figure 2.5: Asphalt binder colloidal structure *(88).*

Maltene components are highly vulnerable to oxidation. This time-dependent activity starts when oxygen contacts with asphalt binder through air voids in the asphalt mix *(18)*. Oxygen reacts with maltenes to generate carbonyl groups and sulfuric groups associated with polar species *(87)*. It is widely accepted that increased polar functional groups polar-polar interactions and yield a sol-gel transition. Oxidation generates a detectable change in the rheological property of the asphalt binder, which stiffens the binder. This reaction between diffused oxygen and asphalt binder is known as "oxidative aging" *(87)*. The newly developed asphaltenes change binder molecular structures. The asphaltenes associate with polar functional groups, resulting in a continuous stiffening and embrittlement of the binder *(18)*.

Binder components, pavement structures, and environmental conditions are factors that all affect the oxidative aging progress. High pavement temperatures and large interconnected voids in the mix lead to faster and more intense oxidative aging *(90)*. Using modifiers such as rubber and SBS, however, appears to slow oxidative aging *(91)*.

Oxidative aging causes hardening and stiffening of the binder. This stiffer binder, in turn, increases the stiffness of the asphalt mix *(92)*. Irreversible stiffening has numerous negative impacts. Mirza and Witczak *(19)* found that oxidative aging significantly affected the asphalt mix properties within 20 mm (0.75 in.) of the pavement surface because of its exposure to atmospheric oxygen. The aged asphalt mix is more vulnerable to adhesion failure between the binder and aggregate. This aged asphalt mix is susceptible to spalling, raveling, moisture damage, top-down cracking, low-temperature cracking, and fatigue cracking. These distresses shorten the service life of asphalt mix significantly *(93,94)*.

Oxidative aging in the pavement is a complex chemical-physical process. Although aggregate is not sensitive to aging (only weathering), aggregate properties (i.e., chemical constituents, gradation, water absorption) can affect the aging process. Different aggregates absorb different amounts of binder, which in turn affects film thicknesses *(94)*. Differences in film thickness lead to differences in oxygen diffusion, which, in turn, affects the rate of oxidative aging. Air-void contents influence the amount of oxygen that contacts the binder. Therefore, an aging gradient typically exists in the asphalt mix, with maximum aging at the surface and less aging at the bottom of the layer *(81)*.

According to AASHTO R 30 *(95)*, short-term laboratory-aging of HMA is achieved by oven-aging of the loose mix, which simulates the oxidative aging process during mix production. Long-term

aging of HMA is achieved by oven-aging compacted specimens to simulate aging after placement and compaction of the layer. Accidentally specimen collapses are observed during the long-term aging protocol, which damages the specimen before further laboratory testing. Recent studies *(81)* recommended to long-term oven-age loose mixes to prevent specimen collapses and reduce the aging gradient. The loose mix allows maximum contact with air, which promotes uniform laboratory aging. Specimens can be compacted with the aged mixes for testing.

Researchers from North Carolina State University, Arizona State University, and Western Research Institute *(96)* compared the aging in loose mixes and compacted specimens. They found that loose mix-aging was more severe than compacted specimen aging. There was an aging gradient in the compacted specimen due to oxygen diffusion. This aging gradient could be eliminated by reducing the specimen size. For example, using a specimen with 38 mm diameter and 100 mm height instead of the standard specimen size with 100 mm diameter and 150 mm height. They found that the best method to eliminate the aging gradient was to shorten the oxygen diffusion route in the mix by aging loose mix instead of compacted specimens *(96)*. This modification excludes the aging gradient effect on aged specimens. The long-term loose mix aging protocol was further investigated in this study.

2.2.1   Development of Aging Models

Researchers work towards understanding the mechanism of oxidative aging and modeling aging progress, with the goal of predicting the performance of asphalt mix at a given aging state. Most aging models predict binder viscosity changes using material parameters that include binder properties, aggregate properties, pavement structure, air-void content, depth of the layer from the

surface, and pavement temperatures. This section briefly describes three representative aging models.

One well-known model is the global aging system (GAS) model developed by Mirza and Witczak in 1995. This aging model predicts the binder viscosity change using a regression model of large-scale field data *(19)*. The database includes 2,308 measurements from 47 in-service projects.

Regression methods were applied to this database to generate the GAS model. The GAS model captures the increases in oxidative-related viscosity at 6 mm below the pavement surface. The basic equations used in the GAS model are given in Equations 2.1, 2.2, and 2.3.

$$log\ log\ \eta = A_R + VTS\ log\ T_R \qquad\qquad\qquad 2.1$$

$$log\ \frac{\eta}{13,000} = \frac{-8.5\ log\frac{Pen}{Pen_{T_{RB}}}}{5.42+log\frac{Pen}{Pen_{T_{RB}}}} \qquad\qquad\qquad 2.2$$

$$log\ log\ \eta_{aged} = \frac{log\ log\ \eta_{t=0}+At}{1+Bt}F_v \qquad\qquad\qquad 2.3$$

Where:

$A = -0.004166 + 1.41213C + C\ log(MAAT) + D\ log\ log\ \eta_{t=0}$

$B = 0.197725 + 0.068384\ log\ C$

$C = 10^{274.4946-193.831\ log\ T_R+33.9366\ log(T_R)^2}$

$D = -14.5521 + 10.47662\ log\ T_R - 1.88161\ log(T_R)^2$

η = viscosity measured by a penetration test in centipoise.

T_R = temperature in degree Rankine where the viscosity is estimated (°R= °F+459.7).

A_R = regression line intercept.

VTS = slope that defines the viscosity-temperature susceptibility.

η_{aged} = aged viscosity in centipoise, which represents the viscosity at an assumed depth of 6.3 mm (0.25 in.) from the surface.

η_t = viscosity at mixing/laydown in centipoise. Subscript (t) is the in-service time in months.

Parameter *A* = a function of the mean annual air temperature (MAAT) together with the viscosity at mix/laydown.

Parameter *B* = a function of the temperature of interest.

Parameter *FV* = adjustment factor for optional air void content

In Equation 2.1, measured binder penetrations and softening points are converted to viscosity over a broad range of temperatures at the initial stage before aging occurs. The slope of double-logarithmic viscosity versus logarithmic temperature represents the binder temperature susceptibility. In Equation 2.2, T_{RB} is the temperature measured at the softening point using a ring and ball test. The viscosity after mixing/laydown can be calculated with Equation 2.2. The viscosity of aged binders can be predicted using Equation 2.3.

The GAS model develops an empirical correlation between in-service time and binder viscosity at multiple temperatures. Since this model is only calibrated for dense-graded mixes containing conventional unmodified binders, it is not appropriate for modeling polymer- or rubber-modified asphalt mixes, including gap- and open-graded mixes.

In 2005, Houston et al. *(20)* developed another representative aging model using the data from field aging and laboratory pressure aging vessel (PAV)-aging. The PAV-aging is an accelerated laboratory protocol to accelerate the oxidative aging of asphalt binders by pressurizing air and elevating temperatures. This accelerated test is designed to simulate long-term oxidative aging and hardening of binders in the field, according to AASHTO R 28 *(97)*.

In the Superpave PG system, two laboratory-accelerated aging protocols are specified by AASHTO *(97,98)*. The Rolling Thin Film Oven (RTFO)-aging simulates short-term aging during production and placement of asphalt mixes *(99)*. The PAV-aging conducted at 2.1 MPa at an elevated temperature (typically 90°C to 110°C) simulates five to ten years of field aging of asphalt binders *(100)*.

There are several limitations to these laboratory aging protocols. For example, the range of five to ten years in the PAV-aging is rather broad, and the procedure does not support prediction outside

this range. The test method also does not account for a reduction in air-void content over time caused by densification under traffic loading. This change is apparent for pavements that are not well compacted during construction. To address these limitations, Houston et al. *(20)* proposed the following PAV-aging model to estimate field aging from PAV-aged binders.

$$t_{aging} = exp\left[\frac{\left(\frac{T_{PAV}}{0.445445 \times VA_{orig}^{0.378370}}\right) - 109.9632 + 78.2945 \times (log\ log\ \eta_{RTFO,60°C})^2}{2.132432 + 0.193560 \times (log\ log\ \eta_{RTFO,60°C})^2 \times MAAT}\right] \qquad 2.4$$

Where:
VA_{orig} = initial percent air-void content after construction.
$\eta_{RTFO,\ 60°C}$ = viscosity of RTFO residue at 60°C.
$MAAT$ = mean annual air temperature in °F.

During the PAV-aging model development, Houston et al. *(20)* found that the difference between laboratory-aging and field-aging could not be ignored. Aging of asphalt mixes with air-void contents higher than eight percent in the laboratory protocol was more severe than in the pavement after aging of seven to ten years. This situation was reversed when the mixes had air-void contents of less than eight percent.

Morian et al. *(102,103)* further investigated the influence of air-void contents on oxidative aging. They found that the slope of carbonyl group increment (or kinetics parameter) was significantly correlated to air void contents in the asphalt mix. The properties of the PAV-aged binders were close to those of the aged binders extracted from the mix when mix air-void content was over 11 percent. The difference between these two aging protocols grew when mix air-void content decreased, with PAV-aged binders being more conservative than those measured on field mixes.

The third aging model discussed is the dual-rate aging model developed by Glover et al. from Texas A&M University *(18)*. This model predicts physical properties after aging from chemical component changes and is described in detail in Section 2.2.3.

2.2.2   Measurement of Aging Components

As mentioned at the beginning of Section 2.2, asphalt binder contains various chemical components. Carbonyl and sulfoxide components have been identified as aging products that develop during oxidative aging *(85,104)*. The sulfoxide component is generated in the initial stages of aging. Its growth is usually terminated because of its instability over a long-term duration *(104)*. In contrast, the carbonyl component continues accumulating as long as these fractions have access to oxygen. The carbonyl component is the primary aging product in the long-term aging stages *(18,91)*. Consequently, the carbonyl component instead of the sulfoxide component should be used as the aging indicator for tracking oxidative aging in asphalt binders.

The carbonyl component contains a carbon atom with a double bond to an oxygen atom (C=O). This structure can further bond with other atoms or functional groups to form ketone, carboxylic acid, and anhydride *(85)*. Figure 2.6 sketches these component groups. Ketone contains a C=O bond and two attached carbon atoms. Carboxylic acid has a hydroxide (OH-) and an undefined functional group (R) attached to the C=O bond. Anhydride has one oxygen atom that bridges two C=O bonds, and each of them bonds with another undefined functional group (R and R').

Although there are numerous forms of carbonyl groups, major carbonyl groups in asphalt binders are primarily ketones with a long hydrocarbon chain *(105)*. Fourier transform infrared spectroscopy (FTIR) can precisely measure chemical components and track chemical component changes in asphalt *(106,107)*.
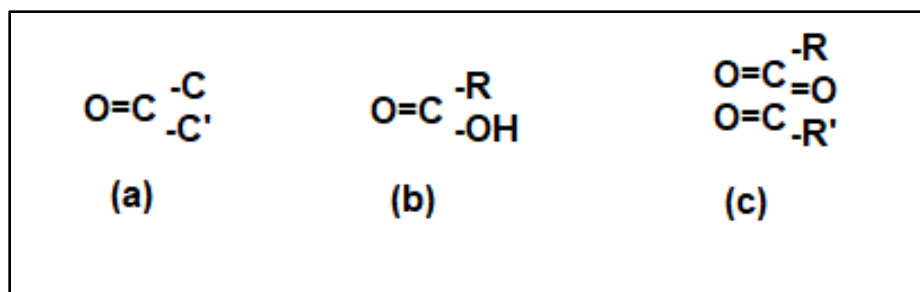
Figure 2.6. Illustration of carbonyl components: (a) ketone, (b) carboxylic acid, and (c) anhydride *(105)*.

Radiation is the functional core of the FTIR measurement. Material molecules and atoms absorb a distinctive wave of incident radiation. An absorbance spectrum can be used to identify the corresponding component *(108)*. The radiation travels in a sinusoidal waveform. One wave cycle of radiation travel is defined as the wavelength. The wavelength can be converted to wavenumber with Equation 2.5 *(109)*:

$$w = \frac{1}{\lambda} \qquad\qquad 2.5$$

Where:
w = wavenumber of light in cm^{-1}.
λ = wavelength of light in cm.

Figure 2.7 shows an FTIR spectrum of asphalt binder with wavenumber ranging from 4,000 cm^{-1} to 400 cm^{-1} using Bruker FTIR equipment. The spectrum plots wavenumber on the horizontal axis and the absorbance unit on the vertical axis. The absorbance unit is generated from Equation 2.6 *(109)*:

$$A = log\left(\frac{l_0}{l_1}\right) \qquad\qquad 2.6$$

Where:
A = specimen absorbance with arbitrary units.
l_0 = intensity of the background scanned at a specific wavenumber.
l_1 = intensity of the specimen scanned at the same wavenumber.

38

A background scan is always the first activity of the FTIR test. Background scans capture the absorbance of components not related to the specimen, and these are removed from the final spectrum. Twenty-four scans are applied to each specimen, and an average detected absorbance unit is obtained as the measurement result. The final specimen absorbance unit is calculated by subtracting the background absorbance from the detected absorbance. Peaks on the spectrum show specific components in specimens. The detailed settings of FTIR used in this study are documented in Section 4.2.2.
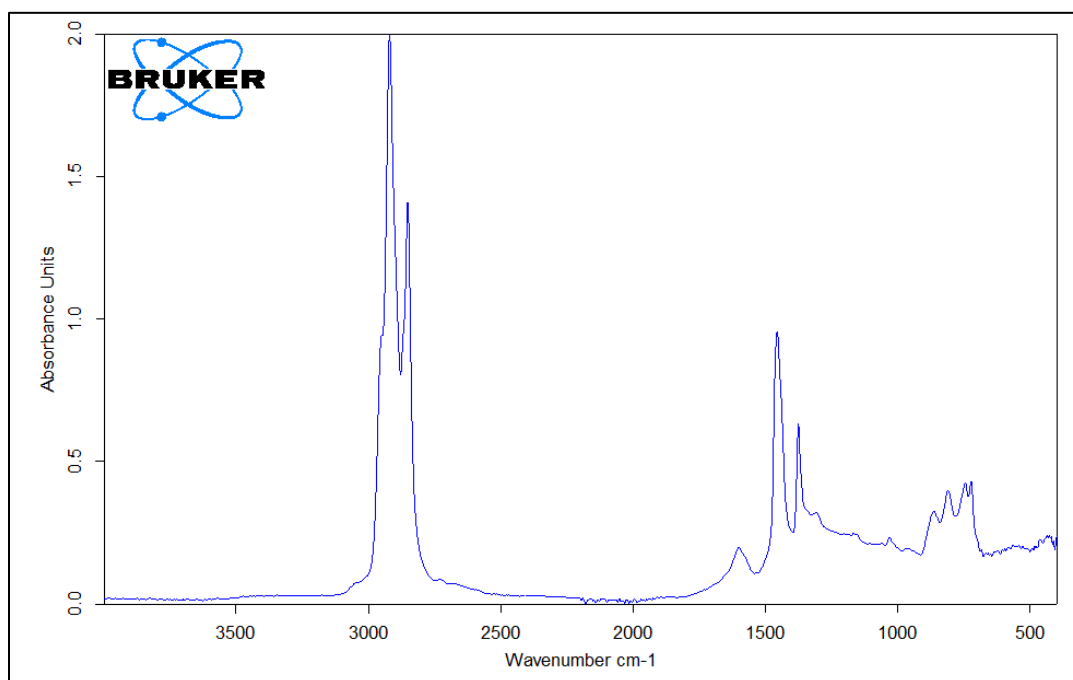
Figure 2.7: An example of the FTIR spectrum of asphalt binder.

2.2.3   Dual-Rate Aging Models

Glover et al. *(18,87,94,110)* divide oxidative aging into short- and long-term aging. In the short-term stage, chemical components rapidly react with oxygen since sufficient maltenes are available for oxidative reactions. The highest reaction rate occurs at the very beginning of oxidative aging, and it gradually decreases over time. This short-term oxidative aging mostly occurs during

production and placement and possibly the first few months after construction *(91)*. After that, long-term oxidative aging continues. The rate of oxidative aging reduces to a relatively slow but constant rate throughout the remaining service life of asphalt mix *(90,92)*. Figure 2.8 is a sketch of these two phases defined by the dual-rate aging theory *(18)*.

The dual-rate aging model developed by Glover et al. in 1992 *(18,87,94,110)* captures the change in chemical components and viscosities of the asphalt binder. In the short-term aging stage, aging products grow at a fast rate. An initial increase in viscosity occurs, shown as point A to point C in Figure 2.8. Point A refers to the binder at unaged status. Point B is considered as representative of the RTFO-aged binder, which is obtained from short-term laboratory aging. Point C is defined as the beginning point of the long-term aging stage, where aging products start to accumulate at a slow but constant rate. This constant-rate region is modeled by an Arrhenius expression with temperature and pressure parameters.
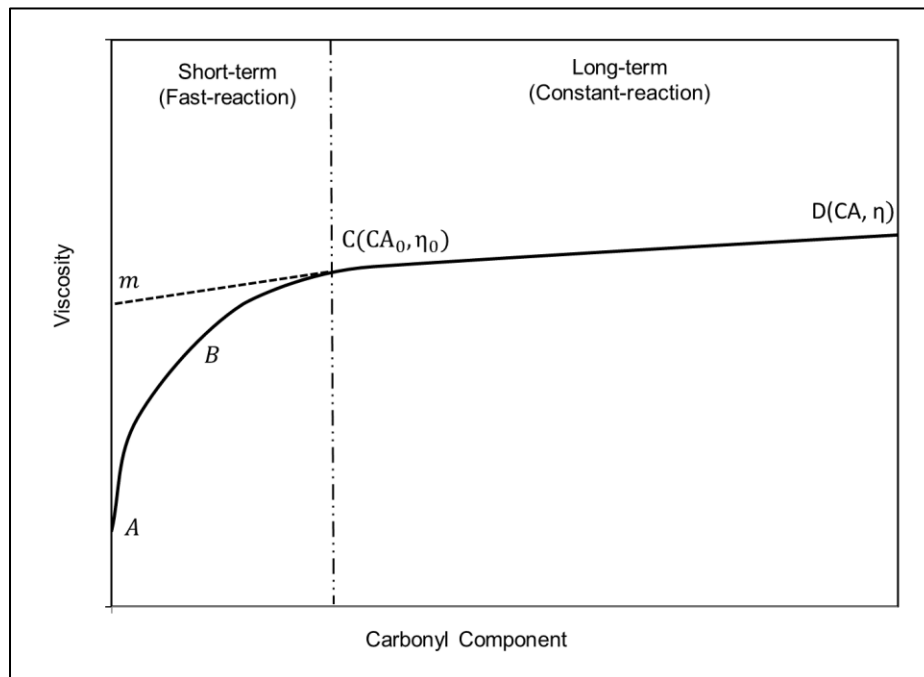
Figure 2.8: Oxidative aging phase defined in the dual-rate model *(18)*.

In the dual-rate model, the correlation between aging products and low-shear viscosity (LSV) at 60°C and 1.59E-05 Hz (0.0001 radians/second) can be modeled using Equation 2.7 and 2.8 *(111)*:

$$\ln \eta^* = \ln \eta_0^* + r_\eta t \qquad\qquad 2.7$$

$$CA = CA_0 + r_{CA}t \qquad\qquad 2.8$$

Where:
   η^* = complex viscosity.
   CA = numerical integration of the FTIR carbonyl area groups with a wavenumber from 1,650 cm^{-1} to 1,820 cm^{-1}.
   Subscript 0 = initial aging point of the long-term aging stage.

It should be noted that the η^*_0 and CA_0 values are higher than the values of RTFO-aged binders, as shown by the difference between point B and point C in Figure 2.8. The oxidative kinetic (r_{ca}) can be calculated from the Arrhenius equation (Equation 2.9) *(18)*:

$$r_a = A_a p^\alpha \exp \left(^{-E_a}/_{RT} \right) \qquad\qquad 2.9$$

Where:
   A = pre-exponential factor.
   P = oxygen partial pressure.
   $E\alpha$ = activation energy, and subscript α is the selected specific rate.
   R = universal gas constant.
   T = temperature.

The hardening susceptibility (HS) is used to calculate the hardening rate (r_η) from the oxidative kinetic (r_{ca}), as shown in Equation 2.10. This HS parameter is binder dependent at a given atmospheric pressure, as shown in Equation 2.11 *(87)*. A low HS value is favorable for resisting age-hardening effects *(91)*. The increasing rate of low shear viscosity is dependent on carbonyl growth.

$$\frac{d \ln \eta^*}{d t} = \frac{d \ln \eta^*}{d CA} \frac{d CA}{d t} \qquad\qquad 2.10$$

$$HS = \frac{d \ln \eta^*}{d CA} = \frac{r_\eta}{r_{CA}} \qquad\qquad 2.11$$

Where:

dCA/dt = growth rate of carbonyl area index (CA), representing the oxidative kinetic (r_{ca}).

HS = a correlation parameter, acting as a surrogate of the hardening rate.

Accelerated laboratory aging can be used to obtain the HS parameter. Hours of aging of the asphalt binder at high-temperatures in the laboratory can be converted to equivalent months or years of field-aging *(87)*. Several studies that investigated the possibility and accuracy of using accelerated aging approaches to match field-aging are presented in the following paragraphs.

Texas A&M Transportation Institute (TTI) conducted accelerated laboratory-aging on asphalt binders to predict the oxidative kinetic and hardening parameter for the dual-rate aging model *(94)*. The aging protocol entailed pouring a 1-mm thick binder film into pressure oxidation vessels (POV) at five different temperatures. Table 2.1 summarizes the setting of the laboratory aging protocol. The kinetic parameter (r_{ca}) obtained from the POV-aged binder fitted in the dual-rate aging model reasonably well. Results showed that oxidative kinetics and age-hardening models built on accelerated aging protocol could predict the oxidation and age-hardening *(94)*. These findings confirmed that POV-aging was a quick and reliable aging protocol to obtain the dual-rate aging model parameters.

Table 2.1: Texas A&M Laboratory Aging Test

Aging Temperature (°C)	Aging Duration (Days)
60	2, 5, 10, 15, 20, 30, 45, 60, 75, 90
70, 80	1, 3, 5, 7, 10, 20, 30, 40, 50, 60
89, 98	1, 2, 4, 6, 10, 15, 20, 25, 30

TTI also compared the PAV-aging at 2.1 MPa to the POV-aging at 0.1 MPa, which is normal atmospheric pressure. The results indicated that the PAV-aging generated a higher constant-reaction rate than the POV-aging. The activation energy of the PAV-aged binder was linear to that

of the POV-aged binder *(94)*. This finding revealed that a linear correlation could be used to relate short-duration PAV-aging results to those from long-term POV-aging.

The University of Nevada, Reno, conducted another POV-aging at an atmospheric air pressure near 0.08 MPa to represent local conditions. Table 2.2 summarizes the experimental factors. The results indicate that the aging rate of an individual binder was source dependent. Therefore, generalizations about asphalt binder aging should be made with caution *(105)*. Their second aging phase was conducted by PAV-aging, with durations of 20, 40, and 60 hours at 2.1 MPa. Comparison between PAV-aging and POV-aging showed an apparent difference between these two aging protocols. This study concluded that a full evaluation of field weather conditions and appropriate PAV-aging protocol setting are necessary for an accurate simulation of field-aging *(112)*.

Table 2.2: Reno Laboratory Aging Test

Aging Temperature (°C)	Aging Duration (Days)
50	4 to 320
60	2 to 160
85	0 to 40
100	0 to 12

In general, the carbonyl component increase showed the same tendency as the asphaltene increase during oxidative aging *(113-115)*. Lin et al. *(113)* further expanded the basic dual-rate aging model (Equation 2.10) to include the asphaltene function. In Equation 2.12, $(\partial \ln\eta^*/\partial AS)$ defines the asphaltene effect on binder stiffening, where $(\partial AS/\partial CA)$ is the asphaltene formation susceptibility. $(\partial AS/\partial CA)$ defines the maltene capacity to produce new asphaltenes. Along with oxidative aging, the amount of maltene reduces, and the rate of oxidative aging slows. The newly formed

asphaltenes affect binder viscosity. This reaction followed the Pal-Rhodes rule, as shown in

Equation 2.13 *(114)*.

$$r_\eta = \frac{d\ln\eta^*}{d\,t} = \frac{\partial\ln\eta^*}{\partial AS}\frac{\partial AS}{\partial CA}\frac{\partial CA}{\partial t} \qquad\qquad 2.12$$

$$\eta^* = \eta_m^*(1 - K\%AS)^{-v} \qquad\qquad 2.13$$

Where:
  $\eta_m{}^*$ = maltene viscosity.
  K = asphaltene solubility.
  $\%AS$ = asphaltene content in the binder.
  v = asphaltene particle shape parameter.

Chipps et al. *(115)* investigated rubber-modified binder aging and proposed an aging model based

on Lin's model. This study evaluated the asphaltene and macromolecule rubber particle analogy

effect on oxidative aging. The model was developed in Pal-Rhodes format, as shown in Equation

2.14.

$$\eta^* = \eta_m^*(1 - K_1\%AS - K_2\%p)^{-v_{avg}} \qquad\qquad 2.14$$

Where:
  K_1 and K_2 = constant parameters for asphaltene and rubber.
  p = weight amount fraction of tire rubber.

This equation was considered to provide approximate values because it ignored the proportion of

changes between asphaltene and the rubber during oxidative aging. This proportion change led to

the polar aromatics converting to asphaltene, which was not considered in the equation. Chipps et

al. *(115)* developed the following equation to calculate the HS of the rubber-modified binder:

$$HS = \frac{\partial\ln\eta}{\partial CA} = \frac{v_{avg}\left(K_1\frac{\partial\%AS}{\partial CA} + \frac{\partial K_2 p}{\partial CA}\right)}{1 - K_1\%AS - K_2\%p} \qquad\qquad 2.15$$

They also found that the HS value of rubber-modified binder remained approximately constant during aging due to the combined effects of parameters (∂%AS/∂CA) and (K_1%AS). The HS value is lower in a rubber-modified binder than in a conventional binder. The results indicate that relatively low HS values slowed the oxidative age-hardening *(115)*.

Jin et al. *(116)* later improved the dual-rate aging model to include both fast- and constant-rate reactions. The growth of the carbonyl component in the full aging phase is calculated using Equations 2.16, 2.17, and 2.18:

$$\frac{d\,CA}{d\,t} = M_{RTFO}r_f e^{-r_f t} + r_c \qquad\qquad 2.16$$

$$r_f = A_f p^\alpha e^{(-E_{af}/_{RT})} \qquad\qquad 2.17$$

$$r_c = A_c p^\alpha e^{(-E_{ac}/_{RT})} \qquad\qquad 2.18$$

Where:
    M_{RTFO} = limited amount of carbonyl component generated during the fast-reaction period.
    r_f and r_c = fast- and constant-reaction rates, which are dependent on the temperature.
    p = oxygen partial pressure,
    α = reaction order concerning P, whose average value is 0.27.

Based on carbonyl values calculated using the above equations, LSV at 60°C and 1.59E-05 Hz (0.0001 radians/second) after aging can be predicted by Equation 2.19, which is the integration format of Equation 2.11 *(117)*.

$$\eta_{LSV} = e^{HS \times CA + m} \qquad\qquad 2.19$$

In summary, the dual-rate aging model predicts oxidative aging through the following steps:

1. The carbonyl component after aging is determined using Equation 2.16 through Equation 2.18 at any aging temperature and atmospheric pressure conditions.

2. The LSV value after aging can be calculated using Equation 2.19 based on the carbonyl component and HS parameter obtained from laboratory tests. Practically, asphalt binder kinetics (E_a, A) and asphalt binder hardening parameters (HS, m) can be determined from measurements of accelerated laboratory aging of binders or mixes at several stages of aging (i.e., different aging temperatures over different durations).

The foundation of the dual-rate aging model is built on the kinetic rate of carbonyl components. This dual-rate aging model develops a regression correlation between oxidative products and rheological properties of the asphalt binder. The age-hardening model correlates carbonyl area group changes to low-shear viscosity increases. One limitation of this model is that it only estimates LSV, while the actual viscosity of the binder in asphalt mixes is mostly beyond this region. This limitation motivated the investigation of predicting viscosity beyond the LSV region in this study.

The original dual-rate aging model was developed on conventional unmodified binders and SBS-modified binders. Only one TR binder with a five percent rubber dosage by weight of the binder was evaluated using this model *(91)*. Further investigation of the dual-rate model on rubber-modified binders is required.

Farrar et al. *(118)* proposed another chemical-mechanical aging model in 2013. This model predicts the change in crossover modulus using a second-order aging kinetics relationship. Crossover modulus is defined as the cross point where storage modulus (G') and loss modulus (G'') is equal in the viscoelastic spectrum. From a structural perspective, the plateau region is a critical part of studying the molecular interaction, as it links with the molecular weight distribution,

which changes along with oxidative aging *(119)*. This change in molecular weight distribution, in turn, correlates to the carbonyl components *(118)*.

Farrar modified the dual-rate aging model by considering that fast-rate oxidative kinetics might not be practically significant for in-service pavements. This model introduced a continually changing rate of crossover modulus, and a reasonable prediction of crossover modulus for long-term aging was identified. The two original equations are Equation 2.20 and 2.21 *(118)*.

$$\frac{1}{G_C^*(t)} = \frac{1}{G_{C0}^*} + rt \qquad\qquad 2.20$$

$$r = AP^\alpha e^{-E/RT} \qquad\qquad 2.21$$

Where:
   $G_C^*(t)$ = crossover modulus as a function of time.
   G_{C0}^* = initial crossover modulus after production and placement.
   r = reaction rate that is also calculated using the Arrhenius equation.

This model receives less attention than the Glover dual-rate model, probably due to the crossover modulus alone providing limited information about binder performance. However, credit for results reported by Farrar is that rheological changes beyond low shear viscosity could be estimated from aging products. It further inspired the study of predicting binder viscosity beyond the LSV region in this study.

2.3   Aging Mechanisms in Rubber-Modified Binders

Oxidative- and age-hardening rates are mostly affected by binder components when sufficient oxygen is accessible. Consequently, oxidative aging can be altered by adding modifiers to asphalt binders *(96,102,104)*. Crumb rubber modifier is one such modifier. Huang and Pauli *(4)* found that rubber-modified binders were less brittle than their base binder after long-term oxidative aging, with crumb rubber appearing to act as an antioxidant.

47

Glover et al. and Farrar *(115,120)* found that rubber-modified binders showed slower oxidative aging than conventional binders. This improved aging resistance may be attributed to two mechanisms. Rubber either slows down the oxidative rate (chemical effect, rubber changes the oxidation of the binder) or reduces the age-hardening effect on binder properties (physical effect, oxidation continues but with limited stiffness increase), or a combined effect of these two mechanisms.

Specifically, for the physical effect, it may be credited to rubber particles that influence the viscosity together with the base binder *(8)*. Rubber-modified binders produced at relatively low temperatures (<200°C) yields a slow hardening rate and a low HS value. The swelling of rubber particles elevates the bulk viscosity by building gel-microstructures. In contrast, the high temperatures (>240°C) degrade long polymer chains and matrix structures in the binder. It diminishes rubber particle swelling and results in the aging product dominating the viscosity. Rubber-modified binder, after blending at high temperatures (>240°C), has relatively less aging resistance than those produced under low temperatures (<200°C). However, HS values were still lower than the base binder due to the increased resistance to oxygen diffusion *(8,115)*.

Modeling of oxidative aging in the rubber-modified binder is complicated because of two reasons. Firstly, the dual-rate aging model discussed in Section 2.2.3 only considers the viscoelastic behavior at LSV levels. This strain level does not accurately represent binder or mix performance. The magnitude difference in stiffness between aggregate and binder causes high strain levels to localize within the asphalt binder. Average binder strains are about eight times larger than the macroscopic bulk strain of the mix. Thus, strain levels in the asphalt binder are usually beyond the LSV range *(121-123)*. Secondly, the measurement of rheological properties is not accurate when using the current Superpave PG system, as discussed in Section 2.1.6. The potential offset of

rheological measurement can mislead the analysis of the age-hardening effect on rubber-modified binders, especially for those containing large rubber particles over 250 microns.

The complexity of evaluating oxidative aging also exists in the asphalt mix phase. Temperatures during mixing and paving operations can be highly variable. Air-void contents also vary in the mix, which results in inconsistent oxygen exposure. These uncertainties complicate the validation of asphalt binder models in asphalt mixes *(124)*. Therefore, using the aged mix to validate the binder aging model is warranted.

One possible solution is to reduce the mix specimen size to study oxidative aging in asphalt mixes *(96,125)*. Fine aggregate matrix (FAM) mixes containing the fine portion of the aggregate matrix (i.e., materials smaller than 2.36 mm, passing the #8 sieve) in an asphalt mix seems appropriate to be a connection between the binder and the full-gradation mix. Underwood *(125)* have already built a FAM aging model to connect binder and mix performance. However, there is still an aging gradient through the FAM mix specimen, and an appropriate methodology of producing FAM mix specimens is under discussion. Different methodologies have been proposed by different researchers *(96,126-128)*.

Another possible solution is to age the loose mix to exclude the aging gradient. The extracted binder from the aged asphalt mix could then be used to validate the aging model *(96)*. One limitation of this methodology is that the air-void content impact cannot be directly modeled based on loose mix aging alone. Besides, the extraction and recovery process may soften the recovered binder. Yazeed *(129)* compared the different solvents used in the extraction and found that the solvent type changed the recovered binder properties (i.e., complex modulus, phase angle). He also

suggested to complete the whole extraction and recovery test within 17 hours to limit the solvent effect on recovered binders.

2.4 Pavement Performance Using Rubber-Modified Mixes

Oxidative aging mostly occurs on the top surface, where easily exposed to oxygen. Luo et al. *(130)* found that oxidative aging could happen beyond the immediate top surface. In some cases, materials deeper than the top 25 mm (1") may be influenced by oxidative aging. The oxidative aging can change the pavement performance as the aged asphalt mix is stiff and brittle. Brittleness is mostly unfavorable for the pavement performance, while the consequence of stiffness change depends on the structure and the material response to loadings and temperature fluctuations.

One typical distress in service is low-temperature cracking caused by thermal fatigue under cycles of temperature fluctuation. This cracking initiates at the pavement surface, and it penetrates to the bottom of the layer. Oxidative aging causes the asphalt binder to become brittle and more susceptible to thermal cracking *(120)*.

Aged binder is stiffer than the original unaged binder and whether this stiffening leads to a beneficial effect on fatigue performance or not is layer thickness-dependent *(93)*. Bottom-up fatigue cracking is influenced by traffic loading, mix stiffness, and the relationship between stiffness and fatigue life to the tensile strain at the bottom of the layer. The standard rule is "stiffer mixes are better for thick pavements, and softer mixes are better for thin pavements". Figure 2.9 illustrates this statement graphically.

This rule points out the stiffness change effect on the mix fatigue life. A mechanistic analysis is required for different scenarios, with the consideration of mix stiffness and fatigue performance under different strains *(131)*.

In a relatively thin layer, fatigue performance is generally strain-controlled. Stiffening of binder reduces the asphalt mix's ability to dissipate the energy caused by traffic loading and environmental factors (i.e., daily temperature fluctuation creates thermal stress). When dynamic and thermal energies in asphalt mix beyond its withstanding capability, cohesive failure happens, resulting in pavement distresses, including top-down thermal-cracking and bottom-up fatigue cracking.

Conversely, in a thick asphalt layer, fatigue performance is mainly stress-controlled. Although brittle aged binder still impairs cracking resistance, this stiff binder can reduce the bending tensile strain at the bottom of the layer. This stiff material can reduce the risk of reflective and fatigue cracking attributed to the high stiffness generates a lower strain than the soft material. The performance of the thick pavement has to be analyzed through careful consideration of material properties and structural response to stress.
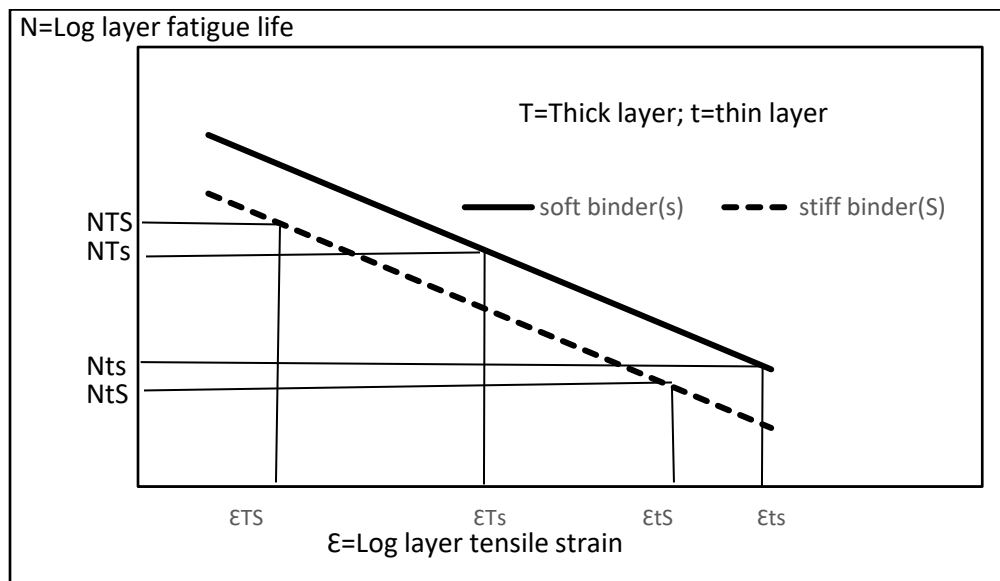
Figure 2.9: General rules of fatigue resistance and stiffness *(131).*

Rubber-modified binders appear to slow the aging compared to unmodified binders, indicating that RHMA would remain flexible for a longer duration *(123)*. In Figure 2.9, rubber-modified binder performance after long-term oxidative aging is plotted as the solid line, and conventional unmodified binder is plotted as a dashed line. In the thin layers, a soft binder (rubber-modified binder) provides a longer fatigue life under certain strain levels. Greene et al. *(31)* and Mohammad et al. *(132)* found that RHMA in a thin surface layer provided better cracking resistance than conventional HMA, attributing to the soft rubber-modified binder after a long-term of oxidative aging.

In thick layers, soft mixes can generate more significant tensile strains than stiffer mixes at certain stress levels, as shown in Figure 2.9. The rubber-modified mix performance in thick surface layers and other structural layers is not well evaluated and is the focus area of this study.

3 PROBLEM STATEMENT AND STUDY METHODOLOGY

3.1 Research Gaps

The following knowledge gaps identified from the background and literature review in Chapter 1 and Chapter 2 are addressed in this study:

1. Refinement of the Rheological Measurement for Rubber-Modified Binders

The current Superpave PG system cannot precisely measure Rubber-modified binders with large rubber particles (>250 microns) due to swelled rubber particles dominating the measurements inside of the binder. Certain modifications to current PG methods are necessary to evaluate these rubber-modified binders. This study further advanced the modified Superpave PG system to analyze the aging mechanism of rubber-modified binders and the performance of PG+X binders. The refinement included a modification of the laboratory aging protocol to match field aging and a modification of the PG test at intermediate temperatures (around 25°C).

2. Investigation into the Oxidative Aging of Rubber-Modified Binders and Mixes

An investigation into the oxidative aging mechanisms of rubber-modified binders and mixes was conducted in this study. This study planned to validate the Glover dual-rate model using accelerated aging in UCPRC. The prediction of the viscosity beyond the low shear viscosity region was also studied, which is necessary to better understand oxidative aging. A refinement of the age-hardening model (HS model) was proposed to make it more capable of predicting the viscosity beyond the low shear viscosity region. This refined model was calibrated and validated using unmodified binders, SBS-modified binders, and RAP binders. This model was further investigated to model age-hardening on rubber-modified binders.

In the asphalt mix studies, the first step was to age the mix with the consideration of eliminating the aging gradient effect. Aging the loose mixes instead of the compacted specimen was used to maximize the mix exposure to oxygen and minimize the aging gradient. After this aging protocol, mix properties were evaluated and compared to those before aging. The refined binder age-hardening model (generic hardening susceptibility [GHS] model) was calibrated and validated using the data from aged asphalt mixes. The oxidative aging effects on the mix stiffness and fatigue performance were evaluated.

3. Performance Evaluation of PG+X Binders

The performance of rubber-modified binder containing five and ten percent rubber by weight of the binder (PG+X binders) was evaluated using the refined Superpave PG system. The measured performance included rheological properties (complex modulus and phase angle) at multiple temperatures and frequencies, stress recoveries at high temperatures, and creep stiffnesses at low temperatures. A comprehensive analysis of the rubber effect on the performance of rubber-modified binders was conducted.

4. Evaluation of the Use of PG+X Mixes in Different Pavement Structures

This study investigated new types of rubber-modified mixes containing low rubber contents (five and ten percent by weight of the binder) in dense-gradations (PG+X mixes) *(17)*. A series of laboratory tests were conducted to evaluate the mix stiffness, rutting resistance, moisture damage resistance, fatigue performance, and thermal-cracking resistance.

The field performance of rubber-modified asphalt mix was simulated and analyzed using the mechanistic-empirical design software (*CalME*). In addition, to understand the PG+X mix performance in a relatively thin layer scenario (thinner than 60 mm), the performance of thicker

54

PG+X mix layers was also analyzed. Evaluation of the use of PG+X materials in various pavement structures was evaluated with mechanistic-empirical design methods.

5.   Recommendations for using PG+X Materials.

Recommendations for using PG+X mixes were made based on findings from this study, with a specific focus on material properties, pavement structures, and climate conditions.

3.2   Questions to Be Answered

This study focused on the following questions to fill in knowledge gaps regarding the oxidative aging and aging-related performance of rubber-modified binders and mixes:

Question set 1.   Investigation of asphalt binder aging mechanisms.

   a. How do binder components (i.e., carbonyl and sulfoxide components) change during oxidative aging?

   b. How do binder dynamic moduli change after oxidative aging?

   c. How can the age-hardening model (HS model) proposed by the Glover team be modified to accommodate the prediction of viscosities beyond the low shear viscosity region?

   d. How well does the modified age-hardening model (GHS model) predict the properties of the different asphalt binders considered in this study?

Question set 2.   Application of the modified age-hardening model (GHS model) for rubber-modified binders.

   a. What is an appropriate methodology for measuring the rheological properties (i.e., complex modulus, phase angle) of rubber-modified binders, especially for those

containing large incompletely digested rubber particles (up to 2.36 mm [passing the #8 sieve])?

b. How do aging products (i.e., carbonyl and sulfoxide components) accumulate in rubber-modified binders during oxidative aging? What is the crumb rubber modifier effect on oxidative aging of the binder?

c. How can the age-hardening of rubber-modified binders be predicted using GHS model?

Question set 3.   Evaluation of oxidative aging of the asphalt mix.

a. Will the loose mix aging protocol used in this study cause high variability in binder contents, mix stiffnesses, and fatigue lives of the compacted specimens?

b. Can the binder GHS model be used for the recovered binders from aged asphalt mixes?

c. How does oxidative aging affect mix stiffness?

d. How does oxidative aging affect mix fatigue performance?

Question set 4.   Performance evaluation of PG+X binders and mixes.

a. How do PG+X binders perform in the laboratory?

b. Can PG+X materials be effectively used in dense-graded mixes?

c. How do PG+X mixes perform in the laboratory in terms of rutting, fatigue, and thermal cracking?

d. What are the appropriate uses of PG+X mixes in different pavement structures and climates?

3.3 Study Objectives and Tasks

The objectives of this dissertation were to investigate oxidative aging and to evaluate its influence on asphalt binders and mixes. This study also aimed to investigate the performance of PG+X materials using laboratory tests and to optimize their application in mechanistic-empirical design. Completion of the following tasks was required to achieve these objectives.

Task set 1:   Understand existing knowledge through a literature survey.

Task set 2:   Investigation of asphalt binder oxidative aging mechanisms:

    a. Measurement of chemical components under a variety of aging conditions and determination of an appropriate tracking indicator for oxidative aging.

    b. Measurement of the rheological property changes of asphalt binders under different aging conditions.

    c. Modification of the age-hardening model (HS model) to be capable of predicting viscosities beyond the low shear viscosity region.

    d. Validation of the modified age-hardening model (GHS model).

Task set 3:   Application of the modified age-hardening model (GHS model) for rubber-modified binders.

    a. Modification of the current laboratory-aging protocol to simulate field-aging during RHMA mix production.

    b. Validation and refinement of the modified Superpave PG system.

    c. Measurement of chemical component changes in rubber-modified binders.

    d. Calibration of the GHS model using rubber-modified binders.

Task set 4:   Evaluation of oxidative aging of the asphalt mix.

    a. Laboratory aging of loose mixes to simulate the field aging of asphalt mixes.

b. Calibration of the binder GHS model using the data obtained from aged asphalt mixes.

c. Analysis of the oxidative aging effect on mix stiffness

d. Analysis of the oxidative aging effect on mix fatigue performance.

Task set 5:   Performance evaluation of PG+X binders and mixes.

a. Evaluation of rubber-modified binders containing low contents of crumb rubber modifier.

b. Mix design of the rubber-modified dense-graded mixes containing low contents of crumb rubber modifier.

c. Performance evaluation of PG+X materials using laboratory tests.

d. Understanding how PG+X materials can best be used in a pavement structure using *CalME* simulation.

3.4   Structure and Content

The subsequent chapters of this dissertation are structured as follows:

- Chapter 4 discusses the study of oxidative aging. This chapter answers the questions in Question set-1 in Section 3.2 by accomplishing the work listed in Task set-2. The chemical component changes during oxidative aging were analyzed. In terms of viscosity changes beyond the low shear viscosity region, physical properties were predicted with the modified age-hardening model (GHS model). Different types of binders were tested to calibrate and validate the modified age-hardening model.

- Chapter 5 documents the investigation of oxidative aging on rubber-modified binders. This chapter answers questions in Question set-2 in Section 3.2 by accomplishing the work listed in Task set-3. Changes in chemical components owing to the crumb rubber and

oxidative aging were measured. A refined performance-grading system was validated, which was used to measure the rheological properties of rubber-modified binders. The modified age-hardening model (GHS model) developed in Chapter 4 was calibrated for rubber-modified binders.

- Chapter 6 summarizes the analysis of oxidative aging in asphalt mixes. This chapter answers the questions in Question set-3 in Section 3.2 by accomplishing the work listed in Task set-4. The modified binder age-hardening model (GHS model) was validated using the data from testing extracted binders from laboratory-aged mixes. The mix stiffness and fatigue life after laboratory-aging were evaluated. The correlations between carbonyl component changes in extracted binders and the mix performance (stiffness and fatigue life changes) were analyzed.

- Chapter 7 summarizes the performance evaluation of PG+X materials under different aging conditions. This chapter answers the Question set-4 in Section 3.2 by accomplishing the work listed in Task set-5. The PG+X binders were performance-graded. The mix tests included the Hamburg wheel track test, unconfined repeated load triaxial test, flexural frequency sweep test, flexural fatigue test, and uniaxial thermal stress and strain test. Mechanistic-empirical pavement performance simulation procedures were used to evaluate PG+X performance for a range of pavement structures, traffic loadings, and environmental conditions. A comparison of simulated performance between the PG+X mixes and the conventional mixes was made based on these simulation results.

- Chapter 8 summarizes the findings and conclusions of this study and provides recommendations for future studies.

Figure 3.1 illustrates the framework for this study.
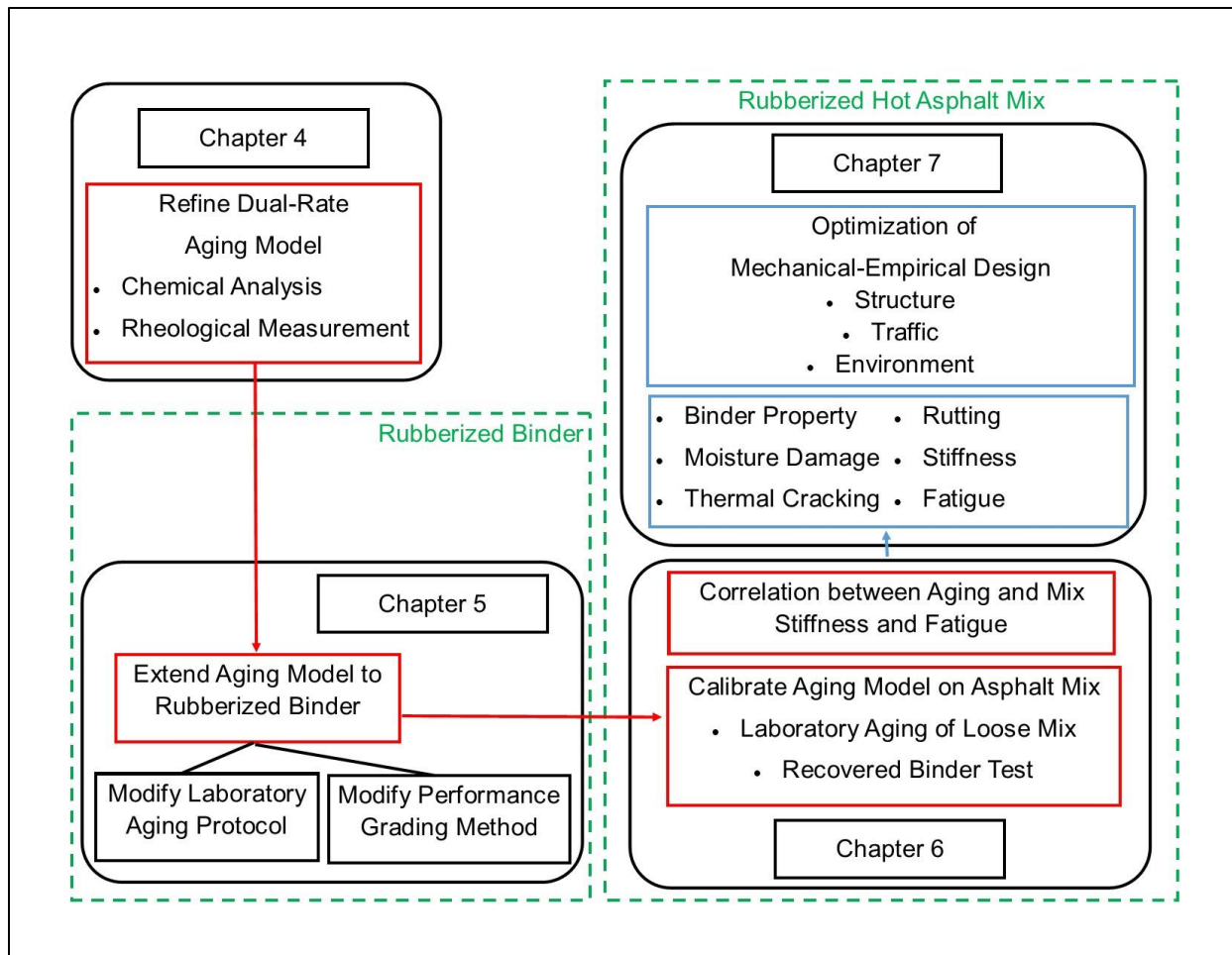
Figure 3.1: Framework for the study.

4   INVESTIGATION INTO ASPHALT BINDER AGING MECHANISMS

4.1   Introduction

This chapter presents the investigation into oxidative aging mechanisms of asphalt binders. The objective of this chapter was to analyze oxidative aging in different types of binders. The following questions were addressed:

- How do binder components (i.e., carbonyl and sulfoxide components) change during oxidative aging?

- How do binder dynamic moduli change after oxidative aging?

- How can the age-hardening model (HS model) proposed by the Glover team be modified to accommodate the prediction of viscosities beyond the low shear viscosity region?

- How well does the modified age-hardening model predict the properties of the different asphalt binders considered in this study?

The steps taken to address these questions were:

1. Measurement of chemical components under a variety of aging conditions and determination of an appropriate tracking indicator for oxidative aging.

2. Measurement of the rheological property changes of asphalt binders under different aging conditions.

3. Modification of the age-hardening model (HS model) to be capable of predicting viscosities beyond the low shear viscosity region.

4. Validation of the modified age-hardening model (generic hardening susceptibility [GHS] model).

4.2 Experimental Design and Test Methodology

4.2.1 Material Preparation and Experimental Factors

Nine binders were evaluated in this chapter, including five unmodified binders, two SBS binders, and two AR binders. Table 4.1 summarizes the binder information. These binders were produced from different oil sources. The PGs of these binders represent the usual PGs used in California. The PGs of the base binders for AR binders instead of their final PGs are presented in Table 4.1 due to the geometry limitation discussed in Section 2.1.6 *(75,76)*. The performance grading of AR binders is discussed in Chapter 5.

Table 4.1: Summary of Experimental Materials

Binder ID	Modifier and Dosage	Source	Binder PG
PG 64-10_1	-	Refinery 1	64-10
PG 64-16_1	-	Refinery 1	64-16
PG 64-28PM_1	4%SBS	Refinery 1	64-28 PM
PG 64-16_2	-	Refinery 2	64-16
PG 70-10_2	-	Refinery 2	70-10
PG 58-28_3	-	Refinery 3	58-28
PG 76-22PM_3	4%SBS	Refinery 3	76-22 PM
AR_4	20% CRM	Refinery 4	64-16 (Base)
AR_5	20% CRM	Refinery 5	64-16 (Base)

These binders were aged according to the RTFO-aging protocol at 163°C for 85 minutes to simulate short-term aging during mix production and placement *(98,101)*. These RTFO residues were then divided into two groups for long-term aging. The accelerated field-and laboratory-aging were conducted separately. The objective of these two aging protocols was to obtain aged specimens in a relatively short period of time. The material preparation process was based on Hofko and Alavi *(133)*.

The field-aging and the PAV-aging were considered as the accelerated aging protocol. For field aging, binder samples were loaded with thin binder films on glass plates that maximized the field aging progress. On the other hand, the PAV-aging is an accelerated laboratory aging test that simulates five to ten years of field-aging (*97*). These two accelerated aging protocols were analyzed and compared in this study.

In the field-aging protocol, six aging racks were constructed on the west side of the UCPRC grounds in June 2016. Figure 4.1 shows the site of these racks with a red mark, which is located at (38°32'03"N, 121°47'41"W). The UCPRC facility experiences a Mediterranean climate with hot daytime temperatures and generally no rainfall during the hottest months between May and September.

Figure 4.1: Arial view of UCPRC and location of the aging racks (source from Google Map).

Figure 4.2 shows that each rack consists of an outer frame, which was mounted to two poles. The outer frame carries a set of eight L-shaped sections, which supports glass plates. Each rack provides a maximum capacity of 40 glass plates. A total of 240 glass plates can be exposed to field aging simultaneously. The frames are angled at five degrees towards the south, which ensures a direct exposure to sunlight that avoids shadowing from trees or nearby buildings.

Figure 4.2: Six aging racks (left), an unloaded aging rack (center), and aging rack loaded with glass plates (right).

Each type of binder was applied onto a series of eight glass plates. They were located in the aging rack in a row. The glass plate (20×20 cm^2) was wrapped by a cardboard frame that provided a 12.6×12.6 cm^2 square area in the plate center. The target coating thickness was 1 mm in this framed area. A total of 16.3 g binder was required to reach this coating with a presumed binder density of 1.02 g/cm³. Before coating, the empty glass plate was weighed (m_1), and the hot binder was then poured onto the plate. The hot binder was evenly spread across the plate using a 20 cm wide palette knife. After the coated binder had cooled down to ambient temperature (around 25°C), the cardboard frame was carefully removed, and the coated glass plate was weighed again (m_2). The exact dimensions of the coated area were recorded (l_1 and l_2). The theoretical binder film thickness (b) was then calculated using Equation 4.1:

$$b = \frac{m_2 - m_1}{(1.02/l_1 - l_2)}$$ <div align="right">4.1</div>

Where:

    b = binder film thickness in mm.

    m_1 = glass plate weight in grams.

    m_2 = glass plate weight after application of binder in grams.

    l_1 and l_2 = dimensions of the coated area in mm.

Samples with a coat thicker than 1.3 mm or thinner than 0.7 mm were discarded from the study. The median thickness of all 72 samples was 1.0 mm, and 75 percent of these specimens had a thickness between 0.9 mm and 1.2 mm. The production of aging specimens started on June 27th, 2016 and was completed by August 4th, 2016. The aging racks were loaded on August 8th, 2016, which was the start date of this field-aging protocol. Table 4.2 summarizes the test factors and factorial levels.

<div align="center">**Table 4.2: Field-Aging Experimental Factors**</div>

Factor	Factor Level	Detail
Binder Type	3	Five unmodified binders, two SBS modified binders, two AR binders
Aging Temperature	-	Actual temperatures recorded
Aging Duration	6	Specimens were collected after six different aging times
Aging Pressure	1	0.1 MPa

The original plan was to age these binders for two years. However, a lack of adhesion between the binder specimens and the glass plates was observed after early rains (Nov 15th, 2016), which forced a pause in the study about three months after its start date. Table 4.3 presents the sampling schedule in these first 98 days. The daily temperatures from August 8th to November 15th were assumed as the approximate temperature inside the thin binder films. A high temperature is expected to accelerate oxidative aging, as the Arrhenius equation (Equation 2.9) shows *(18)*. Temperature fluctuations during the aging period could cause variability of the oxidative aging in the field.

Theoretically, the pavement surface is the location where maximum aging occurs in the field *(134)*.

The glass plate was used to provide a way to simulate the maximum aging in the field in a short

period of time. The thinness of the binder layer coated on the glass sheets in this study accelerates

the aging progress by maximizing exposure to oxygen.

Table 4.3: Sampling of Field-Aged Binder

Date	Cumulative Field-Aging in Days for Each Date	Average Field Temperature (°C)	Maximum Temperature (°C)	Days of Max Temperature over 30°C
08/23/2016	15 days	24.2	38.9	15
09/06/2016	29 days	21.2	32.2	11
09/20/2016	43 days	22.5	37.2	10
10/18/2016	70 days	19.0	32.2	10
11/15/2016	99 days	14.0	28.9	0

A small amount of binder was scratched off from the plate using a spatula at the intervals listed in

Table 4.3. The samples were then transferred into small tins, sealed, labeled, and stored for further

laboratory testing.

Figure 4.3 shows a comparison between a newly produced specimen and a 60-day aged specimen.

The original black color was faded in the aged binder. The binder film was thinner than the original

binder film, which was attributed to volatilization and oxidative aging *(85)*.
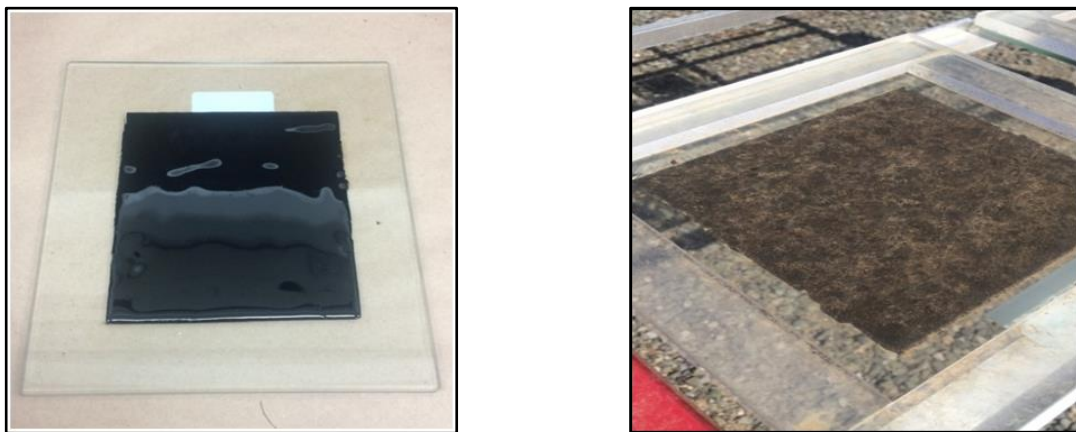
Figure 4.3: Binder film before field-aging (left) and after 60 days of field-aging (right).

For the accelerated laboratory aging protocol, a series of PAV-aging were conducted to simulate the in-service long-term oxidative aging at a selected temperature, following AASHTO R 28 *(97)*. The PAV-aging was conducted to obtain aged binders in a short time and to compare their properties to those subject to the field aging protocol for validating the aging kinetic model. The PAV-aging also provided data for developing a refined age-hardening model. Table 4.4 summarizes the experimental factors and factorial levels for the accelerated aging protocol.

Table 4.4: Laboratory Accelerated Aging Experimental Design Factors and Factorial Levels

Factor	Factor Level	Detail
Binder Type	3	Five unmodified binders, two SBS modified binders, two AR binders (same binders used in field aging protocol)
Aging Temperate	2	90°C and 100°C
Aging Duration	3	20 hours, 40 hours, and 60 hours
Aging Pressure	1	2.1 MPa

One modification of the PAV-aging was made to avoid multiple re-heating cycles of aged residues. Binder specimens were loaded into small tins (32 mm diameter), nine of which were then placed around the outside of the PAV pan (Figure 4.4), instead of just pouring the binder into the standard PAV pans (140 mm diameter). No tin was put in the pan center to ensure that all tins were subjected to the same level of aging. This modification introduced two benefits. First, the binder in individual small tins is easier and quicker to heat to the dynamic shear rheometer (DSR) testing temperature. It is easier to pour it into the DSR test mold or place it into the FTIR scan plate. Second, separated small tins prevent multiple oven heating cycles of specimens, which reduces the operational impact introduced when comparing between field-and laboratory-aging.

Figure 4.4: Modified PAV loading - small tin loaded in standard PAV pan (left), loaded tins put in PAV frame (right).

4.2.2   Measurement of Chemical Components

After the prescribed aging protocols were completed, aged samples were reheated in sealed containers at 163°C for no longer than five minutes to get sufficient workability without overheating. The small amount of scraped samples ensured that the preheating was kept as short as possible to limit additional oxidative aging.

The binder samples were evaluated using a Bruker ALPHA FTIR spectrometer with platinum attenuated total reflection (ATR) that holds a diamond ATR mold. After thoroughly cleaning the optics with citric acid and acetone, a small mass of preheated binder was applied directly onto the FTIR scan plate. A paper spacer was applied over the sample to prevent any contamination of the FTIR equipment. Constant pressure was applied to the paper by the device to ensure full contact between the optics and binder sample. Figure 4.5 sketches the steps of the loading procedure.

Figure 4.5: Application of sample: FTIR device before sample loading (left), with attached sample (center) and with paper spacer and holding arm (right).

This FTIR equipment can record spectra in a reflective mode from 4,000 to 400 cm^{-1} at a resolution of 4 cm^{-1}. The advantage of using the reflective mode is that the specimen does not have to be diluted with any solvents. This simplifies and expedites the sample preparation without losing any spectral information *(133)*.

Each measurement entails 24 scans, and an average value is recorded. Nine replicate measurements were taken to ensure that representative measurements of each binder sample were collected *(133)*. Visible changes were noted in the carbonyl, ether and ester, and sulfoxide components. Consequently, these components were analyzed in this chapter.

The carbonyl (CA) component area is usually defined as the band around the peak at 1,680 cm^{-1}. The ether and ester component area covers a broader band from 1,100 cm^{-1} to 1,260 cm^{-1}, and the sulfoxide (SUL) component area is the band around the peak at 1,030 cm^{-1} *(104,105,133,135)*. The component area for tracking the rubber is butadiene with a peak at 960 cm^{-1} *(136-139)*. This butadiene component is analyzed in Chapter 5.

The upper and lower wavenumbers chosen around the peak are the start and end points of the corresponding component area. Table 4.5 lists wavenumbers applied in this study.

Table 4.5: Wavenumber for Integration of Chemical Area Index

Index	Lower Wavenumber (cm⁻¹)	Upper Wavenumber (cm⁻¹)
Carbonyl	1,675	1,720
Ester and Ether	1,110	1,263
Sulfoxide	982	1,050
Butadiene	950	979

Each area index was calculated separately from the selected wavenumber ranges listed in Table 4.5. These area indices quantitatively measured the corresponding chemical changes in oxidative aging. The respective areas were derived by integrating the absorbance spectrum around the defined band in a tangential integration. Figure 4.6 shows an example of a spectrum and the respective component areas. The spectra were normalized to the aliphatic band at 2,923 cm⁻¹, which is widely acknowledged as not being affected by aging over time *(133,140)*. The normalization was used to eliminate the variability introduced by the operation and background impact. The chemical component area index was then integrated from normalized spectra using Equation 4.2 *(133)*:

$$I_i = \int_{w_{l,i}}^{w_{u,i}} a(w)dw - \frac{a(w_{u,i})+a(w_{l,i})}{2} \times (w_{u,i} - w_{l,i}) \qquad 4.2$$

Where:
I_i = index of area i.
$w_{l,i}$ = lower wavenumber for area i.
$w_{u,i}$ = upper wavenumber for area i.
$a(w)$ = absorbance as a function of wavenumber.
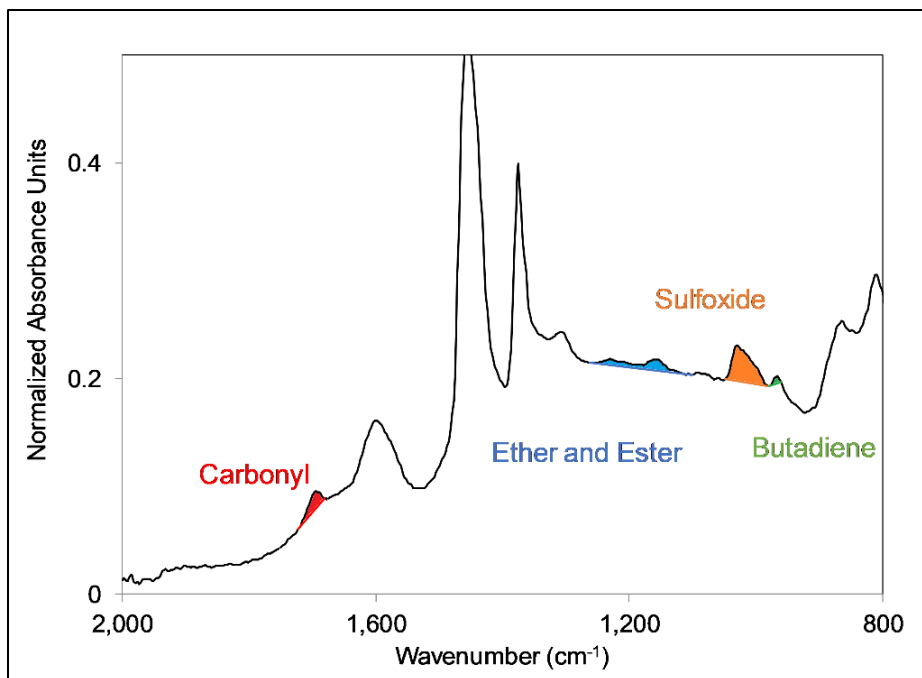
Figure 4.6: Example of normalized FTIR absorbance spectrum with the tangential integration.

4.2.3   Measurement of the Rheological Properties

An Anton Paar DSR was used to measure the binder rheological properties with the frequency sweep test to obtain the complex shear moduli and phase angles at 4°C, 20°C, and 40°C. A parallel plate geometry with an 8-mm diameter plate (PP-8) and a 2-mm gap was used for these tests *(74)*.

In this initial phase, the frequency sweep test was not done at high temperatures (i.e., 50°C and over) because the specified geometry gap is only 1-mm at these temperatures, which is not appropriate for AR binders containing large rubber particles (>250 microns). The offset in the measurement might dramatically increase due to the large rubber particles compressed between the test plates.

The test frequency ranged between 0.0159 Hz and 3.99 Hz (0.1 radians/second and 25.1 radians/second). The strain was set to 0.1 percent to prevent any non-linear viscoelastic behavior

from being measured in the frequency sweep test. The rheological data were used to build the shear

modulus master curves using Equations 4.3, Equation 4.4, and Equation 4.5 *(141,142)*.

$$log|G^*| = \delta + \frac{\alpha}{1+e^{\beta+\gamma\,log(\omega f_r)}}$$ 4.3

$$logf_r = logf + log\alpha_T$$ 4.4

$$log\alpha_T = \frac{E_a}{R(ln10)}\left(\frac{1}{T} - \frac{1}{T_r}\right)$$ 4.5

Where:

G^* = complex shear modulus in kPa.
α = high asymptote of the master curve.
δ = lower asymptote of the master curve.
β and γ = fitting parameters define the slope of the transition region of the master curve.
ω and f = measurement frequency in radians/second and Hz, respectively.
f_r = reduced frequency represents the shifted frequency at reference temperature from the measurement frequency at the test temperature.
α_T = shift factor as a function of temperature.
E_α = activation energy.
T = test temperature in Kelvin.
T_r = reference temperature in Kelvin.
R = ideal gas constant, 8.314 J/ (°K mol).

The symmetric sigmoidal function equation (Equation 4.3) is included in the AASHTOWare

Pavement ME Design software package *(141)*. Equation 4.4 is the Arrhenius shift function, which

provides a reasonable conversion in broad temperature ranges *(142)*. The shift factor (α_T) can be

calculated using the solver function in Microsoft Excel® by minimizing the sum of square error

between the predicted and measured dynamic modulus at each reduced frequency. Figure 4.7

shows an example of the shifting process.
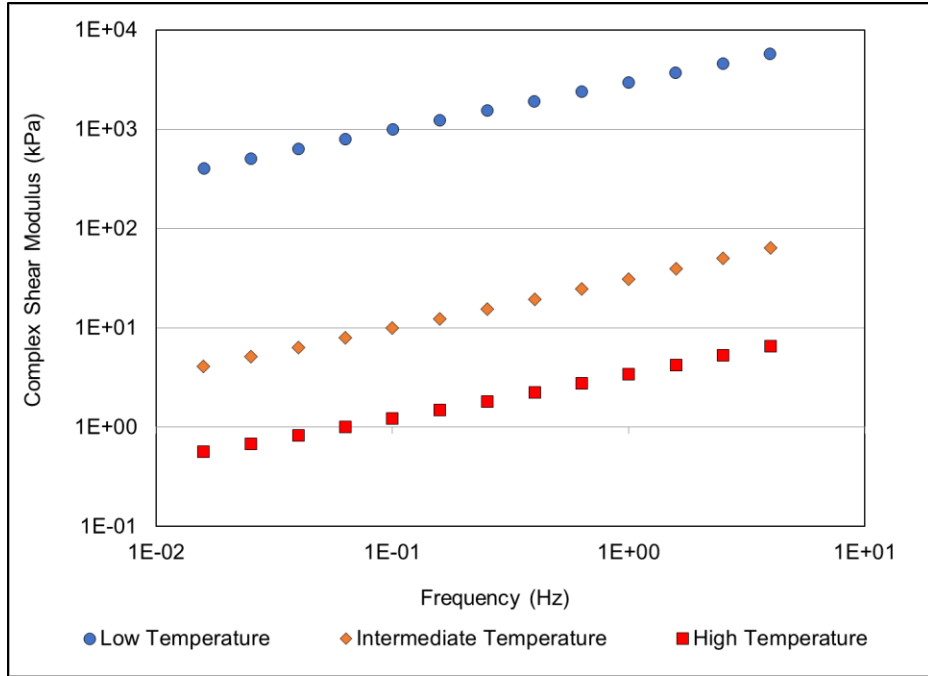
a: Modulus plotted versus frequency for each test temperature.
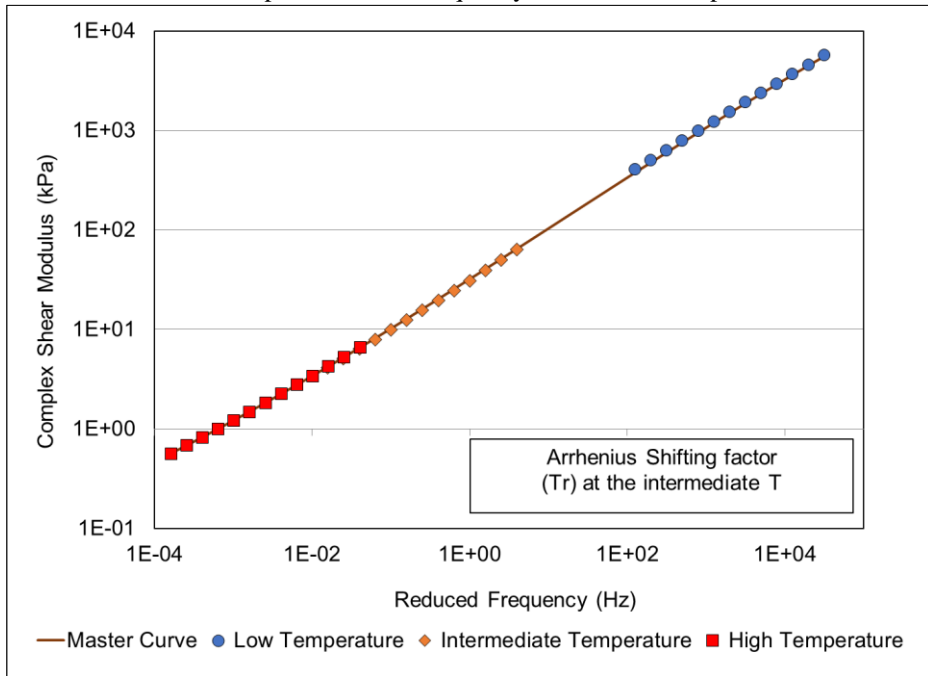
b: Modulus plotted in the shifted frequency.

Figure 4.7: Example of master curve shifting measured data (a) and shifted data (b).

4.3 Evaluation of the Oxidative Aging in Asphalt Binders

4.3.1 Changes of Chemical Components During Oxidative Aging

Figure 4.8 shows the changes in the CA index, along with aging. Some outliers were found in the field aging protocol. These outliers appeared to be caused by the small variations in the binder thickness on the glass plates.

The binder thickness has a critical impact since oxidative aging is influenced by oxygen contact with maltenes *(105)*. The diffusion of oxygen into the binder is prolonged and slow progress *(143)*. Consequently, varied layer thicknesses can significantly affect the oxidative-aging rate. The binder thickness ranged between 0.7 mm and 1.3 mm. Outliers were not entirely avoided due to the limitations of the manual binder application process. Temperature differences among sampling intervals shown in Table 4.3 may have also influenced the aging and caused inconsistent aging.

Figure 4.8 shows that all binders had an increment in the CA index. Although the aging rate varied among binder sources and types, elevating the temperature led to significantly faster aging, as expected. The PAV-aging protocol provided a considerably faster CA index increase than the field-aging protocol. The former led to a higher aging degree than the 99-day aging of the binder samples on the glass plate in this study. An approximately linear relationship between the CA index and the PAV-aging duration was observed. This linearity indicated that a constant aging rate was achieved during PAV-aging. Based on the dual-rate aging theory, this constant aging rate is a symbol of long-term aging *(94,110)*. Following the dual-rate aging theory discussed in Section 2.2.3, the PAV-aged binder residues can be considered long-term aged binders.

The CA indices of RTFO residues are plotted in Figure 4.8as reference points. PG 64-16_1 and PG 70-10_2 had RTFO indices close to zero. These two binders better resisted the short-term aging

74

progress stimulated by the RTFO-aging. On the other hand, AR binders had higher CA indices than other binders after RTFO conditioning. However, they generated the lowest CA indices than other binders after long-term aging (PAV-aging and field plate-aging).

Figure 4.8a to Figure 4.8i also show that the CA index changes were dependent on binder components. Comparing the binder from the same refinery revealed that adding additives (SBS and CRM) appeared to reduce the CA index in these two long-term aging protocols. In general, the soft unmodified binder contained more light oily components (maltenes) than the stiffer modified ones *(87)*. These larger amounts of maltenes in the unmodified binders reacted with oxygen resulting in a higher degree of oxidative aging at the same aging condition compared to modified binders. This phenomenon was more apparent in AR binders than in SBS binders in this study, probably because the SBS content (four percent) was less than the rubber content (20 percent) in these corresponding binders. The higher rubber content further reduced the maltene content in the binder.
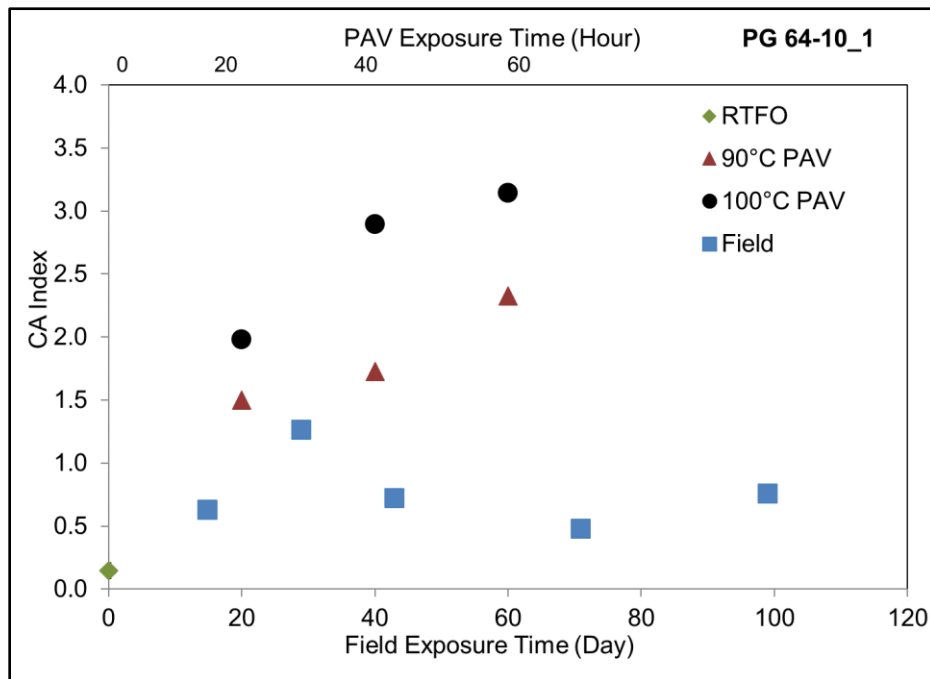
a: PG 64-10_1
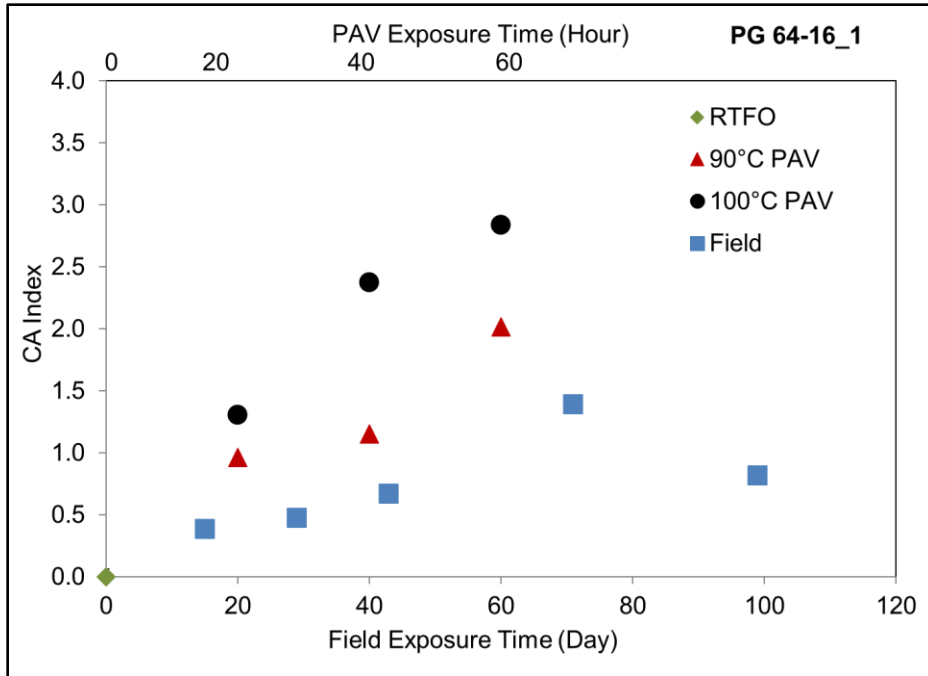
b: PG 64-16_1
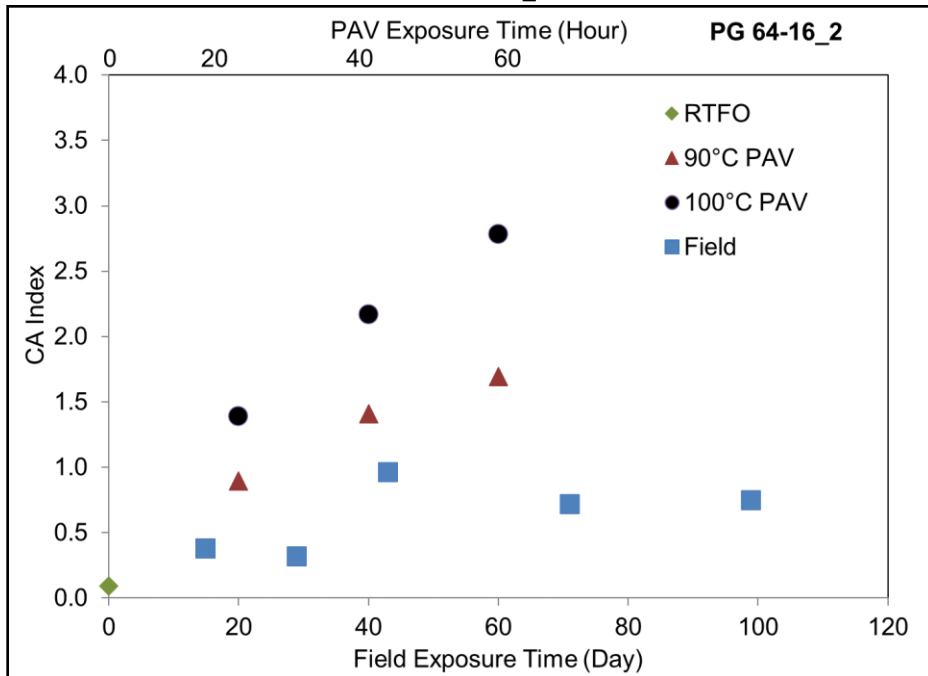
c: PG 64-16_2
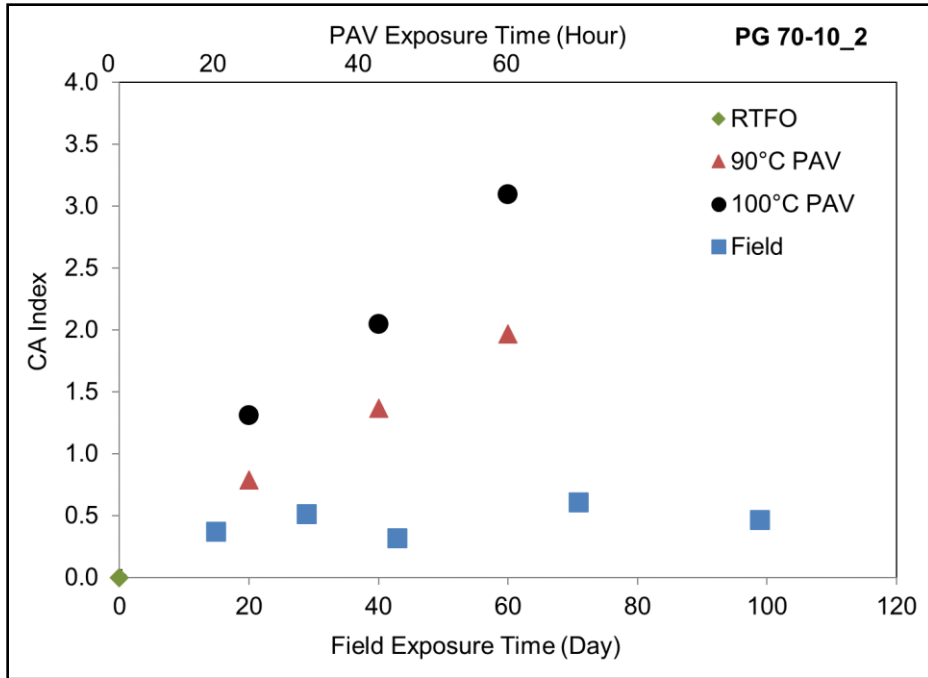
d: PG 70-10_2
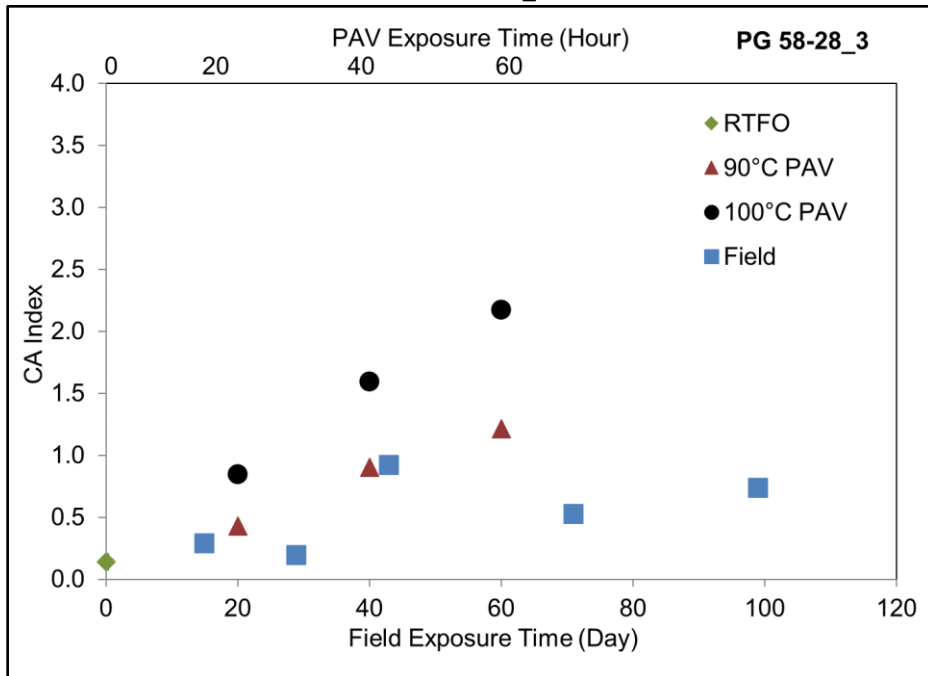
e: PG 58-28_3
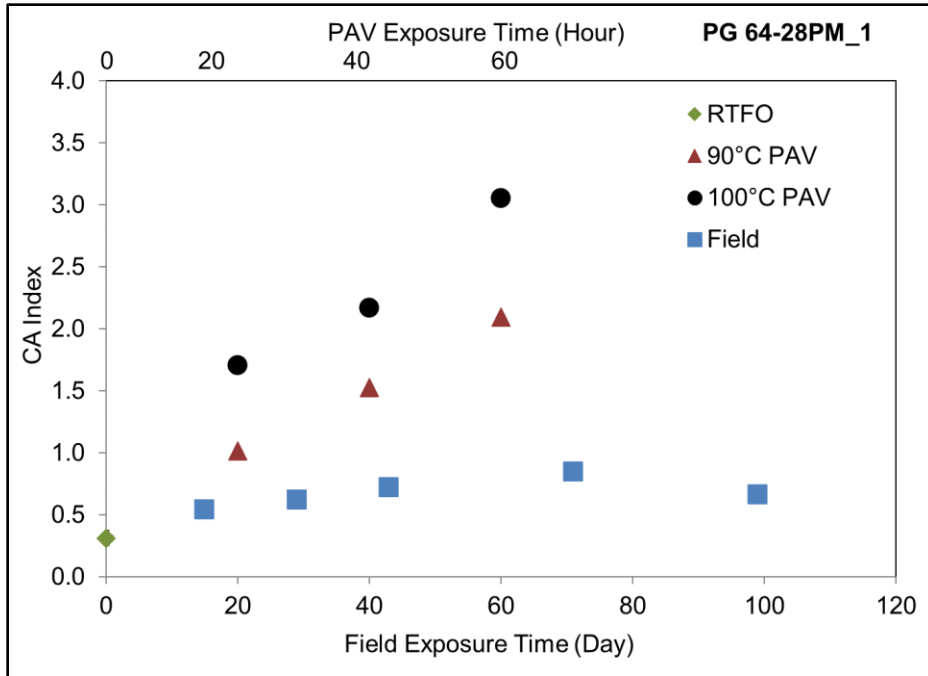
f: PG 64-28PM_1
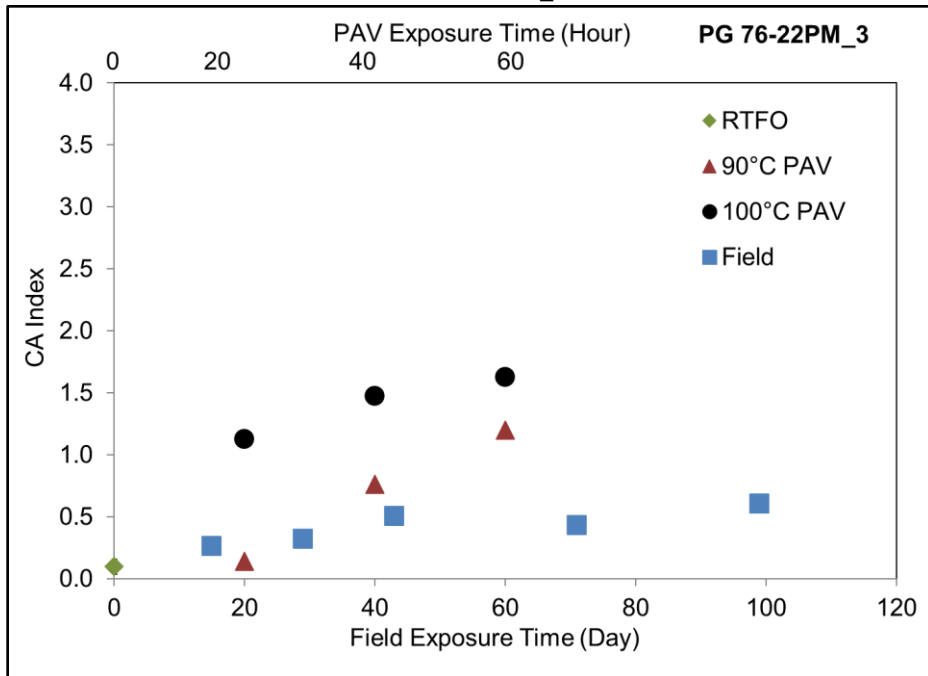
g: PG 76-22PM_3
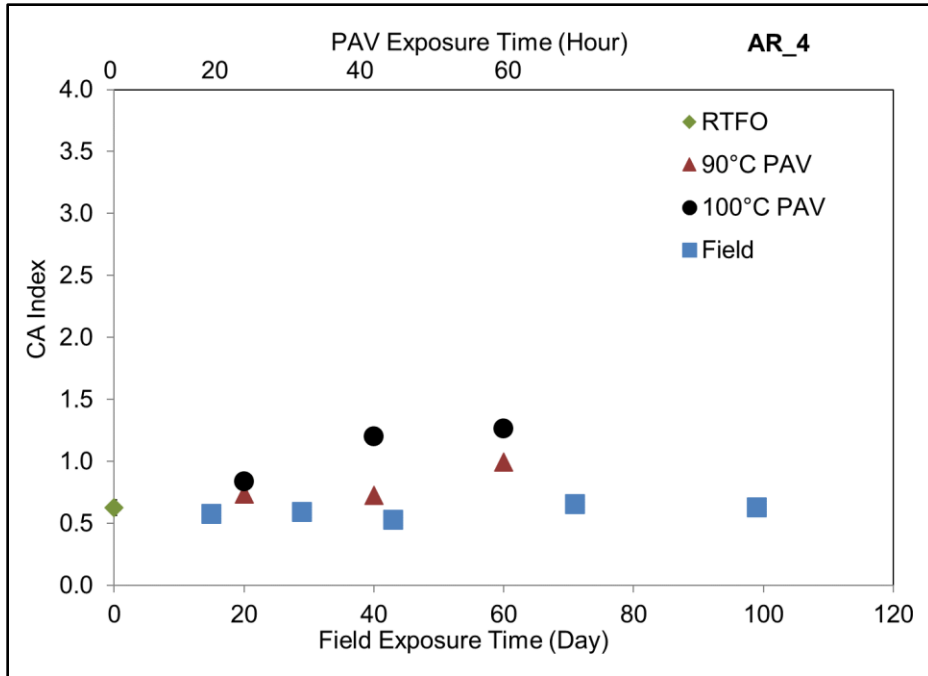
h: AR_4
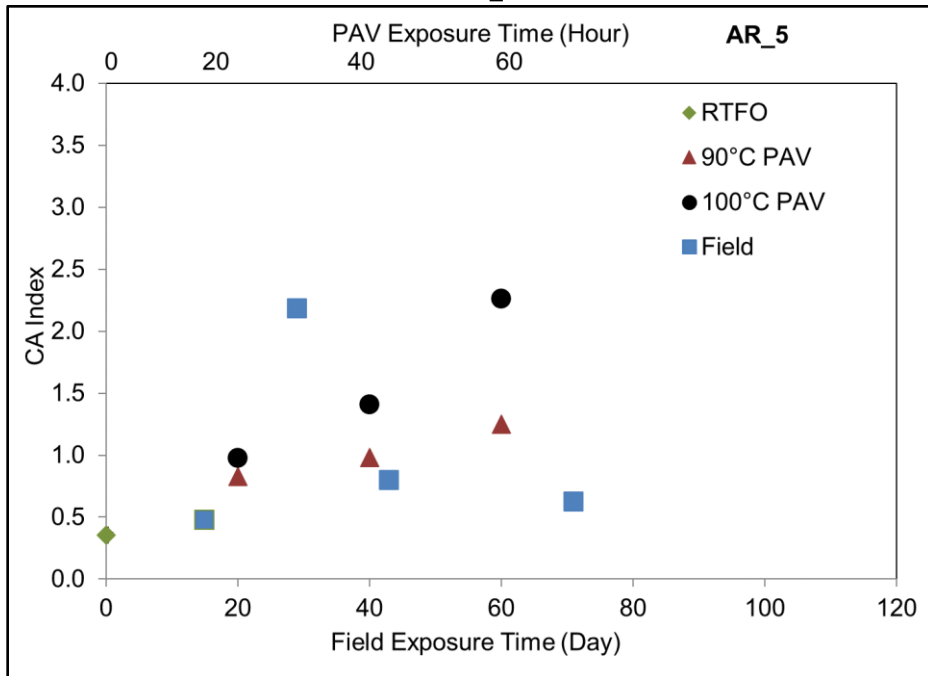
i: AR_5

Figure 4.8: Evolution of carbonyl (CA) area index along with exposure durations for tested binders.

Figure 4.9 shows the changes in ether and ester area indices along with the exposure time. The

broad wavenumber ranges and the relatively less distinct maxima peaks of these two components

79

caused an evident variability in the analysis. An overall observation of these indices was that ether and ester components increased at a faster rate at higher temperatures and appeared to dissolve after a longer aging duration (i.e., 60 hours) in the PAV-aging. No consistent increasing trend was found in the field aging protocol, probably because the relatively low field temperatures (average 20°C to 30°C) limited the ether and ester component changes in the 99 days aging on the glass plate.

The ether and ester area indices mostly remained the same as those of the RTFO residue after 99-day field aging. In the PAV-aging protocol, the increasing trend was relatively apparent, probably because of the high aging temperature (90°C and 100°C). Given the inconsistent growth of these indices in these two aging protocols, it was not fundamentally appropriate to use the PAV-aging protocol (20-hour) to simulate the field aging protocol (99-day) for the ether and ester area indices to shorten the test duration.

There was no apparent correlation between ether and ester area indices and the PAV-aging time, especially for AR binders. A prolonged aging duration degraded the ether and ester components *(144)*. This decrease in indices was attributed to the possible dissolution of ether and ester components after 60 hours of PAV-aging at 90°C for PG 64-16_2, AR_4, and AR_5 binders. This phenomenon also happened after 60 hours of PAV-aging at 100°C for the PG 64-10_1, PG 64-16_1, PG 68-28_3, and AR_4 binders. These observations indicated that the ether and ester area indices were not an appropriate indicator for continuously tracking oxidative aging.
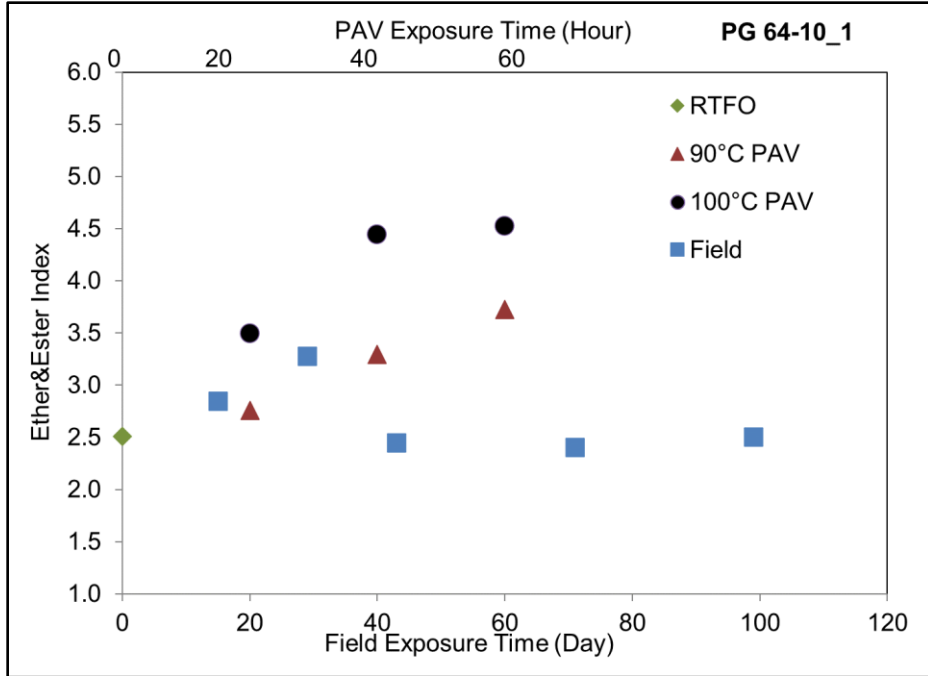
a:PG 64-10_1

b: PG 64-16_1

c: PG 64-16_2

d: PG 70-10_2

e: PG 58-28_3

f: PG 64-28PM_1

g: PG 76-22PM_3

h: AR_4

i: AR_5
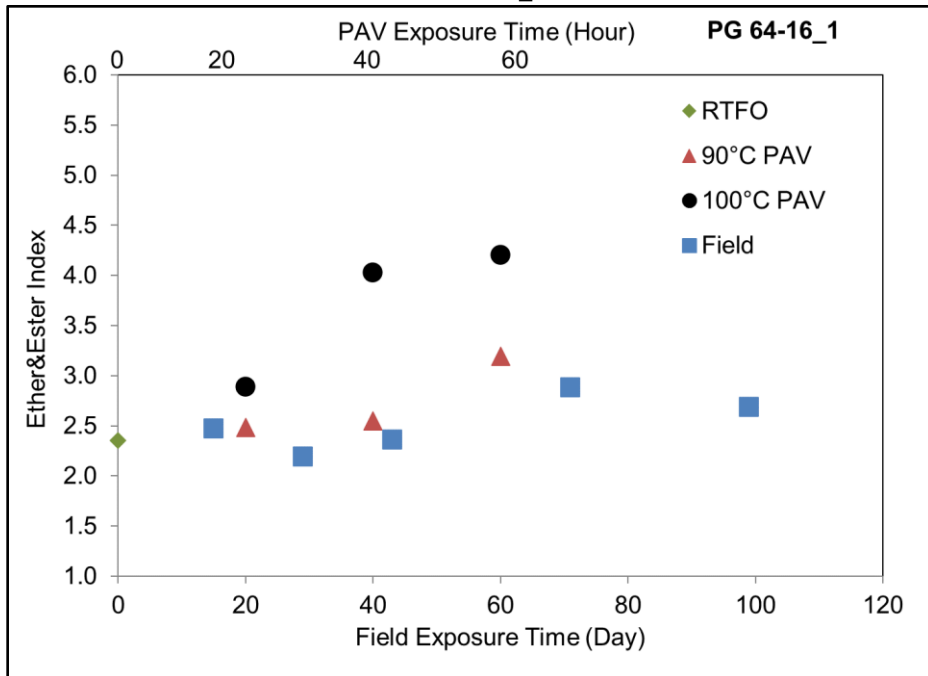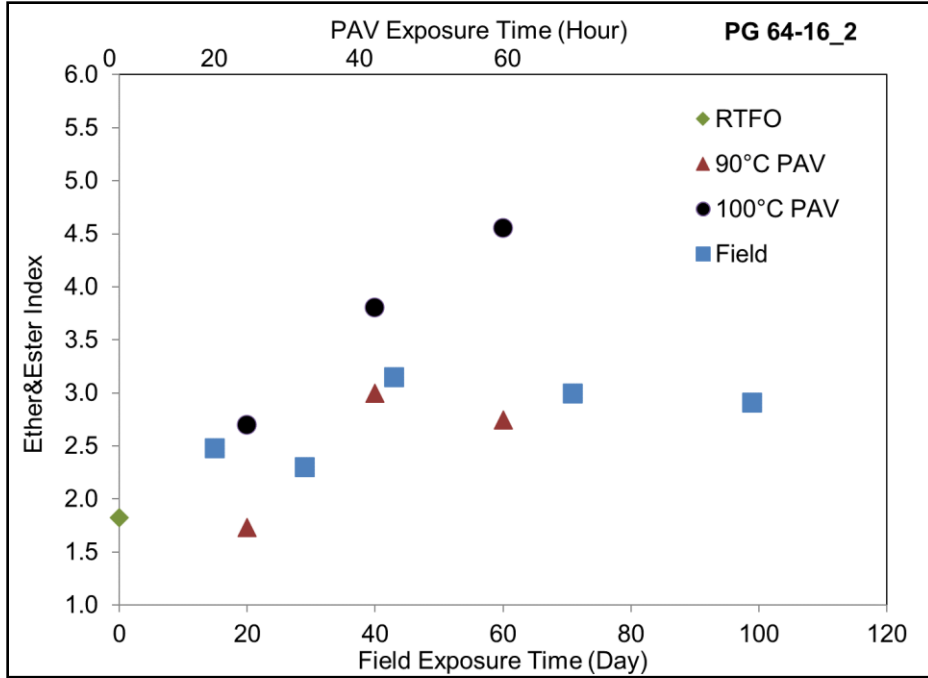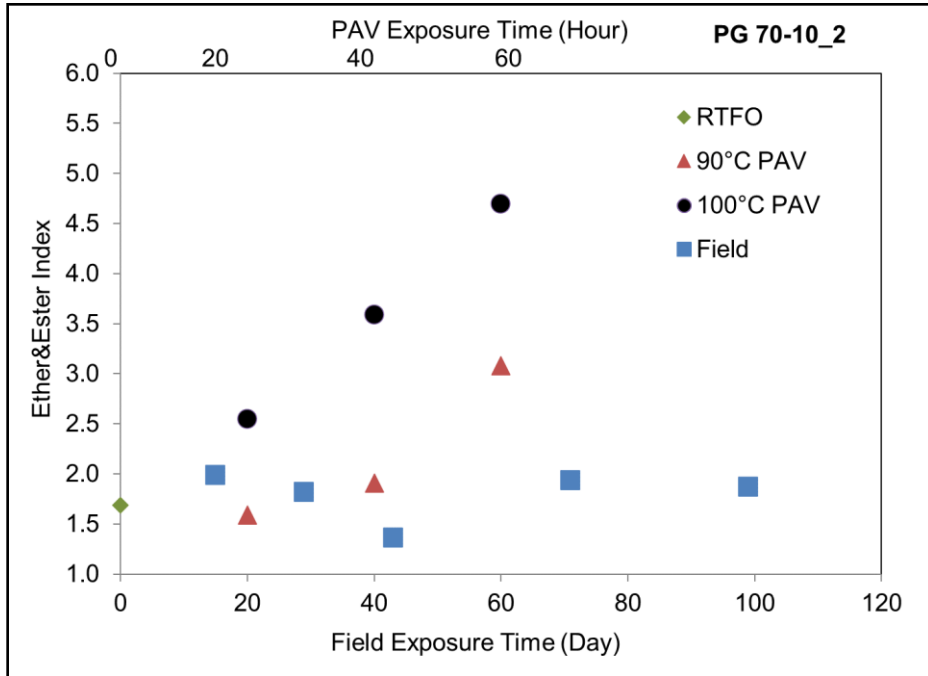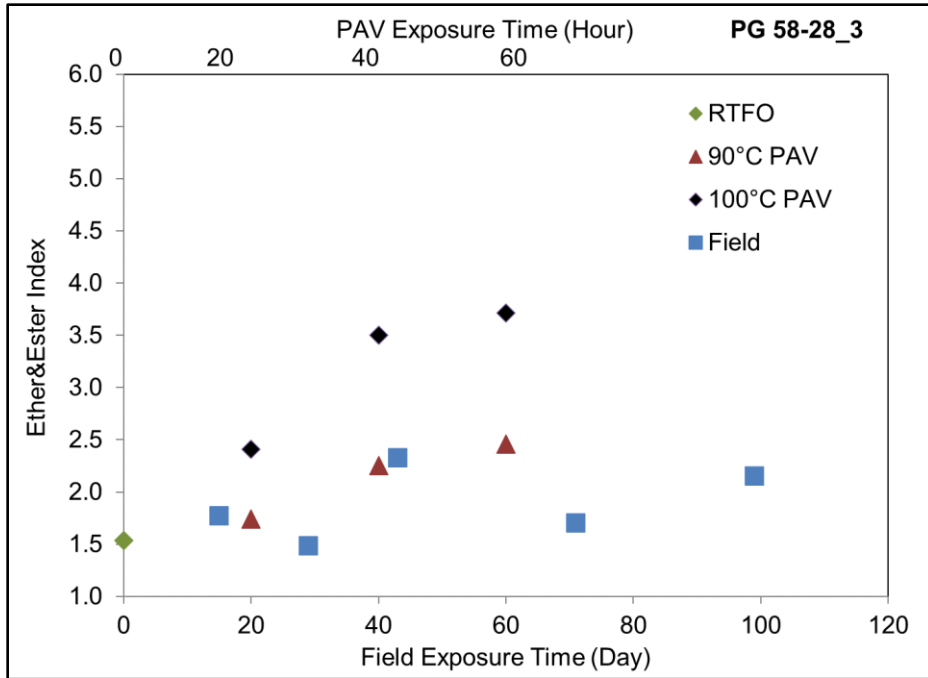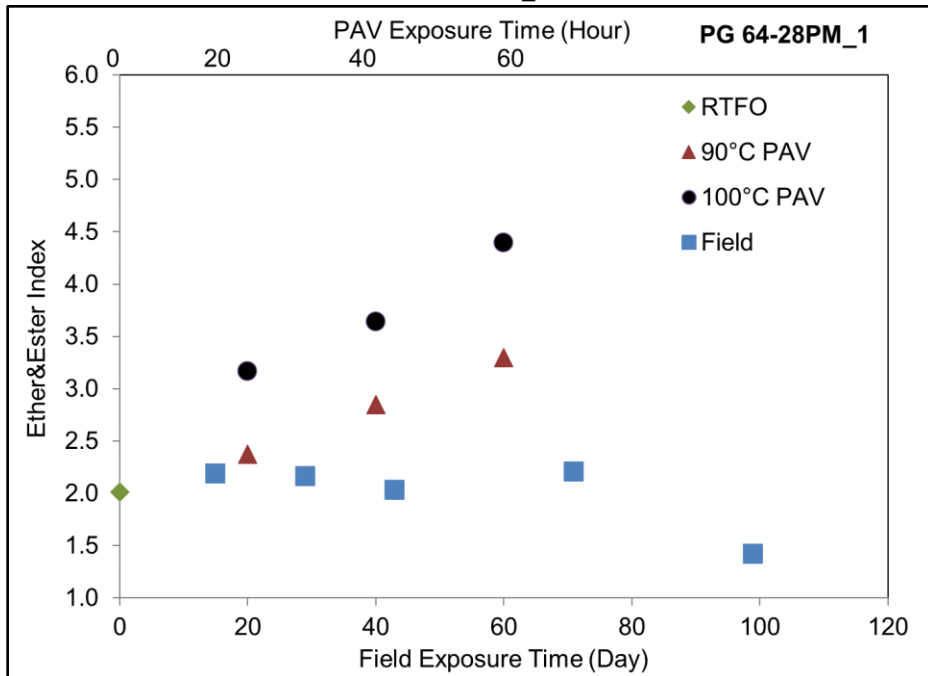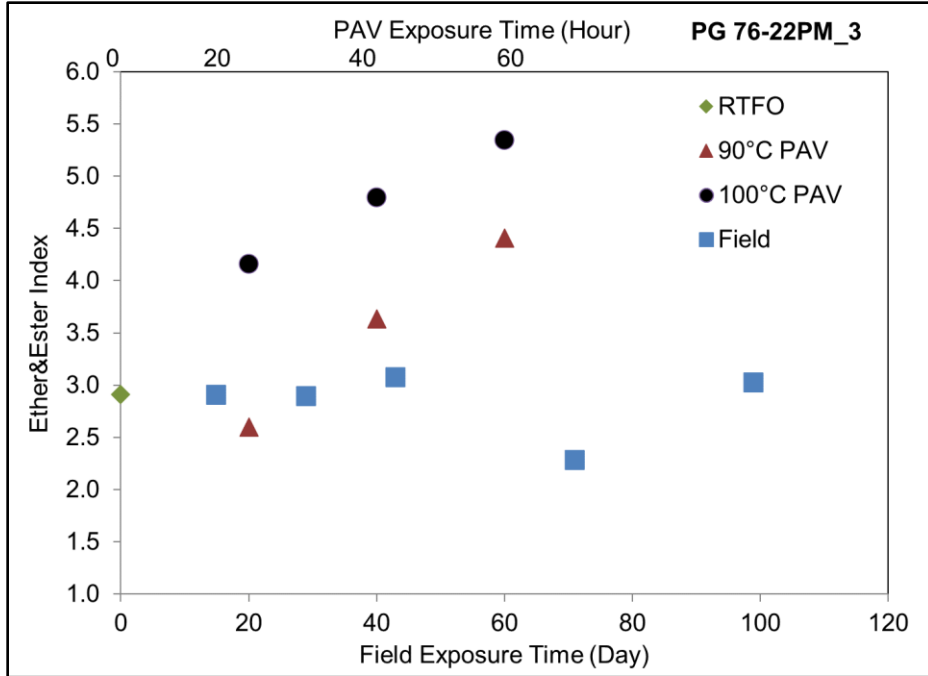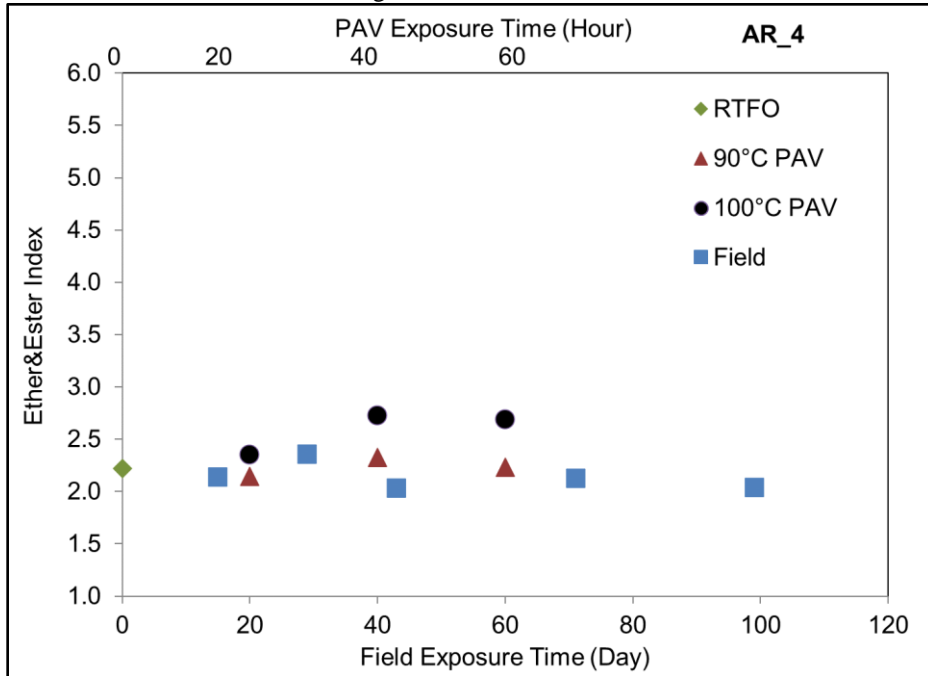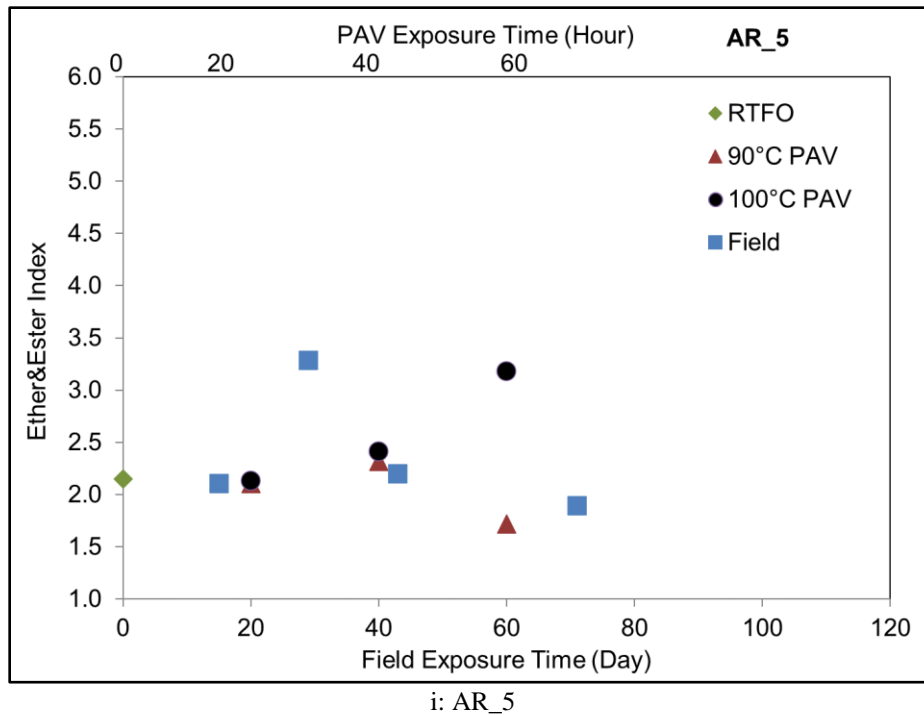
Figure 4.9: Evolution of ether and ester area index along with exposure durations for tested binders.

Figure 4.10 shows the changes in the SUL index along with aging. This index had a generally increasing trend versus time in both aging protocols, but it increased significantly faster in the PAV-aging protocol than in the field-aging protocol.

The accumulation of the SUL index was inconsistent in the PAV-aging. The PG 64-16_2, PG 58-28_3, AR_4, and AR_5 binders had higher sulfoxide indices at 100°C than at 90°C after the same PAV-aging duration. The PG 70-10_2 and PG 76-22PM_3 binders had similar SUL indices after 60-hours of PAV-aging at both 90°C and 100°C. The remaining binders (PG 64-10_1, PG 64-16_1, and PG 64-28PM_1) had even lower SUL indices at 100°C than at 90°C.

This observation was consistent with previous studies *(103,104)* in that the sulfoxide component was mostly developed in the early aging stage, and it was unstable at extreme conditions (high temperatures [>100ºC] under high pressure [2.1 MPa] with long duration [>40 hours]). Its

85

development was terminated, and the amount of the sulfoxide component might not increase when increasing the temperature or duration in PAV-aging. Figure 4.10a, Figure 4.10b, Figure 4.10d, Figure 4.10f, and Figure 4.10g show that the sulfoxide component did not continue increasing when increasing the PAV temperature and prolonging the PAV duration.

Figure 4.10 confirms that this sulfoxide component mostly accumulated in the early aging stage as an evident increase was shown between RTFO residues and PAV residues. The more-severe PAV-aging (high pressure, long duration, and/or high temperature) did not continue producing the sulfoxide component. The amount of sulfoxide component was not necessarily coincident with the degree of aging. Consequently, the SUL index was not considered to be an appropriate indicator for tracking oxidative aging.
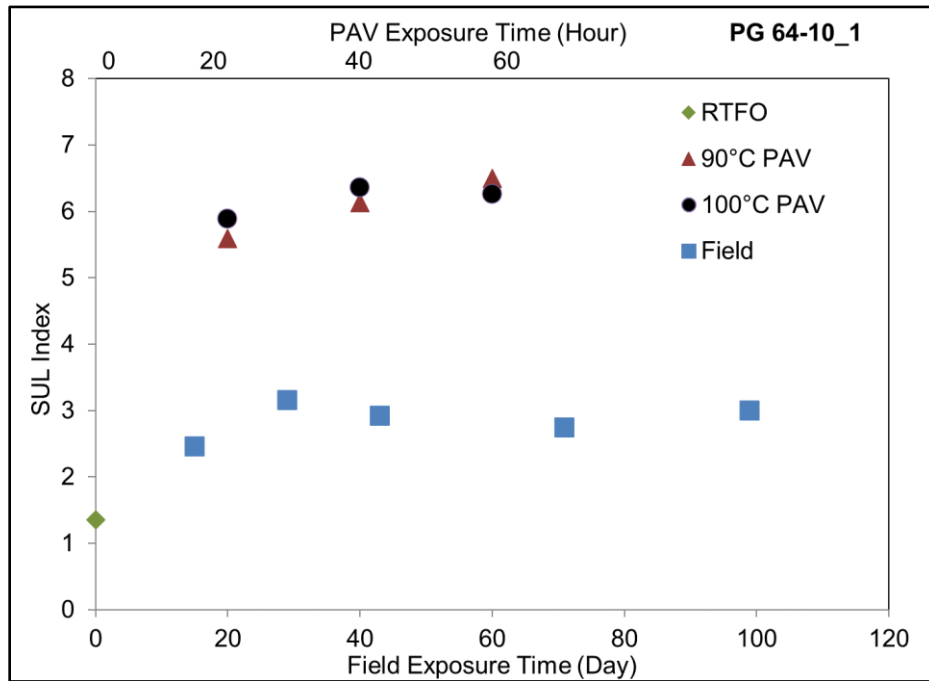
a:PG 64-10_1
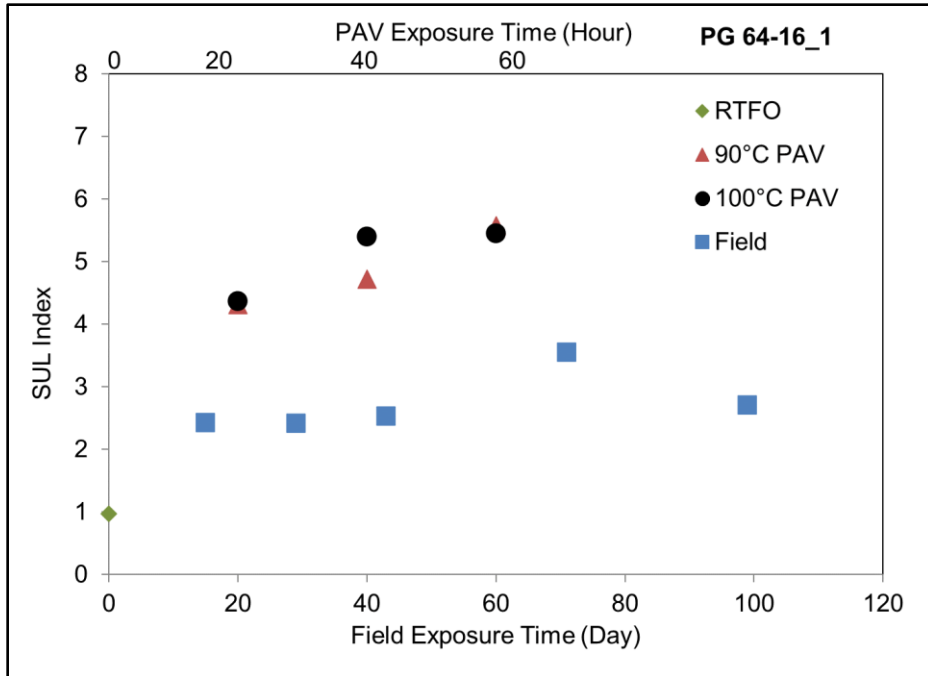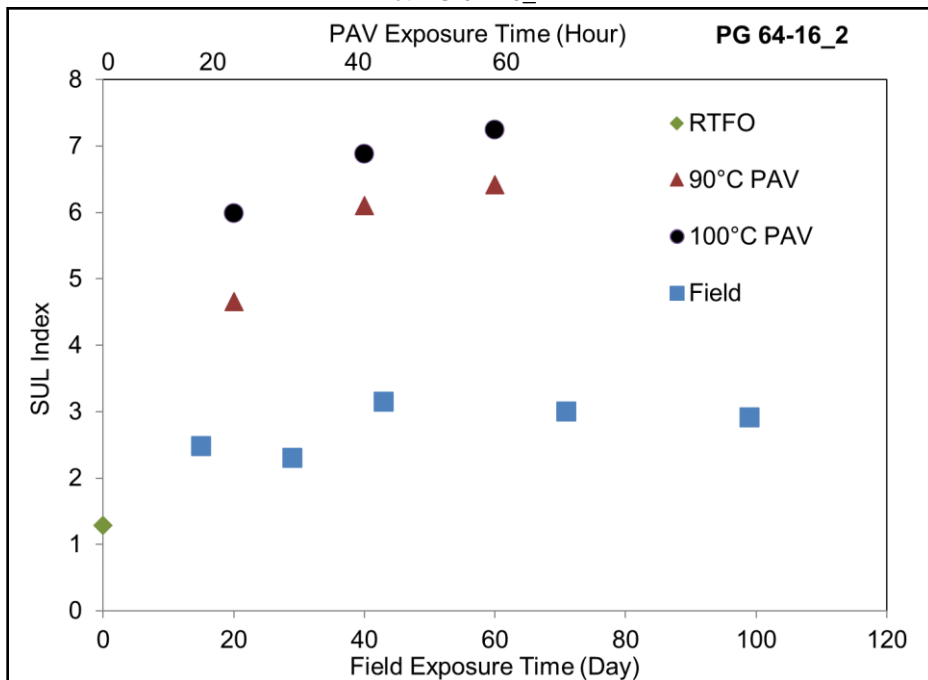
b: PG 64-16_1

c: PG 64-16_2
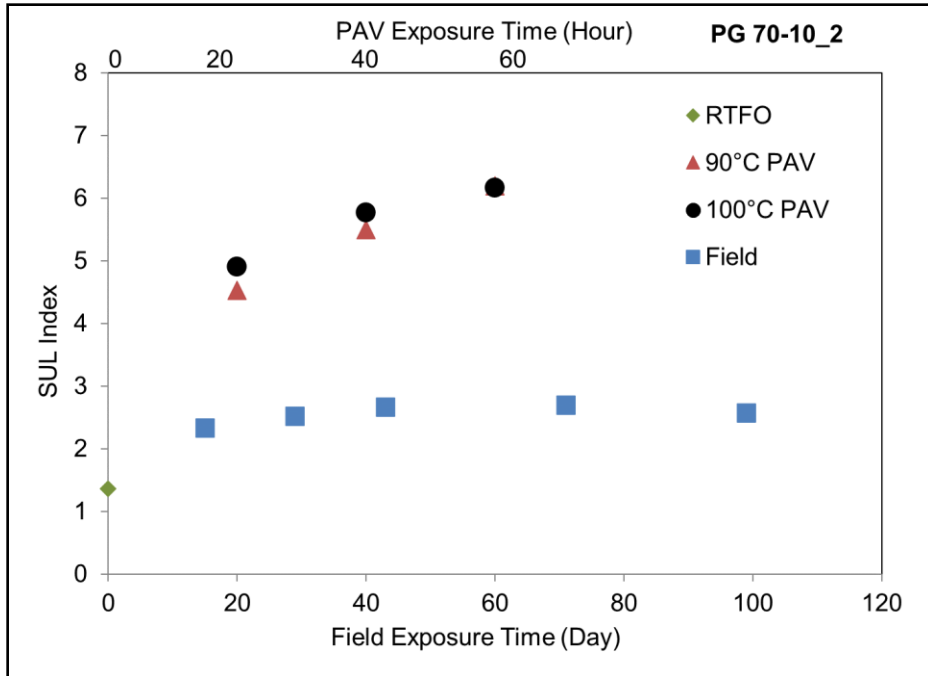
d: PG 70-10_2
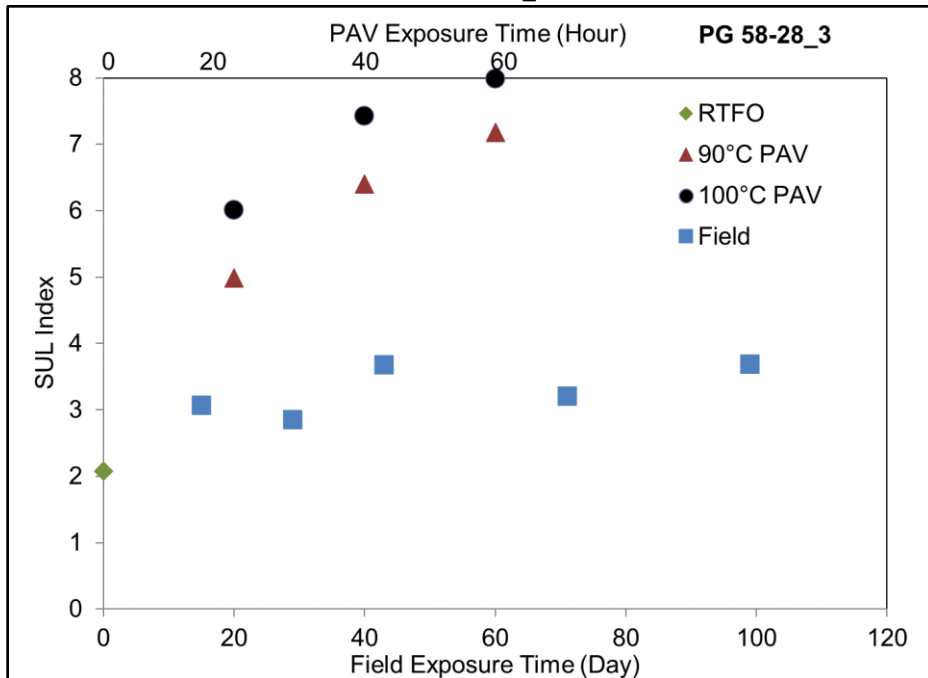
e: PG 58-28_3
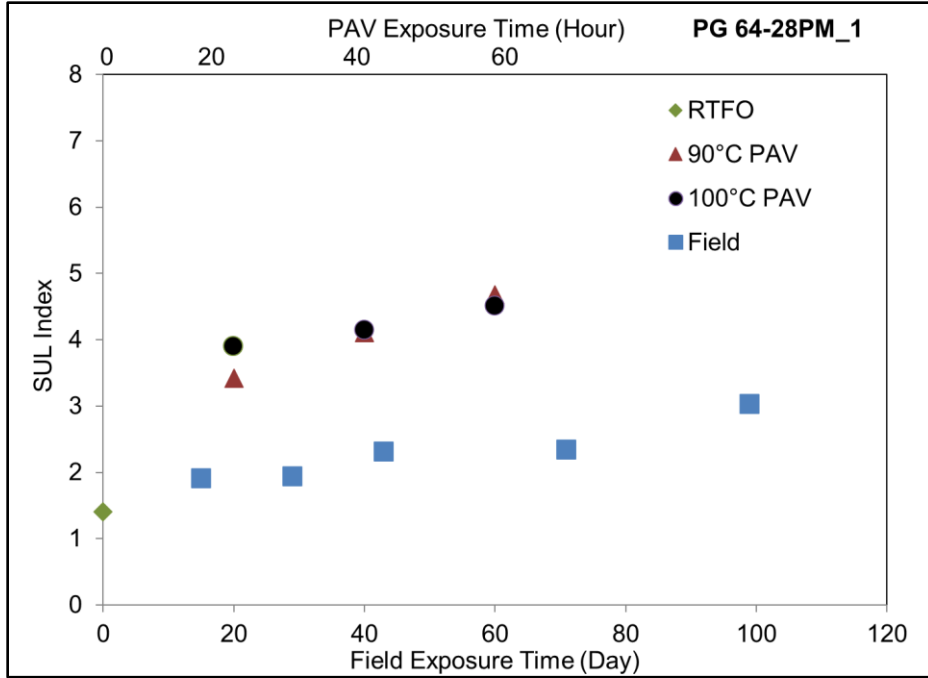
f: PG 64-28PM_1
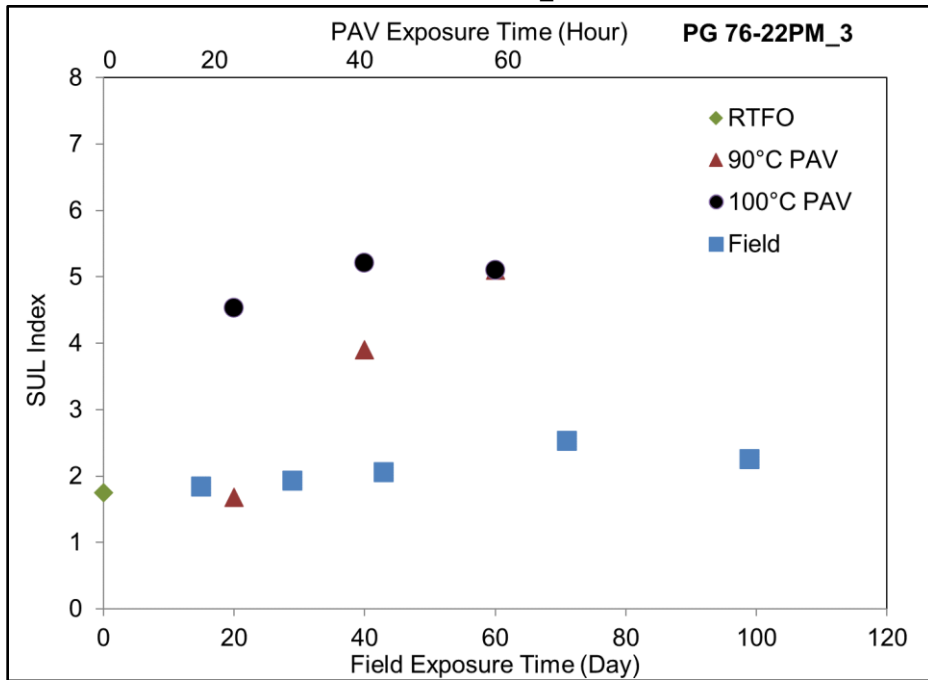
g: PG 76-22PM_3
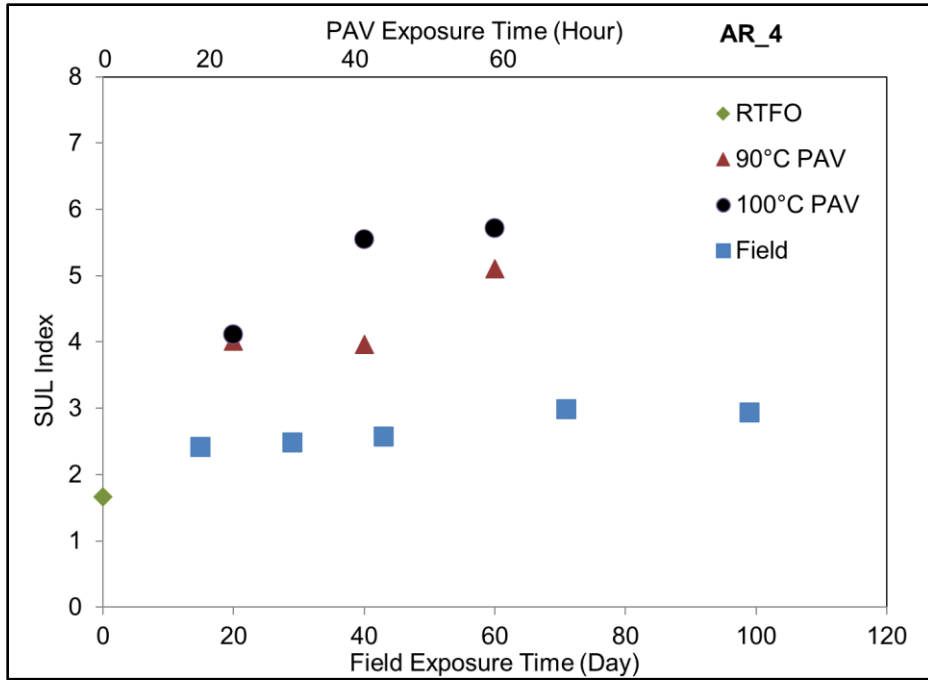
h: AR_4
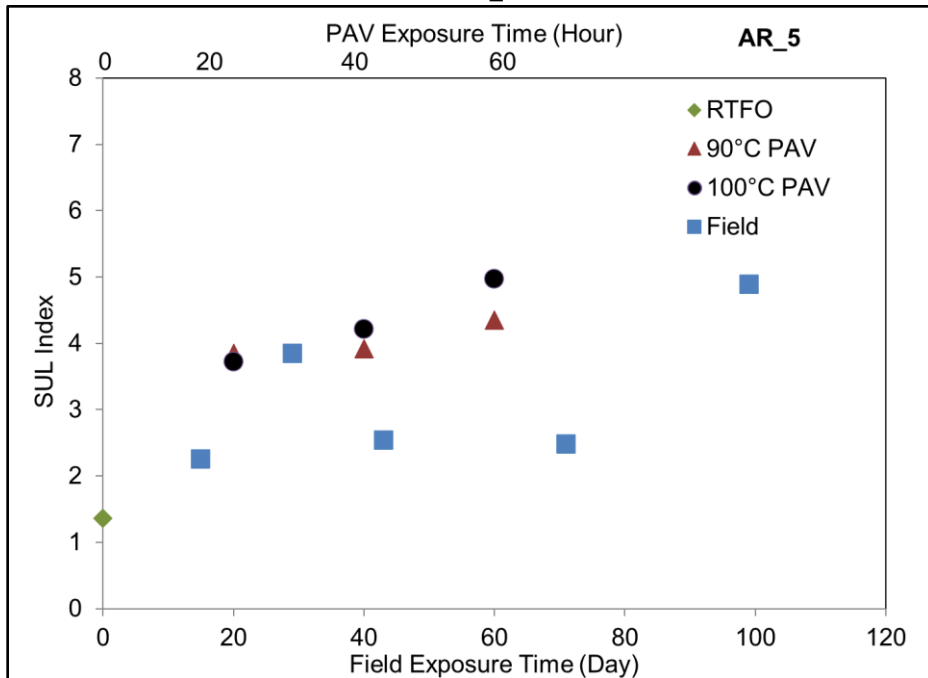
i: AR_5

Figure 4.10: Evolution of sulfoxide (SUL) area index along with exposure durations for tested binders.

One objective of this study was to find an appropriate tracking indicator of oxidative aging. Based

on the above observations, only the CA index continued to increase throughout the aging period

in both the PAV- and field-aging protocols. The CA index was also stable in both protocols, and it did not dissolve into the binder. Hence, the CA index was chosen as the aging indicator for this study.

The rate of increase in the CA index was binder dependent. Glover et al. *(94,112)* proposed that the oxidative kinetic (r_{ca}) during a natural aging protocol (i.e., field aging at room temperature [around 25°C and 1.0 atm atmosphere]) could be predicted using data from the PAV-aging protocol (around 100°C and 20.7 atm air pressure) to obtain the parameters for modeling field aging (i.e., r_{ca}) in a fast laboratory protocol (PAV). This study further validated this theory using the PAV-aged data to generate the model parameters used to predict the CA index of the glass plate-aged binder.

The aging kinetic model (Equation 2.8) is a linear function that works for isothermal and isobaric conditions. In the equation, the CA_0 is the start point of the long-term aging phase, which is plotted as point C in Figure 2.8. The r_{ca} can be determined by Equation 2.9 *(18)*. In this study, the aging kinetic model presented in Equation 2.8 was calibrated using the data from the PAV-aging protocol. Then the data from the field-aging protocol were used to validate the aging kinetic model.

In the PAV-aging protocol, r_{ca} is defined as the slope between the CA value and aging time. Once the r_{ca} has been determined, the activation energy for the PAV ($E_{a,20.7atm}$) condition can be calculated based on the slope between r_{ca} and $(R \times T)^{-1}$ *(94)*.

Figure 4.11a graphically explains this procedure using binder PG 64-10_1 data as an example. The r_{ca} values for this binder were 0.0291 and 0.0207 at 100°C and 90°C, respectively. The reaction rate was higher at a higher PAV temperature, as expected. Figure 4.11b plots these two reaction

rates versus the $(R \times T)^{-1}$ value. The activation energy was, therefore, determined as 38,375 kJ/mol for PG 64-10_1 at the PAV-aging protocol based on the exponential regression.

The kinetic parameters for the field-aging protocol ($E_{a,1.0atm}$, and A) can then be estimated using Equations 4.6 and Equation 4.7. In Equation 4.6, the field atmosphere pressure is 1.0 atm (0.1 MPa), and the pressure in the PAV-aging is equal to 20.7 atm (2.1 MPa) *(94)*.

$$E_{a,1.0atm} = \frac{E_{a,20.7atm} + 94960}{1.9402}$$ 4.6

$$A = 0.0266 \times e^{0.3347 E_{a,1.0atm}}$$ 4.7

Where:
E_a = activation energy in kJ/mol.
A = pre-exponential factor in the Arrhenius equation.

The intercept of the field-aging CA line was considered as the starting point for long-term aging. This CA_0 was obtained by plotting all CA values of the field-aged binder against their aging days. Figure 4.11c presents the determination of CA_0 for the PG 64-10_1 binder.

PG 64-10_1

♦ 90°C PAV   ♦ 100°C PAV

CA = 0.0291×t + 1.5093
R² = 0.90

3.14
2.89
1.98
1.73
2.33
1.50

CA = 0.0207×t + 1.0262
R² = 0.93

Absorbance Index

Hours
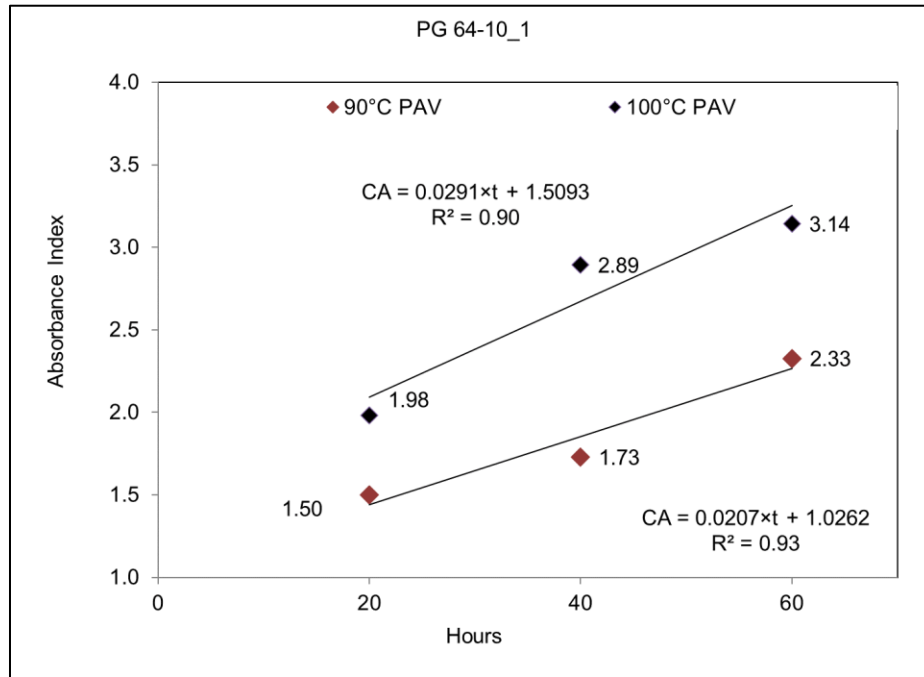
a: Determination of CA increasing rate
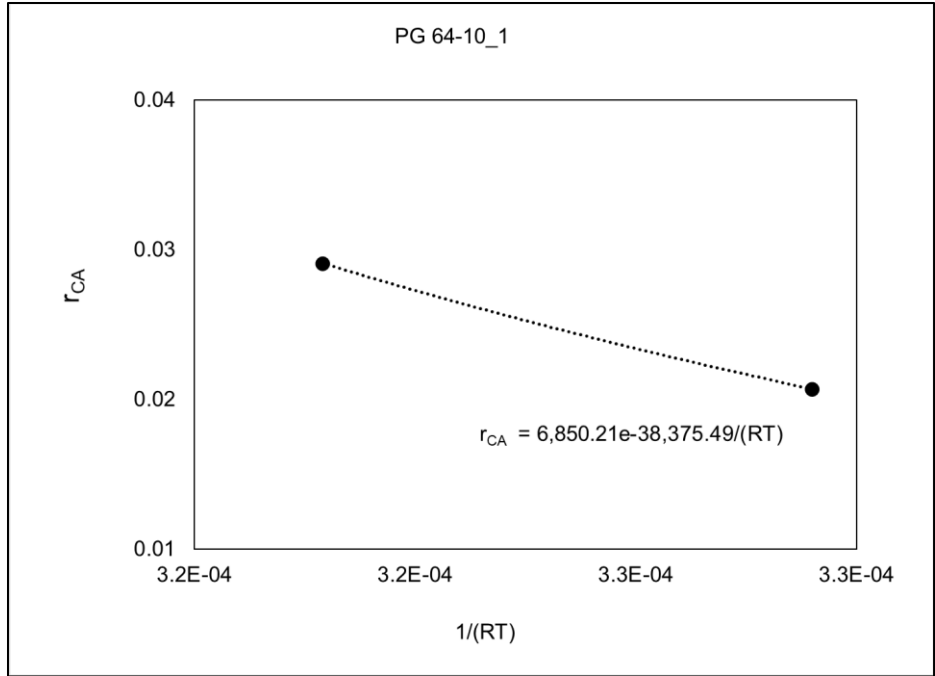
b: Determination of activation energy
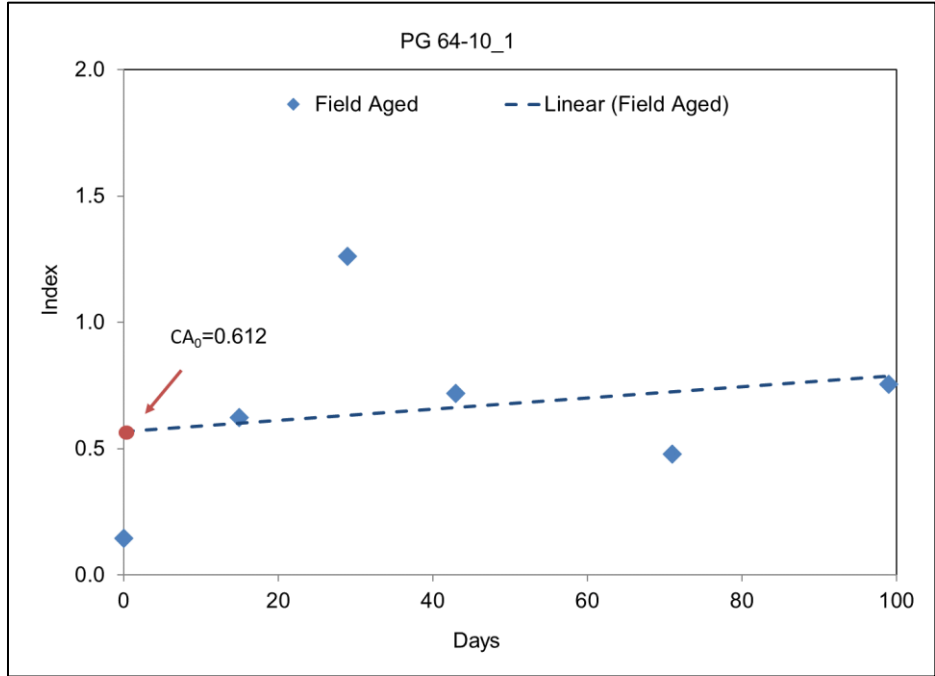
c: Determination of CA_0

Figure 4.11: Example of kinetics parameter determination: CA rate, activation energy, and CA_0.

The kinetic parameters and predicted CA values for the other eight binders were determined using the same methodology. The model-predicted CA values were compared to measured CA values from field-aged samples (labeled with blue bubbles) in Figure 4.12.

Figure 4.12 shows the comparison between measured data and model-predicted data. The RTFO residue CA value is also presented as a blue bubble at day-zero on the y-axis in Figure 4.12. The predicted CA values consistently increased through the aging protocol, owing to the linear format of the kinetic model in Equation 2.8.

PG 64-10_1, PG 70-10_2, PG 64-28PM_1, PG76-22PM_3, and AR_4 binders showed that the predicted CA values matched the observed values reasonably well. Outliers were noted for the other binders. However, there was no consistent offset in terms of the aging time or the binder type. These outliers were mostly attributed to the variations in binder film thickness and to temperature fluctuations.

Visible differences were observed between the intercept of CA_0 with the predicted line and the RTFO residue CA value on day zero on the y-axis. These differences indicated that using the intercept of the field-aging line instead of RTFO residue CA value as CA_0 point was reasonable. This finding was consistent with the principles described by the dual-rate aging model shown in Figure 2.8 *(18)*.

The difference between the RTFO residue CA value and CA_0 value was smaller for the SBS and AR binders than the unmodified binders, implying that these modified binders might not have a significant carbonyl component increase during the short-term aging stage.

The first matchup between the predicted CA values and measured CA values occurred at 15 days, indicating that the short-term aging stage had been completed within 15 days for the binders aged

on the glass plate. Based on these results, aging the thin film of binder on the glass plate was equivalent to several months of field aging on the road, as discussed in Section 2.2.3. This glass plate aging protocol can be used to simulate short-term aging (material production and lay down).
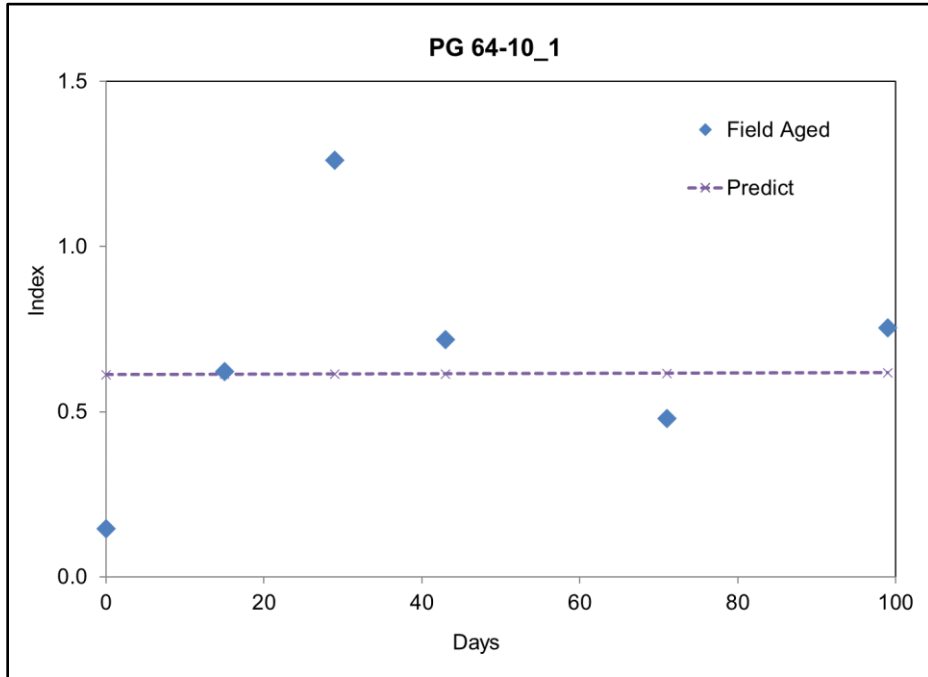

a: PG 64-10_1
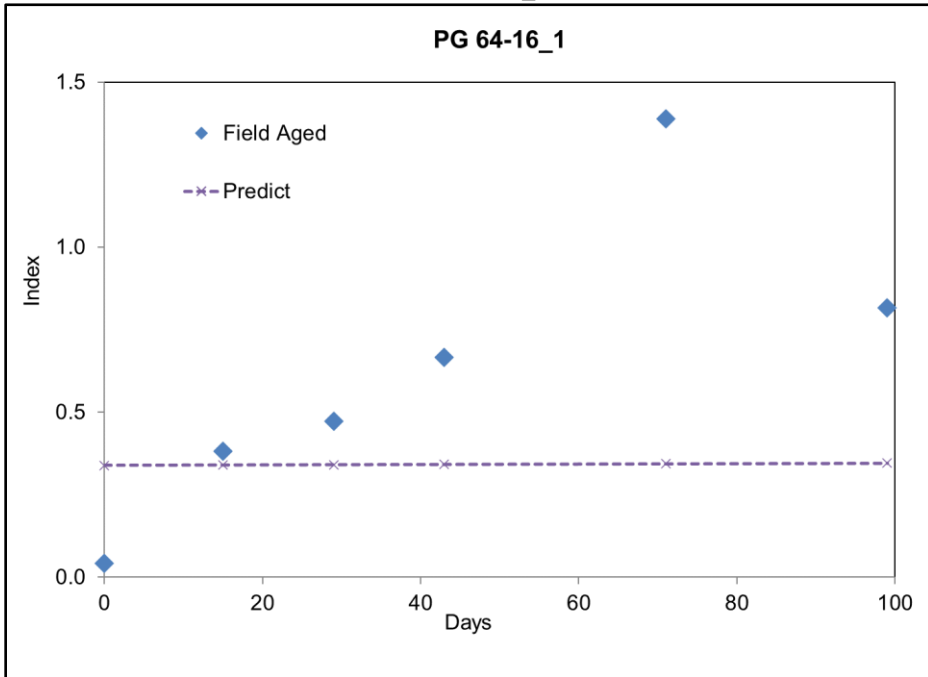

b: PG 64-16_1
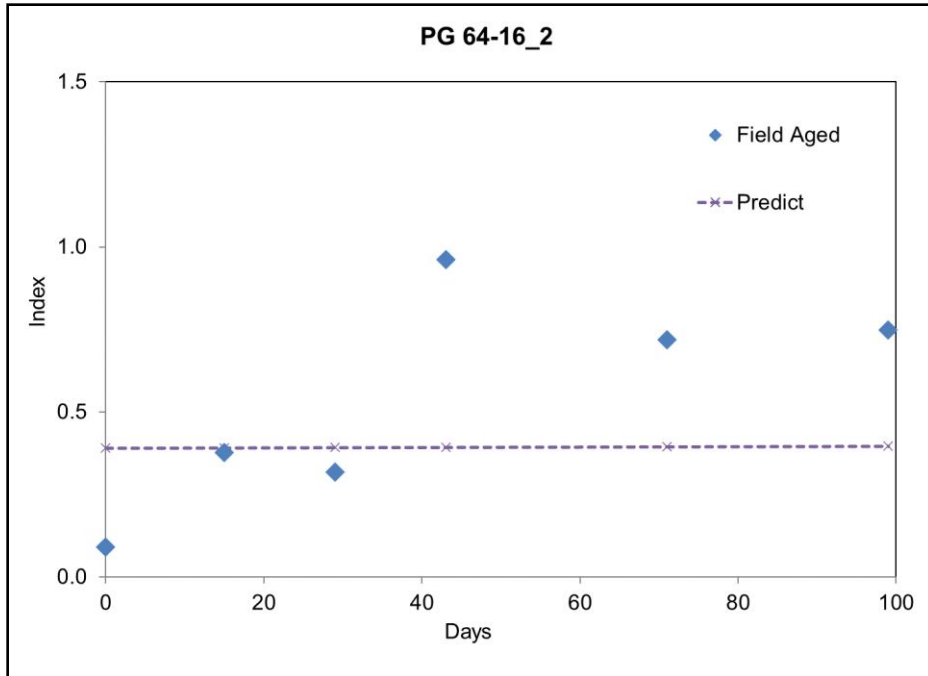
c: PG 64-16_2
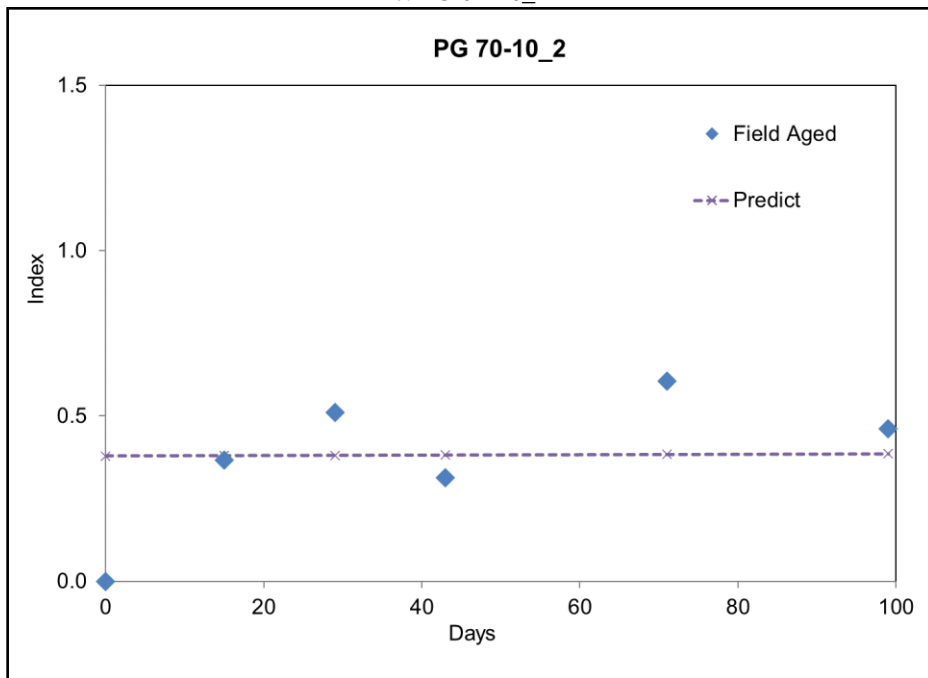
d: PG 70-10_2
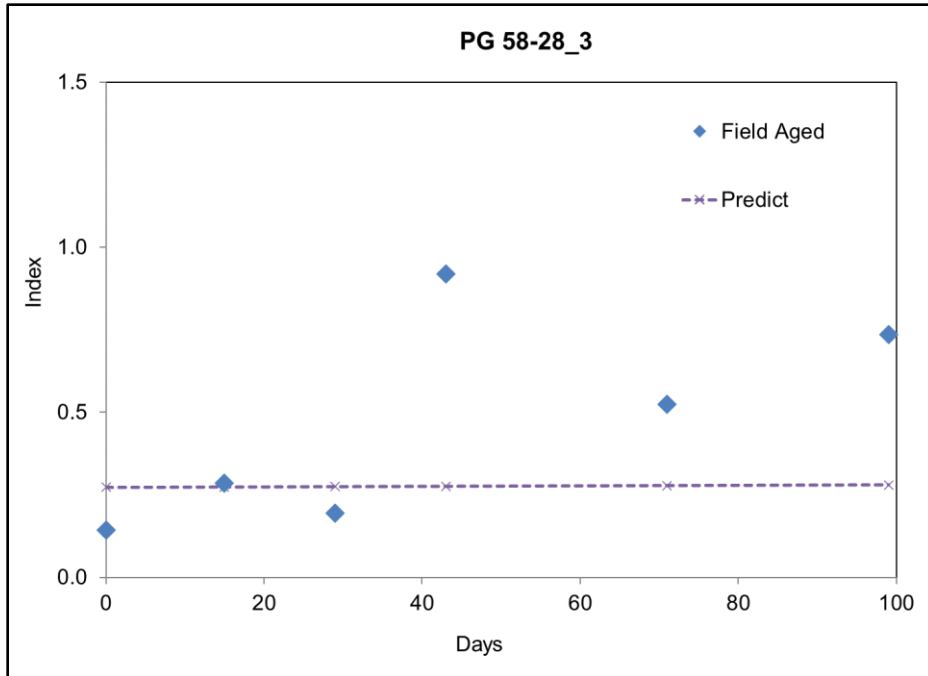
e: PG 58-28_3
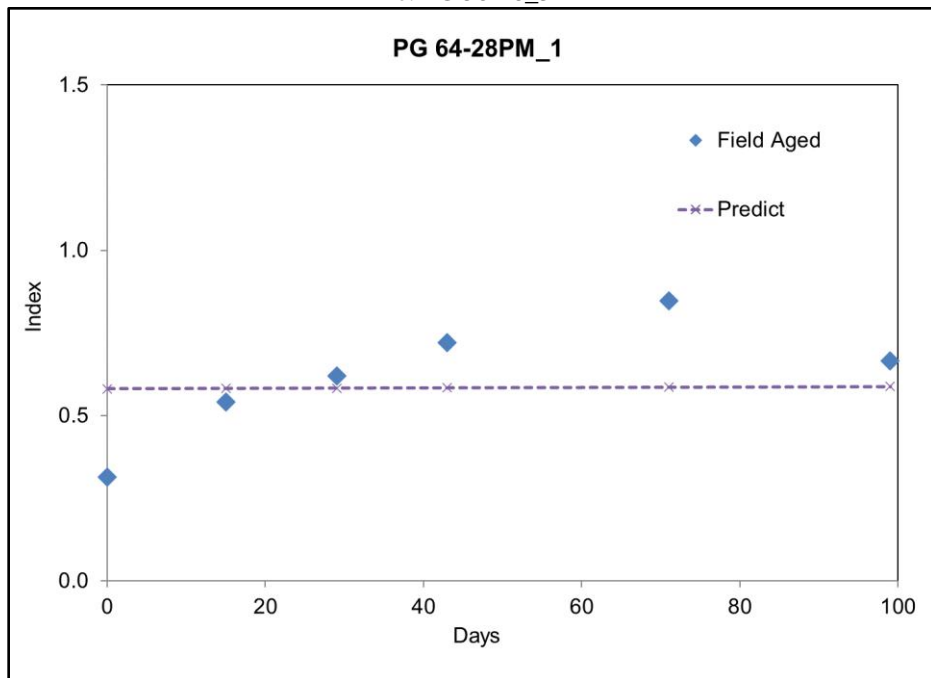
f: PG 64-28PM_1
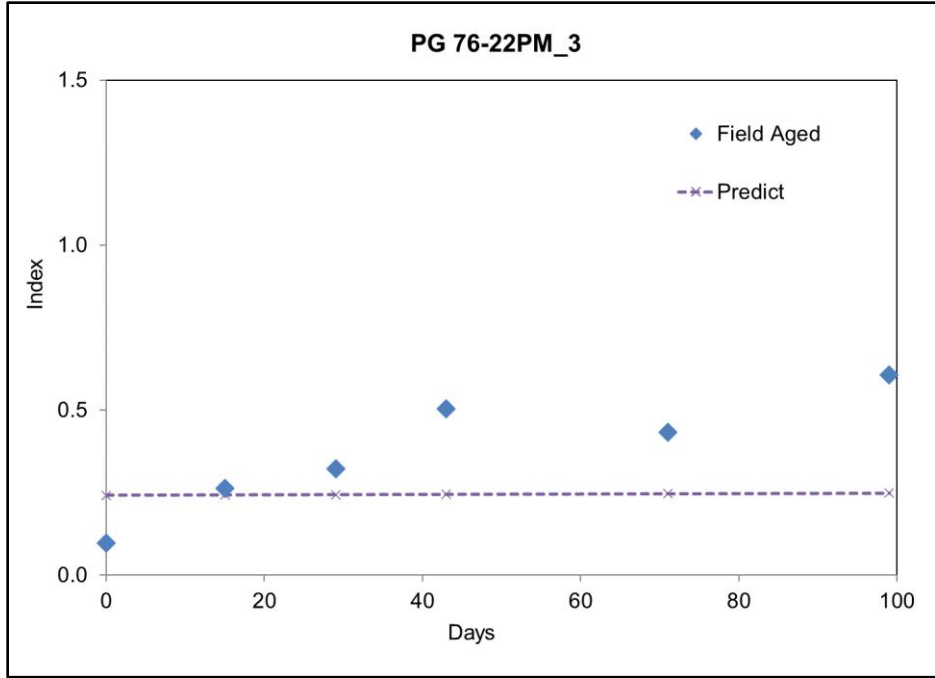
g: PG 76-22PM_3
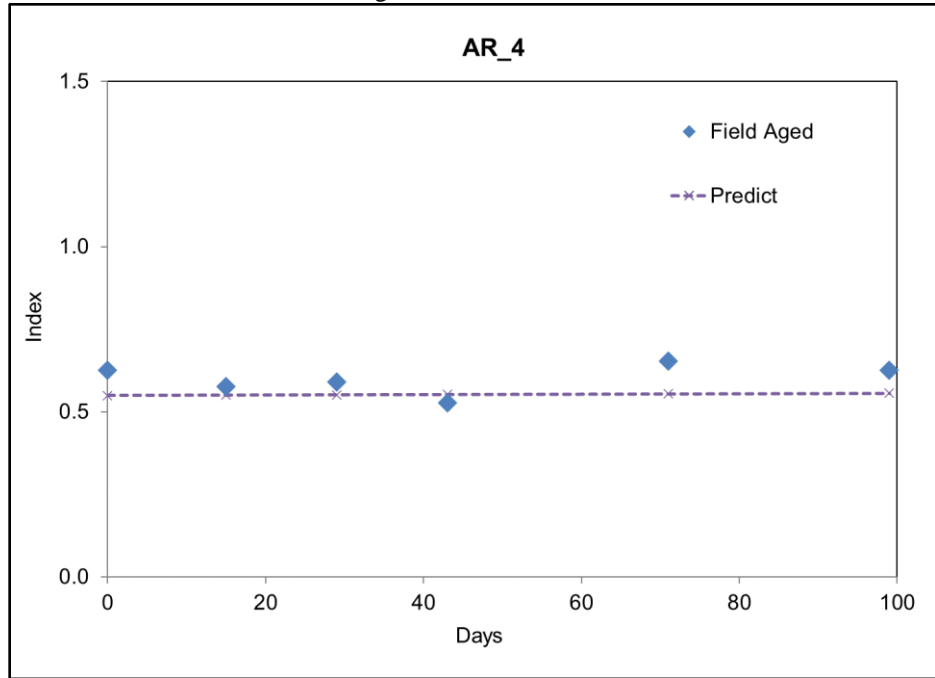
h: AR_4
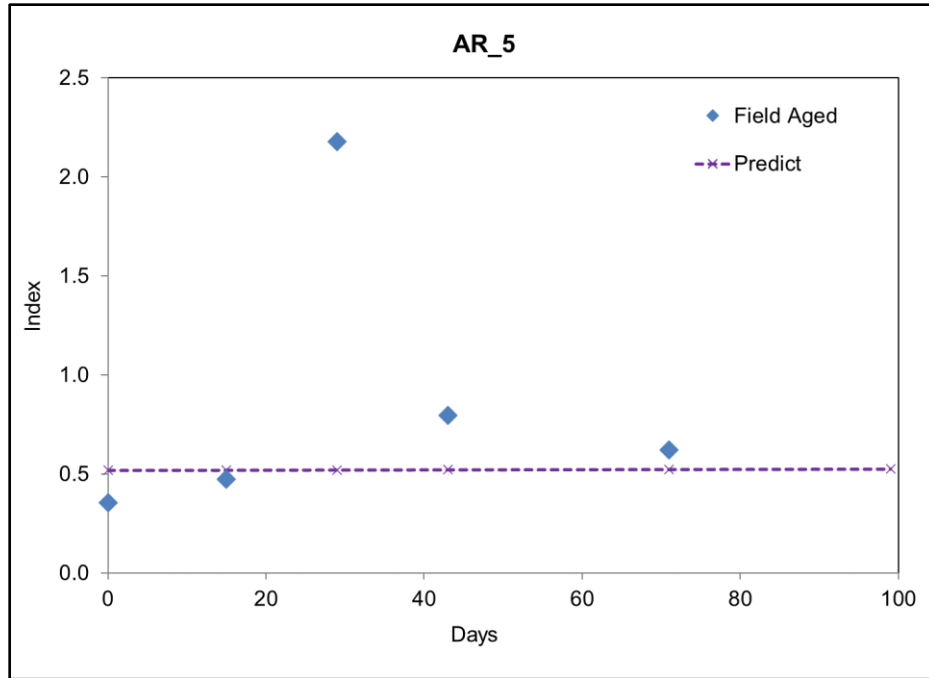
i: AR_5

Figure 4.12: Comparison of field measured CA indices and model predicted CA indices.

4.3.2 Changes of Rheological Properties During Oxidative Aging

The frequency sweep test data were used to build dynamic modulus master curves. Figure 4.13 shows master curves for the nine binders on a logarithmic scale at a reference temperature of 20°C. The reduced frequency at 20°C was determined according to the angular frequency and the shift factor (α_t) using Equations 4.4 and 4.5. The reduced loading frequencies were between 1E-04 Hz and 1E+03 Hz when the raw data were shifted to the reference temperature in this section. Each master curve in Figure 4.13 is the average of two replicate tests.
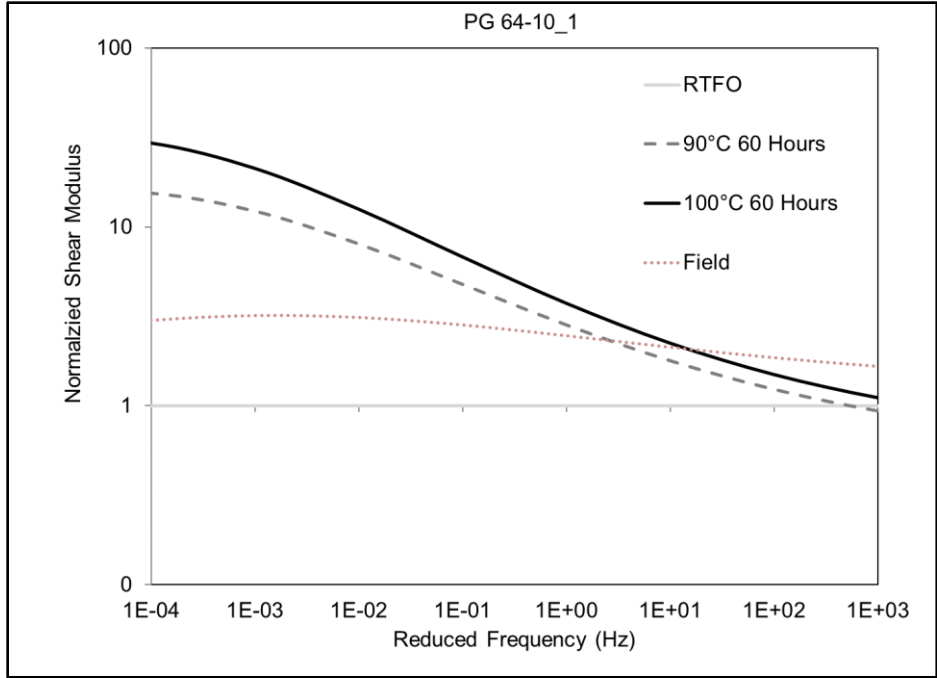
a: PG 64-10_1
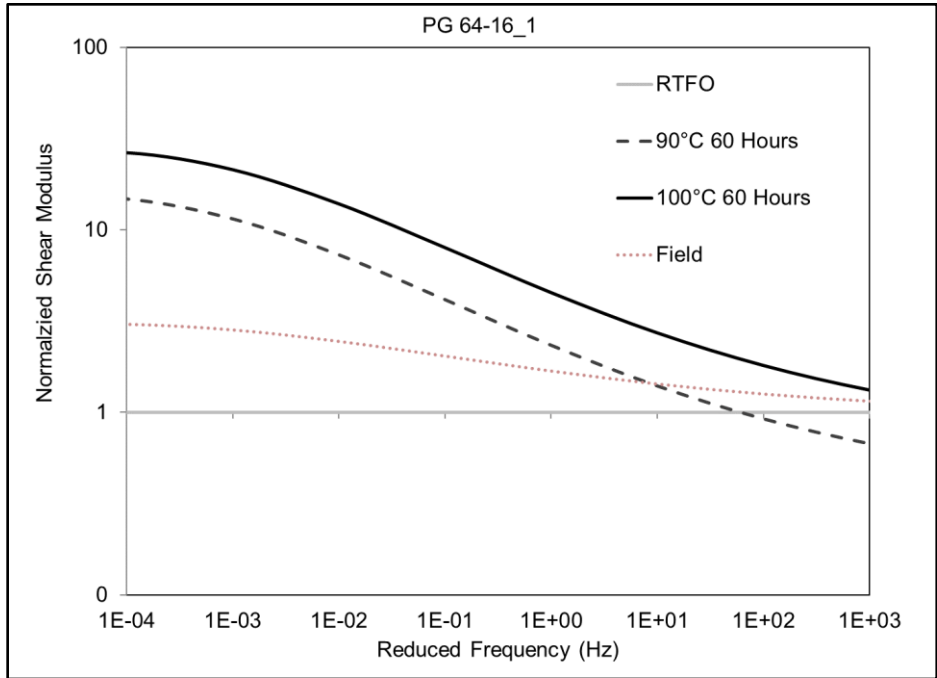
b: PG 64-16_1
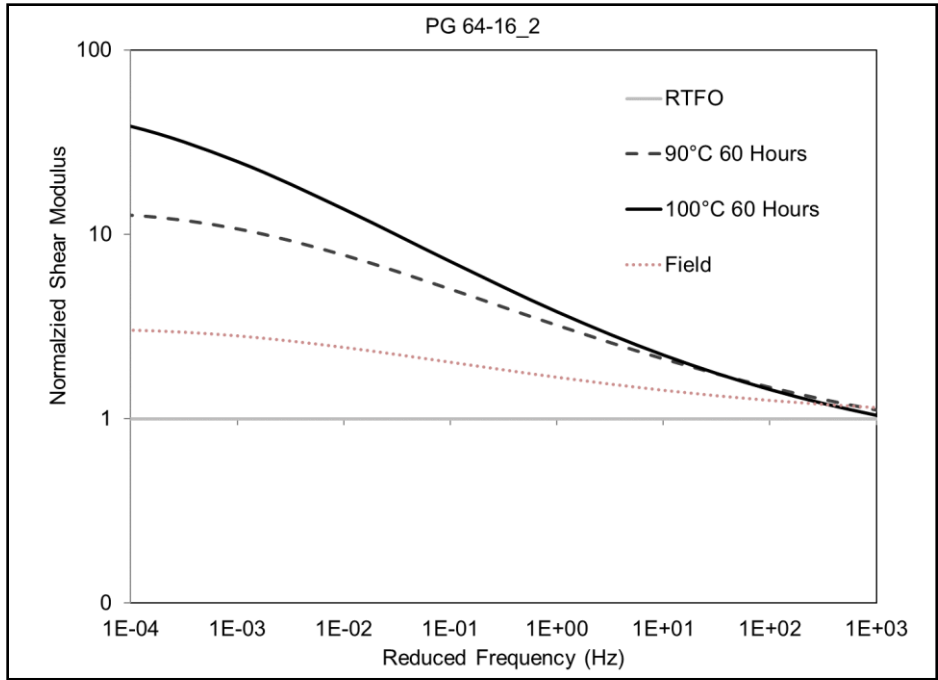
c: PG 64-16_2
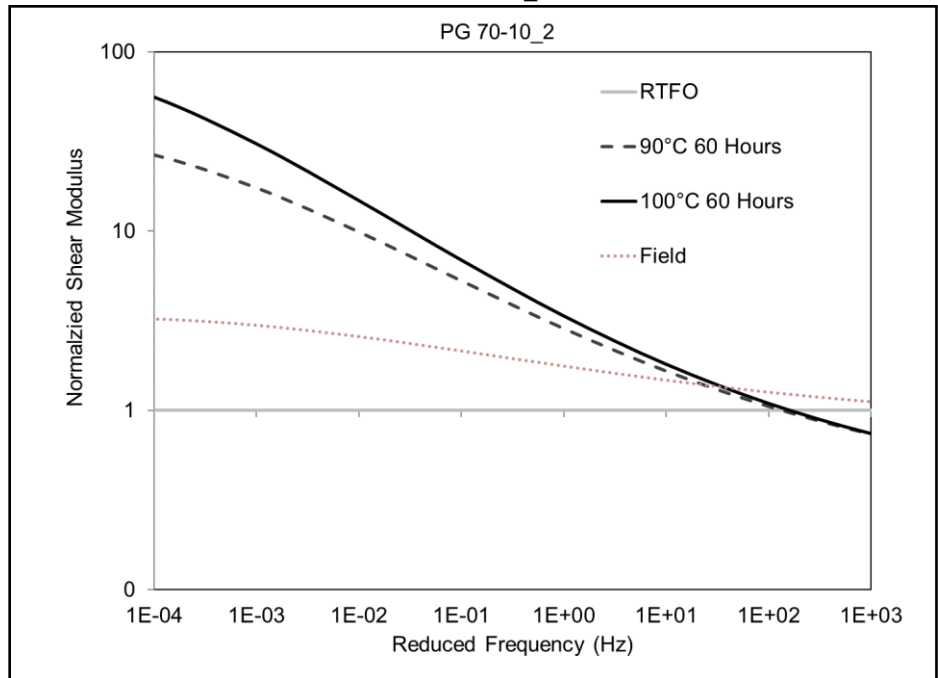
d: PG 70-10_2
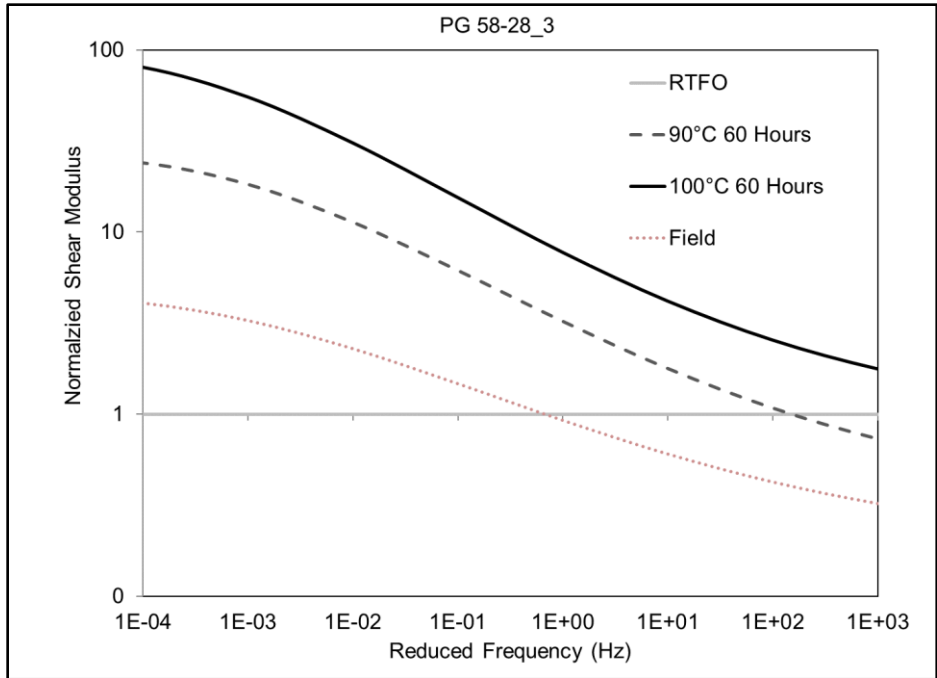
e: PG 58-28_3
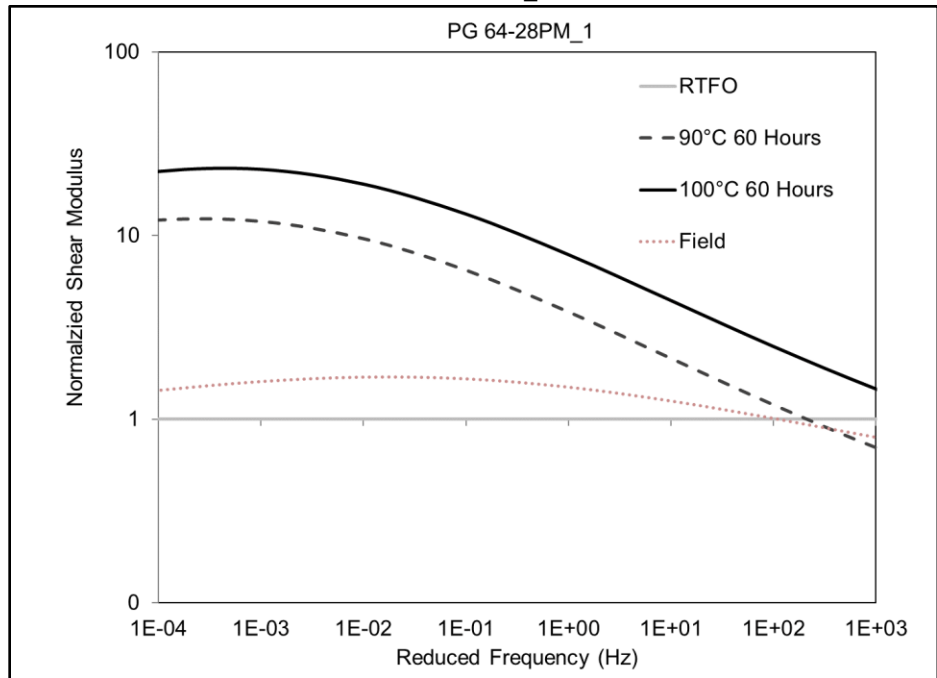
f: PG 64-28PM_1
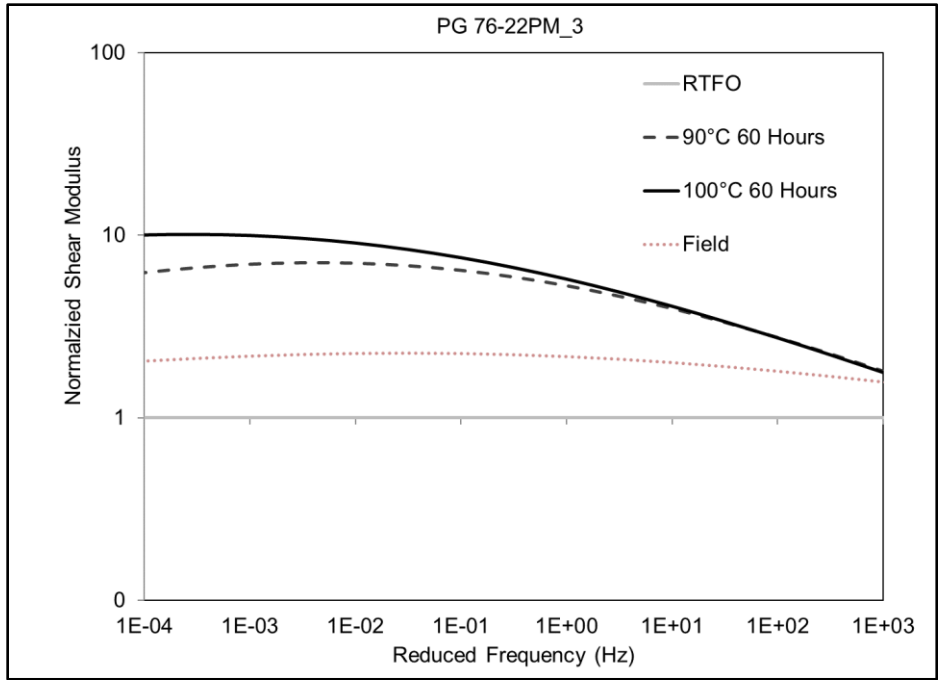
g: PG 76-22PM_3
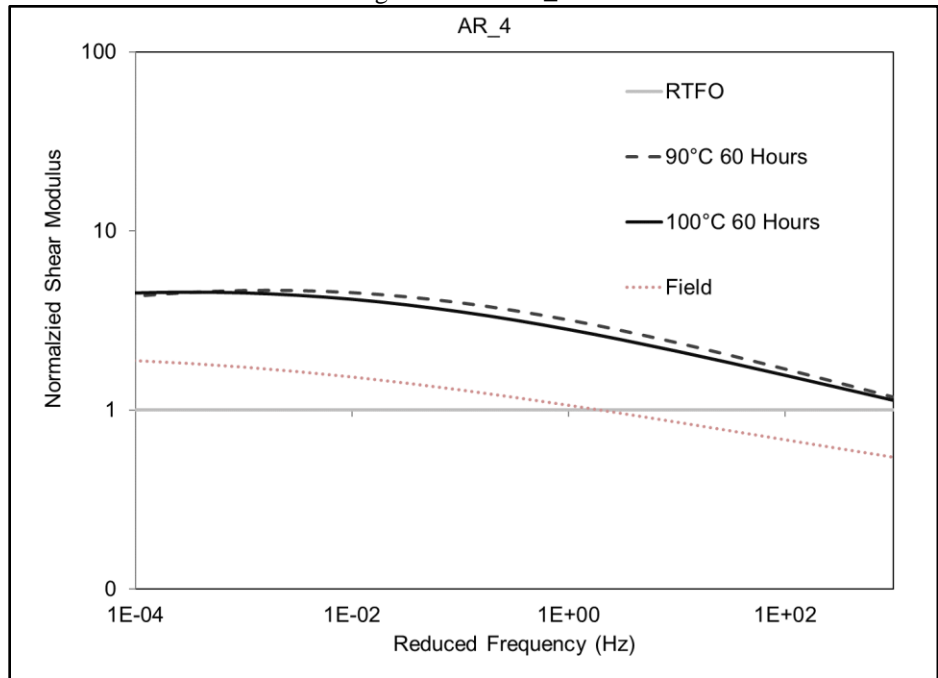
h: AR_4
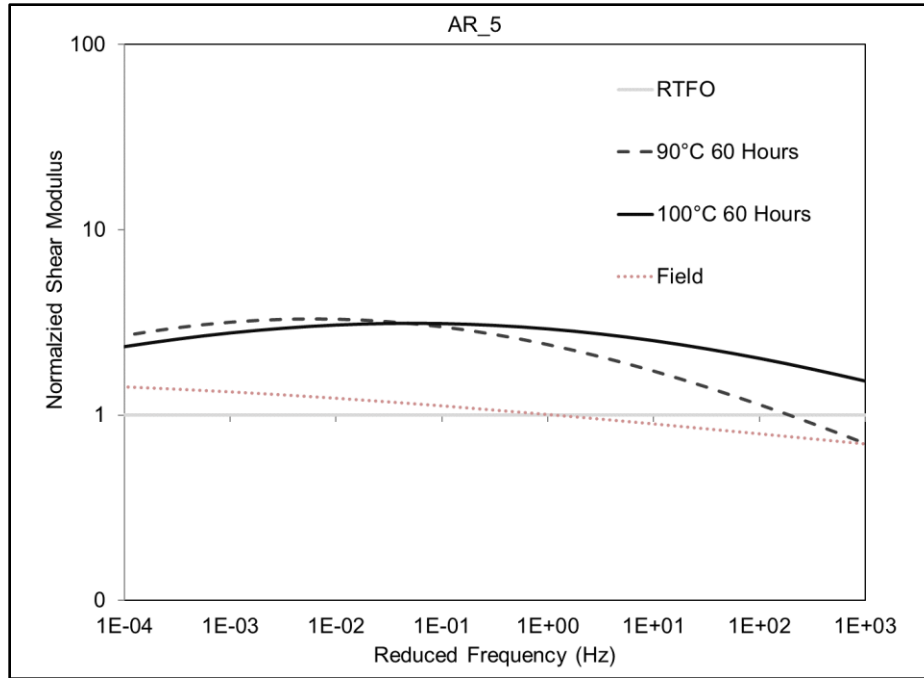
i: AR_5

Figure 4.13: Normalized shear modulus master curves at 20ºC.

Six master curves were developed for the PAV-aging protocol, and five were developed for the field-aging protocol for each binder. The master curves at the maximum aging condition were plotted to avoid overlapped multiple curves. Specifically, master curves for 99-day samples were used to represent the field-aging protocol, and the 60-hour PAV-aging results were used to represent the PAV-aging protocol.

In Figure 4.13, master curves of aged binders were normalized to their corresponding RTFO residue values for a better comparison of the stiffness change along with the degree of long-term oxidative aging. The RTFO residue data are presented as a horizontal line that intercepts with the y-axis at unit one.

The long-term aged PG 64-16_1, PG 58-28_3, PG64-28PM_1, and AR_4 binders showed lower dynamic moduli than those in the RTFO-aged conditions at the high reduced frequency ranges

(>100 Hz). The abnormally low dynamic moduli for long-term aged binders were likely caused by the biased prediction using Equation 4.3 under these high frequencies (the master curve developed at high frequency [>100 Hz at 20ºC] might not be precise) *(74)*. At high frequencies, the elasticity, rather than viscosity, dominates binder properties, which decreases the accuracy of the viscosity estimation *(91,148)*.

A higher shear modulus at a given frequency after aging indicated a higher degree of age-hardening. For the master curve at the intermediate and lower reduced frequency span (i.e., <100 Hz), the long-term aged binders were stiffer than the RTFO-aged binders. These binders experienced a more intensive age-hardening in the PAV-aging protocol than the field one.

The difference in dynamic moduli between the PAV-aging and field-aging protocols was more substantial for unmodified binders than the modified binders, especially the AR binders. This observation indicated that unmodified binders experienced a higher degree of age-hardening than the modified binders did at the same aging condition. The unmodified binders had the largest stiffness increases, followed by SBS-modified binders, and then AR binders, which had the lowest stiffness increase after completion of long-term aging. AR binders did not show a noticeable stiffness difference between RTFO residues and the long-term aged residues, indicating that the presence of rubber reduced the overall age-hardening. Further investigation of the oxidative aging in rubber-modified binders is discussed in Chapter 5.

Figure 4.13 shows that the rate of change in binder stiffness increased when the loading frequency decreased, implying that aged asphalt binders were less vulnerable to permanent deformation (i.e., rutting) after age-hardening, as expected.

At the 20°C and 10 Hz condition, the binder stiffness increased by up to four times after PAV-aging and up to two times after glass plate field-aging. For a thin pavement layer, the stiffening reduces the binder's ability to dissipate the damage energy resulting from traffic loading and thermal gradient stresses *(131)*. Thus, oxidative aging in a thin asphalt mix layer makes it less resistant to fatigue damage. In a thick layer, the age-hardened stiffer binder decreases the bending at the bottom of the layer, which improves fatigue resistance *(131)*. However, the aged binder will still have the same lessened ability to dissipate the damage energy. Fatigue analysis, in these instances, requires evaluating the material properties under various loadings and temperatures, as well as the pavement response to fatigue damage. Additional discussions of aged mix performance are presented in Chapter 6.

4.4   Correlation of Carbonyl Area Index and Viscosity in Long-Term Oxidative Aging

In the long-term aging stage, the logarithmic increase of LSV was linearly correlated to the CA index increase, as shown in Equation 2.11. This correlation is defined as the constant parameter-hardening susceptibility (HS) *(87)*.

Equation 2.11 can be logarithmically transformed to Equation 4.8. The LSV is typically defined at 60°C, 1.59E-05 Hz (0.0001 radians/second), which is simulated in the ring and ball test *(87)*. The LSV can also be estimated from the dynamic modulus and the phase angle using Equation 4.9 *(145)*.

$$\ln \Delta\eta_{LSV} = HS \times \Delta CA + m \tag{4.8}$$

$$\eta = \frac{|G^*|}{\omega} \cdot \left(\frac{1}{\sin(\delta)}\right)^{3.63922+0.13137.\omega-0.0009.\omega^2} \tag{4.9}$$

Where:

    m = regression parameter.

    η = viscosity in Pa·s.

    G^* = complex modulus in Pa.

    ω = loading frequency in radians/second.

The DSR test temperatures were between 4°C and 40°C owing to the geometry limitation (PP-8 is used at intermediate temperatures). This limitation significantly reduces the accuracy of estimating the LSV, which corresponds to a reduced frequency of 1.27E-08 Hz at 20°C. This is beyond the measured data range (1E-04 to 1E+03 Hz) in the section. Thus, no LSV prediction was attempted. Instead, data collected in this section was used to investigate whether the linear correlation between ln(Δη) and ΔCA was valid or not for viscosities other than the LSV.

The linearity between ln(Δη) and ΔCA of PAV-aged binder was evaluated at each combination of temperature and frequency. The calculation of the coefficient of determination (R^2) is shown in Figure 4.14, with the PG 64-10_1 binder at 40°C and 0.0159 Hz (0.1 radians/second) as an example. In this example, the CA index values at six PAV-aged conditions (90°C and 100°C, at 20, 40, and 60 hours) were plotted on the x-axis, and the corresponding viscosities were plotted on the y-axis. The R^2 value calculated from the linear regression of these six data points for this example was 0.89.
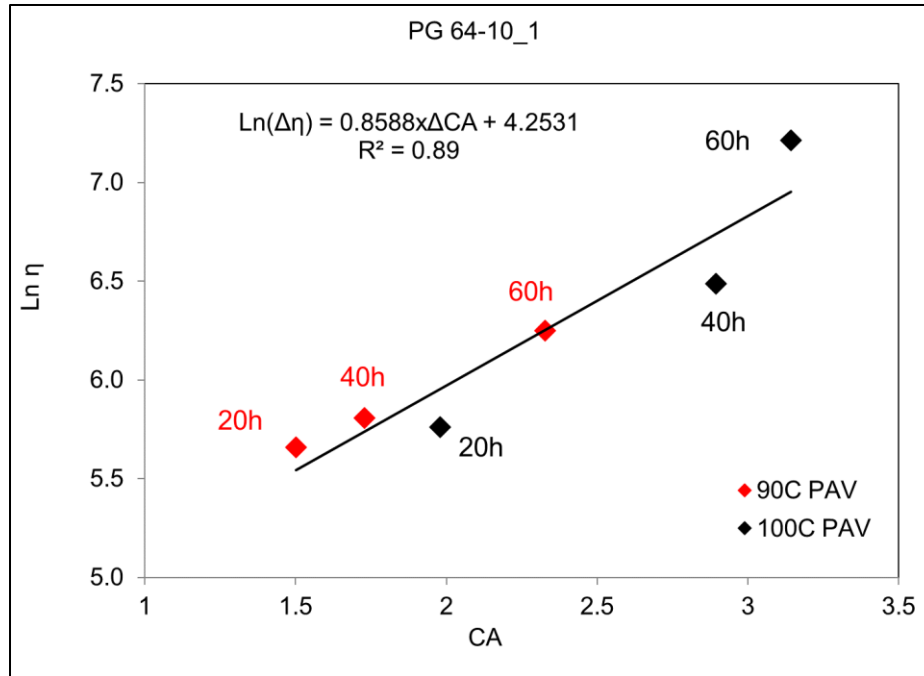
Figure 4.14: Example of determining the linearity between ln (Δη) and ΔCA index.

The linearities of nine binders at measured temperatures (4°C, 20°C, and 40°C) and frequencies (0.0159 Hz to 3.99 Hz [0.1 radians/second to 25 radians/second]) were evaluated using the same methodology shown in Figure 4.14.

Figure 4.15 shows the summary of R^2 values by plotting them along with the reduced frequency at 20°C. Each point represents an R^2 value at the measured frequency. Numerous cases confirmed that the linearity assumption between ln(Δη) and ΔCA was valid using 0.70 as a threshold *(135,146,147)*, indicating that there was a strong linear correlation between ln(Δη) and ΔCA. This threshold is a rough rule of thumb for variables to be considered significant for the regression.

Figure 4.15a shows that R^2 values generally decreased along with the frequency, indicating that the linearity was more evident at high temperatures and slow loading frequencies. The lack of linearity at a relatively low temperature is mainly attributed to the biased viscosity estimation, where elastic properties dominate the binder performance instead of viscosity *(91,148)*. Errors in

phase angle also have a larger effect on the viscosity prediction when the phase angle is considerably small (sin 90° = 1 and sin 0 = 0). When the phase angle is relatively small at low temperatures or faster loading frequencies, the measurement errors are considerably larger relative to the measurement value, which significantly affects the viscosity estimation using Equation 4.9.

When the test temperature increases, viscosity dominates the binder performance. The phase angle is close to 90°, and the measurement errors are relatively small compared to the actual value. At higher temperatures, viscosity can be better estimated using Equation 4.9. In testing discussed in this chapter, unmodified binders had higher R^2 values than modified binders, and AR binders tended to have the lowest R^2 values. The most likely reason for this low linearity was that the DSR measurement of AR binders using parallel plate geometry described above was not sufficiently precise due to the proximity of the incompletely digested rubber particles to the plates.

For the field-aging protocol, the R^2 values for the linearity assumption were also mostly higher than the 0.70 threshold. Figure 4.15b shows the R^2 values for the glass plate-aged binders. The unmodified binders had the highest R^2 values, followed by SBS-modified binders and AR binders. This ranking was the same as that in the PAV-aging.

The valid linearities between $\ln(\Delta\eta)$ and ΔCA indicated that the viscosity beyond the LSV range could be predicted from the CA growth for the unmodified and SBS-modified binders tested in this study. Improvements to the measurement of rheological properties of AR binders were considered to be necessary before validating the linearity assumptions. These rubber-modified binders will be evaluated using the modified Superpave PG system in Chapter 5.
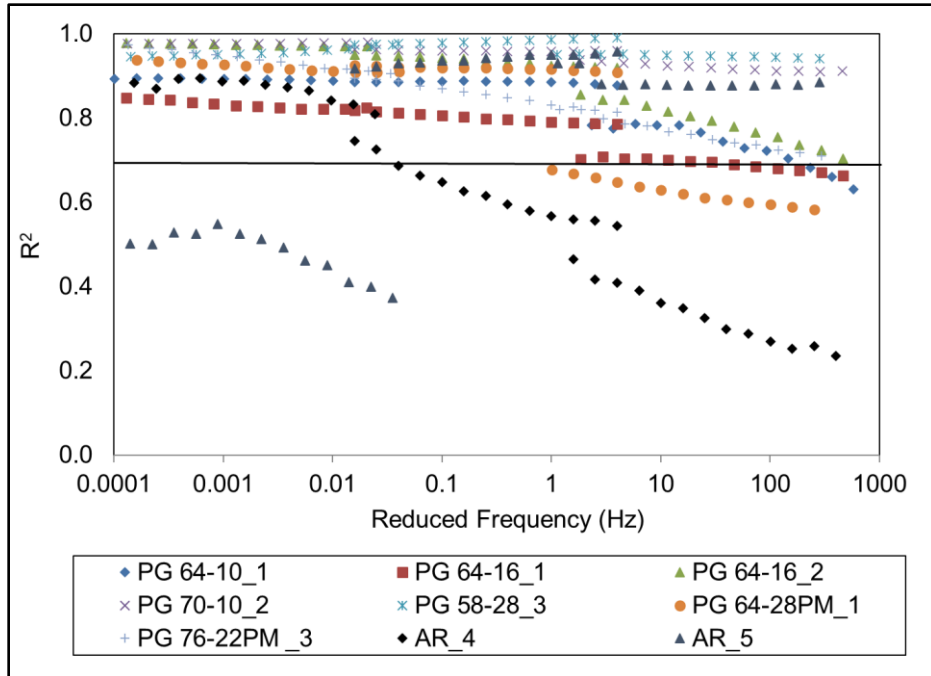
a: PAV-aging protocol
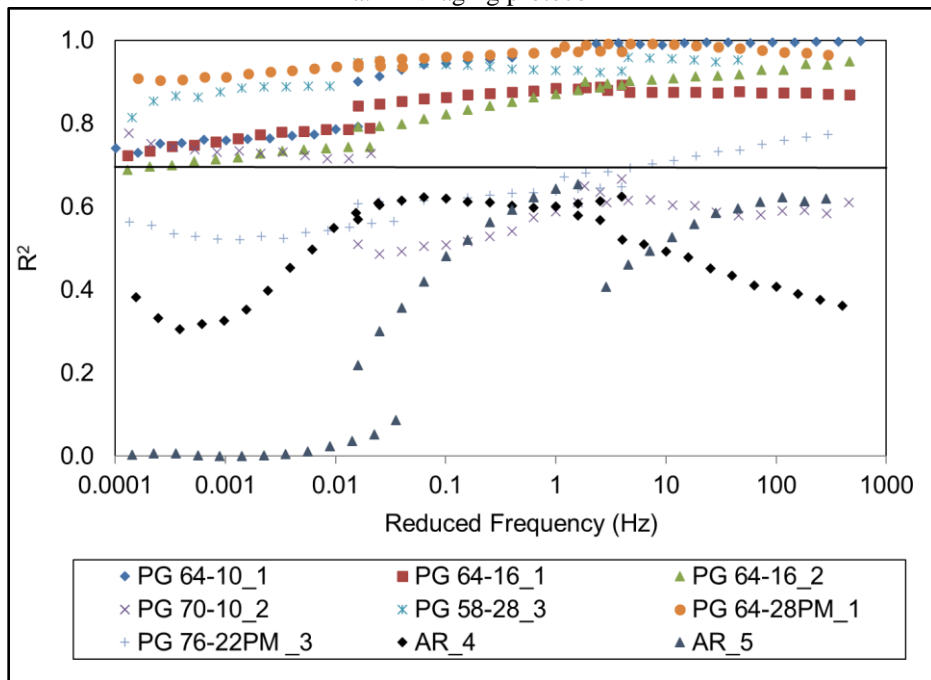
b: Glass plate aging protocol in the field

Figure 4.15: Coefficient of determination (R^2) between $\ln(\Delta\eta)$ and ΔCA index.

An alternative parameter that defines the slope between $\ln(\Delta\eta)$ and ΔCA under general loading conditions is proposed in this study. The generic hardening susceptibility (GHS) is proposed to

distinguish the HS parameter that corresponds to the specific low shear loading condition of 60°C and 1.59E-05 Hz (0.0001 radians/second). With the valid linearity assumption between ln(Δη) and ΔCA, an increase in ln(Δη) based on known ΔCA values in the long-term oxidative aged binder could be predicted using the GHS principle.

One difference between the GHS and the HS is that GHS is not only binder dependent but also temperature and frequency dependent. The HS is a constant value because it only defines the linearity at the specific 60°C and 1.59E-05 Hz (0.0001 radians/second) condition. The GHS principle advances the prediction of age-hardening over a wide range of viscosities, which benefits the performance-related evaluation under different temperatures and loading frequencies.

4.5   Determination of the Generic Hardening Susceptibility

The above observations indicate that the linearity between ln(Δη) and ΔCA was validated for unmodified and SBS-modified binders from 4°C to 40°C at a loading frequency of 0.0159 Hz to 3.99 Hz (0.1 radians/second to 25 radians/second). The GHS parameter can be obtained from an accelerated aging protocol using multiple PAV-aging. When the increment in the CA index is known, the GHS model can be used to predict binder viscosity changes at the required combination of temperature and loading frequency. The original format of the GHS model is given in Equation 4.10.

$$ln\, \Delta\eta = GHS(T, f) \times \Delta CA + m \qquad\qquad 4.10$$

Where:
   $\Delta\eta$ = growth of viscosity in the long-term aging phase.
   ΔCA = increase in carbonyl area index, which is the integrating area between 1,675 cm^{-1} and 1,750 cm^{-1} from the spectrum obtained by the FTIR.
   m = a constant regression parameter.
   T and f = temperatures and loading frequencies for viscosity measurement, respectively.

The preliminary GHS model provides a quick, cost-effective, and well-controlled approach to predict the age-hardening effect on the binder after long-term aging. However, this preliminary GHS model requires data at the beginning of the long-term aging period as the reference status, which needs additional tests to obtain binder properties at this starting point.

According to Figure 2.8, the preliminary GHS model defines age-hardening on viscosity in the long-term aging period, which is plotted from point C to point D. However, the calculation of changes in the viscosity and CA index requires knowledge of these properties at point C. Glover et al. *(94)* suggested that a binder at point C might be aged beyond what would have typically occurred in the asphalt plant and during paving operations. It is difficult to accurately quantify binder properties at point C, leading to considerable uncertainty for determining the starting point of the constant reaction stage. This uncertainty would reduce the accuracy of using the preliminary GHS model.

Consequently, the GHS model was modified to avoid using the changes of viscosity and CA index. This modification limits the uncertainty of using the point C in the constant reaction period. The mathematical logic for this refinement is described in Equation 4.11 through Equation 4.14:

$$\Delta ln\,\eta = GHS(T,f)' \times \Delta CA + m_1 \qquad\qquad 4.11$$

$$m_1 = GHS(T,f)' \times CA_0 + m_2 \qquad\qquad 4.12$$

$$\Delta ln\,\eta = GHS(T,f)' \times \Delta CA + GHS(T,f)' \times CA_0 + m_2 = GHS(T,f)' \times CA + m_2 \qquad 4.13$$

$$l\,n(\eta) = \Delta ln(\eta) + ln(\eta_0) = GHS(T,f)' \times CA + m_2 + ln(\eta_0) = GHS(T,f)' \times CA + m_3 \qquad 4.14$$

Where:
    GHS(T,f)' = linear slope for $\Delta ln\,\eta$ and ΔCA.
    (CA$_0$, η_0) = binder properties at point C.
    η and *CA* = binder properties at any point in the long-term aging period.
    m_1, m_2, and *m_3* = interceptions on the log viscosity axis for each regression, respectively.

In this section, the linearity between delta logarithmic viscosity ($\Delta\ln(\eta)$) and delta carbonyl area index (ΔCA) was checked. After this linearity was confirmed, the preliminary GHS model could be rewritten in the form of Equation 4.11. Since the product of CA_0 and GHS is a constant, the regression parameter (m_1) in Equation 4.11 can be substituted by Equation 4.12. Then Equation 4.13 is obtained by combining Equation 4.11 and Equation 4.12. After verifying the linearity between $\ln(\eta)$ and CA, Equation 4.14 can be implemented by adding the ($\ln \eta_0$) to the left side of Equation 4.13. Equation 4.14 provides the final GHS model that correlates ($\ln \eta$) and the CA index at any given point in the long-term aging phase.

Figure 4.16 provides a graphic description of determining the GHS model using the PG 64-28PM_1 binder at 20°C and 3.99 Hz (25.1 radians/second). The preliminary GHS model in the format of Equation 4.10 is plotted with a black line. The blue line presents the linearity between $\Delta\ln(\eta)$ and ΔCA, which is in the format of Equation 4.11. The finalized GHS model is shown with a red line, which has the same GHS value as the one presented by the blue line. Apparent linearity exists for this binder at 20°C and 3.99 Hz (25.1 radians/second), as the R^2 values were over 0.90 for these three regression models.
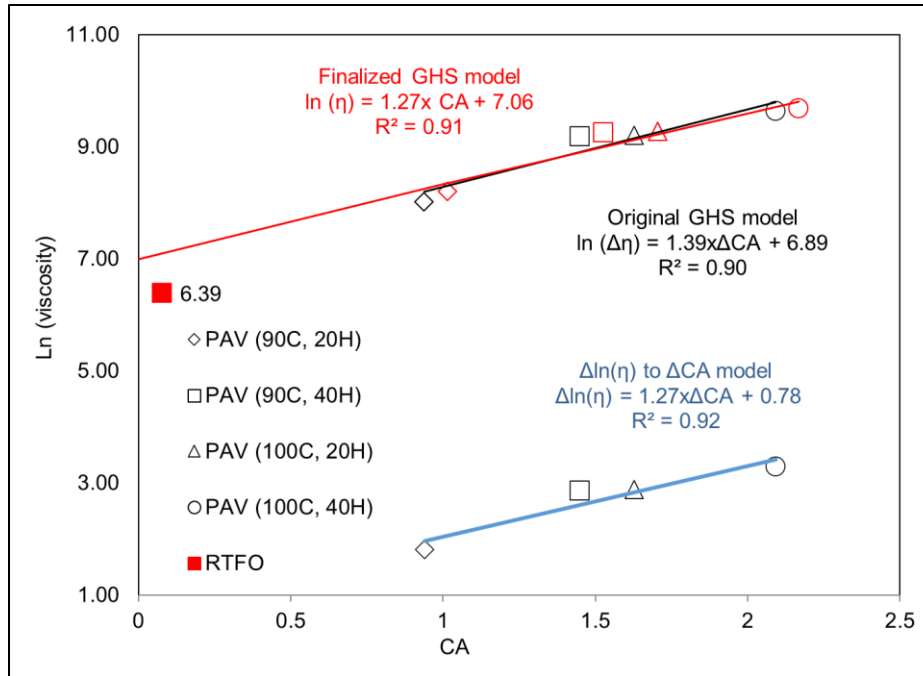
Figure 4.16: Graphic explanation of the GHS model.

The (m) value is 7.06 in the finalized GHS model, which is higher than the corresponding viscosity of the RTFO residue (ln(η) equals 6.39). Given that the (m) value is the interception of the viscosity axis, it is the bottom boundary of the viscosity in the long-term aging phase. This observation indicates that the viscosity at the start of the long-term aging phase (point C) should be higher than that of an RTFO residue. This was consistent with previous observations in terms of the low shear viscosity growth, as shown in Figure 2.8 *(94)*.

4.5.1   Verification of GHS Principle

To verify the linearity between $\Delta \ln(\eta)$ and ΔCA defined Equation 4.11, three unmodified binders and two SBS-modified binders were tested. These binders were first subjected to RTFO-aging at 163°C for 85 minutes. The RTFO protocol corresponds to the aging condition after plant mixing and lay down, which is around point B in Figure 2.8. In this section, the RTFO residue was assumed to be an approximate representation of the oxidative aging at point C. Although it is less

114

aged than the binder at point C, the difference between these two aging statuses is relatively small compared to that occurring during long-term oxidation aging *(116)*. This assumption may bias the intercept of the linearity regression line, but it will not affect the accuracy of linearity validation.

The RTFO residues were subjected to long-term aging using PAV-aging at two temperatures (90°C and 100°C) and two durations (20 and 40 hours). The CA indices and the viscosities of PAV-aged binders were measured.

The ΔCA value was calculated by subtracting the CA value of the RTFO residue from the CA value at a given PAV-aged condition. Similarly, $\Delta \ln(\eta)$ value was calculated by subtracting the $\ln(\eta)$ value of the RTFO residue from the $\ln(\eta)$ value at a given PAV-aged condition. Figure 4.16 plots the $\Delta \ln(\eta)$ on the y-axis and ΔCA on the x-axis. Linear regression was conducted to validate the linearity between $\Delta \ln(\eta)$ and ΔCA, using the method shown by the blue line in Figure 4.16.

Figure 4.17 presents R^2 values for the linearity between $\Delta \ln(\eta)$ and ΔCA at 4°C, 20°C, and 40°C. There were several data points outside the plot boundary at 4°C for the PG 64-16_1 binder because the backcalculated viscosity for the RTFO residue was higher than that of the PAV-aged binders in this case. The $\Delta \eta$ was negative and could not be logarithmically transformed. A reasonable explanation is that the elastic behavior, and not the viscosity, dominates the binder behavior at this low temperature *(148)*, which leads to an inaccurate estimation of the viscosity.

Figure 4.17 shows that linearity existed at intermediate temperatures between 20°C and 40°C. However, it was marginally valid for the cases at 4°C. The red symbol in Figure 4.17b presents the R^2 value of the sample case shown in Figure 4.16.

a: 4˚C
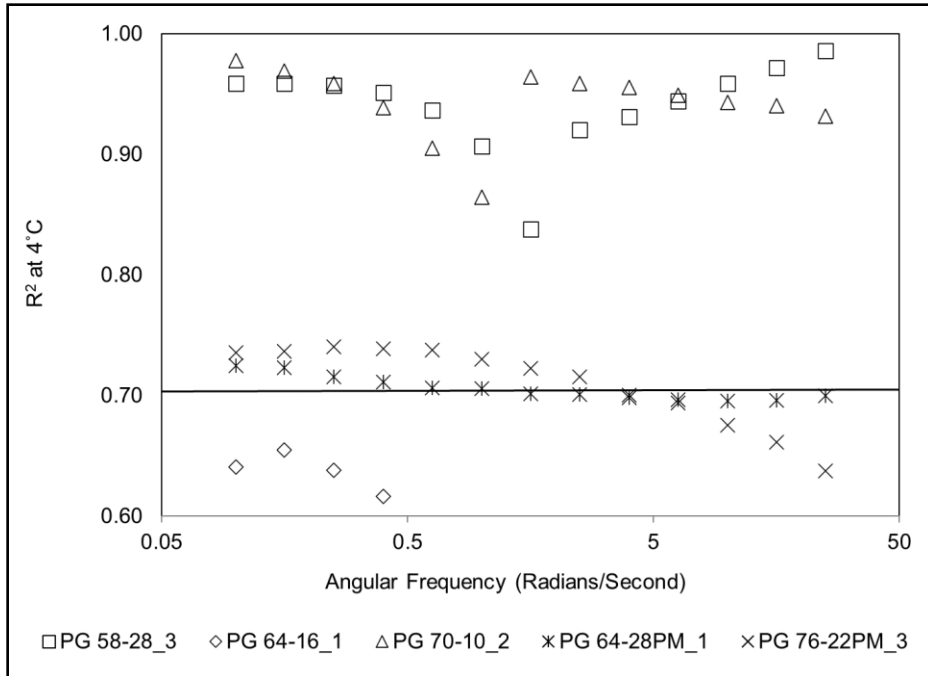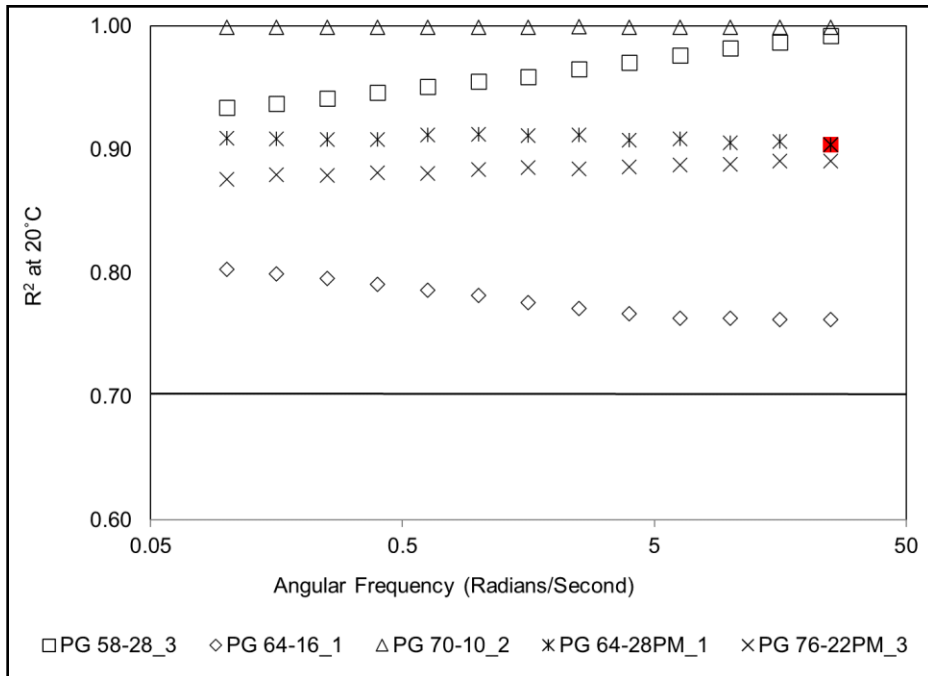
b: 20˚C (Red point presents the R^2 value of the sample case shown in Figure 4.16)
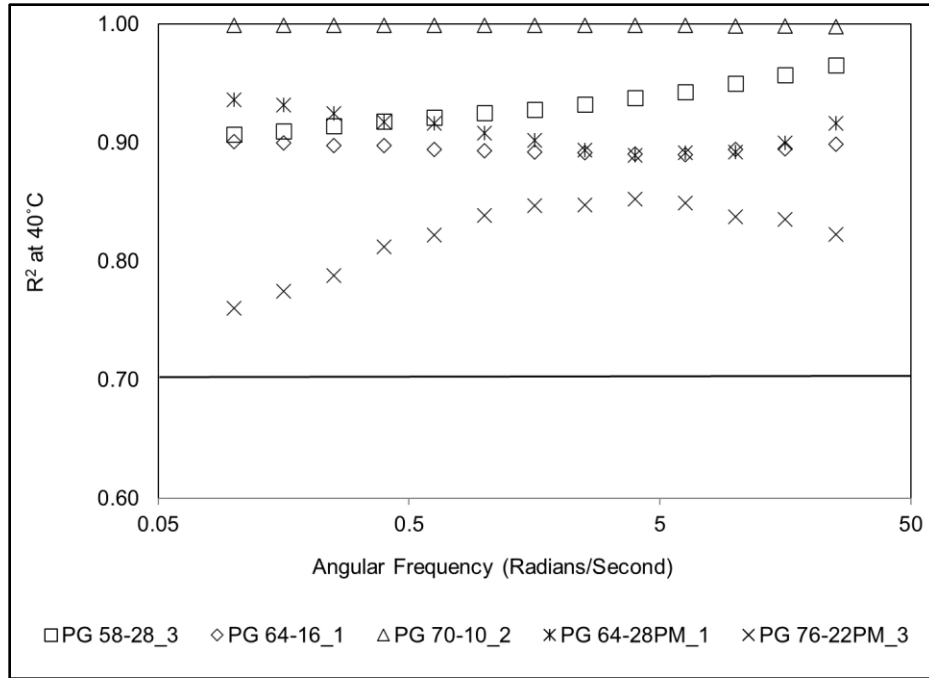
c: 40°C

Figure 4.17: Linearity between Δln(η) and ΔCA at intermediate temperatures.

4.5.2   Development of GHS Model

In this section, the linearity assumption between the ln (η) and the CA index was checked with a linear regression of the ln(η) and CA index without subtracting the values of the RTFO residues, as shown in Figure 4.16. The CA indices and viscosities were measured and calculated at each PAV-aged condition. Data were collected from the same tests conducted in Section 4.5.1. Figure 4.18 shows R^2 values for the linear regression of ln(η) and CA indices. The red dot in Figure 4.18b presents the R^2 value of the sample case shown in Figure 4.16.

In addition to the tests at intermediate temperatures (4°C to 40°C), additional tests at a higher temperature range were conducted to validate the linearity in this section. The second-round frequency sweep tests were run at 60°C and 85°C, with a loading frequency between 0.0159 Hz and 3.99 Hz (0.1 radians/second and 25.1 radians/second).

117

The 25-mm diameter plate parallel plate geometry (PP-25) with a 1-mm gap was used. The frequency sweep tests were run at 1 percent strain. Viscosities were backcalculated from the rheological properties using Equation 4.9. Numerous cases showed that the linearity assumption between $\ln(\eta)$ and CA was valid, as R^2 values were higher than the 0.7 threshold *(135,146,147)*. The refinery and binder source, modifier, and PG did not impact the validation of the linearity.
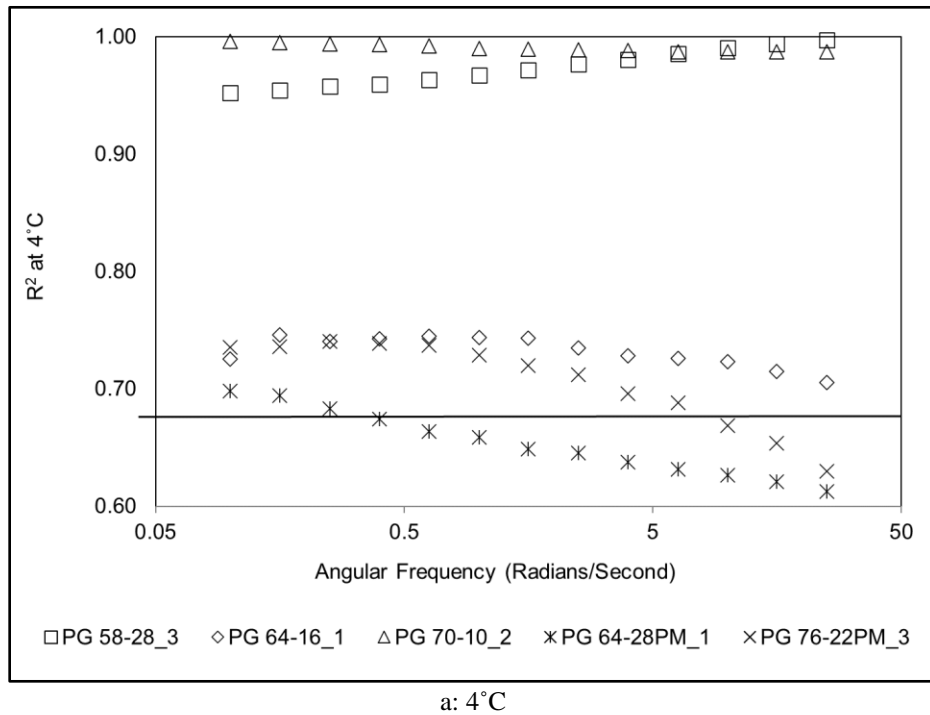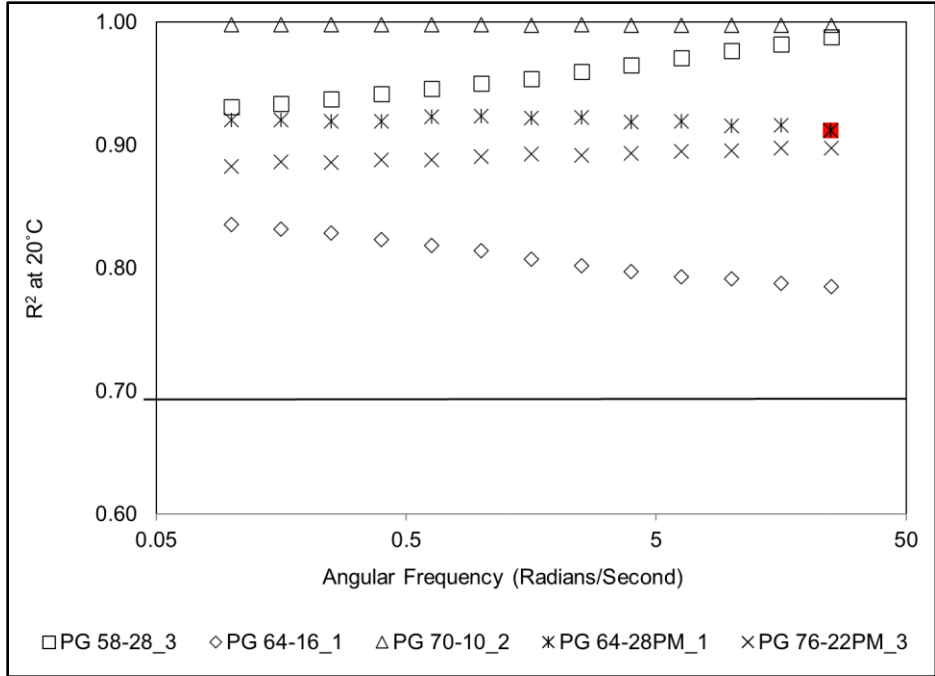
a: 4˚C

b: 20°C (Red point presents the R^2 value of the sample case shown in Figure 4.16)

c: 40°C

119
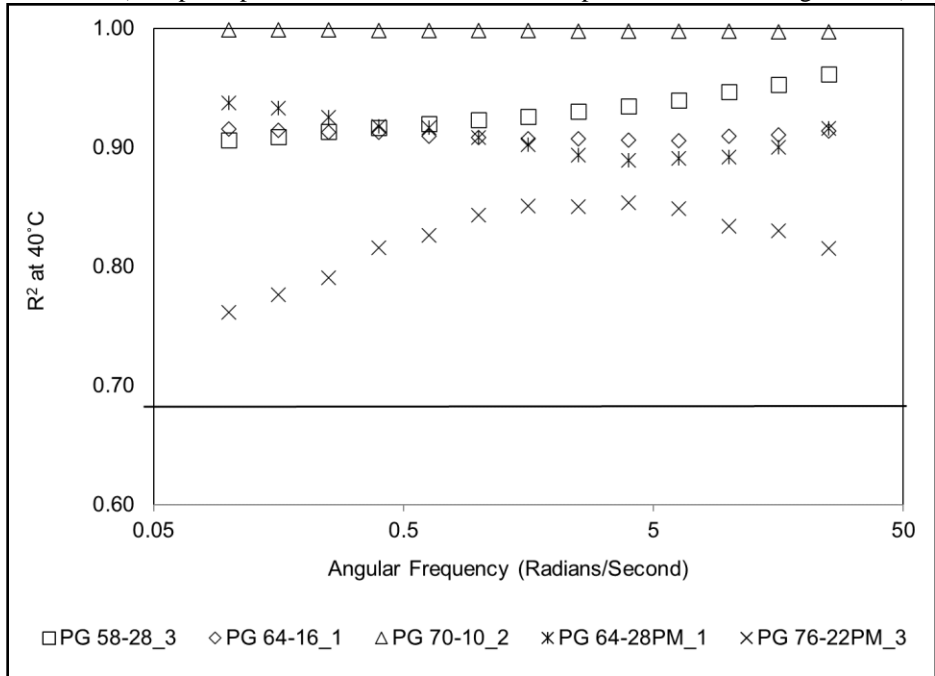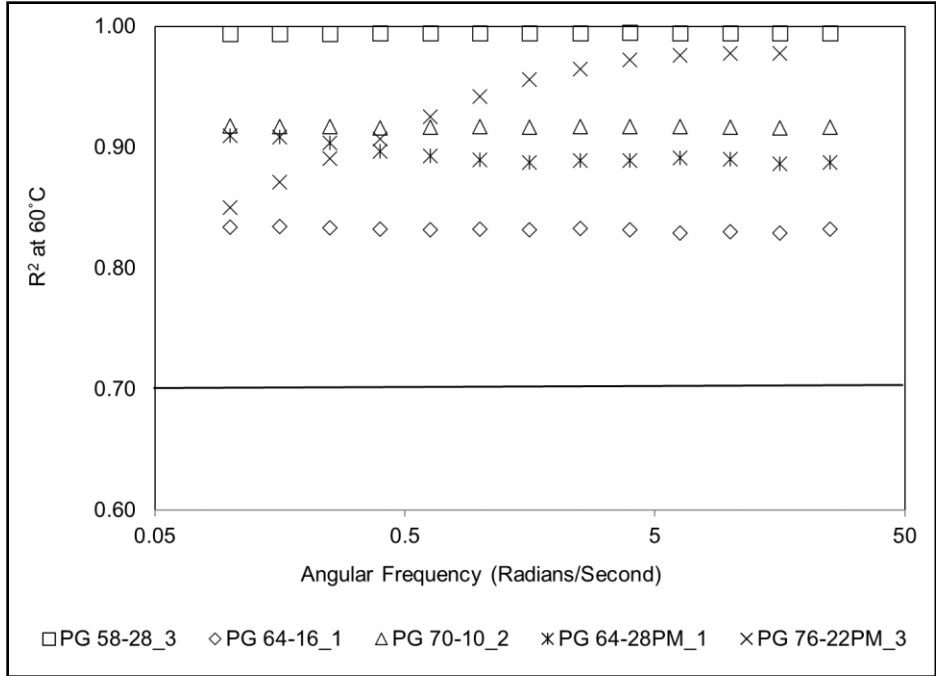
d: 60˚C
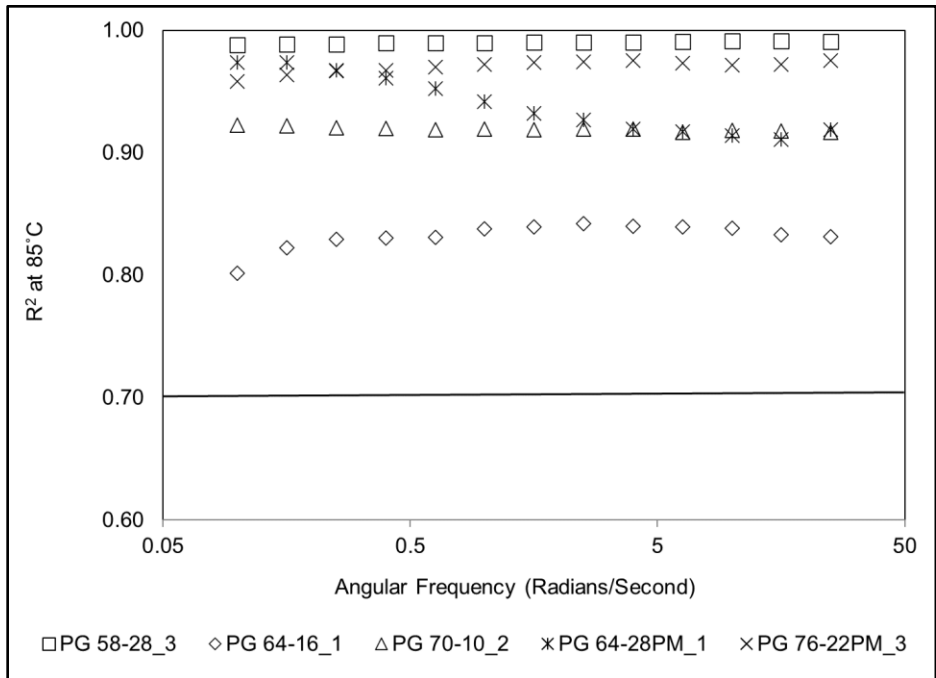
e: 85˚C

Figure 4.18: Linearity between ln(η) and CA at 4°C, 20°C, 40°C, 60°C, and 85°C.

Most of the low R^2 values were observed at the 4°C conditions. Aged binders were stiff, which

made it difficult to trim them in the parallel plate geometry. This poor trimming of the binder

specimen increased the operational error. Since phase angles were small at low temperatures, even a minor measurement offset in the phase angle would lead to a significant viscosity difference when calculated using Equation 4.9.

The linearity increased when the testing temperature was increased, which was attributed to the actual phase angle, being large enough to discount any measurement errors. Increasing the testing temperature from 4°C to 85°C increased the minimum R^2 value from 0.60 to 0.85. In general, the linearity between $\ln(\eta)$ and the CA index was significant for temperatures between 20°C and 85°C with a loading frequency between 0.0159 Hz and 3.99 Hz (0.1 radians/second and 25.1 radians/second). According to the validated linearity of PAV binders, the finalized GHS model is given in Equation 4.15.

$$ln(\eta) = GHS(T, f) \times CA + m \qquad\qquad 4.15$$

Where:
   η = viscosity of long-term aged binder at temperature T(°C) and frequency f (Hz or radians/second).
   CA = carbonyl area index in this binder.
   GHS = slope between viscosity and carbonyl area index.
   m = regression parameter, which defines the minimum binder viscosity in long-term aging.

4.6   Application of the Generic Hardening Susceptibility Model

4.6.1   *Prediction of the Viscosity Using GHS Model*

This section presents the validation of the GHS model using the data from tests on five PAV-aged binders: PG 58-28_3, PG 64-16_1, PG 70-10_2, PG 64-28PM_1, and PG 76-22PM_3. Model parameters were obtained through the method described in Section 4.5. Data points (CA, $\ln(\eta)$) were collected from four PAV-aging: 90°C at 20 hours, 90°C at 40 hours, 100°C at 20 hours, and 100°C at 40 hours.

Figure 4.19 plots the predicted viscosities versus measured viscosities at 20°C and 1.59 Hz (10 radians/second). Although the prediction accuracy varies among binders, the GHS model generally provided reasonably good estimations.

The GHS model had a better prediction for binders that were sensitive to oxidative aging. For example, the viscosity of the PG 58-28_3 binder aged at 100°C for 40 hours was almost ten times higher than the specimen aged at 90°C for 20 hours. The GHS model, in this case, provided a 99 percent accuracy for the viscosity prediction. On the other hand, for the PG 76-22PM_3 binder, the difference was only three times higher between the most and least severe PAV-aging. For this case, the precision of the GHS model was also relatively lower to 0.87. When the aging-related increase in viscosity is relatively small, the bias from random offsets in the test or backcalculation was relatively large compared to the aged binder viscosity. This bias decreased the precision of the GHS model parameters and decreased prediction accuracy.
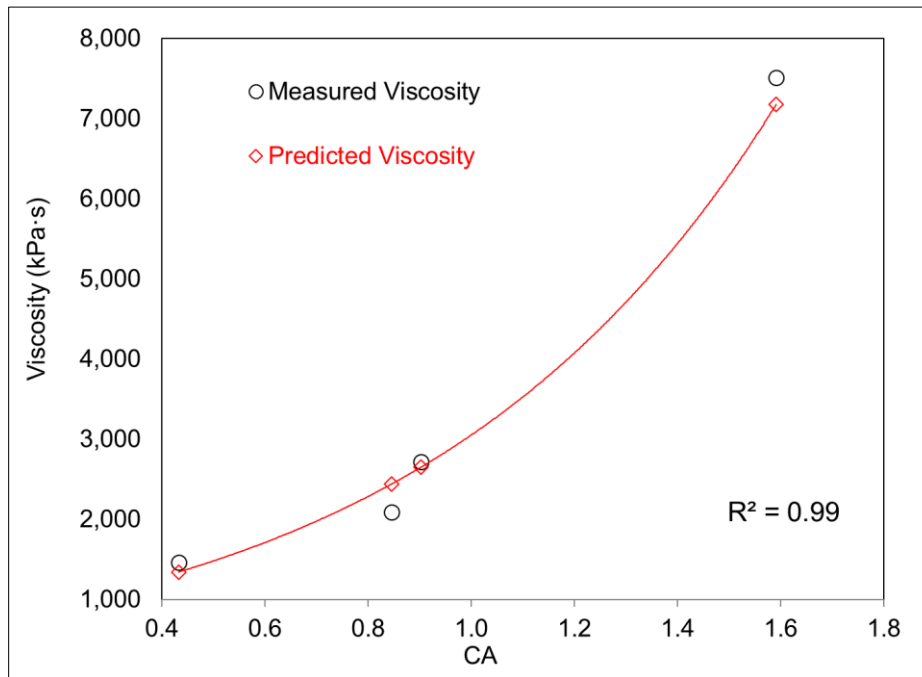
a: PG 64-16_1
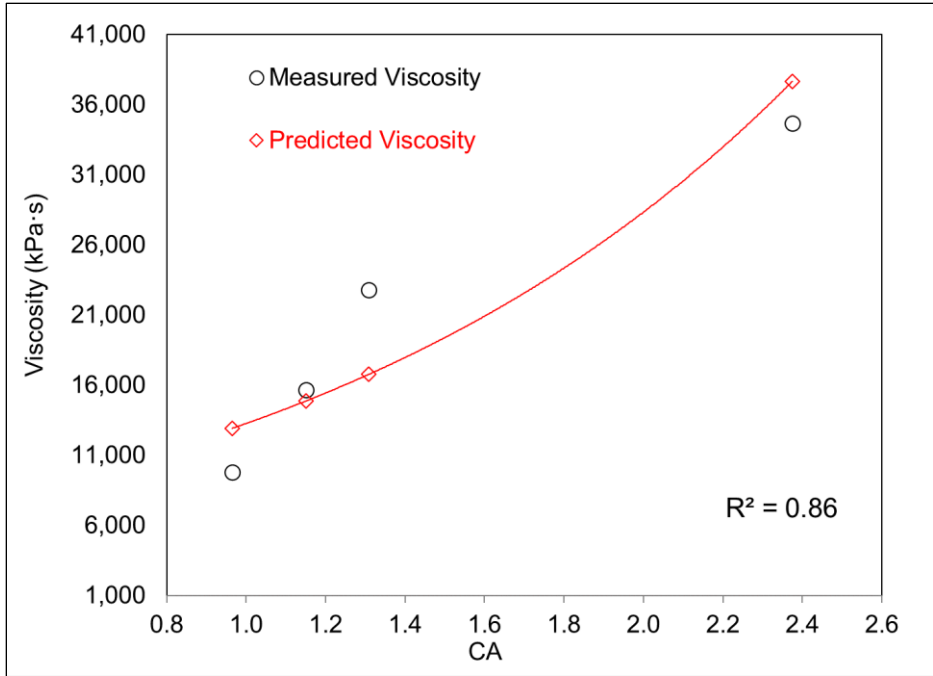
b: PG 70-10_2
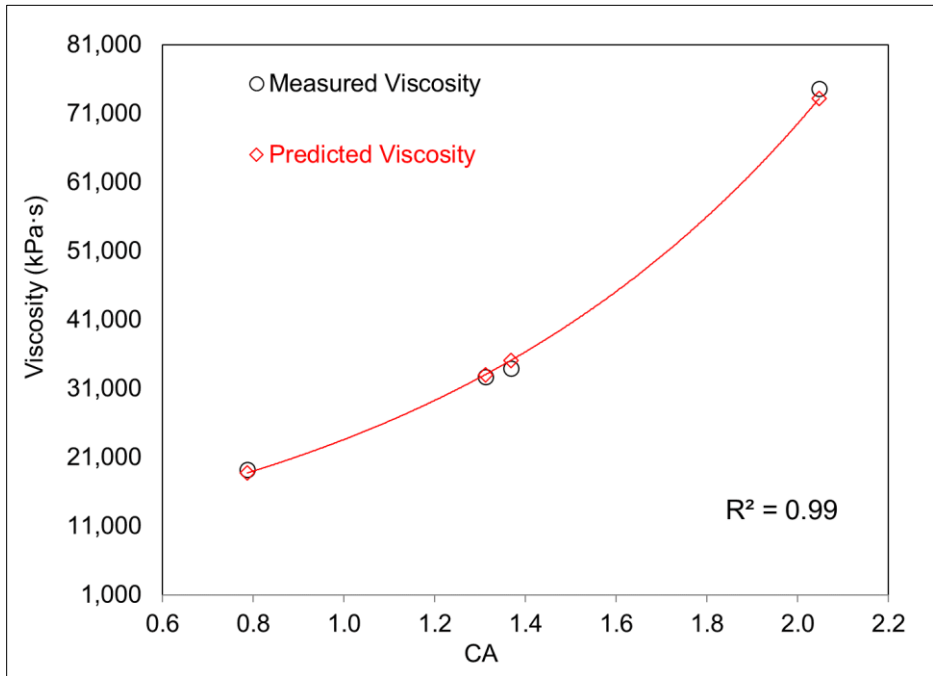
c: PG 58-28_3

123
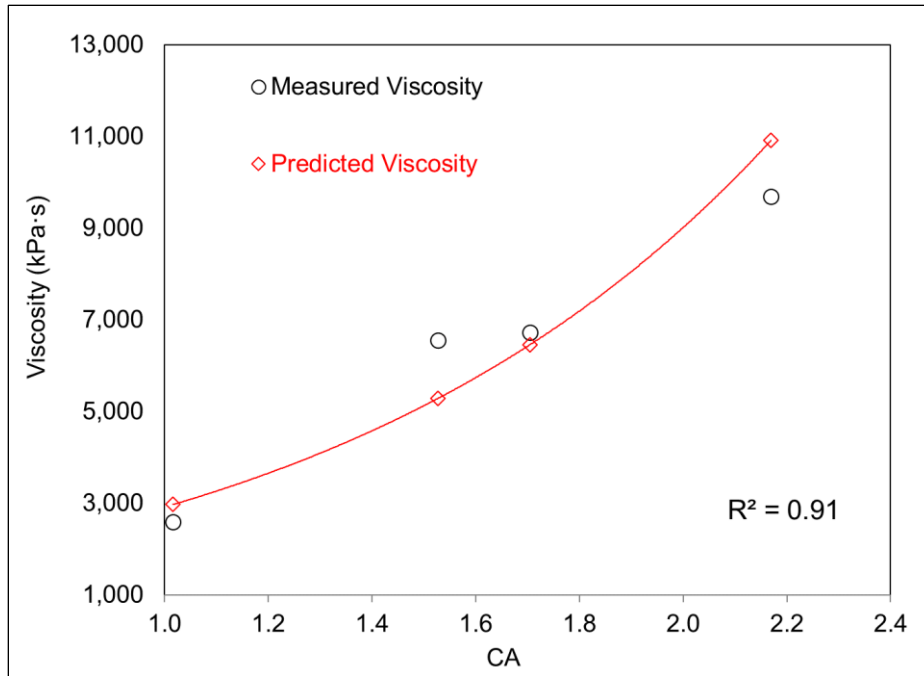
d: PG 64-28PM_1
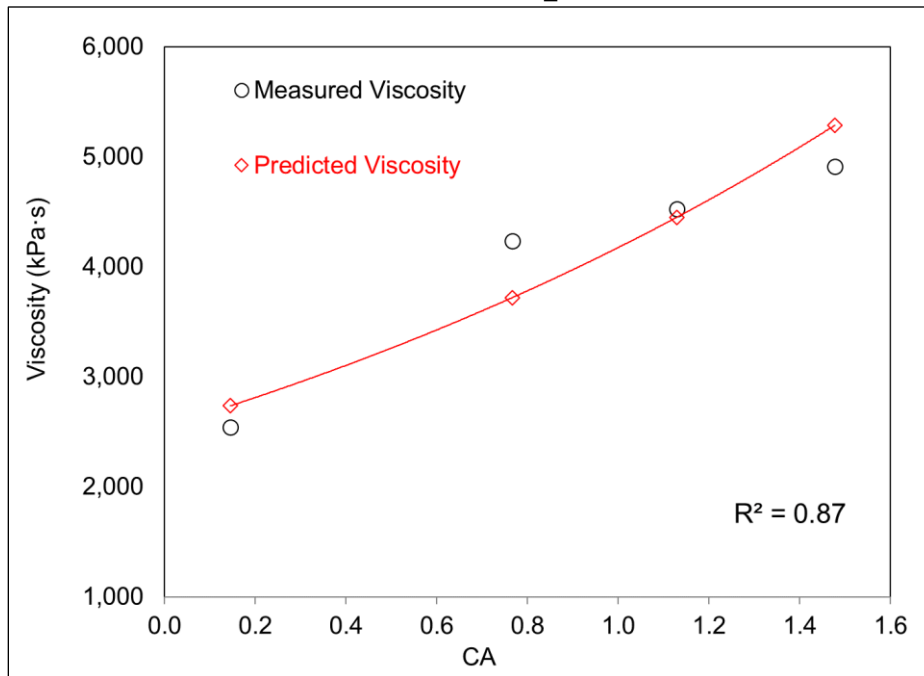
e: PG 76-22PM_3

Figure 4.19: Comparison between measured viscosity and predicted viscosity using GHS model at 20°C and 1.59 Hz (10 radians/second).

Figure 4.20 presents the overall comparison of measured viscosities to model-predicted viscosities in temperatures between 20°C and 85°C with loading frequencies between 0.0159 Hz and 15.9 Hz

124

(0.1 radians/second and 100 radians/second). The R^2 values were above 0.95 for all test temperatures and frequencies, indicating that the GHS model could predict more than 95 percent of the viscosities.

An equilibrium line (1:1 ratio) was added in each plot to present the ideal prediction of the viscosity. The actual predictions locate around this standard line, and the offsets are randomly distributed. No consistently high or low prediction of the viscosity was observed, indicating that the finalized GHS model generally captured age-hardening without missing important correlation factors.

a: PG 64-16_1

b: PG 70-10_2

c: PG 58-28_3

126
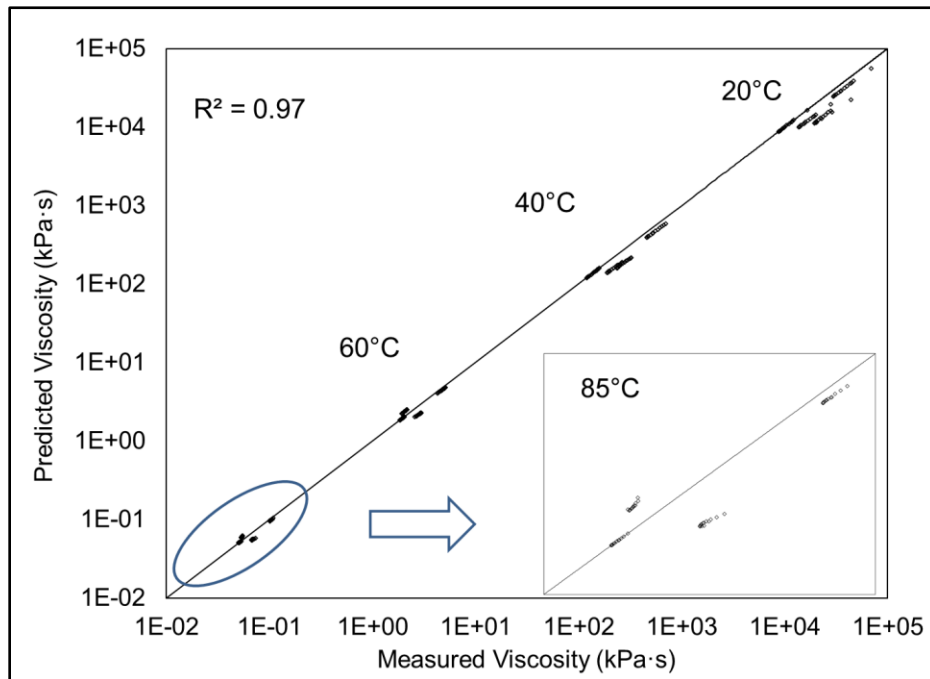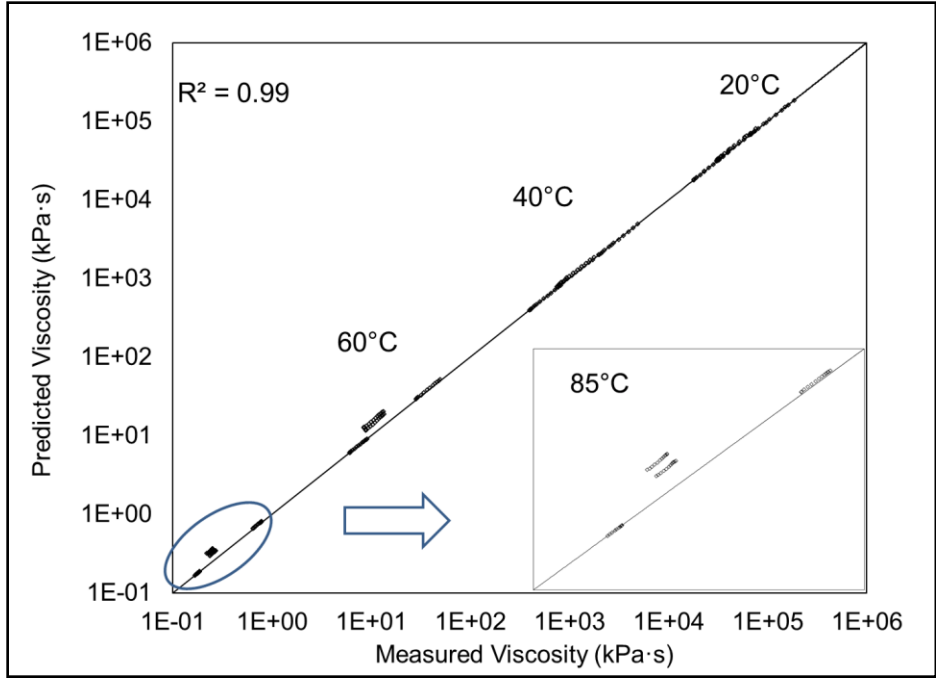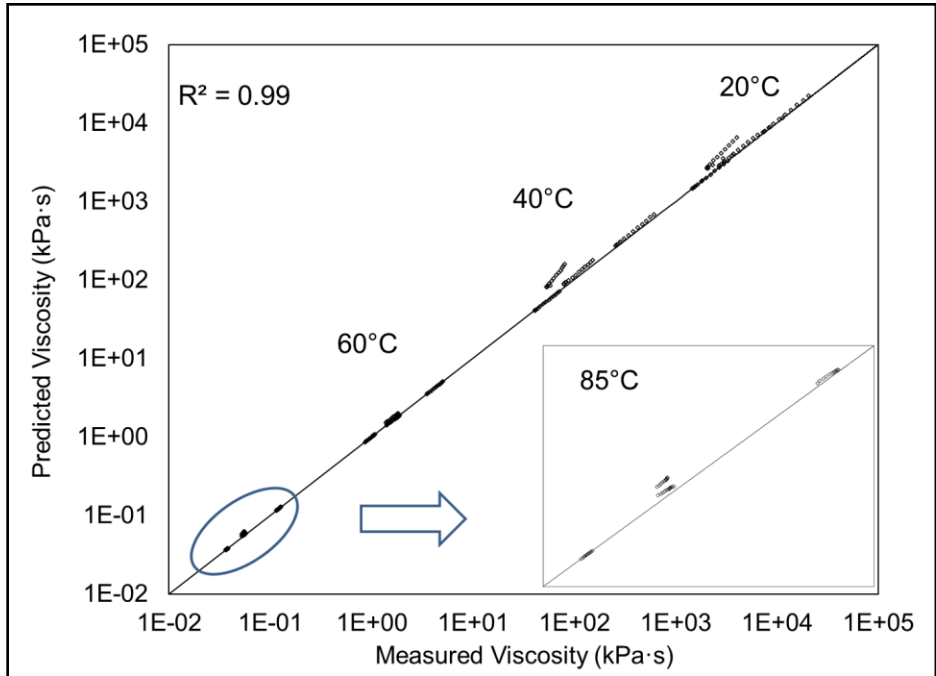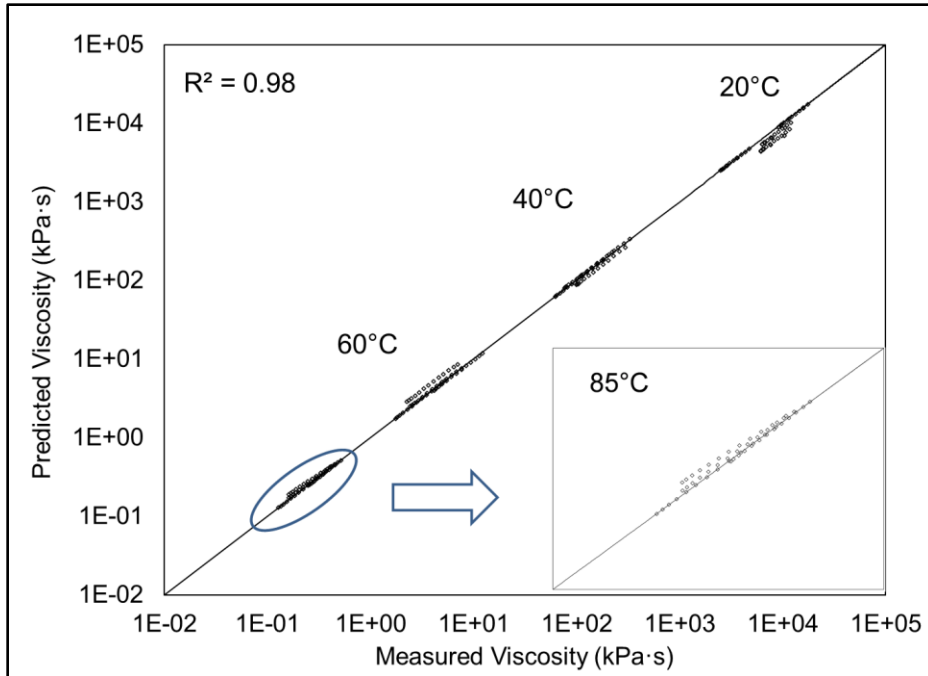
d: PG 64-28PM_1
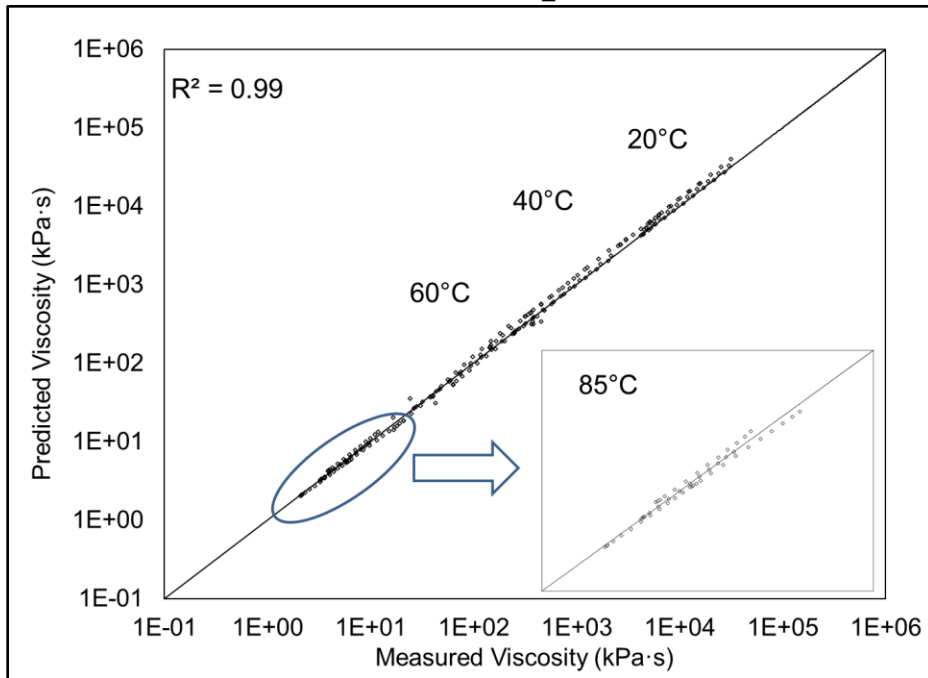
e: PG 76-22PM_3

Figure 4.20: Comparison between the GHS modeled viscosity to the measured viscosity at tested conditions.

At 85°C, binder viscosities were relatively low. Soft binders had phase angles very close to 90°, indicating that they might reach a purely viscous state that tends to flow. This test issue caused the

relatively low prediction accuracy at this state. However, the prediction accuracy was generally high for these binders ($R^2 > 0.95$) at 20°C, 40°C, 60°C, and 85°C.

Comparing the PG 64-16_1 binder to the PG 64-28PM_1 binder revealed that the SBS-modified binder had a lower viscosity than the unmodified binder after PAV-aging. The viscosity difference between the PG 58-28_3 and PG 76-22PM_3 binders was small after PAV-aging. These comparisons of binders from the same refinery indicated that SBS-modified binders experienced less age-hardening during PAV-aging. Section 4.3.1 concludes that the increase in the CA indices of SBS-modified binders was not significantly different from unmodified binders sourced from the same refinery. The low viscosity of the SBS-modified binder indicated that the SBS polymer reduced the age-hardening susceptibility according to the definition of the GHS principle.

Figure 4.20 also shows that viscosities for unmodified binders were discrete from each other at different test temperatures. The maximum and minimum viscosities of SBS-modified binders were within the viscosity range of unmodified binders. This observation indicated that SBS-modified binders had a relatively low temperature susceptibility after PAV-aging *(149)*. These binders can better withstand temperature fluctuations and better resist thermal cracking than unmodified binders.

In summary, the finalized GHS model was validated for PAV-aged unmodified and SBS-modified binders in this section. The validation was binding at temperatures between 20°C and 85°C with loading frequencies between 0.0159 Hz and 15.9 Hz (0.1 radians/second and 100 radians/second).

4.6.2 *Utilization of the GHS Model for the Reclaimed Asphalt Pavement Binders*

This section presents the application of the GHS model on reclaimed asphalt pavement (RAP) binders. RAP is the aged HMA material milled from the existing pavement. As discussed at the

beginning of Section 1.1, aggregates can be reused in paving activities (i.e., new HMA production, pavement rehabilitation) to reduce the dumping of waste materials and consumption of virgin aggregates *(127)*. Using RAP materials in new asphalt mixes has been promoted in recent years. In 2013, Caltrans posted a construction procedure directive that suggested an increase in RAP utilization in new asphalt mixes from 15 percent to 25 percent *(150)*.

A primary concern regarding the use of RAP material is its highly aged binder *(126,151,152)*. Rejuvenators may, therefore, be used to partially recover aged binders to a less aged state in applications where RAP is highly aged and its usage is high in the asphalt mix (i.e., 50 percent by weight of the aggregate) *(153,154)*. Rejuvenators generally introduce extra light oily components that restore the proportion of these components (maltenes) and heavier aging products (asphaltene) *(148,155)*. Consequently, oxidative aging appears to be reversed. The binder stiffness decrease is credited to the restoring of maltene and asphaltene, which is one of the widely accepted explanations of rejuvenation.

Given that the GHS model correlates the CA index and viscosity changes, it is potentially appropriate for assessing the effectiveness of the rejuvenation of aged RAP binders. This application requires validation of the linearity assumption that the CA index and $\ln(\eta)$ is still linearly correlated in the intensely aged RAP binders.

The following tests were conducted to calibrate the GHS model for the rejuvenation of RAP binders. One RAP material was sampled from the Sacramento region, where the average summer (June, July, and August) temperature is around 32°C (according to the U.S. climate database). The aged binder was extracted from RAP materials following AASHTO T 164 *(156)*.

Two types of rejuvenators (bio-based rejuvenator and petroleum-based rejuvenator) were separately added to this RAP binder at a ten percent content by weight of the binder. Table 4.6 presents the FTIR analysis results.

Table 4.6 shows that both rejuvenators contained fewer carbonyl and sulfoxide components than the RAP binder. The petroleum-based rejuvenator had a negative CA index. Its FTIR spectrum showed a concave curve at the carbonyl peak that led to this negative integration, indicating that no carbonyl component existed in the petroleum-based rejuvenator.

Table 4.6: FTIR Analysis of the Rejuvenators

Binder ID	Rejuvenator Type	CA Index	SUL Index
RAP	-	3.340	5.120
REJ_1	Bio-Based	1.927	2.009
REJ_2	Petroleum-Based	-10.262	4.343

A rotational mixer was used to thoroughly blend the rejuvenators with the RAP binder at 163°C and 1,200 revolutions per minute. No visible separation was observed between the rejuvenator and the binder after 20 minutes of blending.

After blending, two aging protocols were conducted on these three binders: RTFO-aging at 163°C for 85 minutes, followed by a PAV-aging at 10°C for 20 hours. The rheological properties of these aged residues were measured according to AASHTO M 320 to obtain parameters for backcalculating the viscosity *(30,74)*. Table 4.7 summarizes the test results. The high PG of the RAP binder was 94, which is lower than the normal PG of RAP binders collected from the central valley in California. The typical high PG of the central valley RAP binder could be over 100 degrees *(157)*.

Table 4.7: Summary of RAP Test Results

Binder ID	Rejuvenator Type	CA Index		SUL Index		Binder PG
		RTFO	PAV	RTFO	PAV	
RAP	-	3.555	4.151	5.347	4.006	94-0
RAP+REJ_1	Bio-Based	3.420	3.959	5.256	4.529	82-6
RAP+REJ_2	Petroleum-Based	1.523	1.738	4.952	4.900	70-16

In this study, samples were randomly collected from rejuvenated RAP binders. The FTIR results showed that the standard deviation of the chemical components was not larger than that of the unrejuvenated RAP binder, indicating that the rejuvenator was well blended with the RAP binder.

Table 4.7 shows that the petroleum-based rejuvenator was more effective than the bio-based rejuvenator. The former better restored the RAP binder properties and showed a larger PG drop than the one containing the bio-based rejuvenator.

The CA and SUL indices reduced after RTFO-aging for the rejuvenated binders, indicating that adding rejuvenators diluted the aging components in the RAP binder. The CA indices increased after PAV-aging, while the SUL indices did not. The continuous accumulation of CA indices indicated that the carbonyl component was more stable after more severe aging. The RAP binders with rejuvenators had lower CA indices than the unrejuvenated RAP binder after PAV-aging, which was attributed to the addition of rejuvenators.

Adding rejuvenators to the RAP binder reduced the sulfoxide components after RTFO-aging, mostly owing to the dilution effect of the rejuvenators. However, the results were inconclusive after PAV-aging. The unrejuvenated RAP binder had a notable reduction in the sulfoxide component, and the bio-based one experienced a lower decrease. In contrast, the petroleum-based one had no significant change in the sulfoxide component.

The sulfoxide component is not a stable aging product, and it is mostly dissolved at severe aging conditions (high temperature and long durations) *(103,104)*. The RAP binder has already been long-term aged in the road. After PAV-aging, the RAP binders started to show fewer sulfoxide components than it was in RTFO-aged condition, probably because the PAV-aging was more intense than the sulfoxide components in RAP binders were capable of withstanding. The petroleum-based rejuvenator better recovered the RAP binder to a less aged state. Therefore, the change in sulfoxide components after PAV-aging compared to after RTFO-aging was minimal. According to the observations of the CA and SUL indices for these binders, the CA index should be selected as the indicator for tracking the rejuvenation.

The frequency sweep test was used to measure the rheological properties of the RAP and rejuvenated RAP binders. The tests were run at 76°C and 88°C for RTFO-aged binders with the PP-25 geometry, and 20°C, 30°C, and 40°C for PAV-aged binders using the PP-8 geometry. These temperatures were chosen to be close to the performance grading temperatures. The angular frequency was from 15.9 Hz to 0.0159 Hz (100 radians/second to 0.1 radians/second). The strains were 1 percent for the PP-25 test and 0.1 percent for the PP-8 test.

The GHS model was developed by plotting $\ln(\eta)$ of these three binders on the y-axis and CA indices on the x-axis. Figure 4.21 shows an example of the GHS model at 20°C and 10 Hz (64 radians/second). The correlation of determination (R^2) for this case was 0.95, indicating that the GHS model was suitable to describe the rejuvenation at this combination of temperature and frequency.
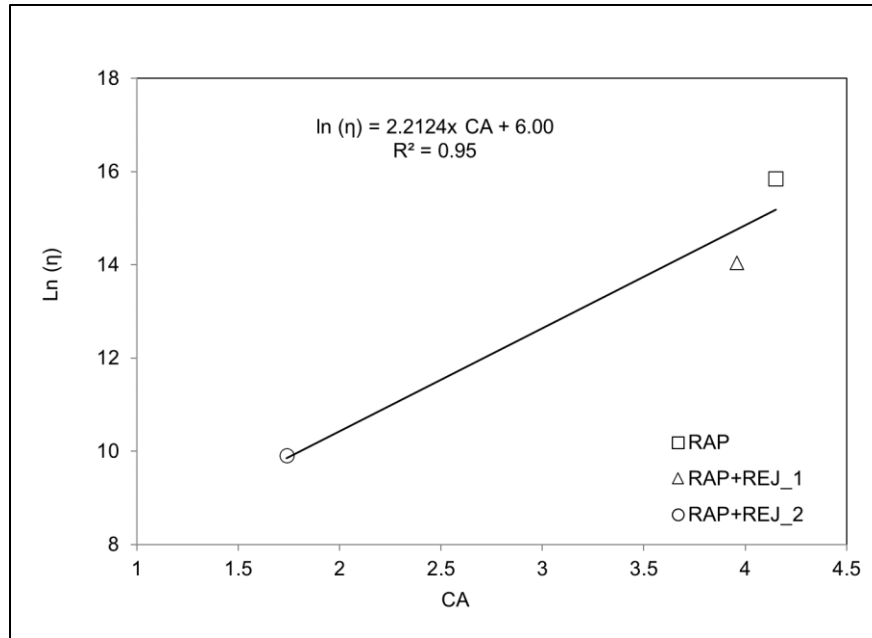
Figure 4.21: Example of determining GHS model for RAP binders.

The R^2 values at all tested temperatures and angular frequencies were calculated and plotted in Figure 4.22. The R^2 values were almost the same at the same test temperature. A difference in R^2 values between high temperatures and low temperatures was observed, mostly attributed to the difference in testing geometries.

Figure 4.22 shows that R^2 values were higher than 0.85 for all cases, indicating that the linearity assumption between the $\ln(\eta)$ and the CA index was valid for RAP binders and rejuvenated RAP binders after RTFO- and PAV-aging. Therefore, the GHS model was capable of tracking rejuvenation.
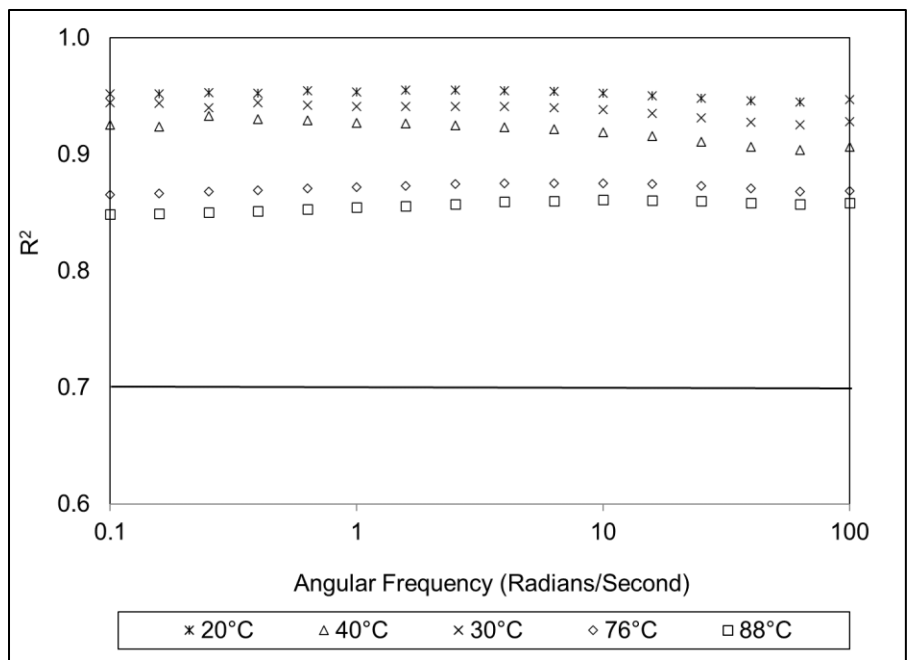
Figure 4.22: Linearity between ln(η) and CA index for RAP binders.

4.7   Summary and Conclusions

This chapter discussed refinements to the dual-rate aging model, with a focus on the investigation of age-hardening effects during long-term aging. Field-and laboratory-aging protocols were conducted to investigate the aging of unmodified, SBS-modified, and AR binders. Field-aging in a hot California climate condition was simulated by thinly spreading binders on glass plates and placing them on an unshaded rack outdoors with the purpose of accelerating the field-aging. Separate accelerated aging was achieved by running a PAV-aging. Based on laboratory test results, the following conclusions were drawn:

1. Question: How do binder components (i.e., carbonyl and sulfoxide components) change during oxidative aging?

   The carbonyl, ether and ester, and sulfoxide components were observed to change after aging. However, only the carbonyl component had a consistently increasing trend throughout the field-aging protocol as well as the PAV-aging protocol. The ether and ester components appeared to not change in the field-aging protocol but increased in the PAV-aging protocol. The sulfoxide component might not continuously increase in the intense PAV-aging protocol (i.e., 60 hours PAV-aging at 100ºC). Therefore, the carbonyl area (CA) index was selected as the most appropriate indicator for tracking oxidative aging in this study.

2. Question: How do binder dynamic moduli change after oxidative aging?

   The dynamic modulus master curves constructed for aged binders showed that oxidative aging stiffened the binder. This stiffening increased when the loading frequency decreased, which corresponds to a high temperature according to the time-temperature superposition principle.

The SBS-modified binders and AR binders experienced less age-hardening than the unmodified binders after the accelerated field and laboratory aging protocols.

3. Question: How can the age-hardening model (HS model) proposed by the Glover team be modified to accommodate the prediction of viscosities beyond the low shear viscosity region?

A linear correlation between $\ln(\eta)$ and CA index was observed for the unmodified and SBS-modified binders. This linearity held in a wide range of loading conditions (between 20°C and 85°C, and between 0.0159 Hz and 15.9 Hz [0.1 radians/second and 100 radians/second]), not just those typically used to represent the low shear condition (i.e., 60°C and 1.59E-05 Hz [0.0001 radians/second]) in the HS model. Accordingly, the generic hardening susceptibility (GHS) model was proposed to define the ratio between the logarithmic viscosity growth, and the carbonyl area index increase in the long-term aging phase.

4. Question: How well does the modified age-hardening model predict the properties of the different asphalt binders considered in this study?

The GHS model was developed to correlate the $\ln(\eta)$ and the CA index in the long-term aging phase (GHS = $(\ln \eta)$/CA). This GHS model was calibrated and validated using unmodified and SBS-modified binders from different refineries. It was also used to track the rejuvenation of RAP binders. The coefficients of determination when using the GHS model to predict the viscosities of unmodified, SBS-modified, and RAP binders were over 0.95 for temperatures between 20°C and 85°C and loading frequencies between 0.0159 Hz and 15.9 Hz (0.1 radians/second and 100 radians/second).

The GHS model developed in this chapter provides a tool to evaluate the age-hardening of long-term aged binders. Chapter 5 further validates this finding with rubber-modified binders. Chapter 6 investigates the application of the GHS model in aged asphalt mixes.

5 APPLICATION OF AGE-HARDENING MODEL ON RUBBER-MODIFIED BINDERS

5.1 Introduction

This chapter investigates the aging mechanism of asphalt binders containing crumb rubber modifiers. The following questions were addressed:

- What is an appropriate methodology for measuring the rheological properties (i.e., complex modulus, phase angle) of rubber-modified binders, especially for those containing large incompletely digested rubber particles (up to 2.36 mm [passing the #8 sieve])?

- How do aging products (i.e., carbonyl and sulfoxide components) accumulate in rubber-modified binders during oxidative aging? What is the crumb rubber modifier effect on oxidative aging of the binder?

- How can the age-hardening of rubber-modified binders be predicted using the GHS model?

The steps to accomplish the investigation in this chapter were:

1. Modification of the current laboratory-aging protocol to simulate field-aging during RHMA mix production.
2. Validation and refinement of the modified Superpave PG system.
3. Measurement of chemical component changes in rubber-modified binders.
4. Calibration of the GHS model using rubber-modified binders.

5.2 Refinement of the Modification of Performance-Grading Tests for Asphalt Rubber Binders

5.2.1 Modification of Accelerated Laboratory Aging Test

Baumgardner et al. *(75)* and Hung et al. *(76)* have modified the Superpave PG system for testing rubber-modified binders. This chapter further validated this grading system and refined part of the test methodology. Issues of laboratory-aging rubber-modified binders were identified in previous research conducted by the UCPRC *(70)*. The standard RTFO-aging is carried out at 163°C, the average temperature at which conventional HMA mixes are produced in asphalt plants. However, RHMA is typically produced at around 190°C and higher *(2)*. The operating temperature changes the swelling and degrading of the rubber significantly *(38,65)*. Consequently, the temperature used in the standard RTFO-aging is not representative of the short-term aging conditions during RHMA production.

Problems of coating in the RTFO bottle and binder leakage at the lower temperatures were also observed during the RTFO-aging of rubber-modified binders following the standard procedure. These observations inspired the review and modification of the RTFO-aging. In 2016, Jones et al. *(69,70)* proposed two modifications to the RTFO-aging to accommodate rubber-modified rubbers:

- An increase in sample size from 35 g to 45 g to better reflect the actual asphalt component. Asphalt rubber binder typically contains 18 to 22 percent rubber by weight of the binder in California *(2)*. Therefore, a standard 35 g RTFO specimen only contains 22 to 29 g of base asphalt binder. Increasing the specimen size to 45 g allows an equivalent of 35 g of base asphalt binders to be aged.

139

- The test temperature was increased from 163°C to 190°C in line with typical RHMA field-production temperatures. It was anticipated that the coating of the RTFO bottles would improve because of the larger sample size and higher testing temperature.

This modified RTFO procedure was further validated in this phase of the study. Figure 5.1 shows a comparison of the binder coating between the standard RTFO-aging and the modified one. The binder coverage in the bottles on the left is poor compared to the bottles on the right. This observation indicated that increasing the test temperature was appropriate to better coat the RTFO bottle. The binder film thickness could not be directly measured through the narrow opening. However, increasing the sample size was considered logical to provide sufficient base asphalt binder to achieve the specified binder film thickness.

| 35 g at 163°C | 35 g at 190°C |
| 45 g at 163°C | 45 g at 190°C |
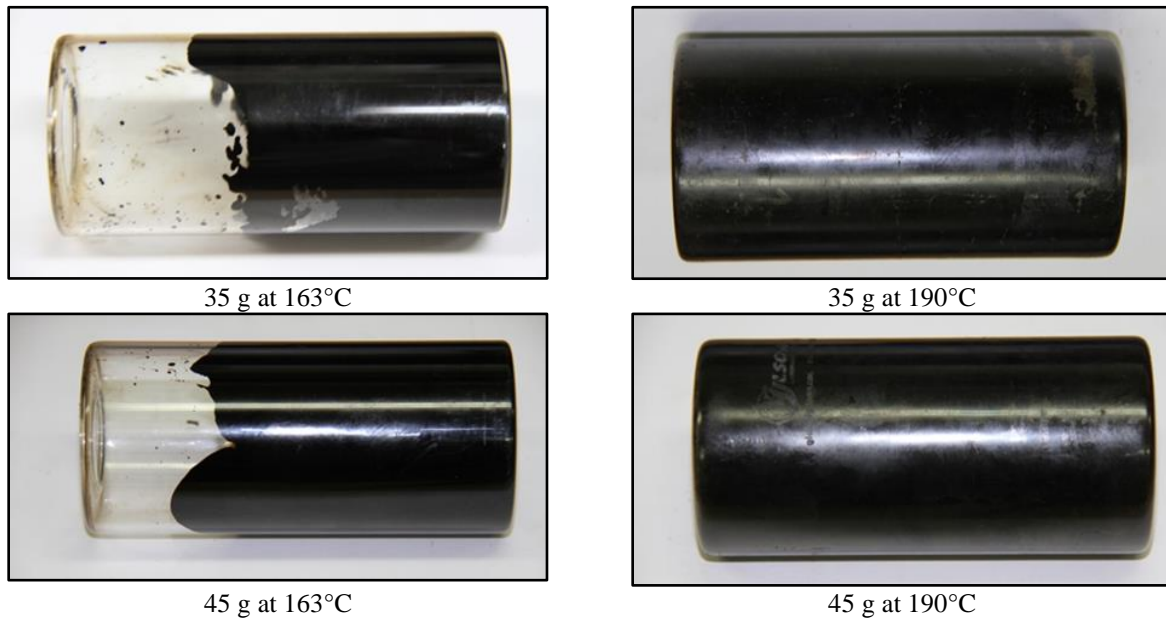
Figure 5.1: Comparison of bottle coating between standard and modified RTFO-aging.

The PAV specimen sizes were also adjusted by the rubber content. These increased specimen sizes were intended to provide an equivalent amount of base asphalt binder in each PAV pan *(97,158).*

5.2.2   Refinement of the Modification of the Performance Grading Test

Rubber-modified binders containing rubber particle sizes larger than 250 microns cannot be measured or performance-graded with sufficient accuracy using the parallel plate geometry specified in the current Superpave performance grading system *(30,74)*. The results are potentially dominated by the individual rubber particles rather than the modified binder. Houston et al. *(159)* proposed to increase the gap in the parallel plate geometry to 3-mm to alleviate the particle issue. However, the following factors would still likely influence the test results:

- Questionable rheological measurements using the 3-mm or smaller gap considering that the gap size should be at least four times the maximum particle size, according to AASHTO T 315 *(30)*. A 3-mm gap is only slightly larger than the maximum rubber particle size of 2.36 mm used in AR binders. In parallel plate geometry testing, the moduli are proportional to the sample radius to the power of four. A two percent error in radius implies a 16 percent error in moduli.
- Poor trimming due to the increased gap size and presence of large rubber particles causes the irregular shape of the specimen.
- Increased gap size and edge-effect cause unrepresentative measurements.

Researchers *(75,76)* have been studying alternative geometries to obtain a realistic measurement of rubber-modified binders. The concentric cylinder (CC) or "cup-and-bob" geometry appears to be an appropriate substitution for the parallel plate geometry. Baumgardner and D'Angelo *(75)* used the concentric cylinder geometry to test rubber-modified binders with rubber particles up to 840 microns at 64°C, 70°C, and 76°C. They concluded that this geometry was a suitable alternative to the parallel plate geometry. Hung et al. *(76)* used the concentric cylinder geometry to test

unmodified, SBS-modified, and terminal-blended binders (rubber particles smaller than 250 microns) at 58°C and 64°C. The results further confirmed that the concentric cylinder geometry could provide consistent measurements *(76)*.

A statistical analysis of the concentric cylinder geometry test at high temperatures (≥58°C) was conducted in this section. The application of concentric cylinder geometry at intermediate temperatures (around 25°C) was also investigated. A modified test method for grading rubber-modified binders at intermediate temperatures was therefore proposed.

The concentric cylinder geometry used in this study includes a disposable cylinder 56-mm high × 29 mm in diameter, with different sizes of spindles. The combination of the cylinder and various spindles provides different gaps to accommodate the tests for rubber-modified binders at different temperatures. Figure 5.2a shows a sketch of the concentric cylinder geometry. Figure 5.2b shows the spindle (bob) in two sizes: CC-17 (diameter of the measurement region of the spindle is 17 mm) and CC-10 (diameter of the measurement region of the spindle is 10 mm). Figure 5.2c shows the plan view and vertical view of the cylinder and the spindle. The binder specimen is poured into the cylinder (cup) to a certain height to ensure the specimen size. This height is marked before pouring using the size marker shown in Figure 5.2d.
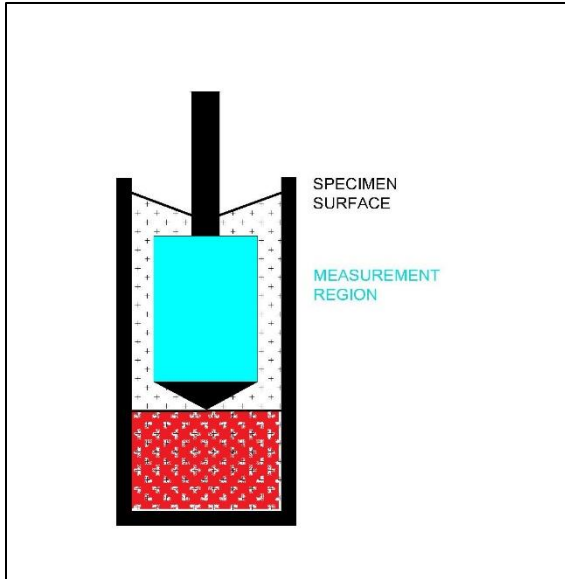
a: Sketch of CC geometry

b: Spindle (bob)

c: Cylinder (cup)

d: Specimen size marker

Figure 5.2: Package for the concentric cylinder geometry.

The concentric cylinder geometry measures the rheological properties of the specimen located within the measuring region, as shown in Figure 5.2a. The space between the cup wall and the spindle defines the gap size. The specimen is required to overflow the spindle to ensure uniformity in the measurement region. The gap size should be large enough to provide a representative element to satisfy the testing, as recommended by the RVE theory *(72)*. However, a large gap

results in shear stress and shear rate difference between the cylinder wall and the spindle. This inconsistent shear causes an unsteady flow and non-homogeneous deformation of the specimen. This non-homogeneity may lead to inaccurate determinations of the viscoelastic behavior *(160)*. Therefore, calibration with a certified reference fluid was used to determine an appropriate gap between the cylinder and the spindle to obtain the correct measurement.

After a series of tests with the reference fluid, the gap used for high temperatures (≥58°C) was set to 6 mm using a 17 mm bob (CC-17). The gap used for intermediate temperatures (16°C to 50°C) was set to 9.5 mm using a 10 mm bob (CC-10). These gaps allow a representative specimen size that alleviates volumetric issues in testing rubber-modified binders.

Another issue of using the concentric cylinder geometry is that the liquid binder shrinks as the temperature drops to low temperatures (i.e., 4°C). The shrinkage leads to the non-homogeneous deformation of the binder surface. After several rounds of calibration, the concentric cylinder test was limited to 16°C and higher to avoid extended shrinkage.

The specimen weight was determined by a trial-and-error method. The specimen should always cover the measurement region (blue section drawn in Figure 5.2a). This requirement limits binder shrinkage from affecting the measurement. Not submerging the spindle correctly causes a relatively lower measurement than the actual value, while submerging the spindle deeper than the recommended limit may lead to an overrated rheological value.

The preliminary setting parameters in this study are summarized in Table 5.1. It should be noted that the binder between the bottom of the spindle and the bottom of the cylinder (area shown in red in Figure 5.2a) does not influence the test result as it is outside the measurement region.

Adjusting the spindle to be deep in the cup will reduce the amount of binder needed for the test.

This adjustment function equates to the trimming function used in the parallel plate geometry.

Table 5.1: Summary of the Experimental Settings for the Concentric Cylinder Test

Spindle	Gap Size (mm)	DSR position (mm)	Specimen Height (mm)	Measurement Region Height (mm)	Test Temperature (°C)
CC-17	6.0	0.0	34.0	25.0	> 58
CC-10	9.5	9.5	37.5	15.0	16 to 50

The shear stress (τ) and shear strain (γ) for the concentric cylinder geometry can be calculated using Equations 5.1 and 5.2 *(76)*.

$$\tau = \frac{T}{2\pi h R_s^2}$$ 5.1

$$\gamma = \frac{\omega R_b}{R_c - R_s}$$ 5.2

Where:
T = torque, in mN·mm.
h = specimen thickness or the gap, in mm.
R_s and R_c = radii of the spindle and the cylinder, in mm.
ω = angular rotation of the spindle, in radians/second.

No trimming is needed when using the concentric cylinder geometry. This avoids the trimming problems associated with testing stiff rubber-modified binders using the parallel plate geometry. However, the concentric cylinder geometry requires considerably more binder. This geometry also requires an extended conditioning period compared to the parallel plate geometry to achieve the equilibrium test temperature. A minimum of 15-minute conditioning is essential for the CC-17 geometry, and a minimum of 20-minute conditioning is necessary for the CC-10 geometry. The latter conditioning time is longer because the hot binder has to cool down to the intermediate testing temperature. Although the measurement time is the same for these two geometries, an

additional five to 10 minutes are needed for conditioning for the concentric cylinder geometry at each grading temperature.

Before testing rubber-modified binders containing large particles (>250 microns), binders with particles smaller than 250 microns were tested using both geometries (CC and PP) to validate the testing accuracy of using concentric cylinder geometry. Table 5.2 lists the unmodified (UM), SBS modified, and TR binders tested in this validation phase.

Table 5.2: Materials for the Validation of Modified PG Tests

Binder ID	PG	Modifier	Particle
UM-A	64-16	None	None
UM-B	64-16	None	None
UM-C	64-16	None	None
PM-A	64-28	SBS	None
PM-B	64-28	SBS	None
TR-A	64-28	CRM	Rubber ≤ 250 microns
TR-B	64-28	CRM	Rubber ≤ 250 microns

The PG tests for unaged and RTFO-aged binders were completed at 64°C and 1.59 Hz (10 radians/second). Figure 5.3 shows the test results. The G*/sin(δ) values were mostly the same for these two geometries. They were closely located along the equilibrium line (1:1 ratio line), and the data were randomly distributed. These observations indicate that both geometries could precisely capture the rheological properties of these binders.
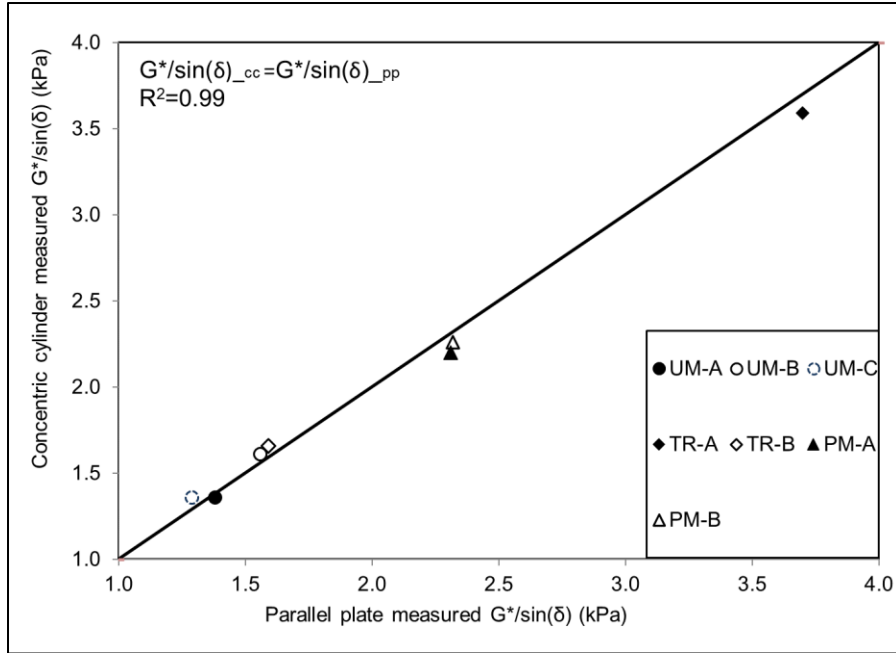
a: Unaged
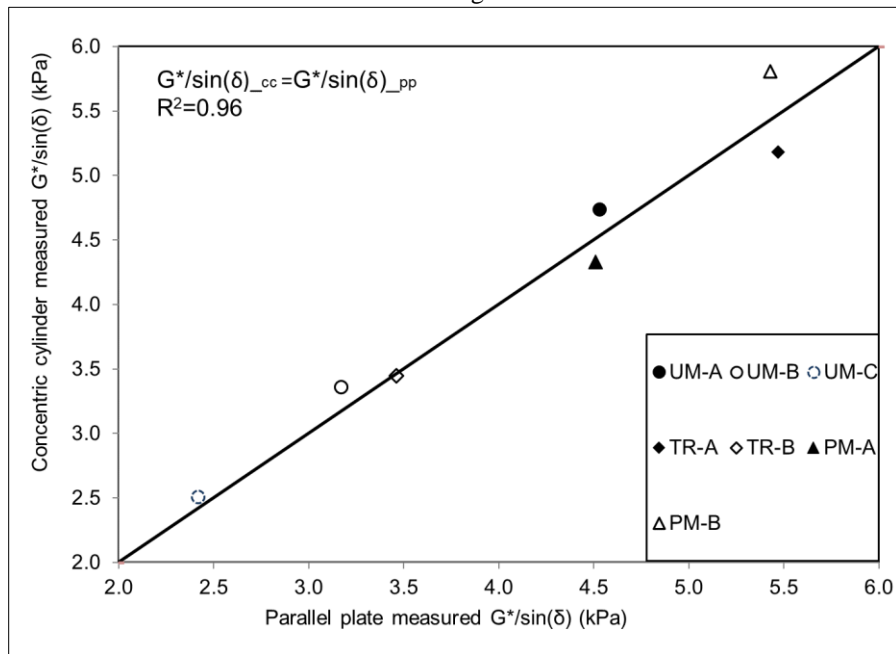
b: RTFO-aged

Figure 5.3: Comparison of G*/sin(δ) values determined using concentric cylinder and parallel plate geometries.

The PAV-aged binders were tested at 25°C and 1.59 Hz (10 radians/second). Figure 5.4 shows the test results. The G*×sin(δ) values were similar for both geometries. The UM binders were stiffer

than the modified binders after PAV-aging, indicating that UM binders were more susceptible to age-hardening, as discussed in Chapter 4.
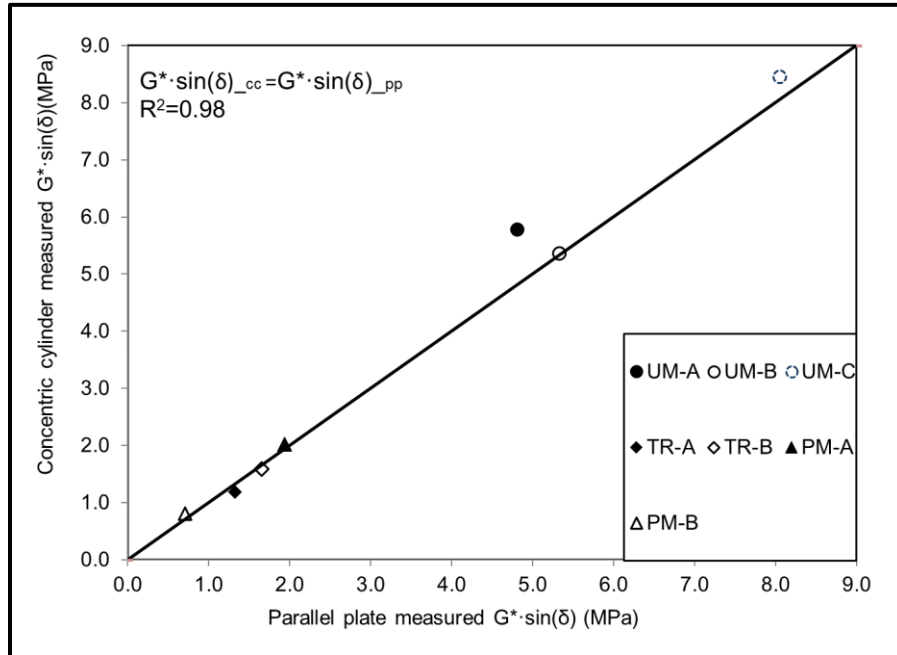
Figure 5.4: Comparison of G*×sin(δ) values determined with concentric cylinder and parallel plate geometries.

Table 5.3 summarizes the statistical analysis of the two geometries. According to AASHTO T 315, acceptable ranges for the single-operator precision are 6.4 percent for the unaged binders, 9.0 percent for RTFO-aged binders, and 13.8 percent for PAV-aged binders *(74)*. The test results confirmed that both geometries (CC and PP) were within the standard single-operator precision range.

The test results from the parallel plate geometry were more consistent than that of the concentric cylinder geometry for unaged and RTFO-aged binders. The maximum variances within the geometry were 1.9 percent for the parallel plate geometry and 4.0 percent for the concentric

cylinder geometry. The relatively large variance using the concentric cylinder geometry was likely attributed to the surface deformation of the specimen.

Table 5.3: Variance in Measurements between Concentric Cylinder Geometry and Parallel Plate Geometry

Binder ID	Unaged Binder			RTFO-Aged Binder			PAV-Aged Binder		
	Variance (%)		Difference	Variance (%)		Difference	Variance (%)		Difference
	PP	CC	(%)	PP	CC	(%)	PP	CC	(%)
UM-A	0.0	3.5	+0.6	1.5	0.1	-2.2	11.8	1.0	-9.3
UM-B	0.3	0.6	-1.6	0.0	0.3	-2.1	8.3	6.6	-0.3
UM-C	0.0	0.7	-2.6	1.9	3.3	-2.0	7.0	6.1	-2.4
TR-A	1.4	4.0	+1.5	0.2	0.9	+2.8	0.8	4.6	+5.5
TR-B	1.3	0.3	-2.0	1.2	0.6	+0.1	1.8	2.8	+2.0
PM-A	0.4	0.5	+2.4	0.3	2.5	+2.0	0.1	2.5	-2.1
PM-B	0.4	2.3	+1.3	0.2	1.5	-3.3	5.9	2.0	-6.5

Note: Sign "+" indicates the PP geometry results higher than CC geometry results; Sign "-" indicates the PP geometry results were lower than the CC geometry results.

The tested strains were set to 1 percent for the CC-17 test and 0.1 percent for the CC-10 test to limit surface deformation. These strain levels were lower than those used in the parallel plate geometry, which are 12 percent for PP-25 and 10 percent for PP-8 *(74)*. Equation 5.1 implies that thicker specimens require a high torque to gain the same shear stress as that for thinner specimens. Since the shear stress equals strain times shear modulus, the larger gap in the concentric cylinder test requires a higher torque to reach the pre-defined strain. Therefore, decreasing the test strain decreases the possibility of overloading the DSR motor. This lower strain should not introduce other measurement errors because it allows the test to be conducted in the linear-viscosity region of the binder *(74)*.

Table 5.3 shows that the results of the concentric cylinder geometry had better repeatability than the parallel plate geometry for PAV-aged binders. However, the variance within the concentric cylinder geometry results was still larger than the variance observed in the results of the unaged

149

and RTFO-aged binder tests owing to the increased binder shrinkage at the intermediate test temperatures (around 25°C).

The concentric cylinder geometry had fewer variances than the parallel plate geometry when testing PAV-aged binders. The variance of the parallel plate geometry substantially increased due to the stiff binder at intermediate temperatures being difficult to trim, which caused a repeatability issue. Table 5.3 shows the variance in results within each geometry and the difference in results between these two geometries.

The differences between parallel plate geometry and concentric cylinder geometry results were between -2.6 percent and +2.4 percent for unaged binders, between -3.3 percent and +2.8 percent for RTFO-aged binders, and between -9.3 percent and + 5.5 percent for PAV-aged binders. The offset between these two geometries was randomly distributed. No constant up or down offsets between these two geometries were observed. These observations indicated that the concentric cylinder geometry did not introduce any equipment error into these test results.

A single-factor ANOVA analysis was used to further compare the results from these two geometries. The independent variable was the geometry type, and dependent variables were $G^*/\sin(\delta)$ for unaged and RTFO-aged binders and $G^* \times \sin(\delta)$ for PAV-aged binders. The null hypothesis was no significant difference between the parallel plate geometry and the concentric cylinder geometry. A normalization within the geometry was made to eliminate the binder difference in dependent variables. The test results for the UM-A binders were selected as standard values, and results of other binders were normalized to the standard values within each geometry.

Table 5.4 summarizes the normalized test values and the ANOVA result. The ANOVA analysis results show that the null hypothesis should be rejected at a 95 percent confidence interval because the p-values are over five percent. Therefore, these two geometries were not statistically different.

<div align="center">Table 5.4: ANOVA Results for the Two Geometries</div>

Binder ID	Unaged Binder		RTFO-Aged Binder		PAV-Aged Binder	
	PP	CC	PP	CC	PP	CC
UM-A	1.00	1.00	1.00	1.00	1.00	1.00
UM-B	1.13	1.18	0.70	0.71	1.11	0.93
UM-C	0.93	1.00	0.53	0.53	1.68	1.46
TR-A	2.68	2.64	1.21	1.09	0.28	0.20
TR-B	1.15	1.22	0.76	0.73	0.34	0.27
PM-A	1.67	1.62	1.00	0.91	0.40	0.35
PM-B	1.68	1.66	1.20	1.23	0.15	0.14
ANOVA						
F critical	4.75		4.75		4.75	
p value >F	0.976		0.833		0.767	

Issues with performance grading of AR binders were also identified in the bending beam rheometer (BBR) test, specifically during the preparation of beams *(70,161)*. The standard mold has a very narrow opening following AASHTO T 313 *(162)*, which makes it difficult to pour a stiff, viscous binder containing incompletely digested rubber particles. The narrow opening results in incomplete filling of the mold, producing specimens that are often irregular in shape with random bubbles, as shown in Figure 5.5a. This problem prompted the review and refinement of the BBR specimen preparation. In 2016, Alavi et al. *(69,70)* proposed a modification to the BBR mold to provide a more uniform BBR specimen.

Figure 5.5 shows a graphic comparison of the standard and modified mold. This modified mold allows operators to pour and spread the binder in the width-dimension as opposed to the thickness-dimension. The resulting specimen dimensions do not change. Figure 5.5b shows that the modified mold provides a uniform beam without bubbles or gaps in the beam corners.
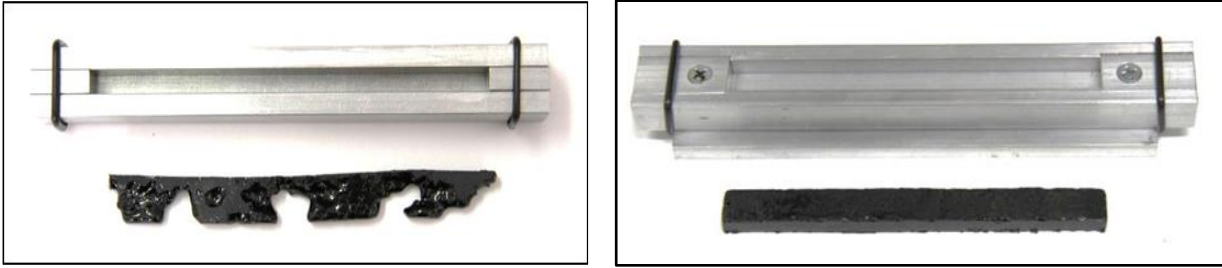
Figure 5.5: Conventional mold and beam (left) versus modified mold and beam (right).

Careful trimming with a sharp blade to slice across the edges of the mold is required to ensure the beam specimen retains the required dimensions. Any irregularity in the thickness significantly affects the test result because the stiffness modulus is a negative third-power of the beam thickness, as shown in Equation 5.3 *(162)*.

$$S(t) = \frac{PL^3}{4bh^3\delta(t)}$$

5.3

Where:
   $S(t)$ = time-dependent flexural creep stiffness, in MPa.
   P = constant load, in mN.
   L = span length, in mm.
   b = width of the beam, in mm.
   h = thickness of the beam, in mm.
   $\delta(t)$ = beam deflection at 60 seconds of testing, in mm.

This modified mold was found to be able to consistently produce acceptable beams. The UM, TR, and SBS binder specimens were fabricated using both the standard and modified mold for validation. The BBR tests were run at -6°C for UM binders, and -18°C for TR and SBS modified binders according to their tested PGs *(162)*. Figure 5.6 shows the measured creep stiffness and m-values of specimens produced with these two molds. These UM, TR, and SBS modified binders passed the stiffness and the m-value criteria at the required measuring temperatures.

The comparison of these two molds showed that there was no apparent difference between molds. The data were randomly distributed along with the equilibrium line (1:1 ratio line), and coefficients of determination were over 0.95. There was no constant up or down offset. These observations

indicated that the modified mold was capable of testing binders without introducing any equipment errors.
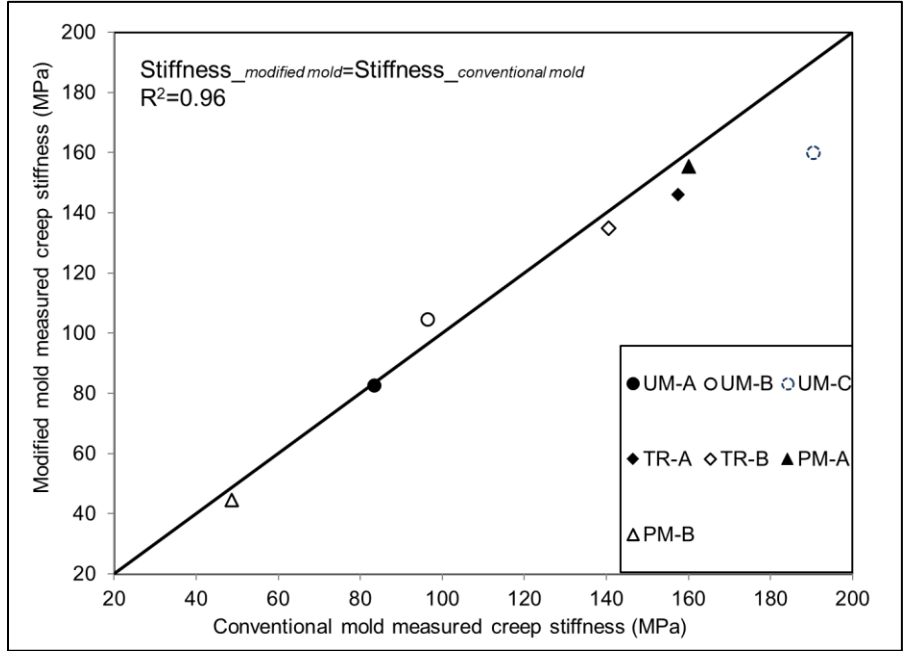
a: Creep stiffness
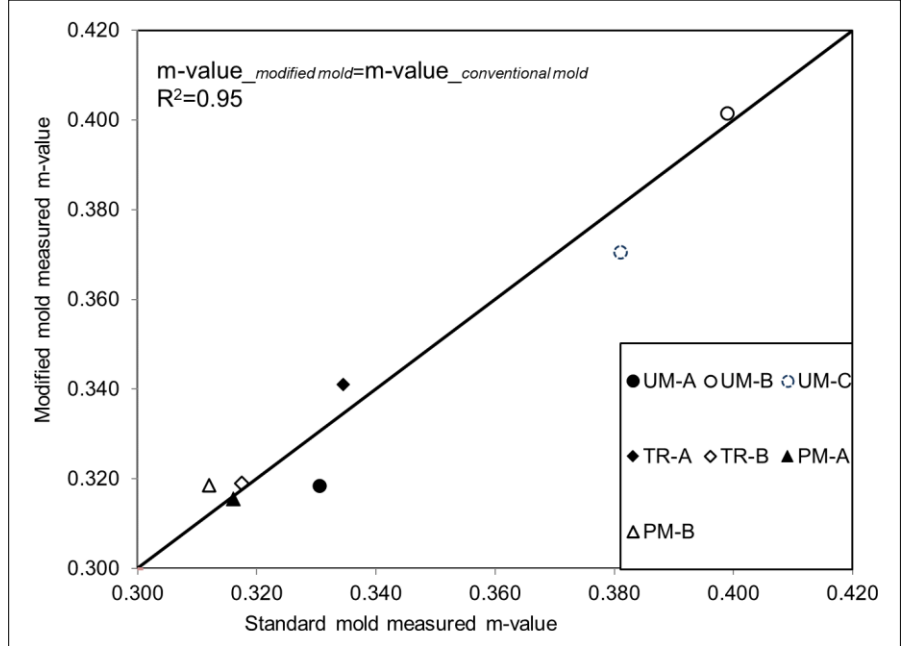
b: m-value

Figure 5.6: BBR test results at measured temperatures.

A single-factor ANOVA analysis was used to compare the variability of these two molds. The type of mold was selected as the independent variable, and rheology parameters (stiffness and m-value) were selected as dependent variables. The null hypothesis was that the two molds were significantly different.

A normalization was made to eliminate the binder type effect on dependent variables. The test results for UM-A binders were selected as the standard value, and results of other binders were normalized to this standard value for each mold type. Table 5.5 summarizes the ANOVA results. The results show that specimens prepared by these two molds were not statistically different at a 95 percent confidence interval using the p-value criteria of five percent. Consequently, the modified mold can be used for beam production of rubber-modified binders.

Table 5.5: ANOVA of Normalized BBR Data for Conventional and Modified Beam Molds

Binder ID	Normalized Stiffness		Normalized m-value	
	Conventional Mold	Modified Mold	Conventional Mold	Modified Mold
UM-A	1.000	1.000	1.000	1.000
UM-B	1.158	1.264	1.207	1.261
UM-C	2.286	1.935	1.153	1.163
TR-A	1.890	1.765	1.012	1.071
TR-B	1.686	1.632	0.961	1.002
PM-A	1.920	1.880	0.956	0.991
PM-B	0.584	0.540	0.944	1.000
ANOVA				
F	4.75		4.75	
p-value>F	0.814		0.529	

In this section, the modified performance grading method was validated. The comparison between the modified performance grading method and the standard one showed that these two methods provided a similar measurement accuracy for testing binders with particles smaller than 250 microns. The ANOVA analysis also showed that using the modified performance grading method did not introduce system errors or equipment errors into the measurement.

This modified performance grading method potentially solves the volumetric issue of testing rubber-modified binders containing large incompletely digested rubber particles (>250 microns). This modified performance-grading method was used to measure the rheological properties (i.e., complex modulus, phase angle) of rubber-modified binders containing incompletely digested rubber particles larger than 250 microns in this study.

5.3   Testing and Analysis of Oxidative Aging in Rubber-Modified Binders

5.3.1   Hypothesis of Rubber Dilution of Aging Products in Rubber-Modified Binders

According to the literature review in Section 2.1.2, rubber swelling is the main rubber-binder interaction in rubber and binder blending at temperatures lower than 220°C. The rubber particles absorb the lighter components from the binder and swell to a larger volume size.

The rubber-modified binders in the study were produced at 190°C, and rubber swelling was the main rubber-binder interaction at this temperature. The swelled rubber particles replace part of the base asphalt binder in a given volume of binder. In other words, rubber appears to dilute the base asphalt binder in the rubber-modified binder.

The rubber dilution effect hypothesis on the oxidative aging of the rubber-modified rubber is proposed to explain the slower aging in the rubber-modified binder compared with the base binder. This dilution hypothesis is based on two assumptions. First, the rubber itself ages differently to the base asphalt binder. Second, the rubber-binder interaction is mainly swelling such that the rubber replaces the base asphalt binder in a unit volume without any chemical interactions.

In this case, the aging products (i.e., carbonyl and sulfoxide components) in the rubber-modified binder can be diluted by the rubber, and the reduction of the aging product should be proportional

to the rubber content. The calculated component indices based on the volumetric correlation between the rubber and the base asphalt binder should be compared to the measured values to test this hypothesis. Equation 5.4 defines the calculated indices.

$$I_C = C_R \times I_R + C_O \times I_O + C_B \times I_B \qquad\qquad 5.4$$

Where:

I_C = calculated chemical index (i.e., CA or SUL) in the rubber-modified binder.
C_R = rubber content, in percent
I_R = measured chemical index in the rubber.
C_O = extender oil content, in percent
I_O = measured chemical index in the extender oil.
C_B = base asphalt binder content, which is (1-C_R-C_O), in percent.
I_B = measured chemical index in the base asphalt binder.

Negative component index values are considered to be zero in Equation 5.4. The integration method used in Equation 4.2 does not automatically reject the negative area index. The negative value indicates that no such component exists in the material, which should be zero in the calculation. Besides the dilution hypothesis, chemical interaction may also explain the aging in the rubber-modified binder. Three hypotheses proposed in this chapter are:

1. Dilution, which is implied if the measured aging products are close to calculated values using Equation 5.4.

2. Chemical interaction where the rubber acts as an antioxidant as discussed in one previous study *(4)*, which is implied if more aging product reductions than dilution alone can explain.

3. Other chemical interactions, which is implied if there are fewer aging product reductions than dilution alone can explain.

In this study, FTIR measured indices were compared to the calculated indices using Equation 5.4. Two criteria were selected to determine whether or not to accept the dilution hypothesis. First, the

calculated indices should be within one standard deviation of the measured indices. Second, the Pearson correlation between the calculated indices and the measured indices should be higher than the 0.7 threshold *(163)*, which is a rule of thumb for accepting "high positive correlation". If the FTIR data met these two criteria, then the dilution hypothesis could be preliminarily accepted. It should be noted that accepting the dilution hypothesis does not deny the possible chemical interactions between rubber and base binder, but the data would then suggest that the chemical interaction effect was not significant compared to the dilution effect posed by the dilution hypothesis. Suppose the FTIR data did not meet the two criteria for accepting the dilution hypothesis. In that case, chemical interaction should be considered the primary mechanism to explain the oxidative aging in the rubber-modified binder.

5.3.2   *Experimental Design for Evaluating the Oxidative Aging of Rubber-Modified Binders*

Twelve binders from four refineries were evaluated in the work discussed in this section. These binders were produced using the field-blending approach with different rubber contents and particle sizes. The blending temperature was 190°C. The ones containing five and ten percent rubber by weight of the binder fit the definition of PG+X materials *(17)*.

These binders can be divided into four groups based on the binder source and rubber type. Group A contains two devulcanized rubber binders and their base binder. A devulcanization process was used to reduce the rubber into fine particles smaller than 250 microns. Group B includes four rubber-modified binders and their base binder from the second producer. Their rubber particle sizes are smaller than 1.18 mm (passing the #16 sieve) or 2.36 mm (passing the #8 sieve), depending on the mix. Group C and Group D include two standard AR binders. They were field blended with 20 percent rubber by weight of the binder. AR binders in Group C and Group D

contained four percent extender oil by weight of the binder. The refineries added this extender oil to improve the rubber swelling. This is a standard practice in California *(25)*. Table 5.6 summarizes the binder information.

The purpose of this work was to evaluate the oxidative aging of various rubber-modified binders produced using different production approaches used in the industry. In this study, the producer conducted the rubber-binder blending process and delivered the rubber-modified binders to the UCPRC laboratory. The devulcanization effect could not be analyzed as the laboratory received no devulcanized rubber particles. Considering that Group A, Group B, Group C, and Group D binders used different rubber types and base binders, the rubber effect analysis was based on a group-by-group scenario.

Table 5.6: Summary of Materials in Experiment Design

Group	Binder ID[1]	CRM Dosage (%)	Maximum CRM Size (mm)	Extender Oil (%)	Specific Gravity	Binder PG
A	Base_A	0	N/A	None	1.035	64-22
	A_5_0.25	5	0.25		1.036	70-22
	A_10_0.25	10	0.25		1.037	70-22
B	Base_B	0	N/A	None	1.032	64-22
	B_5_1.18	5	1.18		1.034	70-22
	B_10_1.18	10	1.18		1.039	82-22
	B_5_2.36	5	2.36		1.043	70-22
	B_10_2.36	10	2.36		1.045	76-22
C	Base_C	0	N/A	None	1.035	64-16
	C_20_2.36	20	2.36	4	~1.070	88-16
D	Base_D	0	N/A	None	1.035	64-16
	D_20_2.36	20	2.36	4	~1.070	88-16

[1] Binder ID format: source-rubber-content in percent-maximum particle size in mm.

Table 5.6 includes the specific gravities of these binders. Since specific gravities of the base binders were approximately similar, the specific gravity changes after adding rubber were compared to the original binder base. Figure 5.7 shows the specific gravity change along with the rubber content and the rubber particle size. The results indicated that increasing the rubber content

would lead to a higher specific gravity. The rubber specific gravity is typically around 1.12 g/cm^3, which is denser than the base binder *(2)*. In one-unit volume, part of the binder was replaced by the heavier rubber particles. Naturally, delta specific gravity was positively correlated to the rubber content. The increase in specific gravity indicated that adding the crumb rubber diluted the base asphalt binder in rubber-modified binders.
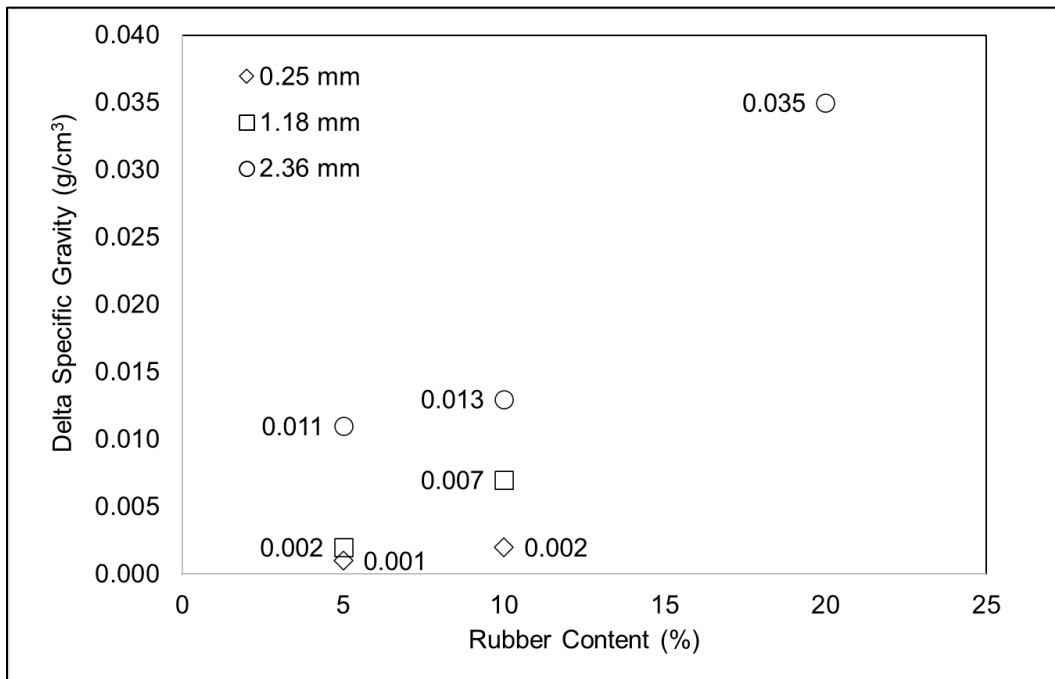
Figure 5.7: Changes in specific gravities after adding rubber particles.

The rubber-modified binders in Group A had similar particle size gradations as traditional terminal blended binders. These binders can be performance-graded using the current Superpave PG system. Therefore, the RTFO-aging for Group A binders was set at 163°C for 85 minutes following AASHTO T 240 *(98)*. The PAV-aging was done at 100°C and 2.1 MPa pressure for 20 hours following AASHTO R 28 *(97)*. An Anton Paar DSR machine was used to measure the rheological properties of the unaged binders and aged residues with a parallel plate geometry according to AASHTO T 315 and AASHTO T 320 *(30,74)*.

The rubber-modified binders in Group B, Group C, and Group D contained large incompletely digested rubber particles (>250 microns). One local manufacturer provided the crumb rubber modifier used in this study. Figure 5.8 shows the rubber gradation. The CRM_1.18 is the fine rubber used in Group B., and the CRM_2.36 is the coarse rubber used in Group B, Group C, and Group D.

Figure 5.8 shows that most rubber particles were between 0.25 mm and 1.00 mm. These large rubber particles can cause volumetric issues using the current Superpave PG system, as discussed in Section 2.1.6. The modified PG system discussed in Section 5.2 was used to evaluate these rubber-modified binders.
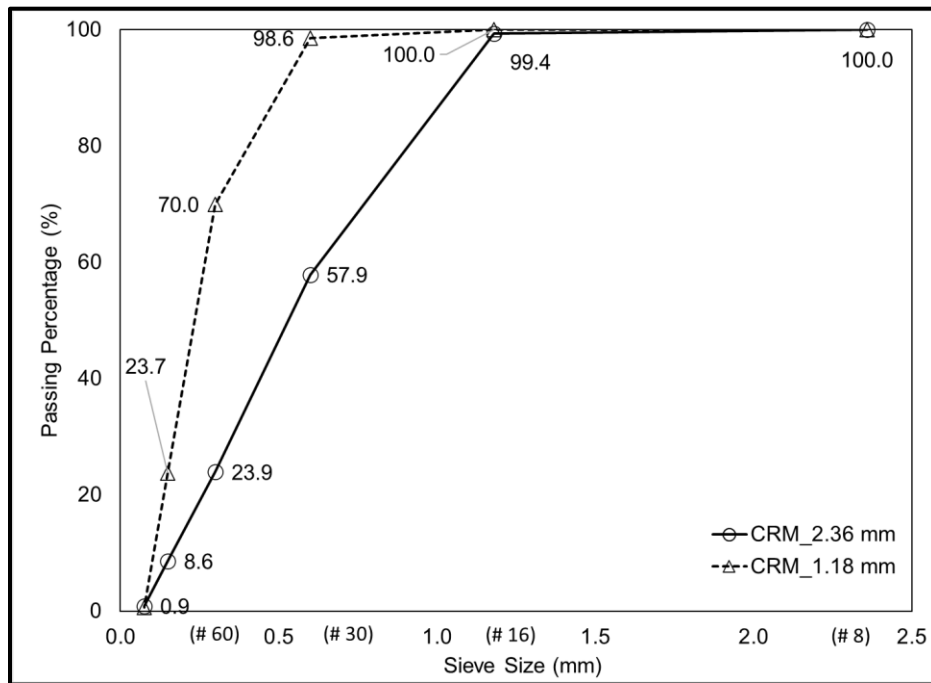
Figure 5.8: Sieve analysis of the rubber gradations.

The laboratory-aging protocols for aging the base binders and Group A binders followed the standard RTFO-aging (AASHTO T 240) *(98)* and PAV-aging specification (AASHTO R 28) *(97)*. The rubber-modified binders in Groups B, C, and D were aged using the modified RTFO and PAV

protocols discussed in Section 5.2.1. The specimen sizes in the RTFO bottles and PAV pans were adjusted by the rubber content to obtain the same amount of base asphalt binder aged in the standard aging protocol.

In this chapter, the RTFO specimen weights for rubber-modified binders in Group B were 37 g for binders containing five percent rubber and 39 g for the ones containing ten percent rubber. The RTFO specimen size in Groups C and D was 44 g, corresponding to the 20 percent rubber by weight of the binder in these two groups. The PAV specimen sizes for rubber-modified binders in Groups B, C, and D were also increased according to the rubber content. A 53 g specimen was used for the rubber-modified binder containing five percent rubber; a 56 g specimen was used for the ones containing ten percent rubber, and a 63 g specimen was used for the ones containing 20 percent rubber. Table 5.7 provides the setting of the test.

This setting was selected according to the rubber particle size in the rubber-modified binders. The inconsistency of the temperature used in RTFO-aging may influence the analysis after RTFO-aging. Additionally, the Base-B binder was also RTFO-aged at 190°C to evaluate the RTFO-aging temperature effect in the base binder.

After aging, carbonyl components, sulfoxide components, and butadiene components were measured using the FTIR. The corresponding area indices were calculated using the same methodology presented in Section 4.2.2.

The FTIR returns the average spectrum of 24 scans for each sample. A total of nine replicate samples were tested for each binder. These nine samples were randomly collected from the binder tin after heating the binder to the liquid condition and thoroughly stirring it. The binder sample was then transferred to the FTIR optics using the glass stick.

However, the optics diameter is only 2 mm, and it measures the chemical components of the sample within this 3.14 mm^2 ($1^2 \times \pi$) area of the optics. Considering the maximum rubber particle size can be as large as 2 mm, and the digested or incompletely digested rubber particles may not necessarily distribute uniformly in the FTIR sample, the measurement results could vary. The results discussed in the following sections include the average measurement and the standard deviation of the nine replicate measurements for each binder.

Table 5.7: Experiment Design for Evaluation of the Aging in Rubber-Modified Binders

Group	Binder ID[1]	CRM Dosage (%)	Maximum CRM Size(mm)	Extender Oil (%)	RTFO Temperature (°C)	PAV Temperature (°C)
A	Base_A	0	N/A	0	163	100
	A_5_0.25	5	0.25			
	A_10_0.25	10	0.25			
B	Base_B	0	N/A	0	163 (190)	
	B_5_1.18	5	1.18		190	
	B_10_1.18	10	1.18			
	B_5_2.36	5	2.36			
	B_10_2.36	10	2.36			
C	Base_C	0	N/A	0	163	
	C_20_2.36	20	2.36	4	190	
D	Base_D	0	N/A	0	163	
	D_20_2.36	20	2.36	4	190	
E	Base_E	0	N/A	0	163	
	Control_E	0	N/A			
	E_2.5	2.5	2.36		190	
	E_5	5	2.36			
	E_10	10	2.36	4		
	E_18	18	2.36			
	E_22	22	2.36			
	E_30	30	2.36			
	E_35	35	2.36			

[1] Binder ID format: source-rubber content in percent-maximum particle size in mm.

An additional group (Group E) of rubber-modified binders was prepared with seven different rubber amounts (2.5, 5, 10, 18, 22, 30, and 35 percent by weight of the binder) to test the rubber dilution hypothesis. The modified RTFO and PAV protocols discussed in Section 5.2.1 were applied to the rubber-modified binders in Group E. The specimen sizes in the RTFO bottles and

PAV pans were adjusted by the rubber content to obtain the same amount of base asphalt binder aged in the standard aging protocol.

These Group E binders were prepared in the laboratory using the Base_D binder and the coarse rubber (CRM_2.36) shown in Figure 5.8. Similar to the field-blending approach used in Group C and Group D, the four percent of extender oil by weight of the base binder was added during the blending process *(25)*. The extender oil amount was fixed for the rubber-modified binders in Group E; this was done to ensure the same amounts of chemical components were brought in by extender oil and keep this as a fixed value in the factorial level in the analysis of Group E. However, it is acknowledged that excess extender oil not consumed by the rubber and may have influenced the test results.

The blending process for Group E was conducted at 190˚C using a shear mixer in the laboratory. This is the same blending temperature used in other binder groups. The constant amount of extender oil and the required amount of rubber were added to a 300 ml base binder sample and then blended at 1,200 revolutions per minute for 45 minutes. The control binder in Group E was produced by blending the extender oil in the base binder at 190˚C and 1,200 revolutions per minute for 45 minutes. Fixing the extender oil content and the blending duration instead of making extender oil content proportional to the rubber content ensured the quantitative analysis of rubber dilution, with the assumption that no chemical interaction occurs between the extender oil, rubber, and binder.

It should be noted that the extender oil may influence the digestion of rubber. However, the rubber digestion could not be studied because of the nature of the FTIR measurement. The FTIR equipment measures the whole specimen that contacts the measurement unit (optics). In the

rubber-modified binder, the rubber components (digested or incompletely digested) absorb the same wavelengths of incident radiation. Azevedo et al. *(164)* found that the FTIR measured butadiene content was lower than the content reported by the rubber supplier. This finding implied that undigested rubber might not be counted in the FTIR measurement result. Therefore, the FTIR can quantitatively analyze the amount of digested or incompletely digested rubber in the binder but not the undigested rubber. In other words, it cannot determine the level of rubber digestion.

5.3.3 Oxidative Aging of Crumb Rubber Modifiers

The chemical components in the crumb rubber modifier before and after aging were evaluated. No RTFO-aging was conducted on the rubber particles due to safety concerns. The small rubber particles could be forced out of the RTFO bottle by the air that blows over the sample, resulting in a dust explosion risk.

The two crumb rubber modifiers (gradations are shown in Figure 5.8) were directly PAV-aged to evaluate the oxidative aging effect on the rubber particles before blending with asphalt binder. After PAV-aging at 100°C for 20 hours, chemical components were compared to those determined before aging. Table 5.8 lists the results.

The CA indices in the rubber were negative before and after aging. In the FTIR spectra, a concave curve over the carbonyl peak was observed. This concave curve led to a negative integration of the CA index, indicating no carbonyl component as defined by the 1680 cm^{-1} peak was in the crumb rubber modifiers.

Table 5.8 shows that the PAV-aging appeared to not age these rubber particles. The carbonyl and sulfoxide components did not increase after PAV-aging. This proved the first assumption of the rubber dilution hypothesis proposed in Section 5.3.1. Aging the rubber itself does not produce

carbonyl or sulfoxide components, which are the main aging products produced in asphalt binder aging. Adding the aging-resistant rubber into the asphalt binder is anticipated to effectively dilute the aging components generated in the base asphalt binder.

Table 5.8: Average Chemical Indices for the Rubber in Unaged and PAV-Aged Conditions

Maximum Rubber Size	Aging Condition	Average CA[1] Index	SD[2] of CA Index	Average SUL[3] Index	SD[2] of SUL[3] Index	Average Butadiene Index	SD[2] of Butadiene Index
2.36 mm	Unaged	-1.359	1.007	0.556	0.368	0.215	0.032
	RTFO[4]	0	-	0.530	-	0.236	-
	PAV	-1.569	1.026	0.503	0.371	0.256	0.042
1.18 mm	Unaged	-1.401	1.071	0.493	0.412	0.255	0.058
	RTFO[4]	0	-	0.468	-	0.249	-
	PAV	-1.477	1.019	0.443	0.415	0.243	0.045

[1] CA-Carbonyl. [2] SD-Standard Deviation. [3] SUL-Sulfoxide. [4] RTFO-Calculated as the average of those indices in unaged and PAV-aged rubber.

Table 5.8 shows that the butadiene area index before and after aging did not constantly increase or decrease for these two sizes of rubber. The measured butadiene area indices were only around 0.25, while the variations were around 0.05. The variations of the butadiene area index measured were 20 percent of the average value.

An ANOVA analysis was applied to these butadiene area indices, and the results showed that no significant difference was found before and after aging at the 95-confidence level (p-value =0.56 > 0.05). For unmodified binders containing no butadiene component before adding the rubber, the distinctive butadiene area index could be used to track the amount of digested and incompletely digested rubber in the binder, as previous studies have suggested *(136,137)*.

The indices (CA, SUL, and butadiene) in the rubber in RTFO-aged conditions were required in the calculation to inspect the rubber dilution hypotheses proposed in Section 5.3.1 for rubber-modified binders in RTFO-aged condition. Since the actual values could not be obtained in the

laboratory, the indices (CA, SUL, and butadiene) in the rubber in RTFO-aged condition were assumed to be the averages of those in the unaged and PAV-aged rubber. Table 5.8 shows that rubber did not contain any carbonyl components, and the CA index values were considered zero in the rubber in unaged, RTFO-aged, and PAV-aged conditions. For SUL and butadiene area indices in rubber, the values in RTFO-aged conditions were calculated using Equation 5.5. Table 5.8 summarizes calculated indices in the rubber for the RTFO-aged conditions.

$$I_{RTFO} = \frac{(I_{Unaged} + I_{PAV})}{2}$$ 5.5

Where:
I_{RTFO} = component index in the rubber in RTFO-aged condition.
I_{Unaged} = component index in the rubber in unaged condition.
I_{PAV} = component index in the rubber in PAV-aged condition.

5.3.4 Accumulation of Carbonyl Components in Rubber-Modified Binders

Figure 5.9 shows the CA indices of tested binders before and after aging. Error bars for the nine replicates were added in the figure to show the variation of the measurement. The data used for plotting are summarized in Appendix A.
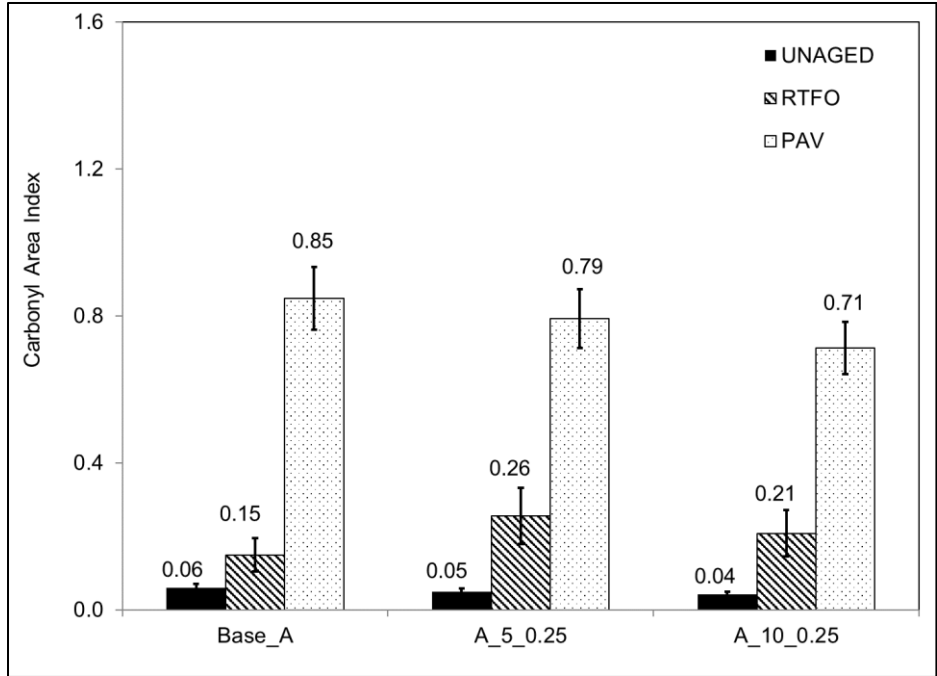
a: Group A (Binder ID format: source_rubber content in percent_maximumrubber size in mm)
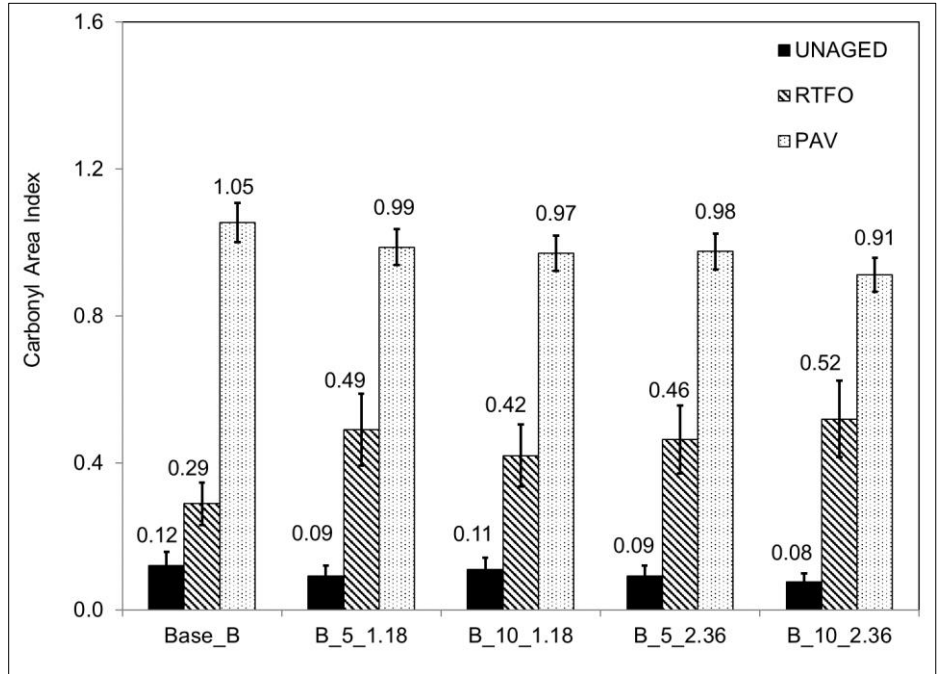
b: Group B (Binder ID format: source_rubber content in percent_maximum rubber size in mm)

167
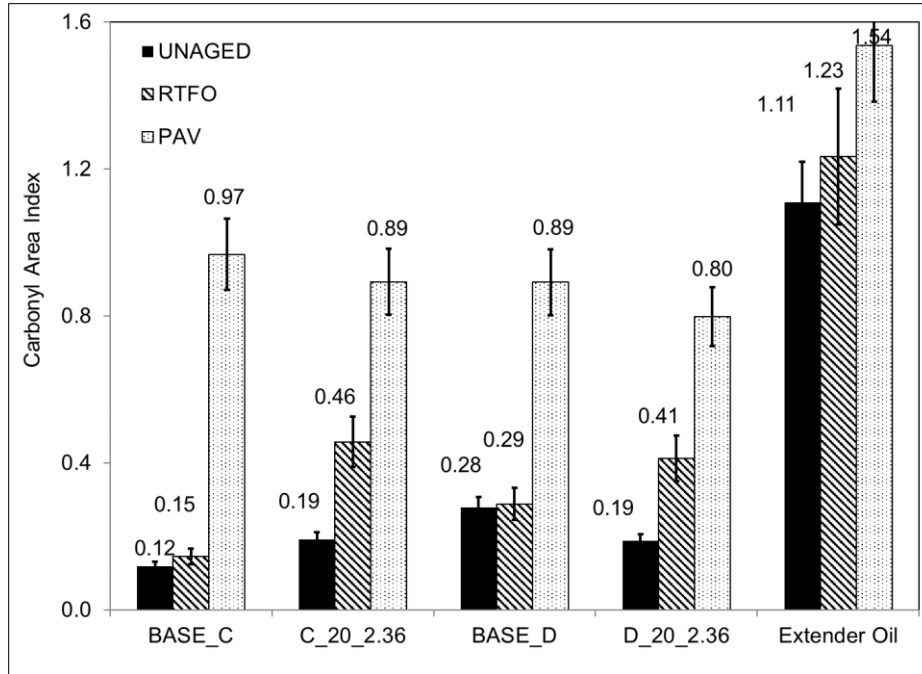
c: Group C and Group D (Binder ID format: source_rubber content in percent_maximum rubber size in mm)
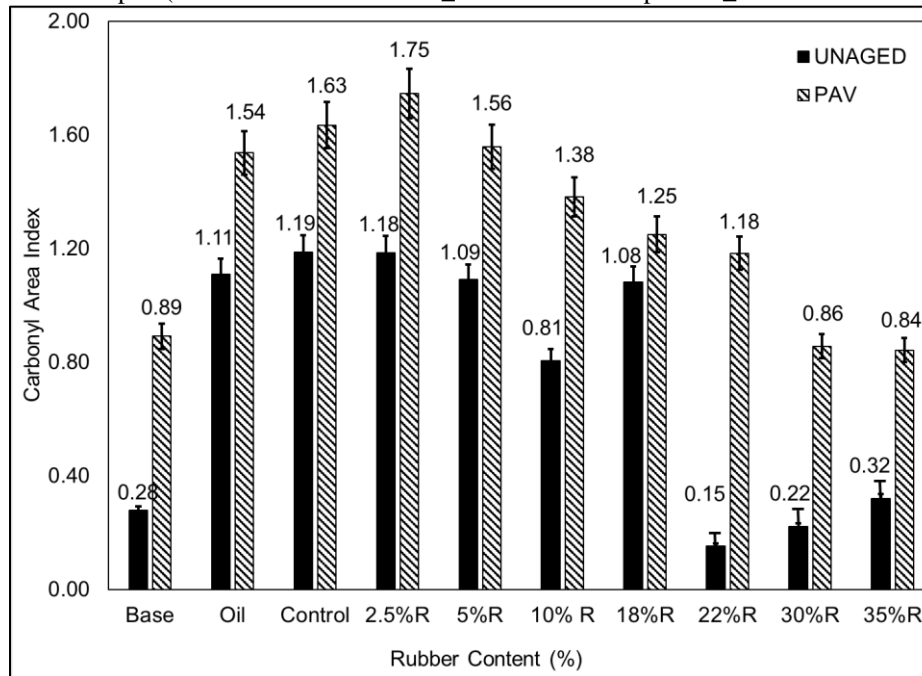
d: Group E

Figure 5.9: Changes of CA index of rubber-modified binders after RTFO- and PAV-aging.

In the unaged condition, Groups A and B binders show that the CA indices of the rubber-modified

binders were generally smaller than those of their base binders, which appeared to be attributed to

168

the rubber digesting in the binder phase. The reduced aging is hypothesized to be because the rubber effectively diluted carbonyl components in the rubber-modified binders in those groups. Different observations were found in Groups C, D, and E, where part of the rubber-modified binders had higher CA indices than the base binders. The difference between Group A and B binders to Group C, D, and E binders was that the latter contained extender oil.

Figure 5.9c shows that the extender oil used in this study contained higher amounts of carbonyl components than the base binder and the rubber (Table 5.8 shows that the rubber did contain any carbonyl components). This extender oil was added to the base binder simultaneously with the rubber, which could cause the CA index to increase in the final rubber-modified binder. The control binder in Group E was a mixture of base binder and the four percent extender oil, which showed an even higher CA index than the extender oil itself. This indicated that chemical interaction between the base binder and extender oil might occur during blending. Table 5.9 and Table 5.10 show the statistical analysis results for the CA index.

The CA indices of devulcanized rubber in Group A were assumed to be the same as those in CRM_1.18 since no devulcanized rubber samples were received by the laboratory. However, even if devulcanized rubber was available, the FTIR used in this study could not precisely measure the devulcanized rubber because the maximum particle size of devulcanized rubber is 250 microns, which is too small to fully cover the FTIR optics [2-mm diameter]).

Table 5.9: Comparison of Carbonyl Area Index

Binder ID	Extender Oil Content (%)	Unaged Binder				RTFO-Aged Binder				PAV-Aged Binder			
		I_M	SD	I_c	C	I_M	SD	I_c	C	I_M	SD	I_c	C
Base_A	0	0.061	0.017	0.061		0.150	0.065	0.150		0.848	0.102	0.848	
A_5_0.25	0	0.050	0.019	0.058	Yes	0.255	0.084	0.143	No	0.793	0.026	0.806	Yes
A_10_0.25	0	0.043	0.013	0.055	Yes	0.208	0.073	0.135	No	0.713	0.051	0.763	Yes
Base_B	0	0.121	0.053	0.121		0.289 (0.360)	0.058 (0.090)	0.289 (0.360)		1.054	0.051	1.054	
B_5_1.18	0	0.093	0.029	0.115	Yes	0.491	0.039	0.275 (0.342)	No (No)	0.987	0.042	1.001	Yes
B_10_1.18	0	0.110	0.042	0.109	Yes	0.420	0.034	0.260 (0.324)	No (No)	0.971	0.036	0.949	Yes
B_5_2.36	0	0.093	0.032	0.115	Yes	0.464	0.092	0.275 (0.342)	No (No)	0.976	0.037	1.001	Yes
B_10_2.36	0	0.077	0.024	0.109	No	0.520	0.037	0.260 (0.324)	No (No)	0.912	0.053	0.949	Yes
Base_C	0	0.119	0.025	0.119		0.146	0.045	0.146		0.968	0.125	0.968	
C_20_2.36	4	0.191	0.085	0.140	Yes	0.457	0.055	0.166	No	0.893	0.072	0.836	Yes
Base_D	0	0.279	0.025	0.279		0.289	0.029	0.289		0.892	0.125	0.892	
D_20_2.36	4	0.188	0.025	0.268	No	0.412	0.055	0.280	No	0.798	0.043	0.775	Yes
E_Control	4	1.190	0.105	1.190						1.630	0.047	1.630	
E_2.5	4	1.180	0.357	1.160	Yes					1.750	0.049	1.589	No
E_5	4	1.090	0.053	1.131	Yes					1.560	0.047	1.549	Yes
E_10	4	0.810	0.022	1.071	No					1.380	0.030	1.467	No
E_18	4	1.080	0.052	0.976	No					1.250	0.060	1.434	No
E_22	4	0.150	0.046	0.928	No					1.180	0.026	1.271	No
E_30	4	0.220	0.091	0.833	No					0.860	0.240	1.141	No
E_35	4	0.320	0.063	0.774	No					0.840	0.127	1.060	No

SD= standard deviation of the measured index (I_M).

C= testing criterion to check whether the calculated index (I_C) is within one standard deviation of the measured index or not.

Yes and No = it is "Yes" if I_c is within one standard deviation of I_M. Otherwise, it is "No".

For Group B binder x(x)= results are calculated based on RTFO-aged Base_B binder at 163°C and 190°C, respectively (the one in the brackets represents the data in 190°C). The 190°C temperature is the same RTFO temperature used for the RTFO-aging of the rubber-modified binders in Group B.

Table 5.10: Pearson Correlation of I_M and Ic for Carbonyl Area Index

Extender Oil Content (%)	Group	Unaged Binder	RTFO-Aged Binder	PAV-Aged Binder
0	A, B	0.90	0.98	0.96
4	C, D, E	0.56	N/A*	0.65

*Group C, D, and E binders only contain two data points (I_M) in RTFO-aged condition that Pearson correlation is not valid to use.

In the unaged condition, the calculated CA indices were mostly within one standard deviation of the measured CA indices for Groups A and B, none of which had extender oil. In contrast, the calculated CA indices were mostly not within one standard deviation of the measured CA indices for Groups C, D, and E, which did have extender oil in the binders with rubber. The Pearson correlation between measured CA indices and calculated indices was 0.90 for unaged Group A and B binders (>0.7 threshold), but it was 0.56 for the unaged Groups C, D, and E binders. This indicated that the dilution appeared to be evident for rubber-modified binder containing five and ten percent rubber without extender oil but not valid for those binders containing extender oil.

Nakason et al. *(165)* and Govedarica et al. *(166)* suggested that the extender oil reduced the cohesive forces between polymer chains and increased the polymer chain mobility. Adding the extender oil promoted chemical interaction between the rubber and the binder. This may explain why the dilution hypothesis alone could not explain the chemical changes in rubber-modified binders containing extender oil.

Figure 5.9d shows that increasing the rubber content decreased the carbonyl components in the Group E binders in the unaged condition. Some variability was identified, e.g., the binder with 18 percent rubber showed higher CA indices than the one with 10 percent rubber, and the binder with 22 percent rubber showed lower CA indices than the one with 30 percent rubber. These variabilities were attributed to limitations with the FTIR equipment. As discussed in Section 5.3.2, the measuring optics are small, and one drop of the binder is often larger than the optics. When the rubber content was high, the possible range of measured rubber content in one drop of the binder increased. The FTIR equipment could only measure part of the sample resulting in inconsistent CA index changes in Group E binders. Although these variabilities existed, a decreasing tendency of the CA indices with increasing rubber content from 2.5 percent to 35 percent was found.

Table 5.9 shows that the measured CA indices were generally lower than the calculated CA indices in Group E binders. In this case, chemical interaction between the rubber, extender oil, and binder appeared to occur as the second hypothesis proposed in Section 5.3.1. The rubber might be an antioxidant that further decreased the CA index than the dilution effect alone would explain. The inconsistent CA index changes in Group E indicated that the extender oil amount and blending time appeared to influence the chemical interaction in Group E rubber-modified binders.

After RTFO-aging, increases of CA indices were observed for all binders in each group. The rubber-modified binders had higher CA indices than their base binders regardless of the differences in RTFO-aging temperatures. For binders in Group A, the standard RTFO-aging (163°C) was conducted with adjustment of the sample size to account for the rubber content. The standard deviation of the measured CA index was relatively high compared to the total amount of the CA index, making it difficult to determine the CA index changes after RTFO-aging for Group A binders. For binders in Groups B, C, and D, the modified RTFO-aging was operated at a higher temperature (190°C) than the standard RTFO-aging (163°C). The elevated RTFO-aging temperature might result in additional aging that generated larger CA indices.

A second RTFO-aging of Base_B at 190°C was conducted, and the data were added in Table 5.9. The calculated CA indices using the data for 190°C were still beyond the one standard deviation of the measured CA indices for rubber-modified binders, which indicated that elevating the RTFO temperature alone could not explain the high CA indices in rubber-modified binders.

After RTFO-aging, the measured CA indices were always higher than the calculated CA indices for the rubber-modified binders tested in the section. Increasing the rubber content reduced the measured CA indices, which showed the same tendency as the calculated CA indices. Therefore,

173

the Pearson correlation was high (0.98) for RTFO-aged Group A and B binders. The observed higher CA indices for rubber-modified binders than for the base binder indicated that the rubber dilution hypothesis was not valid for RTFO-aged binders. This observation was found for Groups A and B (no extender oil) and Groups C and D (four percent extender oil), indicating that the chemical interaction occurred during RTFO-aging, which apparently changed the CA index.

The PAV-aging protocol resulted in higher CA indices than those recorded after RTFO-aging, as expected. In Group A, the CA indices of PAV-aged binders were triple those of RTFO-aged binders. In Groups B, C, and D, the CA indices of PAV-aged binders were double those of the RTFO-aged ones. Although the aging rate varied among binder sources and types, adding crumb rubber modifiers into binders decreased the CA indices compared with the base binders after PAV-aging. In each binder group, base binders experienced the highest increase in the CA index during PAV-aging. These observations were consistent with the findings discussed in Section 4.3.1 in that rubber-modified binders had lower CA indices than the unmodified binder after field-aging.

Figure 5.9 shows that increasing the rubber content decreased the CA indices in rubber-modified binders after PAV-aging compared to the base binders. Table 5.9 shows that the calculated CA indices were within one standard deviation of the measured CA indices for Group A and Group B binders, which contained no extender oil. Table 5.10 shows that the Pearson correlation between measured and calculated CA indices was 0.96 for these PAV-aged binders. In this case, the dilution of CA indices appeared to be valid.

On the other hand, when extender oil was used in Groups C, D, and E, the calculated CA indices were not always within the one standard deviation of the measured CA indices. Table 5.10 also shows that the Pearson correlation between measured and calculated CA indices was 0.56, which

174

was lower than the 0.7 threshold. Groups C and D binders showed that the measured CA indices were higher than the calculated values. Group E binders showed that the measured CA indices were lower than the calculated CA indices when the rubber content was more than five percent. In this case, chemical interaction occurred during the PAV-aging that the dilution hypothesis was not valid for explaining the CA index changes.

In summary, the crumb rubber modifier used in this study did not contain any carbonyl components. Chemical interactions existed between the extender oil and the base binder, as the E_Control binder showed. Therefore, the extender oil and the aging condition affected the rubber-binder interaction. In the unaged condition, the rubber dilution effect could explain the carbonyl component changes in the rubber-modified binders without extender oils. In contrast, the rubber appeared to be an antioxidant in the rubber-modified binders containing extender oils, which showed fewer carbonyl components than the calculated values based on the dilution hypothesis.

After RTFO-aging, the rubber-modified binders showed greater carbonyl component increases than the calculated values by the dilution effect. This observation was found in all tested binders with or without extender oils. It indicated that chemical interaction between rubber and binder occurred at elevated temperatures (>160°C) that considerably changed the measured CA indices.

In the PAV-aged condition, the rubber dilution of carbonyl components hypothesis appeared to be valid for binders without extender oils. In contrast, the dilution effect alone could not explain the carbonyl component changes for binders with extender oils.

5.3.5 Change of Sulfoxide Components in Rubber-Modified Binders

Figure 5.10 shows the baseline SUL indices in the unaged condition and how they changed after RTFO and PAV-aging. For Groups A and B binders without extender oils, the SUL indices of rubber-modified binders were generally smaller than those of the base binders in the unaged condition. The rubber decreased the sulfoxide components in rubber-modified binders, similar to the carbonyl components. This observation was not found for the binders in Groups C, D, and E, which contained extender oils. Figure 5.10d shows the SUL indices of Group E binders. Comparing the extender oil and the base binder showed that the extender oil used in this study contained more sulfoxide components than the base binder in the unaged condition. The E-Control binder produced by adding extender oils to the base binder showed a higher SUL index than the extender oil, indicating that chemical interaction between the base binder and extender oils could occur during the blending process.
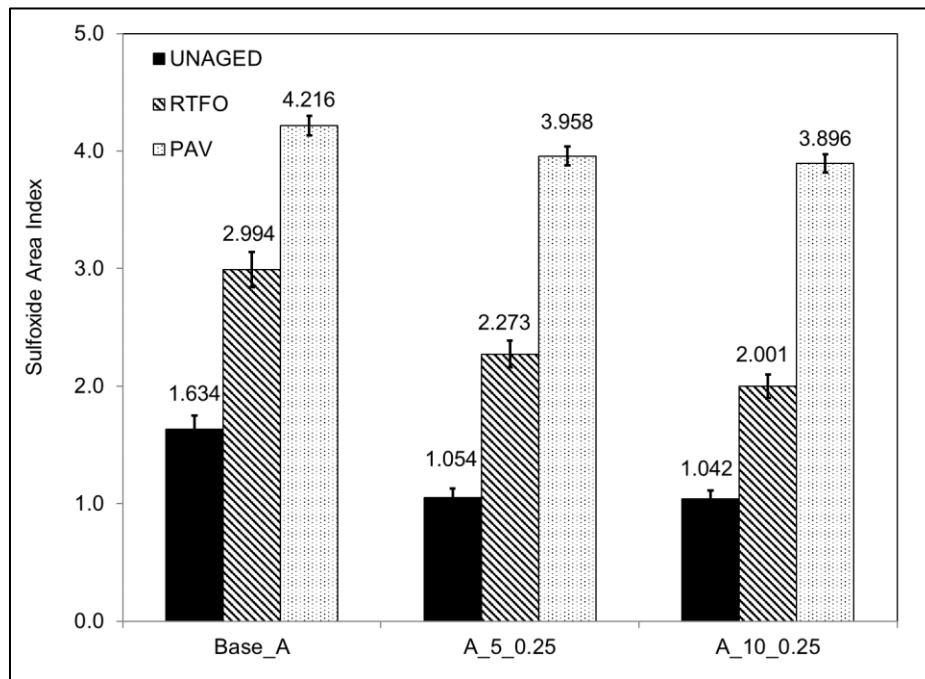
a: Group A (Binder ID format: source_rubber content in percent_maximum rubber size in mm)
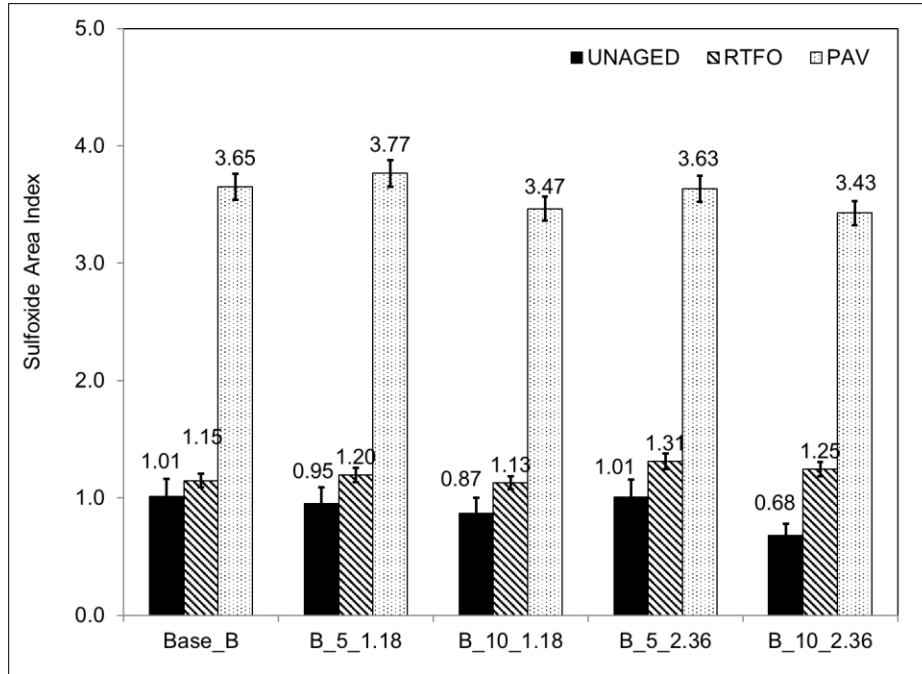
b: Group B (Binder ID format: source_rubber content in percent_maximum rubber size in mm

c: Group C and Group D (Binder ID format: source_rubber content in percent_maximum rubber size in mm)

177
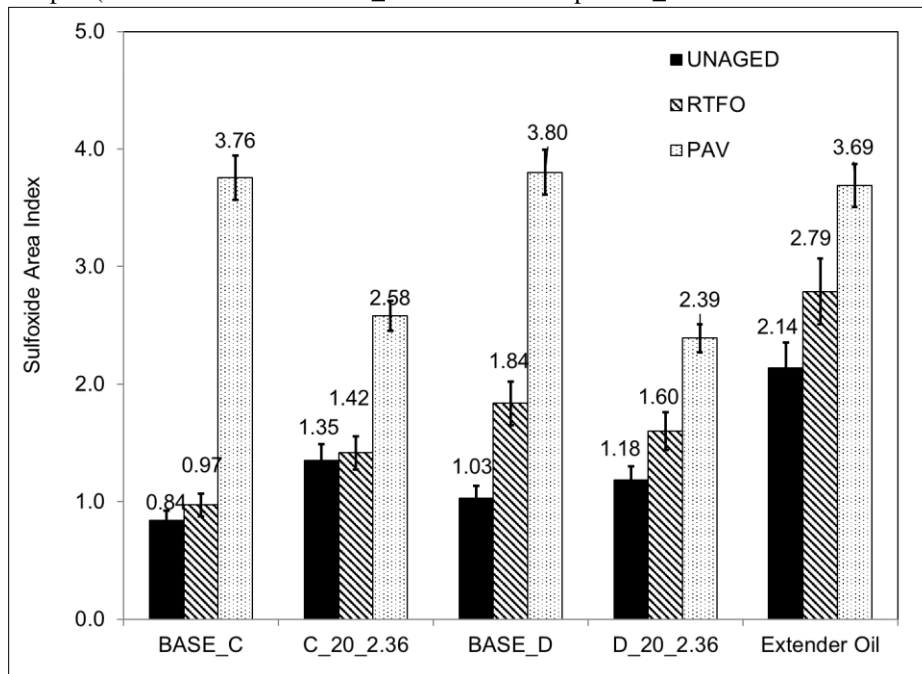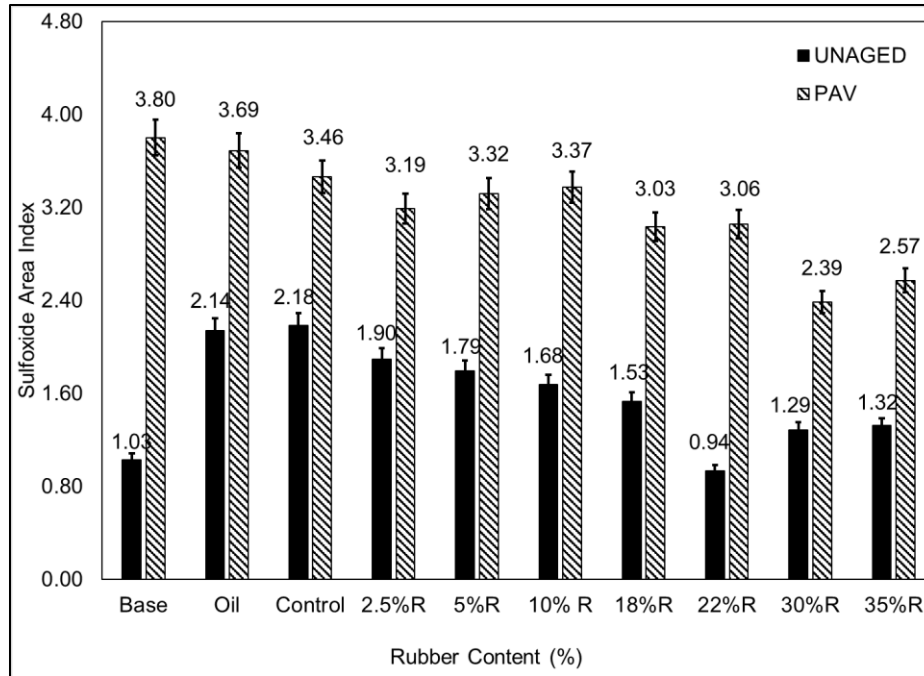
d: Group E

Figure 5.10: Changes of SUL index of rubber-modified binders after RTFO- and PAV-aging.

To inspect the hypotheses proposed in Section 5.3.1, calculated SUL indices using Equation 5.4 were compared to the measured SUL indices. In the calculation, the SUL indices of the rubber in RTFO-aged condition were assumed to be the averages of those in the unaged and PAV-aged rubber as discussed in Section 5.3.3. Table 5.11 and Table 5.12 show the calculation results for SUL indices.

In the unaged condition, the calculated SUL indices were not always within one standard deviation of the measured SUL indices for these binders in all groups. The measured SUL indices were lower than the calculated SUL indices, except for the C_20_2.36 and D_20_2.36 binders. The exception was caused by the calculated SUL indices listed in Table 5.11, which were calculated from the base binder for these two rubber-modified binders. It did not account for the SUL index increase because of the chemical interaction between the base binder and the extender oil. The E_Control

binder showed that the chemical interaction between the base binder and the extender oil resulted in a higher SUL index than that in the extender oil. Using 2.140 (SUL index of extender oil) as the input for the SUL index calculation would result in a value of 1.855 for the C_20_2.36 and D_20_2.36 binders, which was higher than their measured SUL indices. In this case, all measured SUL indices were lower than the calculated SUL index. Table 5.12 shows that the Pearson correlation between measured and calculated SUL indices was not above the 0.7 threshold. Therefore, adding the rubber appeared to act as an antioxidant that resulted in lower SUL indices than the calculated SUL indices based on the dilution hypothesis alone.

Therefore, the extender oil amount and blending time could influence the chemical interaction in the Group E rubber-modified binders. In future studies of the chemical interaction between the rubber and the binder containing extender oils, it is recommended that the extender oil amount and blending time are proportional to the rubber content to better explain chemical interactions between the two.

Table 5.11: Comparison of Sulfoxide Area Index

Binder ID	Extender Oil Content (%)	Unaged Binder				RTFO-Aged Binder				PAV-Aged Binder			
		I_M	SD	Ic	C	I_M	SD	Ic	C	I_M	SD	Ic	C
Base_A	0	1.634	0.057	1.634		2.994	0.067	2.994		4.216	0.045	4.216	
A_5_0.25	0	1.054	0.169	1.577	No	2.273	0.136	2.868	No	3.958	0.038	4.027	No
A_10_0.25	0	1.042	0.065	1.526	No	2.001	0.09	2.741	No	3.896	0.161	3.839	Yes
Base_B	0	1.01	0.212	1.01		1.147 (1.219)	0.04	1.147 (1.219)		3.651	0.036	3.651	
B_5_1.18	0	0.949	0.045	0.984	Yes	1.197	0.037	1.113 (1.181)	No (Yes)	3.766	0.089	3.491	No
B_10_1.18	0	0.871	0.155	0.958	Yes	1.129	0.071	1.079 (1.144)	Yes (Yes)	3.465	0.337	3.330	Yes
B_5_2.36	0	1.008	0.109	0.987	Yes	1.313	0.069	1.116 (1.181)	No (No)	3.634	0.091	3.494	No
B_10_2.36	0	0.679	0.150	0.965	No	1.246	0.055	1.085 (1.144)	No (No)	3.428	0.195	3.336	Yes
Base_C	0	0.842	0.031	0.842		0.973	0.068	0.973		3.757	0.132	3.757	
C_20_2.36	4	1.353	0.292	0.870	No	1.416	0.087	0.996	No	2.581	0.268	3.254	No
Base_D	0	1.031	0.088	1.031		1.836	0.362	1.836		3.802	0.099	3.802	
D_20_2.36	4	1.183	0.287	1.022	Yes	1.601	0.177	1.686	Yes	2.392	0.106	3.290	No
E_Control	4	2.180	0.036	2.180						3.464	0.171	3.464	
E_2.5	4	1.900	0.042	2.139	No					3.192	0.041	3.390	No
E_5	4	1.790	0.110	2.099	No					3.320	0.035	3.316	Yes
E_10	4	1.680	0.078	2.018	No					3.373	0.044	3.168	No
E_18	4	1.530	0.190	1.888	No					3.034	0.124	3.139	Yes
E_22	4	0.940	0.076	1.823	No					3.057	0.038	2.813	No
E_30	4	1.290	0.698	1.693	Yes					2.390	0.240	2.576	Yes
E_35	4	1.320	0.457	1.612	Yes					2.570	0.438	2.428	Yes

SD= standard deviation of the measured index (I_M).

C= testing criterion to check whether the calculated index (I_C) is within one standard deviation of the measured index or not.

Yes and NO = it is "Yes" if Ic is within one standard deviation of I_M. Otherwise, it is "No".

For Group B binder x(x)= results are calculated based on RTFO-aged Base_B binder at 163°C and 190°C, respectively (the one in the bracket represents the result in 190°C). The 190°C temperature is the same RTFO temperature used for the RTFO-aging of the rubber-modified binders in Group B.

Table 5.12: Pearson Correlation of I_M and Ic for Sulfoxide Area Index

Extender Oil Content (%)	Group	Unaged Binder	RTFO-Aged Binder	PAV-Aged Binder
0	A, B	0.64	0.96	0.93
4	C, D, E	0.70	N/A*	0.45

*Group C, D, and E binders only contain two data points (I_M) in RTFO-aged condition that Pearson correlation is not valid to use.

Figure 5.10 shows that the SUL indices increased after RTFO-aging. For binders in Group A, Figure 5.10a shows that both rubber-modified binders had lower SUL indices than the base binder after standard RTFO-aging (163°C).

When the modified RTFO-aging protocol (190°C) was applied to the Groups B, C, and D rubber-modified binders, the SUL indices were higher than the base binder (standard RTFO-aging). The second round of RTFO-aging for the Base_B binder was conducted at 190°C. Part of the calculated SUL indices based on the Base_B binder (RTFO-190°C) was still not within one standard deviation of the measured SUL indices, which indicated that dilution alone could not explain the SUL index changes in RTFO-aging.

PAV-aging increased the SUL index, as shown in Figure 5.10. Although the aging rate varied among binder sources and types, the presence of rubber decreased the SUL indices.

For binders in Groups A and B, the calculated SUL indices could be within one standard deviation of the measured SUL indices because a high standard deviation was found for the A_10_0.25, B_10_1.18, and B_10_2.36 binders. Although the Pearson correlation between measured and calculated SUL indices for Group A and B binders was 0.93, this was not high enough to support a conclusion that dilution alone could explain the aging for these binders because it did not meet the standard deviation criterion for accepting the dilution hypothesis.

For Groups C, D, and E binders, the calculated SUL indices could be within one standard deviation of the measured SUL indices for the E_18, E_30, and E_35 binders, which had a high standard deviation of the measured SUL indices. Although the measured SUL indices were randomly offset among calculated SUL indices, the Pearson correlation between measured and calculated SUL

indices was only 0.45 in this case. Therefore, dilution alone could not explain the SUL index changes for those binders after PAV-aging.

In summary, the dilution hypothesis was not valid for explaining the changes in the SUL index. Table 5.8 shows the rubber itself contained sulfoxide components. The E_Control binder showed that chemical interactions could occur between the base binder and the extender oil before adding the rubber. In the unaged condition, adding the rubber appeared to have antioxidant effects that resulted in SUL indices lower than the calculated SUL indices based on the dilution hypothesis. After RTFO- and PAV-aging, chemical interaction occurred in the rubber-modified binders that changed the SUL indices considerably, such that the dilution hypothesis was not valid.

5.3.6   Change in Butadiene Components in Rubber-Modified Binders

Figure 5.11 shows the changes in the butadiene area index along with aging. In the unaged condition, base binders and the extender oil showed small butadiene area indices. The butadiene area indices of PAV-aged base binders were even negative in several cases. This was not to say that the butadiene amount changed in the base binder after PAV-aging, but that the calculated value changed because of the integration method used in this study.

Figure 4.6 shows that the defined wavenumber of the butadiene area index is bonded to the SUL index wavenumber. Considering that the sulfoxide component increased after PAV-aging, the baseline of integrating the butadiene area in an FTIR spectrum curve was raised. A negative integration of the butadiene area index would occur when the baseline was above the peak of the defined butadiene area. A general decrease of the butadiene area index was observed for all binders by comparing the butadiene area index under RTFO- and PAV-aging. Therefore, the analysis of

183

the butadiene area index should be made under each aging condition individually to mitigate the calculation errors.

Figure 5.11 shows that the base binders and the extender oil used in this study did not contain butadiene components, except for the Base_A binder. The butadiene area index increased after adding rubber. Increasing the rubber content would increase the butadiene area index regardless of the aging condition. Binders in Groups C and D experienced a greater increase of the butadiene area index than the binders in Groups A and B, because of the higher rubber content (20 percent rubber in Groups C and D, compared to five and ten percent rubber in Groups A and B) used in former groups.
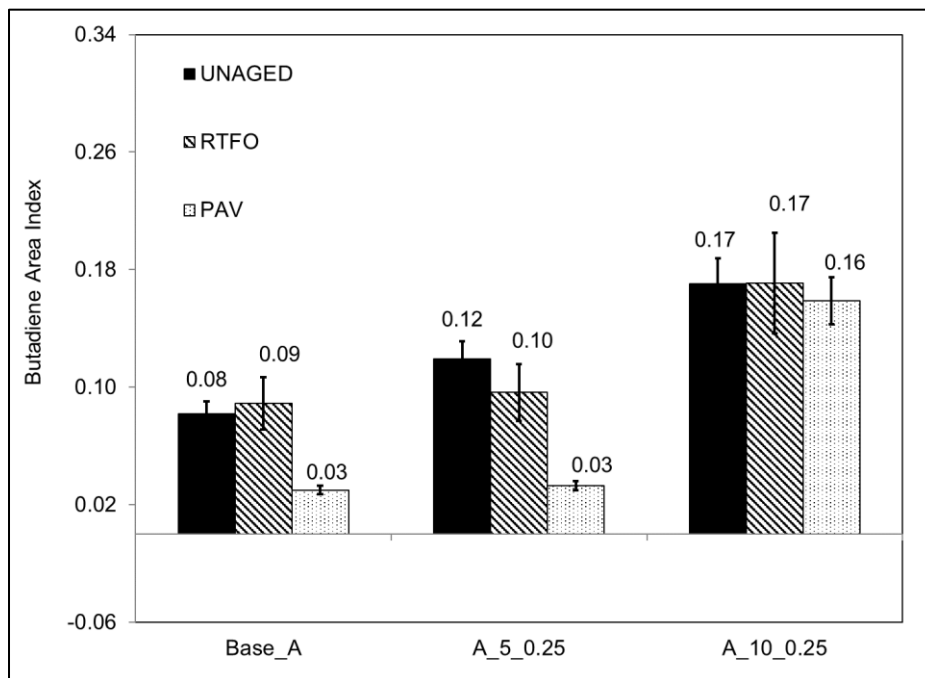

a: Group A (Binder ID format: source_rubber content in percent_maximum rubber size in mm)
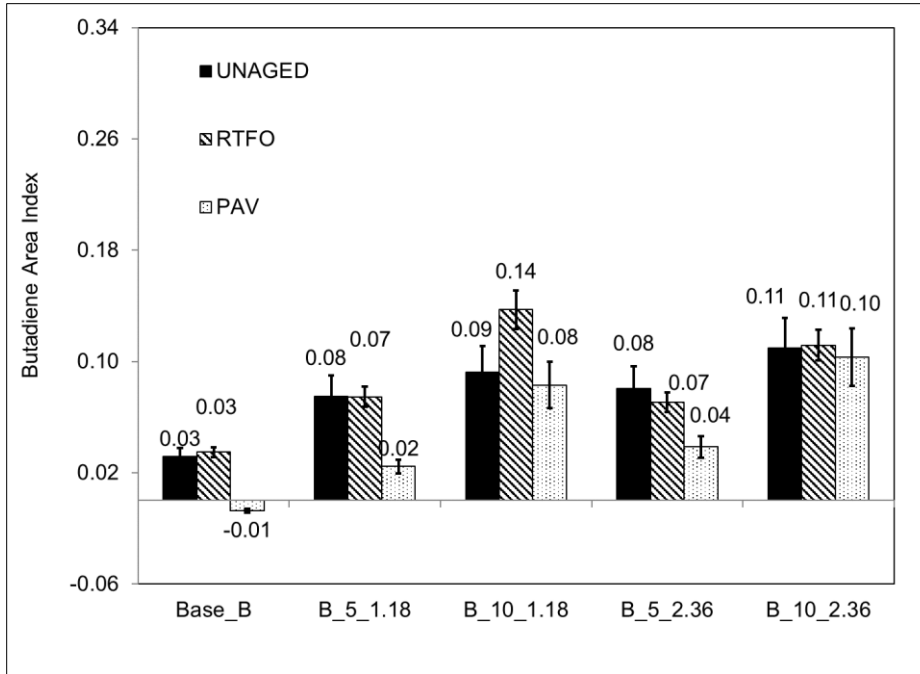
b: Group B Binder ID format: source_rubber content in percent_maximum rubber size in mm
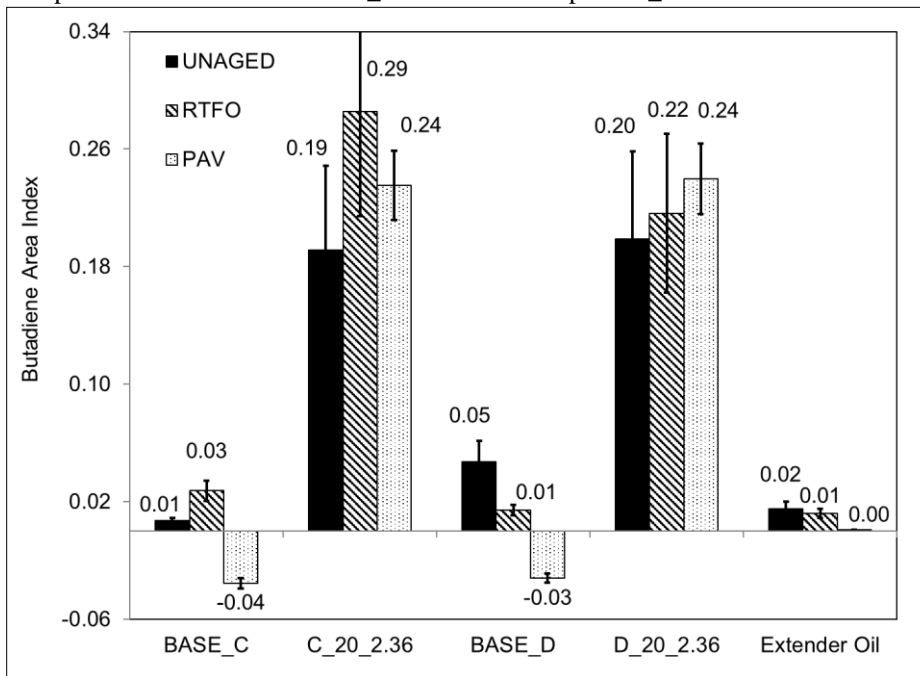
c: Group C and Group D Binder ID format: source_rubber content in percent_maximum rubber size in mm
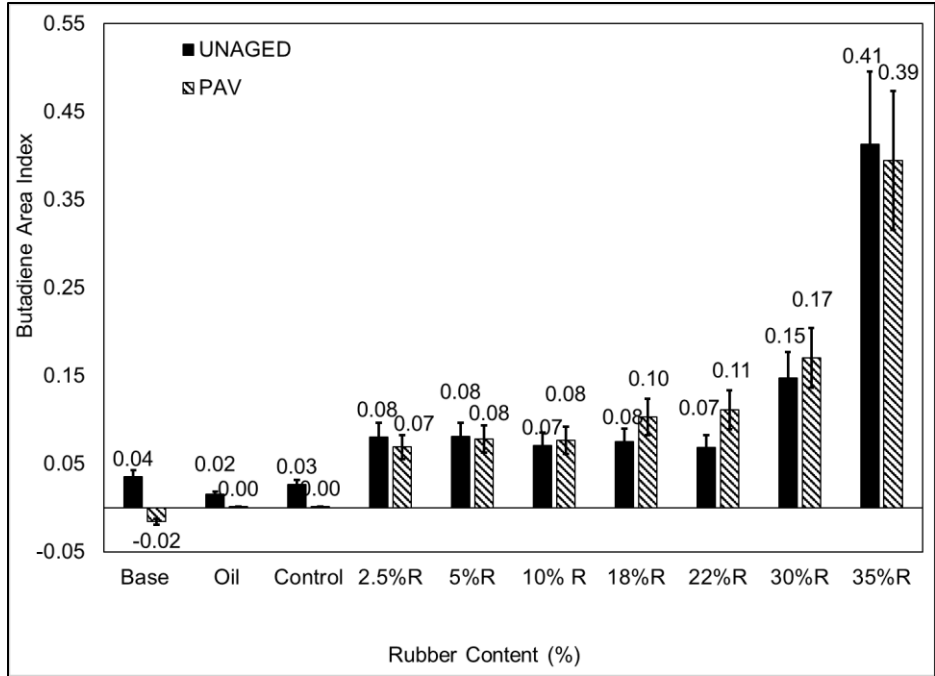
d: Group E

Figure 5.11: Changes in butadiene area index of rubber-modified binders after RTFO- and PAV-aging.

To test the hypotheses proposed in Section 5.3.1, the calculated butadiene area indices were compared to the measured butadiene indices. The negative butadiene area indices in the base binders were substituted with a zero value in the calculation. The butadiene area index of RTFO-aged rubber was assumed to be the average values of those in the unaged and PAV-aged conditions. Table 5.13 and Table 5.14 show the statistical analysis results of the butadiene area index.

Table 5.13 shows that the calculated butadiene area indices were generally lower than the measured butadiene area indices. The difference between the calculated and measured butadiene area indices increased with increasing rubber content.

This finding was observed for all tested binders, excepted for the A_5_0.25 binder. The Base-A binder was abnormal because the measured butadiene area indices in the Base_A binder were high. These butadiene area indices did not necessarily imply butadiene components existed in Base_A,

although it was one possibility. The high butadiene area indices in the Base_A binder raised the calculated butadiene area indices for the A_5_0.25 and A_10_0.25 binders. Therefore, the calculated butadiene area indices were higher than the measured values for the A_5_0.25 binder.

Another possibility to explain the observation in Group A was that this group used devulcanized rubber, which might have contained different amounts of butadiene than the ambient-temperature ground rubber (CRM_1.18 and CRM_2.36). The assumption of using the butadiene area index of CRM_1.18 to represent that in devulcanized rubber might be not valid. The calculated butadiene area indices of the A_10_0.25 binder were even larger than the C_20_2.36 and D_20_2.36 binders, which contained 20 percent rubber. Table 5.14 shows that the minimum Pearson correlations between measured and calculated butadiene area indices were 0.62. Although it was lower than the 0.7 threshold, a Pearson correlation over 0.6 still indicated that the measured and calculated butadiene area indices had moderate positive correlations *(163)*. The increase in the butadiene area index in Group A was still introduced by the added rubber.

The data in Table 5.13 shows that the measured butadiene area indices were higher than the calculated values for most rubber-modified binders in all groups. The integration of the butadiene area index possibility caused high measured values. The defined wavenumbers of the butadiene area indices were bonded to those of SUL indices. The value of the butadiene area index was smaller than that of SUL indices. Table 5.11 and Table 5.13 show that the SUL indices were at least ten times larger than the butadiene area indices in these binders. Therefore, changes in the sulfoxide component could significantly change the absolute area between the measured spectrum and the baseline for the butadiene component. Figure 5.10 shows that the SUL indices in the rubber-modified binders with 20 percent rubber were lower than those in the rubber-modified binders with five or ten percent rubber. The low SUL indices lowered the baseline for integrating

the butadiene area index in the rubber-modified binders with a high rubber content, which enlarged the integrated butadiene area index. Figure 5.11 and Table 5.14 show that increasing the rubber content increased the difference between the measured butadiene area index and the calculated butadiene area index. This observation appeared to prove the assumption that the larger measured butadiene area indices compared to the calculated values based on the dilution hypothesis were caused by the biased integration in the measured values.

In summary, increasing the rubber content increased the butadiene area indices in the rubber-modified binders before and after aging. However, the butadiene area index changes in these tested binders did not support the dilution hypothesis. Considering the possible integration issues for the butadiene area index, the dilution hypothesis should be tested with the CA and SUL indices, as they were discussed in Section 5.3.4 and Section 5.3.5.

Table 5.13: Comparison of Butadiene Area Index

Binder ID	Unaged Binder				RTFO-Aged Binder				PAV-Aged Binder			
	I_M	SD	Ic	C	I_M	SD	Ic	C	I_M	SD	Ic	C
Base_A	0.082	0.013	0.082		0.089	0.016	0.089		0.030	0.012	0.030	
A_5_0.25	0.119	0.007	0.091	No	0.096	0.035	0.097	Yes	0.033	0.012	0.041	Yes
A_10_0.25	0.171	0.020	0.095	No	0.171	0.026	0.105	No	0.159	0.006	0.051	No
Base_B	0.032	0.012	0.032		0.035 (0.040)	0.014	0.035 (0.040)		-0.007	0.008	0	
B_5_1.18	0.075	0.016	0.043	No	0.075	0.012	0.046 (0.050)	No (No)	0.025	0.008	0.012	No
B_10_1.18	0.093	0.009	0.054	No	0.137	0.016	0.056 (0.060)	No (No)	0.083	0.021	0.024	No
B_5_2.36	0.081	0.019	0.041	No	0.071	0.017	0.045 (0.050)	No (No)	0.039	0.012	0.013	No
B_10_2.36	0.109	0.015	0.050	No	0.112	0.015	0.055 (0.060)	No (No)	0.103	0.019	0.026	No
Base_C	0.007	0.011	0.007		0.028	0.011	0.028		-0.035	0.023	0	
C_20_2.36	0.191	0.066	0.049	No	0.286	0.087	0.070	No	0.235	0.014	0.051	No
Base_D	0.047	0.024	0.047		0.014	0.022	0.014		-0.032	0.020	0	
D_20_2.36	0.199	0.014	0.081	No	0.216	0.014	0.059	No	0.240	0.020	0.051	No
E_Control	0.030	0.110	0.030						0.000	0.014	0.000	
E_2.5	0.080	0.015	0.035	No					0.070	0.024	0.006	No
E_5	0.080	0.020	0.039	No					0.080	0.017	0.013	No
E_10	0.070	0.011	0.049	No					0.080	0.026	0.026	No
E_18	0.080	0.015	0.063	No					0.100	0.014	0.046	No
E_22	0.070	0.013	0.071	Yes					0.110	0.021	0.056	No
E_30	0.150	0.051	0.086	No					0.170	0.090	0.077	No
E_35	0.410	0.047	0.095	No					0.390	0.014	0.090	No

SD= standard deviation of the measured index (I_M).

C= testing criterion to check whether the calculated index (I_C) is within one standard deviation of the measured index or not.

Yes and NO = it is "Yes" if Ic is within one standard deviation of I_M. Otherwise, it is "No".

For Group B binder x(x)= results are calculated based on RTFO-aged Base_B binder at 163°C and 190°C, respectively (the one in the bracket represents the data in 190°C). The 190°C temperature is the same RTFO temperature used for the RTFO-aging of the rubber-modified binders in Group B.

Table 5.14: Pearson Correlation of I_M and Ic for Butadiene Area Index

Extender Oil Content (%)	Group	Unaged Binder	RTFO-Aged Binder	PAV-Aged Binder
0	A, B	0.87	0.62	0.66
4	C, D, E	0.67	N/A*	0.78

*Group C, D, and E binders only contain two data points (I_M) in RTFO-aged condition that Pearson correlation is not valid to use

The summary of the findings in Section 5.3.3 through Section 5.3.6 shows that adding rubber decreased the CA and SUL indices and increased the butadiene area indices in rubber-modified binders. The dilution effect could explain the CA index changes in unaged and PAV-aged conditions for binders without extender oil. In other cases, chemical interactions occurred that apparently changed the measured index values. The measured values were beyond the reductions in those indices that could be explained by the rubber dilution alone.

Figure 5.12 shows FTIR spectra for a control binder and a rubber modified binder for Group D and Group E as an example. A butadiene area index peak is not observed in the control binder. In contrast, a peak is evident in the rubber-modified binder, indicating that the presence of butadiene can be attributed solely to the rubber. Both the CA and SUL indices increased after PAV-aging for base binder and rubber-modified binder samples. Adding rubber decreased the accumulation of these aging products, especially the CA indices after PAV-aging. Section 5.3.3 shows that the rubber particles were not susceptible to oxidative aging. Their presence in the rubber-modified binders decreased the carbonyl and sulfoxide components, indicating that rubber-modified binders are likely to age at a slower rate than the base binders from which they are produced. The rubber appeared to dilute the carbonyl component for binders without extender oils in unaged and PAV-aged conditions. When extender oil was used, indications were that chemical interactions could occur in unaged and PAV-aged conditions and that dilution was not valid for explaining the component changes.
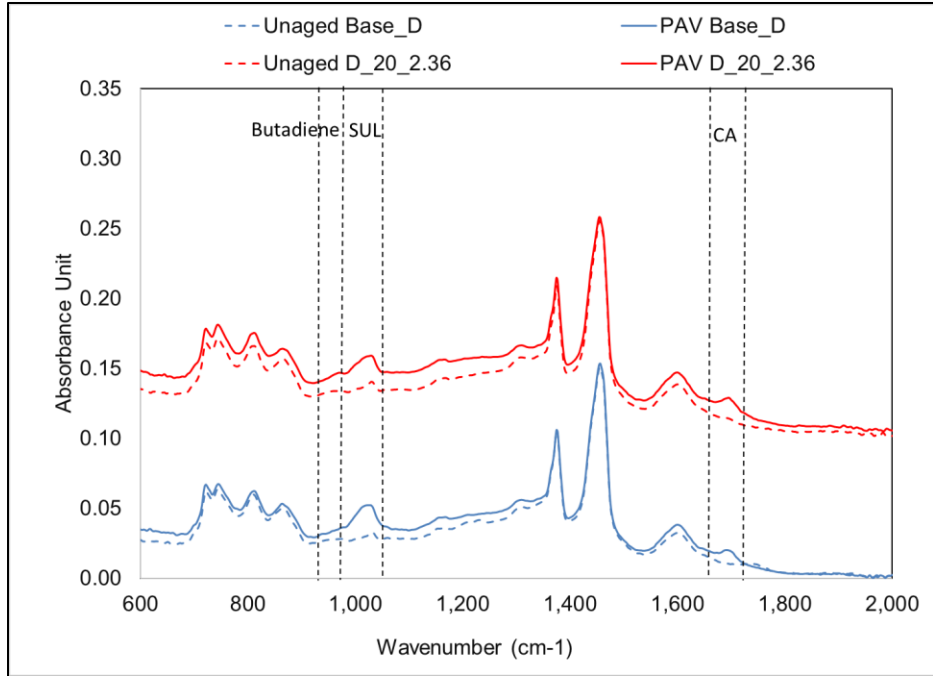
a: Binders in Group D
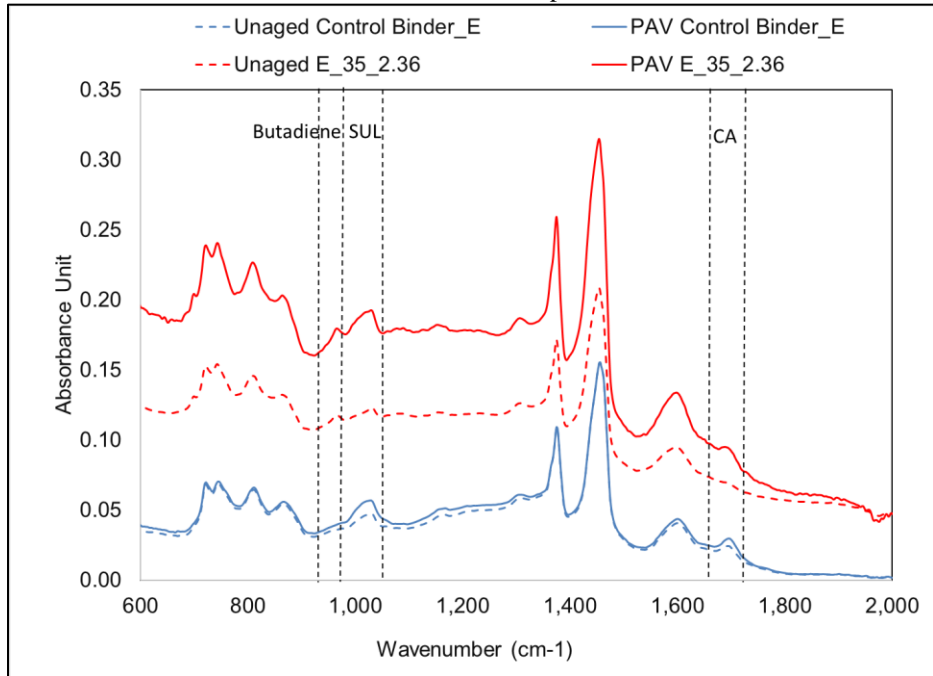
b: Binders in Group E

Figure 5.12: Comparison of FTIR spectrum before and after PAV-aging.

5.4 Calibration of GHS Model for Rubber-Modified Binders

5.4.1 Experimental Design for Validating the GHS Model for Rubber-Modified Binders

Section 5.3 shows that oxidative aging produces carbonyl and sulfoxide components in rubber-modified binders at a lower rate than in the corresponding base binders. The crumb rubber modifier is not susceptible to oxidative aging. Increasing the rubber content decreases the carbonyl and sulfoxide components in rubber-modified binders after PAV-aging.

In this section, four levels of PAV-aging were conducted to further evaluate oxidative aging in rubber-modified binders and prepare aged specimens for validating the GHS principle. Four levels of PAV-aging were conducted in this section, namely 100˚C for 20 hours and 40 hours, and 110˚C for 20 hours and 40 hours, respectively. Since the GHS principle had already been validated for unmodified binders in Chapter 4, only one base binder (Base_C) was tested and analyzed in Groups C and D.

The rheological properties of the base and rubber-modified binders in Group A were determined using the standard performance grading system following AASHTO T 315 and AASHTO T 320 *(30,74)*. The parallel plate geometry was used to test rubber-modified binders in Group A and the base binders in other groups. The rubber-modified binders in Groups B, C, and D were measured using the concentric cylinder geometry described in Section 5.2.2. Frequency sweep tests were run at 20°C, 40°C, 60°C, 85°C with the loading frequency between 0.0159 Hz and 15.9 Hz (0.1 and 100 radians/second).

The measured complex moduli and phase angles were backcalculated to viscosities using the method described in Section 4.4. These viscosities and CA indices of aged binders were used to validate the GHS principle for rubber-modified binders.

193

5.4.2 *Evaluation of Chemical Component Changes with PAV-Aging*

Figure 5.13 shows the changes in the CA index along with aging. At the same aging temperature, doubling the aging duration from 20 hours to 40 hours led to a higher increase in the CA index for all binders.

A comparison of the binders aged at 100°C and 110°C within the same binder group revealed that elevating the temperatures increased the CA index, indicating that increasing the aging temperature accelerated oxidative aging, as expected.

Although the CA index increasing rates were dependent on binder source and type, the rubber-modified binders generally had a lower increase in the CA index than their corresponding base binders. The base binders had the highest CA indices in each binder group. The difference between rubber-modified binders and base binders increased with increasing rubber content. These observations revealed that the rubber decreased the carbonyl components in the rubber-modified binders after PAV-aging, with levels proportional to testing temperature and duration.
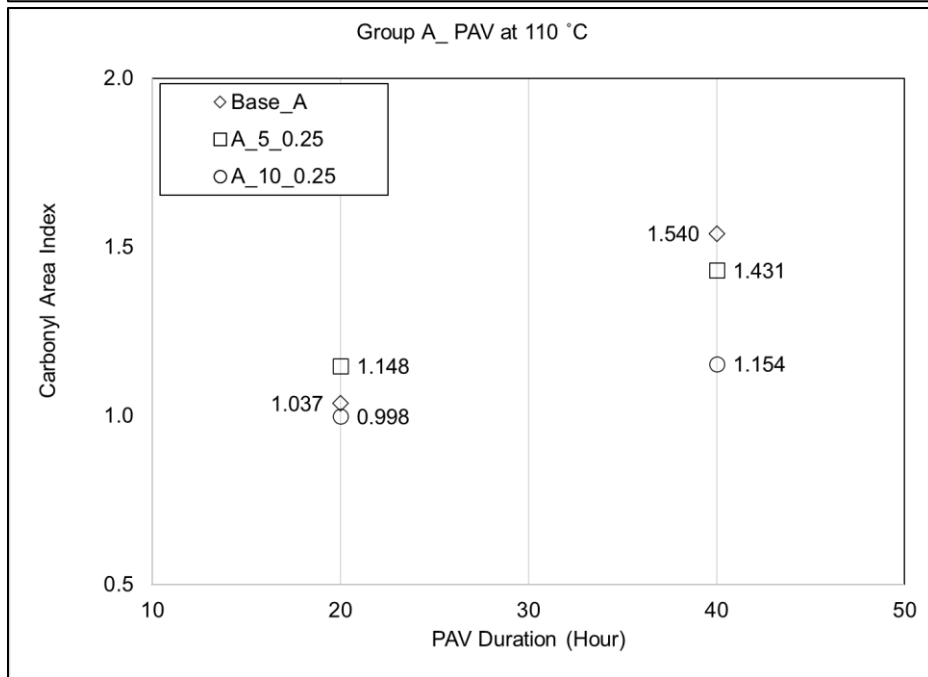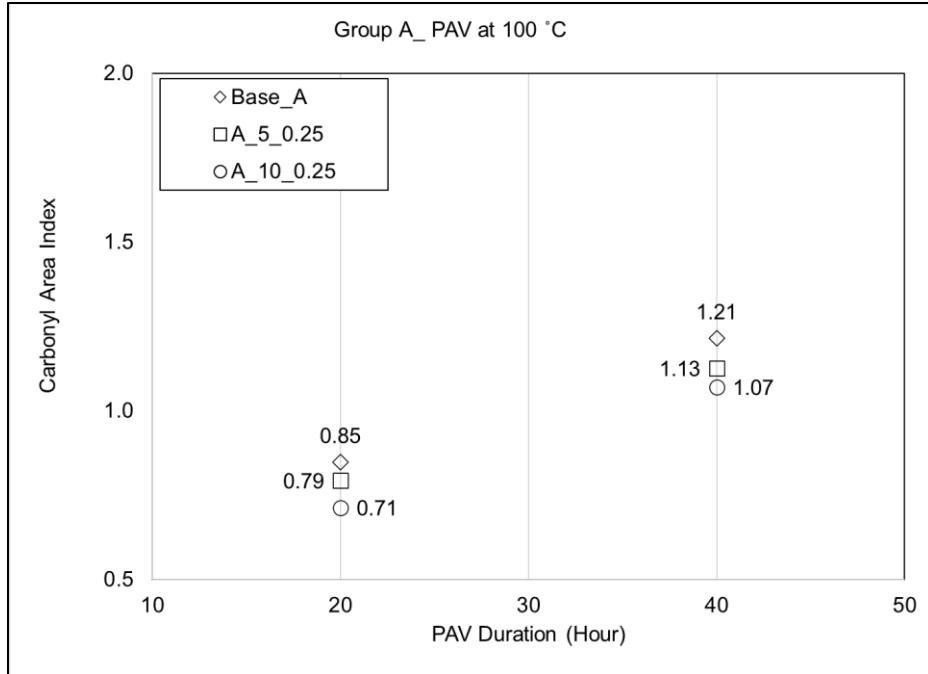
a: Group A (Binder ID format: source_rubber content in percent_maximum rubber size in mm)
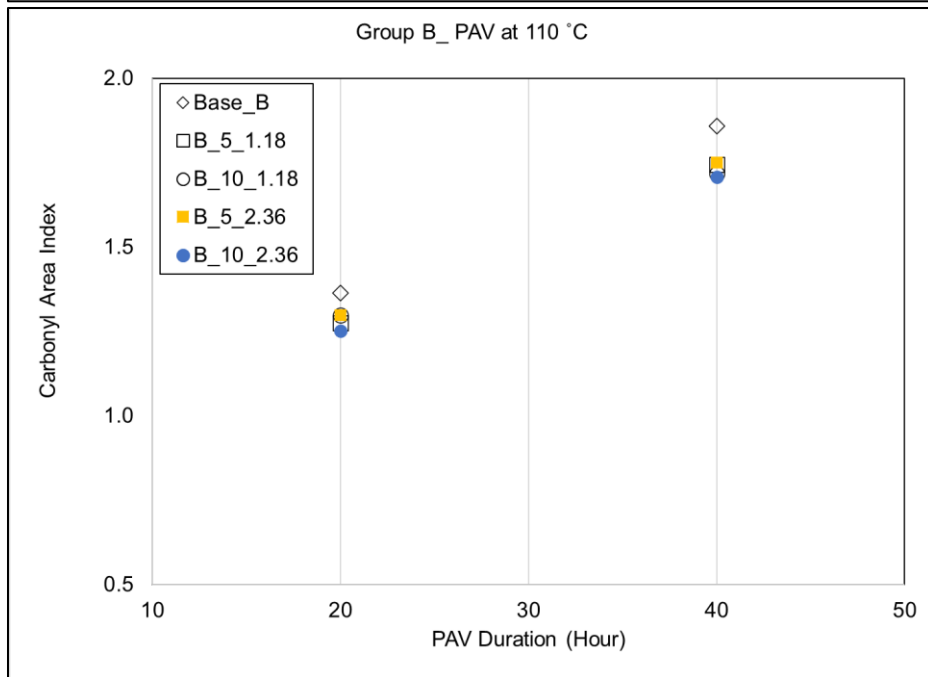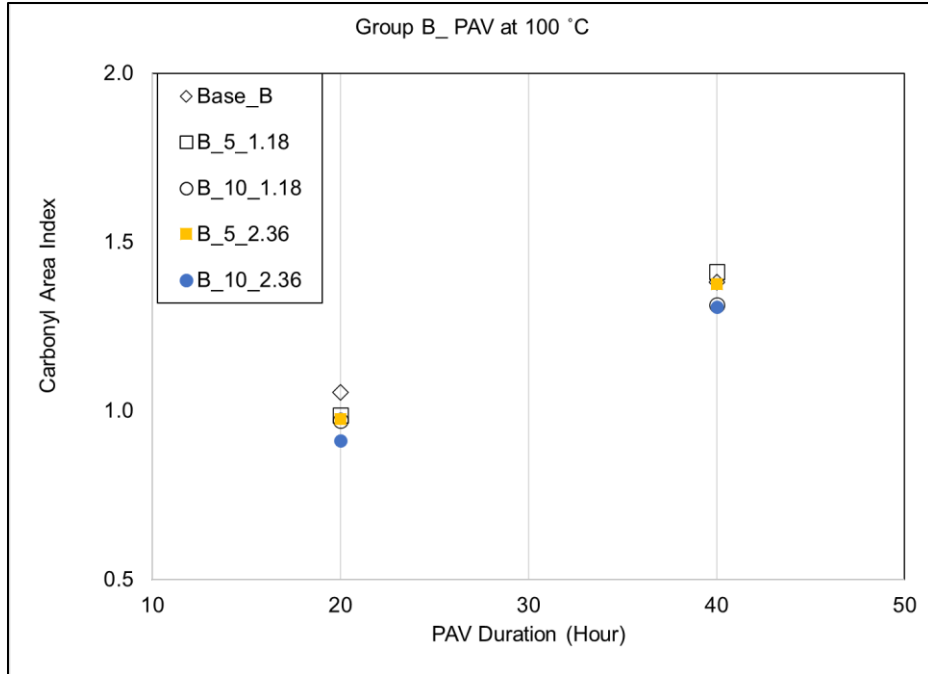
b: Group B (Binder ID format: source_rubber content in percent_maximum rubber size in mm)
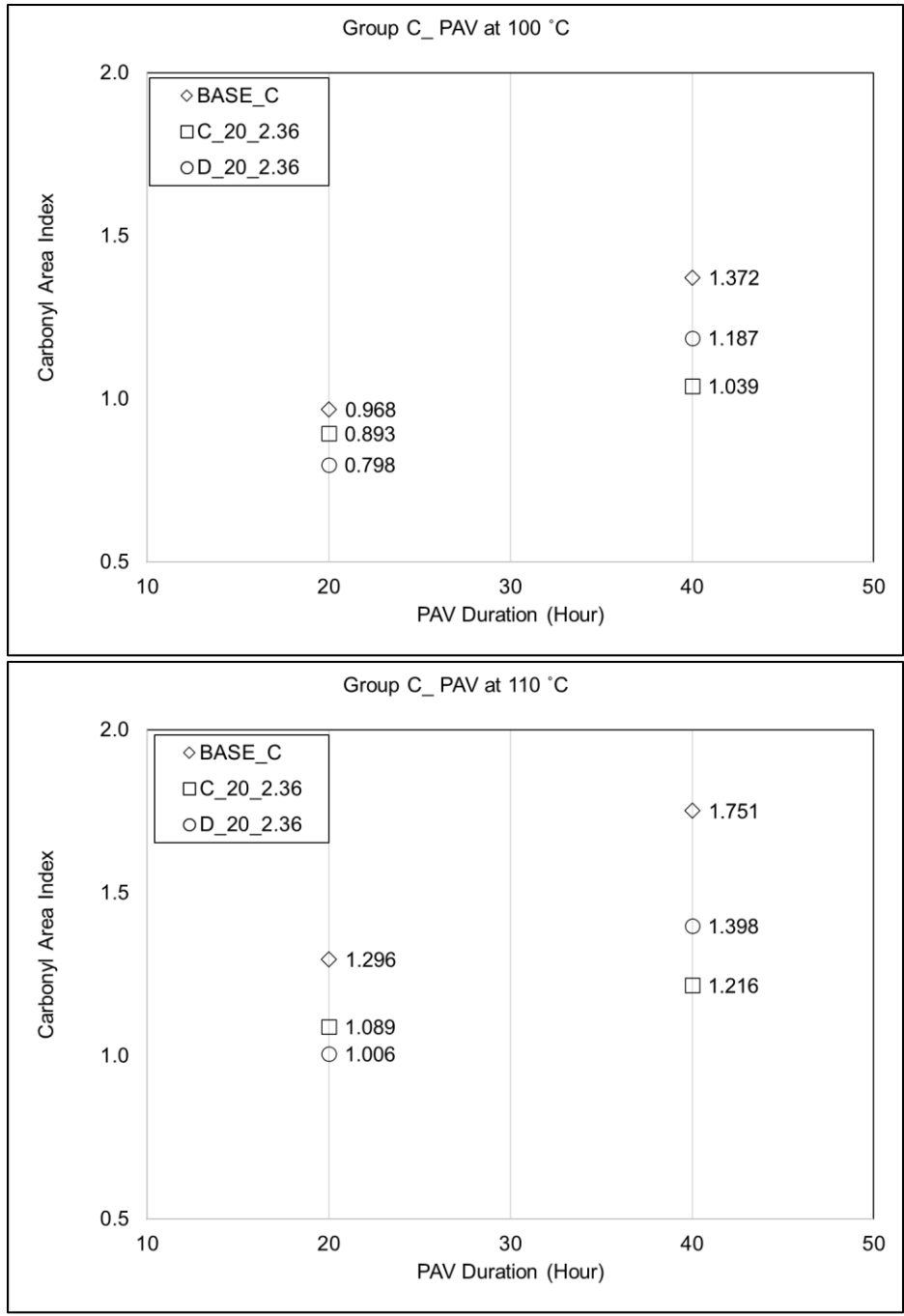
c: Group C and Group D (Binder ID format: source_rubber content in percent_maximum rubber size in mm)
Figure 5.13: Evolution of CA indices with exposure durations for base and rubber-modified binders.

The discussion in Section 5.3.4 shows that dilution could explain the CA index changes for PAV-aged binders without extender oils. This section further tests this hypothesis using the data from multiple PAV-aged conditions. Table 5.15 shows that the calculated CA indices were within one

standard deviation of the measured CA indices for Group A and B binders at these four PAV-aged conditions. The Pearson correlation was 0.97 for Group A and B binders, indicating a strong correlation between calculated and measured CA indices. Therefore, the dilution hypothesis was valid for CA indices after PAV-aging for binders without extender oils. The available data for Groups C and D binders show that dilution alone appeared unable to explain the CA index changes for binders containing extender oils.

Table 5.15: Comparison of Carbonyl Area Index after PAV-Aging

Binder ID	100°C and 20 Hours				100°C and 40 Hours				110°C and 20 Hours				110°C and 40 Hours			
	I_M	SD	Ic	C	I_M	SD	Ic	C	I_M	SD	Ic	C	I_M	SD	Ic	C
Base_A	0.848	0.102	0.848		1.215	0.366	1.215		1.037	0.318	1.037		1.540	0.259	1.540	
A_5_0.25	0.793	0.026	0.806	Yes	1.126	0.346	1.154	Yes	1.148	0.364	0.985	Yes	1.431	0.443	1.463	Yes
A_10_0.25	0.713	0.051	0.763	Yes	1.070	0.073	1.094	Yes	0.998	0.305	0.933	Yes	1.154	0.328	1.386	Yes
Base_B	1.054	0.051	1.050		1.380	0.433	1.380		1.360	0.078	1.360		1.860	0.629	1.860	
B_5_1.18	0.987	0.042	0.998	Yes	1.410	0.426	1.311	Yes	1.270	0.036	1.292	Yes	1.740	0.55	1.767	Yes
B_10_1.18	0.971	0.036	0.945	Yes	1.310	0.533	1.242	Yes	1.300	0.409	1.224	Yes	1.720	0.517	1.674	Yes
B_5_2.36	0.976	0.037	0.998	Yes	1.380	0.415	1.311	Yes	1.300	0.392	1.292	Yes	1.750	0.113	1.767	Yes
B_10_2.36	0.912	0.053	0.945	Yes	1.310	0.423	1.242	Yes	1.250	0.378	1.224	Yes	1.710	0.519	1.674	Yes
Pearson Correlation between I_M and Ic for Group A and B																
0.97																
Binder ID	100°C and 20 Hours				100°C and 40 Hours				110°C and 20 Hours				110°C and 40 Hours			
	I_M	SD	Ic	C	I_M	SD	Ic	C	I_M	SD	Ic	C	I_M	SD	Ic	C
Base_C	0.968	0.125	0.970		1.370	0.045	1.370		1.300	0.125	1.300		1.750	0.125	1.750	
C_20_2.36	0.893	0.072	0.838	Yes	1.040	0.115	1.158	No	1.090	0.170	1.102	Yes	1.220	0.072	1.462	No
Base_D	0.892	0.125	0.970		N/A	N/A	N/A		N/A	N/A	N/A		N/A	N/A	N/A	
D_20_2.36	0.798	0.043	0.838	Yes	1.190	0.055	N/A	N/A	1.010	0.043	N/A	N/A	1.400	0.043	N/A	N/A

SD= standard deviation of the measured index (I_M).

C= testing criterion to check whether the calculated index (I_C) is within one standard deviation of the measured index or not.

Yes and NO = it is "Yes" if Ic is within one standard deviation of I_M. Otherwise, it is "No".

Figure 5.14 shows the changes in the SUL index with PAV-aging. Figure 5.14a shows that this index had an overall increasing trend with increasing aging time when binders were PAV-aged at 100°C. When the PAV-aging temperature was increased to 110°C, the Base_A binder had a lower SUL index at 40 hours than at 20 hours. Similar findings were shown in Figure 4.10 that the development of sulfoxide components appeared to terminate during the long PAV-aging protocols. Morian et al. *(103)* and Peterson et al. *(104)* also suggested that the sulfoxide component was mostly produced in the early aging stage. Therefore, the SUL index was not necessarily consistent with the PAV-aging protocol, which increased the complexity of the analysis.

Table 5.16 shows the comparison between measured SUL indices and the calculated SUL indices using Equation 5.4. For Group A binders, the rubber-modified binders had higher SUL indices than the Base_A binder after PAV-aging at 100°C. When the PAV-aging temperature was increased to 110°C, the A_5_0.25 binder had similar SUL indices to the Base_A binder, while the A_10_0.25 binder had lower SUL indices than the Base_A binder.

The Base_B and Base_C binders had higher SUL indices after 40 hours of PAV-aging than at 20 hours. Adding rubber reduced the accumulation of sulfoxide components, as shown in Figure 5.14b and Figure 5.14c. The rubber-modified binders had lower SUL indices after PAV-aging, and this trend was more apparent for the rubber-modified binders containing 20 percent rubber in Groups C and D, indicating that adding a higher amount of rubber could decrease the amount of the sulfoxide component developed during aging.
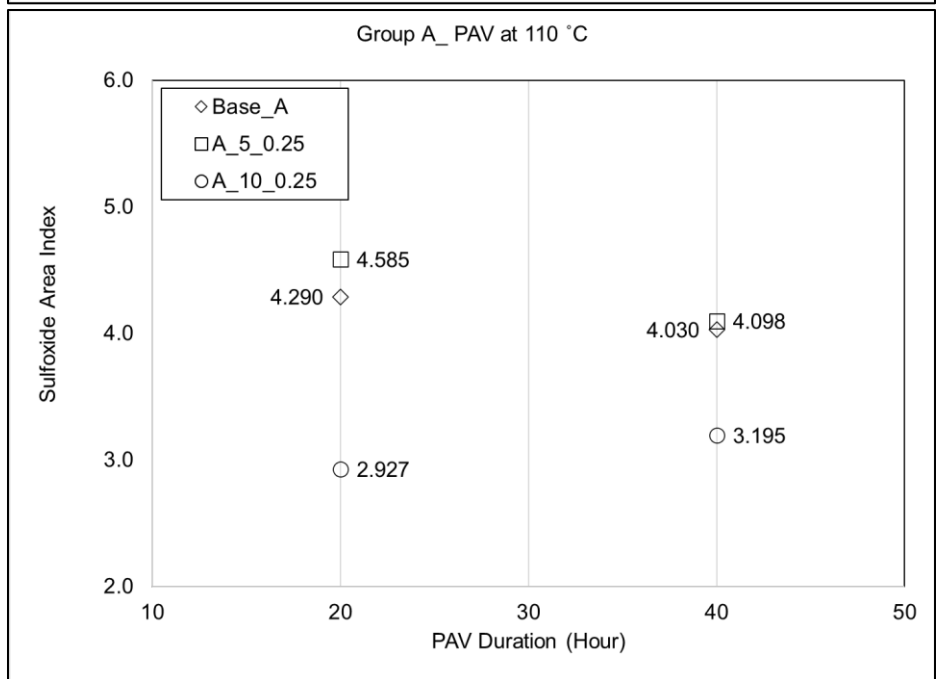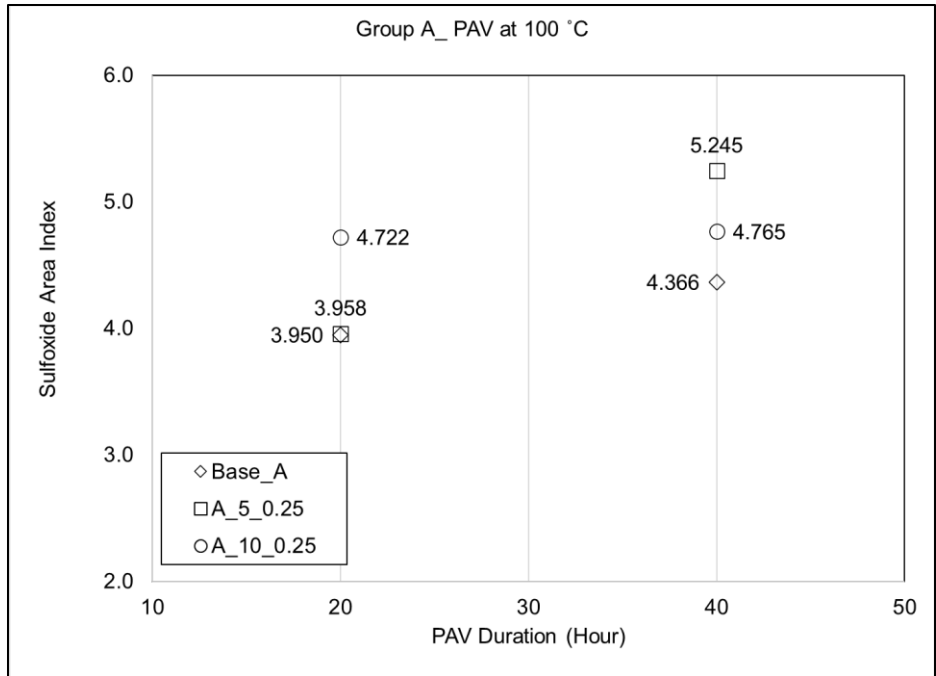
Group A_ PAV at 100 ˚C

Group A_ PAV at 110 ˚C

a: Group A (Binder ID format: source_rubber content in percent_maximum rubber size in mm)
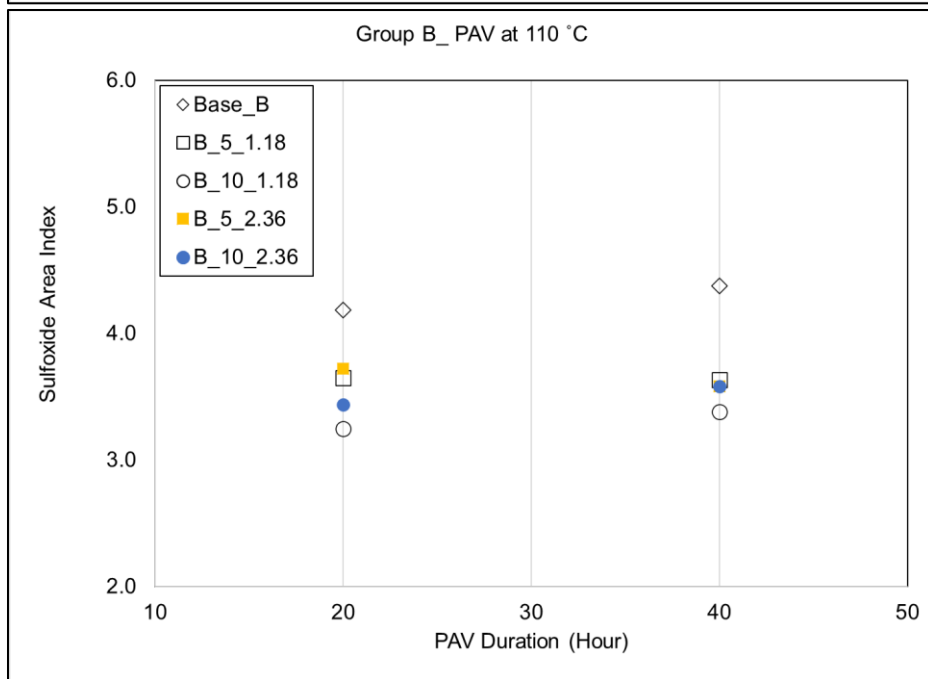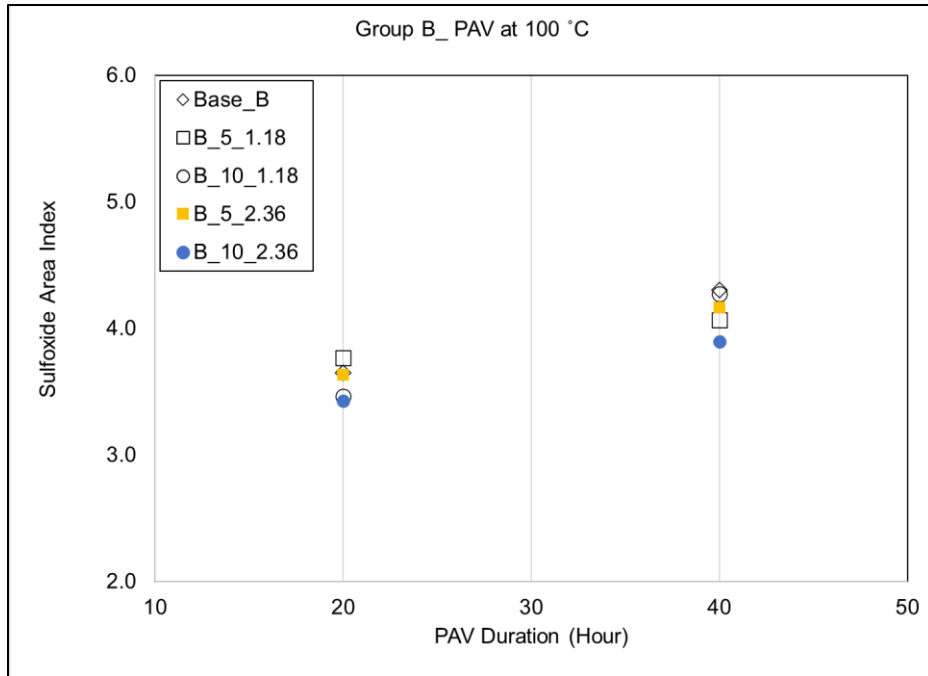
b: Group B (Binder ID format: source_rubber content in percent_maximum rubber size in mm)
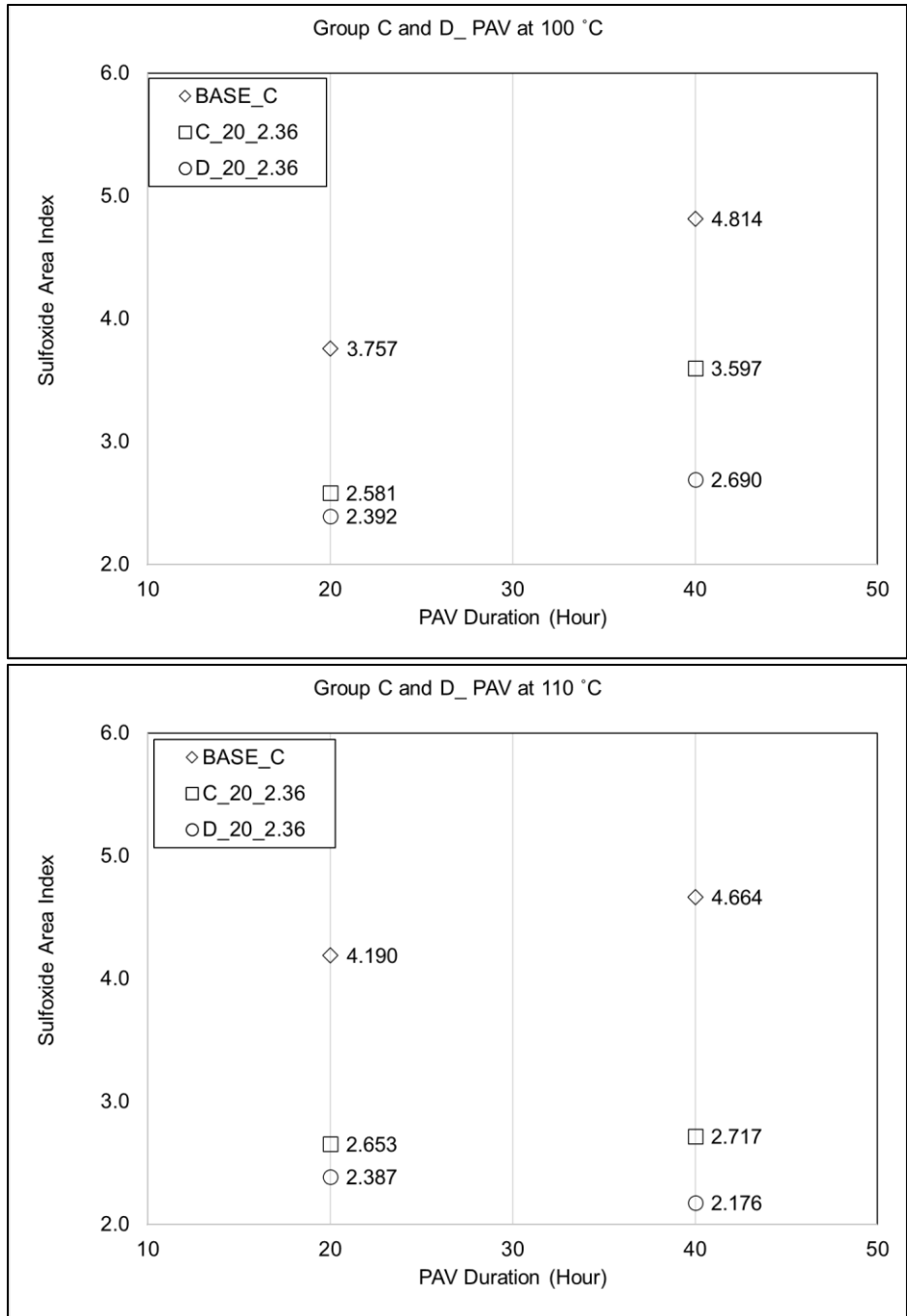
c: Group C (Binder ID format: source_rubber content in percent_maximum rubber size in mm)

Figure 5.14: Evolution of SUL indices along with exposure durations for base and rubber-modified binders.

Table 5.16 shows that the calculated SUL indices were not always within one standard deviation

of the measured SUL indices, and the Pearson correlation between measured and calculated SUL

indices for Groups A and B binders was only 0.42. This indicated that the dilution hypothesis was

not valid for the SUL index after PAV-aging. The chemical interaction between the rubber and the binder changed the sulfoxide components in rubber-modified binders after PAV-aging. Although using the FTIR test could not identify the chemical interaction, the data shown in Figure 5.14 and Table 5.16 indicated that increasing the rubber content generally decreased the sulfoxide components in rubber-modified binders after PAV-aging beyond the reduction that could be explained by dilution.

Table 5.16: Comparison of Sulfoxide Area Index after PAV-Aging

Binder ID	100°C and 20 Hours				100°C and 40 Hours				110°C and 20 Hours				110°C and 40 Hours			
	I_M	SD	Ic	C	I_M	SD	Ic	C	I_M	SD	Ic	C	I_M	SD	Ic	C
Base_A	4.216	0.045	4.216		4.370	0.366	4.370		4.290	0.318	4.290		4.030	0.259	4.030	
A_5_0.25	3.958	0.038	4.027	No	5.240	0.602	4.174	No	4.590	0.137	4.098	No	4.100	0.177	3.851	No
A_10_0.25	3.896	0.161	3.839	Yes	4.770	0.077	3.977	No	2.930	0.080	3.905	No	3.190	0.095	3.671	No
Base_B	3.651	0.036	3.651		4.300	0.433	4.300		4.190	0.078	4.190		4.370	0.629	4.370	
B_5_1.18	3.766	0.089	3.491	No	4.070	0.426	4.107	Yes	3.650	0.036	4.003	No	3.630	0.550	4.174	Yes
B_10_1.18	3.465	0.337	3.330	Yes	4.272	0.533	3.914	Yes	3.246	0.409	3.815	No	3.383	0.517	3.977	No
B_5_2.36	3.634	0.091	3.494	No	4.166	0.415	4.110	Yes	3.720	0.392	4.006	Yes	3.582	0.113	4.177	No
B_10_2.36	3.428	0.195	3.336	Yes	3.898	0.423	3.920	Yes	3.436	0.378	3.821	No	3.584	0.519	3.983	Yes
Pearson Correlation between I_M and Ic for Group A and B																
0.42																
Binder ID	100°C and 20 Hours				100°C and 40 Hours				110°C and 20 Hours				110°C and 40 Hours			
	I_M	SD	Ic	C	I_M	SD	Ic	C	I_M	SD	Ic	C	I_M	SD	Ic	C
Base_C	3.757	0.132	3.757		4.814	0.693	4.814		4.190	0.048	4.190		4.664	0.123	4.664	
C_20_2.36	2.581	0.268	3.254	No	3.597	0.174	4.099	No	2.653	0.094	3.600	No	2.717	0.312	3.979	No
Base_D	3.802	0.099	3.802		N/A	N/A	N/A		N/A	N/A	N/A		N/A	N/A	N/A	
D_20_2.36	2.392	0.106	3.290	No	2.690	0.055	N/A	N/A	2.387	0.043	N/A	N/A	2.176	0.043	N/A	N/A

SD= standard deviation of the measured index (I_M).

C= testing criterion to check whether the calculated index (I_C) is within one standard deviation of the measured index or not.

Yes and NO = it is "Yes" if Ic is within one standard deviation of I_M. Otherwise, it is "No".

Figure 5.15 shows the change in butadiene area index for the different aging protocols. The butadiene area indices generally increased with increasing rubber content. Increasing the rubber particle size did not significantly change the butadiene area index, as shown in Figure 5.15b because the FTIR can quantitatively analyze the rubber content, but it could not determine the rubber particle sizes. Increasing the temperature or aging duration did not show a significant change in the butadiene area index other than random fluctuations, indicating that the rubber content in the rubber-modified binder was constant after different PAV-aging procedures.

Figure 5.15 shows that the butadiene area indices in base binders were close to zero after PAV-aging at the different temperatures and durations. Comparing the rubber-modified binders to their corresponding base binders confirmed that adding rubber increased the butadiene component measured in rubber-modified binders.

The Group B binder results showed that butadiene area indices of the fine rubber gradations (≤1.18 mm) were not significantly different to those of the coarse gradations (≤2.36 mm) under the same aging condition owing to the fact that the FTIR cannot distinguish rubber particle size. Reducing the rubber particle size does not change the chemical component structure in the rubber. The component structure in different rubber particles reflects the same distinctive wave of the incident radiation that can be measured by FTIR *(108)*.
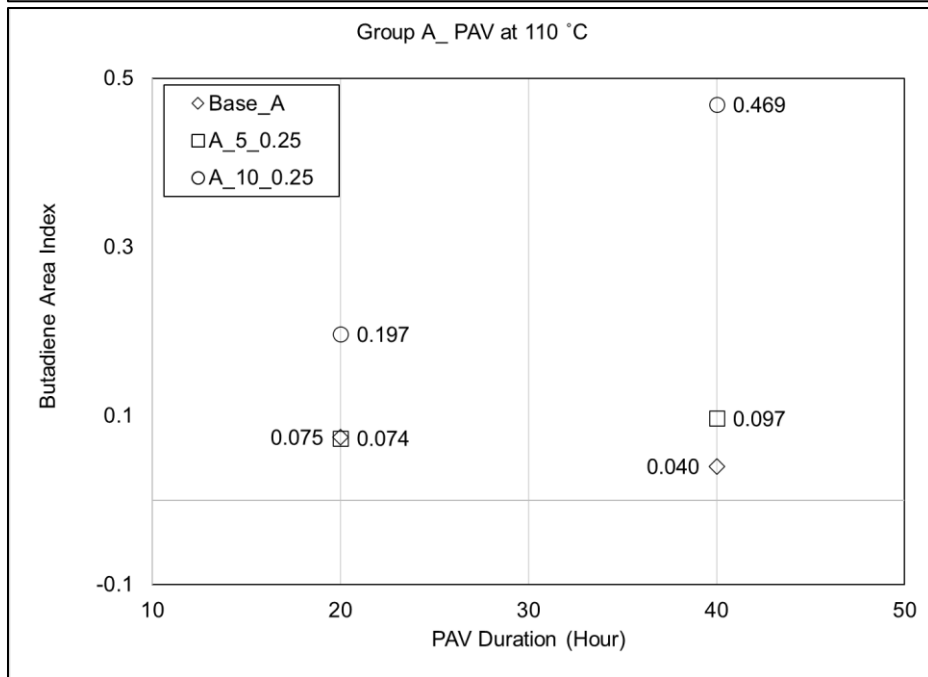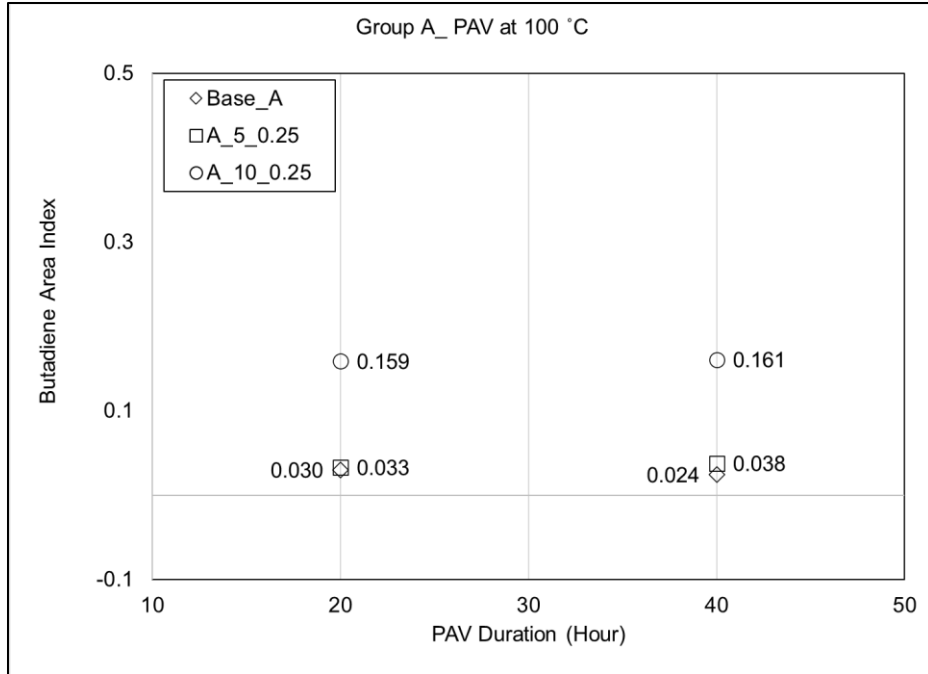
a: Group A (Binder ID format: source_rubber content in percent_maximum rubber size in mm)
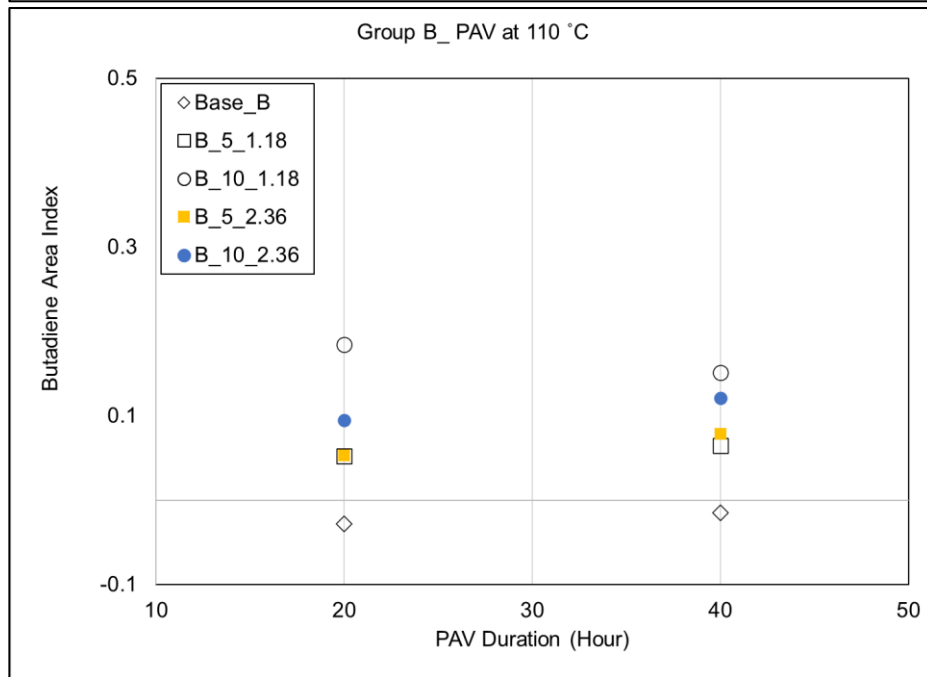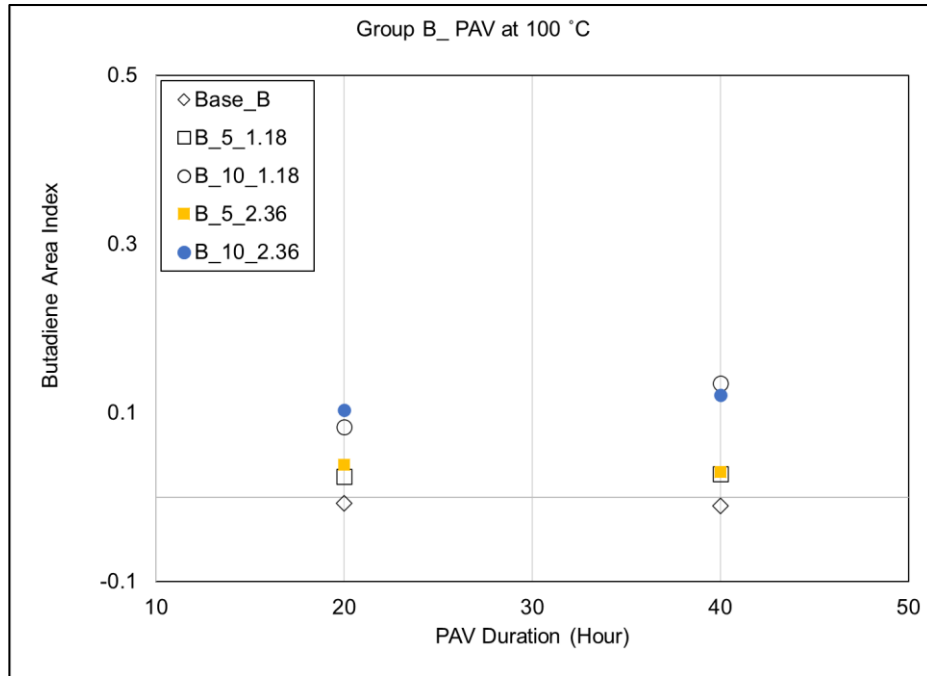
b: Group B (Binder ID format: source_rubber content in percent_maximum rubber size in mm)
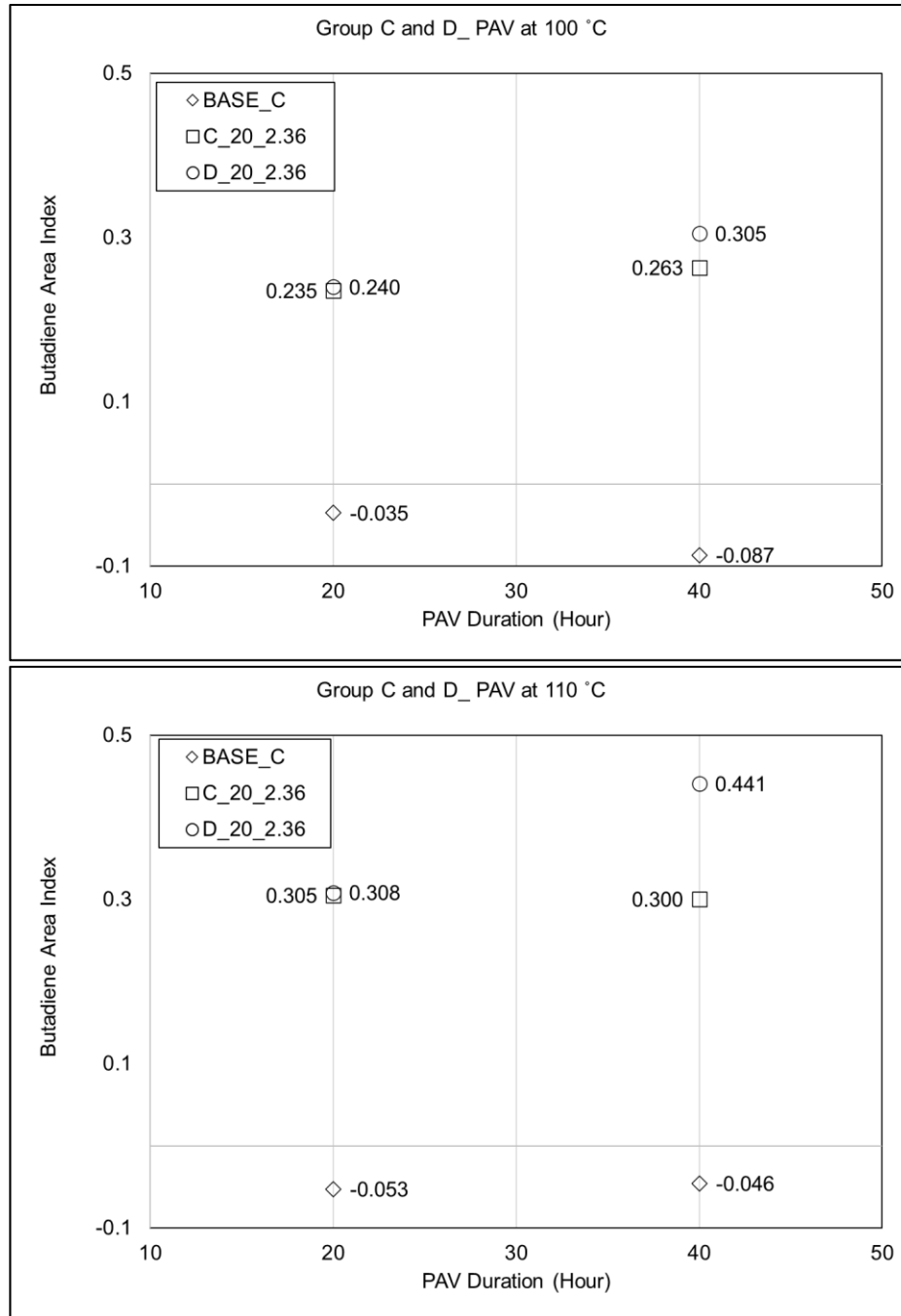
c: Group C and Group D (Binder ID format: source_rubber content in percent_maximum rubber size in mm)
Figure 5.15: Evolution of butadiene area indices along with exposure durations for base and rubber-modified binders.

Table 5.17 shows that the calculated butadiene area indices generally were not within the one standard deviation of the measured butadiene area indices. Increasing the rubber content resulted

in higher than calculated butadiene area indices based on the dilution hypothesis. This finding was consistent with that in Section 5.3.6, which was caused by the potentially biased integration of the butadiene area index.

Table 5.17: Comparison of Butadiene Area Index after PAV-Aging

Binder ID	100°C and 20 Hours				100°C and 40 Hours				110°C and 20 Hours				110°C and 40 Hours			
	I_M	SD	Ic	C	I_M	SD	Ic	C	I_M	SD	Ic	C	I_M	SD	Ic	C
Base_A	0.030	0.012	0.030		0.020	0.010	0.020		0.070	0.028	0.070		0.040	0.019	0.040	
A_5_0.25	0.033	0.012	0.041	Yes	0.040	0.033	0.031	Yes	0.070	0.021	0.079	Yes	0.097	0.021	0.050	No
A_10_0.25	0.159	0.006	0.051	No	0.161	0.017	0.042	No	0.197	0.018	0.087	No	0.469	0.022	0.060	No
Base_B	-0.007	0.014	0		-0.010	0.024	0		-0.028	0.037	0		-0.015	0.016	0	
B_5_1.18	0.025	0.008	0.012	No	0.027	0.019	0.012	Yes	0.052	0.032	0.012	No	0.065	0.033	0.012	No
B_10_1.18	0.083	0.021	0.024	No	0.135	0.056	0.024	No	0.185	0.023	0.024	No	0.151	0.047	0.024	No
B_5_2.36	0.039	0.012	0.013	No	0.030	0.015	0.013	No	0.053	0.024	0.013	No	0.078	0.03	0.013	No
B_10_2.36	0.103	0.019	0.026	No	0.121	0.033	0.026	No	0.095	0.032	0.026	No	0.121	0.014	0.026	No
Pearson Correlation between I_M and Ic for Group A and B																
0.50																
Binder ID	100°C and 20 Hours				100°C and 40 Hours				110°C and 20 Hours				110°C and 40 Hours			
	I_M	SD	Ic	C	I_M	SD	Ic	C	I_M	SD	Ic	C	I_M	SD	Ic	C
Base_C	-0.035	0.023	0		-0.087	0.036	0		-0.053	0.021	0		-0.046	0.0197	0	
C_20_2.36	0.235	0.014	0.051	No	0.236	0.083	0.051	No	0.305	0.095	0.051	No	0.300	0.091	0.051	No
Base_D	-0.032	0.020	0		N/A	N/A	N/A		N/A	N/A	N/A		N/A	N/A	N/A	
D_20_2.36	0.240	0.020	0.051	No	0.305	0.055	N/A	N/A	0.308	0.043	N/A	N/A	0.441	0.043	N/A	N/A

SD= standard deviation of the measured index (I_M).

C= testing criterion to check whether the calculated index (I_C) is within one standard deviation of the measured index or not.

Yes and NO = it is "Yes" if Ic is within one standard deviation of I_M. Otherwise, it is "No".

5.4.3 Application of the GHS Model in Rubber-Modified Binders

Section 5.4.1 shows that the carbonyl component accumulated continuously in the rubber-modified binders during PAV-aging, while the sulfoxide component did not. The accumulations of the carbonyl component in the rubber-modified binders were similar to those of their corresponding base binders regardless of rubber content (range between 5 and 35 percent) and particle size (range between ≤250 microns and ≤2.36 mm), but at a lower rate. On the other hand, the level of increase in the butadiene component corresponded with increasing rubber content. These observations indicated that adding rubber decreased the carbonyl components and increased the butadiene components in rubber-modified binders.

Considering that the rubber itself did not contain carbonyl components, the GHS principle could still be applied to these rubber-modified binders as along as the linearity between ln (η) and CA index for the rubber-modified binder is valid. This section aims to verify the possibility of applying the GHS principle to rubber-modified binders.

The viscosities of the rubber-modified binders were backcalculated from the frequency sweep test data using Equation 4.9. The parallel plate geometry was then used to measure the rheology of the rubber-modified binders produced with fine rubber gradations (≤250 microns [passing the #60 sieve]), while the concentric cylinder geometry was used for rubber-modified binders with the coarse rubber gradations (≤2.36 mm [passing the #8 sieve]).

The testing temperatures were 20°C, 40°C, 60°C, and 85°C, and the loading frequency was between 0.0159 Hz and 15.9 Hz (0.1 radians/second and 100 radians/second). The Group A binders and the base binders in Group B and Group C were Superpave performance-gradable with the parallel plate geometry. The PP-25 geometry with a 1-mm gap with a constant strain of 1

percent was used for testing at higher temperatures (60°C and 85°C). The PP-8 geometry with a 2-mm gap with a constant strain of 0.1 percent was used for testing at intermediate temperatures (20°C and 40°C).

The concentric cylinder geometry was used to test rubber-modified binders in Group B, Group C, and Group D. The CC-17 geometry with a strain of 1 percent was used for testing at 60°C and 85°C. The CC-10 geometry with a strain of 0.1 percent was used for testing at 20°C and 40°C.

The data obtained during the testing discussed in Section 5.4.1 provided the CA indices data for validating the GHS principle. The linearity assumption was inspected by calculating the coefficient of determination (R^2) between the $\ln(\eta)$ and the CA index at each combination of temperature and loading frequency. The calculation methodology was the same as that presented in Figure 4.18. Figure 5.16 shows an example of the determination of R^2 for the A_5_0.25 binder at 20°C and 15.9 Hz (100 radians/second). The R^2 value was 0.9 for this case, indicating that the GHS principle was reasonable for this binder at this condition.
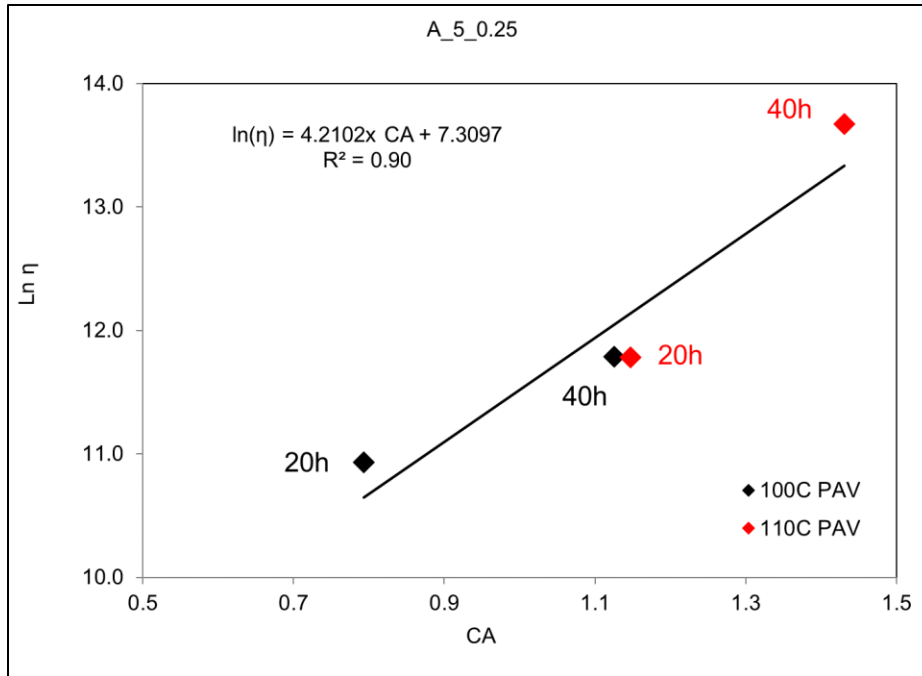
Figure 5.16: Example of determining the linearity between the ln(η) and CA index for rubber-modified binders.

Figure 5.17 summarizes the R^2 values for the Group A binders. The red symbol in Figure 5.17 represents the example case shown in Figure 5.16. Figure 5.17 shows that the linearity assumption between ln(η) and CA was valid for binders in Group A. The R^2 values were higher than the 0.7 threshold, which was the same criterion used for evaluating the unmodified binders discussed in Chapter 4 *(135,146,147)*.

Figure 5.17 also indicates that the base binder appeared to have better linearity between ln(η) and CA than the rubber-modified binders produced with it. One explanation was that rubber particles appeared to affect the accuracy of the frequency sweep test since the rubber-modified binder was difficult to trim in the parallel plate geometry. Nevertheless, this reduced linearity was still within the acceptable range for the linearity determination (over the 0.7 threshold). The GHS model was therefore considered applicable for the rubber-modified binders tested in Group A.
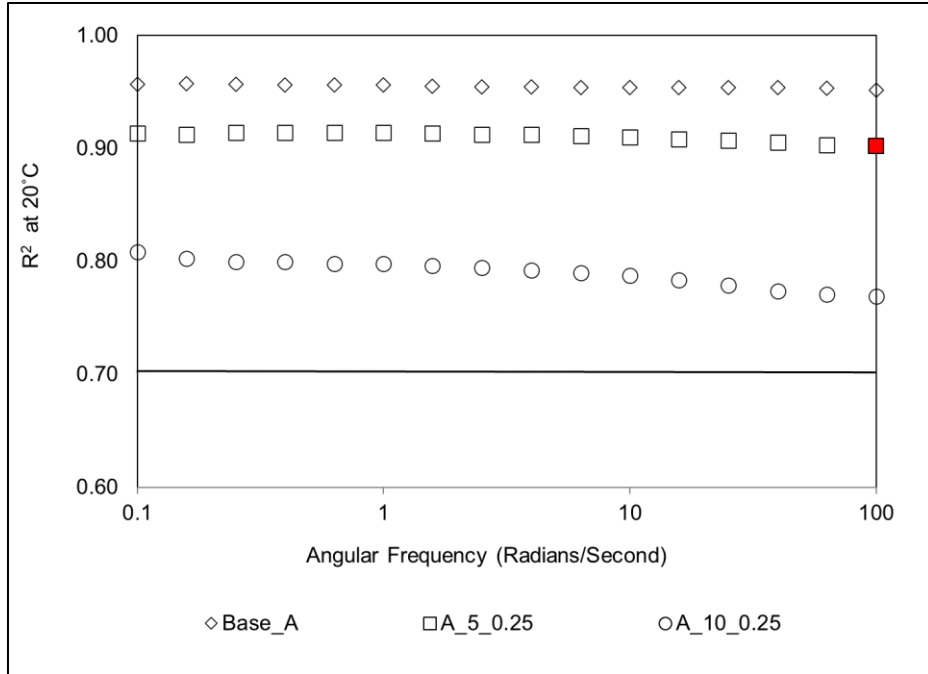
a: 20˚C (red symbol presents the sample R^2 value shown in Figure 5.19)

b: 40˚C

215
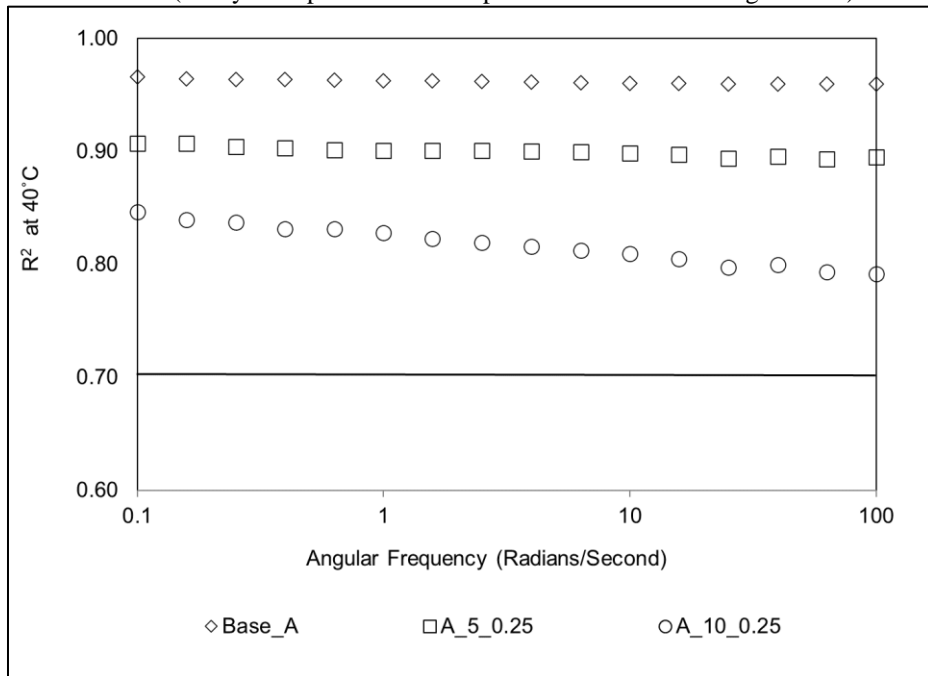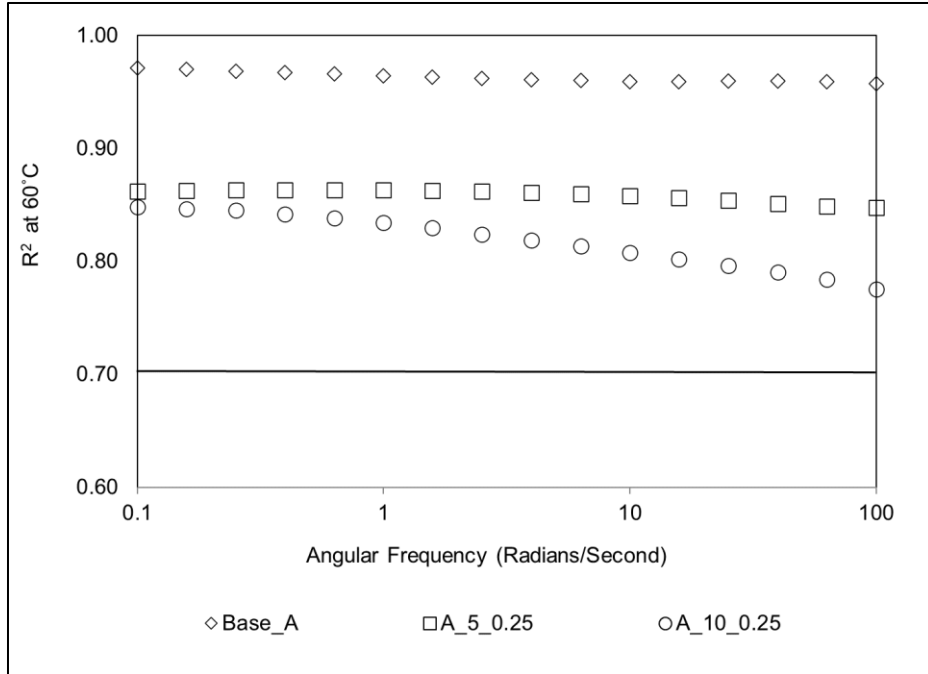
c: 60˚C
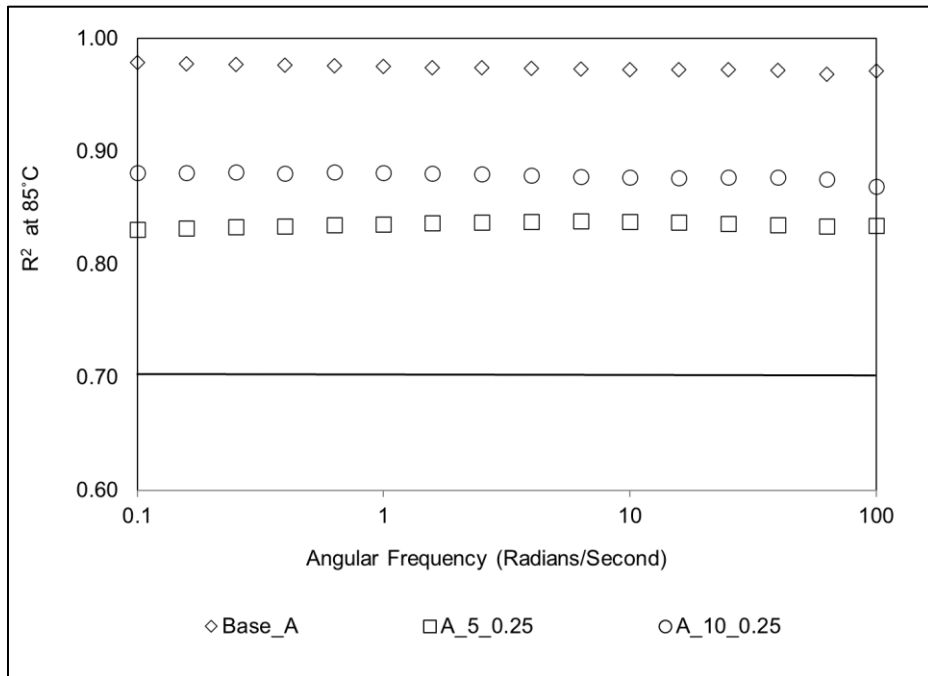
d: 85˚C

Figure 5.17: Linearity between the ln(η) and CA index of rubber-modified binders in Group A.

Figure 5.17 also shows that increasing the temperature and decreasing the angular frequency could increase R^2 values. The linearity was more significant at a high temperature and a lower loading frequency, where the viscosity dominated the binder properties rather than the elasticity.

Figure 5.18 plots R^2 values for the binders in Group B. These R^2 values were all higher than the 0.7 threshold line. There was no significant difference between the rubber-modified binders containing five percent rubber and those containing ten percent rubber by weight of the binder.

In Group B, the R^2 values of the rubber-modified binders were higher than the base binder at the intermediate testing temperatures (20°C and 40°C), which was opposite to the results for the Group A binders. This was attributed to the improved accuracy of the rheological measurement. No trimming was needed for the concentric cylinder geometry, which improved the measurement accuracy for the rubber-modified binders, compared to the Group A binders, which required trimming prior to testing in the parallel plate geometry. The R^2 values were randomly distributed after increasing the rubber content and rubber particle size. This random distribution indicated that adding the rubber should not impede the linearity between the $\ln(\eta)$ and CA index.

Another observation from the Group B binder results was that changes of R^2 values along with the angular frequency were less smooth than those in Group A. This observation was obvious for the data at 20˚C. It was found that the inaccurate measurement of phase angle was the primary reason for these variabilities of R^2 values. The rubber-modified binder was relatively stiff at this relatively low temperature, resulting in the DSR applying a high torque to provide the necessary shear stress to reach the defined shear strain. This high torque could overwhelm the friction between the cylinder wall and the DSR housing, which created a slight movement of the cylinder itself that diminished the accuracy of the measured phase angle.
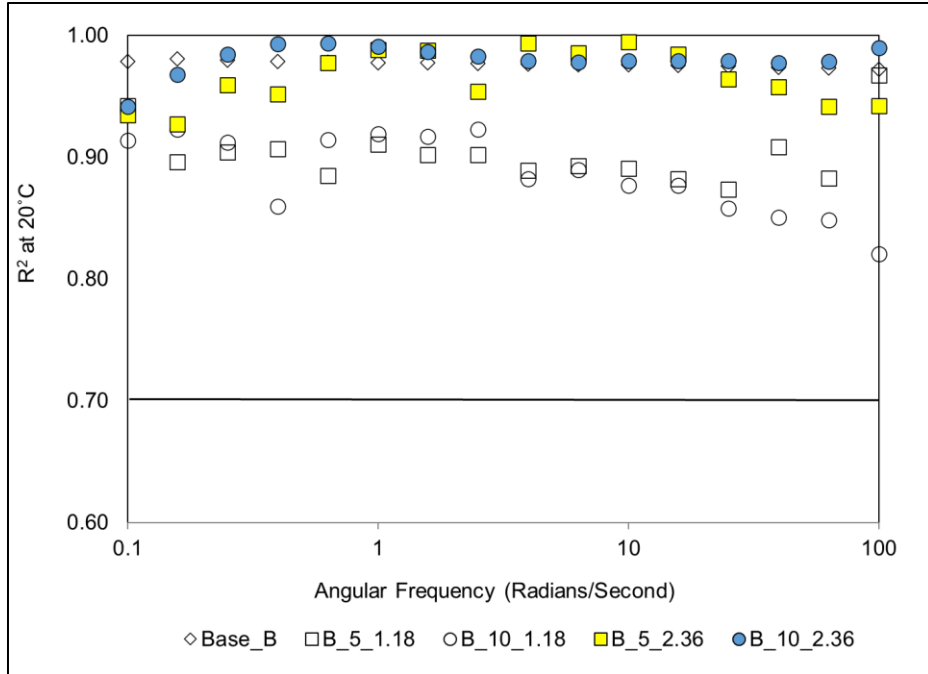
a: 20˚C
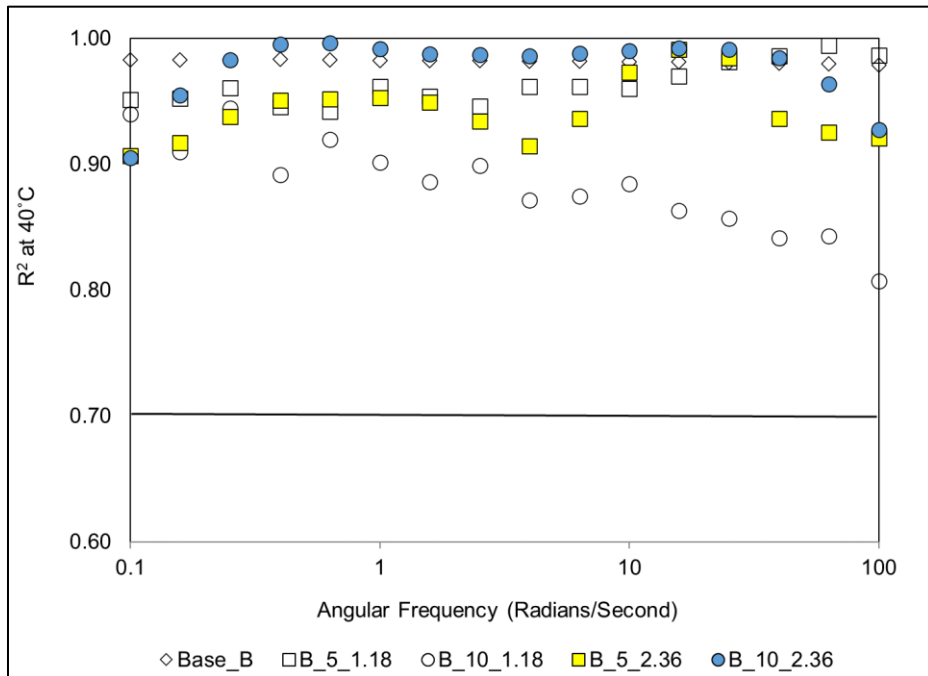
b: 40˚C
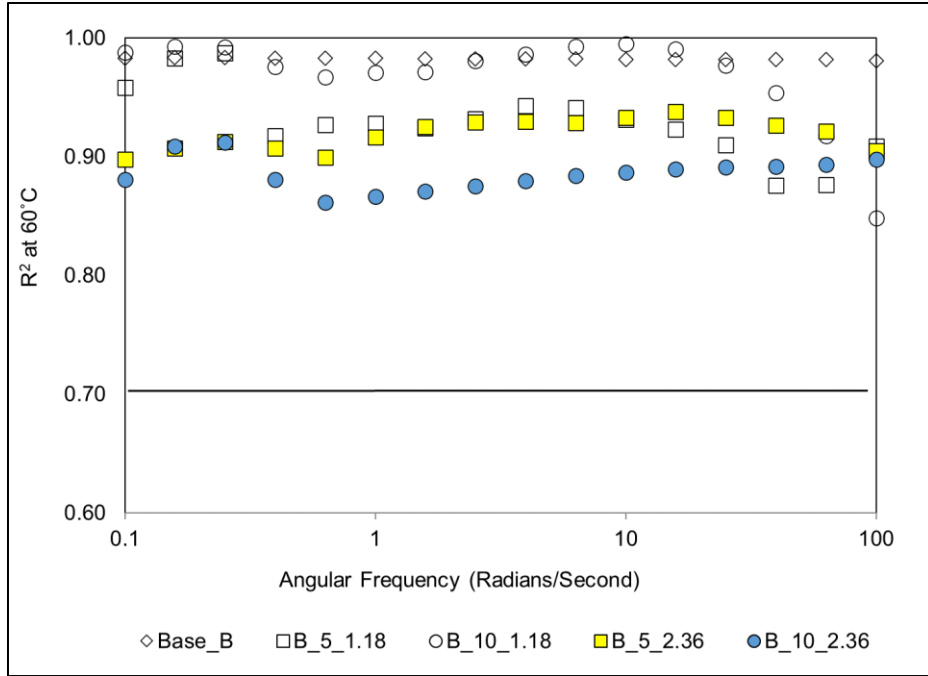
c: 60°C
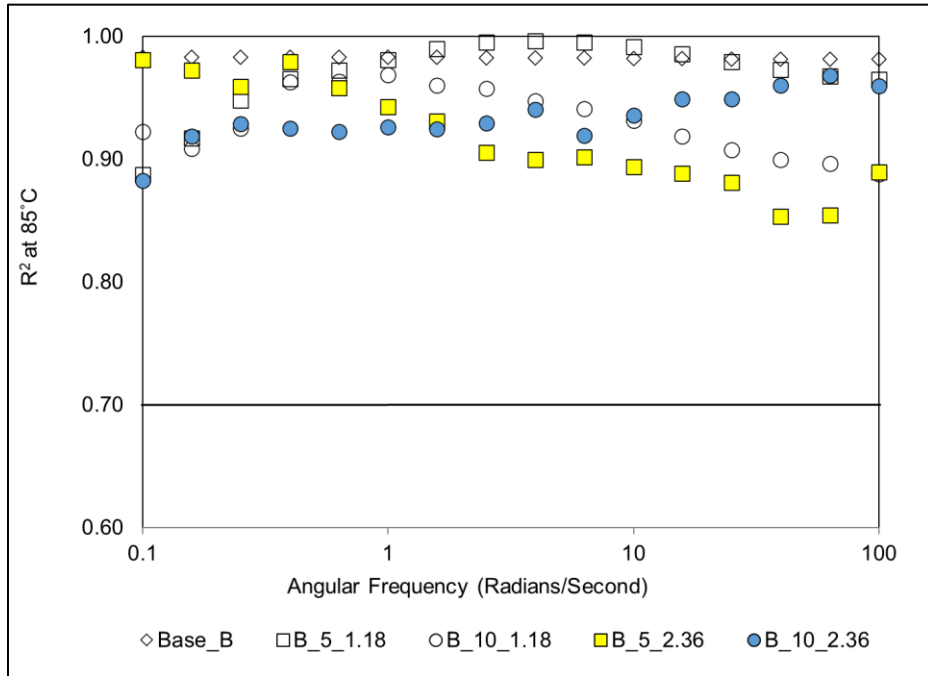
d: 85°C

Figure 5.18: Linearity between ln(η) and CA index of rubber-modified binders in Group B.

The shear strain used for testing binders in Groups C and D was, therefore, reduced to 0.01 percent to avoid inaccurate measurements caused by the movement of the cylinder during testing, as

observed during testing of the Group B binders. This test strain was still within the linear viscoelastic region of the binder. Figure 5.19 shows the R^2 values for binders in Group C and Group D.

Figure 5.19 shows the results were smoother along with the angular frequency than the tests under the 0.1 percent strain, shown in Figure 5.18. The generally high R^2 values indicated that the $\ln(\eta)$ and CA index were linearly correlated for the rubber-modified binders containing 20 percent rubber with particles smaller than 2.36 mm. Comparing the R^2 values between rubber-modified binders to the base binder showed that adding the rubber did not impair this linearity.
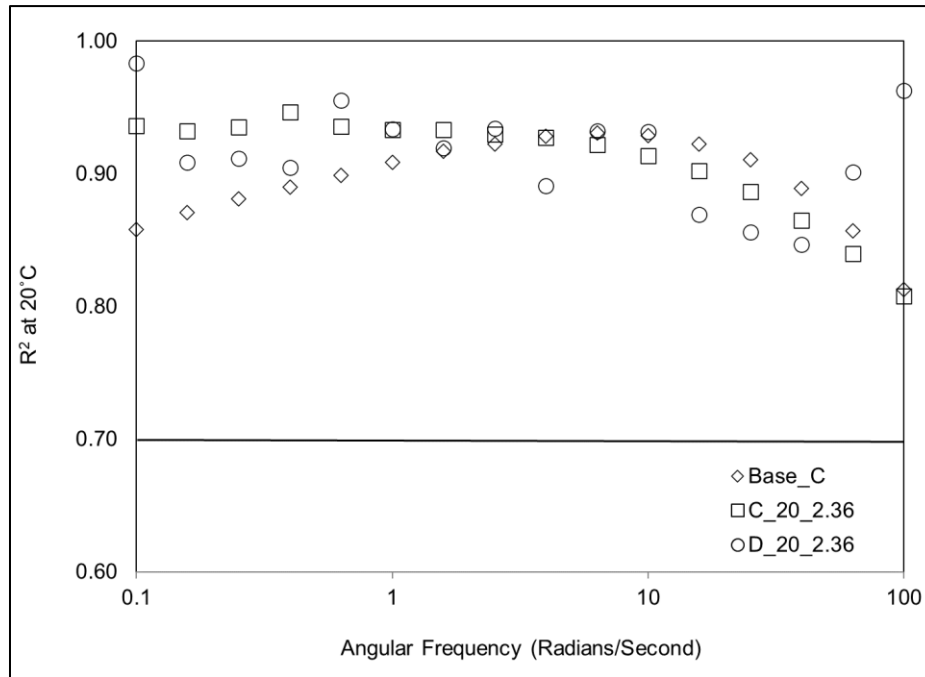
a: 20˚C
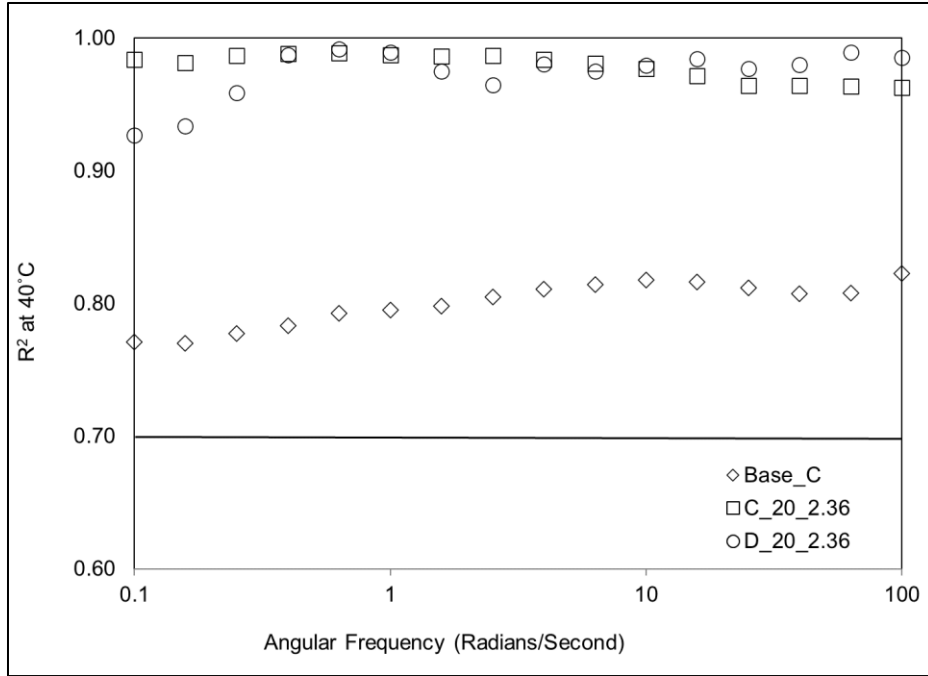
b: 40˚C
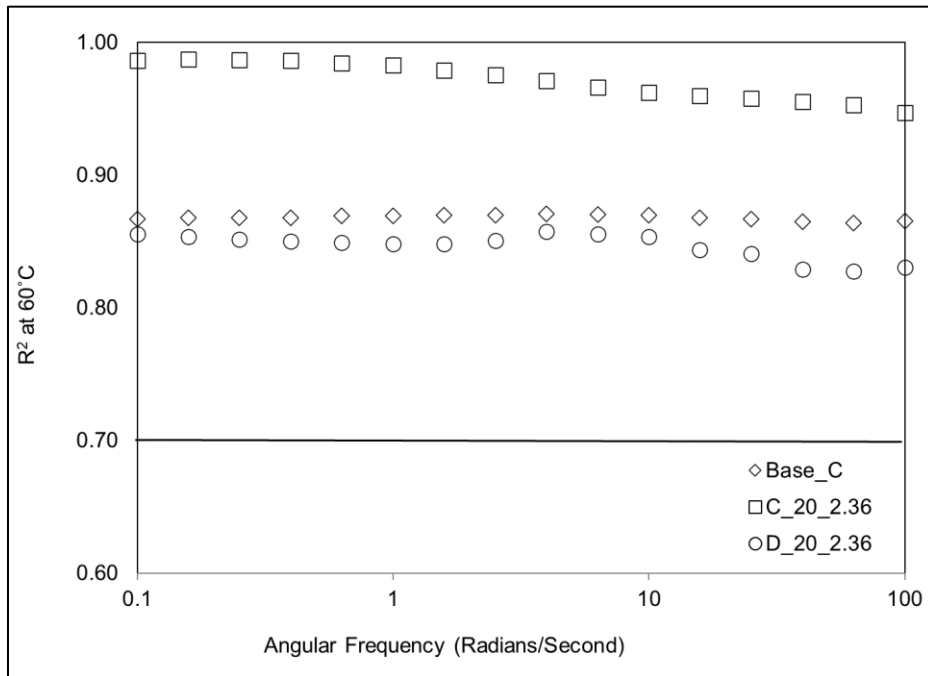
c: 60˚C
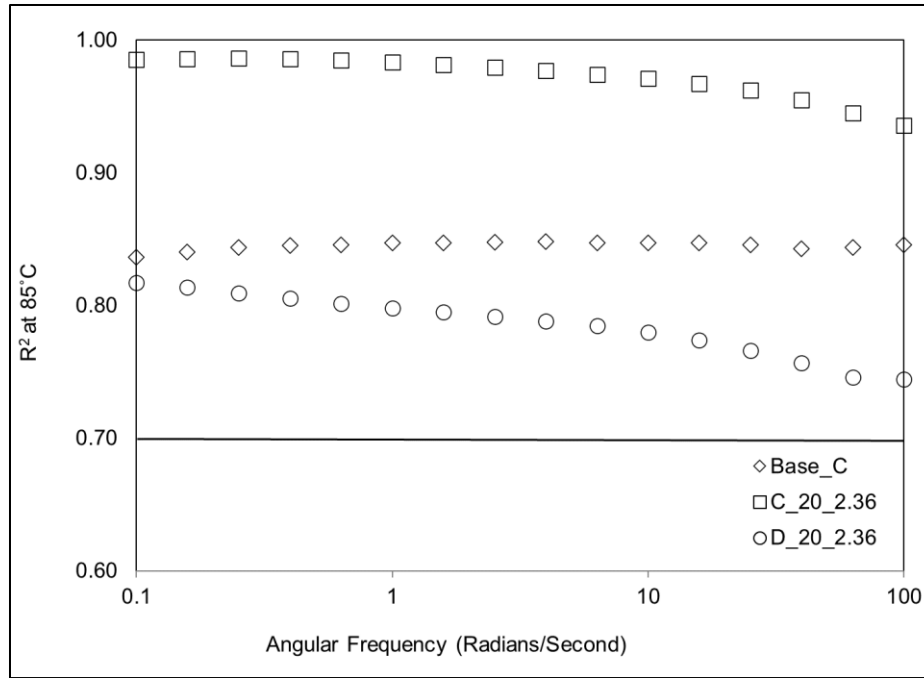
d: 85˚C

Figure 5.19: Linearity between ln(η) and CA index of rubber-modified binders in Group C and Group D.

The above test results indicated that the linearity assumption between ln(η) and CA was valid for the rubber-modified binders tested in this study. Therefore, the GHS principle was considered appropriate for predicting the viscosity changes in rubber-modified binders after PAV-aging.

5.4.4   Validation of the GHS Model for Rubber-Modified Binders

Figure 5.20 compares the measured viscosities to the GHS model-predicted viscosities for rubber-modified binders. These data were based on a series of tests including four PAV-aged conditions, four testing temperatures (20°C, 40°C, 60°C, and 85°C), and 16 testing frequencies (between 0.0159 Hz and 15.9 Hz [0.1 and 100 radians/second]) for a total of 256 data points for each binder.

The coefficients of determination were all above 0.95 at the testing temperatures and frequencies. The data points were located around the equilibrium line (1:1 ratio line), and the offsets were randomly distributed along this line. These observations indicated that the GHS model could

accurately predict the viscosities of PAV-aged rubber-modified binders using the CA indices and the GHS parameters.
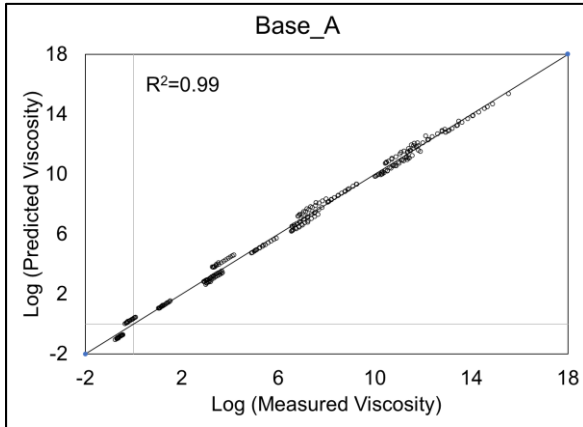
a: Base_A
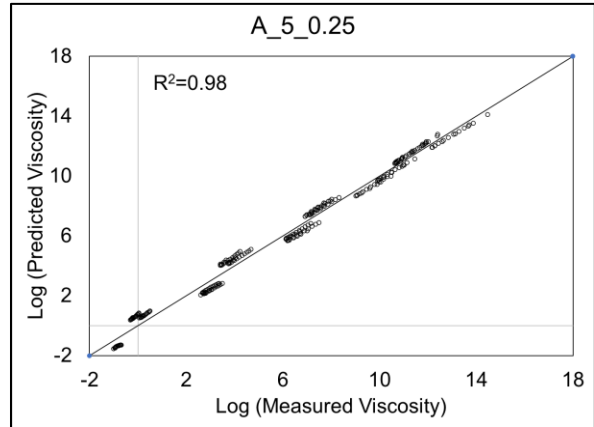
b: A_5_0.25
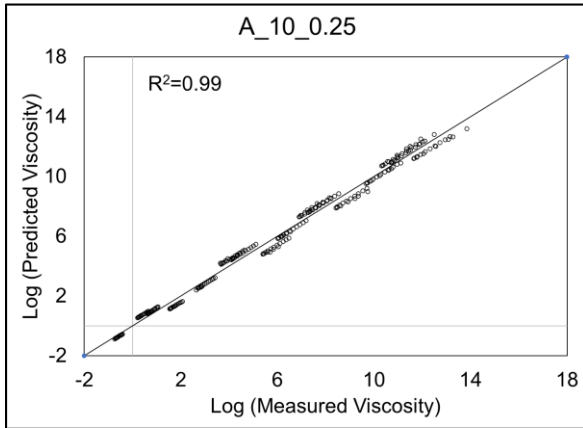
c: A-10_0.25

d: Base_B

e: B_5_0.60

f: B_10_0.60

g: B_5_2.36

h: B_10_2.36

i: Base_C

j: C_20_2.36

k: D_20_2.36
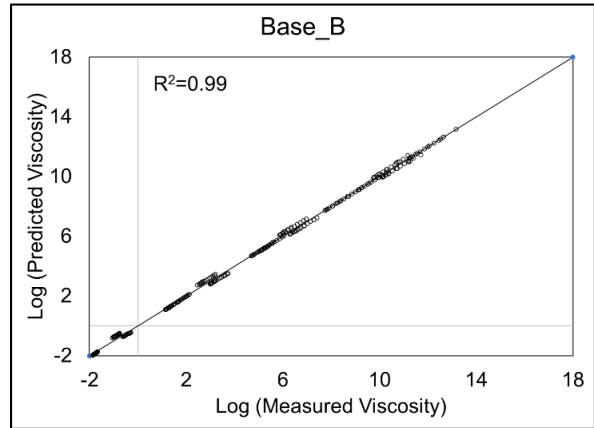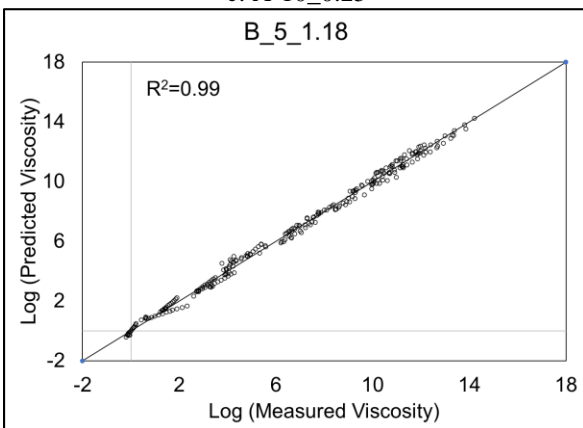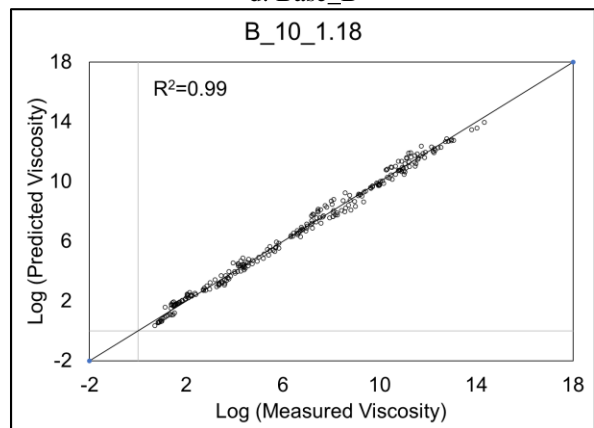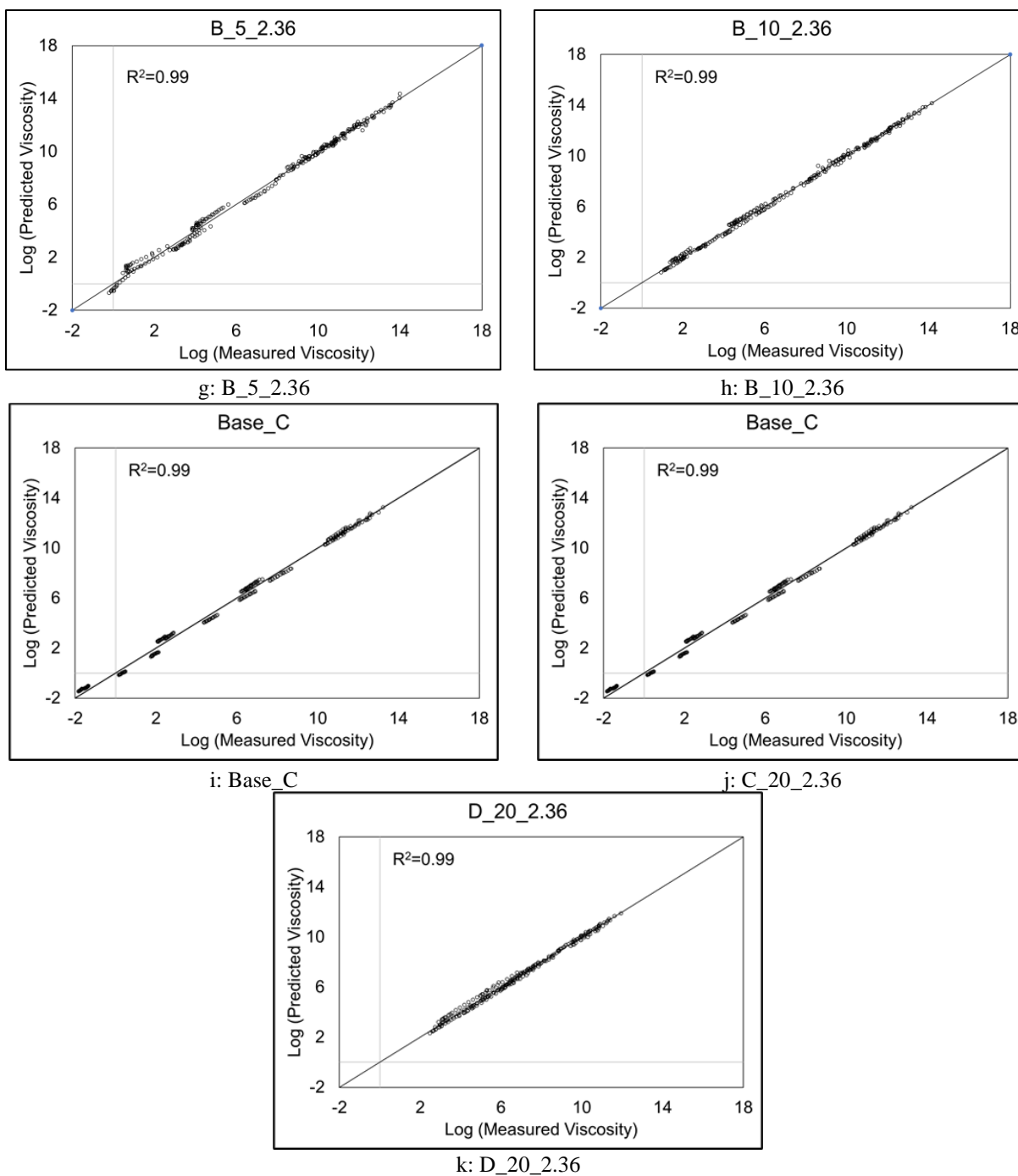
Figure 5.20: Validation of the GHS model under tested conditions.

Figure 5.20 also shows that the minimum viscosities of the rubber-modified binders were higher

than those of their corresponding base binders, while the maximum viscosities were almost the

same. These observations indicated that the viscosity of rubber-modified binder was less susceptible to temperature changes after PAV-aging.

The prediction error of the GHS model is summarized in Table 5.18. The percentage error was calculated by dividing the measured logarithmic viscosity by the prediction error. The average percentage error and its standard deviation for each binder type were also calculated.

Table 5.18: Summary of Prediction Error Using the GHS Model

Binder ID	Average Percentage Error (%)	Standard Deviation of the Error (%)
Base_A	7.8	8.1
A_5_0.25	7.8	10.9
A_10_0.25	8.3	11.5
Base_B	8.8	12.1
B_5_1.18	5.2	4.2
B_10_1.18	5.4	4.6
B_5_2.36	8.3	11.6
B_10_2.36	3.3	2.5
Base_C	8.9	8.5
C_20_2.36	2.0	0.1
D_20_2.36	3.0	0.3
p-value (tested between base binders and rubber-modified binders)		
p-value	0.07	0.23

Table 5.18 shows that the maximum prediction error of rubber-modified binders was 8.3 percent, which was lower than that of the base binder (8.9 percent). Similarly, the maximum standard deviation of the error for rubber-modified binders was lower than that of the base binder. An ANOVA analysis of these criteria (average percentage error and standard deviation of the error) shows that the predictions for base binders and rubber-modified binders were not significantly different from each other (p-value>0.05). This statistical analysis indicated that the GHS model was capable of predicting age-hardening for rubber-modified binders without missing significant variables. This model was validated for temperatures between 20°C and 85°C and loading frequencies between 0.0159 Hz and 15.9 Hz (0.1 and 100 radians/second).

5.5   Summary and Conclusions

This chapter investigates the oxidative aging of rubber-modified binders. The Superpave performance grading method was refined to address the issues identified for testing rubber-modified binders containing large rubber particles (up to 2.36 mm). The RTFO temperature was elevated to 190°C in line with typical field-production of RHMA, and the sample size in the RTFO bottle was adjusted by the rubber content to obtain the equivalent amount of base asphalt binder being aged as that in standard RTFO-aging. After subjecting the binders to the RTFO- and PAV-aging protocols, an FTIR was used to measure the binder chemical changes, and the DSR was used to measure the binder rheological properties. The GHS model was calibrated and validated for eight rubber-modified binders tested in this study. The following conclusions were drawn from these test results:

1. Question: What is an appropriate methodology for measuring the rheological properties (i.e., complex modulus, phase angle) of rubber-modified binders, especially for those containing large incompletely digested rubber particles (up to 2.36 mm [passing the #8 sieve])?

    This chapter validated the modification of the RTFO- and PAV-aging protocols. It was recommended to perform the RTFO-aging at 190°C to better simulate RHMA production temperatures in the field. The sample amount of the rubber-modified binder in each RTFO bottle was adjusted according to the rubber content to provide an equivalent base asphalt binder amount as in RTFO-aging of unmodified binders. Similarly, the sample size used in PAV-aging was also increased to account for the rubber. This chapter further validated the high temperature performance-grading test (≥58°C) and the BBR specimen preparation method developed in the previous research. The results showed that the concentric cylinder geometry

226

(cup-and-bob geometry) provided an equivalent accuracy to the parallel plate geometry for testing binders without large particles (<250 microns [passing the #60 sieve]). The concentric cylinder geometry was capable of measuring the rheological properties of rubber-modified binders containing large particles (<2.36mm [passing the #8 sieve]). For the BBR test, a modified beam mold was fabricated. This mold provided a larger opening with a shallower depth for pouring the binder than the standard mold. The laboratory results showed that there was no statistical difference between the modified mold and the conventional mold when testing conventional binders. The beam produced by the modified mold had a regular shape without entrapping air bubbles. This chapter initialized the rheological measurement of rubber-modified binders at intermediate temperatures (16°C to 50°C). A reference liquid was used to calibrate the concentric cylinder geometry setting. The test was calibrated to use a 10 mm spindle with a 9.5-mm gap for the tests at intermediate temperatures. The statistical analysis showed that this setting provided the same accuracy as the parallel plate geometry when testing conventional binders containing particles smaller than 250 microns. The concentric cylinder geometry could be considered as a potential geometry for measuring the rheological properties of rubber-modified binders containing large rubber particles (<2.36 mm [passing the #8 sieve]).

2. Question: How do aging products (i.e., carbonyl and sulfoxide components) accumulate in rubber-modified binders during oxidative aging? What is the crumb rubber modifier effect on oxidative aging of the binder?

The carbonyl components in rubber-modified binders continuously increased along with oxidative aging. Consequently, the carbonyl area index was used to track the oxidative aging in rubber-modified binders.

The carbonyl and sulfoxide components in rubber-modified binders decreased after adding the rubber. Increasing the rubber content decreased the carbonyl components in rubber-modified binders before and after PAV-aging. The rubber did not contain the carbonyl component before and after PAV-aging, and it did not show sulfoxide or butadiene component changes after PAV-aging. Considering that the carbonyl and sulfoxide components are the main aging products developed during oxidative aging of the base asphalt binder, the measurement results indicated the crumb rubber modifier itself was found to oxidatively age differently from the base binder in PAV-aging. Adding the rubber might decrease the aging products in the rubber-modified binders because part of the base binder was replaced by digested rubber particles. In other words, the rubber might dilute the aging products in the rubber-modified binders.

The comparison between FTIR-measured component indices and calculated component indices based on the dilution hypothesis indicated that the rubber dilution effect could explain the carbonyl component changes for binders without extender oils in unaged and PAV-aged conditions. In RTFO-aging, chemical interaction occurred in the rubber-modified binders at elevated temperatures (>160˚C). This interaction apparently changed the carbonyl components in the rubber-modified binders such that the dilution effect was not valid for explaining those changes.

The extender oil contained carbonyl and sulfoxide components, and these two components increased in the extender oil after RTFO- and PAV-aging. When extender oil was used, chemical interactions occurred in the rubber-modified binders after blending (unaged) and during RTFO- and PAV-aging, which changed the measured carbonyl component values considerably. The carbonyl component changes were beyond the reductions that could be explained by dilution.

228

The FTIR data also indicated that the dilution could not explain the sulfoxide component changes for rubber-modified binders (with and without extender oils) in unaged, RTFO-aged, and PAV-aged conditions.

Although the carbonyl and sulfoxide components increased with aging in rubber-modified binders as they did in the conventional unmodified binders, the rates of increase of these aging products in the rubber-modified binders were lower than those of their base binders. Increasing the rubber content also increased the butadiene area index in the rubber-modified binder. The amounts of the butadiene components were positively correlated to the rubber contents in the rubber-modified binders tested in this chapter.

3. Question: How can the age-hardening of rubber-modified binders be predicted using the GHS model?

The linearities between logarithmic viscosity and carbonyl area index for rubber-modified binders were validated at temperatures between 20°C and 85°C and loading frequencies between 0.0159 Hz and 15.9 Hz (0.1 radians/second and 100 radians/second). The GHS model provided a reasonable estimation of the viscosity for PAV-aged rubber-modified binders. The prediction error of using the GHS model was not significantly different between rubber-modified binders and their base binders. This observation indicated that the GHS model could model the age-hardening of rubber-modified binders containing up to 20 percent rubber with particle sizes up to 2.36 mm.

6 EVALUATION OF THE OXIDATIVE AGING OF ASPHALT MIXES

6.1 Introduction

This chapter investigates the oxidative aging of asphalt mixes. The following questions were answered:

- Will the loose mix aging protocol cause high variations in binder contents, mix stiffnesses, and fatigue lives of the specimens?

- Can the binder GHS model be used to predict the properties of recovered binders in aged asphalt mixes?

- How does oxidative aging affect mix stiffness?

- How does oxidative aging affect mix fatigue performance?

The steps taken to answer these questions included:

1. Laboratory aging of loose mixes to simulate the field aging of asphalt mixes.

2. Calibration of the binder GHS model using the data obtained from aged asphalt mixes.

3. Analysis of the oxidative aging effect on mix stiffness

4. Analysis of the oxidative aging effect on mix fatigue performance.

6.2 Experimental Design and Test Methodology

6.2.1 Material Preparation

One dense-graded mix (Mix D) produced with an unmodified binder (PG 64-16) and one gap-graded mix (Mix G) produced with an asphalt rubber binder were evaluated in this part of the study. The asphalt rubber binder used in the gap-graded mix was produced from a PG 64-16 base binder (different to the one used in Mix D) with a rubber content of 20 percent by weight of the binder. The asphalt rubber binder met Caltrans specifications (i.e., rubber particle gradation with 100 percent smaller than 2.36 mm [passing the #8 sieve], four percent extender oil by weight of the binder) *(25)*. These two mixes were sampled from the plant produced mixes. The plant mixes were quartered and well blended before compaction or testing in the laboratory following the standard sample size reduction procedure specified in AASHTO R 47 *(167)*.

The first purpose of this part of the study was to calibrate the binder GHS model for the binders in aged mixes by checking the linearity between logarithmic viscosity and the carbonyl area index. The second purpose was to study the effect of aging on mix stiffness and fatigue performance.

The aggregate gradations for these two mixes are plotted in Figure 6.1 on a 0.45 power curve. Both mixes had a nominal maximum aggregate size of 19 mm (3/4" sieve). The blue dashed line presents the maximum density curve at the maximum aggregate size of 25 mm (1" sieve). Some deviations of the maximum density gradation are necessary to provide spaces for asphalt binders. Mix D deviated slightly from the maximum density curve, while the gradation curve of Mix G deviated significantly, as expected, because of the designed gaps between 12.5 mm (1/2" sieve) and 0.6 mm (#30 sieve). These offsets in the gradation curve provide gaps to accommodate the asphalt binder containing incompletely digested rubber particles.
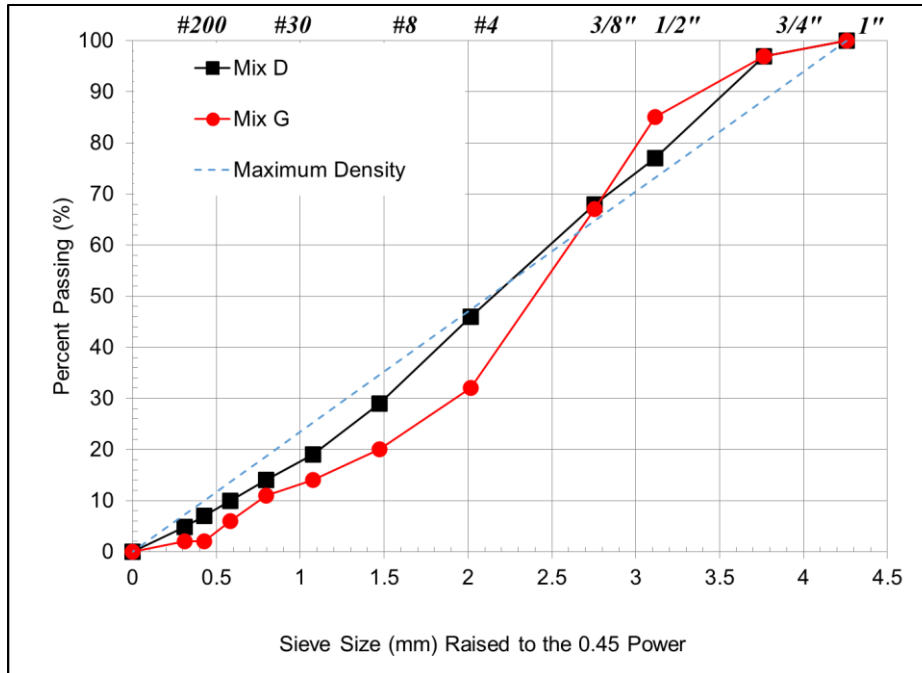
Figure 6.1: Aggregate gradation on 0.45 power graph.

The dense-graded Mix D includes a RAP bin, which is common practice in California to use more recycled materials for reducing the cost. This RAP material contained a 4.96 percent aged conventional binder by weight of the RAP. After thoroughly blending with the aggregate, the RAP itself was assumed to be similar in each batch, and it was not considered as a variable when analyzing the difference between different Mix D mixes.

Table 6.1 lists the volumetric design results. Both mixes met the current mix design criteria specified by Caltrans *(2)*. The voids in mineral aggregate (VMA) in Mix D was 14.4, which was within the requirement (13.5-16.5) for Type-A HMA mix following Caltrans specifications. The VMA in Mix G was 18.4, which was within the requirement (18 to 23) for RHMA-G mixes following Caltrans specifications. The VMA in Mix G was higher than Mix D because of the large spaces in the batched aggregates. Mix G also had a higher optimum binder content than Mix D (because the gap-gradation requires more binder) but a lower dust proportion.

232

Table 6.1: Volumetric Design Data for Mix D and Mix G

Mix ID	Optimum Binder Content by Weight of the Mix (%)	Air-Void Contents (%) at N-Design (85 Gyrations)	Voids in Mineral Aggregate (%)	Voids Filled with Asphalt (%)	Dust Proportion
Mix D	5.0	4.0	14.4	72.0	1.2
Mix G	7.8	4.0	18.4	-	0.3

6.2.2   Specimen Preparation and Laboratory Aging of Asphalt Mixes

The batched aggregates were mixed with the binders using the binder contents shown in Table 6.1. The uncompacted loose mixes were short-term oven-aged at 135°C for four hours following AASHTO R 30 *(95)*. After short-term oven-aging (STOA), the Mix D samples were divided into three groups, and the Mix G samples were divided into four groups. One sample in each group was used for control purposes and was not subjected to long-term oven-aging (LTOA). Two samples in each group were subjected to LTOA at 85°C for 72 and 120 hours, respectively. The fourth Mix G sample was aged for 44 hours and was added because a high variability of mix properties (i.e., stiffness, fatigue performance) was expected in the gap-graded mixes *(23,37)*. Note that 120 hours is the standard LTOA duration specified by AASHTO R 30 *(95)*. The mixes without LTOA (Mix D-0H and Mix G-0H) and the mixes with different LTOA (Mix D-72H, Mix D-120H, Mix G-44H, Mix G-72H, and Mix G-120H) provided data for the mixes at different aging conditions. These mixes were used to calibrate the GHS model and to quantitatively analyze the properties of aged mixes at different aging conditions.

During LTOA, the loose mixes were turned over in the shallow pan twice a day. Note that STOA and LTOA are conducted on loose mixes instead of compacted specimens, as specified in AASTHO R 30 *(95)*, because aging the loose mixes mitigates the development of aging gradients

in the compacted specimen that are a function of specimen dimensions and avoids problems associated with changes in specimen dimensions that can occur when aging compacted specimens *(96)*.

After completing LTOA, the oven temperature was raised to the compaction temperature, and the aged loose mixes were preheated for two hours before compaction. These conditioned mixes were then compacted into fatigue beams following the rolling-wheel compaction method *(168)*. Two slabs were produced in each group. These slabs were cut into beams with a dimension of 50 mm × 63 mm × 380 mm for fatigue test following AASHTO T 321 *(169)*. The air-void contents of these beams were required to be 7±1 percent, which was measured using the CoreLok method following AASHTO T 331 (*170*).

6.2.3 *Experimental Design for Evaluation of the Aged Asphalt Mixes*

Beams produced from the aged loose mixes were used to run frequency sweep tests at temperatures of 10˚C, 20˚C, and 30˚C, and frequencies between 0.01 Hz and 15 Hz.

Beams selected for the fatigue test were conditioned in the temperature chamber at 20˚C for two hours before starting the test. The controlled-strain flexural beam fatigue test was then conducted at 20˚C and 10 Hz. Table 6.2 summarizes the test strains in this section. Three replicates for each mix were applied under each test strain. The fatigue life was determined at the peak of the product of flexural stiffness and load cycles *(169)*.

Table 6.2: Strains Settings for Fatigue Tests

Mix ID	0 Hour LTOA (microstrain)			44 Hour LTOA (microstrain)			72 Hour LTOA (microstrain)			120 Hour LTOA (microstrain)		
Mix D	300	400	500	Not tested			270	300	400	250	330	400
Mix G	450	600	800	450	600	750	500	600	700	400	500	600

Specifically for analyzing the binder properties (i.e., carbonyl area index and viscosity), beams tested at the same strains were selected to collect the aged binders by extraction and recovery. The constant strain was 400 microstrain for Mix D and 600 microstrain for Mix G. These two strain levels were selected so that the beams would fail at around 1E+05 cycles. Three replicate beams were tested under each aging condition. The beams were prepared at the same target air-void content using the same method, and the tests on these beams were all conducted at the same strain level. This uniformity was used to exclusively evaluate the aging effect on beam performance without the influence of variables in aggregate gradation, air-void content, and test settings.

Aged binders were extracted and recovered from tested fatigue beams following AASHTO T 164 and ASTM D1856 *(156,171)*. The recovery method specified in ASTM D1856 is the Abson method. These two test methods are listed in the 2018 Caltrans specification as the standard procedure to extract and recover binders from HMA *(2)*.

The Abson method was developed in the 1930s, and it was the standardized method for decades *(172)*. However, issues with using the Abson method were identified, including repeatability issues and the amount of residual solvent remaining in recovered binders *(173,174,175)*. Test repeatability will be discussed in the analysis in the following sections. Recovery was conducted immediately after extraction to limit the time that the binders were in contact with the solvent to address the residual solvent issue. Although the solvent's effect on the binder properties (i.e., viscosity) could not be fully avoided, the same extraction and recovery procedure and time frame were followed for each beam to limit any variability from solvent contact.

The findings in Chapter 4 and Chapter 5 show that the CA index is an appropriate aging index for tracking oxidative aging. Hence, the CA index was measured on these recovered binders using the FTIR equipment. The test procedure followed the same methodology discussed in Section 4.2.2.

A series of frequency sweep tests (temperatures of 20˚C, 40˚C, 60˚C, and 85˚C, and frequencies between 0.0159 Hz and 15.9 Hz [0.1 radians/second and 100 radians/second]) were conducted on the recovered binders. These tests followed the same procedure discussed in Section 4.2.3. During extraction, incompletely digested rubber particles were separated from the binder and left in the aggregates following the current procedure listed in AASHTO T 164 *(156)*. Consequently, it was expected that any subsequent binder tests might not necessarily be fully representative of the asphalt rubber binder in the mix. Given the absence of any incompletely digested particles, the DSR parallel plate geometry could be used to test all binders. Viscosity was backcalculated from the rheological measurements. The correlation between the $\ln(\eta)$ and the CA index was analyzed to calibrate the GHS principle for the aged asphalt mixes.

6.3   Calibration of the Binder GHS Model for Asphalt Mixes

Table 6.3 and Table 6.4 present the measured properties of the recovered binders. No information was obtained from Mix G-72H-1 as this beam was not properly stored before extraction and recovery. Before testing the carbonyl component and the binder viscosity, the measured binder contents were calculated based on quantities of binder collected after recovery to evaluate the variation of the binder content in beams produced from aged loose mixes. Mix D-0H and Mix G-0H mixes were selected as the control mixes. The variations of the binder contents in long-term oven aged mixes were compared to those in the control mixes. The effective binder contents and binder film thicknesses were calculated to further evaluate any binder content changes in the mixes.

The effective binder content is the binder that is not absorbed by the aggregate, which can be calculated from the measured binder content and mix properties using Equation 6.1 and Equation 6.2 *(176)*:

$$Pbe = Pm - (Pba/100) \times Ps \tag{6.1}$$

$$Pba = 100 \times (Gse - Gsb)/(Gsb \times Gse) \times Gb \tag{6.2}$$

Where:
  Pbe = percent effective binder content.
  Pm = percent measured binder content.
  Pba = apparent binder content.
  Ps = percentage of aggregate in the beam, equal to one hundred minus the measured binder content.
  Gse = effective specific gravity of the aggregate, which was 2.750 g/cm^3 for Mix D and 2.749 g/cm^3 for Mix G.
  Gsb = bulk specific gravity, which was 2.661 g/cm^3 for mix D and 2.525 g/cm^3 for Mix G.
  Gb = binder specific gravity, which was 1.020 g/cm^3 for mix D and 1.120 g/cm^3 for Mix G.

Table 6.3: Measured Binder Properties of Mix D

Beam ID	Measured Binder Content (%)	Range and SD[1] for Measured Binder Content (%)	Effective Binder Content (%)	Binder Film Thickness (microns)	Binder Viscosity at 20°C and 10 Hz (kPa·s)
0H-1	5.01	0.22 SD=0.100	3.83	8.69	3,164
0H-2	5.01		3.83	8.69	4,647
0H-3	4.79		3.61	8.17	4,641
72H-1	4.28	0.58 SD=0.240	3.09	6.96	15,218
72H-2	4.86		3.68	8.33	18,981
72H-3	4.55		3.37	7.60	11,862
120H-1	4.31	0.20 SD=0.080	3.12	7.03	23,063
120H-2	4.51		3.33	7.50	13,884
120H-3	4.43		3.24	7.32	27,741

[1] SD= Standard Deviation.

Table 6.4: Measured Binder Properties of Mix G

Beam ID	Measured Binder Content (%)	Range and SD[1] for Measured Binder Content (%)	Beam Binder Content with Rubber (%)	Effective Binder Content (%)	Binder Film Thickness (microns)	Binder Viscosity at 20°C and 10 Hz (kPa·s)
0H-1	5.27	0.02 SD=0.009	7.77	3.84	16.47	2,267
0H-2	5.25		7.75	3.82	16.38	1,947
0H-3	5.25		7.75	3.82	16.38	2,265
44H-1	5.36	0.04 SD=0.022	7.86	3.93	16.89	1,863
44H-2	5.37		7.87	3.94	16.93	3,645
44H-3	5.41		7.91	3.98	17.12	2,118
72H-1	N/A	0.09 SD=0.045	N/A	N/A	N/A	N/A
72H-2	5.13		7.63	3.69	15.82	6,337
72H-3	5.22		7.72	3.78	16.24	7,713
120H-1	5.44	0.05 SD=0.021	7.94	4.01	17.26	12,209
120H-2	5.42		7.92	3.99	17.17	9,355
120H-3	5.47		7.97	4.04	17.40	12,187

[1] SD= Standard Deviation.

Since the extraction procedure separated the rubber particles from the binder, the measured binder contents for Mix G samples were generally two percent lower than the optimum binder content values listed in Table 6.1, including Mix G-0H without LTOA. Therefore, the binder contents were recalculated to include the designed 20 percent rubber based on the assumption that all rubber

would have been separated during the extraction process. Based on these results, the total binder contents in Mix G beams met the target optimum binder contents listed in Table 6.1 and Table 6.4 shows that the LTOA procedure appeared not to change the binder contents for Mix G mixes.

Figure 6.2 shows the measured binder contents for each beam. The LTOA Mix D binder contents were slightly lower than the designed binder contents (about 0.5 percent lower than 5.0 OBC), while the binder contents in Mix G remained similar to the designed binder contents. The effective binder contents showed similar trends, indicating that the binder absorbed by the aggregates was not different after LTOA. This observation indicated that aging the loose mix should not change the level of absorption by the aggregate.

Table 6.3 and Table 6.4 also show the range and standard deviation of the binder content measured from the beams produced using the loose mixes from each aging duration. It should be noted that the Abson method measurements generally had high variability for the calculated binder content. Stroup-Gardiner et al. *(173),* Peterson et al. *(177),* and Rodezno et al. *(178)* found that the error in measurement of the binder content could be as high as 0.75 percent.

AASHTO T 164 specifies that the acceptable range of two tests for a single operator is 0.58, and the standard deviation is 0.21 *(156).* Table 6.3 and Table 6.4 show that only the Mix D-72H beam group failed the standard deviation requirement. However, the ANOVA test for Mix D-72H and Mix D-0H shows the two groups were not statistically different at a 95 percent confidence level (p-value = 0.90 > 0.05). The measured binder contents listed in Table 6.3 and Table 6.4 show that long-term oven-aging the loose mixes produced similar variations in the binder contents to those mixes without LTOA. Therefore, the loose mix aging protocol should not introduce additional variability in measured binder contents based on the tested results in Table 6.3 and Table 6.4. The

high variability in Mix D-72H is owing to the Mix D-72H-1 beam, which might be caused by the

variability in the plant sampled mixes used for the laboratory test.
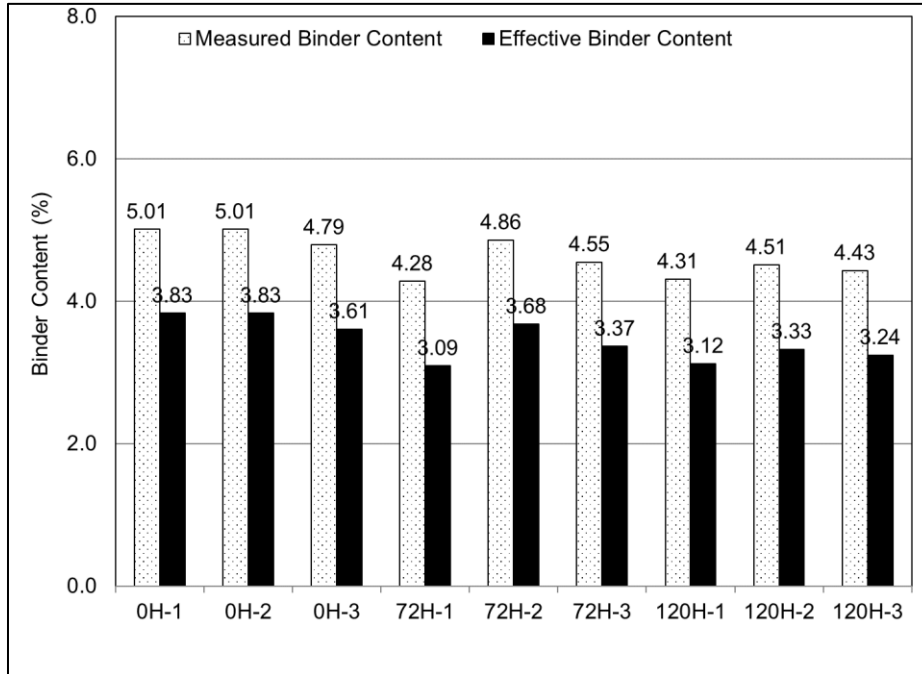
a: Mix D
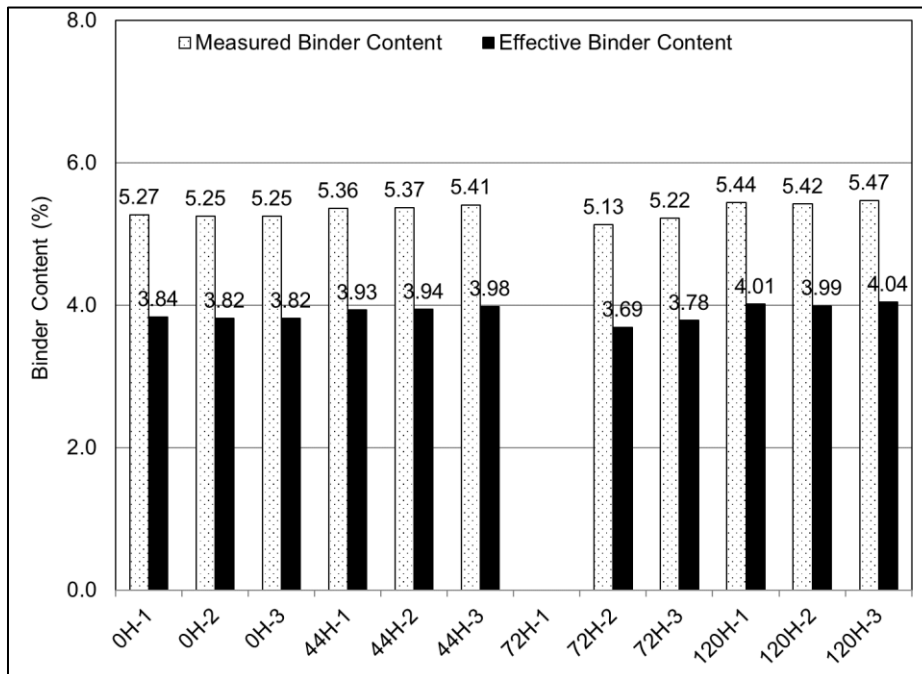
b: Mix G

Figure 6.2: Measured binder contents and effective binder contents for beams.

Regarding the aging in the loose mix, Lau et al. *(87)* noted that the diffusion of oxygen could significantly affect the aging rate. A thick binder film slows the oxygen diffusion rate and, therefore, decreases the rate of aging in a given period *(134,179,180)*. The binder film thicknesses in these beams were calculated using Equation 6.3 and Equation 6.4 *(181)*:

$$AFT = Pbe \times 4870/(Ps \times SA) \hspace{4cm} 6.3$$

$$SA = 2 + 0.02 \times a + 0.04 \times b + 0.08 \times c + 0.14 \times d + 0.30 \times e + 0.60 \times f + 1.60 \times g \hspace{1cm} 6.4$$

Where:
   AFT = asphalt binder film thickness in microns.
   Pbe = effective binder content.
   Ps = percentage of the aggregate weight.
   SA = calculated aggregate surface area in ft^2/lb.
   Parameters(a-g) = percent of aggregate passing 4.75, 2.36, 1.18, 0.60, 0.30, 0.15, and 0.075 mm.

Table 6.3 and Table 6.4 show the calculated binder film thicknesses for each beam. The results showed that Mix G binder film thicknesses were generally twice as thick as those measured for Mix D. This thicker binder film would slow the oven-aging effect in Mix G.

The binder viscosities at 20˚C and 10 Hz are listed in Table 6.3 and Table 6.4. The results indicate that oven-aging increased the binder viscosity in both mixes. The viscosities of Mix G binders were lower than those of Mix D binders in the same aging condition, which was attributed to a lower degree of aging in Mix G.

Figure 6.3 shows box plots of CA indices measured in the recovered binders. These indices increased with aging duration, which indicated that carbonyl components were continuously generated during oven-aging. Therefore, the CA index can be used to track oxidative aging in asphalt mixes, confirming findings from previous research *(96)*.
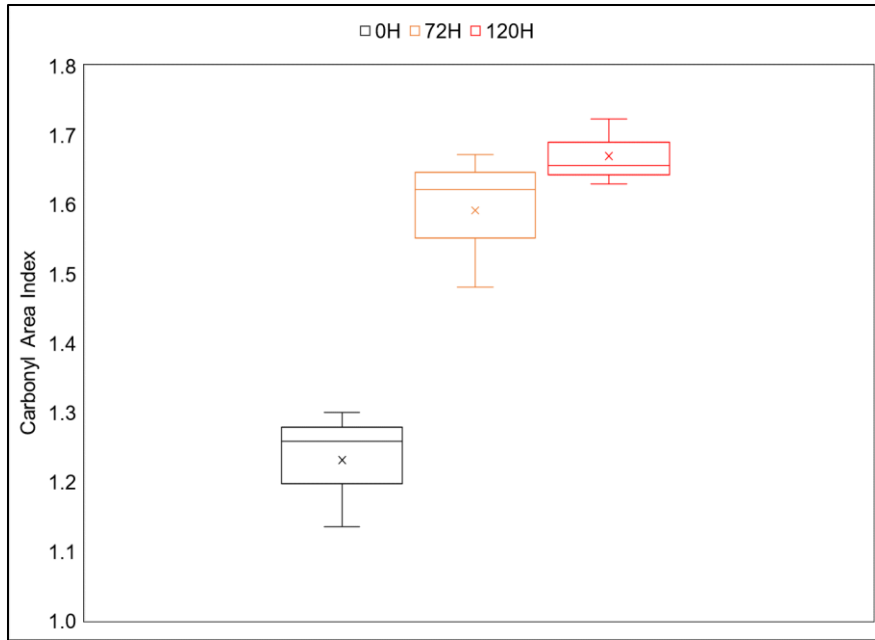
a: Mix D
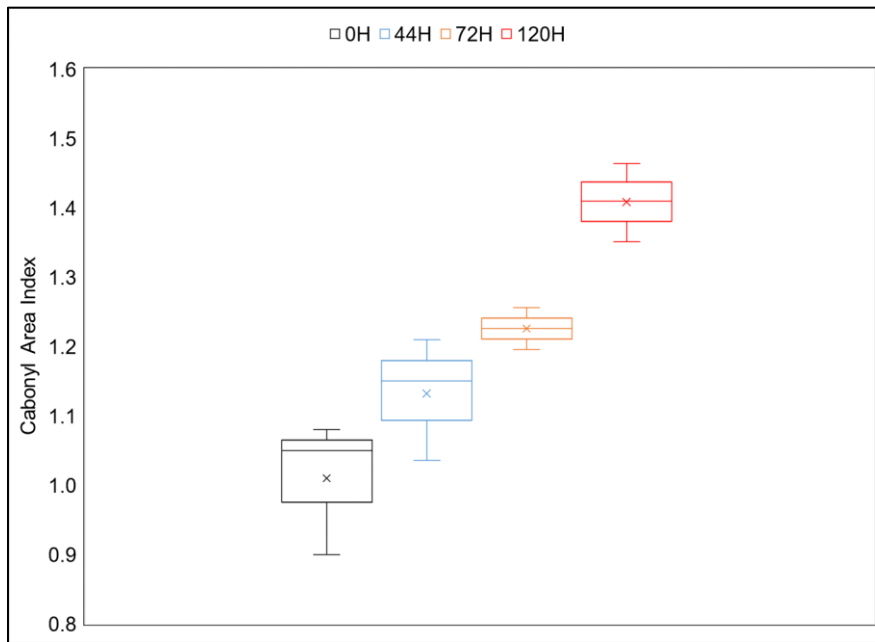
b: Mix G

Figure 6.3: CA indices measured in binders extracted from beams.

Figure 6.4 shows that the butadiene area indices for recovered binders from Mix D and Mix G after different aging durations. The Mix D butadiene area indices were negative, which indicated that no butadiene component existed in the unmodified binders used in Mix D. Positive butadiene

area indices were found in the recovered binders in Mix G. Although incompletely digested rubber particles were separated from the binder during the extraction procedure, the digested rubber was identified in the recovered binders.
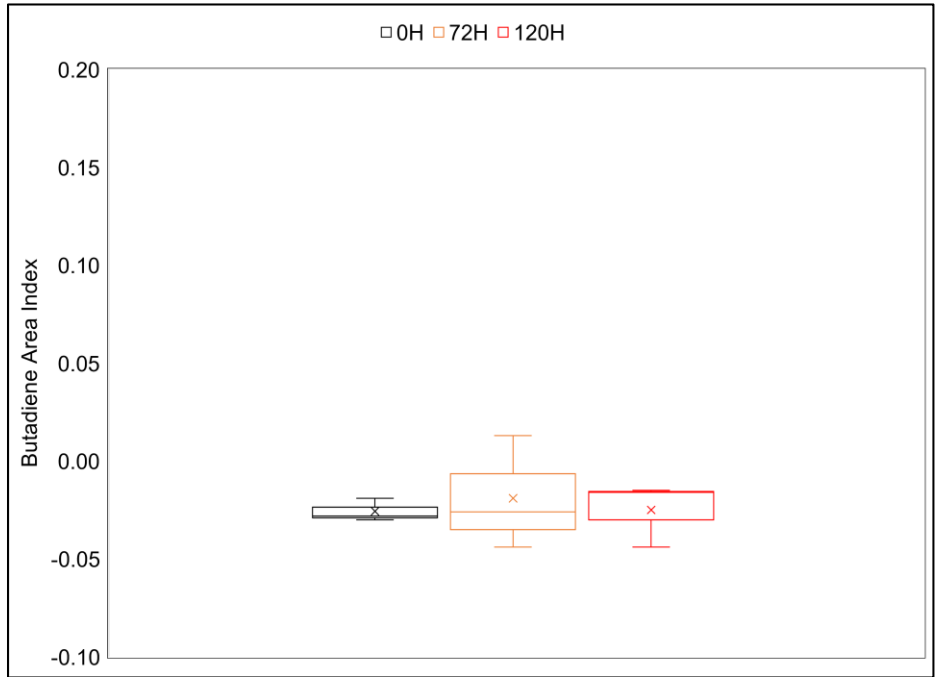
a: Mix D
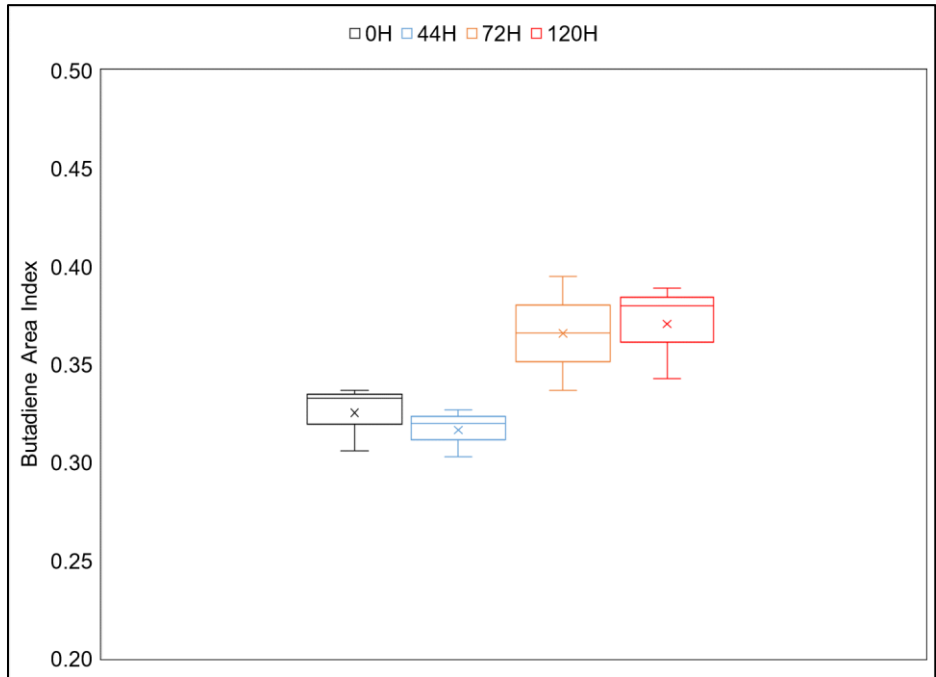
b: Mix G

Figure 6.4: Butadiene area indices measured from beams.

The viscosities of the recovered binders at the testing temperatures (20°C, 40°C, 60°C, and 85°C) and frequencies (between 0.0159 Hz and 15.9 Hz) were calculated using Equation 4.9. The validation of the linearity assumption between the ln(η) and the CA index followed the same method discussed in Figure 4.18.

Figure 6.5 shows examples of the linearity validation process at 20°C and 10 Hz. The R^2 values of the linearity between the ln(η) and CA index value were 0.87 for Mix D and 0.81 for Mix G. They both exceeded the 0.7 threshold *(135,146,147)*, which indicated that the linearity assumption was valid for these two aged mixes at 20°C and 10 Hz.

Mix D

$$\ln(\eta) = 4.09 \times CA + 3.50$$
$$R^2 = 0.81$$

Mix G
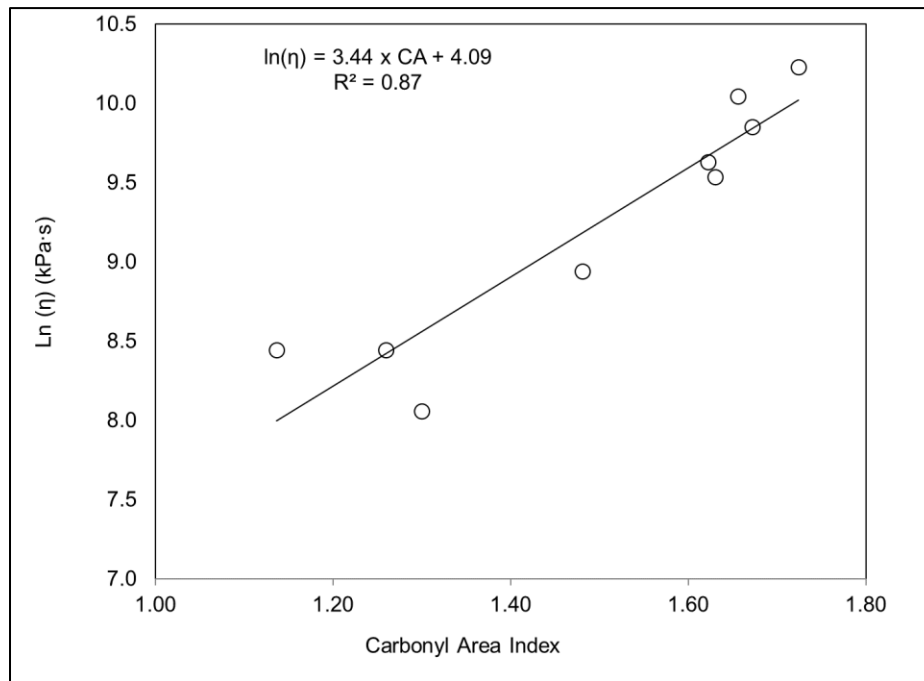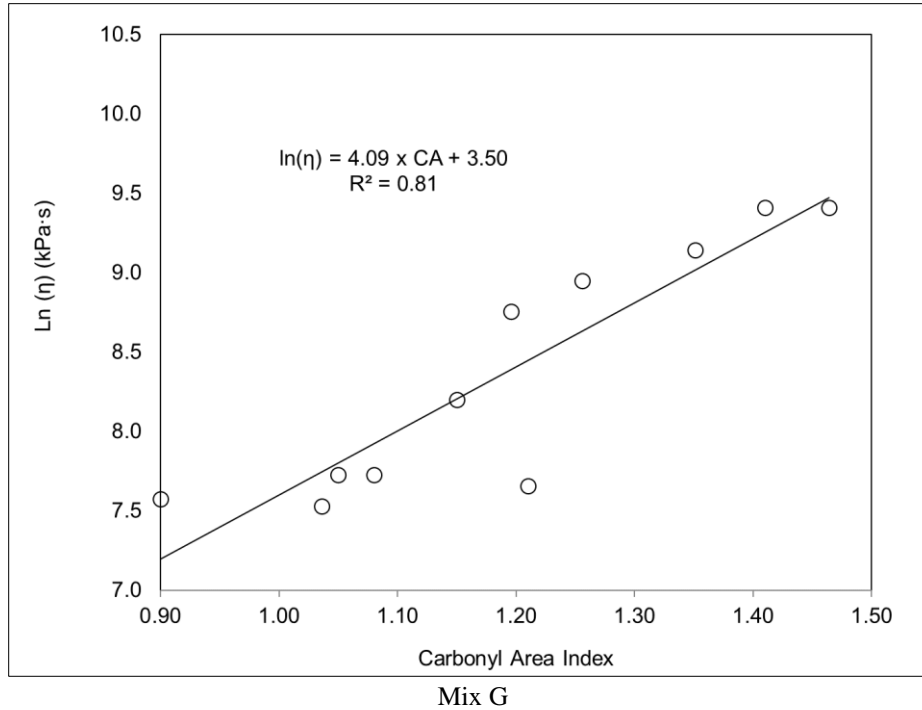
Figure 6.5 Determining the linearity between ln(η) and CA index for recovered binders.

The linearity assumption was then checked at additional temperatures and frequencies for these two mixes. Figure 6.6 summarizes the R^2 values. The red points in Figure 6.6 represent the examples shown in Figure 6.5.

For both mixes, the R^2 values had apparent differences between higher temperatures (60°C and 85°C) and intermediate temperatures (20°C and 40°C). The differences were mostly attributed to the DSR testing geometry and the preparation of the samples before testing. A PP-25 geometry with a 1-mm gap was used for high temperature tests, while the PP-8 geometry with a 2-mm gap was selected for intermediate temperature tests. The gap difference between the PP-25 and PP-8 could result in different trimming-effects for the test, which could have introduced the difference in R^2 values between high temperatures and intermediate temperatures.

245

Figure 6.6a shows that the R^2 values were higher at high temperatures than at intermediate temperatures, which was consistent with the binder test results discussed in Chapter 4 and Chapter 5. This observation indicated that the linearity between the $\ln(\eta)$ and CA index was more apparent when the precision of the backcalculated viscosity was higher at high temperatures than it was at intermediate temperatures. However, Figure 6.6b shows the opposite tendency. This was because the recovered Mix G binder was much softer than the Mix D binders, as Table 6.3 and Table 6.4 show. The Mix G binder was easier to trim at the intermediate temperatures than the Mix D binder, which reduced the repeatability issues in PP-8 testing for the Mix G binder.
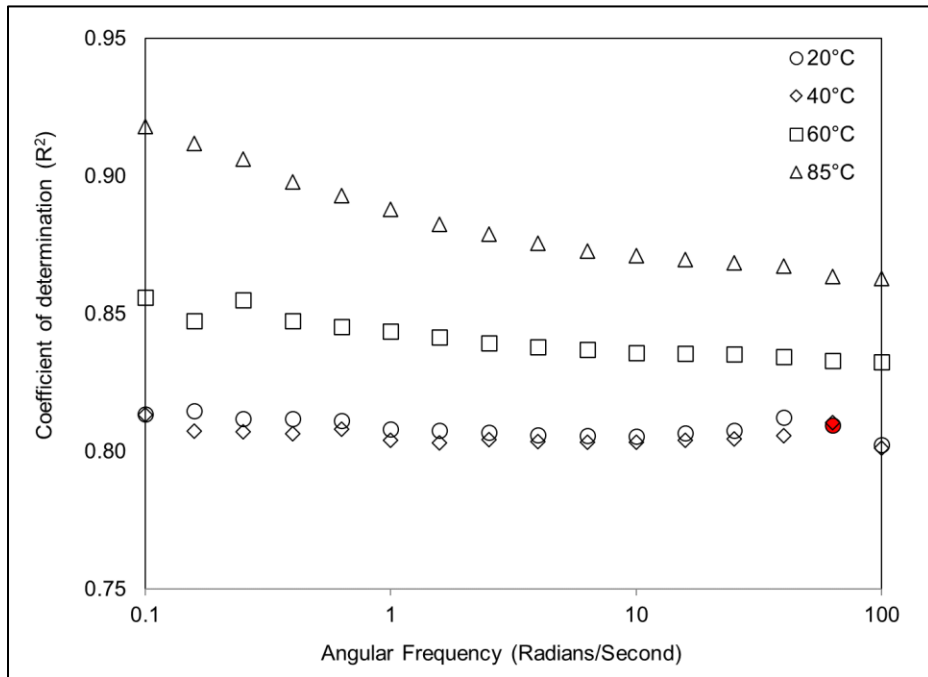
a: Mix D (red bubble presents the example case in Figure 6.5a)
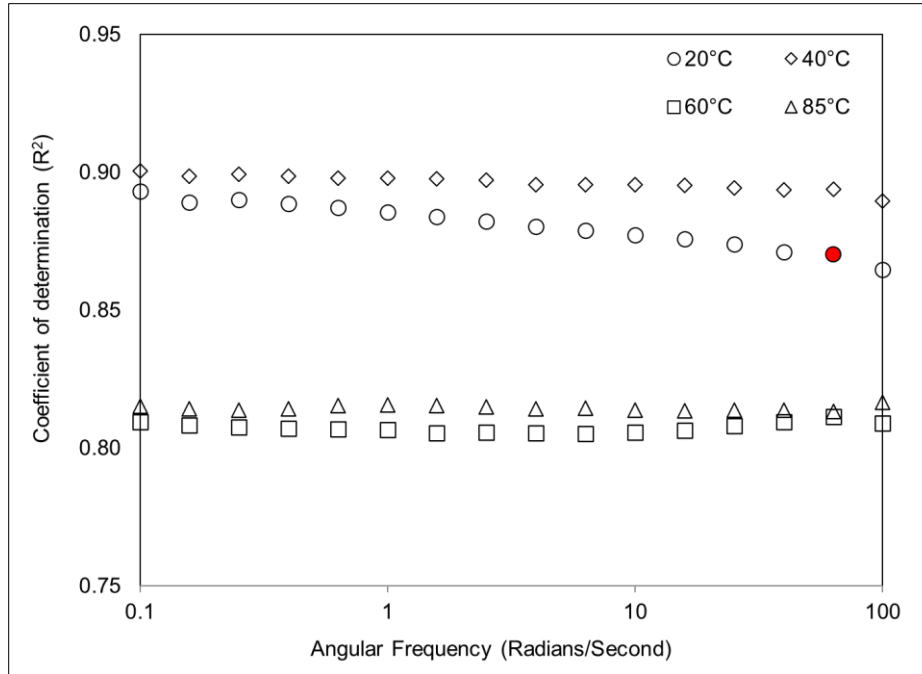
b: Mix G (Red bubble presents the example case in Figure 6.5b)

Figure 6.6: Validation of the linearity between the ln(η) and CA index for recovered binders.

Figure 6.6 shows that the linearity assumption between the ln(η) and CA index was valid for recovered binders from these LTOA mixes, as all R^2 values were higher than the 0.7 threshold line *(135,146,147)*.

The GHS model was used to model the oxidative aging in these asphalt mixes. The performance of the GHS model was evaluated by comparing the measured and model-predicted viscosities. The 95 percent confidence interval of the GHS model was used to evaluate the probability that the model would provide a satisfactory prediction of the viscosity. The upper and lower boundaries of the model-predicted viscosities at the 95 percent confidence intervals were calculated using Equation 6.5 to Equation 6.8 *(182)*.

$$M = e^{z\sqrt{var(\ln{(\eta)})}}$$ 6.5

$$var\ (ln\ \eta) = s^2 \times (1 + \frac{1}{n} + (\frac{(X-\bar{X})^2}{q \times \sum(X_P-\bar{X})^2}))$$ 6.6

$$S^2 = \frac{\sum_{k=1}^{d} WSS_k}{n-d}$$ 6.7

$$WSS_k = \sum_{i=1}^{nk}(\ln \eta_i - \ln \eta_k)^2$$ 6.8

Where:
$Z = 1.64$ for design reliability of 95 percent.
Var (ln η) = variability of viscosities estimated at the CA index level.
S^2 = variance in the logarithm of measured viscosities.
n = number of tested specimens.
$X = \ln$ (CA) at which $\ln$ (η) must be predicted.
$\bar{X}$ = average $\ln$ (CA).
q = number of replicate specimens at each CA index level.
WSS_k = within sum of squares for the factor level (CA index level).
d = number of factor level (CA index level).
ln η$_i$ = logarithm of measured viscosities for specimen *i*.
ln η$_k$ = average logarithm of measured viscosities for factor level *k*.
n_k = number of replicates at factor level *k*.

Nine Mix D specimens were tested with a CA index factor level of three (corresponding to the three aging conditions [0H, 72H, and 120H]). Three replicates were tested at each factor level. The S^2 of Mix D was calculated to be 0.134 using the measured viscosities. For Mix G, ten specimens were tested with a CA index factor level of four (four aging conditions [0H, 44H, 72H, and 120H]). Three replicates were tested at each factor level. The S^2 of Mix G was calculated to be 0.092. Table 6.5 and Table 6.6 summarize the predicted viscosities of the recovered binders and the boundaries of the 95 confidence intervals based on the above calculations. Figure 6.7 plots model-predicted binder viscosities versus measured binder viscosities at 20°C and 10 Hz. The measured viscosities were mostly within the 95 confidence intervals of the predicted viscosities, with more exceptions for Mix G than Mix D.

The coefficient of determination (R^2) values between measured and predicted viscosities were close to 0.9 and above the 0.7 threshold *(135,146,147)*, which means the observed viscosities were

well predicted by the GHS model. In summary, these results indicated that the GHS model provided a reasonable prediction of the recovered binder viscosity.

Table 6.5: Comparison of Measured and GHS Model-Predicted Viscosities for Mix D

Beam ID	Measured Viscosity (kPa·s)	Predicted Viscosity (kPa·s)	Upper Boundary of 95% Confidence Interval	Lower Boundary of 95% Confidence Interval
0H-1	3,164	5,511	7,569	4,013
0H-2	4,647	4,790	6,714	3,417
0H-3	4,641	3,144	4,878	2,026
72H-1	15,218	16,596	22,342	12,328
72H-2	18,981	19,694	26,871	14,435
72H-3	11,862	10,242	13,561	7,735
120H-1	23,063	18,645	25,320	13,729
120H-2	13,884	17,057	23,006	12,646
120H-3	27,741	23,532	32,682	16,944

Table 6.6: Comparison of Measured and GHS Model-Predicted Viscosities for Mix G

Beam ID	Measured Viscosity (kPa·s)	Predicted Viscosity (kPa·s)	Upper Boundary of 95% Confidence Interval	Lower Boundary of 95% Confidence Interval
0H-1	2,267	2,427	2,917	2,020
0H-2	1,947	1,314	1,694	1,020
0H-3	2,265	2,744	3,276	2,298
44H-1	1,863	2,292	2,764	1,901
44H-2	3,645	3,654	4,328	3,084
44H-3	2,118	4,670	5,532	3,942
72H-1	N/A	N/A	N/A	N/A
72H-2	6,337	4,410	5,221	3,725
72H-3	7,713	5,637	6,701	4,741
120H-1	12,209	13,197	16,471	10,574
120H-2	9,355	8,313	10,043	6,881
120H-3	12,187	10,582	12,980	8,627
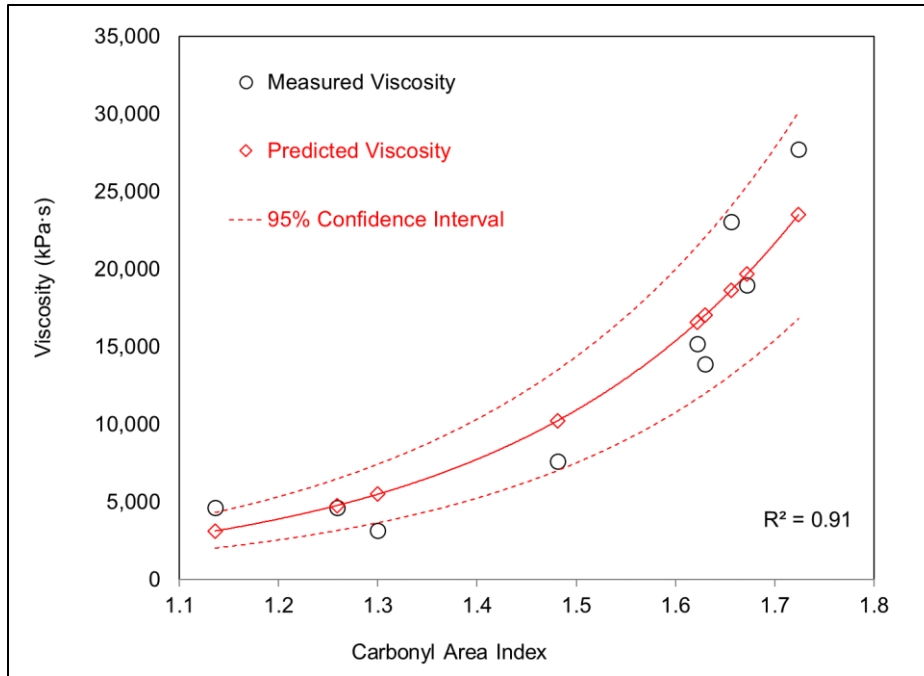
a: Mix D
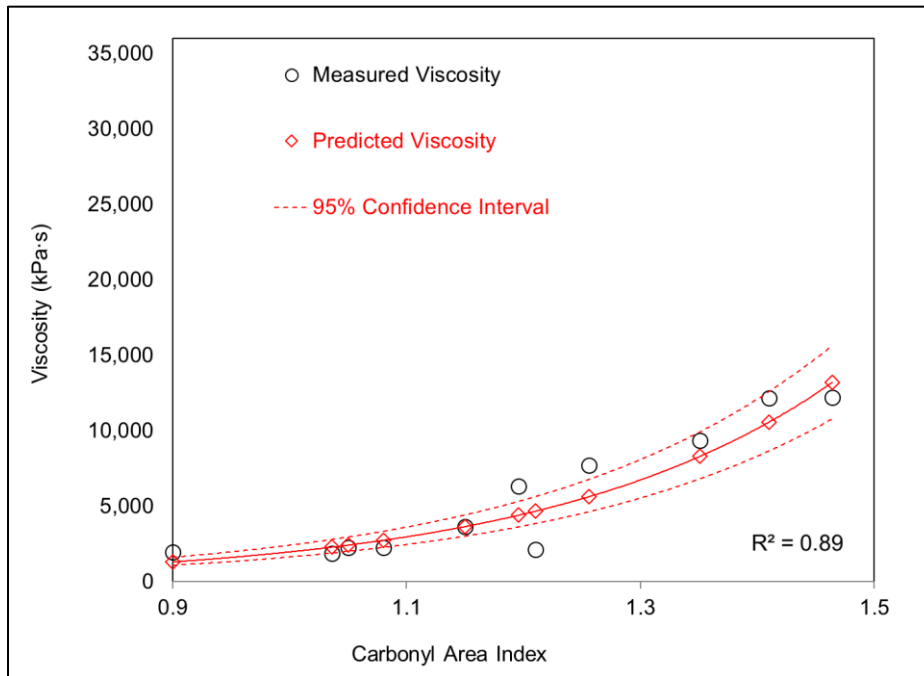
b: Mix G

Figure 6.7: Comparison between measured and predicted viscosity using GHS model at 20°C and 10 Hz.

6.4 Correlation between Binder Properties and Mix Stiffness

Section 6.3 showed that oven-aging of asphalt mixes changes chemical components and physical properties in the binder. These changes in the binder properties, in turn, affect the mix properties. This section studies the influence of aging on mix stiffness.

The frequency sweep test data for beams produced with the loose mixes were horizontally shifted to the stiffness master curve at 20°C. This shifting was conducted using the symmetric sigmoidal function *(141)* and the Williams-Landel-Ferry shift function *(183)*. Figure 6.8 shows that the LTOA protocol stiffened the mixes.
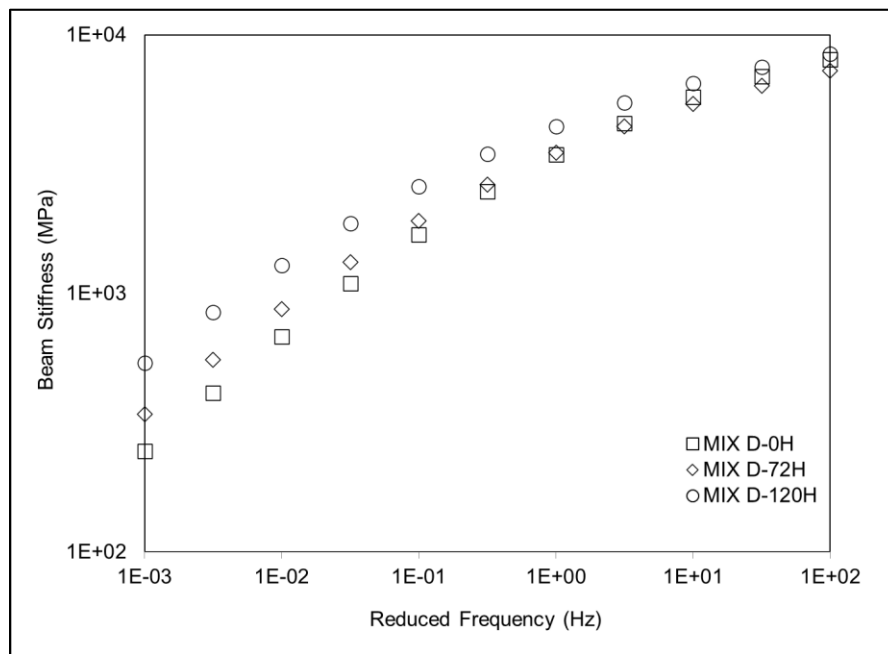
a: Mix D
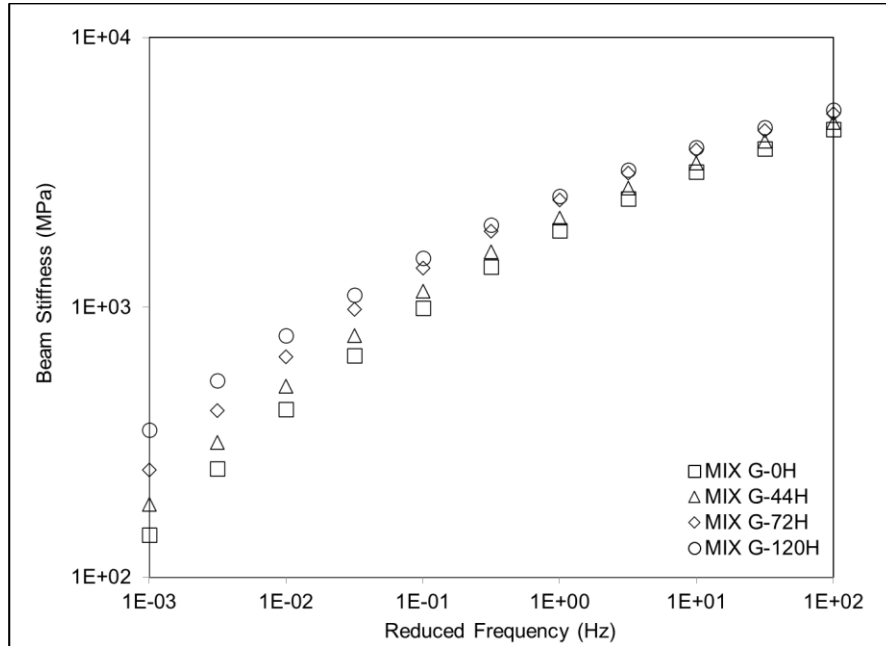
b: Mix G

Figure 6.8: Master curve at 20°C of the beams made with loose mixes subjected to LTOA.

Table 6.7 and Table 6.8 present the measured mix properties. Measured air-void contents of these beams all met the target range (7±1 percent). The air-void contents indicated that the loose mix aging protocol might not impact the workability of the aged mixes. At the compaction temperatures (150˚C for Mix D and 170˚C for Mix G), the aged loose mixes could be compacted to the design air-void content. From this perspective, aging loose mixes in the laboratory might not create compaction issues.

Table 6.7: Measured Mix D Beam Properties

Beam ID	Air-Void Content (%)	Initial Stiffness at 20°C and 10 Hz (MPa)	Average Initial Stiffness (MPa)	Range and SD[1] of Initial Stiffness (MPa)	COV[2]
0H-1	7.7	6,059			
0H-2	7.9	5,950	5,602	1,270 SD=562	0.10
0H-3	7.5	4,800			
72H-1	7.7	4,469			
72H-2	7.7	6,339	5,698	1,852 SD=866	0.15
72H-3	7.8	6,286			
120H-1	7.6	7,075			
120H-2	7.4	6,361	6,473	1,117 SD=462	0.07
120H-3	7.5	6,011			

[1] SD= Standard Deviation, [2] COV= Coefficient of Variation.

Table 6.8: Measured Mix G Beam Properties

Beam ID	Air-Void Content (%)	Initial Stiffness at 20°C and 10 Hz (MPa)	Average Initial Stiffness (MPa)	Range and SD[1] of Initial Stiffness (MPa)	COV[2]
0H-1	7.1	2,352			
0H-2	7.7	2,285	2,435	316 SD=167	0.07
0H-3	6.6	2,668			
44H-1	7.0	2,328			
44H-2	6.6	3,014	2,769	686 SD=313	0.11
44H-3	7.0	2,966			
72H-1	N/A	N/A			
72H-2	8.0	2,800	2,785	29 SD=14	0.01
72H-3	7.9	2,771			
120H-1	6.9	3,125			
120H-2	7.2	3,162	3,128	67 SD=27	0.01
120H-3	7.4	3,095			

[1] SD= Standard Deviation, [2] COV= Coefficient of Variation.

Table 6.7 and Table 6.8 show the initial beam stiffnesses determined at the 50th cycle in the fatigue tests (*169,184*). Mix D LTOA-72H-1 and Mix G-44H-1 were considered to be outliers that caused variances in the corresponding aging groups. The coefficient of variation (COV) values of the initial stiffnesses for the beams produced with long-term aged loose mixes (Mix D-72H, Mix D-120H, Mix G-44H, Mix G-72H, and Mix G-120H) were not statistically different from the ones produced by the mixes without LTOA (Mix D-0H and Mix G-0H).

To better understand the variations in the initial stiffness of the beams produced with the loose mix aging protocol, the standard deviation and COV of all fatigue tested beams were calculated following the test plan in Table 6.2 (three beams in each fatigue test strain in each LTOA condition). In each aging condition, nine beams were used in the calculation. Table 6.9 shows the statistical analysis results. The standard deviation and COV of the beams produced with loose mixes after LTOA (Mix D-72H, Mix D-120H, Mix G-44H, Mix G-72H, and Mix G-120H) did not show apparent differences from those produced from loose mixes without LTOA (Mix D-0H and Mix G-0H). This observation indicated that extending the duration of aging in the loose mix aging protocol from zero to 120 hours should not increase variability in the initial stiffnesses of the beams.

The variations of the initial stiffness in the loose mix aging protocol were compared to the compacted specimen aging protocol. Table 6.9 shows two types of aged beams produced using mixes with California Valley and Coastal binders, which have very different aging characteristics *(185)*. These two types of beams were laboratory-mixed and laboratory-compacted. They contained approximately 5.5 percent binder, which is similar to the binder contents in Mix D and the base binder contents (without rubber) in Mix G. The air-void contents were between seven and nine percent for the Valley and Coastal binder beams, which are also close to the air-void contents in Mix D and Mix G. The beams were long-term oven-aged at 85°C for 72 and 144 hours. Comparing the standard deviations and COVs in each aging condition showed that the variations of the initial stiffnesses in the loose mix aging protocol were similar to those in the beam aging protocol.

Table 6.9: Comparison of the Initial Stiffness Variations for Different LOTA Protocols

Aging Condition	Beam ID	Average Stiffness (MPa)	SD[1] (MPa)	COV[2]
No LTOA (LTOA-0H)	Mix D-0H	5,612	531	0.09
	Mix G-0H	2,424	229	0.09
	Valley-0H	6,230	260	0.04
	Coastal-0H	1,832	183	0.10
Middle LTOA (LTOA-44H and LTOA-72H)	Mix D-72H	5,957	690	0.12
	Mix G-44H	2,803	440	0.16
	Mix G-72H	3,025	217	0.07
	Valley-72H	7,908	399	0.05
	Coastal-72H	N/A	N/A	N/A
Long LTOA (LTOA-120H and LTOA-144H)	Mix D-120H	5,918	482	0.08
	Mix G-120H	3,249	149	0.05
	Valley-144H	8,256	435	0.05
	Coastal-144H	3,288	325	0.10

[1] SD= Standard Deviation, [2] COV= Coefficient of Variation.

Figure 6.9 plots the initial stiffnesses of fatigue beams grouped by LTOA duration using the data in Table 6.7 and Table 6.8. The initial mix stiffnesses generally increased after LTOA, indicating that oven-aging stiffened the mix. This observation was consistent with the results from the mix frequency sweep tests. This stiffening was also consistent with the viscosity increases measured in the extracted binders. When extending the LTOA duration, the age-hardening effect further stiffened the binder, which then increased the mix stiffness.
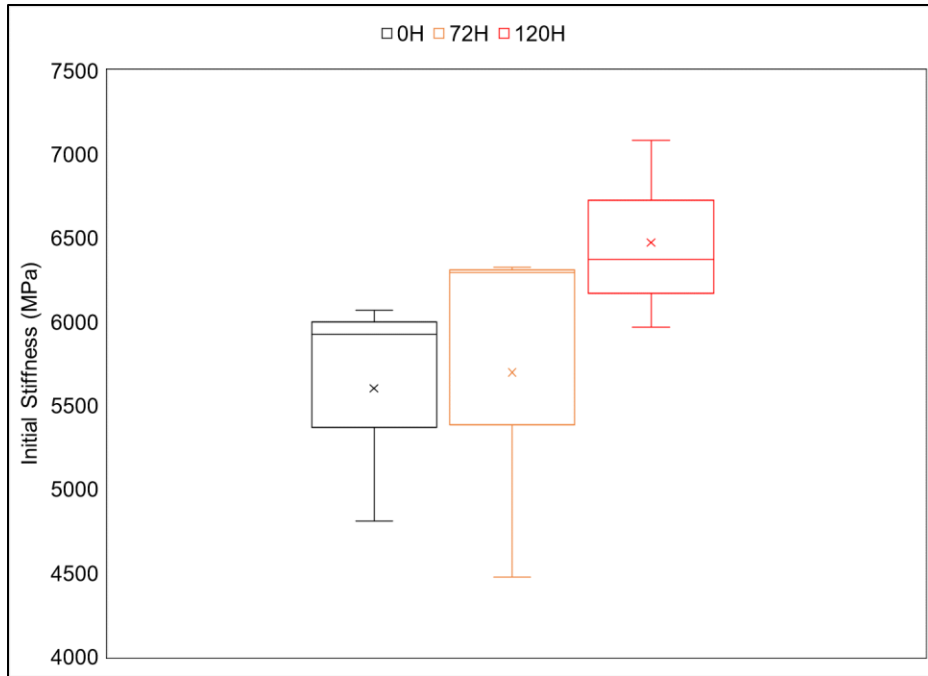
a: Mix D
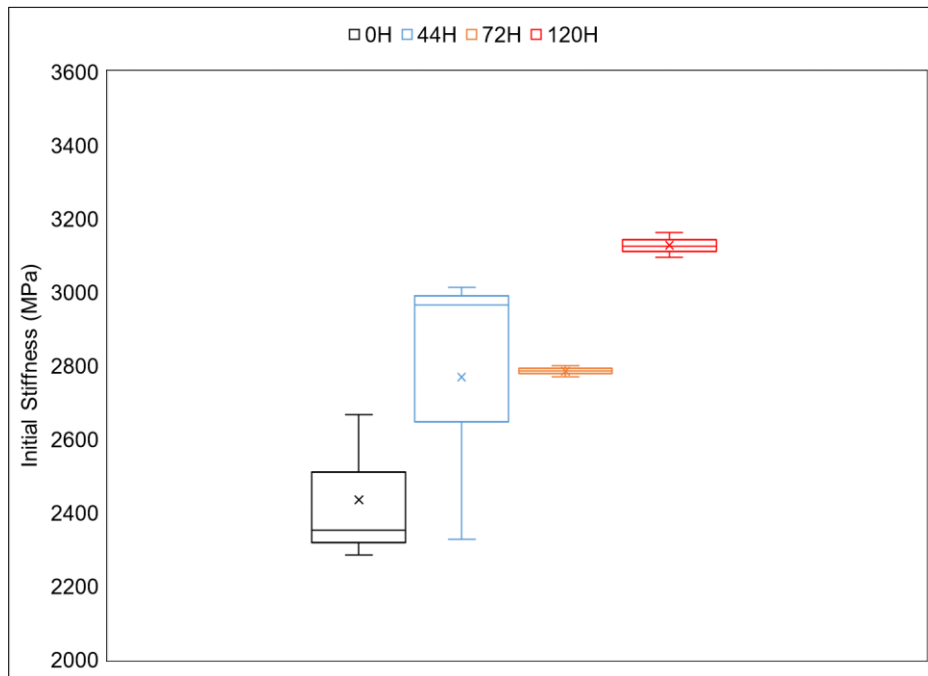
b: Mix G

Figure 6.9: Measured mix stiffness versus measured binder viscosity at 20°C and 10 Hz.

The changes in mix stiffness can be modeled from the binder properties using Equation 6.9. This stiffness prediction model was proposed by Andrei, Witczak, and Mirza in 1999 *(142,186)*, which can predict the mix stiffness using binder viscosity and mix volumetric parameters.

$$log_{10}(E^*) = -1.2499 + 0.0292\rho_{200} - 0.0018(\rho_{200})^2 - 0.0028\rho_4 - 0.0581V_a - (0.8821V_{be})/(V_{be} + V_a) +$$
$$(3.8720 - 0.021\rho_4 + 0.0040\rho_{38} - 0.000017(\rho_{38})^2 + 0.0055\rho_{34})/\left(1 + e^{(-0.6033 - 0.3133logf - 0.3935log\eta)}\right)$$

6.9

Where:
    E^* = mix modulus in ksi.
    η = binder viscosity in 10^6 poise.
    f = loading frequency in Hz.
    V_a = mix air-void content in percent.
    V_{be} = effective binder content in percent.
    ρ_{xx} = aggregate cumulative retained on 19, 9.50, 4.75, and 0.075 mm sieve in percent.

This Andrei-Witczak-Mirza stiffness prediction model was used to estimate the mix stiffness of each beam using the data listed in Table 6.1, 6.3, 6.4, 6.7, and 6.8.

Figure 6.10 compares the predicted mix stiffnesses to the measured initial beam stiffnesses in the fatigue test. The R^2 values of Mix D were lower than those of Mix G, probably because the variations in the measured stiffnesses of Mix D were higher than those of Mix G, as Table 6.7 shows. The initial stiffnesses of Mix D-0H-3 and Mix D-72H-1 were 1,000 MPa lower (approximate equal to 20 percent of the total stiffness) than other Mix-D beams, which caused the high variation among Mix D beams. The Mix D-120H group showed lower variabilities than the other two groups (Mix D-0H and Mix D-72H), as Table 6.7 shows. Therefore, the variability was not caused by the loose mix aging protocol. The plant sampled mixes might have had some variability in the mixes before laboratory aging.

The increase in beam stiffness due to increased aging could be predicted from the recovered binder viscosities and mix parameters. For both mixes, using the GHS model-predicted viscosities

resulted in higher R^2 values than using the measured viscosities to predict the mix stiffness. Burr et al. *(187)*, Bahia et al. *(188)*, and Wakefield *(189)* concluded that using the Abson method caused repeatability issues for the measurement of viscosities in recovered binders. Using the GHS model-predicted viscosities instead of the measured viscosities, removed the variations in measured binder viscosities. This increased accuracy of the binder viscosity could, in turn, increase the precision of mix stiffness prediction.

The only variable that could be identified to increase the stiffness was the aging of loose mixes. The data shown in this chapter indicated that aging the loose mix produced new carbonyl components in the binder, and this aging also increased binder viscosity. In turn, this aged binder stiffened the mix.

The results from this study indicated that using the GHS model-predicted viscosity and Andrei-Witczak-Mirza stiffness prediction model to estimate the stiffness of aged mixes is promising. It should be noted that only two types of mixes were studied. Further evaluation of this application using different mixes under different aging conditions is warranted. Calibration of this application using field data is also recommended.
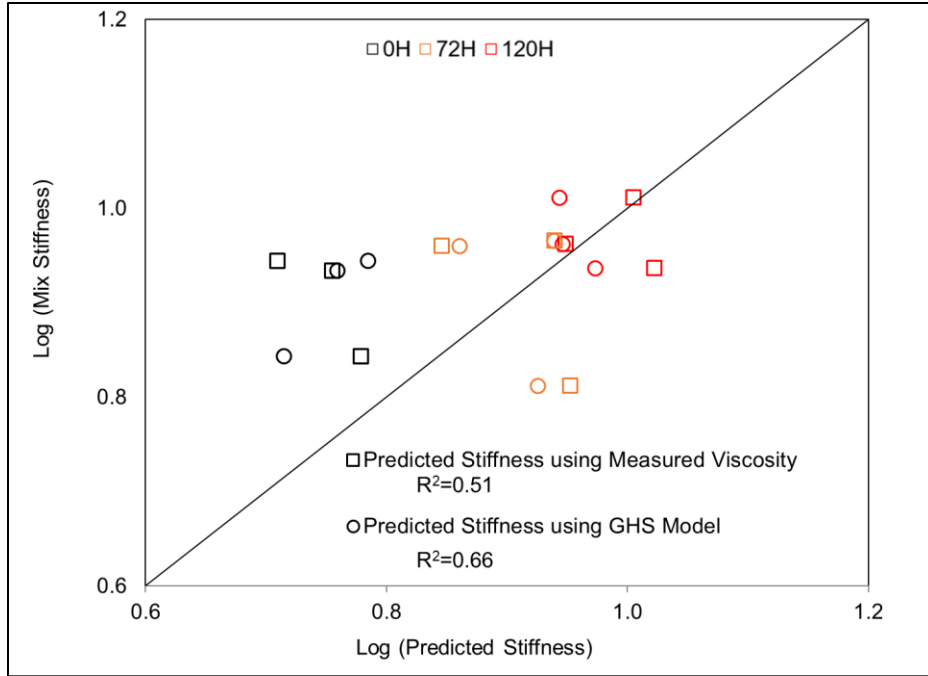
a: Mix D
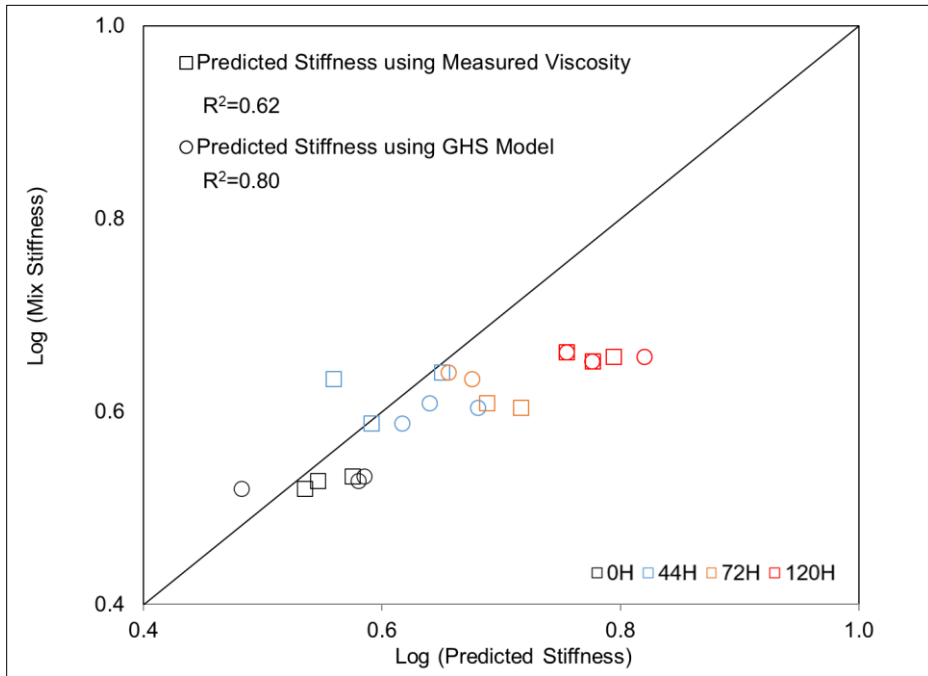
b: Mix G

Figure 6.10: Comparison of predicted stiffness to initial beam stiffness at 20°C and 10 Hz.

259

6.5 Correlation between Binder Properties and Mix Fatigue Performance

This section analyzes the effect of binder property changes on mix fatigue performance due to oven aging. The fatigue life (Nf) values at the peak stiffness versus load cycles for each beam are summarized in Table 6.10 and Table 6.11. The Nf values decreased with the degree of aging, as expected. Given that test settings were the same for each mix (test temperature, frequency, and strain), a reasonable assumption was that the changes inside the mix itself caused this decrease in fatigue life.

Table 6.10: Measured Mix D Beam Properties

Beam ID	Air-Void Content (%)	Fatigue Life (Cycles)	Average and SD[1] of Fatigue Life (Cycles)	COV[2]
0H-1	7.7	230,000	274,167 SD=147,257	0.54
0H-2	7.9	120,000		
0H-3	7.5	472,500		
72H-1	7.7	32,000	129,500 SD=140,012	1.08
72H-2	7.7	29,000		
72H-3	7.8	327,500		
120H-1	7.6	29,000	30,667 SD=14,337	0.47
120H-2	7.4	49,000		
120H-3	7.5	14,000		

[1] SD= Standard Deviation, [2] COV= Coefficient of Variation.

Table 6.11: Measured Mix G Beam Properties

Beam ID	Air-Void Content (%)	Fatigue Life (Cycles)	Average and SD[1] of Fatigue Life (Cycles)	COV[2]
0H-1	7.1	270,000	1,483,333 SD=1,779,931	1.20
0H-2	7.7	4,000,000		
0H-3	6.6	180,000		
44H-1	7.0	312,500	221,667 SD=76,658	0.35
44H-2	6.6	227,500		
44H-3	7.0	125,000		
72H-1	N/A	N/A	178,750 SD=21,250	0.12
72H-2	8.0	200,000		
72H-3	7.9	157,500		
120H-1	6.9	57,000	91,500 SD=25,420	0.28
120H-2	7.2	117,500		
120H-3	7.4	100,000		

[1] SD= Standard Deviation, [2] COV= Coefficient of Variation.

The COVs of the Nf values for the Mix D-72H group and Mix G-0H group were significantly higher than other groups because the larger Nf values of Mix D-72H-3 and Mix G-0H-2 were considered to be outliers. The variations of Nf values in the loose mix aging protocol were compared to those from the beam aging protocol. The beam fatigue tests were set at 20°C and 10 Hz for all these mixes. The Nf values of the Valley- and Coastal-binder mixes were obtained from the beam fatigue test at 600 microstrain *(185)*. Table 6.12 shows the comparison of results. No differences in the variations of Nf values were found between these two aging protocols, except for the Mix D-72H group and Mix G-0H group owing to the two outliers (Mix D-72H-3 and Mix G-0H-2). Therefore, the loose mix aging protocol did not introduce a high variation of fatigue life in Mix D and Mix G.

Table 6.12: Comparison of the Fatigue Life Variations for Different LOTA

Aging Condition	Beam ID	Average Nf (Cycles)	SD[1] (Cycles)	COV[2]
No LTOA (LTOA-0H)	Mix D-0H	274,167	147.257	0.54
	Mix G-0H	1,483,333	1,779,931	1.20
	Valley-0H	23,560	N/A	N/A
	Coastal-0H	91,883	37,947	0.41
Middle LTOA (LTOA-44H and LTOA-72H)	Mix D-72H	129,500	140,012	1.08
	Mix G-44H	221,667	76,658	0.35
	Mix G-72H	178,750	21,250	0.12
	Valley-72H	18,003	7,155	0.40
	Coastal-72H	N/A	N/A	N/A
Long LTOA (LTOA-120H and LTOA-144H)	Mix D-120H	30,667	14,337	0.47
	Mix G-120H	91,500	25,420	0.28
	Valley-144H	30,675	4,492	0.15
	Coastal-144H	26,660	7,739	0.29

[1] SD= Standard Deviation, [2] COV= Coefficient of Variation.

Besides fatigue life, four additional variables were not the same among these beams: mix stiffness, air-void content (AV), asphalt content (AC), and binder properties. The results discussed in Section 6.3 showed that the changes in binder properties during LTOA could be modeled with the GHS model. Therefore, the CA index was selected as the most appropriate parameter to represent

the binder properties. A statistical analysis was conducted to identify the potential variables that decreased the mix fatigue life after LTOA.

A backward selection method was used to remove insignificant variables to the dependent variable-fatigue life *(190,191)*. The essential steps of a backward selection include the following:

1. Start with all the candidates.
2. Delete variables that contribute the least to the regression.
3. Repeat Step 2 until the remaining variables are significant to the regression model or until the regressing criterion is reached.

The ANOVA test was used to check the significance of variables at a 95 percent confidence level for the backward selection in this study. The fatigue life was the dependent variable, and the mix stiffness, AV, AC, and CA were independent variables.

- Step 1: An ANOVA test with all four variables returned that an essentially perfect fit was unreliable since the initial four independent variables were not totally independent. It was found that mix stiffness and the binder CA index were correlated. The stiffness could be predicted from the CA index using the GHS model and stiffness prediction model, as shown in Section 6.4. Therefore, the CA index was kept as it was directly correlated to oven-aging, while mix stiffness was removed from the regression.

- Step 2: A three-way ANOVA statistical analysis was run to determine the significance of AV, AC, and CA to the dependent variable. The null hypothesis was that neither of these three factors or the interactions among factors caused fatigue life changes. Table 6.13 shows the ANOVA results. The null hypothesis was rejected using the significance level of 5 percent (p-value < 0.05). For Mix D, the AV variable had the highest p-value, and it

was therefore removed from the regression. For Mix G, the AC variable had the highest p-value, and it was therefore removed from the regression.

Table 6.13: Three-Way ANOVA Test Results for Mix Fatigue Performance

Mix ID	Variable	AC	AV	CA	AC: AV	AC: CA	AV: CA	AC: AV: CA
Mix D	F value	0.307	0.205	28.150	1.789	4.282	0.707	0.490
	P(>F)	0.678	0.730	0.119	0.409	0.287	0.638	0.611
Mix G	F value	0.710	21.99	34.55	0.644	18.87	8.099	3.889
	P(>F)	0.461	0.018	0.010	0.481	0.023	0.065	0.143

AC-asphalt content in mix, AV-air-void content of the mix, CA-carbonyl area index of the recovered binder.

- Step 3: Repeating the process in Step 2. A two-way ANOVA was run for Mix D and Mix G with the remaining independent variables. Table 6.14 shows the ANOVA results. In this step, the AC variable did not qualify as a significant variable for Mix D since its p-value was higher than 0.05. For Mix G, the AV variable had a p-value exceeding 0.05, and it was also removed from the regression.

Table 6.14: Two-Way ANOVA Test Results for Mix Fatigue Performance

Mix ID	Variable	AC	CA	AC: CA
Mix D	F value	0.394	36.121	5.479
	P(>F)	0.558	0.002	0.066
Mix G	F value	4.786	17.609	17.371
	P(>F)	0.065	0.004	0.004

AC-asphalt content in mix, AV-air void content of the mix, CA-carbonyl area index of the recovered binder.

- Step 4: A one-way ANOVA was run to check the correlation between the CA index and the fatigue life. The null hypothesis was that the fatigue life change was not related to the change of the CA index. Table 6.15 shows the ANOVA results. The null hypothesis was rejected at a 95 percent confidence level. For both mixes, the fatigue life had a significant correlation to the change of the CA index.

263

Table 6.15: One Way ANOVA Test Results for Mix Fatigue Performance

Variable	Criterion	Mix D	Mix G
CA Index	F value	23.255	5.44
	P(>F)	0.002	0.045

The ANOVA analysis confirmed that the AC and AV variables were not significant to the fatigue life changes in this controlled testing. In this study, the loose mixes were oven-aged and then compacted to a target air-void content. No statistical difference was found for the asphalt contents among beams after LTOA. These two variables (AC and AV) should not influence the fatigue life significantly since they were controlled by the experimental parameters. The above statistical analysis results confirmed the assumption that aging increased the CA indices of the binders, and hence the mix stiffnesses (because of the correlation between CA index and mix stiffness was found in backward selection Step 1), which in turn shortened the fatigue lives of the aged asphalt mixes.

Figure 6.11 plots fatigue life against the CA index in a semi-logarithm plot. The Mix D-72H-3 and Mix G-0H-2 beams were removed from the data since their much higher fatigue lives were considered outliers. Both the Mix D and Mix G results had coefficients of determination values over 0.7, indicating that the shorter mix fatigue lives after LTOA was correlated to the increase in CA index.
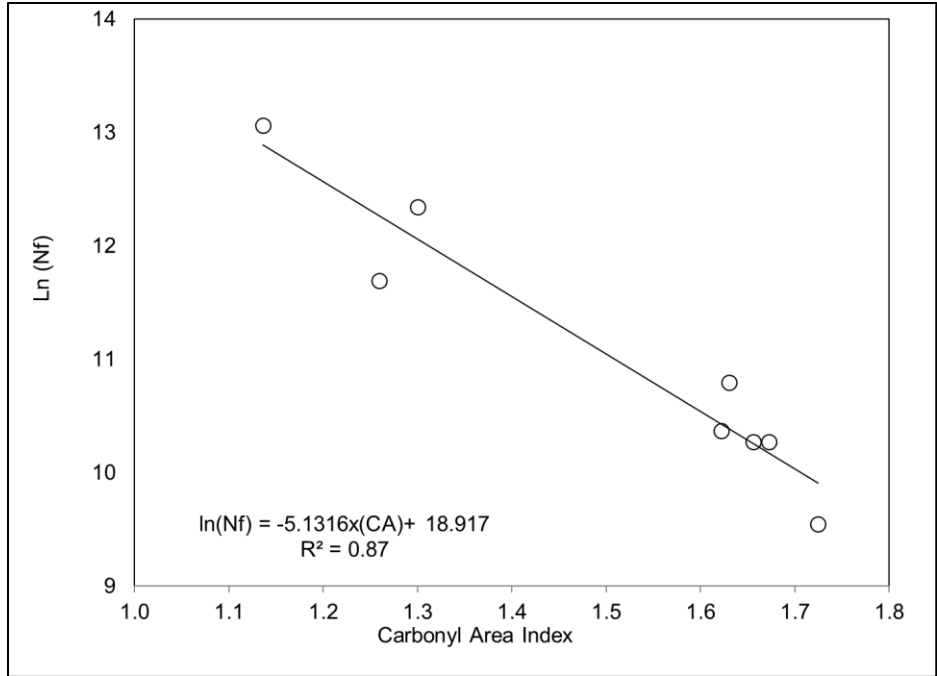
a: Mix D
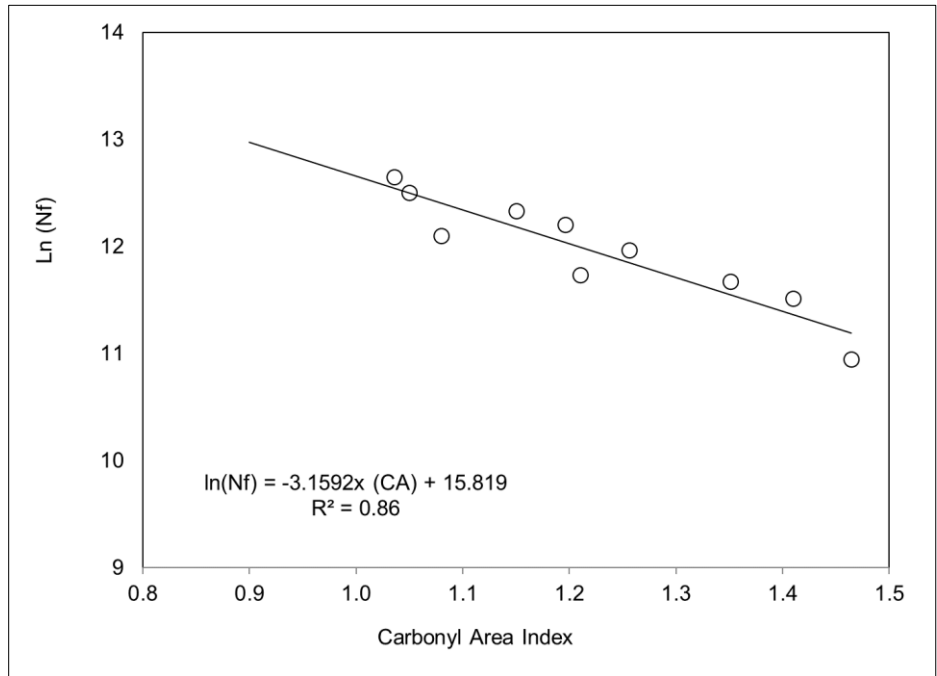
b: Mix G

Figure 6.11: Correlation between the CA index and beam fatigue life at 20°C and 10 Hz.

The correlation between ln (Nf) and the CA index is modeled in Equation 6.10. This ln (Nf)-CA

model was expected to predict the aging effect on the mix fatigue life while excluding the influence

of other mix volumetric parameters. This describes the Nf-CA index correlation at a specific testing temperature, loading frequency, and strain. Further validation of the ln (Nf)-CA model in different mixes and test conditions is warranted.

$$ln(N_f) = \alpha(CA) + ln\ (\beta)\ or\ N_f = \beta e^{\alpha(CA)}$$ 6.10

Where:
    α = slope of the $ln(N_f)$-CA curve.
    $ln(\beta)$ = intercept of $ln(N_f)$-CA curve.

The ln (Nf)-CA models used to predict fatigue lives for Mix D and Mix G are presented in Equation 611 and Equation 6.12, respectively. A comparison between the predicted and measured Nf values for each beam are presented in Figure 6.12.

$$ln(N_f) = -5.13 \times (CA) + 18.92\ or\ N_f = 164{,}266{,}390 \times e^{-5.13(CA)}$$ 6.11

$$ln(N_f) = -3.16 \times (CA) + 15.82\ or\ N_f = 7{,}422{,}303 \times e^{-3.16(CA)}$$ 6.12

The performance of the ln (Nf)-CA model was evaluated by comparing the measured and the model-predicted fatigue lives. The reliability of the ln (Nf)-CA model uses the 95 percent confidence intervals. If most points fall within that interval, it was assumed that the model would provide a satisfactory prediction of the fatigue lives. The reliability of the ln (Nf)-CA model was analyzed using the same method described in Section 6.3, with changing viscosity to fatigue life in Equation 6.5 to Equation 6.8. For Mix D, eight specimens were tested with a CA index factor level of three (corresponding to the three aging conditions [0H, 72H, and 120H]). Three replicates were tested at each factor level. The S^2 of Mix D was calculated to be 0.347 using the measured fatigue lives. For Mix G, ten specimens were tested with a CA index factor level of four (four aging conditions [0H, 44H, 72H, and 120H]). Three replicates were tested at each factor level. The

S^2 of Mix G was calculated to be 0.139 using the measured fatigue lives. The estimated boundaries of the ln (Nf)-CA model-predicted fatigue lives were then calculated using Equation 6.5 and Equation 6.6.

Table 6.16 and Table 6.17 summarize the predicted fatigue lives and the boundaries at 95 confidence intervals based on the above calculations. Figure 6.12 plots model-predicted fatigue lives versus measured fatigue lives at 20°C and 10 Hz. The measured fatigue lives were within the 95 confidence intervals of the predicted fatigue lives. The coefficient of determination (R^2) values between measured and predicted fatigue lives were larger than 0.8 and above the 0.7 threshold *(135,146,147)*, which means the observed fatigue lives were well predicted by the ln (Nf)-CA model. In summary, these results indicated that the ln (Nf)-CA model provided a reasonable prediction of the fatigue lives of the beams produced with laboratory-aged loose mixes.

Table 6.16: Comparison of Measured and Ln (Nf)-CA Model-Predicted Fatigue Lives for Mix D

Beam ID	Measured Fatigue Lives (Cycles)	Predicted Fatigue Lives (Cycles)	Upper Boundary at 95% Confidence Interval	Lower Boundary at 95% Confidence Interval
0H-1	230,000	208,130	621,230	69,730
0H-2	120,000	256,867	766,883	86,038
0H-3	472,500	482,870	1,442,768	161,608
72H-1	32,000	39,877	118,850	13,379
72H-2	29,000	30,852	91,937	10,353
72H-3	Outlier	N/A	N/A	N/A
120H-1	29,000	33,492	99,810	11,239
120H-2	49,000	38,273	114,066	12,842
120H-3	14,000	23,626	70,392	7,930

Table 6.17: Comparison of Measured and Ln (Nf)-CA Model-Predicted Fatigue Lives for Mix G

Beam ID	Measured Fatigue Lives (Cycles)	Predicted Fatigue Lives (Cycles)	Upper Boundary at 95% Confidence Interval	Lower Boundary at 95% Confidence Interval
0H-1	270,000	268,874	395,745	182,677
0H-2	Outlier	N/A	N/A	N/A
0H-3	180,000	244,556	347,417	172,150
44H-1	312,500	281,037	422,053	187,136
44H-2	227,500	196,025	265,127	144,934
44H-3	125,000	162,170	216,622	121,406
72H-1	N/A	N/A	N/A	N/A
72H-2	200,000	169,505	226,599	126,797
72H-3	157,500	140,230	188,375	104,390
120H-1	57,000	72,676	115,496	45,731
120H-2	117,500	103,864	146,454	73,660
120H-3	100,000	86,198	128,286	57,918
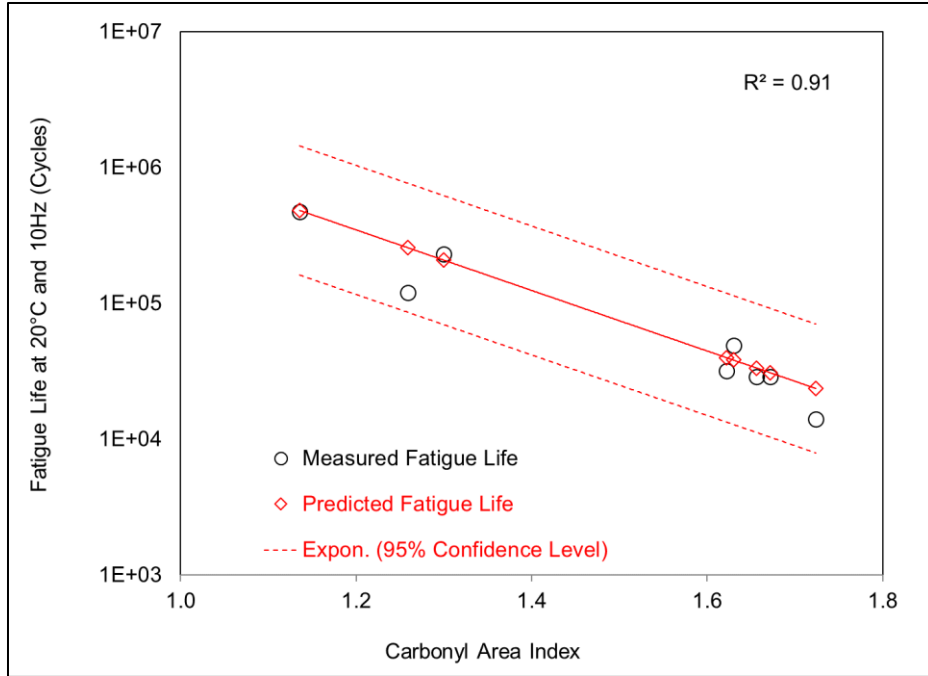
a: Mix D
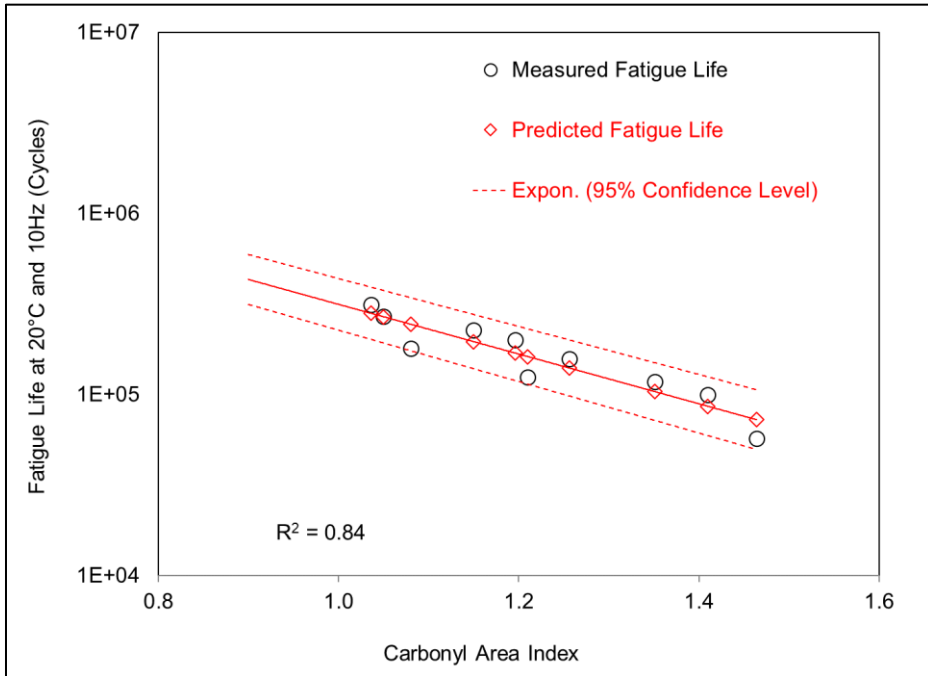
b: Mix G

Figure 6.12: Comparison of measured and predicted fatigue lives at 20°Cand 10 Hz.

269

6.6   Aging Effect on Mix Fatigue Performance

The fatigue test results for Mix D and Mix G following the test plan in Table 6.2 are analyzed in this section. Figure 6.13 and Figure 6.14 show the test results in a log-log plot. Figure 6.14c shows an apparent variability among the Mix G-72H beams. Three more beams, produced from 72-hour aged loose mix, were tested, and the results were added to the plot. However, the regression still showed a low R^2 value (0.54). A statistical analysis table was used to evaluate the variations of the fatigue lives for these beams.

The plot shows Log (Nf) on the y-axis ranging from 1E+04 to 1E+06 and Log (ε) on the x-axis ranging from 1E-04 to 1E-03. The regression equation is $y = 9\text{E-}10x^{-4.193}$ with $R^2 = 0.72$.
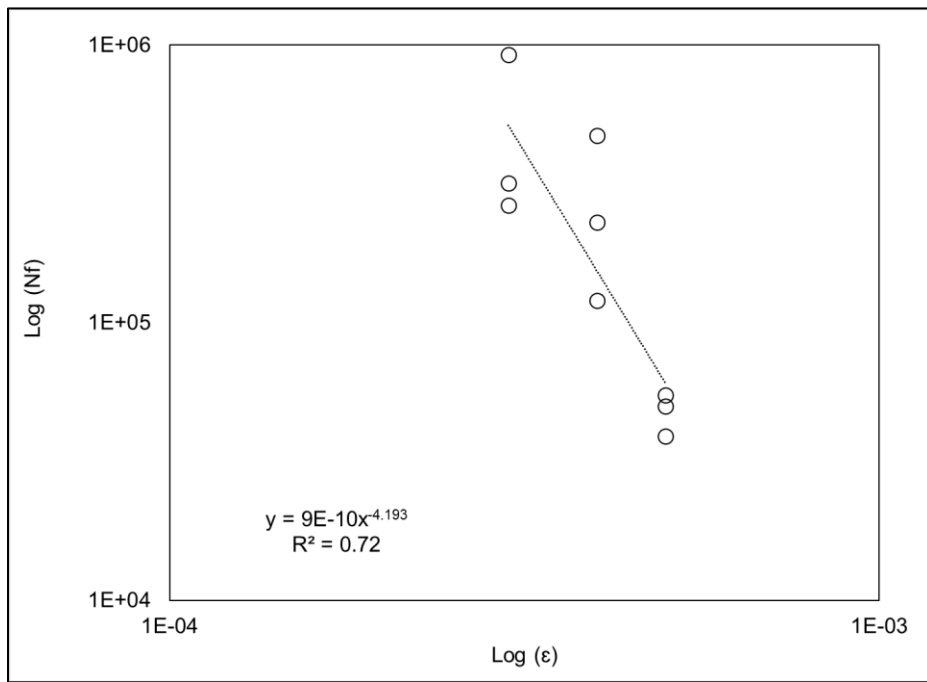
a: Mix D-0H
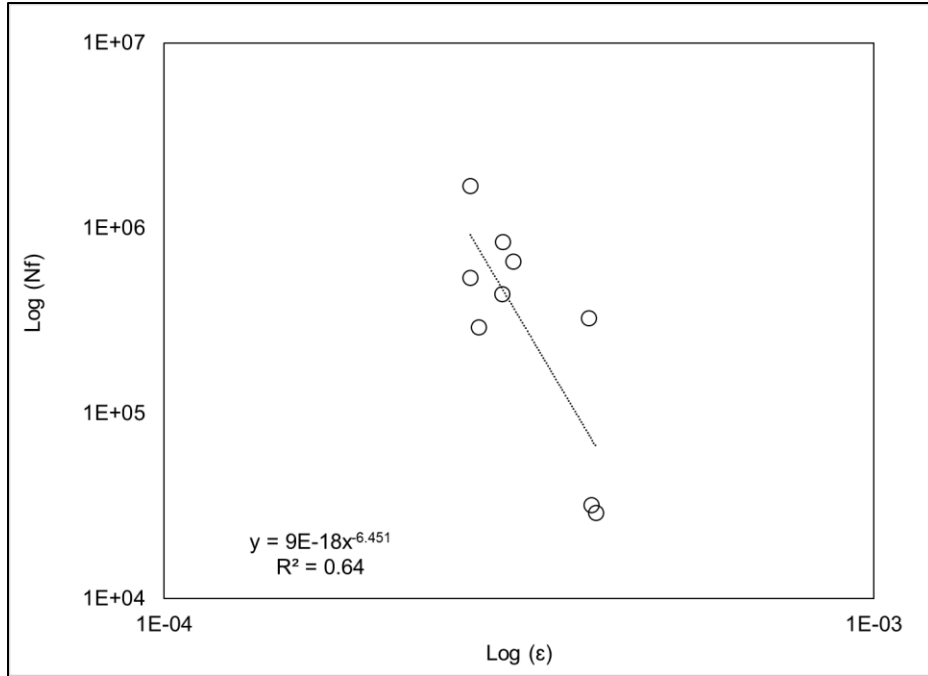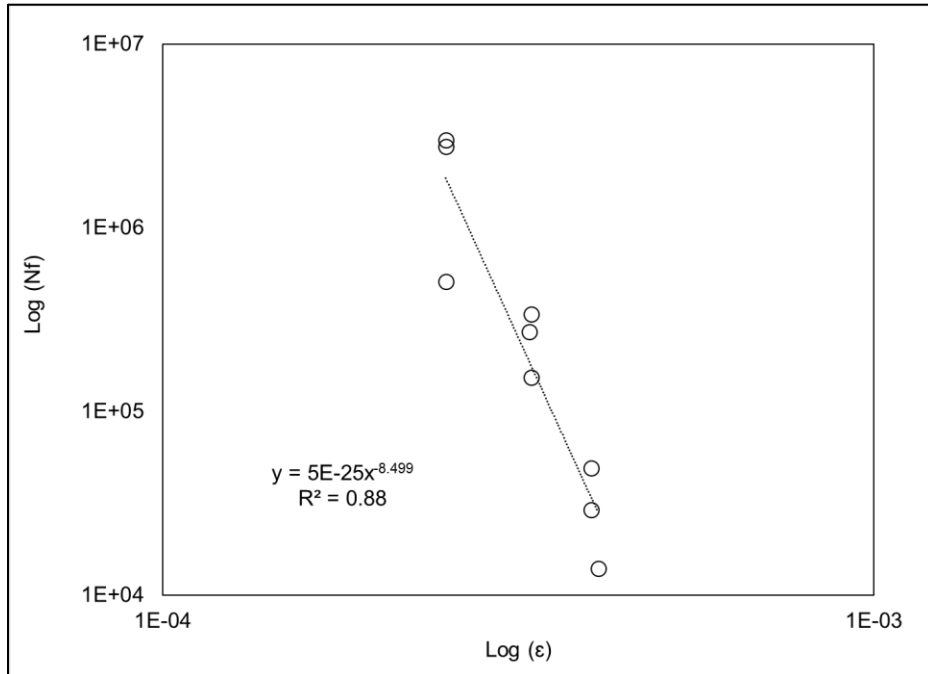
b: Mix D-72H

c: Mix D-120H

Figure 6.13: Fatigue lives of Mix D beams at 20°C and 10 Hz.

271
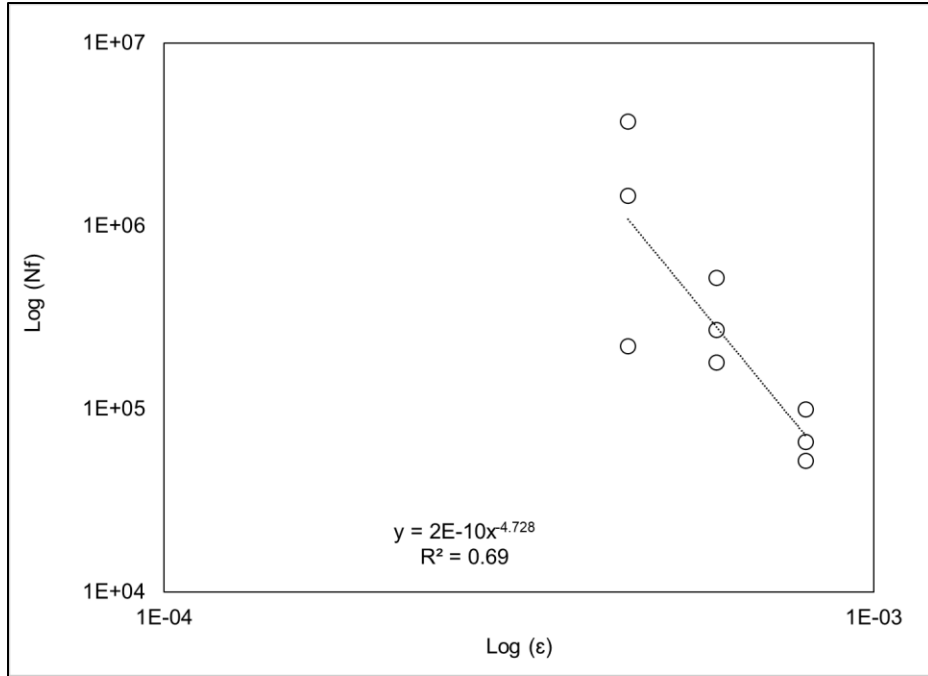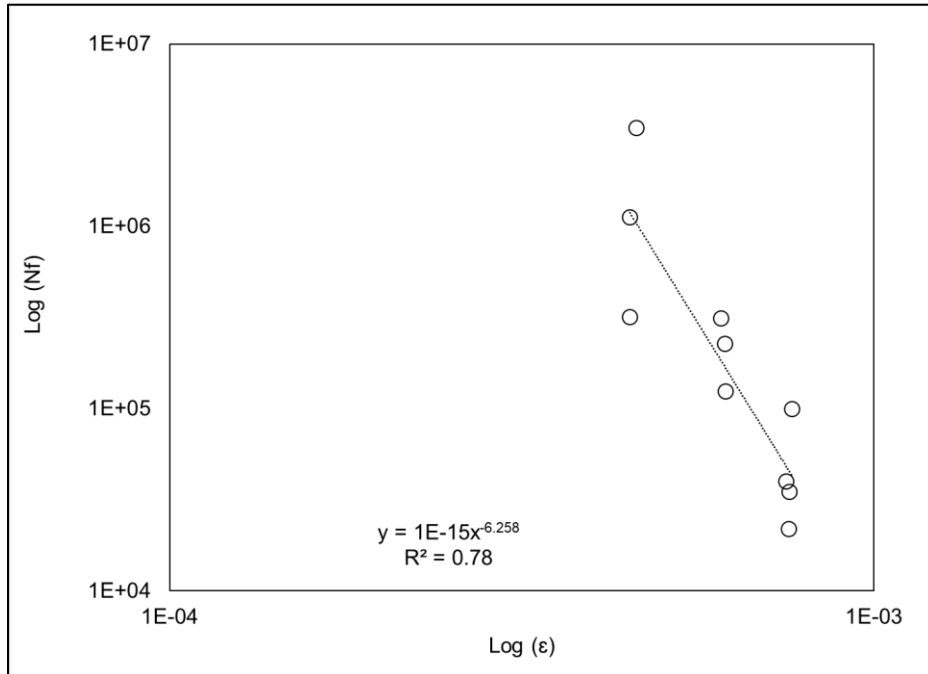
a: Mix G-0H

b: Mix G-44H
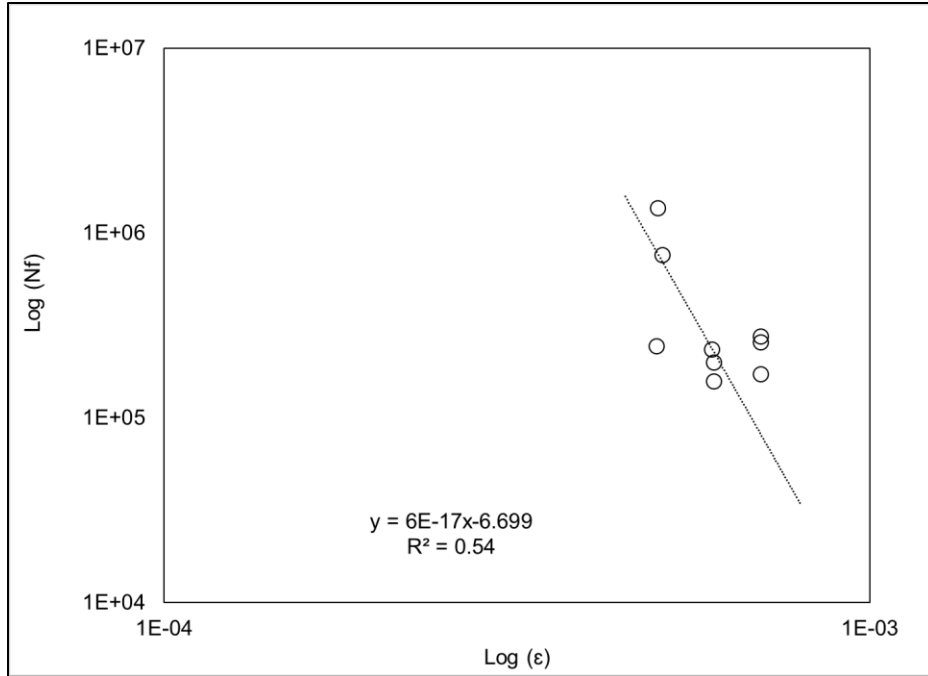
c: Mix G-72H
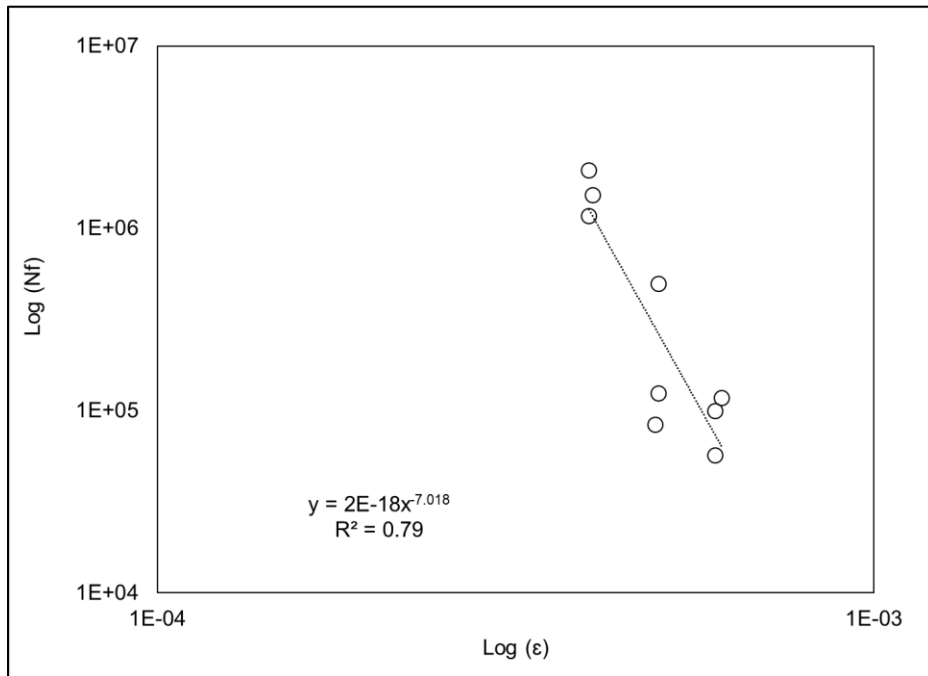
d: Mix G-120H

Figure 6.14: Fatigue lives of Mix G beams at 20°C and 10 Hz.

Table 6.18 summarizes the fatigue test results for Mix D and Mix G. Mix D-72H-3 and Mix G-0H-2 had extremely long fatigue lives (327,500 cycles for Mix D-72H-3 and 400,000 cycles for

Mix G-0H-2) and were considered to be outliers, as discussed in Section 6.5. These two beams led

to the low R^2 values of fatigue life regression versus tensile strain for Mix D-72H and Mix G-0H

beams. For Mix G-72H beams, the average Nf value at 700 microstrain was larger than the Nf

values at 600 microstrain, which dropped the R^2 values of the fatigue life regression for Mix G-

72H beams. Comparing the COVs between different aging conditions showed no consistent

changes in the COVs with increasing aging duration. The COVs among different aging conditions

were randomly distributed, indicating that the variations in fatigue lives were not caused by the

loose mix aging protocol but appeared to be caused by the variations among the sampled plant

mixes.

Table 6.18: Summary of Mix D and Mix G Beam Fatigue Test Results

Beam ID	Strain (Microstrain)	Average Nf (Cycles)	SD (Cycles)	COV	Nf=a(ε)^b		
					a	b	R²
Mix D-0H	300	502,500	299,520	0.60	9E-10	-4.193	0.72
	400	274,167	147.257	0.54			
	500	48,000	6,683	0.14			
Mix D-72H	270	840,000	607,731	0.72	9E-18	-6.451	0.64
	300	649,167	163,571	0.25			
	400	129,500	140,012	1.08			
Mix D-120H	250	2,090,833	1,121,503	0.54	5E-25	-8.499	0.88
	330	253,333	76,440	0.30			
	400	30,667	14,337	0.47			
Mix G-0H	450	1,807,500	1,456,292	0.81	2E-10	-4.728	0.69
	600	1,483,333	1,779,931	1.20			
	800	72,667	20,155	0.28			
Mix DG-44H	450	1,641,667	1,340,798	0.82	1E-15	-6.258	0.78
	600	221,667	76,658	0.35			
	750	49,250	30,028	0.61			
Mix G-72H	500	790,000	457,730	0.58	6E-17	-6.699	0.54
	600	178,750	21,250	0.12			
	700	235,833	45,522	0.19			
Mix G-120H	400	1,591,667	373,253	0.23	2E-18	-7.018	0.79
	500	235,500	186,017	0.79			
	600	91,500	25,420	0.28			

SD= Standard Deviation, COV= Coefficient of Variation.

The fatigue life (Nf) versus strain (ε) curves were developed for these tested beams using the power equations obtained from Figure 6.13 and Figure 6.14. Figure 6.15 presents the calculated fatigue lives between 100 microstrain and 1,000 microstrain strain on a log-log scale.

Figure 6.15 shows that extending the aging duration of the loose mixes led to a steep Nf- ε curve for beams produced with these mixes, which caused the beams to be more sensitive to changes in strain. At higher strain levels, such as 300 microstrain and above, beams produced with aged mixes that experienced the longer aging durations had lower fatigue lives than those under shorter aging durations, while it was the opposite at low strain levels. The log (Nf)-log(ε) curve of Mix G-72H was not in between the curves of Mix G-44H and Mix G-120H because of the high variability in the fatigue test results of Mix G-72H that might impact the accuracy of the log (Nf)-log(ε) curve, as Table 6.18 shows.
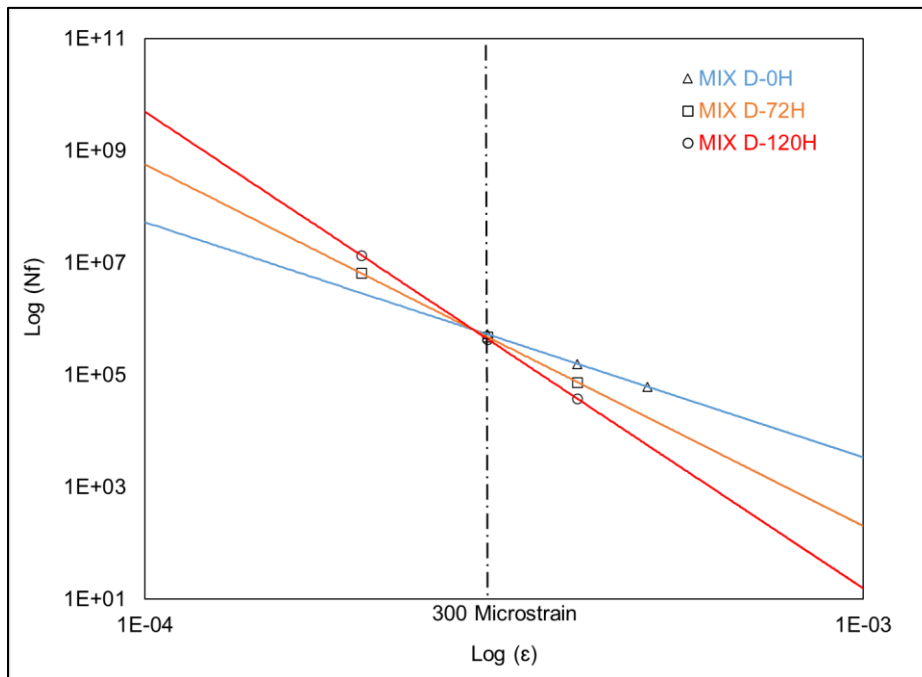
a: Mix D
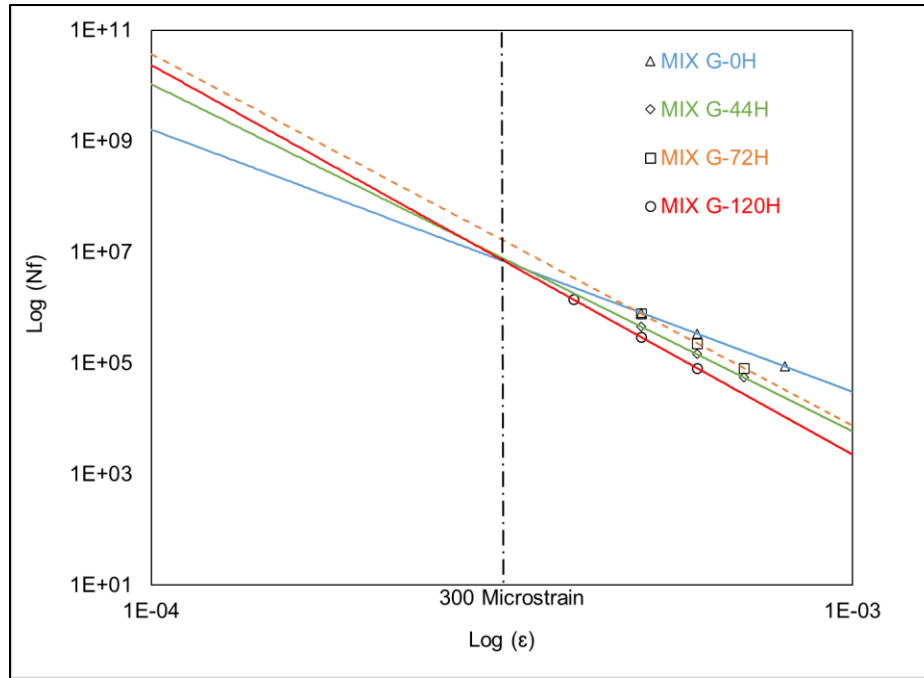
b: Mix G
Figure 6.15: Fatigue life versus strain curves on a log-log scale at 20°C and 10 Hz.

As described in Section 2.4, classical theories suggest that softer mixes have longer service lives than stiffer mixes in a thin layer (i.e., ≤60 mm thick) where performance is mainly strain-controlled (*131*). The performance of aged mixes in a relatively thin layer (<approximately 60 to 100 mm) has been widely studied *(31,132,185,192,193)*. Aged mixes are stiffer than unaged mixes. In thin layers, the strain at the bottom of the layer is normally high under a given traffic load (i.e., approximate 600 microstrain when applying an 80 kN single load on a 60-mm thick layer, standard contact area size, and layer stiffness of 6,000 MPa). Although these aged mixes in a thin layer might experience a lower strain than the unaged soft mixes, the fatigue lives of aged mixes are shorter than the unaged mixes in high strain conditions (>300 microstrain). The aged mixes also have less capacity to withstand the damage generated by traffic and the environment (i.e., daily and seasonal temperature fluctuations). The age-stiffened binders also tend to have a cohesive

276

failure that results in fatigue cracking and reflective cracking. When the strain in the thin layer is relatively high (i.e.,>300 microstrains), aging shortens the fatigue life, as Figure 6.15 shows.

In relatively thick layers (>approximately 60 to 100 mm), a stiff mix can reduce the structural bending moment, which benefits the fatigue life (*131*). The in-service aging mostly occurs in the layer surface, and it gradually reduces with depth due to less accessibility of oxygen to the mix. The layer surface becomes stiff and transfers lower stresses to the bottom of the layer. The asphalt at the bottom of the layer is less aged, and they are at a low strain level. When the strain in this thick layer is relatively low (i.e., <300 microstrain), the fatigue life of the mix at the low strain is longer. From this perspective, age-stiffening of the mix may not necessarily decrease the service life in a thick layer.

6.7 Summary and Conclusions

This chapter investigated long-term oven-aging and its effect on asphalt mixes. Two types of loose mixes (dense-graded mix [Mix D] and gap-graded mix [Mix G]) were short-term oven-aged (STOA) at 135°C for four hours. The STOA mixes were then divided into the control group and the long-term oven aging (LTOA) group. Long-term laboratory aging was simulated in an oven on loose mixes at 85°C for different durations. Flexural frequency sweep and fatigue tests were conducted on beam specimens produced with mixes subjected to LTOA and without LTOA. Binders were extracted from these beams produced with control mixes and LTOA mixes after the fatigue test. Changes in binder chemical components were tracked using the CA indices measured with an FTIR. Changes in binder rheological properties were determined by running frequency sweep tests in a DSR. The following conclusions were drawn:

1. Question: Will the loose mix aging protocol cause high variations in binder contents, mix stiffnesses, and fatigue lives of the specimens?

   Fatigue beams can be compacted to the target air-void content from loose mixes after LTOA. The loose mix aging protocol showed similar variations in binder contents, mix stiffnesses, and fatigue test results among different aging durations as those in the compacted specimen aging protocol.

2. Question: Can the binder GHS model be used for the recovered binders in aged asphalt mixes?

   The GHS model provided a reasonably accurate prediction of the binder viscosity using measured CA indices of the extracted and recovered binders from aged mixes. The binder GHS model was validated using rheology test results for the recovered binders tested at temperatures

between 20°C and 85°C with frequencies between 0.0159 Hz and 15.9 Hz (0.1 and 100 radians/second).

3. Question: How does oxidative aging affect mix stiffness?

Aging the loose mix resulted in a continuous increase in the CA index in the recovered binder. The CA index of the recovered binder was used to track the oxidative aging in the asphalt mix. Increases in the CA index increased binder viscosity. The age-hardened binder stiffened the mix. The degree of age-hardening or stiffening of the two mixes (dense-graded mix [Mix D] and gap-graded mix [Mix G]) tested in this study could be predicted using the Andrei-Witczak-Mirza stiffness prediction model and the GHS model-predicted binder viscosity.

4. Question: How does oxidative aging affect mix fatigue performance?

A linear correlation between the logarithmic fatigue life (ln Nf) of these beams produced with aged loose mixes at a given strain and the CA indices of the binders recovered from the beams was found for Mix D and Mix G. An ln (Nf)-CA model that describes the correlation between ln Nf and CA index was proposed ($N_f = \beta e^{\alpha(CA)}$). This model defines the aging effect on fatigue life for the tested mixes at the defined mix volumetric parameters and fatigue testing conditions. Fatigue test results for beams produced with long-term oven-aged loose mixes showed lower fatigue lives at higher strains (>300 microstrain) than the ones without long-term oven-aging, while it was opposite at lower strain levels (<300 microstrain). In a thin layer (i.e., <60 mm) where high strains are common, the aged mixes may experience a lower strain than the unaged mixes, but the former still provide shorter fatigue lives at higher strains. In a thick layer where lower strains are typical, aging stiffens the layer surface, and the stiff surface transfers lower stresses to the bottom of the layer. The asphalt at the bottom of the layer is less

aged, and it is at a lower strain level, which may result in longer fatigue lives for thick asphalt layers.

The findings of laboratory test results (validation of GHS model, age-stiffening, and fatigue changes with long-term oven-aging) point to a general framework for studying the aging effect on asphalt binders and mixes. The logarithmic fatigue life at a single strain was linearly correlated to the CA index of the recovered binder. Once this correlation is established for a given mix, changes in binder viscosity and mix fatigue life with the CA index can be predicted. Additional validation of this Nf-CA principle using field data under different aging conditions is warranted.

It should be noted that aging in the mix is an ongoing chemical-physical interaction. General correlations should be made with caution. Additional tests of different LTOA mixes are recommended following the procedure in this chapter (loose mix aging protocol, beam fatigue test, extraction and recovery of the binder from the beam, FTIR and DSR testing of the recovered binder). It is anticipated that a general correlation can be developed between binder aging and mix aging based on a large database. This correlation can then be used to estimate mix stiffness and fatigue performance after LTOA by testing the binder instead of testing the mix. This approach could save cost and time in laboratory testing.

The test results in this chapter show that the performance (i.e., stiffness and fatigue performance) of the aged mix is different from the unaged mix, as expected. This observation implies that using unaged mix performance to predict the performance of in-service pavements may not be appropriate. It seems realistic to use the mix performance test results after aging instead of those in unaged condition to estimate in-service performance. However, the appropriate aging conditions

may vary by mix and binder types, and this additional aging protocol could increase testing time and cost.

7 PERFORMANCE EVALUATION OF RUBBER-MODIFIED BINDERS AND MIXES

7.1 Introduction

This chapter summarizes the evaluation of rubber-modified binders and dense-graded mixes containing low contents of crumb rubber modifier. The motivation in this chapter was to evaluate the performance of rubber-modified binders in dense-graded mixes using laboratory tests and mechanistic-empirical (ME) simulations. A relatively small amount of rubber is defined as five to ten percent rubber by weight of the binder or 0.25 to 0.50 percent rubber by weight of the aggregate (*17*). These materials were collectively labeled "PG+X" materials, meaning that the binder meets or exceeds the PG of the base binder with X percent rubber added.

Four tasks should be completed to evaluate any new material, including PG+X materials. First, testing and analysis of example materials to determine their capability of meeting Superpave PG specifications. This task includes asphalt binder and mix testing. Second, evaluation of the effects of mix properties on pavement performance in different thicknesses of overlays and new/reconstructed asphalt pavements using the *CalME* mechanistic-empirical analysis and design program for different levels of traffic and different climate regions. Third, life cycle cost analysis should be performed, which includes identification of cost and performance data, and analysis of the net present value, with sensitivity analysis. Fourth, life cycle assessment should be performed, which includes the development of environmental flow data, calculation of impacts, and interpretation and reporting of the results.

The first and second tasks were addressed in this chapter by answering the following questions:

- How do PG+X binders perform in the laboratory?

- Can PG+X materials be effectively used in dense-graded mixes?

- How do PG+X mixes perform in the laboratory in terms of rutting, fatigue, and thermal cracking?

- What are the appropriate uses of PG+X mixes in different pavement structures and climates?

The steps to accomplish the work in this chapter were:

- Evaluation of rubber-modified binders containing low contents of crumb rubber modifier.

- Mix design of the rubber-modified dense-graded mixes containing low contents of crumb rubber modifier.

- Performance evaluation of PG+X mixes using laboratory tests.

- Understanding how PG+X mixes can best be used in a pavement structure using *CalME* simulation.

7.2 Experimental Design and Test Methodology

In this chapter, four different approaches were used to prepare PG+X mixes. Three of these approaches used wet-process binders, and the one remaining approach used dry-process rubber. All these mixes were produced using laboratory mixing and laboratory compaction methods. One uniform aggregate gradation was used in these four approaches without adjusting the gradation for dry-process rubber. The same aggregates and RAP materials were used in the laboratory batching. The differences between different PG+X mixes were the binder source and the rubber type (i.e., rubber content, rubber particle size, rubber production method).

The Superpave performance-grading was used to obtain the binder PGs for wet-process binders. The multiple stress creep recovery test was used to evaluate the rubber effect on binder performance. The rotational viscosity test was used to determine the mixing and compaction temperatures for PG+X mixes. Volumetric mix design was conducted after completing the binder tests. Mix stiffness, moisture damage resistance, rutting resistance, and fatigue damage resistance were evaluated for all mixes. The evaluation of the thermal cracking resistance was conducted on three approaches (two approaches using the wet-process binders and one approach using the dry-process rubber). The one remaining approach using the wet-process binder did not test the thermal cracking resistance because the other two approaches using the wet-process binders showed that the thermal cracking resistance was mainly influenced by the binder properties (i.e., intermediate PG), which did not require measurement of mix properties.

7.2.1 Material Classification and Preparation

7.2.1.1 Classification of PG+X Materials

The material preparation followed the approaches identified by Caltrans and industry in 2016 (*17*):

284

Approach-1: PG+X for binders with five and ten percent rubber by weight of the binder that meet the current Caltrans PG-M (modified binder) specification *(2)*. Aggregate gradations were not adjusted to accommodate the rubber in the binder. The Approach-1 binder suppliers' understanding was that the PG+X binder they delivered needed to meet the same high and low PG grade as the control binder.

Approach-2: PG+X asphalt rubber binders that meet the requirements (i.e., PG) similar to those in the anticipated PG-AR (asphalt rubber) specifications using the modified Superpave PG system *(70)*. It was anticipated that binders prepared using the same approach currently being used to prepare asphalt rubber binders for gap- and open-graded mixes (i.e., rubber particles smaller than 2.36 mm [passing the #8 sieve]) and in chip seals (i.e., rubber particles smaller than 1.41 mm [passing the #14 sieve]), but at lower rubber contents (five to ten percent), and potentially smaller rubber particles would fall into this category. Dense aggregate gradations were not adjusted to accommodate the rubber in the binder. The Approach-2 binder suppliers' understanding was that the PG+X binder they delivered should use the control binder as the PG+X base binder, and the PG+X binder did not need to meet the same high and low PG grade as the control binder.

Approach-3: Addition of between 0.25 and 0.50 percent rubber per ton of asphalt mix (~ 5 to 10 lb/ton [2.3 to 4.5 kg/ton]) using a dry-process. Mixes prepared in this way must still meet all Caltrans specifications. The PG of the binder should not be affected if this approach is followed since the rubber is not blended into the binder. No adjustment to the gradation was made to accommodate the rubber.

Approach-4: Same as Approach-2, but using other recycled tire rubber formulations typically with a finer rubber particle size, such as devulcanized tire rubber, which can be field-blended to produce a binder containing between five and ten percent rubber by weight of the binder that still meets PG-M binder specifications *(2)* but with potentially some relaxation of the solubility and/or separation parts of the specification. Agreement between Caltrans and industry allowed that the addition of the rubber might result in a change to the PG of the base binder. Dense aggregate gradations were not adjusted to accommodate the rubber in the binder. The Approach-4 binder suppliers' understanding was that the PG+X binder they delivered should use the control binder as the PG+X base binder, and the PG+X binder did not need to meet the same high and low PG grade as the control binder.

Table 7.1 summarizes the PG+X binders and mixes evaluated in this chapter. The asphalt binders were provided to UCPRC with the acknowledgment by the suppliers that their binders met the requirements of the selected approach listed above.

The Approach-1 PG+X binders were blended at the suppliers' refineries/terminals, which is known as a terminal blend process. The base asphalt binder was blended with crumb rubber particles reported by the supplier as smaller than 250 microns (passing the #60 sieve) at a 25 percent concentration by weight of the binder. This mixed binder was then blended with a low PG binder (i.e., PG 58-28) and some other additives (i.e., SBS) to accommodate the required final binder PG (i.e., PG 64-16). This production process was summarized from the oral communication between the laboratory and the supplier. The supplier guaranteed that the final PG+X binders contained the required amount of rubber (five and ten percent rubber by weight of the binder), and these binders met all PG-M binder criteria listed in the Caltrans Section 92 specification *(2)*. The laboratory did

not know the exact additives used in the Approach-1 binders. The laboratory used the standard Superpave PG system to grade the binders received from the suppliers.

The field blend process was used to produce the Approach-2 rubber-modified binders at a local asphalt plant. The Approach-2 binders are the Group B binders discussed in Chapter 5. The binder profile provided by the supplier showed that the rubber particles used in these Approach-2 PG+X binders were smaller than 2.36 mm and 1.18 mm, respectively. The gradations of the coarse and fine rubber particles used in these binders are shown in Figure 5.8. No additional additives or extender oils were used. The blending was conducted at 190˚C. Blending of the five and ten percent rubber contents took 30 and 60 minutes, respectively. The laboratory used the modified Superpave PG system to grade the received binders with the understanding that no additives other than rubber were used in Approach-2 binders.

Table 7.1: Material Factors Summary

Approach	Refinery Code	Blending Type	Rubber Content (%)	Maximum Rubber Particle Size(mm)	Binder ID[1]	Mix ID
1	A	Control	0	N/A	A-64-16	A
	A	Terminal Blend	5	<0.25	A-64-16-5-0.25	B
	A	Terminal Blend	10	<0.25	A-64-16-10-0.25	C
	A	Control	0	N/A	A-70-10	D
	A	Terminal Blend	5	<0.25	A-70-10-5-0.25	E
	A	Terminal Blend	10	<0.25	A-70-10-10-0.25	F
2	B	Base	0	N/A	B-64-22	S
	B	Field Blend	5	<2.36	B-64-22-5-2.36	T
	B	Field Blend	10	<2.36	B-64-22-10-2.36	U
	B	Field Blend	5	<1.18	B-64-22-5-1.18	
	B	Field Blend	10	<1.18	B-64-22-10-1.18	
3	A	Dry		<2.36	A-64-16-DRY-5-2.36	G
	A	Dry	10	<2.36	A-64-16-DRY-10-2.36	H
4	C	Base	0	N/A	C-64-22	J
	C	Terminal Blend	5	<0.25	C-64-22-5-0.25	K
	C	Terminal Blend	10	<0.25	C-64-22-10-0.25	L

[1] Binder ID format: source-PG-rubber content in percent-maximum rubber size in mm.

Approach-3 mixes were produced using a dry mixing process. As defined by the production methodology, no modified binder was used in the mix. The unmodified control binder used in Mix A was also used to produce the mixes with dry-process rubber. The crumb rubber was the same coarse rubber (<2.36 mm [passing the #8 sieve]) used in Approach-2, and these rubber particles were directly blended with the aggregate and binder in the mixing unit. No binder test was used in Approach-3 since the dry-process procedure did not modify the binder before mixing. The laboratory did not use any additives other than rubber in the Approach-3 mixes.

For Approach-4 materials, a California refinery provided the PG 64-22 base binder. Approach-4 binders are the Group A binders discussed in Chapter 5. The supplier guaranteed that the

devulcanized rubber used in their product had particles smaller than 250 microns (passing the #60 sieve). The base binder was delivered to the rubber recycling company to blend with devulcanized rubber particles at 190˚C to produce a concentrated binder with a rubber content of 25 percent. This concentrated binder was then further diluted at the UCPRC laboratory with the same base binder at 163˚C to obtain the final two products containing equivalent rubber dosages of five percent and ten percent, respectively. The laboratory conducted Superpave performance-grading on the received binders with the understanding that no additives other than rubber were used in these Approach-4 binders.

The laboratory test results showed that the solubilities were 97.5 percent for the Approach-4 rubber-modified binder containing five percent rubber and 95.2 percent for the one containing ten percent rubber. The test results indicated that Approach-4 rubber-modified binders with ten percent rubber did not meet the 2018 Caltrans specification *(2)* solubility requirement for modified binders, which is a minimum of 97.5 percent. This solubility criterion has been relaxed in Florida and Louisiana *(31,32)*, considering that all other binder properties meet the specification criteria (i.e., PG).

7.2.1.2   Aggregate and RAP

A dense-graded job mix formula (JMF) from a local asphalt plant was used to prepare mixes for this part of the study. Table 7.2 shows the aggregate gradation. Five virgin aggregate bins (3/4" manufactured aggregate [MA], 1/2" MA, 3/8" MA, 1/4" dust, and sand bins) plus 3/8" RAP were blended to meet the target gradation. RAP was used in this dense-graded mix following the common practice in California *(2,194)*. The quartering and splitting of the RAP materials were strictly controlled in the laboratory to ensure that the RAP contents in each mix were similar *(167)*,

such that the use of RAP was not considered as an active factor in the analysis because the control mixes and PG+X mixes contained the same RAP.

Virgin aggregates were oven-dried at 110ºC, and the RAP was oven-dried at 60°C for at least 20 hours to remove the moisture. All dried aggregates and RAP materials were stored in sealed barrels or buckets until batching.

Table 7.2: Aggregate Bin and Mix Gradation

Bin Size	3/4" MA[1]	1/2" MA	3/8" MA	1/4" x Dust	Sand	3/8" RAP
Bin Percentage (%)	15.0	12.0	27.0	22.0	9.0	15.0
Sieve Size (mm)	**19**	**12.5**	**4.75**	**2.36**	**0.60**	**0.075**
Laboratory Gradation Passing Percentage (%)	99.3	89.6	48.8	31.5	16.6	4.5

[1] MA: Manufactured Aggregate.

7.2.2 Experimental Design for Rubber-Modified Materials Testing

A series of laboratory tests were used to evaluate the PG+X binders. The performance-grading was used for Approach-1, Approach-2, and Approach-4 binders. The performance evaluation focused on the Approach-2 and Approach-4 binders, which contained the required five and ten percent rubber without other additives.

The performance grading tests were used to grade Approach-1, Approach-2, and Approach-4 binders following AASHTO M 320 *(30)*. Binders in Approach-1 and Approach-4 were produced with fine rubber particles smaller than 250 microns (passing the #60 sieve) and were therefore tested following the standard AASHTO T 315 procedure *(74,162)*. The refined performance-grading system discussed in Chapter 5 was followed for testing the Approach-2 PG+X binders, which contained coarse rubber particles (>250 microns). Accordingly, the standard RTFO-aging following AASHTO T 240 *(98)* and PAV-aging following AASHTO R 28 *(97)* were applied to all

base binders and the Approach-1 and Approach-4 PG+X binders. The modified aging protocols were used for Approach-2 PG+X binders.

A multiple stress creep recovery (MSCR) test was performed on RTFO-aged binders following AASHTO T 350 *(195)*. This test was used to evaluate the rutting resistance of the Approach-2 and Approach-4 PG+X binders *(196,197)*. A test temperature of 64°C was selected for this testing based on the PG of the base binders.

A rotational viscometer test was used to determine the mixing and compaction temperature for Approach-2 and Approach-4 PG+X mixes following AASHTO T 316 *(198)*. The mixing and compaction temperatures for Approach-1 binders were given in the binder profiles provided by the supplier. These profiles showed that Approach-1 PG+X binders shared the same mixing and compaction temperatures with their control binders at the same PG.

A Brookfield DV-II viscometer was used to determine the viscosities of the Approach-2 and Approach-4 PG+X binders. The tests were conducted at 135°C and 165°C. An SC4-27 spindle with a 10-mm diameter was used to run the test at these temperatures. No tests were run above 165°C due to the limitations of the geometry used. The viscosity at higher temperatures (>165°C) is lower than the minimum viscosity that can be measured by the SC4-27 spindle (approximate measuring range between 250 and 5,000,000 cPa·s), which implies that a larger spindle-SC4-21 (approximate measuring range between 50 to 1,000,000 cPa·s) should be used. This SC4-21 spindle has a diameter of 15-mm, and the cup used to load the binder has a diameter of 18 mm. The Approach-2 coarse rubber particles (<2.36 mm) were, therefore, larger than the gap (~1 mm) between the SC4-21 spindle and the cup in the rotational viscometer, which would have a significant impact on the test. The viscosity curves were plotted using the measured points at

135°C and 165°C in Section 7.3.3. The laboratory mixing and compaction temperatures were determined at the temperatures where binder viscosity reached 0.17 Pa·s and 0.28 Pa·s, respectively *(2)*.

PG+X mix testing included the mix design followed by a series of mechanical tests to assess the performance of PG+X binders in dense-graded mixes.

Section 7.3.5 to Section 7.3.9 discusses the performance of Approach-1, Approach-2, Approach-3, and Approach-4 mixes. Although the Approach-1 binders were not ideal for evaluating the rubber effect because of the uncertainty surrounding the base binder PG and other additives used by the binder producer, analysis of the Approach -1 mix performance was necessary to validate the application of a small amount of rubber through the approaches identified in the material classification (Section 7.2.1).

The laboratory test plan included the Hamburg wheel track test (HWTT), unconfined repeated load triaxial (RLT), flexural frequency sweep (FS), flexural beam fatigue (FAT), and uniaxial thermal stress and strain test (UTSST). Table 7.3 summarizes the conditions for these tests.

The HWT and RLT tests were conducted at high service temperatures (i.e., 50°C) to evaluate moisture damage and rutting resistance, respectively. The beam FS tests at temperatures of 10°C, 20°C, and 30°C were used to characterize the mix stiffness, and the beam FAT tests were used to evaluate the mix fatigue performance at 20°C, as this temperature is recommended in AASHTO T 321. The UTSST was conducted to characterize the thermal cracking resistance at low temperatures (i.e., the test starts from 20°C and cools down at 10°C per hour).

Table 7.3: Summary of Mix Test Factors

Test	Temperature (°C)	Air-Void Content (%)	Testing Parameters	Replicates
HWTT	50	7.0±1.0	Submerged specimen	4 Specimens
RLT	50	7.0±0.5	Unconfined specimen	5 Specimens
FS	10, 20, 30	7.0±1.0	Strain controlled (100 microstrain) at 0.01 Hz to 15 Hz	3 Specimens
FAT	20	7.0±1.0	Three strain levels (200, 300, 400 microstrain) at 10 Hz	3 Specimens per strain level
UTSST	-Δ10/hour	7.0±1.0	Unconfined specimen	2 Specimens

The HWTT followed AASHTO T 324 *(200)*. The specimens were tested in a submerged condition at 50°C and up to 35,000 loading cycles. The rut depth was continuously measured throughout the whole test process.

Rutting resistance under dry conditions was evaluated using the RLT test in an asphalt mixture performance tester (AMPT), following AASHTO T 378 *(201)*. Harvey et al. *(202)* found that the unconfined RLT test was more sensitive to the temperature than the confined RLT test, which indicated that the unconfined RLT test might provide better results than the confined one because field rutting is sensitive to temperatures. Yuan *(203)* found that the unconfined RLT test was faster and easier to perform than the confined RLT test, and the former had less variability because it resulted in fewer repetitions to failure. Pang's research *(204)* showed that the differences between unconfined and confined RLT tests were smaller when using the 483 kPa deviator stress than using other deviator stresses (207 kPa and 340 kPa).

In this study, the unconfined RLT test with deviator stress of 483 kPa was used for comparing the flow numbers between PG+X mixes and their control mixes. In the RLT test, flow number is defined to be the number of loading cycles corresponding to the minimum rate of change of permanent axial strain (PAS) *(201)*. The permanent strains were recorded until they reached five

percent of PAS or until the end of the test if the number of loading cycles needed to reach five percent of PAS was more than 20,000.

The FS test was conducted to provide a measure of mix stiffness under various loading frequencies and temperatures following AASHTO T 321 *(169)*. The test temperatures were 10°C, 20°C, and 30°C, and loading frequencies ranging from 0.1 Hz to 15 Hz. A sinewave frequency was applied to produce a tensile strain of 100 microstrain on the longitudinal surface of the beam. The measured flexural stiffnesses and phase angles were horizontally shifted into master curves at 20°C using Equation 4.3, Equation 4.4, and the Williams-Landel-Ferry (WLF) shift function *(183)*.

$$log(\alpha_T) = \frac{-C_1(T-T_r)}{C_2+(T-T_r)}$$ 7.1

Where:
   α_T = shift factor as a function of temperature T.
   T = test temperature in Kelvin (°K).
   T_r = reference temperature in Kelvin (°K).
   C_1 and C_2 = fitting parameters.

The flexural beam fatigue test was performed following AASHTO T 321 at 20°C and 10 Hz *(169)*. Three strain levels (low, medium, and high) were applied to each mix type, targeting 1E+04, 1E+05, and 1E+06 repetitions to failure. The beam fatigue life was determined at the peak of the product of flexural stiffness and load cycles to evaluate the mix response to the damage under repeated loadings *(169)*.

The UTSST was developed at the University of Nevada, Reno (UNR) to characterize fracture resistance to thermal cracking *(205)*. Before the UTSST test, compacted specimens were oven aged at 85°C for 120 hours to simulate long-term aging following AASHTO R 30 *(95)*. The standard LTOA protocol, instead of the loose mix aging protocol, was followed because the former was the proposed aging protocol that UNR used to prepare specimens for UTSST. During the test,

aged specimens were conditioned at 20°C. An initial tensile load of 20±10 N was then applied, followed by cooling at a rate of 10°C per hour until the restrained specimen failed. The fracture temperature is defined as the temperature at which the applied loading reduces by 25 percent, or a global fracture is observed. The test result is presented by the cracking resistance index (CRI$_{Env}$), which is adjusted using the environmental adjustment factor (F$_{Env}$) calculated using Equations 7.2 and 7.3 *(205)*.

$$CRI_{Env} = \frac{A_V + A_i(1 + \frac{A_V}{A_V + A_i} + \frac{A_p}{A_p + A_i})}{(\sigma_{vgt}/\sigma_f)} \times F_{Env} \qquad 7.2$$

$$F_{Env} = \frac{A_{vgt-F}}{A_{vgt-crit}} \qquad 7.3$$

Where:
A_V = area of viscous behavior in mm^2.
A_i = area of crack initiation in mm^2.
A_P = area of crack propagation in mm^2.
σ_{vgt} = thermal stress at viscous glassy transition in kPa.
σ_f = thermal stress at fracture in kPa.
A_{vgt-F} = area under the thermal stress-strain plot between the viscous glassy transition temperature and the fracture temperature in mm^2.
$A_{vgt-crit}$ = area under the thermal stress-strain plot between the viscous glassy transition temperature and the required environmental temperature at a given location.

7.3 Laboratory Test Results and Analysis

7.3.1 Performance Grading of Rubber-Modified Binders

Table 7.4 summarizes the continuous grades of the tested binders. The continuous grade is defined at the temperature where the binder rheological properties reach the PG criteria per AASHTO M 320 *(30)*.

Table 7.4 shows that Approach-1 PG+X binders maintained the same PG as the control binders under unaged, RTFO- and PAV-aged conditions. This observation indicated that the Approach-1 PG+X binders provided by the supplier had the same high and low temperature PGs to the control binders, which was noted before that the suppliers understood their objective. For Approach-2 and Approach-4 binders, the PG+X binders had higher continuous grades than their base binders at unaged and RTFO-aged conditions.

For Approach-2 binders, a one-grade bump (+6°C) of the base binder high PG was observed when adding five percent rubber, and a two-grade (+12°C) bump was reached when using ten percent rubber. For Approach-4 binders with rubber particles smaller than 250 microns (passing the #60 sieve), adding five percent rubber increased the high temperature continuous grade by an equivalent of 3°C, and adding ten percent rubber increased the high temperature continuous grade by one grade (+6°C). The results indicated that PG+X binders were stiffer than the base binder at high temperatures after short-term aging that simulated the aging condition after production and placement. These stiff rubber-modified binders had the potential to provide a better high-temperature rutting resistance.

Table 7.4: Binder Continuous Grade

Approach	Binder ID[1]	Unaged Binder (°C)		RTFO Binder (°C)		PAV Binder (°C)	
		G*/sin (δ) =1.00 kPa	Grade Change to Base Binder[2]	G*/sin (δ) =2.20 kPa	Grade Change to Base Binder[2]	G*× sin (δ) =5,000 kPa	Grade Change to Base Binder[2]
1	A-64-16	67.1	-	66.5	-	28.7	-
	A-64-16-5-0.25	67.0	-	67.6	-	23.8	-
	A-64-16-10-0.25	68.3	-	68.5	-	26.0	-
	A-70-10	71.4		70.8		33.3	
	A-70-10-5-0.25	71.9	-	72.2	-	31.6	-
	A-70-10-10-0.25	72.7	-	72.6	-	32.9	-
2	B-64-22	67.7	-	70.1	-	22.8	-
	B-64-22-5-2.36	73.7	+6.0	86.7	+16.6	20.3	-2.5
	B-64-22-10-2.36	84.4	+16.7	90.9	+20.8	19.4	-3.4
	B-64-22-5-1.18	74.6	+6.9	85.2	+15.1	21.8	-1.0
	B-64-22-10-1.18	80.1	+12.4	93.1	+23.0	22.0	-0.8
4	C-64-22	67.6	-	69.1	-	24.3	-
	C-64-22-5-0.25	71.0	+3.4	72.9	+3.8	21.0	-3.3
	C-64-22-10-0.25	75.4	+7.8	76.7	+7.6	20.2	-4.1

[1] Binder ID format: source-PG-rubber content in percent-maximum rubber size in mm
[2] Grade change was the result of subtracting the grade of the PG+X binder from that of its base binder.

For Approach-2 and Approach-4 PG+X binders, Table 7.4 also shows that increasing the rubber content and maximum particle size increased the high temperature continuous grades determined at unaged and RTFO-aged conditions, which indicated that these digested and incompletely digested rubber particles stiffened the binder. The change in the continuous grade appeared to be proportional to the rubber content and rubber particle size.

The Approach-4 PG+X binders containing fine rubber particles (smaller than 250 microns [passing the #60 sieve]) demonstrated an apparent proportional correlation between high temperature

continuous grade increase and rubber content. This correlation in the Approach-2 binders was less apparent, which was attributed to the coarser, incompletely digested rubber particles in the binder.

Figure 7.1 presents the binder phase angles at 70°C. In rheological measurement, a low phase angle corresponds to higher elasticity *(5)*. In an unaged condition, the Approach-2 and Approach-4 PG+X binders had lower phase angles than their base binders, indicating that adding rubber particles improved the elastic properties of rubber-modified binders. The phase angles of RTFO-aged binders were also lower than those of unaged binders.

A comparison of PG+X binders in Approach-2 and Approach-4 showed that increasing the rubber content and rubber particle size generally decreased the phase angle, as expected. The only exception was that the Approach-2 B-64-22-10-2.36 binder showed a higher phase angle than the Approach-2 B-64-22-10-1.18 after RTFO-aging. This was probably because of the difference in the rubber digestion between the coarse rubber (CRM_2.36, maximum particle size smaller than 2.36 mm) in B-64-22-10-2.36 and the fine rubber (CRM_1.18, maximum particle size smaller than 1.18 mm) in B-64-22-10-1.18. The fine rubber (CRM_1.18, maximum particle size smaller than 1.18 mm) digested better than the coarse one in the RTFO-aged condition. The fine rubber better modified the binder, resulting in a larger decrease of the phase angle than the coarse rubber in the RTFO-aged condition.
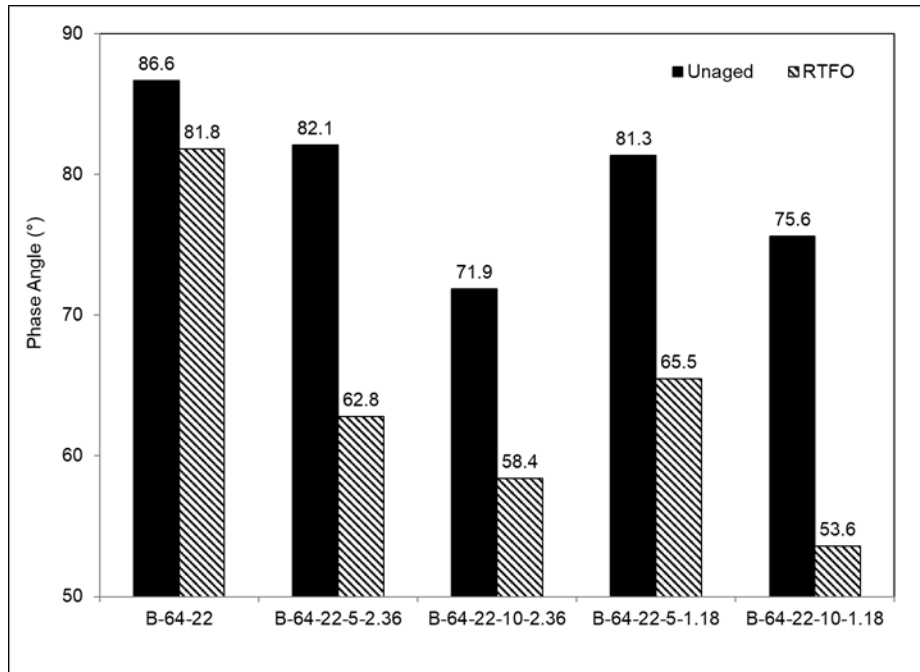
a: Approach-2 Binder (Binder ID format: source_rubber content in percent_maximum rubber size in mm)
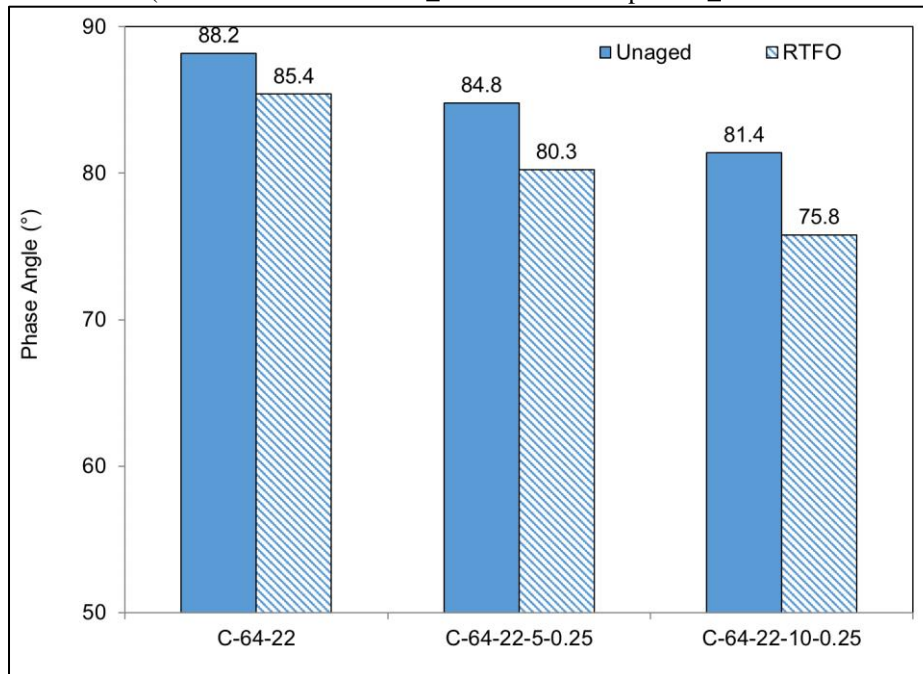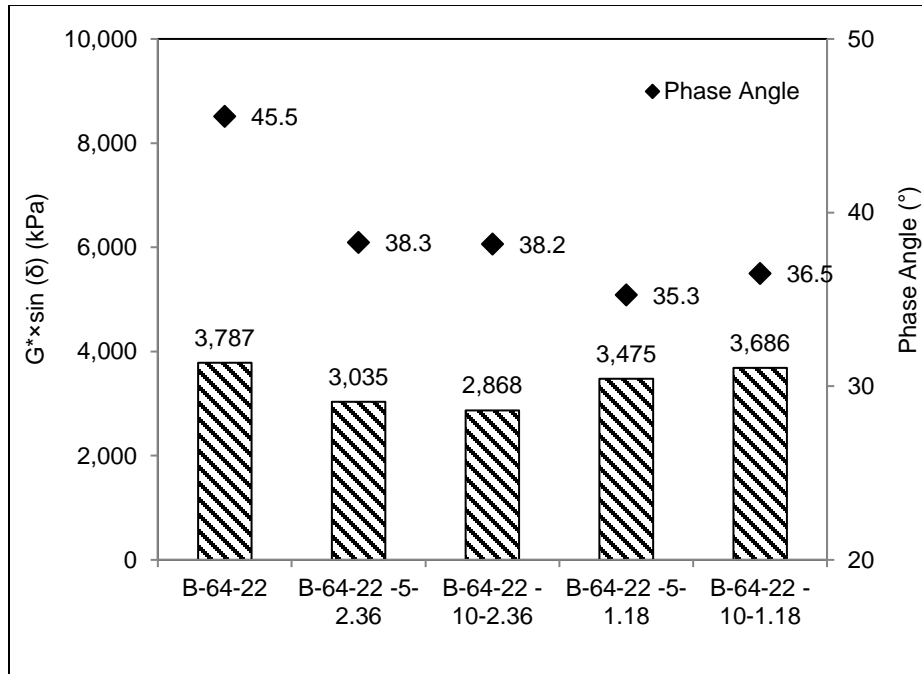

b: Approach-4 Binder (Binder ID format: source_rubber content in percent_maximum rubber size in mm)
**Figure 7.1: Binder phase angles at 70°C.**

Table 7.4 shows that Approach-2 and Approach-4 PG+X binders tended to have lower intermediate continuous grades than their base binders after PAV-aging. Figure 7.2 presents the

grading test results at 25°C and 1.59 Hz (10 radians/second condition). The results show that adding rubber generally decreased the G*×sin (δ) value, which is the criterion used for determining continuous grades at intermediate temperatures. This observation indicated that PG+X binders were softer than the base binder at intermediate temperatures, which led to a potentially better fatigue resistance than the base binder in controlled-strain flexural beam fatigue tests. The change of continuous grade was similar to conventional AR binders containing between 18 and 22 percent rubber by weight of the binder with rubber particles smaller than 2.36 mm (passing the #8 sieve) *(5,70)*, implying that similar effects of rubber modification of the binder could be achieved by this PG+X defined field blend process using a low rubber percentage (i.e., five and ten percent) and small particle sizes (i.e., smaller than 250 microns or 1.18 mm).

The effect at intermediate temperatures of rubber modification is positively related to rubber content and rubber particle size. Increasing the rubber content and particle size decreased the G*×sin (δ) values of the binders within the same approach. The low G*×sin (δ) values indicated a soft binder at intermediate temperatures (i.e., 25ºC), which benefited the fatigue performance in a controlled-strain flexural beam fatigue test.

a: Approach-2 Binder (Binder ID format: source_rubber content in percent_maximum rubber size in mm)
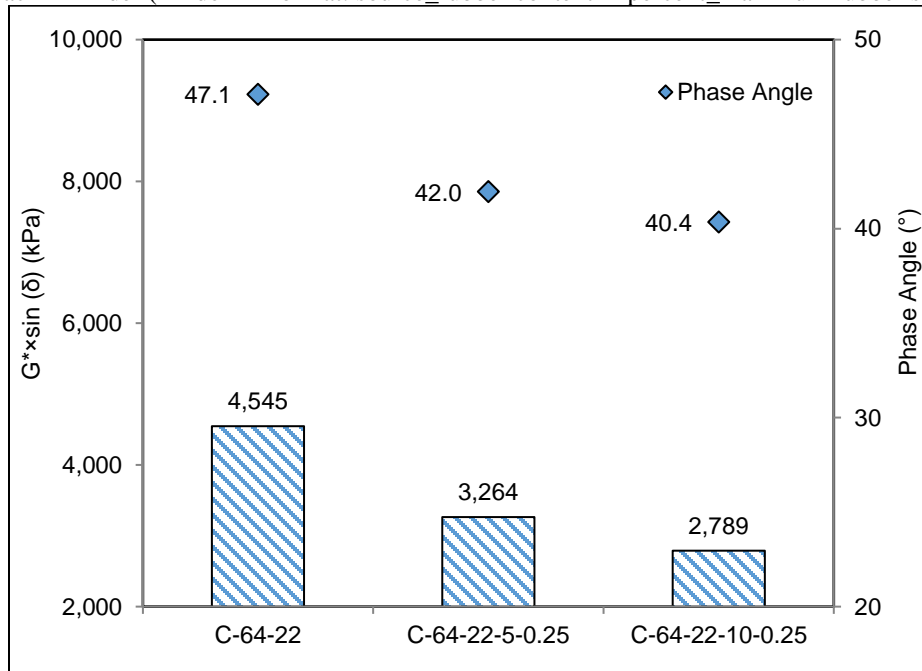
b: Approach-4 Binder (Binder ID format: source_rubber content in percent_maximum rubber size in mm)
Figure 7.2: Grading tests for PAV-aged binders at 25°C and 1.59 Hz (10 radians/second).

The BBR tests were conducted at -12°C according to the low PG of the base binders. The results

shown in Figure 7.3 indicate that PG+X binders had lower creep stiffnesses than their base binders.

Increasing the rubber content decreased the creep stiffness because more rubber particles were blended into the binder, as shown in Figure 5.11. Under the same thermal force caused by cooling, PG+X binders would generate lower thermal stresses than their base binders because of their lower stiffnesses, which lowered the binder's tendency to crack for a given thermal contraction strain.

The m-values of the rubber-modified binders were lower than those of their base binders. Lee et al. and Cong et al. *(52,55)* concluded that the m-value was dominated by base binders rather than the rubber. In the PG+X binders, a proportion of base binder was replaced by rubber particles (in other words, adding rubber reduced the actual base binder amount), which decreased the stress relaxing capability. The rubber-binder interaction that occurred in the rubber-modified binders might also change the m-value.

The contradicting effects of creep stiffness and m-value changes on low-temperature cracking resistance for PG+X binders need further analysis, which is discussed in the following paragraphs.

a: Approach-2 Binder (Binder ID format: source_rubber content in percent_maximum rubber size in mm)

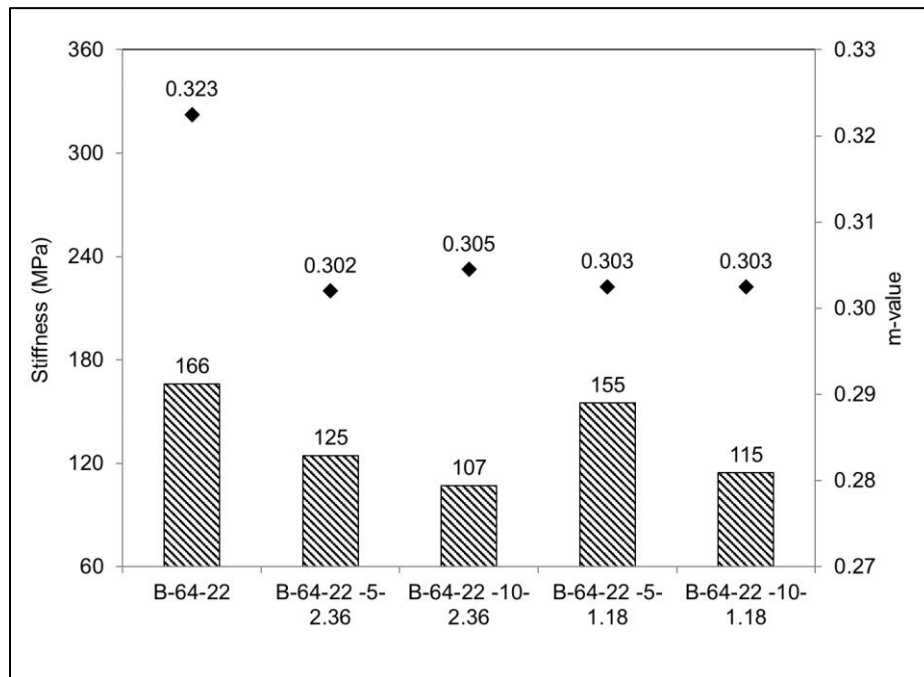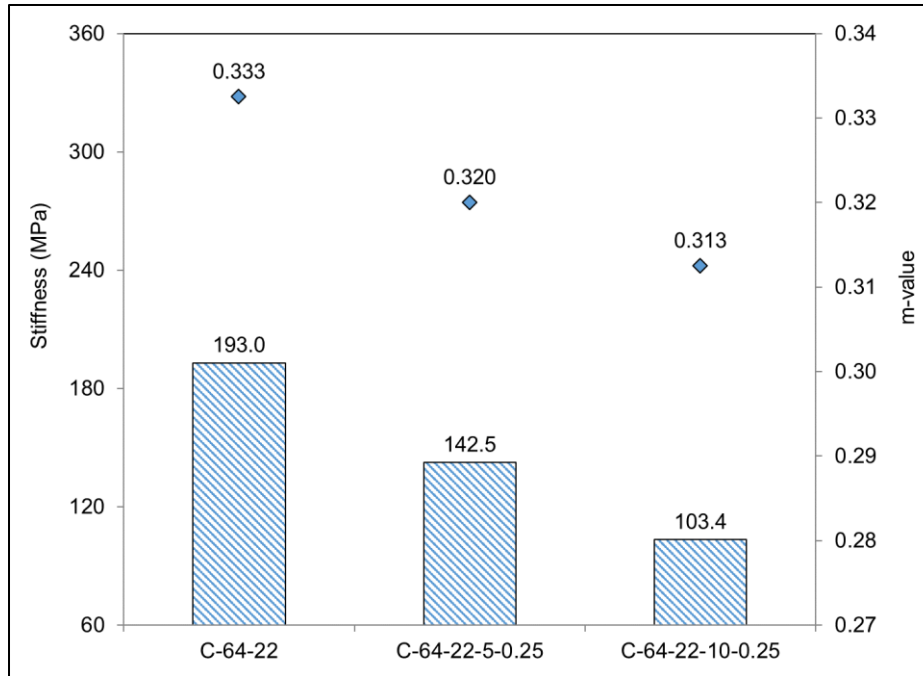b: Approach-4 Binder (Binder ID format: source_rubber content in percent_maximum rubber size in mm)
Figure 7.3: BBR test results for PAV-aged binders at -12°C.

A second round of BBR test was run at lower temperatures (-18°C and -24°C) to calculate the critical temperatures of these binders, defined as the temperature where stiffness equals 300 MPa or m-value equals 0.300. Table 7.5 summarizes the BBR test results. The results show that Approach-2 and Approach-4 PG+X binders had lower critical temperatures calculated by creep stiffness than their base binders, which was credited to the rubber modification. Adding the rubber slightly increased the critical temperature calculated using the m-value, which appeared to be caused by the lower amount of the base binder (replaced by rubber) in the rubber-modified binder and the rubber-binder interaction. These results were consistent with the results of the first round BBR tests.

The difference between the critical temperatures calculated by stiffness and by m-value is termed ΔT_C, which is an index of the binder stress relaxation *(198,199)*. Table 7.5 shows that Approach-

2 and Approach-4 binders had negative ΔT_C, indicating that they were m-value controlled. Increasing the rubber content and rubber particle size increased the absolute value of ΔT_C because adding the rubber decreased the creep stiffness but did not change the m-value much. The difference between the creep stiffness change and the m-value change requires further evaluation of the chemical interaction between the rubber and the binder. This observation was consistent with those from tests on conventional AR binders (>15 percent rubber content and rubber particles <2.36 mm) *(5,70)*. The low-temperature properties of the rubber-modified binders showed consistent changes (decreased the creep stiffness but did not change the m-value much) by adding five to 20 percent rubber with rubber particle sizes smaller than 2.36mm (passing the #8 sieve).

The ΔT_C of Approach-1 binders were also listed in Table 7.5. The unknown additives and base binders affected the BBR results, which brought in noise for analyzing the rubber effect in Approach-1 binders. Still, the Approach-1 PG+X binders met the PG requirement identified for Approach-1.

Table 7.5: Binder BBR Test Results

Approach	Binder ID[1]	$T_{C\text{-stiffness}}$ (°C)	$T_{C\text{-m value}}$ (°C)	ΔT_C (°C)
1	A-64-16	-11.0	-14.5	3.4
	A-64-16-5-0.25	-15.1	-15.3	0.3
	A-64-16-10-0.25	-12.9	-17.2	4.3
	A-70-10	-10.0	-21.9	11.9
	A-70-10-5-0.25	-10.3	-9.7	-0.6
	A-70-10-10-0.25	-8.1	-10.6	2.6
2	B-64-22	-17.3	-14.6	-2.6
	B-64-22-5-2.36	-19.8	-12.2	-7.5
	B-64-22-10-2.36	-24.7	-12.5	-12.2
	B-64-22-5-1.18	-17.9	-12.3	-5.6
	B-64-22-10-1.18	-22.4	-12.3	-10.1
4	C-64-22	-15.6	-14.8	-0.8
	C-64-22-5-0.25	-19.0	-14.4	-4.6
	C-64-22-10-0.25	-20.6	-13.8	-6.8

[1] Binder ID format: source-PG-rubber content in percent-maximum rubber size in mm.

7.3.2 Multiple Stress Creep Recovery Test of Rubber-Modified Binders

MSCR tests were conducted at two stress levels: 0.1 kPa and 3.2 kPa. D'Angelo et al. *(196)* suggested that non-recoverable compliance (Jnr) could be used as an index of rutting resistance. Figure 7.4 and Figure 7.5 plot the MSCR test results at 64°C. The results showed that Approach-2 and Approach-4 PG+X binders both had lower Jnr values than their base binders, indicating that mixes produced with these PG+X binders could have better rutting resistance than mixes produced with their base binders. Using the coarse rubber (<1.18 mm or <2.36 mm) as in Approach-2 binders showed more Jnr-value reductions than using the fine rubber (<250 microns) as in Approach-4 binders. However, the fine rubber appeared to be better digested than the coarser rubber, as the delta Jnr values in Approach-4 binders were proportional to the rubber contents in Figure 7.4b.
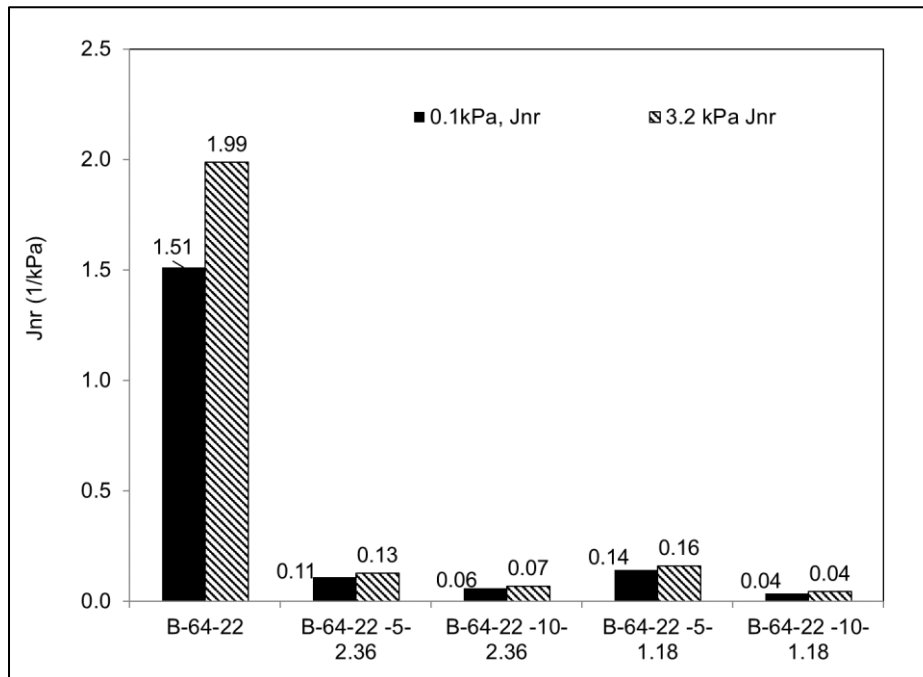
a: Approach-2 Binder (Binder ID format: source_rubber content in percent_maximum rubber size in mm)
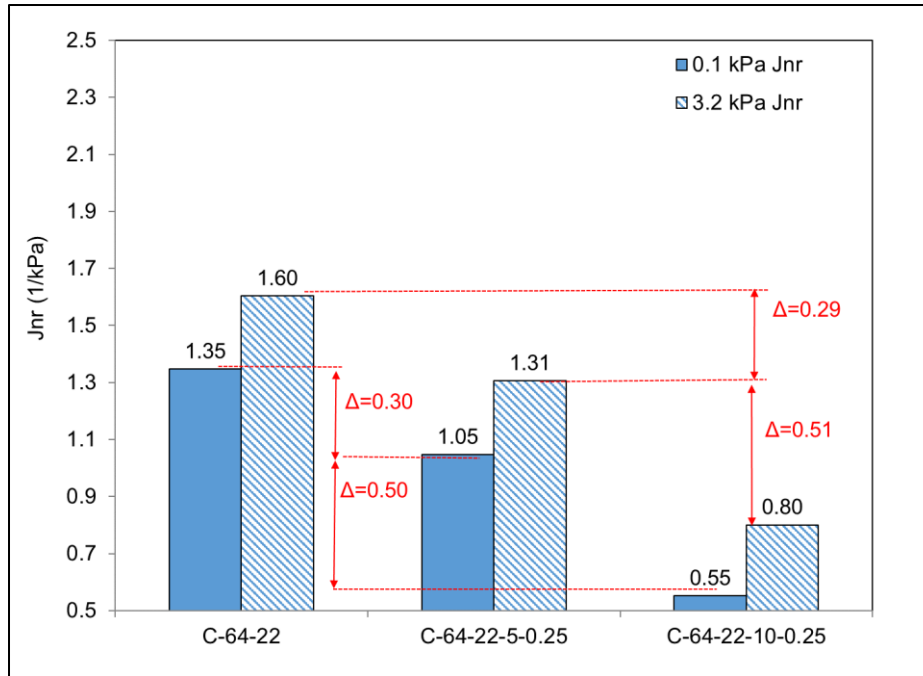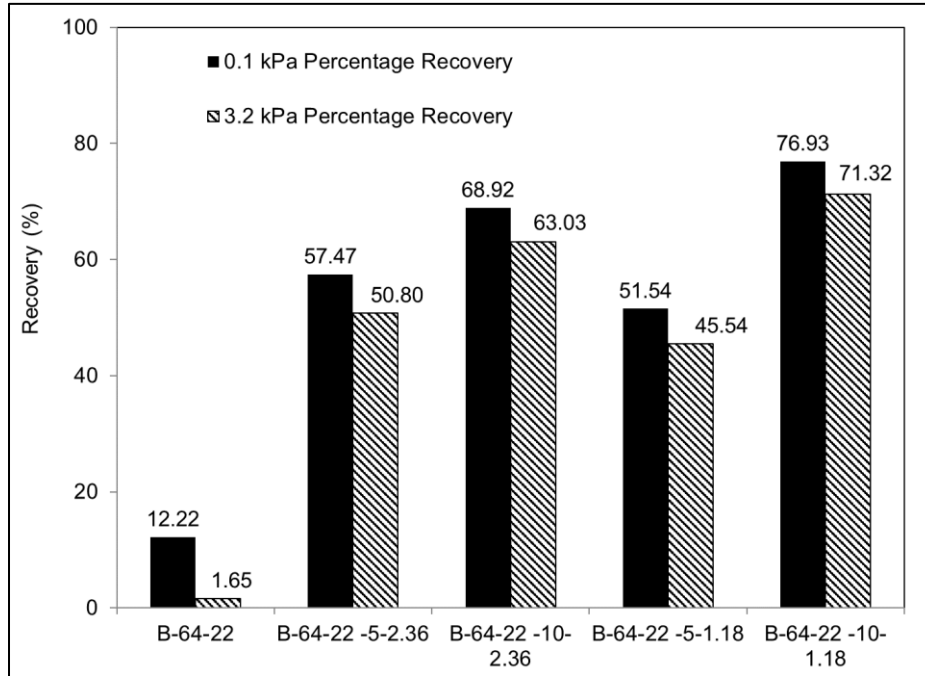
b: Approach-4 Binder (Binder ID format: source_rubber content in percent_maximum rubber size in mm)
Figure 7.4: Non-recoverable compliances of the RTFO-aged binders at 64°C.

Comparing Jnr values from the tests done at 0.1 kPa and 3.2 kPa stress levels revealed that increasing the test stress increased the Jnr values, as expected. Figure 7.4 also shows that increasing the rubber content decreased the Jnr values because the PG+X binders were stiffer than their base binders.

Figure 7.5 shows the percentage recovery during the unloading phase in the MSCR test, which is used to identify the binder's ability to recover the deformation. A low percentage recovery implies that the binder is vulnerable to accumulated permanent deformation *(195,196)*. The test results show that PG+X binders had higher recovery percentages than their base binders when the loadings were removed. Asphalt binder itself is a visco-elastic material *(5)*, and this unmodified binder generally has a low capability of elastic recovery when unloaded at the tested temperature, as Figure 7.5 shows. In contrast, PG+X binders showed a higher recovery percentage, which was

attributed to modification by the elastic rubber. Approach-2 and Approach-4 PG+X binders showed that increasing the rubber content increased the percentage recovery.

a: Approach-2 Binder (Binder ID format: source_rubber content in percent_maximum rubber size in mm)

b: Approach-4 Binder (Binder ID format: source_rubber content in percent_maximum rubber size in mm)

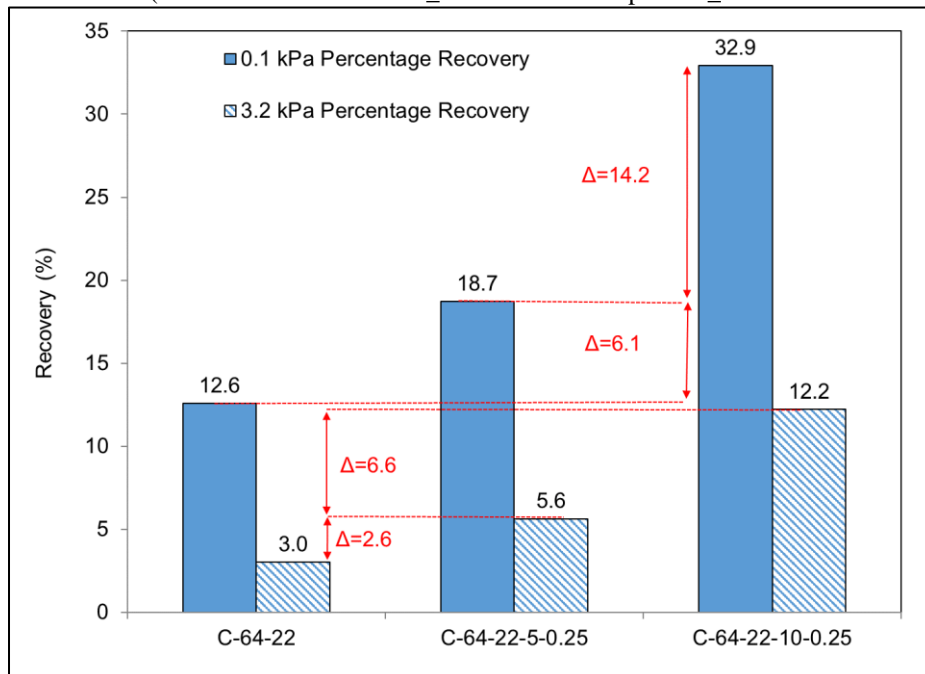**Figure 7.5: Percentage recoveries of the RTFO-aged binders at 64°C.**

Increasing the maximum rubber particle size from smaller than 0.25 mm (passing the #60 sieve) to smaller than 2.36 mm (passing the #8 sieve) further improved the Jnr values and percentage recoveries. The finer particles (smaller than 250 microns [passing the #60 sieve]) used in the Approach-4 PG+X binders appeared to be better digested than the coarser rubber (smaller than 2.36 mm or smaller than 1.18 mm) used in the Approach-2 binders. Figure 7.4 and Figure 7.5 show that delta Jnr values and delta percentage recovery were mostly proportional to the rubber content in the Approach-4 binders.

In summary, the MSCR results indicate that Approach-2 and Approach-4 PG+X binders would be less susceptible to rutting, owing to their lower permanent deformation and higher elastic recovery. Increasing the rubber content and rubber particle size further improved the rutting resistance.

7.3.3 Rotational Viscosity Test of Rubber-Modified Binders

The rotational viscosity test was used to determine the mixing and compaction temperatures for the PG+X binders used in the mix. The mixing and compaction temperatures have to be elevated when rubber is added, if not compensated for in the selection of the base binder and additives, to decrease the binder's viscosity and to improve the binder coating of the aggregates. The standard binder viscosities for mixing and compaction temperatures are 0.17 Pa·s and 0.28 Pa·s, respectively *(2)*.

Figure 7.6 shows the rotational viscosity test results. The results indicate that increasing the rubber content and the rubber particle size increased the binder viscosity, as expected. When the temperature was low (i.e., <165°C), PG+X binders showed higher viscosities than their base binders, which was attributed to the presence and swelling of the rubber particles *(23,39)*. When the temperature was increased (i.e., >135°C), the viscosities of the PG+X binders decreased,

308

indicating that elevating temperature was necessary to facilitate the workability of Approach-2 and Approach-4 PG+X binders.

A steeper curve between the temperature and viscosity was found for these PG+X binders than their base binders. A higher rubber content and coarser rubber particle size amplified the change of temperature-dependent viscosity. The binders containing coarser rubber had higher viscosities than those containing finer rubber based on the results of Approach-2 PG+X binders.
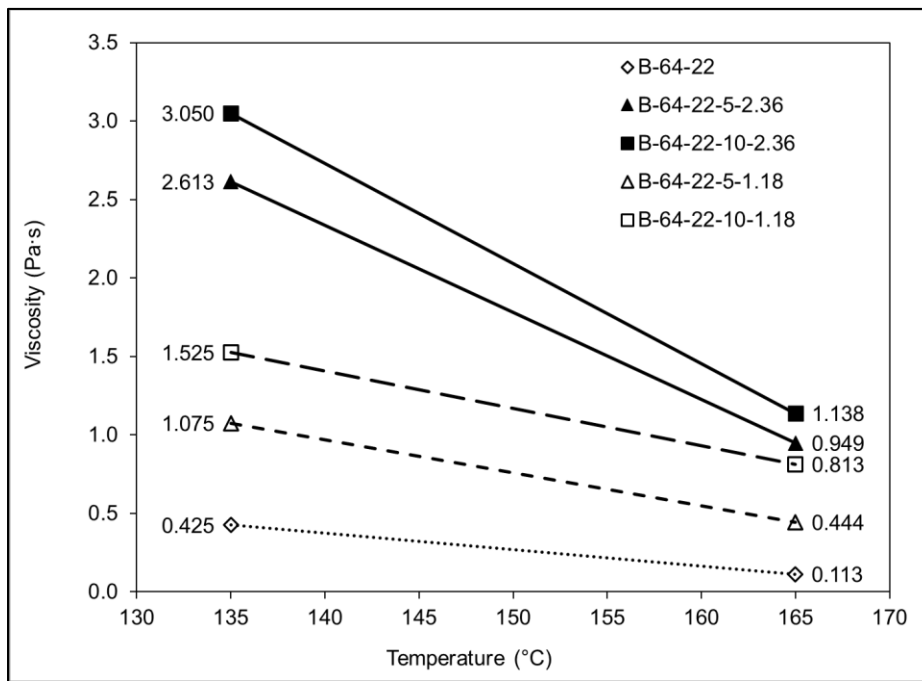
a: Approach-2 Binder (Binder ID format: source_rubber content in percent_maximum rubber size in mm)
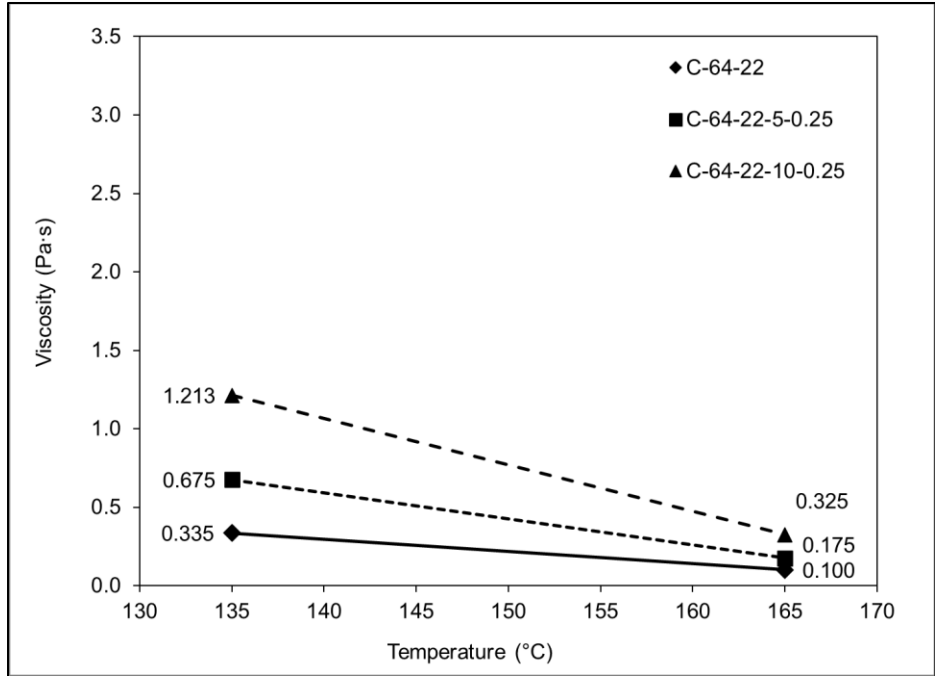
b: Approach-4 Binder (Binder ID format: source_rubber content in percent_maximum rubber size in mm)

Figure 7.6: Rotational viscosity test results.

7.3.4   Volumetric Design of Rubber-Modified Mixes

During mixing, batched virgin aggregates were placed in an oven overnight at 15°C above the mixing temperature to reach the equilibrium temperature needed for aggregates following AASHTO R 35 *(206)*. The preheating temperature of the RAP was 110°C for one hour to prevent overheating of the reclaimed asphalt binder *(2)*. The mixing and compaction temperatures are summarized in Table 7.6.

The mixing and compaction temperatures were determined as the temperatures where the rotational viscosity is 0.17 Pa·s and 0.28 Pa·s, respectively *(2)*. The binders were heated to these elevated temperatures to facilitate the coating of the aggregate surface during mixing and compaction.

Table 7.6 shows that Approach-1 PG+X binders had the same mixing and compaction temperatures as the control binder at the same PG. The mixing and compaction temperature were not changed for the Approach-3 mixes since these mixes with dry-process rubber were prepared with the same unmodified binder. The mixing and compaction temperatures for the Approach-2 and Approach-4 PG+X binders were determined from the rotational viscometer test results shown in Figure 7.6. These elevated temperatures were generally lower than the typical mixing temperatures (>190°C) used for traditional RHMA-G mixes *(2,70)*. The gyratory compactor was set to 600 kPa, which was the same pressure used for conventional dense-graded mixes. This pressure was lower than the gyratory compaction pressure for RHMA-G (825 kPa) *(2,70)*. From this perspective, PG+X materials provide a way of using recycled rubber at lower production temperatures and compaction efforts than conventional RHMA-G mixes.

A common practice for RHMA mix compaction is to hold or square specimens in the mold for 30 to 45 minutes after compaction and before extraction. This prevents expansion of the specimen caused by continued swelling of the rubber particles during cooling *(2,70)*. The squaring durations for different PG+X mixes were determined on a case-by-case scenario. Given the low rubber content in the wet-process binders used in PG+X mixes, no cooling and squaring inside the gyratory mold was applied. Visual observations showed that specimen dimensions did not change and that no visible damage occurred on the specimen surfaces. A 30-minute squaring period was applied to the mixes with dry-process rubber to prevent extended rubber swelling or dilating.

Table 7.6: Mixing and Compaction Settings

Approach	Mix ID	Binder ID[1]	Binder Temp for Mixing (ºC)	Compaction Temp(ºC)	Compaction Pressure (kPa)	Constant Height Squaring Time (Minutes)
1	A	A-64-16	150	140	600	0
	B	A-64-16-5-0.25	150	140	600	0
	C	A-64-16-10-0.25	150	140	600	0
	D	A-70-10	170	155	600	0
	E	A-70-10-5-0.25	170	155	600	0
	F	A-70-10-10-0.25	170	155	600	0
2	S	B-64-22	160	149	600	0
	T	B-64-22-5-2.36	178	176	600	0
	U	B-64-22-10-2.36	180	178	600	0
3	G	A-64-16-DRY-5-2.36	150	140	600	30
	H	A-64-16-DRY-10-2.36	150	140	600	30
4	J	C-64-22	150	140	600	0
	K	C-64-22-5-0.25	165	158	600	0
	L	C-64-22-10-0.25	170	166	600	0

[1] Binder ID format: source-PG-rubber content in percent-maximum rubber size in mm.

A Superpave volumetric design was used to determine the optimum binder contents (OBC) for these mixes to meet Caltrans' Type-A HMA criteria *(2)*. Table 7.7 summarizes the volumetric design results. These volumetric parameters indicated that Approach-1 and Approach-4 PG+X mixes passed the mix design criteria at the same OBC as the control mix. When the rubber particles were small than 250 microns, no adjustment of the binder content was needed. In these PG+X mixes, the base asphalt binder amounts were, in fact, lower than in the control mix when the rubber particles are taken into account. The volumetric parameters (air-void contents, voids in mineral aggregate [VMA], and voids filled by asphalt [VFA]) listed in Table 7.7 show that using these small amounts (five and ten percent by weight of the binder) of fine rubber particles (<250 microns) were not expected to cause any volumetric issues during laboratory mix production.

In contrast, the OBC increased for Approach-2 PG+X mixes compared with the mix using the base binder. Using the large rubber particles (maximum rubber particle size smaller than 1.18 mm and 2.36 mm, which were larger than the fine rubber used in Approach-4) resulted in the OBC increasing 0.3 percent by dry weight of the aggregate (DWA) when adding five percent rubber by weight of the binder, and by 0.6 percent of DWA when adding ten percent rubber. These changes indicated that increasing the OBC to have a similar base asphalt binder amount to the control mix was necessary for using PG+X binders with coarse rubber particles (<1.18mm and <2.36 mm) in a dense-graded mix.

Table 7.7: Summary of Volumetric Mix Design

Approach	Mix ID	Binder ID[1]	Optimum Binder Content (%)	Base Asphalt Binder Content (%)	Air-Void Content (%) at N_{design} (85 Gyrations)[2]	VMA (%)[2]	VFA (%)	Dust Proportion[2]
1	A	A-64-16	5.3	5.3	4.0	14.4	72.4	1.03
	B	A-64-16-5-0.25	5.3	5.0	4.2	14.6	71.4	1.03
	C	A-64-16-10-0.25	5.3	4.8	4.3	14.7	70.8	1.04
	D	A-70-10	5.3	5.3	4.4	14.9	70.7	1.02
	E	A-70-10-5-0.25	5.3	5.0	3.9	14.3	72.6	1.04
	F	A-70-10-10-0.25	5.3	4.8	4.3	14.8	70.6	1.03
2	S	B-64-22	5.3	5.3	4.3	14.8	71.1	0.99
	T	B-64-22-5-2.36	5.6	5.3	4.5	15.3	70.4	0.97
	U	B-64-22-10-2.36	5.9	5.3	3.8	15.5	75.2	0.90
3	G	A-64-16-DRY-5-2.36	6.0	5.7	4.1	16.4	74.7	0.87
	H	A-64-16-DRY-10-2.36	6.8	6.1	4.2	19.3	78.3	0.68
4	J	C-64-22	5.3	5.3	4.1	14.4	72.4	1.03
	K	C-64-22-5-0.25	5.3	5.0	4.0	14.6	71.4	1.03
	L	C-64-22-10-0.25	5.3	4.8	4.0	14.7	70.8	1.04

[1] Binder ID format: source-PG-rubber content in percent-maximum rubber size in mm.
[2] Design criteria *(2)*: Air-void content at N_{design} range is 4 ± 0.5 percent; voids in mineral aggregate range is between 13.5 and 16.5; dust proportion range is between 0.6 and 1.3.

The Approach-3 mixes with dry-process rubber also required an increase in the binder content to meet volumetric design criteria. Since there was no pre-blending between rubber particles and the asphalt binder in the dry-process, rubber particles were considered as part of the aggregate. Increasing the binder content resulted in a lower dust proportion (dust to binder ratio). The swelling and possible dilation of the rubber particles occurred during the mixing and compaction process

when they were exposed to and absorbed the hot binder *(207)*. Consequently, the OBC increased with increasing rubber content along with the increases in VWA and VFA in Approach-3 mixes.

The increases in OBC required for the Approach-3 mixes were consistent with the Approach-2 mixes. However, the mixes with dry-process rubber required more binder than the mixes with wet-process binders to meet the target air-void content at the design gyration count.

The results from the volumetric designs showed that the Approach-3 A-64-16-DRY-10-2.36 mix exceeded the maximum VMA criterion for Type-A HMA mix per Caltrans standards *(2,70)* and that the VFA value was also high. Given that the dense-graded design was not formulated to accommodate rubber particle swelling, problems were expected to occur when they swelled on contact with the asphalt binder. This would affect other volumetric properties. Caution should therefore be used in the use of coarse dry rubber (<2.36 mm [passing the #8 sieve]) in dense-graded mixes.

Figure 7.7 plots the air-void contents for the tested specimens. The results showed that the target requirements were met (7±0.5 for AMPT specimens and 7±1 for beams), indicating that air-void content could be obtained for PG+X mixes using the standard laboratory mixing and compaction method. The beam specimens of Mix B (A-64-16-5-0.25), Mix C (A-64-16-10-0.25), and Mix D (A-70-10) had average air-void contents close to the lower limit allowed in the experiment design (still met the 7±1 percent air-void content requirement for beams). The relatively low air-void contents in these three mixes were taken into consideration in the analysis in the following sections.
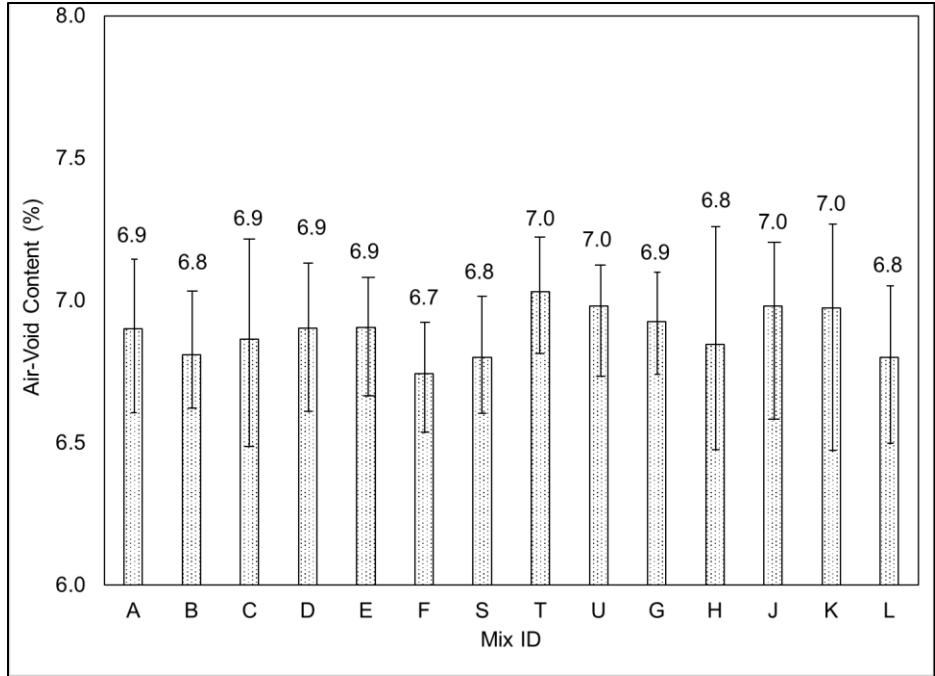
a: Gyratory compacted AMPT specimens
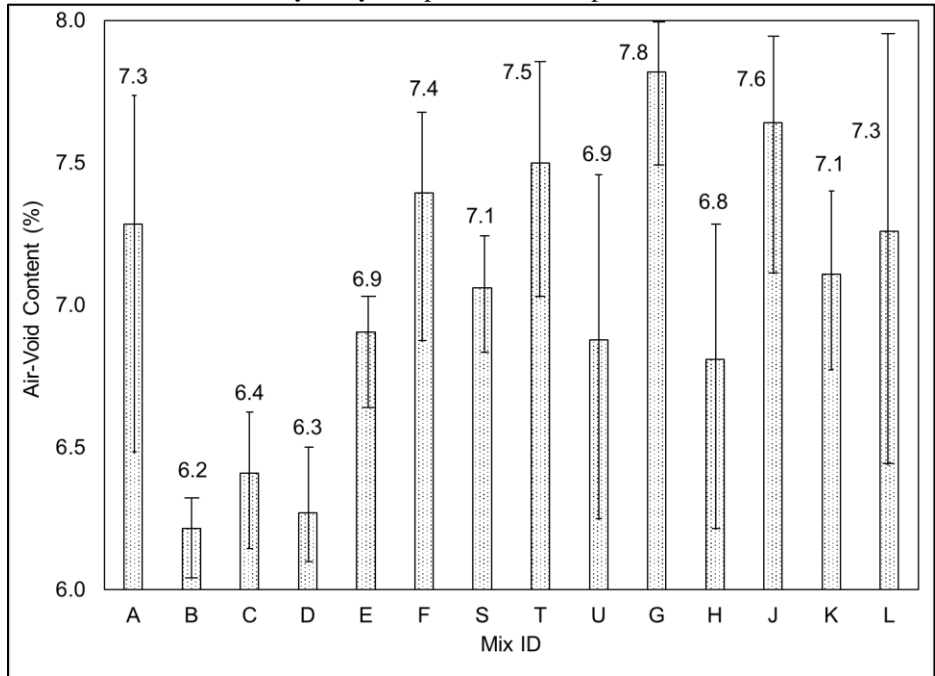
b: Rolling wheel compacted beams

Figure 7.7: Summary of air-void contents for tested specimens.

7.3.5 Evaluation of Mix Stiffness

The mix performance analysis sequence starts with mixes with wet-process binders followed by mixes with dry-process rubber in the following sections.

The measured flexural moduli and phase angles from the flexural frequency sweep tests were horizontally shifted into a master curve using the symmetric sigmoidal fit function *(141)* and Williams-Landel-Ferry shift function *(183)* presented in Equation 4.3, Equation 4.4, and Equation 7.1.

Figure 7.8 shows these master curves at 20°C. There were no apparent visible changes between the control mixes and the Approach-1, indicating that using these PG+X binders, prepared with rubber particles smaller than 250 microns (passing the #60 sieve), in dense-graded mixes should not result in a much stiffness change.

The Approach-2 mixes prepared with binders with coarser rubber particles (<1.18 mm and <2.36 mm) had apparent higher flexural stiffnesses than the control mix between 1E-04 to 1E+02 Hz in the master curves, which indicated that these PG+X mixes were stiffer than the control mix.

For Approach-3 mixes with dry-process rubber, noticeable decreases in flexural stiffness were observed between 1E-04 to 1E+02 Hz in the master curves, indicating that stiffness decreased with the addition of the dry rubber.

The Approach-4 mixes showed a slight stiffness increase at low frequencies (<1E-02 Hz), but no notable stiffness changes at intermediate and high frequencies (>1E-02 Hz) compared to the control mix.
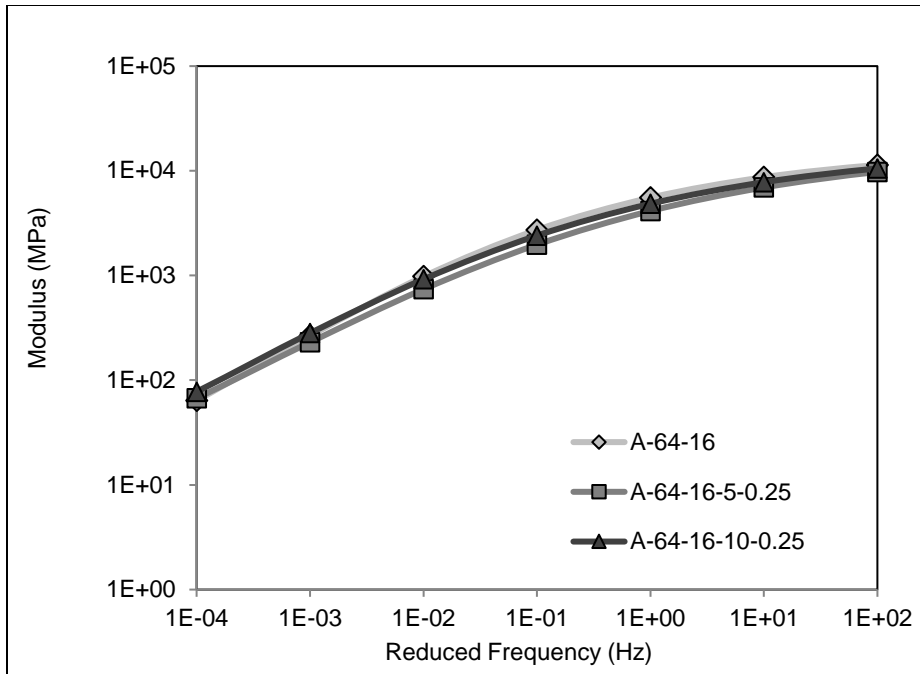
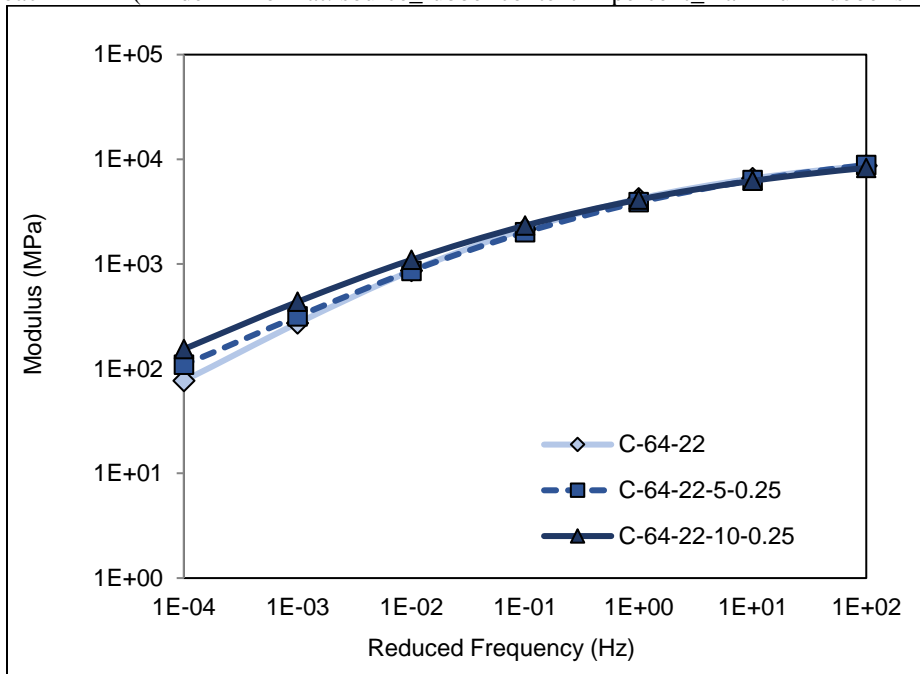a: Approach-1 PG 64-16 Mix (Binder ID format: source_rubber content in percent_maximum rubber size in mm)
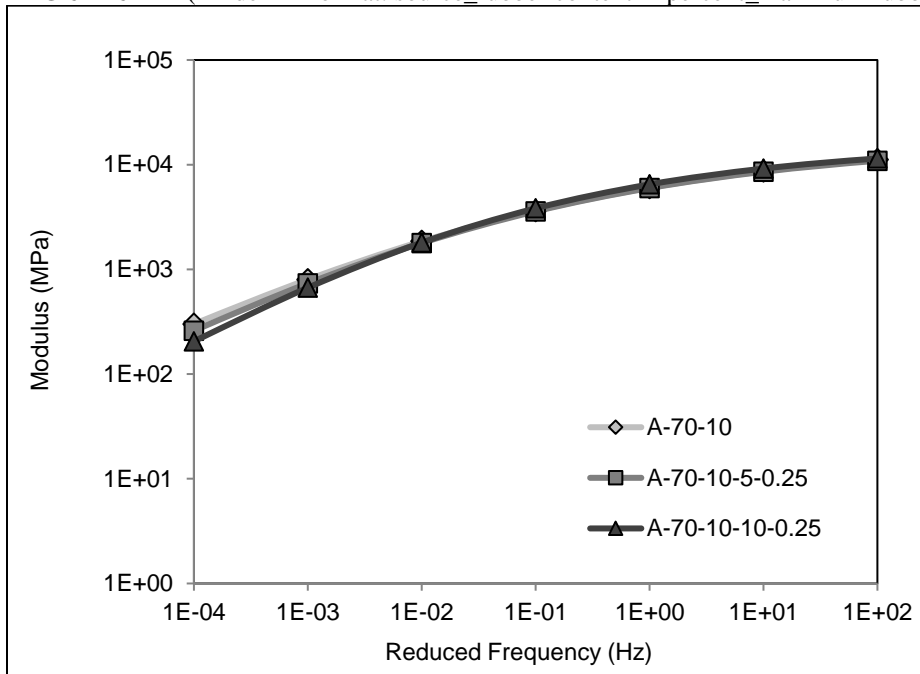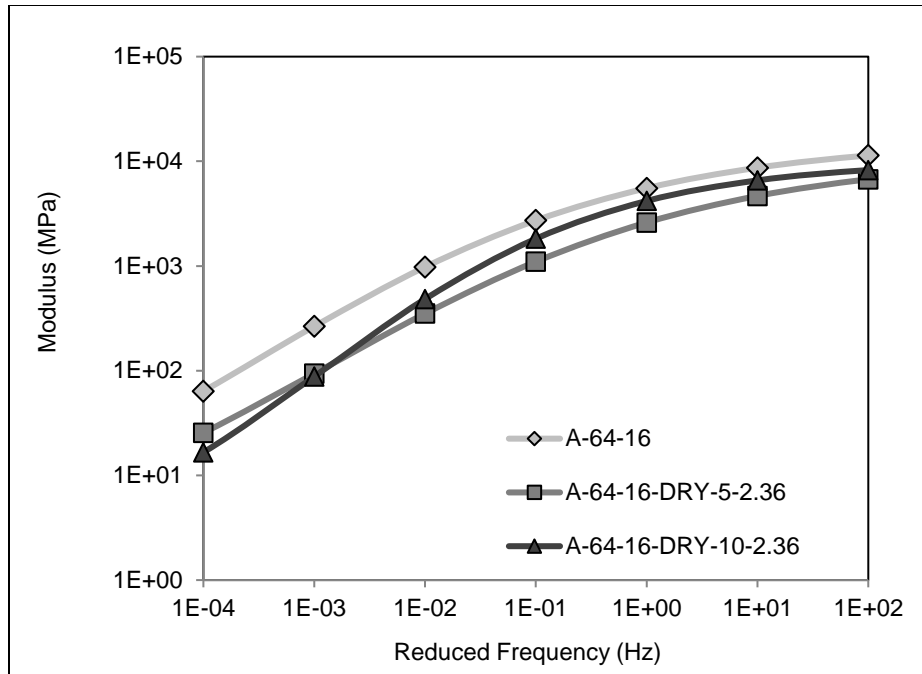

b: Approach-1 PG 70-10 Mix (Binder ID format: source_rubber content in percent_maximum rubber size in mm)
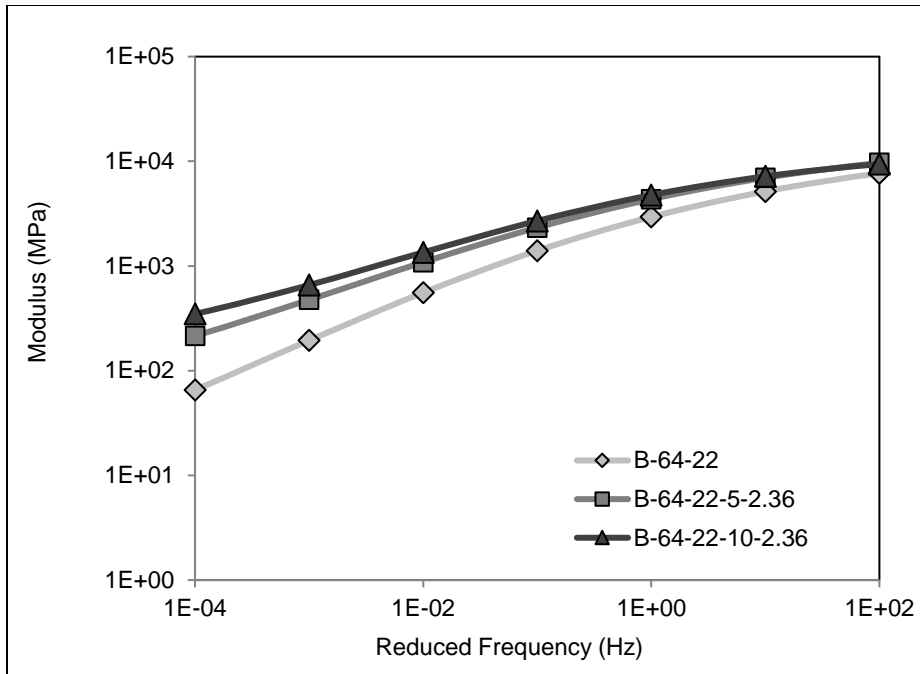
c: Approach-2 Mix (Binder ID format: source_rubber content in percent_maximum rubber size in mm)

d: Approach-4 Mix (Binder ID format: source_rubber content in percent_maximum rubber size in mm)

e: Approach-3 Mix (dry-process) (Binder ID format: source_rubber content in percent_maximum rubber size in mm)

Figure 7.8: Flexural modulus master curves at 20°C.

Normalized master curves were developed to assist with comparing the mixes. The normalized values were calculated as the ratios of PG+X mixes to control mixes at the same frequency. After normalizing, the moduli of the control mixes were equal to one at every frequency, and the moduli of the PG+X mixes were ratio numbers. Figure 7.9 shows these normalized master curves.

For Approach-1 mixes, there was no notable difference in stiffness between different mixes. However, the rubber effect on stiffness was inconclusive because of uncertainties about the base binder and additives. The rubber effect in the Approach-2 and Approach-4 mixes were more apparent. Figure 7.9 shows that the Approach-2 and Approach-4 PG+X mixes were stiffer than their control mixes when the reduced frequency was below 1E-02 Hz.
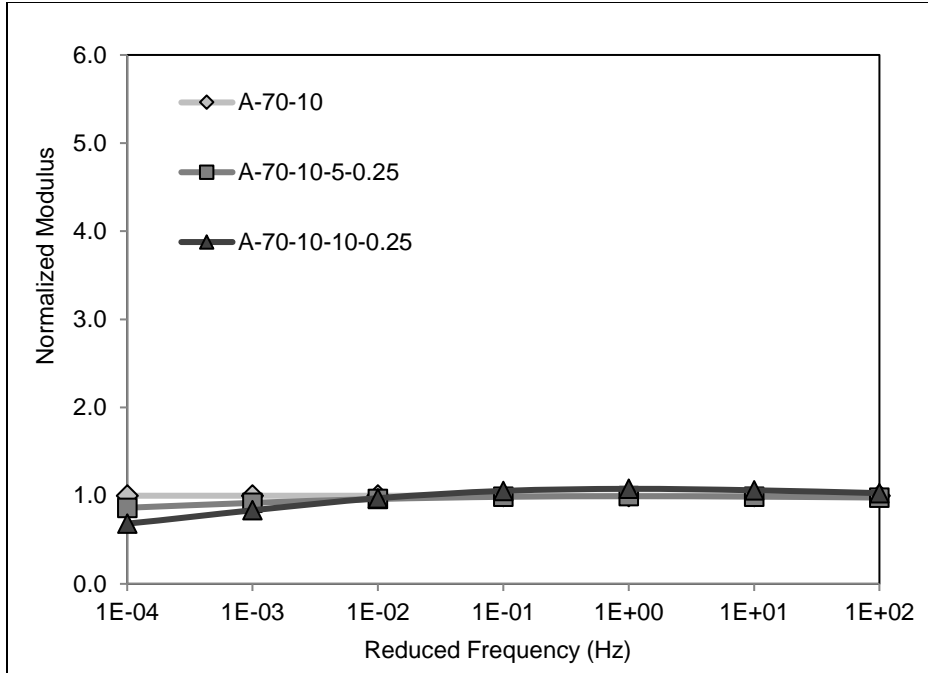
The reduced frequencies below 1E-02 Hz at 20°C correspond to conditions above 42°C and 10 Hz based on the time-temperature superposition principle *(183)*. Therefore, the stiffer Approach-2 and

Approach-4 PG+X mixes would likely provide better rutting resistance than the control mixes at these high temperatures. At intermediate temperature conditions (around 20°C and 10 Hz), Approach-2 PG+X mixes were stiffer than the control mix, which had a potentially shorter fatigue life than the control mix in the controlled-strain flexural beam fatigue test. The Approach-4 PG+X mixes showed similar stiffnesses to the control mix in the intermediate temperature conditions. The controlled-strain flexural beam fatigue tests were used to further evaluate the fatigue performance of the PG+X mixes, and the results were shown in Section 7.3.8.

The Approach-3 mixes with dry-process rubber had lower stiffnesses than the control mix. These mixes would, therefore, likely have poorer rutting resistance at high temperatures (>42°C and 10 Hz) but potentially better fatigue resistance at intermediate temperatures (around 20°C and 10 Hz) than the control mix. A series of laboratory tests presented in Section 7.3.6 to Section 7.3.9 were used to further evaluate these PG+X mixes.
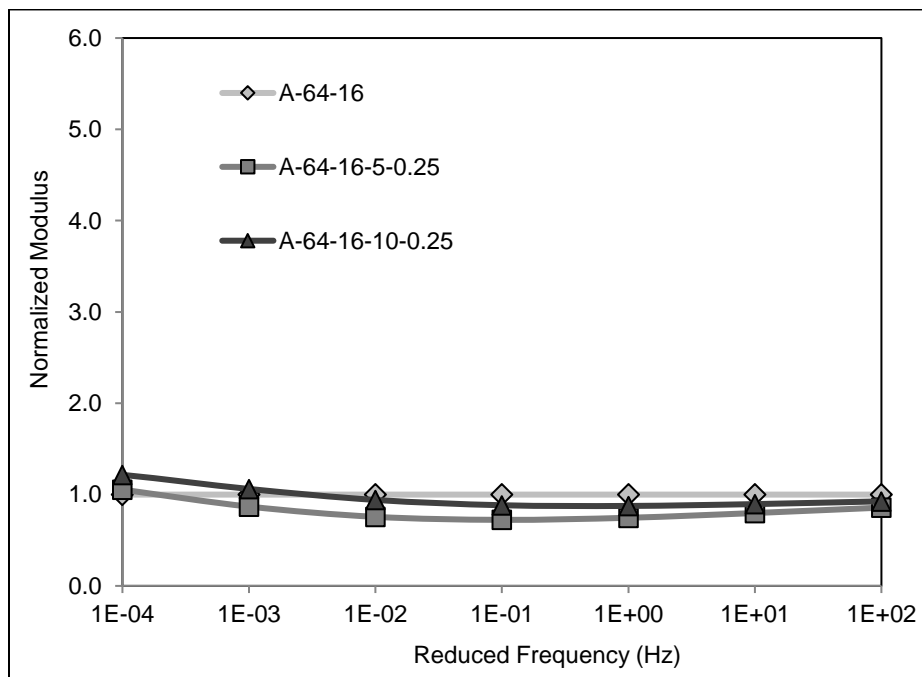
a: Approach-1 PG 64-16 Mix (Binder ID format: source_rubber content in percent_maximum rubber size in mm)

b: Approach-1 PG 70-10 Mix (Binder ID format: source_rubber content in percent_maximum rubber size in mm)

c: Approach-2 Mix (Binder ID format: source_rubber content in percent_maximum rubber size in mm)

322
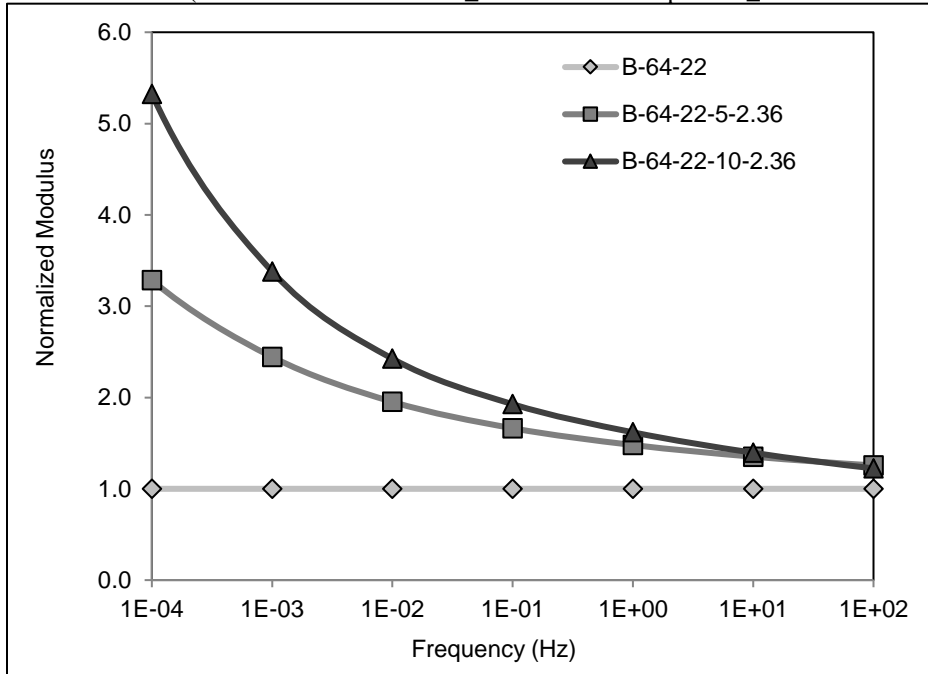
d: Approach-4 Mix (Binder ID format: source_rubber content in percent_maximum rubber size in mm)

e: Approach-3 Mix (Binder ID format: source_rubber content in percent_maximum rubber size in mm)

Figure 7.9: Normalized flexural modulus master curves at 20°C.

Figure 7.10 plots the complex modulus against phase angle plot (black space diagram) for all mixes. The results revealed that PG+X mixes had similar black space trends to their control mixes, especially when fine rubber particles (smaller than 250 microns [passing the #60 sieve]) were used.

a: Approach-1 Mix (Binder ID format: source_rubber content in percent_maximum rubber size in mm)

b: Approach-2 Mix (Binder ID format: source_rubber content in percent_maximum rubber size in mm)
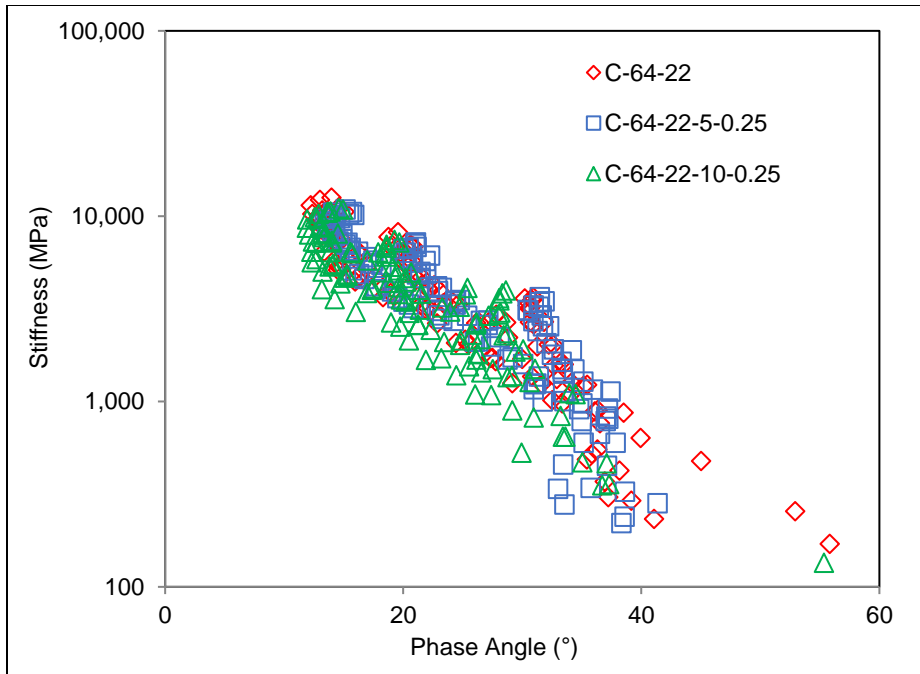
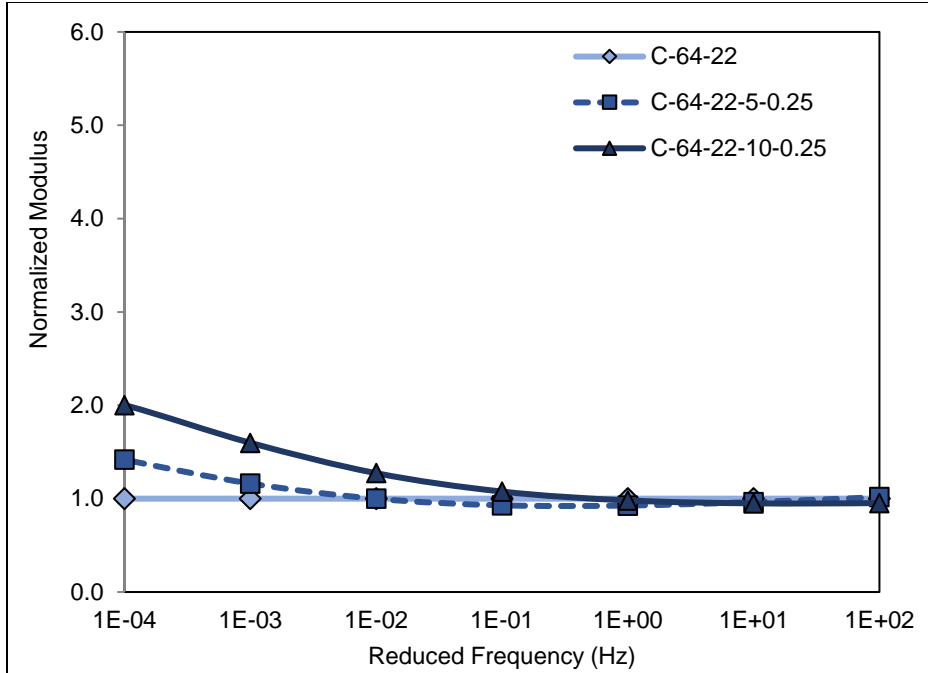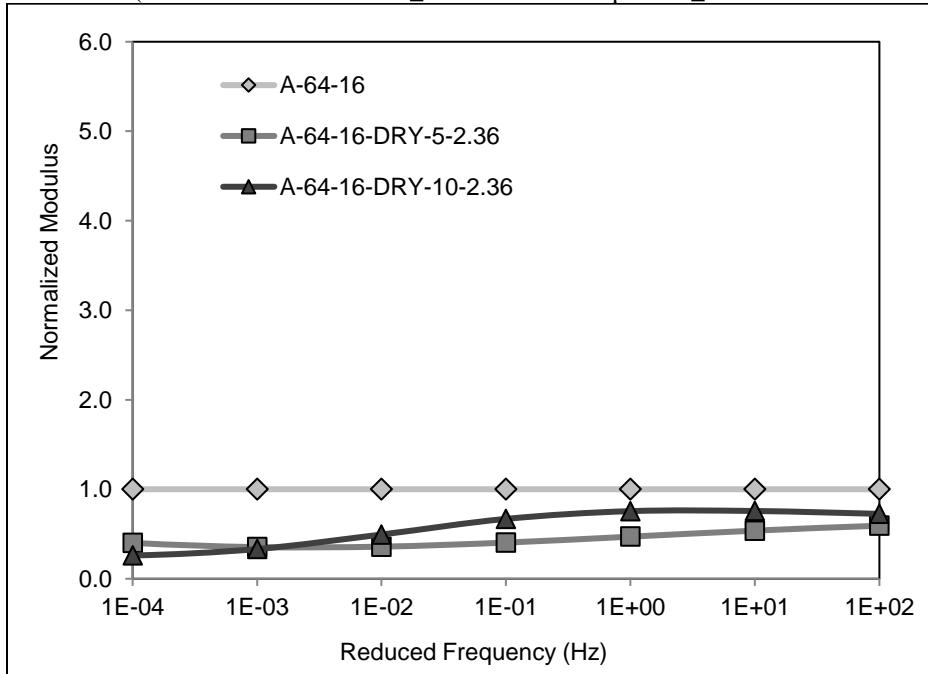c: Approach-4 Mix (Binder ID format: source_rubber content in percent_maximum rubber size in mm)
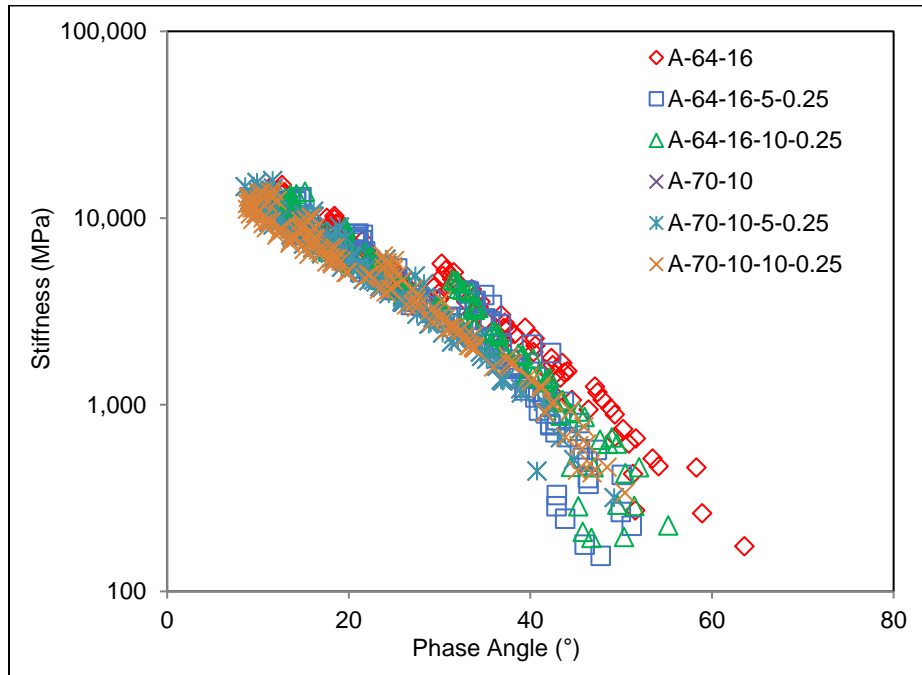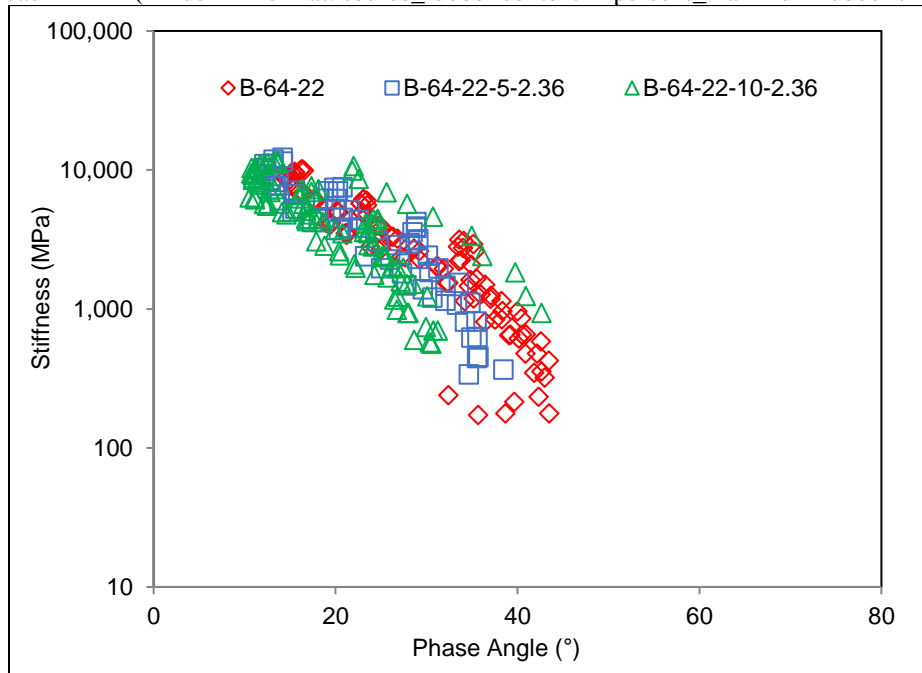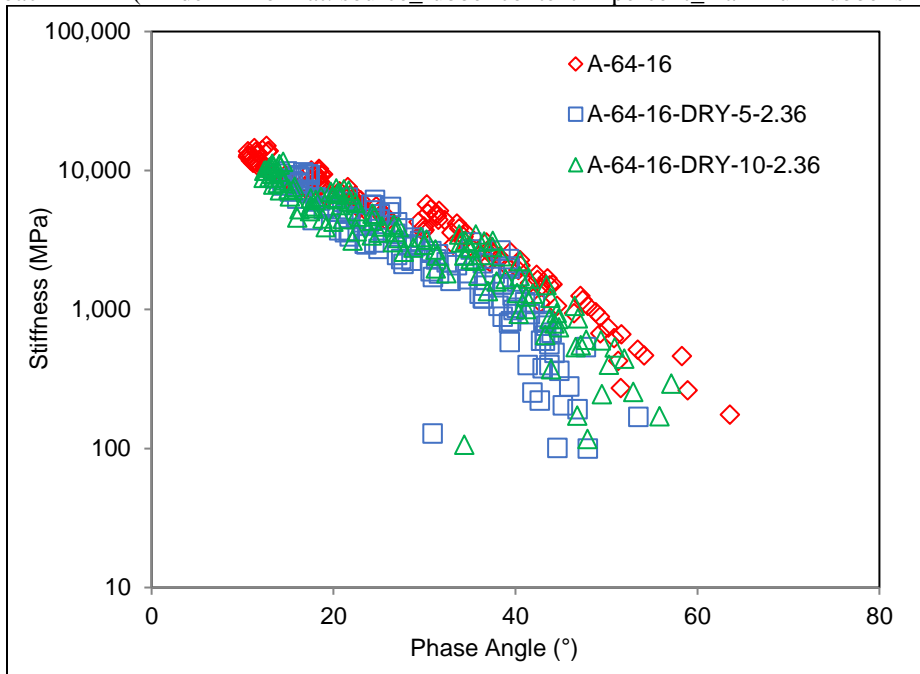

d: Approach-3 Mix (Binder ID format: source_rubber content in percent_maximum rubber size in mm

Figure 7.10: Black diagrams of beam flexural frequency sweep tests.

7.3.6 Evaluation of Moisture Damage Resistance

Figure 7.11 and Figure 7.12 present the HWTT results at 50°C. All mixes rutted less than the Caltrans maximum allowable rut depths for their binder PGs. These limits are 12.7 mm at 15,000 cycles for PG64-XX binders and 20,000 cycles for PG 70-XX binders *(2)*. These mixes showed acceptable rutting resistance and moisture damage simulated by the HWTT. No inflection point was identified for any specimens despite continuing the tests to 35,000 cycles.

The rutting curves of the Approach-1, Approach-2, and Approach-4 mixes indicated that PG+X mixes produced with wet-process binders generally provided better moisture damage resistance than their control mixes. For Approach-1 mixes, PG 70-XX mixes had less rut depth than the PG 64-XX mixes after the same loading cycles, as the binders used in the former are one PG higher and stiffer.

For Approach-2 and Approach-4 mixes, PG+X mixes showed less rut depth than the control mixes. Given that no other additive was used in these mixes, the improvement in moisture-related rutting resistance was attributed to the rubber alone. Similar improvements have also been observed in RHMA-G mixes containing 20 percent rubber by weight of the binder *(81)*. In general, using the wet-process binders in the mix could increase the moisture damage resistance.

a: Approach-1 Mix PG64-16 (Binder ID format: source_rubber content in percent_maximum rubber size in mm)
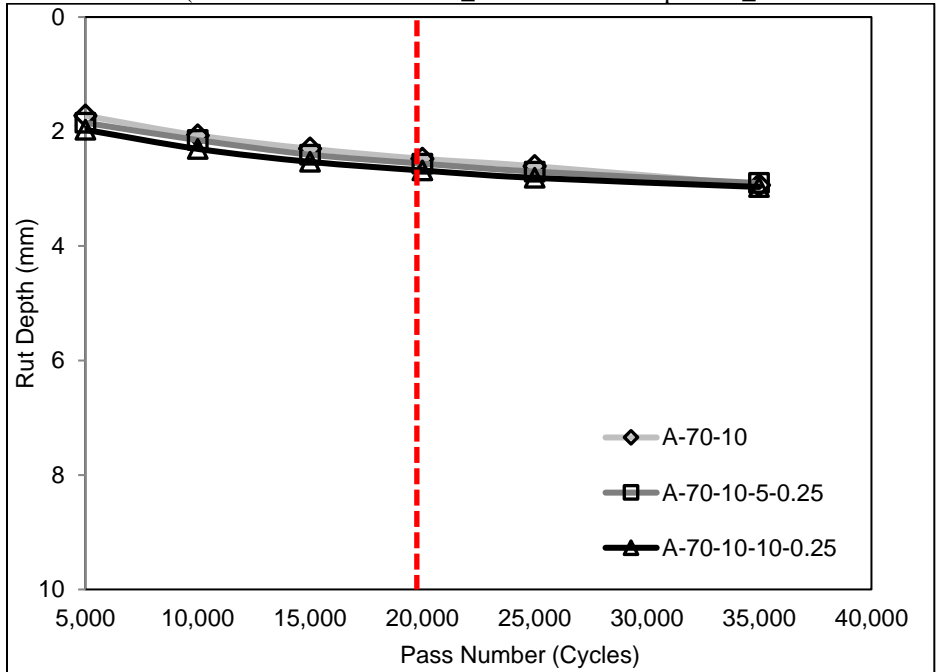
b: Approach-1 Mix PG 70-10 (Binder ID format: source_rubber content in percent_maximum rubber size in mm)
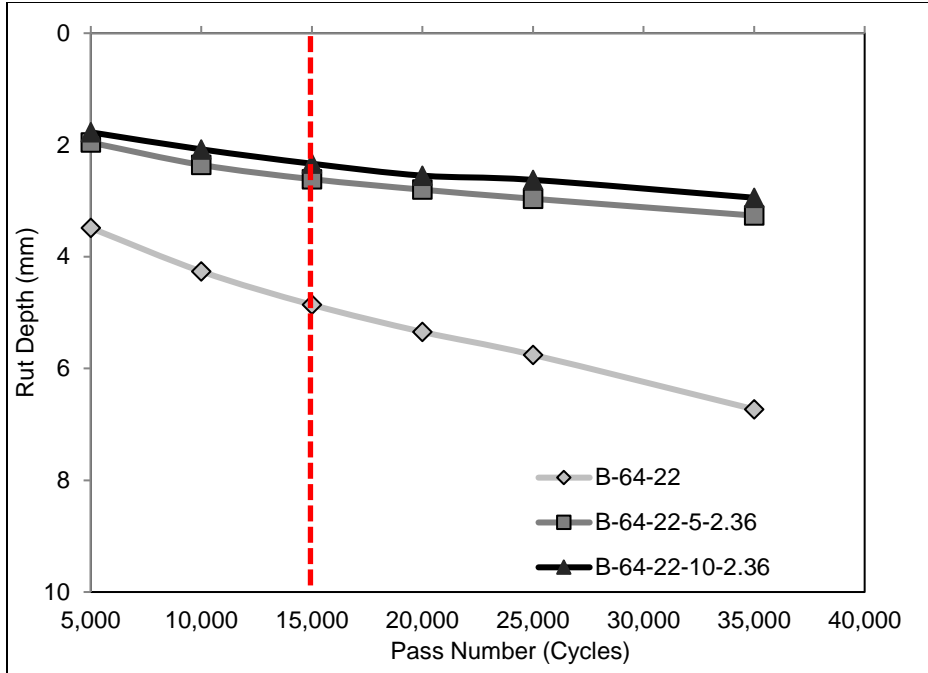
c: Approach-2 Mix (Binder ID format: source_rubber content in percent_maximum rubber size in mm)
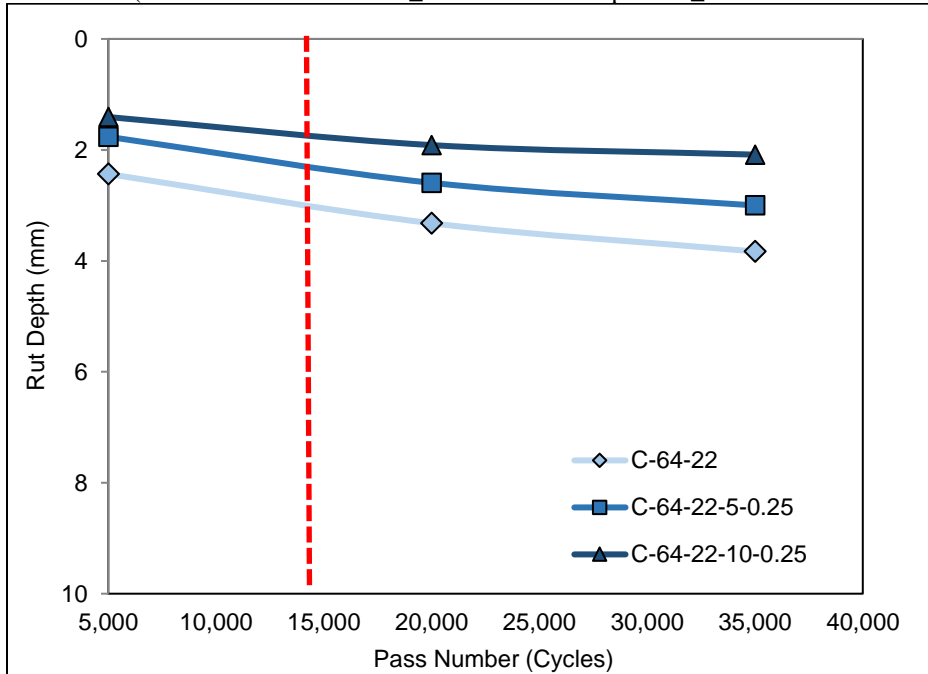
d: Approach-4 Mix (Binder ID format: source_rubber content in percent_maximum rubber size in mm)
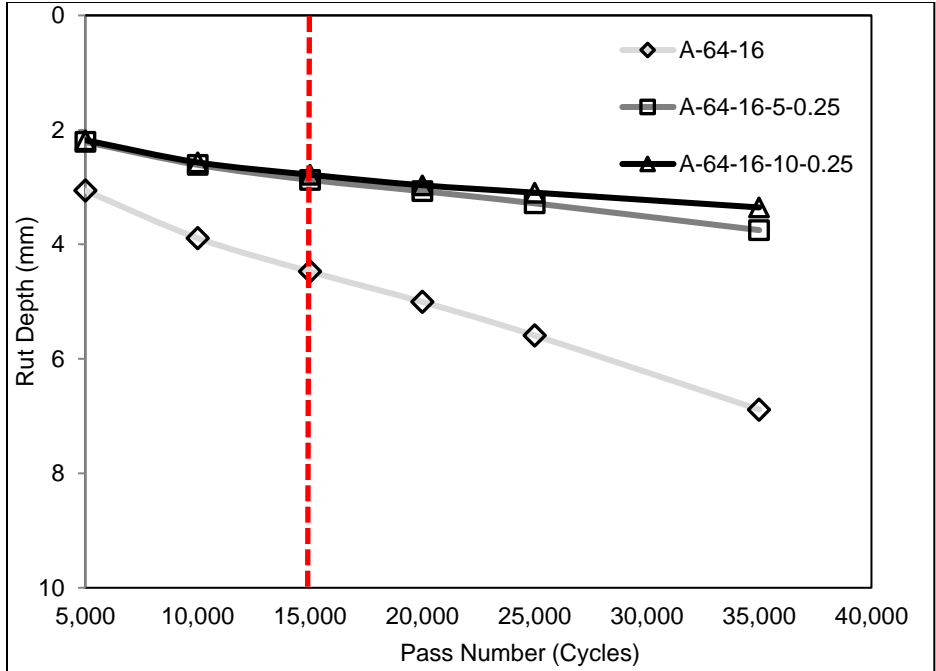**Figure 7.11: HWTT result for mixes with wet-process binders.**

The Approach-3 PG+X mixes with dry-process rubber rutted deeper than the control mix, especially when a higher rubber content (ten percent rubber by weight of the binder) was used, as

shown in Figure 7.12. The swelling of the rubber particles during the mixing and compaction increased the VMA, as shown in Table 7.7. Consequently, water could quickly penetrate the aggregate structure and create moisture-related damage. It should be noted that the mixes with dry-process rubber still provided sufficient rutting resistance to pass the current Caltrans standard *(2)*. However, the high rutting rate in the A-64-16-DRY-10-2.36 mix should be noted. The HWTT results indicated that using 0.5 percent rubber by weight of the aggregates (approximately ten percent rubber by weight of the binder) without adjusting the aggregate gradation for the swelled rubber decreased the moisture damage resistance of the mix.

(Binder ID format: source_rubber content in percent_maximum rubber size in mm)
Figure 7.12: HWTT result for Approach-3 mixes with dry-process rubber.

7.3.7 Evaluation of Rutting Resistance

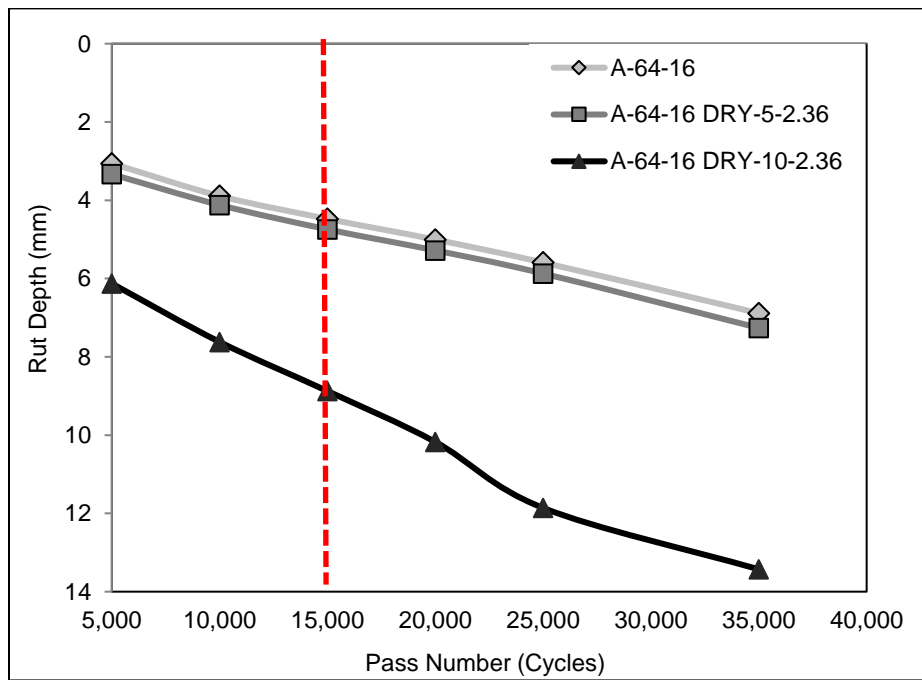This section discusses the unconfined RLT test results at 50°C. Figure 7.13 shows the average flow numbers and the standard deviations for each type of mix. In this study, tested AMPT

specimens had air-void contents within the 7±0.5 tolerance, as shown in Figure 7.7. Although the air-void contents in these specimens met the air-void content requirement, a large variability of the flow numbers within each mix type was still observed.

The AASHTO T 378 test specifies the coefficient of variation for a single operator to be 58.5 percent for mixes with a nominal maximum aggregate size of 19 mm. The flow numbers shown in Figure 7.13 passed this precision requirement. Since the variability of flow numbers within each mix type was high, the differences between PG+X mixes and control mixes might not be fully attributed to the rubber for Approach-1, Approach-3, and Approach-4 mixes. On the other hand, the Approach-2 PG+X mixes showed apparent increases in flow numbers despite the variability.

Figure 7.13a shows the results for Approach-1 mixes. Approach-1 PG+X mixes had higher flow numbers than their control mixes, indicating that Approach-1 PG+X mixes had better rutting resistance. Increasing the rubber content increased the rutting resistance for PG 64-16 mixes and PG 70-10 mixes. The A-64-26-5/10-0.25 mixes containing five and ten percent rubber by weight of the binder had flow numbers similar to the PG 70-10 control mix when they were tested at the same temperature (50°C in this case).

Figure 7.13b and Figure 7.13c show the RLT results for Approach-2 and Approach-4 mixes. These PG+X mixes had higher flow numbers than the control mixes. Increasing the rubber content and rubber particle size increased the flow numbers, which indicated that these PG+X mixes provided a better rutting resistance than their control mixes. The RLT test results followed binder MSCR test results shown in Section 7.3.2 that increasing rubber content decreased the Jnr values and increased the percentage recoveries. This improved rutting resistance in the mix was credited to the higher stiffness of the PG+X binder at this temperature (i.e., 50°C), and also to the increased

elastic recovery introduced by the digested rubber particles. The combination of these two mechanisms reduced the cumulative permanent deformations under repeat loading-unloading cycles.

Figure 7.13d shows the RLT test results for Approach-3 mixes. These mixes with dry-process rubber showed fewer flow numbers than the control mix due to the modified mixes being softer than the control mix, resulting in a faster rate of permanent deformation under repeat loadings. When increasing the rubber content from five percent to ten percent by weight of the binder (0.25 to 0.50 percent by weight of the aggregate), the flow number increased but was still lower than that of the control mix. This increase was not attributed to the mix stiffness because the A-64-16-DRY-5-2.36 mix had a similar stiffness to the A-64-16-DRY-10-2.36 mix at the testing temperature (>42°C and 10 Hz). Instead, the difference was attributed to better recovery after unloading because of the presence of the rubber.
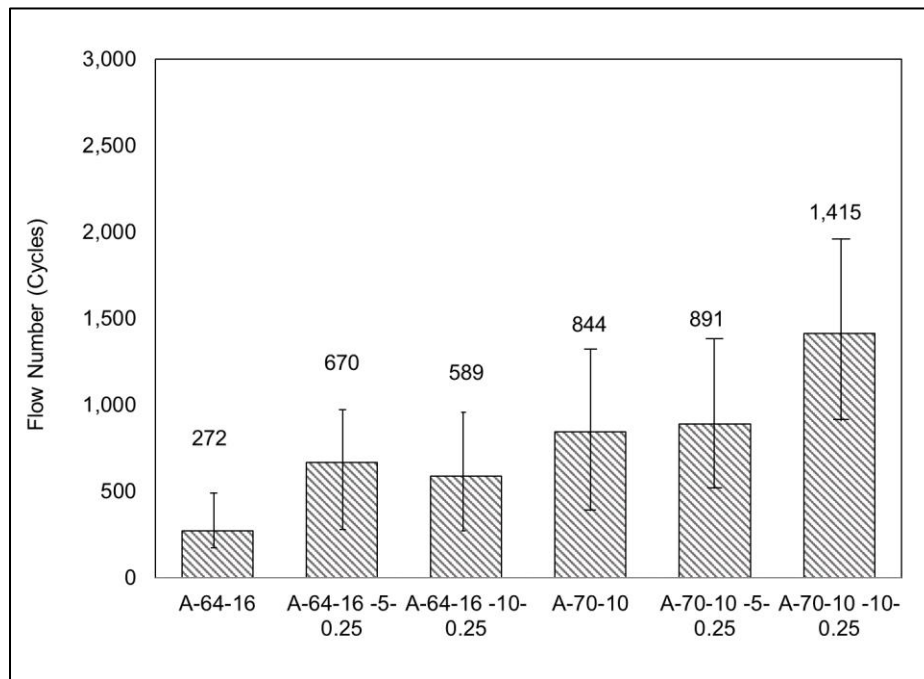
a: Approach-1 Mix (Binder ID format: source_rubber content in percent_maximum rubber size in mm)
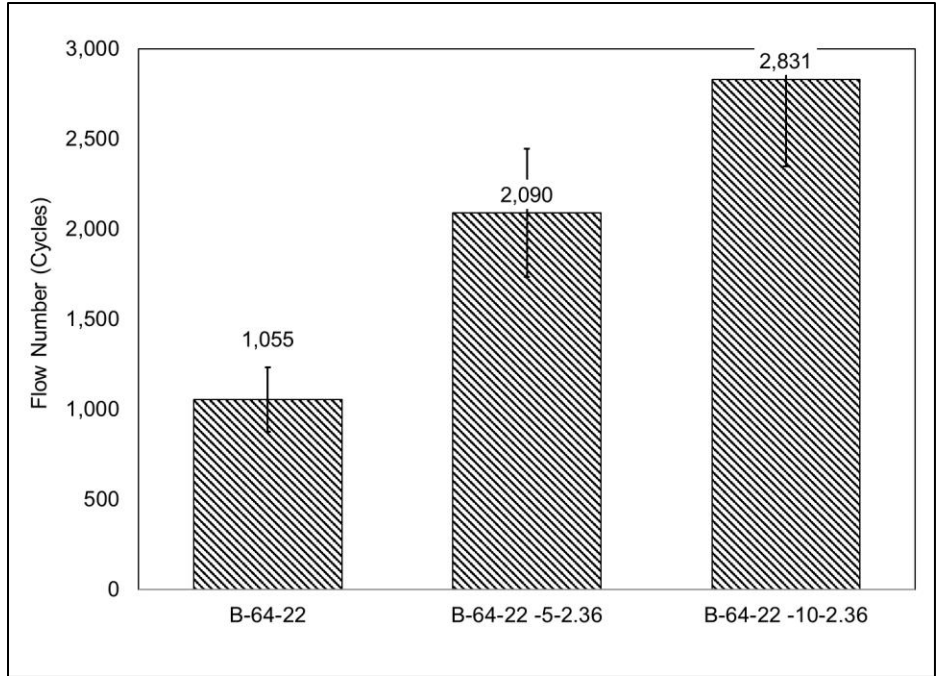
b: Approach-2 Mix (Binder ID format: source_rubber content in percent_maximum rubber size in mm)
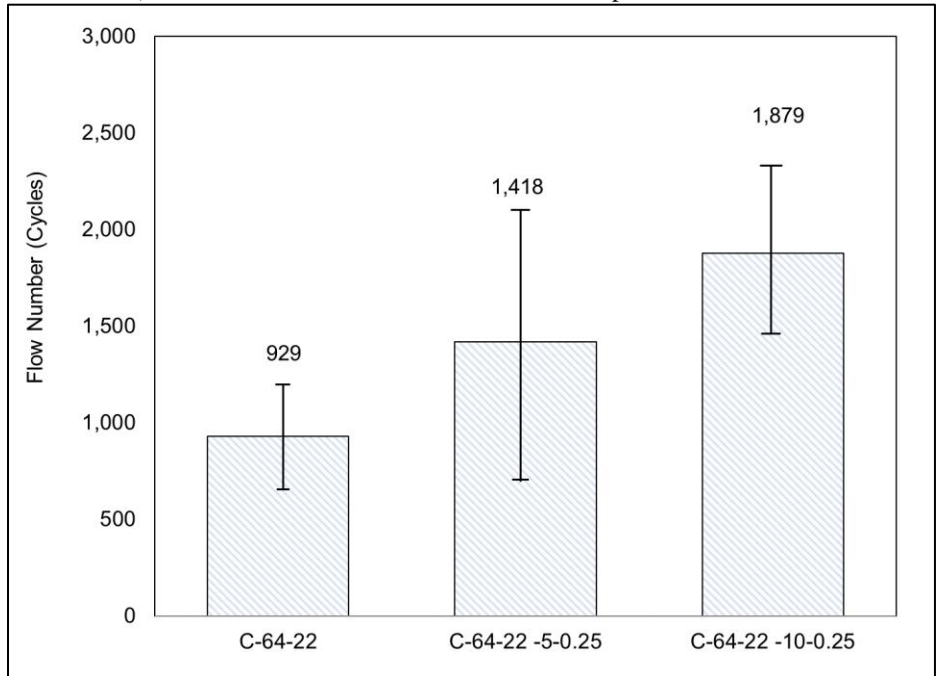
c: Approach-4 Mix (Binder ID format: source_rubber content in percent_maximum rubber size in mm)

d: Approach-3 Mix (Binder ID format: source_rubber content in percent_maximum rubber size in mm)
Figure 7.13: Flow number of rubber-modified mixes at 50°C.

Figure 7.14 shows the plots of average permanent axial strains against loading cycles. The permanent axial strain results showed the same rankings as the flow number results. The PG+X mixes with wet-process binders (Approach-1, Approach-2, and Approach-4) showed flatter permanent strain curves than their control mixes, indicating that these PG+X mixes withstood more loading cycles than their control mixes when they reached the same permanent strain. The Approach-2 PG+X mixes showed the most improvement in rutting resistance among these approaches. The B-64-22-5-2.36 mix withstood double the cycles withstood by the B-64-22 control mix to reach the same average permanent axial strains, and the B-64-22-10-2.36 mix withstood twice as many cycles as the mix with five percent rubber. The Approach-3 mixes with dry-process rubber accumulated permanent strains quickly and at a rate that appeared to be even faster than the control mix after the same number of loading cycles.

a: Approach-1 Mix (Binder ID format: source_rubber content in percent_maximum rubber size in mm)

b: Approach-2 Mix (Binder ID format: source_rubber content in percent_maximum rubber size in mm)
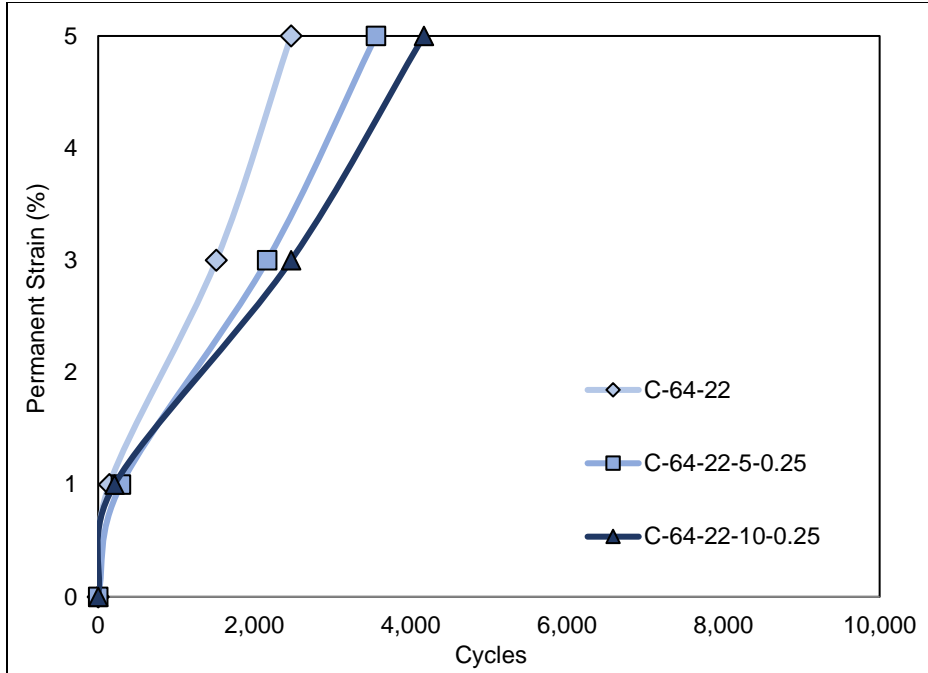
c: Approach-4 Mix (Binder ID format: source_rubber content in percent_maximum rubber size in mm)
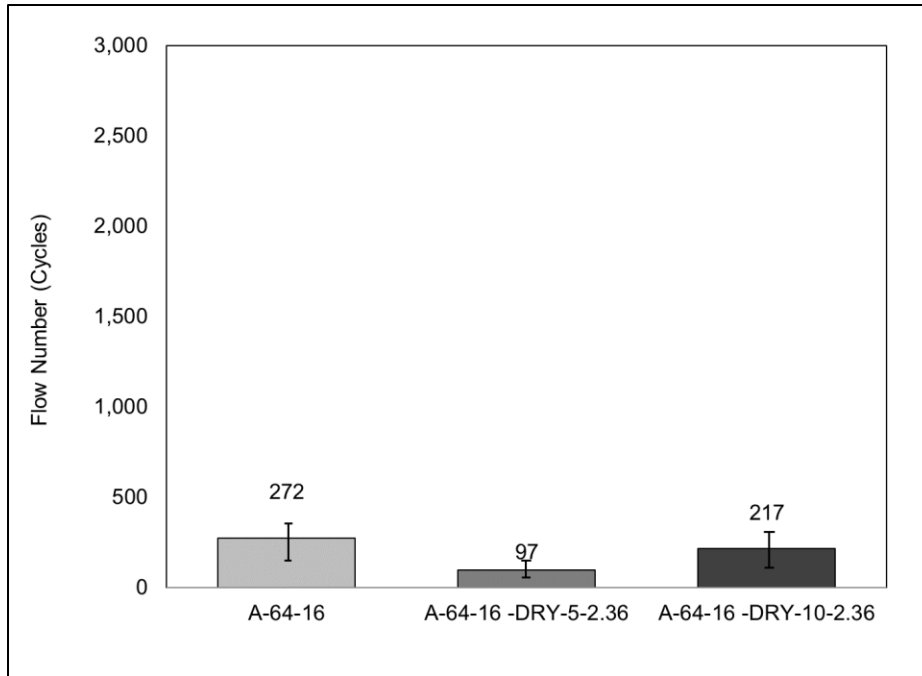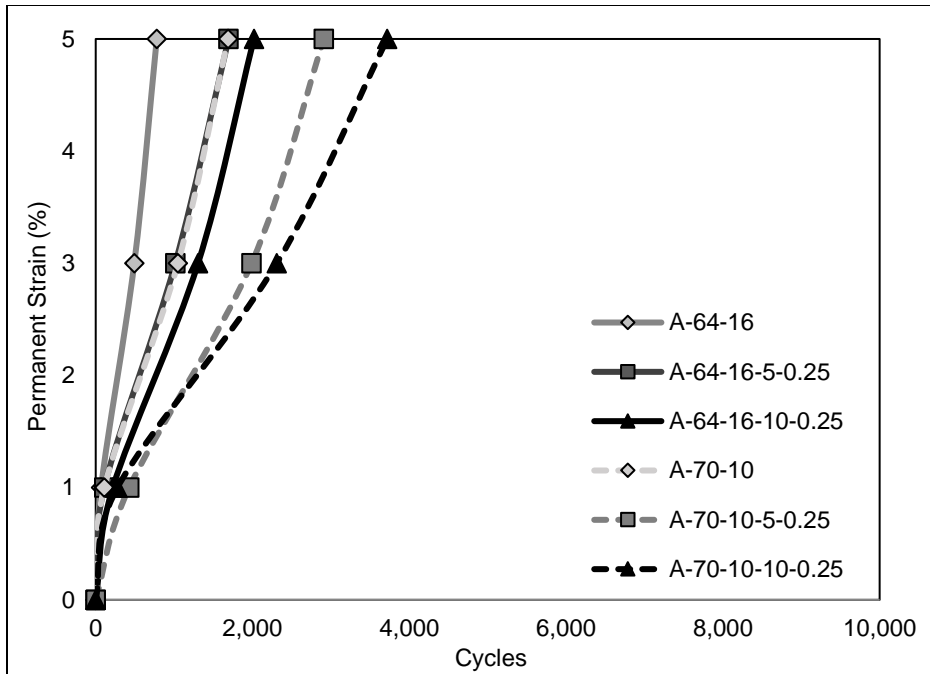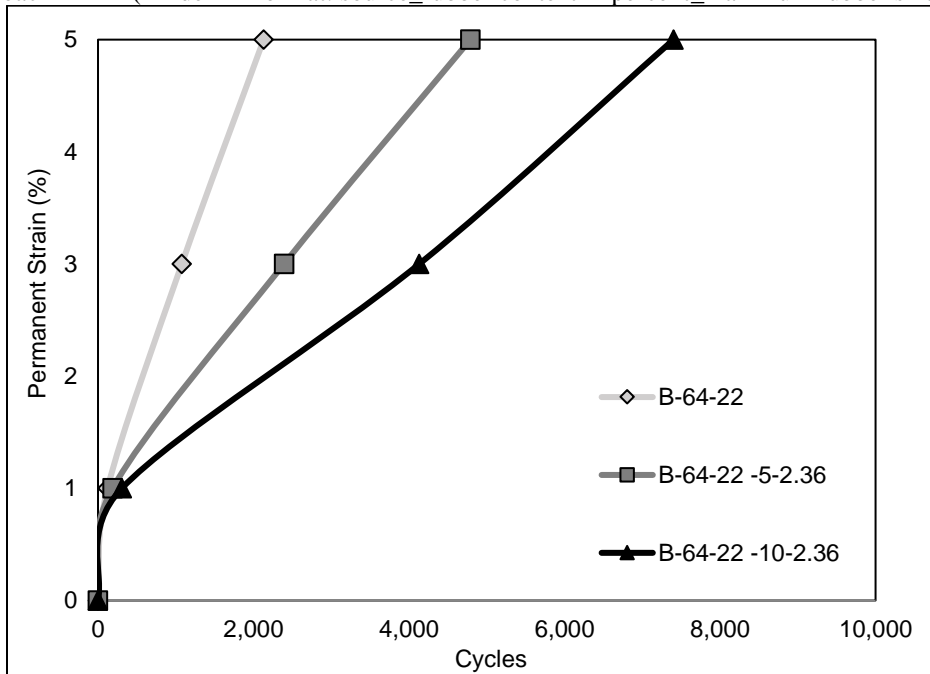

d: Approach-3 Mix (Binder ID format: source_rubber content in percent_maximum rubber size in mm)

Figure 7.14: Average permanent strains versus cycles at 50°C.

7.3.8   Evaluation of Fatigue Damage Resistance

Figure 7.15 shows the controlled-strain flexural beam fatigue test results at 20°C and 10 Hz. The figures plot the predicted fatigue life against applied peak to peak strain on a log-log scale. The fatigue lives were estimated between 100 and 1,000 microstrain to show the difference among mixes.

Increasing the rubber content led to a steeper curve between fatigue life and strain in the PG+X mixes than their control mixes. Figure 7.15 shows that the fatigue lives of all the PG+X mixes were more strain-sensitive than their control mixes.

For Approach-1 PG 64-XX mixes, the predicted fatigue lives for A-64-16-5-0.25 and A-64-16-10-0.25 were higher than the control mix (A-64-16) at low strains (< 400 microstrain), probably attributed to the lower air-void contents in the PG+X mixes, as Figure 7.7 shows. For Approach-1 PG 70-XX mixes, the PG+X mixes (A-70-10-5-0.25 and A-70-10-10-0.25) had longer fatigue lives than the control mix (A-70-10), despite the fact that Approach-1 A-70-10 mixes had relatively lower air-void contents than the other two mixes. For Approach-2 mixes, B-64-22-5-2.36 had higher air-void contents than the control mix (B-64-22), but the PG=X mixes still had higher fatigue lives at most strains in Figure 7.15b.

These observations indicated that air-void content was not the main factor that changed the fatigue lives of the PG+X mixes tested in this chapter. In general, at low strain levels (<400 microstrain), the PG+X mixes had longer fatigue lives than their control mixes, except for the Approach-2 B-64-22-10-2.36 mix. This mix was much stiffer than the control mix (B-64-22), as Figure 7.9c shows. This higher stiffness decreased the fatigue life of the B-64-22-10-2.36 mix in the

controlled-strain flexural beam fatigue test. The comparison between PG+X mixes and their control mixes was inconclusive at higher strains (>400 microstrain).

Figure 7.8 and Figure 7.9 show that the stiffnesses of the PG+X mixes were not notably different from the control mixes for Approach-1 and Approach-4. The Approach-2 PG+X mixes were stiffer than their control mix, but the fatigue lives of the control mix were between these two PG+X mixes. On the other hand, the Approach-3 mixes with dry-process rubber were softer than the control mix, and the former had longer fatigue lives than the control mix when the strain was lower than 600 microstrain.

The fatigue test results implied that the fatigue performance of these PG+X mixes varied and that the fatigue lives of PG+X mixes were more strain-sensitive than their control mixes. To better assess the interaction of stiffness and fatigue life in different applications of the PG+X mixes, the beam test results were analyzed with the *CalME* pavement design software to simulate the pavement responses under various conditions (i.e., pavement structures, climate conditions, and traffic). The simulation results are discussed in Section 7.4.
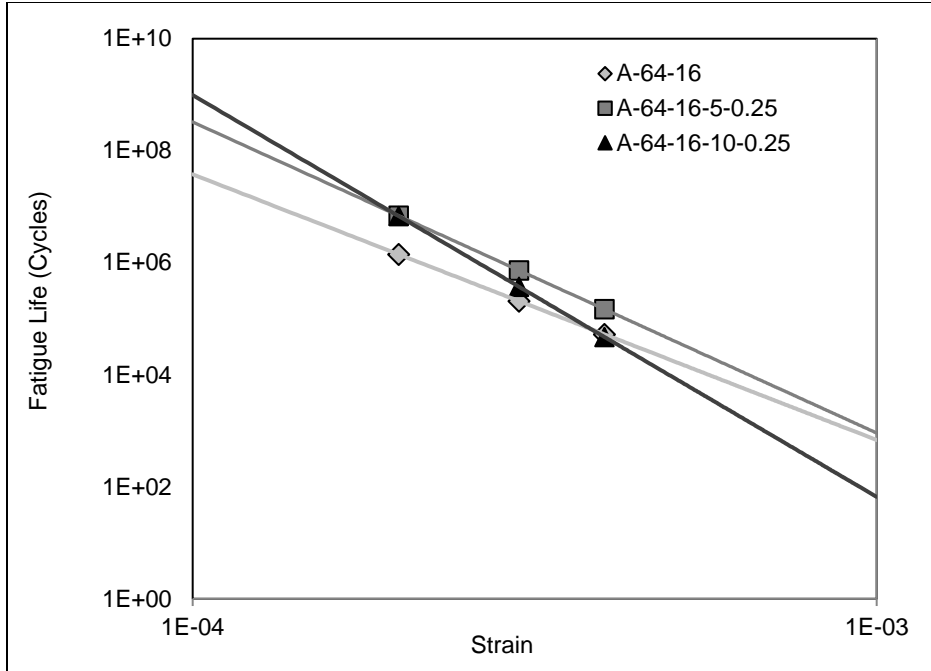
a: Approach-1 PG 64-16 Mix (Binder ID format: source_rubber content in percent_maximum rubber size in mm)

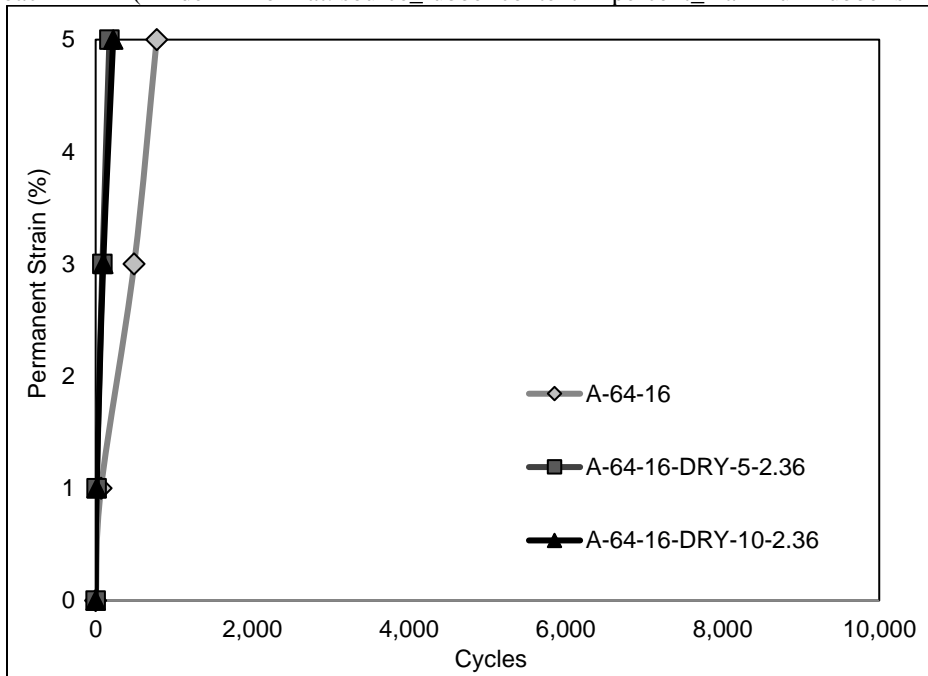b: Approach-1 PG 70-10 Mix (Binder ID format: source_rubber content in percent_maximum rubber size in mm)
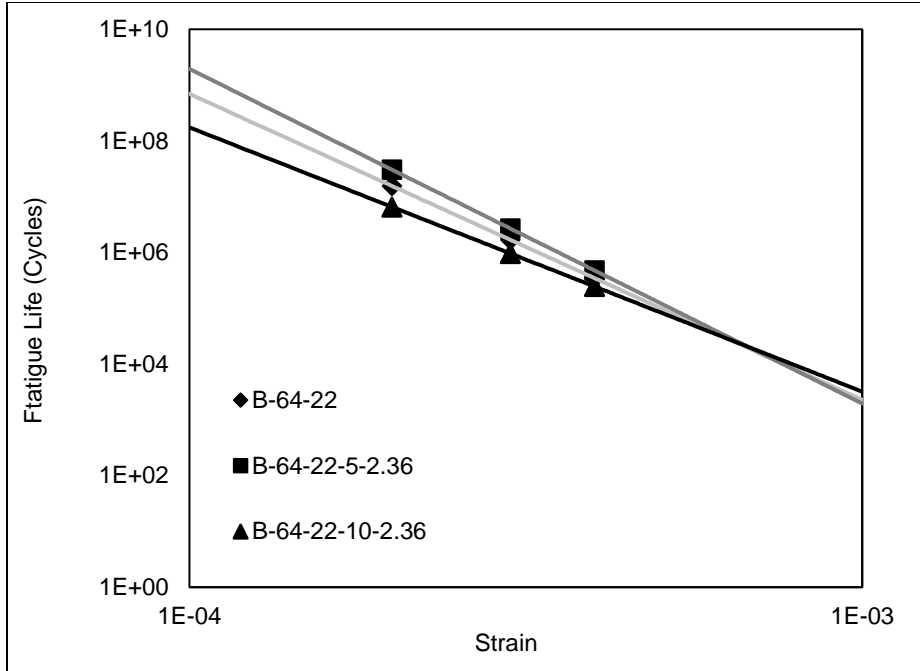
c: Approach-2 Mix (Binder ID format: source_rubber content in percent_maximum rubber size in mm)

d: Approach-4 Mix (Binder ID format: source_rubber content in percent_maximum rubber size in mm)

e: Approach-3 Mix (Binder ID format: source_rubber content in percent_maximum rubber size in mm)
Figure 7.15: Beam fatigue test results at 20°C.

7.3.9 Evaluation of Thermal Cracking Resistance

When asphalt mixes are exposed to the atmosphere, oxygen penetrates the mix over time and oxidizes (ages) the asphalt binder. This aging process changes the chemical composition of the binder, leading to its stiffening and embrittlement. This impairs the long-term performance of the asphalt mix, such as thermal cracking resistance *(135,205)*.

 Figure 7.16 shows the UTSST results for Approach-1, Approach-3, and Approach-4 PG+X mixes after long-term oven-aging. Given that the aggregate gradation was the same among these mixes, the difference in thermal cracking resistance was mostly attributed to the differences between the binders. It was found that cracking temperatures generally matched the low PGs obtained from the BBR tests on these PG+X binders.

340

The PG+X mixes (Approach-1 and Approach-4) containing five percent rubber by weight of the binder generally provided better thermal cracking resistance than their control mixes. These PG+X mixes had the highest CRI_{Env} and the lowest cracking temperature value in each PG group. In contrast, the PG+X mixes containing ten percent rubber by weight of the binder showed the same or slightly lower CRI_{Env} value or fracture temperatures than control mixes. Alavi et al. *(205)* suggested that the CRI_{Env} value of the mix produced using the laboratory mixing and laboratory compaction method should exceed 17 to provide a satisfactory thermal cracking resistance. The PG+X mixes with five percent rubber by weight of the binder appeared to have sufficient thermal cracking resistance following Alavi's recommendations.

The ranking of the thermal cracking resistance (CRI_{Env} value and fracture temperature) within each approach was the same as the ranking of the stiffness of the binder in intermediate and low temperatures (<25ºC in this case). Table 7.4 and Table 7.5 show that the Approach-1 and Approach-4 PG+X binders containing five percent rubber had the lowest $G^* \times \sin(\delta)$ and $\Delta T_{C\text{-stiffness}}$ values in each approach. They were softer than other binders at the intermediate and low temperatures. The soft binders potentially benefited the thermal cracking resistance measured in the UTSST.

The thermal cracking resistance of Approach-3 mixes with dry-process rubber was similar to the control mix. The mixes with dry-process rubber contained higher binder contents (the A-64-16-DRY-5-2.36 mixes had an OBC of 6.0 percent [5.7 percent of base asphalt binder by DWA, the A-64-16-DRY-10-2.36 mixes had an OBC of 6.8 percent [6.1 percent of base asphalt binder by DWA) than the control mix (the A-64-16 mixes contained 5.3 percent binder by DWA), as Table 7.7 shows. This should have benefited the thermal cracking resistance. However, the aggregate gradation was not adjusted for the rubber swelling, which appeared to decrease the stone-on-stone

contact. This decreased the thermal cracking resistance. The conflicting effects of these two mechanisms resulted in inconsistent performance changes for Approach-3 mixes with dry-process rubber using 0.25 and 0.5 percent rubber by weight of the aggregate (approximately five and ten percent rubber by weight of the binder).
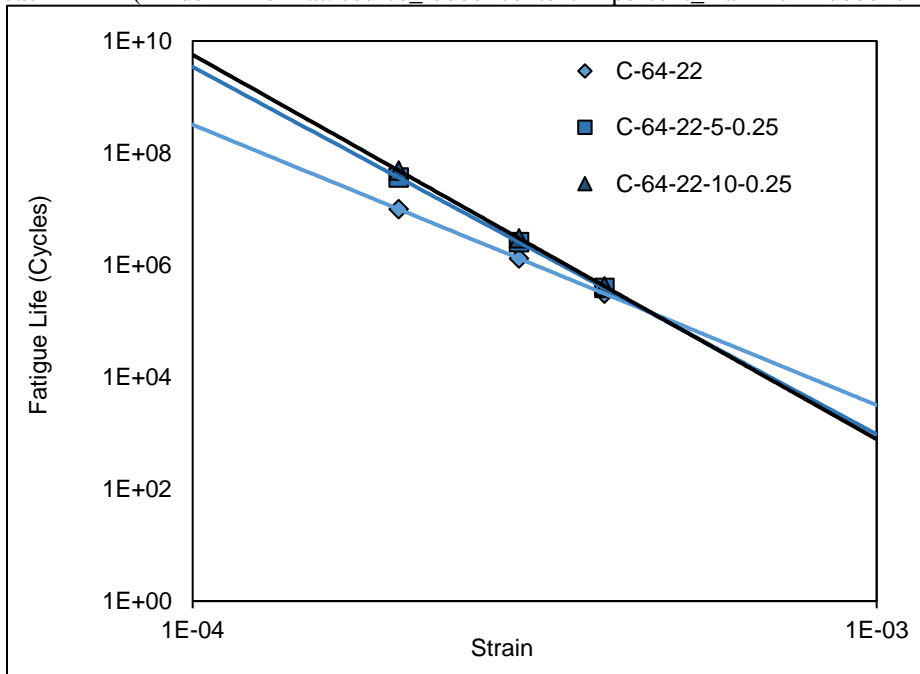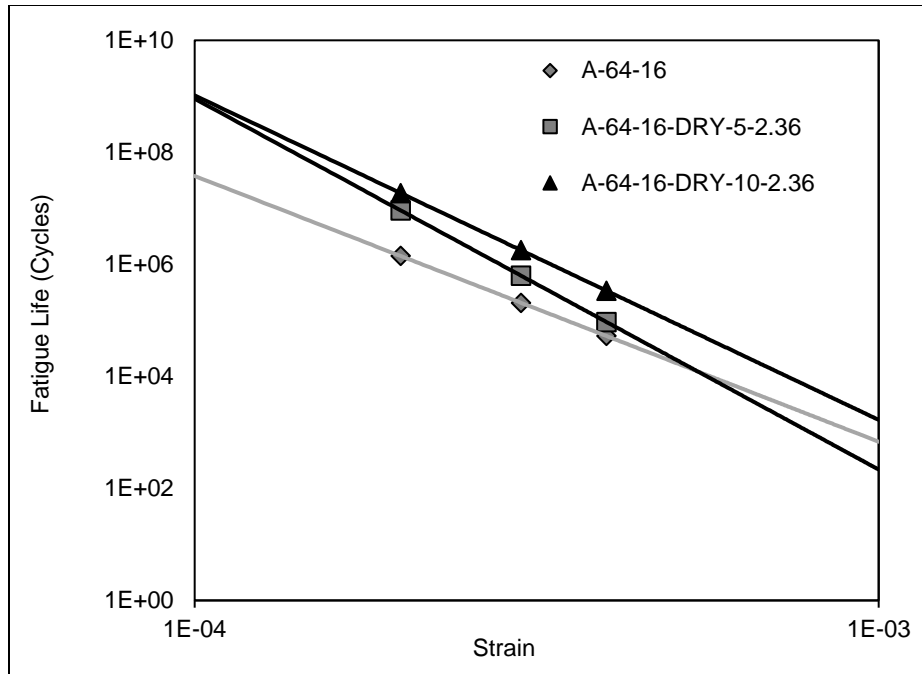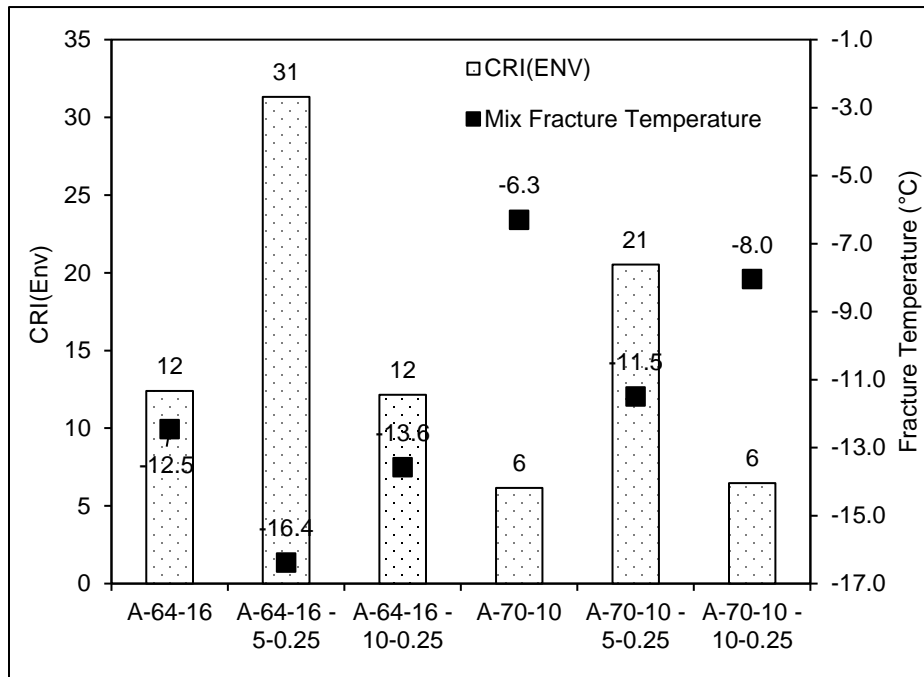

a: Approach-1 Mix (Binder ID format: source_rubber content in percent_maximum rubber size in mm)
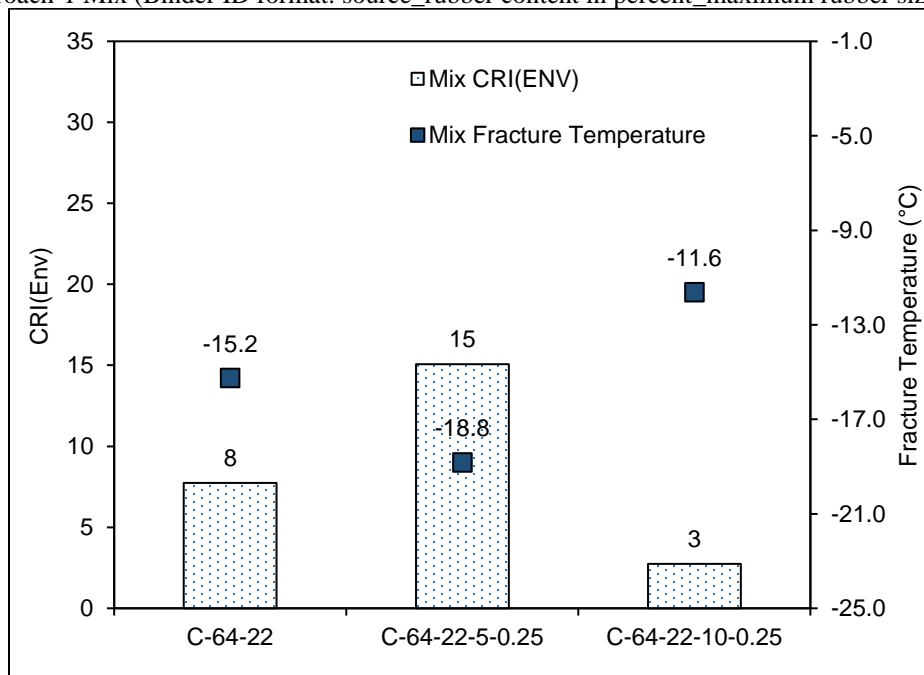
b: Approach-4 Mix (Binder ID format: source_rubber content in percent_maximum rubber size in mm)
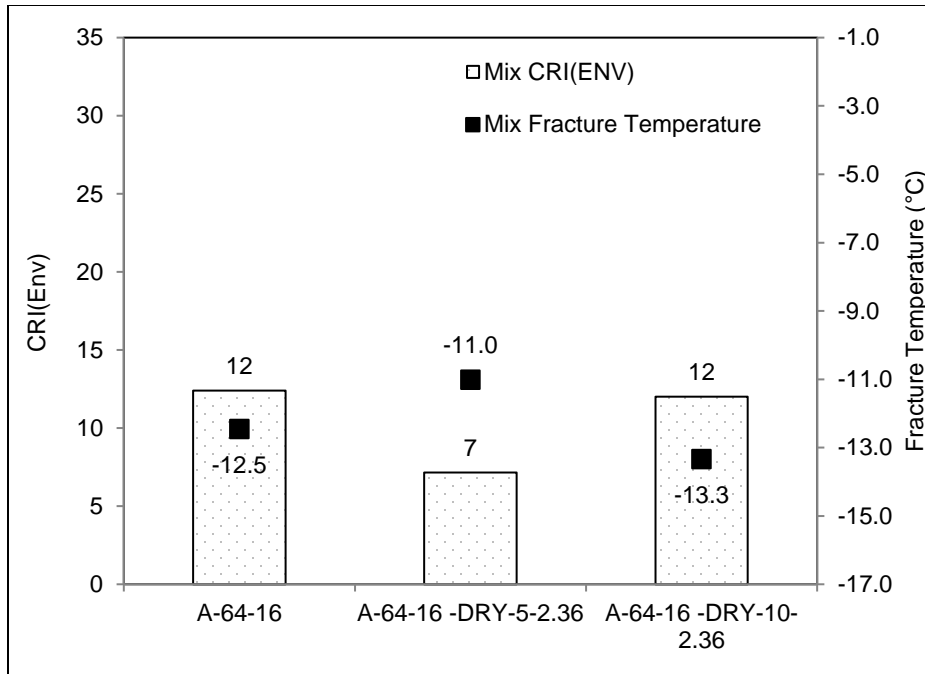
c: Approach-3 Mix (Binder ID format: source_rubber content in percent_maximum rubber size in mm)
Figure 7.16: UTSST results for PG+X mixes.

7.4 Pavement Performance Simulation Using *CalME* Software

In addition to the laboratory evaluation, the field performance of PG+X mixes was simulated under a wide range of structures, climate conditions, and traffic conditions using the *CalME* software *(208-210)*. The purpose of this *CalME* simulation was to predict the PG+X mix performance in different pavement structures and compare this with the performance of conventional dense-graded mixes produced with unmodified binders.

The simulation was based on the road conditions where these mixes would likely be used following the binder PGs. Typical structures used in California were analyzed, namely overlays on a cracked asphalt pavement or cracked concrete pavement, and full-depth asphalt pavement. Representative traffic volumes and temperature fluctuations were applied during the simulation to model loading and environmental impacts. The material parameters were based on the flexural frequency sweep and flexural fatigue test results detailed in Section 7.3.5 and Section 7.3.8.

Simulation results assessed included the development of reflective cracking in overlay cases and fatigue cracking in thick pavement cases. Since rutting is mostly controlled by the surface material properties, and the evaluation of the rutting has been addressed in Sections 7.3.7, no rutting simulation was conducted in this task phase.

7.4.1 CalME Simulation Input

Simulations using the *CalME* software takes into account climate, traffic, material, and pavement structure. The estimation of pavement distress is based on changes in pavement conditions (i.e., stiffness), critical responses (stress, strain, deflection), and the number of loading repetitions over time *(208-210)*. The primary output is the pavement service life, which is the estimated time when

the cracking reaches half a meter per meter squared on the layer surface. The design life was selected to be 20-years for these simulations.

Table 7.8 lists the climate inputs that were used for the simulation. Four typical California climate regions were selected, and then PG+X mixes were selected for a specific climate region based on their binder PGs. The pavement temperatures were calculated on a daily basis using the sinusoidal function option that considers the mean yearly surface temperature, yearly temperature range, and daily temperature range. The temperature in the pavement is calculated from the surface temperature using the finite-difference formulation used in *CalME*.

Table 7.8: *CalME* Climate Input

Mix ID	Binder Grade	Climate	Mean Yearly Surface Temp (ºC)	Range Yearly Surface Temp (ºC)	Range Daily Surface Temp (ºC)
A B C G H	64-16	North Coast (NC)	15.3	12	16
A B C G H	64-16	Inland Valley (IV)	21.4	23	24
D E F	70-10	Desert (D)	26.3	28	22
J K L	64-22	High Desert (HD)	15.4	31	26
S T U	64-22	High Desert (HD)	15.4	31	26

The three different pavement structures evaluated are summarized in Table 7.9 through Table 7.11. In the simulation, the PG+X layer and underlying layers were assumed to be fully bonded.

Table 7.9: AC on AC Overlays

Structure	Material	Thickness (mm)	Stiffness at 20°Cand 10 Hz (MPa)
Layer 1	PG+X	45, 60, 100, 150, 210	Vary by materials
Layer 2	Old HMA	100	5,000
Layer 3	Aggregate Base	300	300
Layer 4	Subgrade (Clay Soil [CL])[1]	Infinite	70

[1] CL is clay soil in the Unified Soil Classification System (USCS).

Table 7.10: Full-Depth Asphalt Mix

Structure	Material	Thickness (mm)	Stiffness at 20°C and 10 Hz (MPa)
Layer 1	PG+X	300	Vary by materials
Layer 2	Aggregate Base	300	300
Layer 3	Subgrade (CL)	Infinite	70

[1] CL is clay soil in the Unified Soil Classification System (USCS).

Table 7.11: AC on PCC Overlays

Structure	Material	Thickness (mm)	Stiffness at 20°C and 10 Hz (MPa)
Layer 1	PG+X	45, 60, 100, 150	Vary by materials
Layer 2	PCC	220	35,000
Layer 3	Aggregate Base	300	300
Layer 4	Subgrade (CL)	Infinite	70

[1] CL is clay soil in the Unified Soil Classification System (USCS).

Two RHMA-G mixes were added to the overlay comparisons to identify the performance differences between PG+X mixes and conventional RHMA-G mixes in different climates. The layer thickness for these comparisons was 60 mm, the current maximum allowable thickness for RHMA-G in Caltrans practice. Table 7.12 summarizes the RHMA-G mix parameters in this simulation. It should be noted that the air-void contents of the RHMA-G mixes were one percent lower than the PG+X mixes (beam air-void content 7±1 percent, as shown in Figure 7.7). The total binder content was at least 8.3 percent by DWA, which equals at least 6.5 percent base asphalt binder content (based on 20 percent rubber content). This is higher than the base asphalt binder content in the PG+X mixes, as Table 7.7 shows. The higher base binder content in RHMA-G increased the binder film thickness, as discussed in Section 6.3, which can potentially slow crack propagation.

Table 7.12: RHMA-G Mix Parameters

Mix ID	Binder Content (%)	Air-Void Content (%)	Mix Gradation	Stiffness at 20°C and 10 Hz (MPa)
RHMA-G#1	8.3	6.0	½'' NMAS[1]	4,329
RHMA-G #2	8.8	6.0	¾'' NMAS[1]	3,786

The simulation of a full-depth thick pavement was used to investigate the potential application of PG+X mixes in a thick pavement structure. The thickness of the asphalt layer was set to multiple lifts totaling 300 mm, which is the same thickness in one of the recent AC long-life project designs for Interstate Freeway 5 in Sacramento (SAC-5). This design structure contains three HMA layers. The combined top and intermediate layer thickness is 240 mm, with a design of four percent air-void content. The bottom layer is 60 mm thick with a two percent design air-void content. The surface layer uses an SBS-modified binder (PG 64-28-SBS) with up to 15 percent RAP, the intermediate layer uses a PG 64-16 binder with 25 percent RAP, and the bottom layer uses a PG 64-16 binder with 15 percent RAP. This SAC-5 design was used as the basis for the *CalME* simulation of a full-depth AC thick pavement.

The traffic input started with a baseline of 1E+06 equivalent single axle loads (ESALs) per year on a 45 mm surface layer for the AC pavement and 2E+05 ESALs on a 45 mm surface layer over the cracked PCC pavement. The traffic volumes increased with increasing asphalt layer thickness. These traffic inputs were applied because they represent reasonable traffic volumes for the corresponding layer thickness. The *CalME* simulations under these traffic volumes should show a clear difference between the different mixes to assist with the comparison between PG+X mixes and control mixes. Given that traffic growth was not a primary concern in this study, the annual traffic was fixed to the defined values showed in Table 7.13.

Table 7.13: *CalME* Traffic Input

AC over AC Surface		AC over PCC Surface		Full-Depth AC	
Thickness (mm)	Traffic (million ESAL[1]/year)	Thickness (mm)	Traffic (million ESAL/year)	Thickness (mm)	Traffic (million ESAL/year)
45	1	45	0.2		
60	2	60	0.2		
100	4	100	1	300	100
150	10	150	2		
210	10	210	N/A		

[1] ESAL: Equivalent Single Axle Load.

7.4.2 *Asphalt Mix over Cracked Asphalt Mix Simulation*

Table 7.14 summarizes the reflective cracking rank for the AC over AC application. The comparison was made within the approach according to the binder PG group. Given that the mixes using binders of different PGs would be used in different climates, no comparison was made across binder groups. In this section, the best-performing material is marked as No.1 and the worst as No.3 in each climate condition. A total of 35 cases were simulated in the overlay application. Ten of these cases used the Approach-1 PG 64-16 mixes (two climate conditions × five thicknesses). Five cases used the Approach-1 PG 70-10 mixes. Approach-2 and Approach-4 mixes were simulated in the high desert climate with five thicknesses for each approach. The remaining ten cases used the Approach-3 mixes (two climate conditions × five thicknesses).

Table 7.14: Reflective Cracking Rank of Thin to Thick Overlay Application

Approach	Binder ID[1]	Mix ID	Inland Valley	North Coast	Desert	High Desert
			Layer Thickness (mm) Considered: 45, 60, 100, 150, 210 mm. The ranking was the same for all thicknesses			
1	A-64-16	A	3	3		
	A-64-16-5-0.25	B	2	2		
	A-64-16-10-0.25	C	1	1		
	A-70-10	D			2	
	A-70-10-5-0.25	E			1	
	A-70-10-10-0.25	F			3	
2	B-64-22	S				1
	B-64-22-5-2.36	T				2
	B-64-22-10-2.36	U				3
3	A-64-16	A	1	1		
	A-64-16-DRY-5-2.36	G	2	2		
	A-64-16-DRY-10-2.36	H	3	3		
4	C-64-22	J				2
	C-64-22-5-0.25	K				3
	C-64-22-10-0.25	L				1

[1] Binder ID format: source-PG-rubber content in percent-maximum rubber size in mm.

The plots of reflective cracking curves in the wheel path are presented in Appendix B. Figure B.1 through Figure B.27 shows no universal optimum rubber content was found for different PG+X approaches when using PG+X mixes in AC over AC applications. The best application was dependent on the material, climate, and structure together rather than the laboratory tested PG+X mix properties (i.e., binder content, mix stiffness, fatigue test result) alone.

The simulation results for Approach-1 and Approach-4 PG+X mixes showed that increasing the rubber content slowed the development of reflective cracking in the AC over AC application in the inland valley and north coast climate for all surface layer thicknesses. Approach-1 and Approach 4 mixes with 10 percent rubber content had the best performance in the dense-graded mix in the inland valley and north coast climates.

Figure 7.10 shows that the Approach-1 and Approach-4 PG+X mixes had similar stiffnesses to the control mixes. The simulated traffic loading would therefore generate similar tensile strains at the bottom of the layer in both these mixes. For the simulation where most strains were lower than 400 microstrain, the PG+X mixes (A-64-16-5/10-0.25, A-70-10-5-0.25, and C-64-22-5/10-0.25) had longer service lives than the control mixes, which was consistent with their fatigue test results shown in Figure 7.15. The simulation of the Approach-1 A-70-10-10-0.25 mix showed the fastest cracking in the desert climate where a wide range of temperature fluctuations happen. The daily temperature fluctuations change the mix stiffness simulated in the surface layer. When the temperature was high, the mix stiffness dropped. The traffic load would generate a higher strain at the bottom of the layer using this less stiff mix soft mix. Therefore, the service life of the Approach-1 PG 70-10-10-0.25 mix was reduced at the higher strains (i.e., >400 microstrain), as the fatigue test results show in Figure 7.15.

The PG+X mixes and RHMA-G mixes were compared at 60 mm thickness. The traffic volume was two million ESAL according to Table 7.13. The results showed that the RHMA-G mixes performed better than the Approach-1 and Approach-4 PG+X mixes. The RHMA-G mix was expected to perform better than the DGAC in terms of reflective cracking performance. These RHMA-G mixes had a higher binder content and relatively lower air void content than the PG+X mixes, which is favorable for reflective cracking resistance *(53)*. The RHMA-G mixes were also softer than the PG+X mixes when comparing the stiffnesses in Figure 7.8 and Table 7.12. The softer mix was preferred in the thin overlay (60 mm) to provide a longer fatigue life than the stiff mix. Without considering the construction cost and other pavement distresses, the RHMA-G mix had better reflective cracking performance than the Approach-1 and Approach-4 PG+X mixes in the 60-mm thick overlay simulation.

Following the *CalME* simulation results, when using an appropriate rubber dosage for Approach-1 and Approach-4, the PG+X mixes showed a lower rate of cracking than the conventional asphalt mix, indicating that these PG+X mixes could be considered as an alternative to conventional mixes in AC over AC applications.

The Approach-2 PG+X mixes had faster crack propagation rates than their control mix in the AC over AC simulation. Increasing the rubber content from five to ten percent further accelerated the rate of cracking. Figure 7.15d shows that the Approach-2 mix with ten percent rubber had a shorter fatigue life than the mix with five percent rubber.

The Approach-3 mixes with dry-process rubber were not suitable for inland valley or north coast climate applications. The control mix withstood the cracking longer than the mixes with dry-process rubber. Under the same traffic loading, the softer mixes with dry-process rubber would transfer higher loadings to the underlying layer than the control mix would, which would accelerate the rate of reflective cracking.

In summary, five simulations showed that the optimum rubber content was five percent in the desert climate using Approach-1 PG 70-10 mixes. Fifteen simulations showed that ten percent rubber was recommended in the inland valley, north coast, and high desert climates using Approach-1 PG 64-16 mixes and Approach-4 PG 64-22 mixes. Approach-2 PG 64-22 mixes would not be recommended in the high desert climate based on the results of the five simulations. The Approach-3 mixes with dry-process rubber were not recommended in the inland valley and north coast climate.

The simulation results indicated that there were no uniform optimum applications of the PG+X mixes in the AC overlay structure. Based on this observation, ME simulations should be used to

select the most appropriate mix for a given set of pavement structure, climate, and traffic conditions in the project.

7.4.3   Full-Depth Asphalt Mix Simulation

Table 7.15 summarizes the fatigue cracking rank in the full-depth pavement structure. A total of seven cases were simulated in the full-depth application. Two cases used the Approach-1 PG 64-16 mixes (two climate conditions). One case used the Approach-1 PG 70-10 mixes in the desert climate. Approach-2 and Approach-4 mixes were simulated in the high desert climate. The remaining two cases used Approach-3 mixes (two climate conditions). The simulation results indicated that there was no universal optimum rubber usage for different approaches in this thick pavement structure.

The plots in Figure B.29 through Figure B.32 show that the fatigue cracking was less than 0.01 percent in most cases because the strain at the bottom of the thick asphalt layer was low. Since the pavement was thick and the traffic-related tensile strain at the bottom of the layer was low, Approach-1 and Approach-4 mixes generally had longer fatigue lives than the control mixes, which was consistent with the laboratory fatigue test results shown in Figure 7.15. In the inland valley, north coast, and desert climates, the Approach-1 mix with five percent rubber outperformed the mix with ten percent rubber. Figure 7.15 shows that the slopes of strain-Nf curves for the ten percent mixes were steeper than the other mixes in Approach-1. When a higher temperature was simulated in the mix, the mix stiffness decreased. The PG+X mixes with ten percent rubber were more strain-sensitive than the other mixes in the same approach, as shown in Figure 7.15. These PG+X mixes with ten percent rubber had shorter fatigue lives in this high strain condition than the other two mixes in the same PG group.

Table 7.15: Fatigue Cracking Rank of Full-Depth Asphalt Mix Application

Layer Thickness (mm)			300			
Approach	Binder ID[1]	Mix ID	Inland Valley	North Coast	Desert	High Desert
1	A-64-16	A	3	3		
	A-64-16-5-0.25	B	1	1		
	A-64-16-10-0.25	C	2	2		
	A-70-10	D			2	
	A-70-10-5-0.25	E			1	
	A-70-10-10-0.25	F			3	
2	B-64-22	S				1
	B-64-22-5-2.36	T				2
	B-64-22-10-2.36	U				3
3	A-64-16	A	1	1		
	A-64-16-DRY-5-2.36	G	2	2		
	A-64-16-DRY-10-2.36	H	3	3		
4	C-64-22	J				3
	C-64-22-5-0.25	K				2
	C-64-22-10-0.25	L				1

[1] Binder ID format: source-PG-rubber content in percent-maximum rubber size in mm.

In a high desert climate, the Approach-4 mix with ten percent rubber had the best reflective cracking performance. This was consistent with the results in Figure 7.15c, which show that the ten percent rubber content mixes generally had longer fatigue lives than the five percent rubber content mixes at the same strain level. The opposite trend was observed for the Approach-2 mixes, with the five percent rubber content mix showing a longer fatigue life at the lower strain level.

The comparison between PG+X mixes and the SAC-5 mixes revealed that the Approach-1 and Approach-4 mixes generally outperformed the SAC-5 mixes. The Approach-2 and Approach-3 mixes did not perform as well as the SAC-5 mixes due to the relatively low stiffnesses of these mixes, which resulted in a higher tensile strain at the bottom of the layer leading to an increased rate of fatigue cracking damage.

In the inland valley and north coast climate, the SAC-5 mixes outperformed the conventional dense-graded mixes, because the rich bottom layer limited the initiation of bottom-up cracking.

The Approach-1 and Approach-4 PG+X mixes provided equivalent performance to the SAC-5 mixes in terms of the rate of fatigue cracking in thick full-depth pavement structures.

In the desert climate, the SAC-5 mixes were unable to withstand the design traffic volume, as expected. These SAC-5 mixes were designed for the inland valley and used a PG 64-XX binder instead of a stiffer PG 70-XX binder. Therefore, SAC-5 mixes experienced high strains in the desert climate, which increased the rate of fatigue cracking damage.

In summary, the five percent rubber content was the optimum rubber dosage for using Approach-1 mixes in the inland valley, north coast, and desert climate for the full-depth application. The ten percent rubber content was recommended for use in Approach-4 mixes in the high desert climate. The use of Approach-2 and Approach-3 mixes would not be recommended in full-depth applications as the three simulation cases show.

7.4.4   Asphalt Mix over Cracked Portland Cement Concrete Simulation

Table 7.16 summarizes the reflective cracking rankings for the AC over PCC application. A total of 28 cases were simulated in the overlay application. Eight of these cases used the Approach-1 PG 64-16 mixes (two climate conditions × four thicknesses). Four cases used the Approach-1 PG 70-10 mixes in the desert climate. Approach-2 and Approach-4 mixes were simulated in the high desert climate with four thicknesses for each approach. The remaining eight cases used the Approach-3 mixes (two climate conditions × four thicknesses).

For the Approach-1 A-64-16 PG+X mixes, the 10 percent rubber content improved the reflective cracking resistance in the inland valley and north coast climates. These PG+X mixes had similar stiffness to the control mix, but generally longer fatigue lives at lower strains (<400 microstrain) in the selected climates. Therefore, Approach-1 A-64-16 PG+X mixes slowed the rate of reflective cracking development, as shown in Figure B.33, Figure B.38, Figure B.45, and Figure B.50 in Appendix B.

Figure B.35, Figure B.42, Figure B.47, and Figure B.52 show that the Approach-1 A-70-10 PG+X mixes performed worse than the control mixes in the desert climate. The Approach-1 A-70-10-10-0.25 mix had the fastest rate of cracking in this climate. The higher temperature in the desert softened the mix resulting in the traffic load generating a high strain in this soft mix. The Approach-1 A-70-10-10-0.25 mix was more strain-sensitive than the other two mixes in the same approach as Figure 7.15 shows, which damaged faster in this high strain condition.

Figure B.37, Figure B.44, Figure B.49, and Figure B.54 show that the Approach-2 PG+X mixes generally showed lower rates of cracking than the control mix. Figure 7.9d shows that the Approach-2 PG+X mixes were generally stiffer than the control mix, which decreased the loading

transferred to the underlying, cracked PCC. Therefore, using these PG+X mixes to overlay the cracked PCC slowed the rate of reflective cracking.

Table 7.16: Reflective Cracking Rank of AC over PCC Application

Approach	Binder ID[1]	Mix ID	Layer Thickness (mm) Considered: 45, 60, 100, 150 mm. The ranking was the same for all thicknesses			
			Inland Valley	North Coast	Desert	High Desert
1	A-64-16	A	3	3		
	A-64-16-5-0.25	B	1	1		
	A-64-16-10-0.25	C	2	2		
	A-70-10	D			1	
	A-70-10-5-0.25	E			2	
	A-70-10-10-0.25	F			3	
2	B-64-22	S				3
	B-64-22-5-2.36	T				1
	B-64-22-10-2.36	U				2
3	A-64-16	A	1	1		
	A-64-16-DRY-5-2.36	G	2	2		
	A-64-16-DRY-10-2.36	H	3	3		
4	C-64-22	J				1
	C-64-22-5-0.25	K				3
	C-64-22-10-0.25	L				2

[1] Binder ID format: source-PG-rubber content in percent-maximum rubber size in mm.

Figure B.36, Figure B.43, Figure B.48, and Figure B.53 show that the Approach-4 PG+X mixes performed worse than the control mix in the high desert climate. The Approach-4 PG+X mixes had larger stiffness fluctuations when the temperature changed, and their fatigue lives decreased under high strains, as shown in Figure 7.15. Since the fatigue lives of the Approach-4 PG+X mixes were more strain-sensitive than the control mix, the former damaged faster in the high strain conditions.

Approach-3 mixes did not perform well in AC over PCC applications. These PG+X mixes with dry-process rubber had lower flexural stiffnesses than the control mix, as shown in Figure 7.9c, and they would not withstand the traffic loading and would transfer the higher load to the PCC

layer. This resulted in the PCC layer generating more cracks that reflected rapidly through the damaged AC layer.

In the 60-mm thick overlay case, RHMA-G mixes generated similar or even slower cracking rates than the PG+X mixes. This was attributed to the higher binder content in the gap-gradation, which decreased the rate of reflective cracking compared to that of the dense-graded/lower binder content mix. The RHMA-G mix also had lower air-void contents than the PG+X mix, which also led to a better reflective cracking resistance.

In summary, the five percent rubber content is the optimum rubber content for the inland valley, north coast, and high desert climates using the Approach-1 PG 64-16 and Approach-2 mixes for overlays over PCC in the 12 simulation cases. In contrast, using the Approach-1 PG 70-10, Approach-3, and Approach-4 PG+X mixes in overlays over PCC was not recommended based on the results from the other 16 simulation cases.

7.4.5 *CalME Simulation Summary*

This section summarizes the *CalME* simulations of PG+X mixes used in different pavement structures. The following conclusions were drawn based on these simulation results:

- The PG+X mixes with wet-process binders (Approach-1, Approach-2, and Approach-4) were generally suitable as alternatives to dense-graded mixes produced with conventional binders in overlay cases and thick full-depth AC cases when appropriate rubber contents were used. The optimum rubber content depended on project-specific factors, including mix properties, pavement structures, traffic, and climate conditions. The Approach-3 PG+X mixes with dry-process rubber performed worse than the control mix.

- The RHMA-G mixes performed better than PG+X mixes in the thin (60 mm) overlay simulation cases, which was attributed to the combination of the higher binder content and the gap-gradation.

- The comparison between the SAC-5 mixes and PG+X mixes in the full-depth pavement structure (300-mm thick) indicated that the PG+X mixes with wet-process binders could provide similar performance to the SAC-5 mixes.

- The *CalME* simulation results indicated that the optimum rubber content used in dense-graded mixes in different pavement structures depended on the specifics of each scenario, including mix properties, pavement structures, traffic, and climate conditions. This finding pointed out that the laboratory tests at a specific temperature and strain condition alone might not necessarily represent the overall field performance, owing to the fluctuation of stresses and strains caused by traffic loadings under daily and seasonally varying temperature gradients. Therefore, laboratory tests and a field performance simulation based on mechanistic-empirical principles are recommended for asphalt pavement design and mix selection.

- The *CalME* simulation also indicated that PG+X (Approach-1, Approach-2, and Approach-4) mixes with wet-process binders could be considered for use in the inland valley, north coast, and high desert climate when appropriate rubber dosages were applied. In contrast, the mixes with dry-process rubber (Approach-3) containing coarse rubber (smaller than 2.36 mm [passing the #8 sieve]) had faster cracking development than the conventional mix in the desert climate.

In summary, these PG+X binders containing between five and ten percent crumb rubber modifier are suitable in dense-graded mixes. The mixes with these binders are likely to provide equal or

better performance to the conventional mixes when appropriate rubber dosages were determined according to the pavement structure, traffic, and climate. It is recommended that ME simulations are used to select the mix based on the pavement structure, climate, and traffic conditions in the project.

7.5   Summary and Conclusions

This chapter summarizes the laboratory evaluation of PG+X binders and mixes, and the *CalME* simulation results. The following conclusions were drawn:

1. Question: How do PG+X binders perform in the laboratory?

    Using as low as five percent rubber by weight of the binder could improve the performance of asphalt binders. The Approach-2 and Approach-4 PG+X binders showed an increase in high PG, a decrease in the intermediate PG, and no change or a decrease in the low PG, compared to their base binders. Adding rubber also decreased the creep stiffness at low temperatures. These rubber-modified binders were found to have lower non-recoverable compliances and higher percentage recoveries than their base binders. These modifications in the binder changed the binder performance that was valid at five and ten percent rubber contents, and maximum rubber particle sizes ranging from fine (smaller than 250 microns [passing the #60 sieve]) to coarse (smaller than 2.36 mm [passing the #8 sieve]).

2. Question: Can PG+X materials be effectively used in dense-graded mixes?

    Using a small amount of rubber (five and ten percent by weight of the binder) elevated the required mixing and compaction temperatures when the binder PG changed. The laboratory mixing and compaction method produced PG+X mix specimens that met the target air-void

content. The volumetric mix design results indicated that the wet process PG+X binders (Approach-1, Approach-2, and Approach-4) were suitable for use in dense-graded mix structures. The Approach-3 mix with dry-process rubber showed that using coarse rubber particles (smaller than 2.36 mm [passing the #8 sieve]) in a dense-graded mix created high-VMA when no adjustment of the aggregate gradation was made for the swelled rubber. The mixes with dry-process rubber could result in poor compaction due to the rubber particles swelling when they contact the hot binder. This, in turn, would impair mix stiffness, moisture damage resistance, and rutting resistance.

3. Question: How do PG+X mixes perform in the laboratory in terms of rutting, fatigue, and thermal cracking?

The flexural frequency sweep test showed that using fine rubber particles (smaller than 250 microns [passing the #60 sieve]) in Approach-1 did not show much stiffness change compared to the control mix. The Approach-4 PG+X mixes had higher stiffnesses at high temperatures (<1E-02 Hz at 20ºC) than the control mix with the unmodified binder with the same PG, but only marginal stiffness differences at intermediate temperatures (between 1E-02 Hz and 1E+02 Hz at 20ºC). The Approach-2 mixes with the PG+X binders containing coarse rubber particles (<1.18 mm and <2.36 mm) were stiffer than their control mix. The Approach-3 mixes with dry-process rubber (<2.36 mm) had lower stiffnesses than their control mixes due to the swelling of the rubber after compaction. Performance tests showed that PG+X mixes with wet-process binders (Approach-1, Approach-2, and Approach-4) had better resistance to moisture damage and permanent deformation than their control mixes. The Approach-3 mixes with dry-process rubber showed worse moisture damage and rutting resistance than their control mix. The fatigue performance of the PG+X mixes depended on the test strains. The flexural fatigue

test results showed that Approach-1, Approach-3, and Approach-4 PG+X mixes had longer fatigue lives than their control mixes at strains lower than 400 microstrain. The fatigue results for the Approach-2 PG+X mixes were also inconsistent across range of strains, with the control mix performance generally falling between the five percent rubber content mix (longer fatigue life than the control) and the ten percent rubber content mix (shorter fatigue life than the control). The Approach-1 and Approach-4 PG+X mixes with five percent rubber by weight of the binder appeared to have improved thermal cracking resistance compared to the control mix after long-term oven-aging, based on the UTSST test results.

4. Question: What are the appropriate uses of PG+X mixes in different pavement structures and climates?

The *CalME* simulation results indicated that the optimum rubber content in dense-graded PG+X mixes would be dependent on project-specific factors, including mix properties, pavement structure, traffic, and climate conditions. The *CalME* simulations showed that PG+X (Approach-1, Approach-2, and Approach-4) mixes with wet-process binders could be considered as an alternative to dense-graded mixes produced with conventional unmodified binders in the inland valley, north coast, and high desert climates. The mixes with dry-process rubber (Approach-3) produced with coarse rubber particles (smaller than 2.36 mm [passing the #8 sieve]) had poorer performance than the control mix in the desert climate. This finding showed that laboratory tests conducted at one specific temperature and strain condition might not necessarily represent the overall field performance, owing to the fluctuation of stresses and strains caused by traffic loadings and temperature gradients. Therefore, a complete factorial of laboratory tests followed by field performance simulation based on mechanistic-empirical

principles is recommended. A specific PG+X mix can be selected for designing the pavement with consideration of the pavement structure, climate, and traffic conditions in the project.

In summary, these wet-processed PG+X binders containing low crumb rubber modifier contents (five to ten percent) are potentially suitable for use in dense-graded mixes. Mixes with these PG+X binders are likely to provide equal or better performance to the conventional mixes when appropriate rubber contents are determined based on the pavement structure, traffic, and climate. Using PG+X material in the asphalt pavement also provides a use for waste tires that may otherwise be dumped in landfills.

8 CONCLUSIONS AND RECOMMENDATIONS

8.1 Summary of Completed Tasks

This study investigated the oxidative aging of asphalt binders and mixes. Chemical and rheological changes in binders after laboratory aging were measured and analyzed. The modified Superpave performance-grading system was refined to test rubber-modified binders containing large rubber particles (up to 2.36 mm). The age-hardening effect was measured and modeled for unmodified, SBS-modified, and rubber-modified binders. This age-hardening model was calibrated and validated for extracted binders from laboratory-aged mixes. Additionally, dense-graded mixes with relatively small amounts of crumb rubber modifier (PG+X) were designed and preliminarily evaluated in this dissertation. The following tasks were completed:

1. Analysis of changes in binder components (carbonyl, ether and ester, sulfoxide, and butadiene components) and binder viscosities after oxidative aging.

2. Development of a generic hardening susceptibility (GHS) model that correlates carbonyl components to binder viscosities after long-term oxidative aging.

3. Refinement of laboratory aging protocols and modification of the Superpave performance-grading system for testing rubber-modified binders containing large rubber particles (up to 2.36 mm).

4. Evaluation of long-term oxidative aging in rubber-modified binders.

5. Investigation of aging effects on mix stiffness and fatigue performance.

6. Evaluation of the performance of rubber-modified binders and mixes containing a low content of rubber (five and ten percent by weight of the binder).

7. Simulation of the performance of PG+X mixes for different pavement structures, traffic, and climate conditions using the *CalME* mechanistic-empirical design software.

8.2   Contributions to the Knowledge

This study proposed to fill in knowledge gaps regarding the oxidative aging of asphalt binders (unmodified, SBS-modified, RAP, and rubber-modified binders) and mixes (one dense-graded mix and one gap-graded mix). The application of a small amount of crumb rubber modifier in dense-graded mixes was also investigated. The following questions were answered:

1. Investigation into asphalt binder aging mechanisms.

    Question: How do binder components (i.e., carbonyl and sulfoxide components) change during oxidative aging?

    The carbonyl, ether and ester, and sulfoxide components were observed to change after aging. However, only the carbonyl component had a continuously increasing trend throughout the field-aging protocol as well as the PAV-aging protocol. The ether and ester components appeared to not change in the field-aging protocol but increased in the PAV-aging protocol. The sulfoxide component might not continuously increase after intense PAV-aging (i.e., 60 hours of PAV aging at 100ºC). Based on these results, the carbonyl area (CA) index was selected as the most appropriate indicator for tracking oxidative aging in this study.

    Question: How do binder dynamic moduli change after oxidative aging?

    The dynamic modulus master curves constructed for aged binders showed that oxidative aging stiffened the binder. This stiffening increased when the loading frequency decreased, which corresponds to a high temperature according to the time-temperature superposition principle. The SBS-modified binders and AR binders experienced less age-hardening than the

unmodified binders after being subjected to the accelerated field- and laboratory-aging protocols.

Question: How can the age-hardening model be modified to accommodate the prediction of viscosities beyond the low shear viscosity region?

A linear correlation between logarithmic viscosity (lnη) and CA index was observed for the unmodified and SBS-modified binders. This linearity held in a wide range of loading conditions (between 20°C and 85°C, and between 0.0159 Hz and 15.9 Hz [0.1 radians/second and 100 radians/second]), in addition to those typically used to represent the low shear condition (i.e., 60°C and 1.59E-05 Hz [0.0001 radians/second]). Accordingly, the generic hardening susceptibility (GHS) was proposed to define the ratio between the logarithmic viscosity growth, and the carbonyl area index increase in the long-term aging phase.

Question: How precise is the modified age-hardening model for different asphalt binders?

The GHS model was developed to correlate the ln(η) and the CA index in the long-term aging phase (GHS = (lnη)/CA). This GHS model was calibrated and validated using unmodified and SBS-modified binders from different refineries. It was also used to track the rejuvenation of RAP binders. The coefficient of determination of using the GHS model to predict the viscosities of unmodified, SBS-modified, and RAP binders was over 0.95 for temperatures between 20°C and 85°C and for loading frequencies between 0.0159 Hz and 15.9 Hz (0.1 radians/second and 100 radians/second).

2. Application of age-hardening model on rubber-modified binders.

Question: What is an appropriate methodology for measuring the rheological properties (i.e., complex modulus, phase angle) of rubber-modified binders, especially for those containing large incompletely digested rubber particles (up to 2.36 mm [passing the #8 sieve])?

This study validated the modification of the RTFO- and PAV-aging protocols. Based on the study results, RTFO-aging should be done at 190°C to simulate the RHMA production temperature in the field. The sample amount of the rubber-modified binder in each RTFO bottle was adjusted according to the rubber content to provide an equivalent amount of base asphalt binder to that used for RTFO-aging of conventional binders. Similarly, the sample size for PAV-aging was also increased proportionally to account for the rubber. This study further validated the high temperature performance-grading test (≥58ºC) and the BBR specimen preparation method developed in earlier research. The results showed that the concentric cylinder geometry (cup-and-bob geometry) provided an equivalent accuracy to the parallel plate geometry for testing binders with no large particles (<250 microns [passing the #60 sieve]). The concentric cylinder geometry was capable of measuring the rheological properties of rubber-modified binders containing large incompletely digested particles (<2.36mm [passing the #8 sieve]). For the BBR test, a modified beam mold was fabricated. This mold provided a larger opening with a shallower depth for pouring the binder than the standard mold. The laboratory results showed that there was no statistical difference in the results obtained from using the modified and conventional molds. The beams produced with the modified mold had a regular shape without entrapping air bubbles. This study initialized the rheological measurement of rubber-modified binders at intermediate temperatures (16°C to 50°C) for rubber-modified binders. A reference liquid was used to calibrate the concentric cylinder geometry setting. The test was calibrated to use a 10 mm spindle with a 9.5-mm gap for the

tests at intermediate temperatures. Statistical analysis showed that this setting provided the same accuracy as the parallel plate geometry when testing conventional binders containing particles smaller than 250 microns. The concentric cylinder geometry can therefore also be considered as a potential geometry to measure the rheological properties of rubber-modified binders containing larger rubber particles (<2.36 mm [passing the #8 sieve]).

Question: How do aging products (i.e., carbonyl and sulfoxide components) accumulate in rubber-modified binders during oxidative aging? What is the crumb rubber modifier effect on oxidative aging of the binder?

The carbonyl and sulfoxide components in rubber-modified binders decreased after adding the rubber. The rubber did not contain the carbonyl component before and after PAV-aging, and it did not show sulfoxide or butadiene component changes after PAV-aging. Considering that the carbonyl and sulfoxide components are the main aging products developed during oxidative aging of the base asphalt binder, the measurement results indicated that the crumb rubber modifier might age differently to the oxidative aging of the asphalt binder. Adding the rubber might decrease the aging products in the rubber-modified binders because part of the base binder is replaced by digested rubber particles. In other words, the rubber might dilute the aging products in the rubber-modified binders.

The comparison between FTIR-measured component indices and calculated component indices based on the dilution hypothesis indicated that the rubber dilution effect could explain the carbonyl component changes for binders without extender oils in unaged and PAV-aged conditions. During RTFO-aging, chemical interactions occurred in the rubber-modified binders at elevated temperatures (>160˚C). This interaction apparently changed the carbonyl

368

components in the rubber-modified binders such that the dilution effect alone could not explain those changes.

The extender oil contained carbonyl and sulfoxide components, and these two components increased after RTFO- and PAV-aging. When extender oil was used, chemical interactions occurred in the rubber-modified binders in the unaged condition and after RTFO- and PAV-aging, which changed the measured carbonyl component values considerably. The carbonyl component changes were beyond the reductions that could be explained by dilution.

The FTIR data also indicated that dilution could not explain the sulfoxide component changes for rubber-modified binders (with and without extender oils) in unaged, RTFO-aged, and PAV-aged conditions.

Although the carbonyl and sulfoxide components also increased with aging in rubber-modified binders as they did in the conventional unmodified binders, the increasing rates of these aging products in the rubber-modified binders were lower than their base binders. The butadiene area index was measured in the rubber used in this study, but not in most base asphalt binders or the extender oil. Increasing the rubber content increased the butadiene area index in the rubber-modified binder. The amounts of the butadiene component were positively correlated to the rubber contents in the rubber-modified binders tested in this study.

Question: How can the age-hardening of rubber-modified binders be predicted using the GHS model?

The linearities between ln (η) and CA index for rubber-modified binders were validated at temperatures between 20°C and 85°C and loading frequencies between 0.0159 Hz and 15.9 Hz (0.1 radians/second and 100 radians/second). The GHS model provided a reasonable

estimation of the viscosity for PAV-aged rubber-modified binders. The prediction error of using the GHS model was not significantly different between rubber-modified binders and their base binders. This observation indicated that the GHS model could model the age-hardening of rubber-modified binders containing up to 20 percent rubber with particle sizes up to 2.36 mm.

3. Evaluation of oxidative aging of the asphalt mix.

   Question: Will the loose mix aging procedure cause high variations in binder contents, mix stiffnesses, and fatigue lives of the specimens?

   Fatigue beams could be compacted to the target air-void content from loose mixes after long-term oven-aging. The loose mix aging protocol showed similar variability in binder contents, mix stiffnesses, and fatigue test results among different aging durations compared to those in the compacted specimen aging protocol.

   Question: Can the binder GHS model be used for the recovered binders in aged asphalt mixes?

   The GHS model provided a reasonably accurate prediction of the binder viscosity using measured CA indices of the extracted and recovered binders from aged mixes. The binder GHS model was validated using rheology test results for the recovered binders tested at temperatures between 20°C and 85°C with frequencies between 0.0159 Hz and 15.9 Hz (0.1 and 100 radians/second).

   Question: How does oxidative aging affect mix stiffness?

   Aging the loose mix resulted in a continuous increase in the CA index in the recovered binder. The CA index of the recovered binder was used to track oxidative aging in asphalt mixes.

Increases in the CA index increased binder viscosity. The age-hardened binder stiffened the mix. The degree of age-hardening or stiffening of the two mixes (dense-graded mix and gap-graded mix) tested in this study could be predicted using the Andrei-Witczak-Mirza stiffness prediction model and binder viscosity could be predicted using the GHS model.

Question: How does oxidative aging affect mix fatigue performance?

A linear correlation between the logarithmic fatigue life (ln Nf) of these beams produced with aged loose mixes at a given strain and the CA indices of the binders recovered from the beams was found for dense- and gap-graded mixes tested in this study. An ln (Nf)-CA model that describes the correlation between ln (Nf) and CA index was proposed ($N_f = \beta e^{\alpha(CA)}$). This model defines the aging effect on fatigue life for the tested mixes at the defined mix volumetric parameters and fatigue testing conditions. Fatigue test results for beams produced with long-term oven-aged loose mixes showed lower fatigue lives at higher strains (>300 microstrain) than the mixes without long-term oven-aging, while the opposite was observed at lower strain levels (<300 microstrain). In a thin layer (i.e., <60 mm) where higher strains are common, the aged mixes may experience slightly lower strains than the unaged mixes, but the former would still provide shorter fatigue lives at high strains. In a thick layer where lower strains are typical, aging stiffens the surface layer, and this stiff surface layer transfers lower stresses to the bottom of the layer. The mixes in the bottom of the layer are less aged and in a low strain state, which may result in a longer fatigue life of the thick asphalt layer.

4. Performance evaluation of rubber-modified binders and mixes.

   Question: How do PG+X binders perform in the laboratory?

Using as low as five percent rubber by weight of the binder could improve the performance of asphalt binders. The Approach-2 and Approach-4 PG+X binders tested in this study showed an increase in high PG, a decrease in the intermediate PG, and no change or a decrease in the low PG, compared to their base binders. Adding rubber also decreased the creep stiffness at low temperatures. These rubber-modified binders were found to have lower non-recoverable compliances and higher percentage recoveries than their base binders. These modifications in the binder changed the binder performance at five and ten percent rubber contents, with maximum rubber particle sizes ranging from fine (smaller than 250 microns [passing the #60 sieve]) to coarse (smaller than 2.36 mm [passing the #8 sieve]).

Question: Can PG+X materials be effectively used in dense-graded mixes?

Using a small amount of rubber (five and ten percent by weight of the binder) elevated the required mixing and compaction temperatures when the binder PG changed. The laboratory mixing and compaction method could produce PG+X specimens that met the target air-void content. The volumetric mix design results indicated that the wet process PG+X binders (Approach-1, Approach-2, and Approach-4) were suitable for use in dense-graded mix structures. Approach-3 mix with dry-process rubber showed that using coarse rubber particles (smaller than 2.36 mm [passing the #8 sieve]) in a dense-graded mix created high VMA when no adjustment of the aggregate gradation was made to accommodate the swelled rubber. Mixes with dry-process rubber could result in poor compaction due to the rubber particles swelling when they contact the hot binder. This would impair mix stiffness, moisture damage resistance, and rutting resistance.

Question: How do PG+X mixes perform in the laboratory in terms of rutting, fatigue, and thermal cracking?

The flexural frequency sweep test showed that using fine rubber particles (smaller than 250 microns [passing the #60 sieve]) in Approach-1 did not show much stiffness change compared to the control mix. The Approach-4 PG+X mixes had higher stiffnesses at high temperatures (<1E-02 Hz at 20°C) than the control mix with the unmodified binder with the same PG, but only marginal stiffness differences at intermediate temperatures (between 1E-02 Hz and 1E+02 Hz at 20°C). The Approach-2 mixes produced with PG+X binders containing coarse rubber particles (<1.18 mm and <2.36 mm) were stiffer than their control mixes. The Approach-3 mixes with dry-process rubber (<2.36 mm) had lower stiffnesses than their control mixes due to the rubber swelling after compaction. The performance tests showed that PG+X mixes with wet-process binders (Approach-1, Approach-2, and Approach-4) had better resistance to moisture damage and permanent deformation than their control mixes. The Approach-3 mixes with dry-process rubber showed worse moisture damage and rutting resistance than the control mix. The fatigue performance of the PG+X mixes depended on the test strains. The flexural fatigue test results showed that Approach-1, Approach-3, and Approach-4 PG+X mixes had longer fatigue lives than their control mixes at strains lower than 400 microstrain, but shorter fatigue lives at larger strains, indicating that they are best used in low-strain applications. The fatigue results for Approach-2 PG+X mixes were also inconsistent across a range of strains, with the control mix performance generally falling between the five percent rubber content mix (longer fatigue life than the control) and the ten percent rubber content mix (shorter fatigue life than the control). The Approach-1 and Approach-4 PG+X mixes with five percent rubber

by weight of the binder appeared to have improved thermal cracking resistance compared to the control mix after long-term oven-aging based on the UTSST test results.

Question: What are the appropriate uses of PG+X mixes in different pavement structures and climates?

The *CalME* simulation results indicated that the optimum rubber content in dense-graded PG+X mixes is dependent on project-specific factors, including mix properties, pavement structure, traffic, and climate conditions. The *CalME* simulations showed that PG+X mixes with wet-process binders (Approach-1, Approach-2, and Approach-4) could be considered as an alternative to dense-graded mixes produced with conventional unmodified binders in the inland valley, north coast, and high desert climates. Mixes with dry-process rubber (Approach-3) produced with coarse rubber (smaller than 2.36 mm [passing the #8 sieve]) had poorer performance than the control mix in the desert climate. This finding showed that laboratory tests conducted at one specific temperature and strain condition might not necessarily represent the overall field performance, owing to the fluctuation of stresses and strains caused by layer thicknesses, traffic loadings, and temperature gradients. Therefore, a complete factorial of laboratory tests followed by field performance simulation based on mechanistic-empirical principles is recommended. Specific PG+X mixes can be selected when designing the pavement along with pavement structure, climate, and traffic conditions for each project.

8.3   Recommendations for Future Work

The following recommendations for future research include, but are not limited to:

1. Additional studies on aging products are recommended to understand oxidative kinetics.

374

a. Different aging protocols at a wide range of temperatures and durations to simulate field-aging are recommended. This will allow correlating aging in the laboratory to that in the field to establish a better laboratory-aging protocol for simulating field-aging of mixes in California.

b. Evaluation of binder molecular group changes during oxidative aging using saturate, aromatic, resin, and asphaltene (SARA) analysis is recommended. The SARA analysis results can be compared to carbonyl and sulfoxide component changes. It is anticipated that this will provide a better understanding of the correlation between the changes in SARA and changes in carbonyl and sulfoxide components. This study may also improve the understanding of the chemical interactions that may have occurred during oxidative aging of rubber modified binders, particularly in those binders with extender oil.

c. Further investigation of the aging mechanism of rubber-modified binders is highly recommended. An interesting topic would be understanding the chemical interaction between the rubber and the binder and its influence on the binder rheological properties (i.e., complex modulus and phase angle) after aging.

2. Further calibration of the GHS model is warranted.

a. A potential correlation of the GHS parameters at one combination of frequency and temperature to another condition would be useful for predicting binder viscosity at the specific conditions of interest (i.e., aging, frequency, temperature) using the data from testable conditions in the laboratory. The calibration of the GHS model using field data is also recommended.

b. Continuing research on rubber-modified binders, especially asphalt rubber binders, is recommended to further validate the GHS model.

c.   Additional studies on aged mixes should be conducted to further validate the GHS principle.

d.   Prediction of mix GHS parameters using those parameters of the binder GHS model is highly recommended.

3.   Validation and calibration of the Nf-CA model is warranted.

a.   Validation of the Nf-CA model for different mixes under different aging conditions is highly recommended.

b.   Calibration of the Nf-CA model using field data is highly recommended.

c.   Validation and calibration of the Nf-CA model under different fatigue test strain levels for mixes with different air-void contents is recommended.

d.   Continuing research on improving the mechanistic-empirical design method with consideration of aging effects is recommended.

e.   Implementation of the Nf-CA model in the mechanistic-empirical design requires further study.

4.   Performance evaluation of rubber-modified binders and mixes requires more study.

a.   Laboratory aging protocols and rheological test methodologies for rubber-modified binders can be further refined and calibrated.

b.   Studying PG+X mixes with dry-process rubber using fine rubber particles (i.e., smaller than 1.41 mm) is recommended.

c.   The evaluation of PG+X mixes in the field is recommended.

d.   Continuing research on rubber-modified binders and mixes is needed to provide appropriate criteria for quality control and quality assurance of these materials.

e. The application of rubber-modified mixes in different pavement structures, traffic, and climate conditions is worth further study.

REFERENCES

1. Raad, L., Saboundjian, S., and Minassian, G. 2001. Field Aging Effects on Fatigue of Asphalt Concrete and Asphalt-rubber Concrete. **Transportation Research Record: Journal of the Transportation Research Board, No.1767,** (pp. 126-134).

2. **California Department of Transportation**. 2015. Standard Specifications. State of California, California State Transportation Agency, Department of Transportation, Sacramento, California.

3. Hu, Z., Zhang, H., Wang, S., and Xu, T. 2020. Thermal-oxidative aging mechanism of asphalt binder based on isothermal thermal analysis at the SARA level. **Construction and Building Materials**, **No. 255,** (119349).

4. Huang, S, and Pauli, A. 2008. Particle Size Effect of Crumb Rubber on Rheology and Morphology of Asphalt Binders with Long-term Aging. **Road Materials and Pavement Design, No.9(1),** (pp. 73-95).

5. Wang, H., You, Z., Beale, J., and Hao, P. 2012. Laboratory Evaluation on High Temperature Viscosity and Low Temperature Stiffness of Asphalt Binder with High Percent Scrap Tire Rubber. **Construction and Building Materials, No. 26(1),** (pp. 583-590).

6. Wang, Q., Li, S., Wu, X., Wang, S., and Ouyang, C. 2016. Weather Aging Resistance of Different Rubber Modified Asphalts. **Construction and Building Materials, No.106,** (pp. 443-448).

7. **Arizona Department of Transportation**.2008. Executive Summary of Arizona's Use of Asphalt Rubber. Tempe, Arizona.

8. **Florida Department of Transportation**. 1998. Long Term Performance Evaluation on Asphalt Rubber Surface Mixes. Tallahassee, Florida (No. FL/DOT/SMO/98-431).

9. Harvey, J., and Popescu, L. 2000. Accelerated Pavement Testing of Rutting Performance of Two Caltrans Overlay Strategies. **Transportation Research Record: Journal of the Transportation Research Board, No. 1716,** (pp. 116-125).

10. Frederick, G. 2002. Formal Policy on the Use of Recycled Materials. **The U.S. Department of Transportation, Federal Highway Administration**.

11. Zhou, H., Holikatti, S., and Vacura, P. 2014. Caltrans Use of Scrap Tires in Asphalt Rubber Products: A Comprehensive Review. **Journal of Traffic and Transportation Engineering (English Edition), No.1(1),** (pp. 39-48).

12. **Northern California Rubberized Asphalt Concrete Technology Center**. 2002. Asphalt Rubber Design and Construction Guidelines., Sacramento, California.

13. **U.S. Environmental Protection Agency**. 2016. Ground Rubber Applications. URL: https://archive.epa.gov/epawaste/conserve/materials/tires/web/html/ground.html

14. **California Department of Resources Recycling and Recovery**. 2019. California Waste Tire Market Report:2018. Sacramento, California.

15. **California Department of Transportation**. 2015. Analysis of Cost Differential between Asphalt Containing Crumb Rubber and Conventional Asphalt for 2013. Sacramento, California.

16. **California Department of Transportation**. 2017. Analysis of Cost Differential between Asphalt Containing Crumb Rubber and Conventional Asphalt for 2014- Public Resource Code Section 42703. Sacramento, California.

17. Jones, D., Liang, Y., and Harvey, J. 2017. **Performance-Based Specifications: Literature Review on Increasing Crumb Rubber Usage by Adding Small Amounts of Crumb Rubber Modifier in Hot Mix Asphalt**. University of California Pavement Research Center, Berkeley and Davis, CA (Report No. TT-2017-05).

18. Liu, M., Ferry, M. A., Davison, R. R., Glover, C. J., and Bullin, J. A. 1998. Oxygen Uptake as Correlated to Carbonyl Growth in Aged Asphalts and Asphalt Corbett Fractions. **Industrial and Engineering Chemistry Research, No.37(12),** (pp. 4669-4674).

19. Mirza, M. W., and Witczak, M. W. 1995. Development of A Global Aging System for Short and Long Term Aging of Asphalt Cements (with Discussion). **Journal of the Association of Asphalt Paving Technologists, No.64,** (pp. 393-418)

20. Houston, W. N., Mirza, M. W., Zapata, C. E., and Raghavendra, S. 2005. **Environmental Effects in Pavement Mix and Structural Design Systems**. National Cooperative Highway Research Program (Report No. 9-23)**.**

21. Bahia, H. U., and Anderson, D. A. 1995. Strategic Highway Research Program Binder Rheological Parameters: Background and Comparison with Conventional Properties. **Transportation Research Record: Journal of the Transportation Research Board, No.1488,** (pp. 32-39).

22. Nokes, W., Stolarski, P., Monismith, C., Harvey, J., Coetzee, N., and Rust, F. 1996. Establishing the California Department of Transportation Accelerated Pavement Testing Program. **Transportation Research Record: Journal of the Transportation Research Board, No. 1540,** (pp. 91-96).

23. Heitzman, M. 1992. Design and Construction of Asphalt Paving Materials with Crumb Rubber Modifier. **Transportation Research Record: Journal of the Transportation Research Board, No.1339,** (pp.1-8).

24. McDonald. C.H. 1975. Elastomeric Pavement Repair Composition for Pavement Failure and A Method of Making the Same. **U.S. Patent 3,891,585.** Washington, DC: U.S. Patent and Trademark Office.

25. **California Department of Transportation**. 2005. Use of Scrap Tire Rubber – State of Technology and Best Practices. Sacramento, California.

26. **University of Wisconsin Research Group**. 2011. The Effects of Digesting Crumb Rubber in Modified Binder (MB). Madison, Wisconsin.

27. **American Section of the International Association for Testing Materials ASTM D6114.** 2019. Standard Specification for Asphalt-Rubber Binder. West Conshohocken, PA.

28. Rezaei, A., and Harvey, J. 2013. **Investigation of Noise, Ride Quality and Macrotexture Trends for Asphalt Pavement Surfaces: Summary of Six Years of Measurements.** University of California Pavement Research Center, Berkeley and Davis, California. (No. UCPRC-RR-2013-11).

29. Harvey, J., R. Wu, I. Guada, Q. Lu, A. Ongel, A. Rezaei, E. Kohler, C. Reyes. 2017. Overview of California Studies on Noise Reduction for Asphalt and Concrete Surfaces. **Bearing Capacity of Roads, Railways, and Airfields: Proceedings of the 10th International Conference on the Bearing Capacity of Roads, Railways and Airfields (BCRRA 2017)**, Athens, Greece

30. **American Association of State and Highway Transportation Officials M 320-10.** 2010. Standard Specification for Performance-Graded Asphalt Binder. Washington, DC.

31. Greene, J., Chun, S., Nash, T., and Choubane, B. 2015. Evaluation and Implementation of PG 76-22 Asphalt Rubber Binder in Florida. **Transportation Research Record: Journal of the Transportation Research Board, No. 2524,** (pp. 3-10).

32. Huang, B., Mohammad, L., Graves, P., and Abadie, C. 2002. Louisiana Experience with Crumb Rubber-Modified Hot-mix Asphalt Pavement. **Transportation Research Record: Journal of the Transportation Research Board, No.1789,** (pp. 1-13).

33. Billiter, T. C., Davison, R. R., Glover, C. J., and Bullin, J. A. 1997. Physical Properties of Asphalt-rubber Binder. **Petroleum Science and Technology, No.15(3-4),** (pp. 205-236).

34. Bai, F., Yang, X., and Zeng, G. 2016. A Stochastic Viscoelastic–Viscoplastic Constitutive Model and Its Application to Crumb Rubber Modified Asphalt Mixtures. **Materials and Design, No.89,** (pp. 802-809).

35. Lastra-González, P., Calzada-Pérez, M. A., Castro-Fresno, D., Vega-Zamanillo, Á., and Indacoechea-Vega, I. 2016. Comparative Analysis of the Performance of Asphalt Concretes

Modified by Dry Way with Polymeric Waste. **Construction and Building Materials, No.112,** (pp. 1133-1140).

36. Way, G. B., Kaloush, K. E., and Biligiri, K. P. 2012. **Asphalt-Rubber Standard Practice Guide**. Rubber Pavements Association, Tempe, Arizona.

37. Liu, S., Cao, W., Fang, J., and Shang, S. 2009. Variance Analysis and Performance Evaluation of Different Crumb Rubber Modified (CRM) Asphalt. **Construction and Building Materials, No.23(7),** (pp. 2701-2708).

38. Abdelrahman, M., and Carpenter, S. 1998. Mechanism of Interaction of Asphalt Cement with Crumb Rubber Modifier. **Transportation Research Record: Journal of the Transportation Research Board, No.1661,** (pp. 106-113).

39. Liang, M., Xin, X., Fan, W., Sun, H., Yao, Y., and Xing, B. 2015. Viscous Properties, Storage Stability and Their Relationships with Microstructure of Tire Scrap Rubber Modified Asphalt. **Construction and Building Materials, No.74,** (pp. 124-131).

40. Zanzotto, L., and Kennepohl, G. 1996. Development of Rubber and Asphalt Binders by Depolymerization and Devulcanization of Scrap Tires in Asphalt. **Transportation Research Record: Journal of the Transportation Research Board, No.1530,** (pp. 51-58).

41. Thives, L. P., Pais, J. C., Pereira, P. A., Trichês, G., and Amorim, S. R. 2013. Assessment of the Digestion Time of Asphalt Rubber Binder based on Microscopy Analysis. **Construction and Building Materials, No.47,** (pp. 431-440).

42. Abdelrahman, M. 2006. Controlling Performance of Crumb Rubber Modified Binders Through the Addition of Polymer Modifiers. **Transportation Research Record: Journal of the Transportation Research Board, No.1962,** (pp. 64-70).

43. Lee, S. J. 2006. **Effects of Reaction Time on Physical and Chemical Properties of Rubber Modified Binders**. Doctoral Dissertation, Clemson University, Clemson, South Carolina.

44. Xiao, F., Putman, B. J., and Amirkhanian, S. N. 2006. Laboratory Investigation of Dimensional Changes of Crumb Rubber Reacting with Asphalt Binder. **In Proceedings of Asphalt Rubber 2006 Conference**, Palms Spring, California.

45. **California Department of Resources Recycling and Recovery**. 2007. Design and Specification Guide. Technology Transfer Series, RAC-103. Sacramento, California.

46. Kök, B. V., and Çolak, H. 2011. Laboratory Comparison of the Crumb-Rubber and SBS Modified Bitumen and Hot Mix Asphalt. **Construction and Building Materials, No. 25(8),** (pp. 3204-3212).

47. Bahia, H. U., and Davies, R. 1995. Role of Crumb Rubber Content and Type in Changing Critical Properties of Asphalt Binders (with Discussion). **Journal of the Association of Asphalt Paving Technologists, No. 64,** (pp. 130-162).

48. Navarro, F. J., Partal, P., Martinez-Boza, F., and Gallegos, C. 2005. Influence of Crumb Rubber Concentration on the Rheological Behavior of a Crumb Rubber Modified Bitumen. **Energy and Fuels, No.19(5),** (pp. 1984-1990).

49. Shen, J., and Amirkhanian, S. 2005. The Influence of Crumb Rubber Modifier (CRM) Microstructures on the High-Temperature Properties of CRM Binders. **The International Journal of Pavement Engineering, No.6(4),** (pp. 265-271).

50. Alavi, Z. 2008. **Evaluating Performance-Related Properties of Asphalt Rubber Binders**, Master's thesis, Sharif University of Technology, Iran.

51. Yousefi Kebria, D., Moafimadani, S. R., and Goli, Y. 2015. Laboratory Investigation of the Effect of Crumb Rubber on the Characteristics and Rheological Behavior of Asphalt Binder. **Road Materials and Pavement Design, No.16(4),** (pp. 946-956).

52. Lee, S. J., Akisetty, C. K., and Amirkhanian, S. N. 2008. The Effect of Crumb Rubber Modifier (CRM) on the Performance Properties of Rubber-modified binders in HMA Pavements. **Construction and Building Materials, No.22(7),** (pp. 1368-1376).

53. Wang, H., You, Z., Mills-Beale, J., and Hao, P. 2012. Laboratory Evaluation on High-Temperature Viscosity and Low-Temperature Stiffness of Asphalt Binder with High Percent Scrap Tire Rubber. **Construction and Building Materials, No.26(1),** (pp. 583-590).

54. Jeong, K. D., Lee, S. J., Amirkhanian, S. N., and Kim, K. W. 2010. Interaction Effects of Crumb Rubber Modified Asphalt Binders. **Construction and Building Materials, No.24(5),** (pp. 824-831).

55. Cong, P., Xun, P., Xing, M., and Chen, S. 2013 Investigation of Asphalt Binder Containing Various Crumb Rubbers and Asphalts. **Construction and Building Materials, No.40,** (pp. 632-641).

56. Cheriet, F., Soudani, K., and Haddadi, S. 2015. Influence of Natural Rubber on Creep Behavior of Bituminous Concrete. **Procedia-Social and Behavioral Sciences, No.195,** (pp. 2769-2776).

57. Sebaaly, P. E., Gopal, V. T., and Epps, J. A. 2003 Low-Temperature Properties of Crumb Rubber Modified Binders. **Road Materials and Pavement Design, No. 4(1),** (pp. 29-49).

58. Kebaïli, N., Zerzour, A., and Belabdelouhab, F. 2015. Influence of Rubber Fine Powder on the Characteristics of the Bitumens in Algeria. **Energy Procedia, No.74,** (pp. 226-233).

59. Linden, R. N., Mahoney, J. P., and Jackson, N. C. 1989. Effect of Compaction on Asphalt Concrete Performance. **Transportation Research Record: Journal of the Transportation Research Board, No.1217,** (pp. 20-28).

60. Bijleveld, F. R., Miller, S. R., de Bondt, A. H., and Doree, A. G. 2016. Aligning Laboratory and Field Compaction Practices for Asphalt–The Influence of Compaction Temperature on Mechanical Properties. **International journal of pavement engineering, No.17(8),** (pp. 727-740).

61. Rechner, K. U. R. T. 2008. **Scrap Tire Recycling-A Summary of Prevalent Disposal and Recycling Methods.** URL: www.entire-engineering.de/Scrap_Tire_Recycling. Pdf.

62. Shen, J., Amirkhanian, S., Xiao, F., and Tang, B. 2009. Influence of Surface Area and Size of Crumb Rubber on High-Temperature Properties of Crumb Rubber Modified Binders. **Construction and Building Materials, No.23(1),** (pp. 304-310).

63. Shatanawi, K. M., Biro, S., Geiger, A., and Amirkhanian, S. N. 2012. Effects of Furfural Activated Crumb Rubber on the Properties of Rubberized Asphalt**. Construction and Building Materials, No.28(1),** (pp. 96-103).

64. Thodesen, C., Shatanawi, K., and Amirkhanian, S. 2009. Effect of Crumb Rubber Characteristics on Crumb Rubber Modified (CRM) Binder Viscosity. **Construction and Building Materials, No.23(1),** (pp. 295-303).

65. Zanetti, M. C., Fiore, S., Ruffino, B., Santagata, E., Dalmazzo, D., and Lanotte, M. 2015. Characterization of Crumb Rubber from End-of-Life Tires for Paving Applications. **Waste Management, No.45,** (pp. 161-170).

66. John W. Oliver. Pavement Binder Composition. 1981. **U.S. Patent No. 4,430,464**. U.S. Patent and Trademark Office, Washington, D.C.

67. Xiao, F., Amirkhanian, S. N., Shen, J., and Putman, B. 2009. Influences of Crumb Rubber Size and Type on Reclaimed Asphalt Pavement (RAP) Mixes. **Construction and Building Materials, No.23(2),** (pp. 1028-1034).

68. Becker, Y., Mendez, M. P., and Rodriguez, Y. 2001. Polymer Modified Asphalt. **Vision Tecnologica**, **No. (9),** (pp. 35-50)

69. Liang, Y. Alavi, M., Jones, D., and Harvey, J. 2018. Development of Performance Grading Testing Procedures for Asphalt Rubber Binders Containing Large Rubber Particles. **Presented in the 97th Transportation Research Board Annual Meeting**, Washington, D.C.

70. Jones, D., Rizvi, H., Liang, Y., Hung, S., Buscheck, J., Alavi, Z., and Hofko, B. 2020. **Developing Performance-Based Specifications for Asphalt Rubber Binder: Interim**

Report on Phase 1 and Phase 2 Testing. University of California Pavement Research Center, Berkeley and Davis, California (No. RR-2017-01).

71. Hill, R. 1963. Elastic Properties of Reinforced Solids: Some Theoretical Principles. **Journal of the Mechanics and Physics of Solids, No.11(5),** (pp. 357-372).

72. Hashin, Z. 1983. Analysis of Composite Materials. **Journal of Applied Mechanics, No.50(2),** (pp. 481-505).

73. Cordova, M, Saw, H., and Villaescusa, E. 2016. Laboratory Testing of Cemented Rock Filled for Open Stope Support. **In Proceedings of the Seventh International Conference and Exhibition on Mass Mining, Sydney, Australia** (pp. 755-762).

74. **American Association of State and Highway Transportation Officials**, T. 315-12. 2012. Standard Method of Test for Determining the Rheological Properties of Asphalt Binder Using A Dynamic Shear Rheometer (DSR). American Association of State and Highway Transportation Officials, Washington, D.C.

75. Baumgardner, G., and D'Angelo, J. 2012. Evaluation of New Dynamic Shear Rheometer Testing Geometry for Performance Testing of Crumb Rubber-modified Binder. **Transportation Research Record: Journal of the Transportation Research Board, No.2293,** (pp. 73-79).

76. Hung, S. S., Farshidi, F., Jones, D., Alavi, M. Z., Harvey, J. T., and Sadraie, H. 2014. **Investigation of Wet-Process Asphalt Rubber Binder Testing with Modified Dynamic Shear Rheometer: Interim Report on Screening Tests.** University of California Pavement Research Center, Berkeley and Davis, California (No. UCPRC-TM-2014-02).

77. Zhu, X., Lu C., and Liang, M. 2009. Rheological Property of Bitumen Modified by the Mix of the Mechanochemically Devulcanized Tire Rubber Powder and SBS. **Journal of Materials in Civil Engineering, No.21(11),** (pp. 699-705).

78. Dong, R., Li, J., and Wang, S. 2011 Laboratory Evaluation of Pre-Devulcanized Crumb Rubber–Modified Asphalt as a Binder in Hot-mix Asphalt. **Journal of Materials in Civil Engineering, No.23(8),** (pp. 1138-1144).

79. Kaloush, K. E., Underwood, B. S., Zeiada, W. A., and Stempihar, J. 2015. Fiber Reinforced Asphalt Concrete: Performance Tests and Pavement Design Consideration. **Bituminous Mixes and Pavements VI, No.313,** (pp. 79-87).

80. Lu, Q., and Harvey, J. 2011. Laboratory Evaluation of Open-Graded Asphalt Mixes with Small Aggregates and Various Binders and Additives. **Transportation Research Record: Journal of the Transportation Research Board, No.2209(1),** (pp. 61-69).

81. Lu, Q., Harvey, J., and Wu, R. 2011.**Investigation of Noise and Durability Performance Trends for Asphaltic Pavement Surface Types: Four-year Results**. University of California Pavement Research Center, Berkeley and Davis, California (No. UCPRC-RR-2010-05).

82. Leng, Z., Lee, C. K., Cheung, L. W., and Hung, W. T. 2017. Exploration of Crumb Rubber Modified Asphalt as a Durable Low Noise Surface in Hong Kon*g*. **In INTER-NOISE and NOISE-CON Congress and Conference Proceedings, No.255(3),** (pp. 4039-4044).

83. Roberts, F. L., Kandhal, P. S., Brown, E. R., Lee, D. Y., and Kennedy, T. 1996. **Hot Mix Asphalt Materials, Mix Design, and Construction**. National Asphalt Pavement Association Education Foundation, Lanham, MD.

84. Shan, L., Tan, Y., Underwood, S., and Kim, Y. 2010. Application of Thixotropy to Analyze Fatigue and Healing Characteristics of Asphalt Binder. **Transportation Research Record: Journal of the Transportation Research Board, No.2179,** (pp. 85-92).

85. Petersen, C. 2009. A Review of the Fundamentals of Asphalt Oxidation: Chemical, Physicochemical, Physical Property, and Durability Relationships. **Transportation Research E-Circular, E-C140**.

86. Fernández-Gómez, W. D., Rondón Quintana, H., and Reyes Lizcano, F. 2013. A Review of Asphalt and Asphalt Mix Aging. **Una revisión. Ingenieria e Investigacion, No.33(1),** (pp. 5-12).

87. Lau, C. K., Lunsford, K. M., Glover, C. J., Davison, R. R., and Bullin, J. A. 1992. Reaction Rates and Hardening Susceptibilities as Determined from Pressure Oxygen Vessel Aging of Asphalts. **Transportation Research Record: Journal of the Transportation Research Board, No.1342,** (pp. 50-57).

88. Loeber, L., Muller, G., Morel, J., and Sutton, O. 1998. Bitumen in Colloid Science: A Chemical, Structural, and Rheological Approach. **Fuel, No.77(13),** (pp. 1443-1450).

89. Corbett, W. 1970. Relationship between Composition and Physical Properties of Asphalt and Discussion. **Association of Asphalt Paving Technologists Proc, No.39,** (pp. 481-491).

90. De Lira, R. R., Cortes, D. D., and Pasten, C. 2015. Reclaimed Asphalt Binder Aging and Its Implications in the Management of RAP Stockpiles. **Construction and Building Materials, No.101,** (pp. 611-616).

91. Glover, C. J., Davison, R. R., Domke, C. H., Ruan, Y., Juristyarini, P., Knorr, D. B., and Jung, S. H. 2005. **Development of A New Method for Assessing Asphalt Binder Durability with Field Validation**. Texas A & M Transportation Institute, Austin, Texas (No. FHWA/TX-14/0-1872-2).

92. Al-Rub, R. K. A., Darabi, M. K., Kim, S. M., Little, D. N., and Glover, C. J. 2013. Mechanistic-Based Constitutive Modeling of Oxidative Aging in Aging-susceptible Materials and Its Effect on the Damage Potential of Asphalt Concrete. **Construction and Building Materials, No.41,** (pp. 439-454).

93. Harvey, J., and Tsai, B. 1997. Long-Term Oven-Aging Effects on Fatigue and Initial Stiffness of Asphalt Concrete. **Transportation Research Record: Journal of the Transportation Research Board, No.1590,** (pp. 89-98).

94. Glover, C. J., Han, R., Jin, X., Prapaitrakul, N., Cui, Y., Rose, A., and Martin, A. E. 2014. **Evaluation of Binder Aging and Its Influence in Aging of Hot Mix Asphalt Concrete**. Texas A & M Transportation Institute, College Station, Texas (No. FHWA/TX-14/0-6009-2).

95. **American Association of State and Highway Transportation Officials**, R 30-02. 2015. Standard Practice for Mixture Conditioning of Hot Mix Asphalt (HMA). American Association of State Highway and Transportation Officials, Washington, D.C.

96. Kim, Y. R., Castorena, C., Rad, F. Y., Elwardany, M., Underwood, S., Farrar, M. J., and Glaser, R. R. 2015. **Long-Term Aging of Asphalt Mixtures for Performance Testing and Prediction. Quarterly Report (April-June, 2015**) National Cooperative Highway Research Program, Washington, D.C.

97. **American Association of State and Highway Transportation Officials**, R. 28-12. 2012.Standard Practice for Accelerated Aging of Asphalt Binder Using a Pressurized Aging Vessel (PAV). American Association of State and Highway Transportation Officials, Washington, D.C.

98. **American Association of State and Highway Transportation Officials**, T. 240-13. 2013. Standard Method of Test for Effect of Heat and Air on a Moving Film of Asphalt Binder (Rolling Thin-Film Oven Test). American Association of State and Highway Transportation Officials, Washington, D.C.

99. Hveem, F.N., Zube, E., and Skog, J. 1963. Proposed New Tests and Specifications for Paving Grade Asphalts. **Proc., Assn. of Asphalt Paving Technologists, No.32,** (pp. 247- 327).

100.   Christensen, D.W., and Anderson, D.A. 1992. Interpretation of Dynamic Mechanical Test Data for Paving Grade Asphalt Cements." **Proc., Assn. of Asphalt Paving Technologists, No.61,** (pp. 67-116).

101.   Arafat, S., and Wasiuddin, N. 2019. Understanding the Short-Term Aging of Warm Mix Asphalt using Rolling Thin Film Oven. **International Journal of Pavement Research and Technology. No.12,** (pp. 638-647)

102.   Morian, N., Hajj, E., Glover, C., and Sebaaly, P. 2011. Oxidative Aging of Asphalt Binders in Hot-mix Asphalt Mixtures. **Transportation Research Record: Journal of the Transportation Research Board, No.2207,** (pp. 107-116).

103.   Morian, N., Hajj, E., and Sebaaly, P. 2013. Significance of Mixture Parameters on Binder Aging in Hot-Mix Asphalt Mixtures. **Transportation Research Record: Journal of the Transportation Research Board, No.2370,** (pp. 116-127).

104.   Petersen, J., and Harnsberger, P. 1998. Asphalt Aging: Dual Oxidation Mechanism and Its Interrelationships with Asphalt Composition and Oxidative Age Hardening. **Transportation Research Record: Journal of the Transportation Research Board, No.1638,** (pp. 47-55).

105.   Morian, N. E. 2014. **Influence of Mixture Characteristics on the Oxidative Aging of Asphalt Binders**. Doctoral Dissertation, University of Nevada, Reno.

106.   Edwards, Y., Tasdemir, Y., and Isacsson, U. 2005. Influence of Commercial Waxes on Bitumen Aging Properties. **Energy and Fuels, No.19(6),** (pp. 2519-2525).

107.   Yao, H., Dai, Q., and You, Z. 2015.Fourier Transform Infrared Spectroscopy Characterization of Aging-related Properties of Original and Nano-modified Asphalt Binders. **Construction and Building Materials, No.101,** (pp. 1078-1087).

108.   Butt, A. A. 2009. **Low Temperature Performance of Wax Modified Mastic Asphalt**. Master's Thesis, KTH Royal Institute of Technology, Sweden.

109.   Smith, B. C. 2011. Fundamentals of Fourier Transform Infrared Spectroscopy. **CRC Press, Taylor and Francis Group**, Boca Raton, Florida.

110.   Jemison, H. B., Burr, B. L., Davison, R. R., Bullin, J. A., and Glover, C. J. 1992. Application and Use of the ATR FT-IR Method to Asphalt Aging Studies. **Fuel science and technology international, No.10(4-6),** (pp. 795-808).

111.   Lau, C. K., Lunsford, K. M., Glover, C. J., Davison, R. R., and Bullin, J. A. 1992. Reaction Rates and Hardening Susceptibilities as Determined from Pressure Oxygen Vessel Aging of Asphalts. **Transportation Research Record: Journal of the Transportation Research Board, No.1342,** (pp. 50-57).

112.   Pournoman, S. 2017. **Oxidative Aging of Binders with High Recycled Asphalt Materials**. Doctoral Dissertation, University of Nevada, Reno.

113.   Lin, M. S., Chaffin, J. M., Liu, M., Glover, C. J., Davison, R. R., and Bullin, J. A. 1996. The Effect of Asphalt Composition on the Formation of Asphaltenes and Their Contribution to Asphalt Viscosity. **Fuel Science and Technology International, No.14(1-2),** (pp. 139-162).

114.   Pal, R., and Rhodes, E. 1989. Viscosity/Concentration Relationships for Emulsions. **Journal of Rheology, No.33(7),** (pp. 1021-1045).

115.   Chipps, J. F., Davison, R. R., and Glover, C. J. 2001. A Model for Oxidative Aging of Rubber-Modified Asphalts and Implications to Performance Analysis. **Energy and Fuels, No.15(3),** (pp. 637-647).

116.   Jin, X., Han, R., Cui, Y., and Glover, C. J. 2011. Fast-Rate-Constant-Rate Oxidation Kinetics Model for Asphalt Binders. **Industrial and Engineering Chemistry Research, No. 29(19),** (pp. 2258-2268).

117.   Lytton, R. L., Uzan, J., Fernando, E. G., Roque, R., Hiltunen, D., and Stoffels, S. M. 1993. **Development and Validation of Performance Prediction Models and Specifications for**

Asphalt Binders and Paving Mixes. Strategic Highway Research Program, Washington, D.C. (No. SHRP-A-357).

118.   Farrar, M.J. 2013. **Discussion AIP Gc* Kinetics**. White paper for NCHRP 9-54, National Cooperative Highway Research Program, Washington, D.C.

119.   Rahalkar, R. R. 1989. Correlation between the Crossover Modulus and the Molecular Weight Distribution using the Doi-Edwards Theory of Repetition and the Rouse Theory. **Rheological Acta, No.28(2),** (pp. 166-175).

120.   Glover, C. J., Davison, R. R., Bullin, J. A., Estakhri, C. K., Williamson, S. A., Billiter, T. C., and Wattanachai, P. 2000. **A Comprehensive Laboratory and Field Study of High-Cure Crumb-Rubber Modified Asphalt Materials**, Texas A and M Transportation Institute, Texas (No. FHWA/TX-01/1460-1).

121.   Masad, E., Huang, C. W., Airey, G., and Muliana, A. 2008. Nonlinear Viscoelastic Analysis of Unaged and Aged Asphalt Binders. **Construction and Building Materials, No.22(11),** (pp. 2170-2179).

122.   Masad, E., and Somadevan, N. 2002. Microstructural Finite-element Analysis of Influence of Localized Strain Distribution on Asphalt Mix Properties. **Journal of Engineering Mechanics, No.128(10),** (pp. 1105-1114).

123.   Chávez-Valencia, L. E., Manzano-Ramírez, A., Alonso-Guzmán, E., and Contreras-García, M. E. 2007. Modelling of the Performance of Asphalt Pavement using Response Surface Methodology—the Kinetics of the Aging. **Building and Environment, No.42(2), (**pp. 933-939).

124.   Michalica, P., Kazatchkov, I. B., Stastna, J., and Zanzotto. 2008. Relationship between Chemical and Rheological Properties of Two Asphalts of Different Origins. **Fuel, No.87(15), (**pp. 3247-3253).

125.   Underwood, B. S. 2015. Multiscale Modeling Approach for Asphalt Concrete and Its Implications on Oxidative Aging. **In Advances in Asphalt Materials: Road and Pavement Construction**, (pp 273-302).

126.   Y. He. 2016. **Interaction between New and Age-hardened Binders in Asphalt Mixes Containing High Quantities of Reclaimed Asphalt Pavement and Reclaimed Asphalt Shingles**. Doctoral Dissertation. University of California-Davis, Berkeley and Davis, CA.

127.   Alavi, M.Z., Jones, D., He, Y., Chavez, P. and Liang, Y. 2016. **Investigation of the Effect of Reclaimed Asphalt Pavement and Reclaimed Asphalt Shingles on the Performance Properties of Asphalt Binders: Phase 1 Laboratory Testing**. University of California Pavement Research Center, Berkeley and Davis, California (No. RR-2016-06).

128.   Hung, S. S., Elkashef, M., Harvey, J. T., and Jones, D. 2019. Development of An Alternative Test Approach for Binder Blending Charts with Fine Aggregate Matrix Mix Testing. **Road Materials and Pavement Design, No.20(sup1),** (pp. 282-298).

129.   AbuHassan, Y. 2016. **Effect of Chemical Solvents on Rheological Properties of Recovered Asphalt Binders**. Master's Thesis, University of Akron. Ohio, Akron.

130.   Luo, X., Gu, F., and Lytton, R. L. 2015. Prediction of Field Aging Gradient in Asphalt Pavements. **Transportation Research Record: Journal of the Transportation Research Board, No.2507,** (pp. 19-28).

131. Harvey, J., Monismith, C., Bejarano, M., Tsai, B. W., and Kannekanti, V. 2004. Long-life AC pavements: A Discussion of Design and Construction Criteria based on California Experience. **In International Symposium on Design and Construction of Long Lasting Asphalt Pavements**, Auburn, Alabama.

132. Mohammad, L.N., Cooper, S.B., and Elseifi, M.A. 2011. Characterization of HMA Mixes Containing High Reclaimed Asphalt Pavement Content with Crumb Rubber Additives. **Journal of Materials in Civil Engineering, No.23(11),** (pp. 1560-1568).

133. Hofko, B., Alavi, M. Z., Grothe, H., Jones, D., and Harvey, J. 2017. Repeatability and Sensitivity of FTIR ATR Spectral Analysis Methods for Bituminous Binders. **Materials and Structures, No.50(3),** (pp 187).

134. Alavi, Z. 2014. **Comprehensive Methodologies for Analysis of Thermal Cracking in Asphalt Concrete Pavements**. Doctoral Dissertation, University of Nevada, Reno.

135. Liang, Y., Wu, R., Harvey, J. T., Jones, D., and Alavi, M. Z. 2019. Investigation into the Oxidative Aging of Asphalt Binders. **Transportation Research Record: Journal of the Transportation Research Board, No.2673,** (pp. 368-378).

136. Braun, D., Esser, E., and Rasch, H. 1998. Chromatographic Investigations of Macromolecules in the Critical Range of Liquid Chromatography. XII. Analysis of Block Copolymers of Styrene and Butadiene. **International Journal of Polymer Analysis and Characterization, No.4(6),** (pp. 501-516).

137. Fernández-Berridi, M. J., González, N., Mugica, A., and Bernicot, C. 2006. Pyrolysis-FTIR and TGA Techniques as Tools in the Characterization of Blends of Natural Rubber and SBR. **Thermochimica Acta, No.444(1),** (pp. 65-70).

138.   Tan, J. H., Wang, X. P., Tai, J. J., Luo, Y. F., and Jia, D. M. 2012. Novel Blends of Acrylonitrile Butadiene Rubber and Polyurethane-Silica Hybrid Networks. **Express Polymer Letters, No.6(7),** (pp. 1462-1477).

139.   Kocevski, S., S, Yagneswaran, F. Xiao, V.S. Punith, D. W. Smith Jr., and S. Amirkhanian. 2012. Modified Ground Rubber Tire by Grafting Acrylic Acid for Paving Applications. **Construction and Building Materials, No.34,** (pp. 83–90).

140.   Lamontagne J, Dumas, P., Mouillet, V., and Kister, J. 2001 Comparison by Fourier Transform Infrared (FTIR) Spectroscopy of Different Ageing Techniques: Application To Road Bitumen. **Fuel, No.80(4,)** (pp. 483–488).

141.   Pellinen, T. K., Witczak, M. W., and Bonaquist, R. F. 2004. Asphalt Mix Master Curve Construction using Sigmoidal Fitting Function with Non-linear Least Suares Optimization. **In Recent Advances in Materials Characterization and Modeling of Pavement Systems**, (pp. 83-101).

142.   Applied Research Associates, Inc. 2004. **Guide for Mechanistic-Empirical Design of New and Rehabilitated Pavement Structures**., National Cooperative Highway Research Program, Washington, D.C. (Project 1-37A).

143.   Han, R., Jin, X., and Glover, C. J. 2013. Oxygen Diffusivity in Asphalts and Mastics. **Petroleum Science and Technology, No.31(15),** (pp. 1563-1573).

144.   Balleza, D., Garcia-Arribas, A., Sot, J., Mirazo, K., and Goni, F. 2014. Ether-versus Ester-Linked Phospholipid Bilayers Containing either Linear or Branched Apolar Chains. **Biophys J., No.107,** (pp. 1364-1374).

145. Bonaquist, R., Pellinen, T., and Witczak, M. W. 1998. **Development of Relationship Between Binder Viscosity and Stiffness. Superpave Support and Performance Models Management.** Department of Civil Engineering, University of Maryland, College Park, Maryland.

146. Chin, W. 1998. The Partial Least Squares Approach for Structural Equation Modeling. **In GA Marcoulides (ed.), Modern Methods for Business Research**, **Lawrence Erlbaum Associates, London** (pp. 295-336)

147. Hair, J., Sarstedt., M., Ringle, C., Mena, J. 2012. An assessment of the use of Partial Least Squares Structural Equation Modeling in Marketing Research. **Journal of the Acad. Mark. Sci. No.40,** (pp. 414-433).

148. Garcia Cucalon, L., King, G., Kaseer, F., Arambula-Mercado, E., Epps Martin, A., Turner, T. F., and Glover, C. J. 2017. Compatibility of Recycled Binder Blends with Recycling Agents: Rheological and Physicochemical Evaluation of Rejuvenation and Aging Processes. **Industrial and Engineering Chemistry Research, No.56(29),** (pp. 8375-8384).

149. Van Gurp, M., and Palmen, J. 1998. Time-Temperature Superposition for Polymeric Blends. **Rheol. Bull, No.67(1),** (pp. 5-8).

150. **California Department of Transportation**. 2013. Construction Procedure Directives, CPD-13-5. Caltrans Division of Construction, Sacramento, CA.

151. Smiljanic, M., J. Stefanovic, H. Neumann, I. Rahimian, and J. Javonovic. Ageing of Asphalt on Paved Roads. 1993. Characterization of Asphalt Extracted from the Wearing Course of the Belgrade. **Nis Highway, Erdol und Kohle, Erdgas, Pertrochemie vereinigt mit Brennstoff-Chemie, No.46 (6),** (pp. 238-244).

152.   Al-Qadi, I., Elseifi, M. Carpenter, S. 2007. **Reclaimed Asphalt Pavement- A Literature Review**. Illinois Center for Transportation, Urbana, IL (No. FHWA-ICT-07-001).

153.   Nazzal, M., Mogawer, W., Austerman, A., Qtaish, L., and Kaya, S. 2015. Multi-Scale Evaluation of the Effect of Rejuvenators on the Performance of High RAP Content Mixtures. **Construction and Building Materials. No.101,** (pp.50-56).

154.   Tran, N., Taylor, A., Turner, P., Holmes, C., and Porot, L. 2017. Effect of Rejuvenator on Performance Characteristics of High RAP Mixture. **Road Materials and Pavement Design. No.18,** (pp.183-208).

155.   Elkashef, M., and Williams, R. C. 2017. Improving Fatigue and Low Temperature Performance of 100% RAP Mixtures Using a Soybean-Derived Rejuvenator. **Construction and Building Materials, No. 151,** (pp 345-352).

156.   **American Association of State and Highway Transportation Officials**, T. 164-18. 2018. Standard Method of Test for Quantitative Extraction of Asphalt Binder from Asphalt Mixtures. American Association of State and Highway Transportation Officials, Washington, D.C.

157.   Adam, H. 2016. RAP, RAS, and Durable Asphalt Pavements. **Presented in the CalAPA Fall Conference**, Sacramento, CA.

158.   Hashim, R., Jones, D., and Liang, Y. 2020. Short-Term Aging of Asphalt Rubber Binders Containing Partially Digested Particles. **Presented in the 99th Transportation Research Board Annual Meeting**, Washington, D.C.

159.   Houston, S., Haichert, R., Houston, G., Berthelot, C., and Podborochynski, D. 2014. Feasibility Study of Performance Grading Particulate Asphalt Rubber Binder. **In the Canadian Technical Asphalt Association,** (pp. 231-247).

160.   Nill, T., and Golalipour, A. 2015. Investigation of Suitable Testing Method for GTR Modified Asphalt Bitumen. **Proceedings Asphalt Conference**. Las Vegas, NV.

161.   Al-Qadi, I., Yang, S. H., Dessouky, S., Masson, J. F., Loulizi, A., and Elseifi, M. 2007. Development of Crack Sealant Bending Beam Rheometer (CSBBR) Testing to Characterize Hot-Poured Bituminous Crack Sealant at Low Temperature. **Asphalt Paving Technology-Proceedings, No.76,** (pp 85).

162.   **American Association of State and Highway Transportation Officials**, T. 313-19. 2019. Standard Method of Test for Determining the Flexural Creep Stiffness of Asphalt Binder Using the Bending Beam Rheometer (BBR). American Association of State and Highway Transportation Officials, Washington, D.C.

163.   Mukaka, MM. 2012. A Guide to Appropriate Use of Correlation Coefficient in Medical Research**. Malawi Medical Journal, No.24(3),** (pp. 69-71).

164.   Azevedo, J., Murakami, L., Ferriera, A., Diniz, M., Silva, L., and Dutrea, R. 2018. Quantification by FT-IR (UATR/NIRA) of NBR/SBR Blends. **Polimeros, No.28,** (pp. 440-449)

165.   Nakason, C., Narathichat, C., Kummerlowe, C., and Vennemann, N. 2013. Thermoplastic Natural Rubber Based on Polyamide-12 Blended with Various types of Natural Rubber: Effect of Processing Oils and Plasticizer, **Journal of Elastomers & Plastics, No.45(1),** (pp. 47-75).

166.   Govedarica, D., Sovtic, N., Bera, O., Kojic, P., Govedarica, O., Jovicic, M., and Pavlicevic, J. 2018. The Influence of Extender Oil Properties on Rubber Performance. **Applied Solid State Chemistry. No.(1)**, (pp. 2-6).

167.   **American Association of State and Highway Transportation Officials**, R 47-19. 2019. Standard Practice for Reducing Samples of Asphalt Mixtures to Testing Size. American Association of State and Highway Transportation Officials, Washington, D.C.

168.   **American Association of State and Highway Transportation Officials**, PP3-94. 1994. Standard Practice for Preparing Hot Mix Asphalt (HMA) Specimens by Means of the Rolling Wheel Compactor. American Association of State and Highway Transportation Officials, Washington, D.C.

169.   **American Association of State and Highway Transportation Officials**, T. 321-17. 2017. Standard Method of Test for Determining the Fatigue Life of Compacted Asphalt Mixtures Subjected to Repeated Flexural Bending. American Association of State and Highway Transportation Officials, Washington, D.C.

170.   **American Association of State and Highway Transportation Officials**, T. 331-13. 2013. Standard Method of Test for Bulk Specific Gravity (Gmb) and Density of Compacted Hot Mix Asphalt (HMA) Using Automatic Vacuum Sealing Method. American Association of State and Highway Transportation Officials, Washington, D.C.

171.   **American Section of the International Association for Testing Materials ASTM D1856.** 2015. Standard Test Method for Recovery of Asphalt From Solution by Abson Method. West Conshohocken, PA.

172.   Abson, G. 1933. Method and Apparatus for the Recovery of Asphalt. **In ASTM proceedings** (pp.704-714)

173.   Stroup-Gardiner, M., and Nelson, J. 2000. **Use of Normal Propyl Bromide Solvents for Extraction and Recovery of Asphalt Cements**. NACT Report 6. National Center for Asphalt Technologies. Auburn, AL.

174.   Hossain, Z., Solanki, P., Zaman, M., Lewis, S. 2011. Influence of Recovery Processes on Properties of Binders and Aggregates Recovered from Recycled Asphalt Pavement. **Journal of ASTM International, No. 9(2),** (pp. 1-18).

175.   Mikhailenko, P., Ataeian, P., and Baaj, H. 2020. Extraction and Recovery of Asphalt Binder: A Literature Review. **International Journal of Pavement Research and Technology. No. 13,** (pp. 20-31).

176.   **American Association of State and Highway Transportation Officials**, R. 35-17. 2017. Standard Practice for Superpave Volumetric Design for Asphalt Mixtures. American Association of State and Highway Transportation Officials, Washington, D.C.

177.   Peterson, R., Soleymani, H., Anderson, R., and McDaniel, R. Recovery and Testing of RAP Binders from Recycled Asphalt Pavement. **Journal of the Association of Asphalt Paving Technologists, No. 69,** (pp. 72-91)

178.   Rodezno, C., and Grant, J. 2018. **Asphalt Binder Extraction Protocol for Determining Amount & PG Characteristics of Binders Recovered from Asphalt Mixtures.** National Center for Asphalt Technology at Auburn University, Auburn, AL (Report No. WHRP 0092-16-02).

179. Prapaitrakul, N. 2009. **Toward an Improved Model of Asphalt Binder Oxidation in Pavements**. Doctoral Dissertation, Department of Chemical Engineering, Texas A&M University, College Station, TX.

180. Han, R., Jin, X., and C. J., Glover. 2013. Oxygen Diffusivity in Asphalts and Mastics. **Petroleum Science and Technology, No. 31(15)**, (pp. 1398-1405)

181. Robert, F., Kandhal, P., Brown, E., Lee, D., and Kennedy, T. 1991. **Hot Mix Asphalt Materials, Mixture Design and Construction**. National Asphalt Pavement Association Research and Education Foundation. Lanham, MD.

182. Harvey, J., Deacon, J., Tsai, B., Monismith, C. 1995. **Fatigue Performance of Asphalt Concrete Mixes and Its Relationship to Asphalt Concrete Pavement Performance in California.** Institute of Transportation Studies, University of California at Berkeley, Berkeley, CA (RTA-65W485-2).

183. Williams, M. L., Landel, R. F., and Ferry, J. D. 1955. The Temperature Dependence of Relaxation Mechanisms in Amorphous Polymers and Other Glass-forming Liquids. **Journal of the American Chemical Society, No.77(14)**, (pp. 3701-3707).

184. Wu, R., Harvey, J., and Monismith, C. 2006. A Mechanistic Model for Reflective Cracking in AC Overlays, **Journal of the Association of Asphalt Paving Technologists, No.75,** (pp. 491-534).

185. Harvey, J., and Tsai, B. 1997. Long-Term Oven-Aging Effects on Fatigue and Initial Stiffness of Asphalt Concrete. **Transportation Research Record: Journal of the Transportation Research Board, No.1590(1),** (pp. 89-98).

186.   Andrei, D., Witczak, M. W., and Mirza, M. W. 1999. **Development of a Revised Predictive Model for the Dynamic (Complex) Modulus of Asphalt Mixtures.**, Department of Civil Engineering, University of Maryland, College Park, MD (Inter Team Technical Report prepared for the NCHRP 1-37A Project).

187.   Burr, B., Davison, R., Glover, C., and Bullin, J. 1990. Solvent Removal From Asphalt. **Transportation Research Record: Journal of the Transportation Research Board, No.1269,** (pp. 1-8).

188.   Bahia, H., and Swiertz, D. 2011. **Design System for HMA Containing a High Percentage of RAS Material.** Department of Civil & Environmental Engineering, University of Wisconsin Madison, Madison, WI (Final Report for RMRC Project 66).

189.   Wakefield, A. 2019. Recovered Asphalt Testing for Acceptance. **Asphalt, No. (34),** (pp. 30-33).

190.   Marill, T., and Green, D. 1963. On the Effectiveness of Receptors in Recognition Systems. **IEEE Transactions on Information Theory. No. 9,** (pp. 11-17).

191.   Halinski, R and Feldt, L. 1970 The Selection of Variables in Multiple Regression Analysis. **Journal of Educational Measurement, No. 7,** (pp. 151-157).

192.   Raad, L., Saboundjian, S., and Minassian, G. 2001. Field Aging Effects on Fatigue of Asphalt Concrete and Asphalt-Rubber Concrete. **Transportation Research Record: Journal of the Transportation Research Board, No.1767(1),** (pp. 126-134).

193.   Glover, C., Martin, A., Chowdhury, A., Han, R., Parpaitrakul, N., Jin, X., and Lawrence, J. 2009. **Evaluation of Binder Aging and Its Influence in Aging of Hot Mix Asphalt**

Concrete: Literature Review and Experimental Design. Texas A & M Transportation Institute, College Station, Texas (No. 0-6009-1)

194. Elkashef, M., Elwardany, M. D., Liang, Y., Jones, D., Harvey, J., Bolton, N. D., and Planche, J. P. 2020. Effect of Using Rejuvenators on the Chemical, Thermal, and Rheological Properties of Asphalt Binders. **Energy and Fuels, No. 34,** (pp. 2152-2159).

195. **American Association of State and Highway Transportation Officials**, T. 350-19. 2019. Standard Method of Test for Multiple Stress Creep Recovery (MSCR) Test of Asphalt Binder Using a Dynamic Shear Rheometer (DSR). American Association of State and Highway Transportation Officials, Washington, D.C.

196. D'Angelo, J., Kluttz, R., Dongre, R. N., Stephens, K., and Zanzotto, L. 2007. Revision of the Superpave High-temperature Binder Specification: the Multiple Stress Creep Recovery Test (with discussion). **Journal of the Association of Asphalt Paving Technologists, No. 76,** (pp. 123-155).

197. Zoorob, S. E., Castro-Gomes, J. P., Oliveira, L. P., and O'Connell, J. 2012. Investigating the Multiple Stress Creep Recovery Bitumen Characterization Test. **Construction and Building Materials, No. 30,** (pp. 734-745).

198. **American Association of State and Highway Transportation Officials**, T. 316-19. 2019. Standard Method of Test for Viscosity Determination of Asphalt Binder Using Rotational Viscometer. American Association of State and Highway Transportation Officials, Washington, D.C.

199.   Anderson, R. M., King, G. N., Hanson, D. I., and Blankenship, P. B. 2011. Evaluation of the Relationship between Asphalt Binder Properties and Non-load Related Cracking. **Journal of the Association of Asphalt Paving Technologists, No. 80,** (pp. 615-644).

200.   **American Association of State and Highway Transportation Officials**, T 324-14. 2014. Standard Method of Test for Hamburg Wheel-Track Testing of Compacted Hot-Mix Asphalt (HMA). American Association of State Highway and Transportation Officials, Washington, D.C.

201.   **American Association of State and Highway Transportation Officials**, T 378-17. 2017. Standard Method of Test for Determining the Dynamic Modulus and Flow Number for Asphalt Mixtures Using the Asphalt Mixture Performance Tester (AMPT). American Association of State Highway and Transportation Officials, Washington, D.C.

202.   Harvey, J., Liu, A., Zhou, J., Signore, J., Coleri, E., and He, Y. 2016. **Superpave Implementation Phase II: Comparison of Performance-Related Test Results**. University of California Pavement Research Center, Berkeley and Davis, CA (No. RR-2015-01).

203.   He, Y. 2016. **Interaction between New and Age-Hardened Binders in Asphalt Mixes Containing High Quantities of Reclaimed Asphalt Pavement and Reclaimed Asphalt Shingles**. Doctoral Dissertation, University of California, Davis, Davis, CA.

204.   Christina Pang. 2019. **Development of Shift Factors between Repeated Load Triaxial and Repeated Simple Shear Test Results**. Master's Thesis, University of California Davis, Davis, CA.

205. Alavi, M. Z., Hajj, E. Y., Morian, N. E., and Sebaaly, P. E., 2013. Low Temperature Characterization of Asphalt Mixtures by Measuring Visco-elastic Properties under Thermal Loadin*g*. **In ISCORD 2013: Planning for Sustainable Cold Regions** (pp. 404-415).

206. **American Association of State and Highway Transportation Officials**, R 35-17. 2017. Superpave Volumetric Design for Asphalt Mixtures. American Association of State and Highway Transportation Officials, Washington, D.C.

207. Willis, J., Plemons, C., Turner, P., Rodezno, C., and Mitchell, T. 2012. **Effect of Ground Tire Rubber Particle Size and Grinding Method on Asphalt Binder Properties.** Auburn University, Auburn, Alabama (NCAT Report No. 12-09).

208. Ullidtz, P., Harvey, J., Basheer, I., Jones, D., Wu, R., Lea, J., and Lu, Q. 2010. *CalME*, A Mechanistic–Empirical Program to Analyze and Design Flexible Pavement Rehabilitation". **Transportation Research Record: Journal of the Transportation Research Board, No. 2153(1),** (pp. 143-152).

209. Wu, R. Harvey, J, and Monismith, C. 2006. A Mechanistic Model for Reflective Cracking in AC Overlays. **Journal of the Association of Asphalt Paving Technologists, No.75,** (pp. 491-534).

210. Wu, R., and Harvey, J. 2012. Calibration of Asphalt Concrete Cracking Models for California Mechanistic-Empirical Design (*CalME*). **The 7ᵗʰ International Conference on Cracking in Pavements**, RILEM, Delft, Netherlands (pp. 537-547).

211. Kim, Y. R., Little, D. N., and Lytton, R. L. 2003. Fatigue and Healing Characterization of Asphalt Mixtures. **Journal of Materials in Civil Engineering, No.15(1),** (pp. 75-83).

212.	**California Department of Transportation**. 2020. Highway Design Manual. Department

of Transportation, Sacramento, California.

A. APPENDIX: FTIR RESULTS FOR RUBBER-MODIFIED BINDERS

Table A 1: Summary of Carbonyl Area Index

Binder ID[1]	Unaged Binder	Deviation	RTFO-Aged Binder	Deviation	PAV-Aged Binder	Deviation
Base_A	0.061	0.017	0.150	0.065	0.848	0.102
A_5_0.25	0.050	0.019	0.255	0.084	0.793	0.026
A_10_0.25	0.043	0.013	0.208	0.073	0.713	0.051
Base_B	0.121	0.053	0.289	0.058	1.054	0.051
B_5_1.18	0.093	0.029	0.491	0.039	0.987	0.042
B_10_1.18	0.110	0.042	0.420	0.034	0.971	0.036
B_5_2.36	0.093	0.032	0.464	0.092	0.976	0.037
B_10_2.36	0.072	0.024	0.520	0.037	0.912	0.053
Base_C	0.119	0.025	0.146	0.045	0.968	0.125
C_20_2.36	0.191	0.085	0.457	0.055	0.893	0.072
Base_D	0.279	0.025	0.289	0.029	0.892	0.125
D_20_2.36	0.188	0.025	0.412	0.055	0.798	0.043

[1] Binder ID format: source_rubber content in percent_maximum rubber size in mm.

Table A 2: Summary of Sulfoxide Area Index

Binder ID[1]	Unaged Binder	Deviation	RTFO-Aged Binder	Deviation	PAV-Aged Binder	Deviation
Base_A	1.634	0.057	2.994	0.067	4.216	0.045
A_5_0.25	1.054	0.169	2.273	0.136	3.958	0.038
A_10_0.25	1.042	0.065	2.001	0.090	3.896	0.161
Base_B	1.010	0.212	1.147	0.040	3.651	0.036
B_5_1.18	0.949	0.045	1.197	0.037	3.766	0.089
B_10_1.18	0.871	0.155	1.129	0.071	3.465	0.337
B_5_2.36	1.008	0.109	1.313	0.069	3.634	0.091
B_10_2.36	0.679	0.150	1.246	0.055	3.428	0.195
Base_C	0.842	0.031	0.973	0.068	3.757	0.132
C_20_2.36	1.353	0.292	1.416	0.087	2.581	0.268
Base_D	1.031	0.088	1.836	0.362	3.802	0.099
D_20_2.36	1.183	0.287	1.601	0.177	2.392	0.106

[1] Binder ID format: source_rubber content in percent_maximum rubber size in mm.

Table A 3: Summary of Butadiene Area Index

Binder ID[1]	Unaged Binder	Deviation	RTFO-Aged Binder	Deviation	PAV-Aged Binder	Deviation
Base_A	0.082	0.013	0.089	0.016	0.030	0.012
A_5_0.25	0.119	0.007	0.096	0.035	0.033	0.012
A_10_0.25	0.171	0.020	0.171	0.026	0.159	0.006
Base_B	0.032	0.012	0.035	0.014	-0.007	0.008
B_5_1.18	0.075	0.016	0.075	0.012	0.025	0.008
B_10_1.18	0.093	0.009	0.137	0.016	0.083	0.021
B_5_2.36	0.081	0.019	0.071	0.017	0.039	0.012
B_10_2.36	0.109	0.015	0.112	0.015	0.103	0.019
Base_C	0.007	0.011	0.028	0.011	-0.035	0.023
C_20_2.36	0.191	0.066	0.286	0.087	0.235	0.014
Base_D	0.047	0.024	0.014	0.022	-0.032	0.020
D_20_2.36	0.199	0.014	0.216	0.014	0.240	0.020

[1] Binder ID format: source_rubber content in percent_maximum rubber size in mm.

B. APPENDIX: *CALME* SIMULATION RESULTS
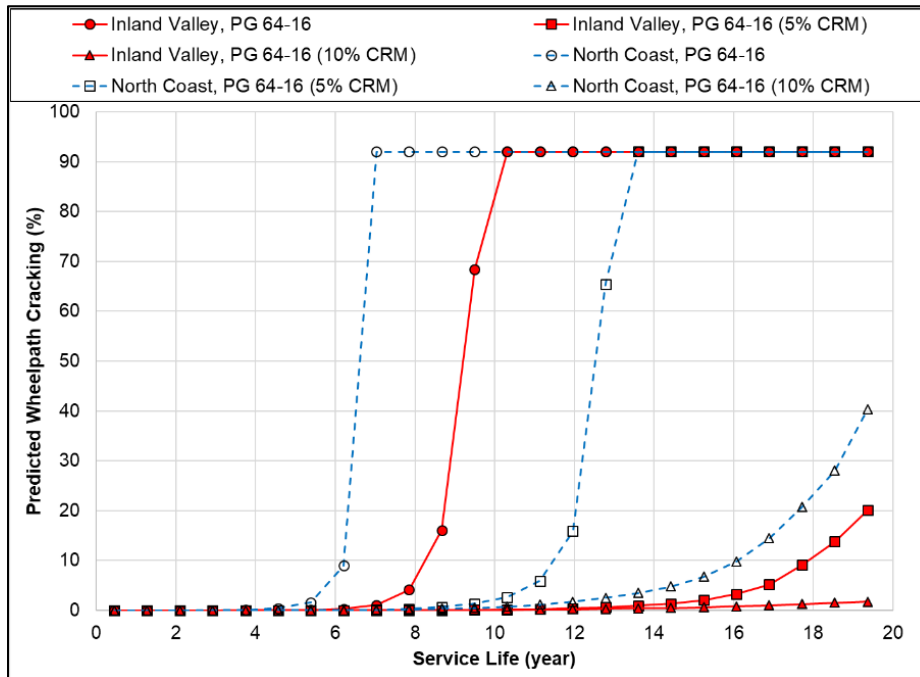
Figure B.1: Asphalt overlay application of Approach-1 Mix A, B, C at 45 mm.
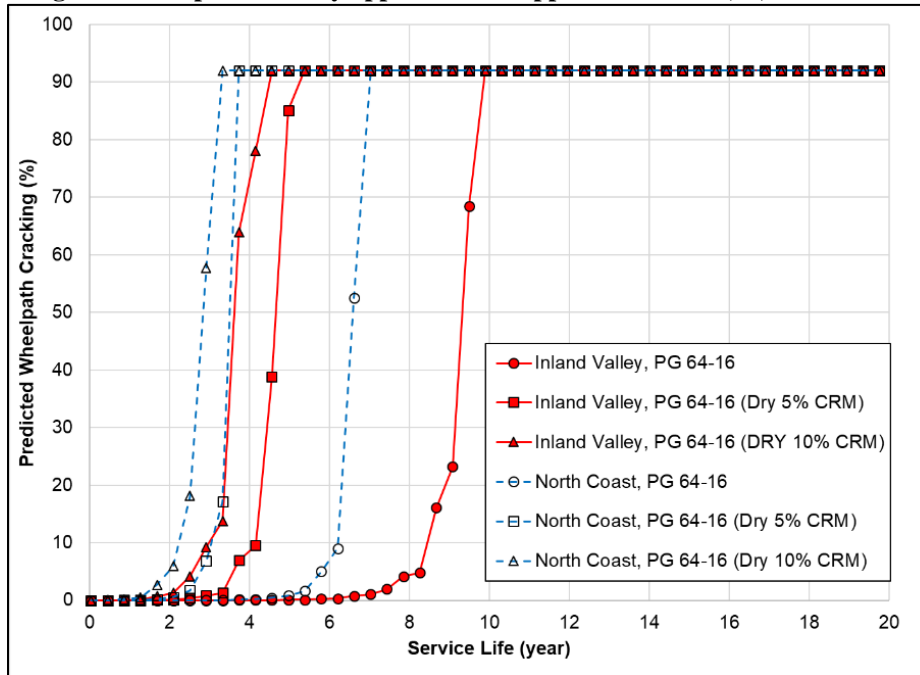
Figure B.2: Asphalt overlay application of Approach-3 Mix A, G, H at 45 mm.
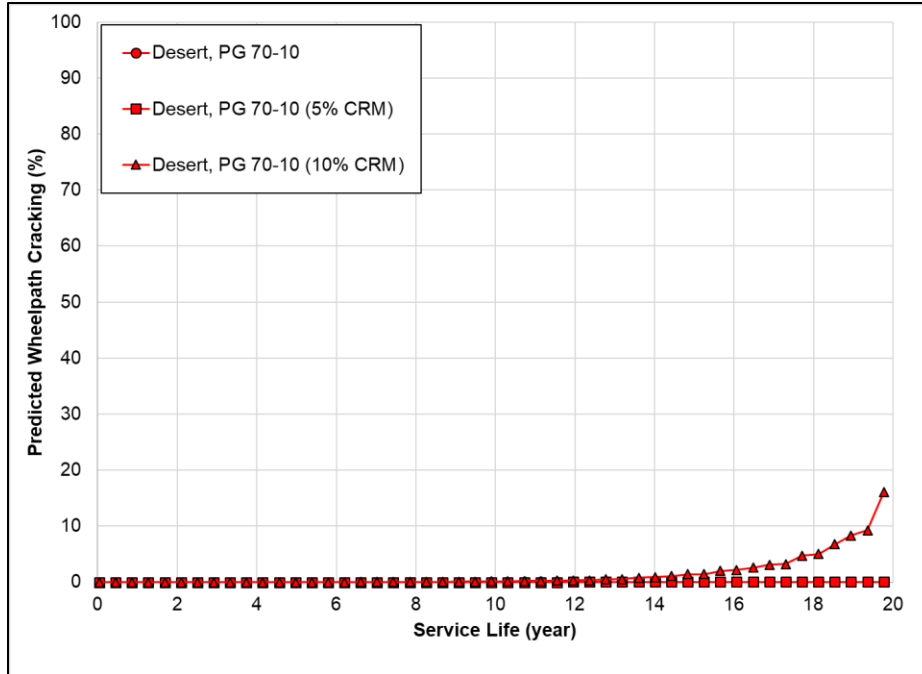
Figure B.3: Asphalt overlay application of Approach-1 Mix D, E, F at 45 mm.
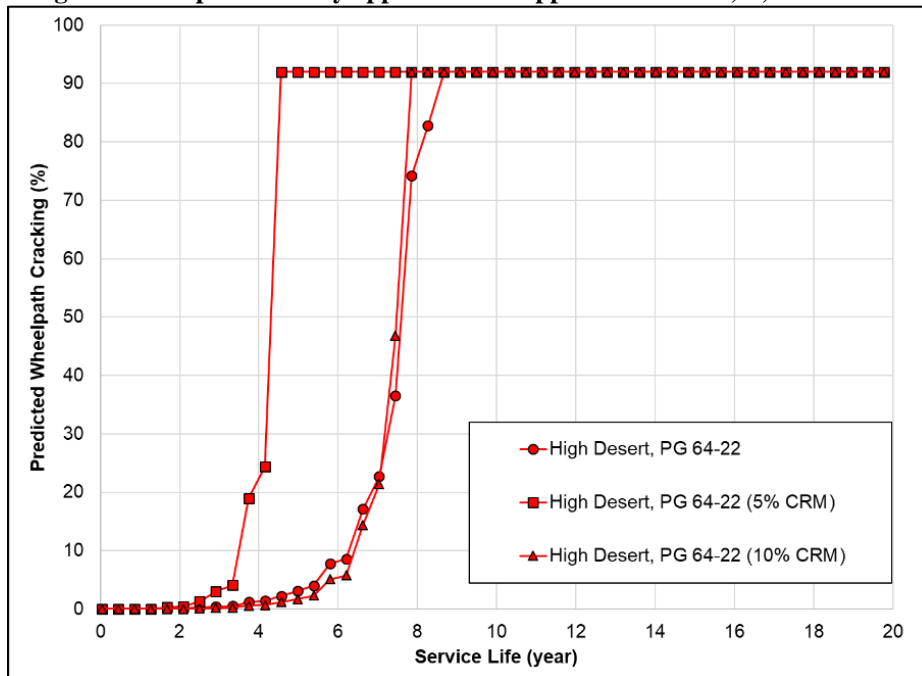
Figure B.4: Asphalt overlay application of Approach-4 Mix J, K, L at 45 mm.
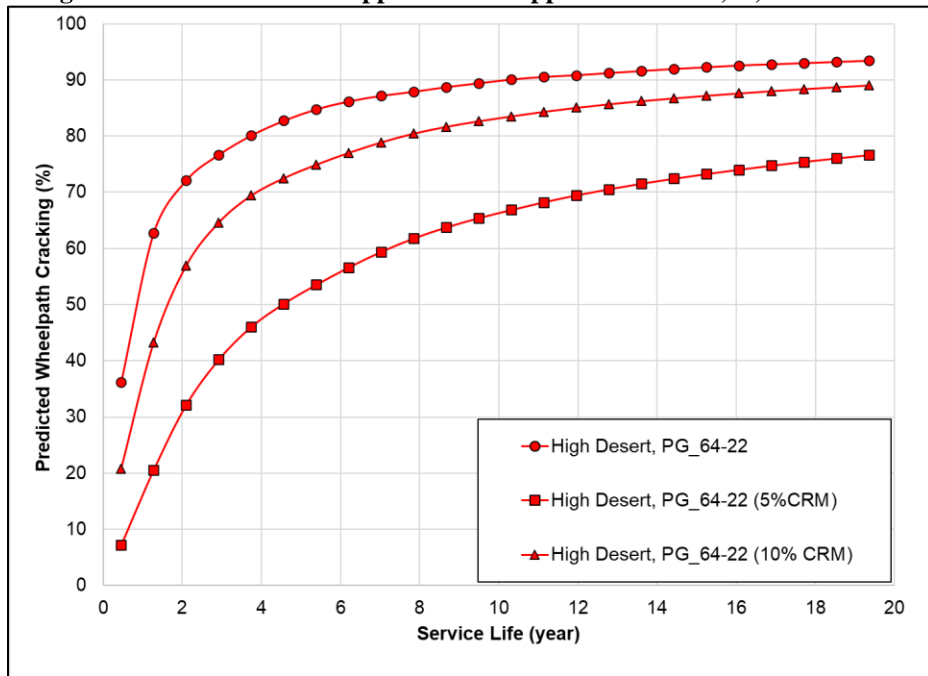
414
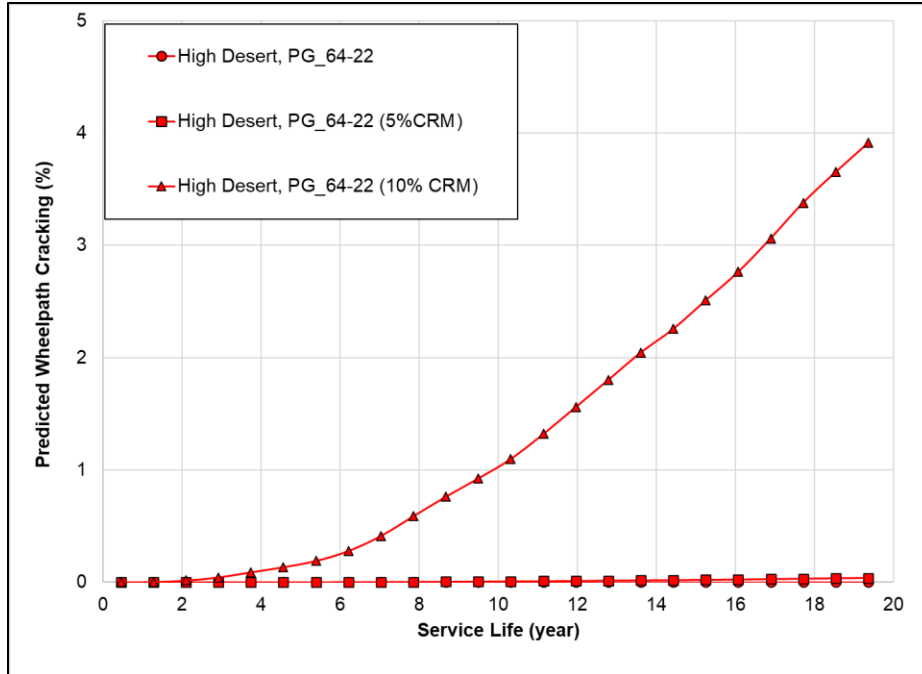
Figure B.5: Asphalt overlay application of Approach-2 Mix S, T, U at 45 mm.
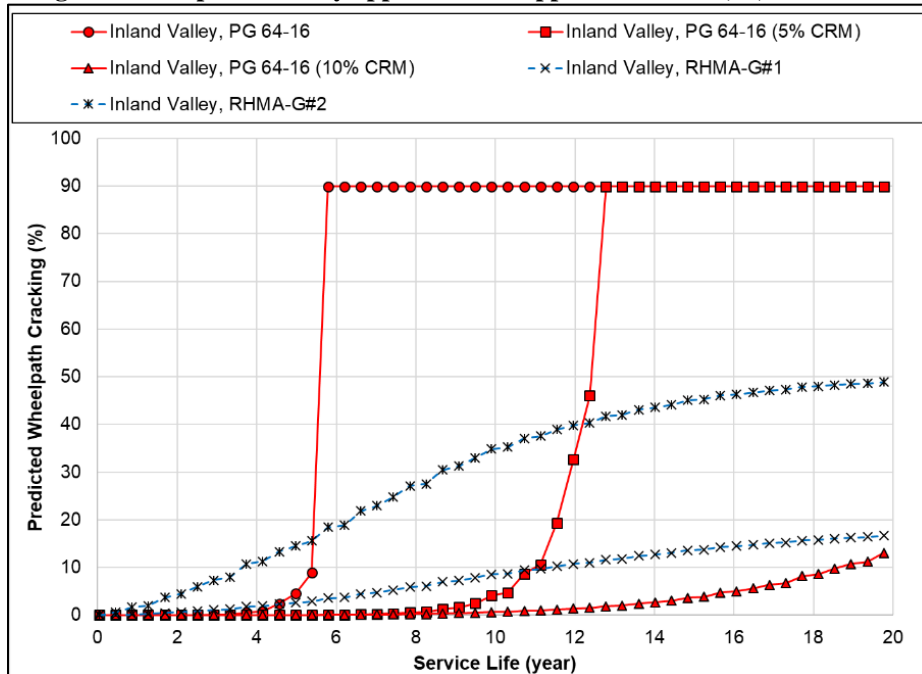
Figure B.6: Asphalt overlay application of Approach-1 Mix A, B, C, and RHMA-G at 60 mm inland valley.
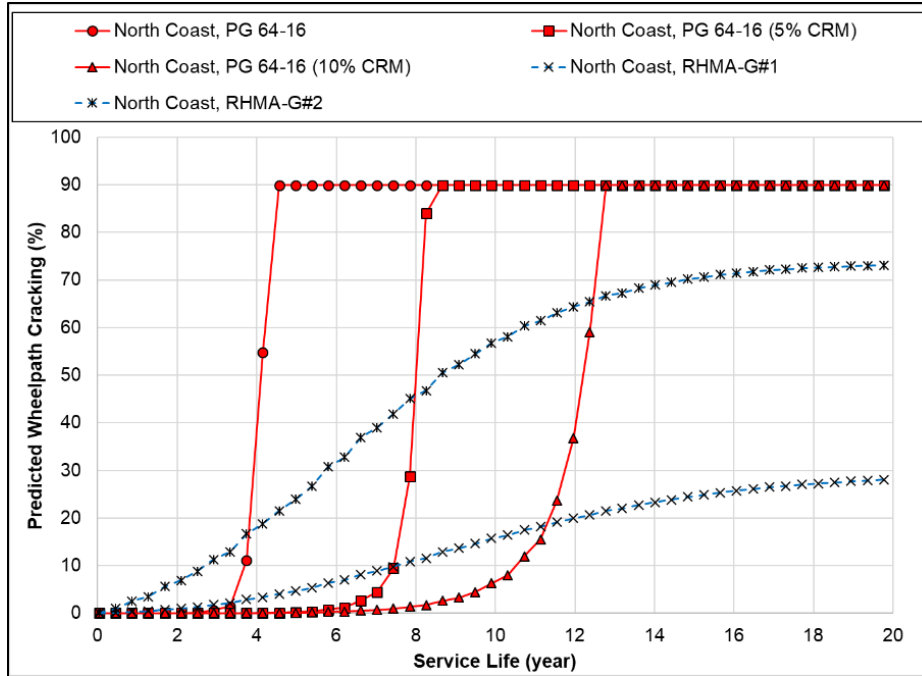
Figure B.7: Asphalt overlay application of Approach-1 Mix A, B, C, and RHMA-G at 60 mm north coast.
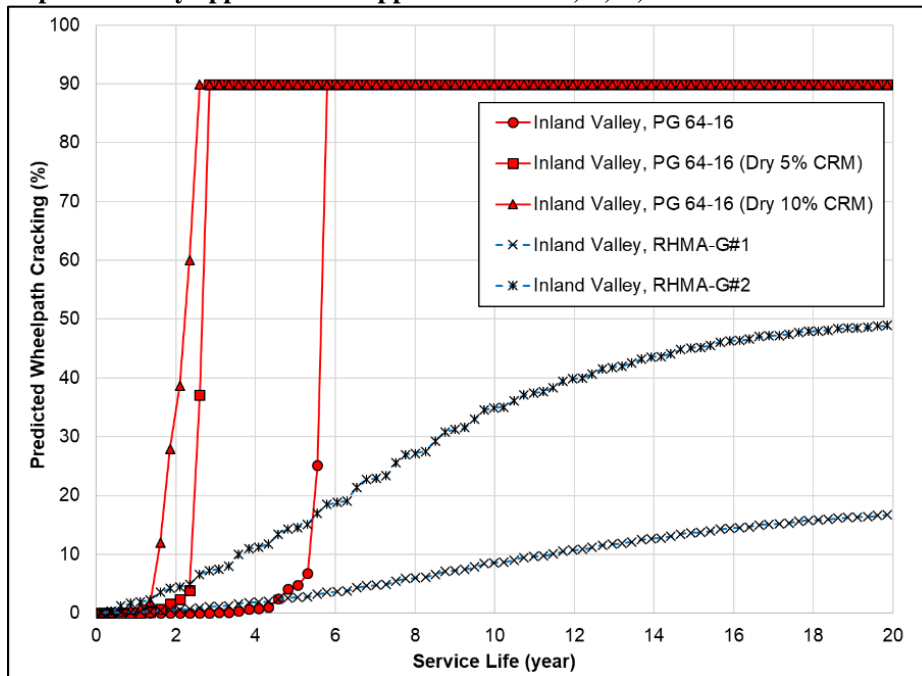
Figure B.8: Asphalt overlay application of Approach-3 Mix A, G, H, and RHMA-G at 60 mm inland valley.

416
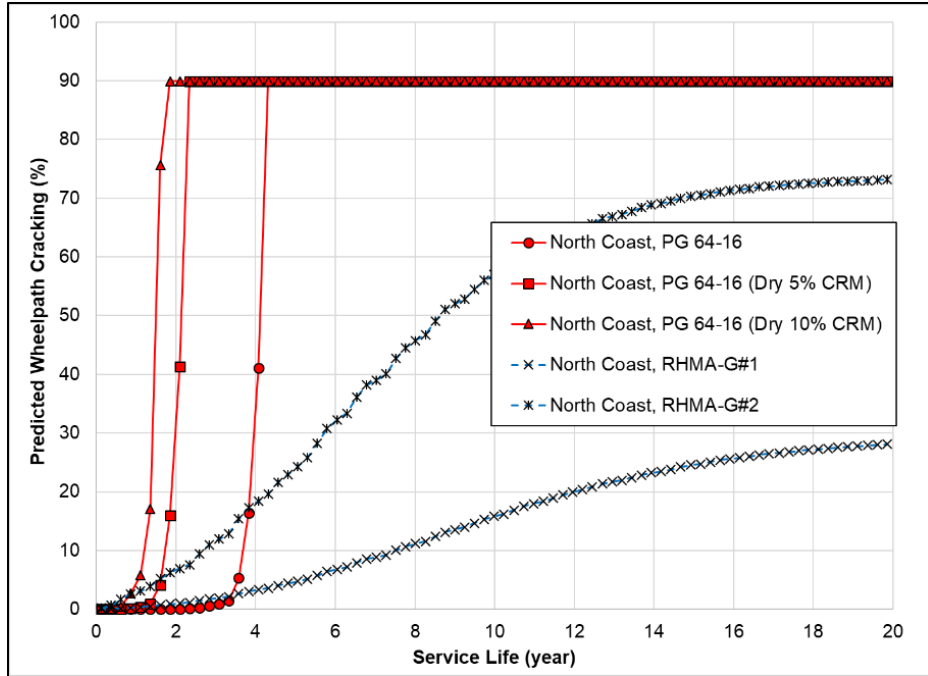
Figure B.9: Asphalt overlay application of Approach-3 Mix A, G, H, and RHMA-G at 60 mm north coast.
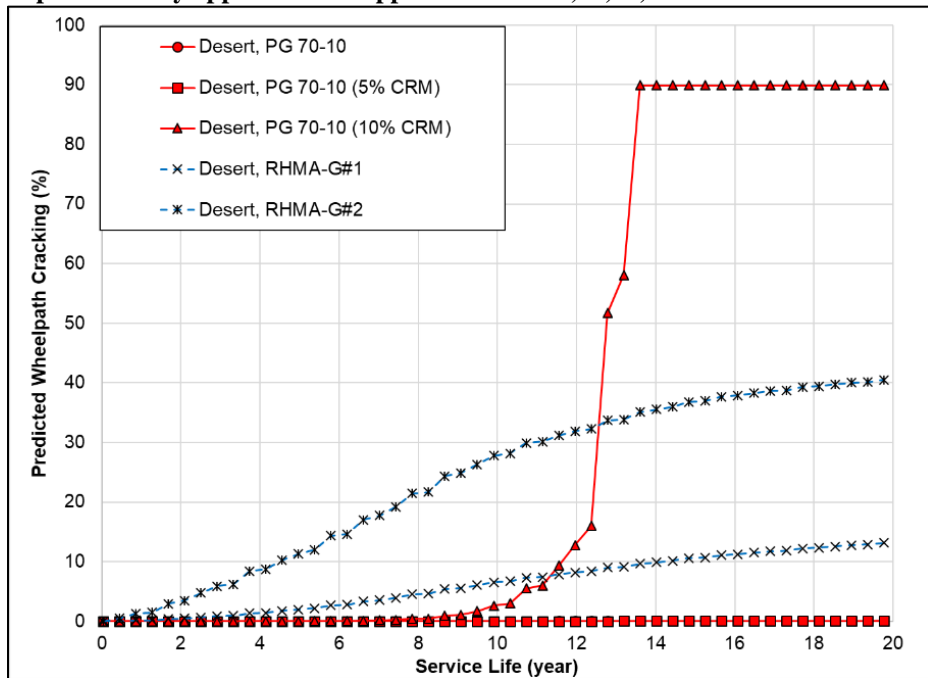
Figure B.10: Asphalt overlay application of Approach-1 Mix D, E, F, and RHMA-G at 60 mm.

417
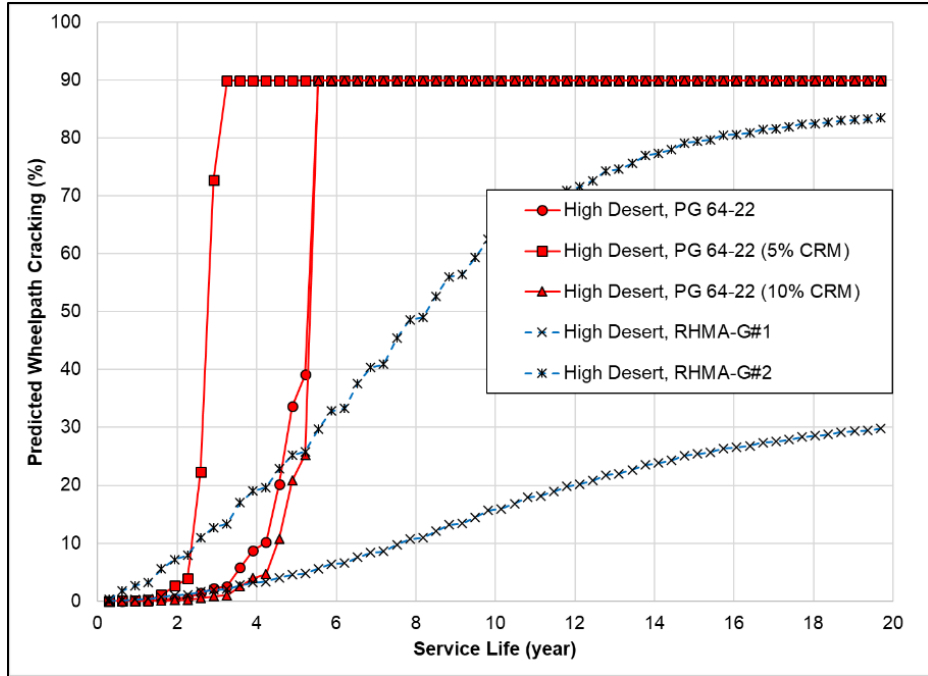
Figure B.11: Asphalt overlay application of Approach-4 Mix J, K, L, and RHMA-G at 60 mm.
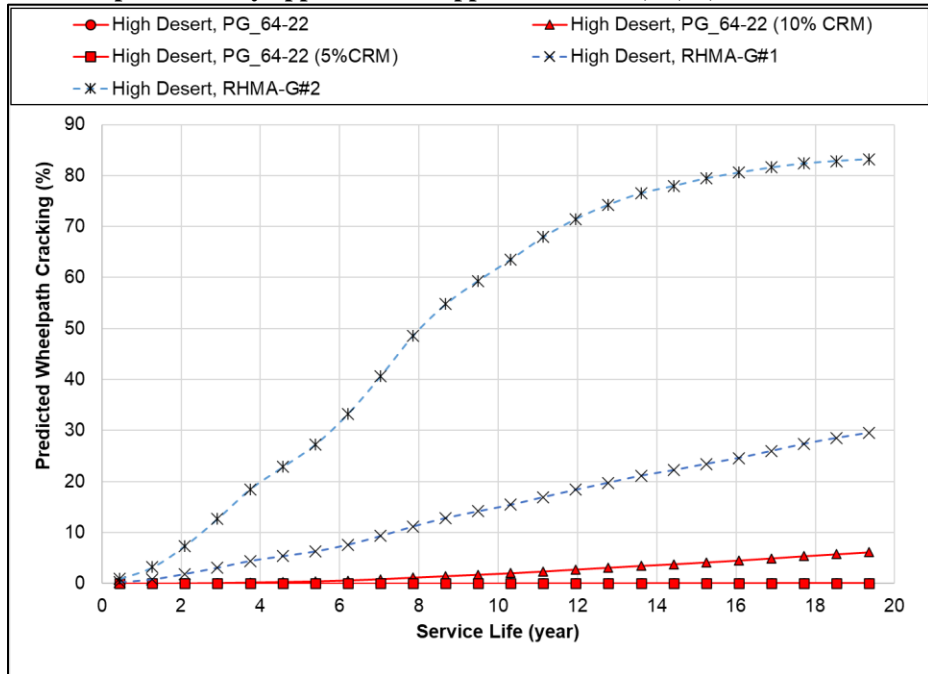
Figure B.12: Asphalt overlay application of Approach-2 Mix S, T, U, and RHMA-G at 60 mm.
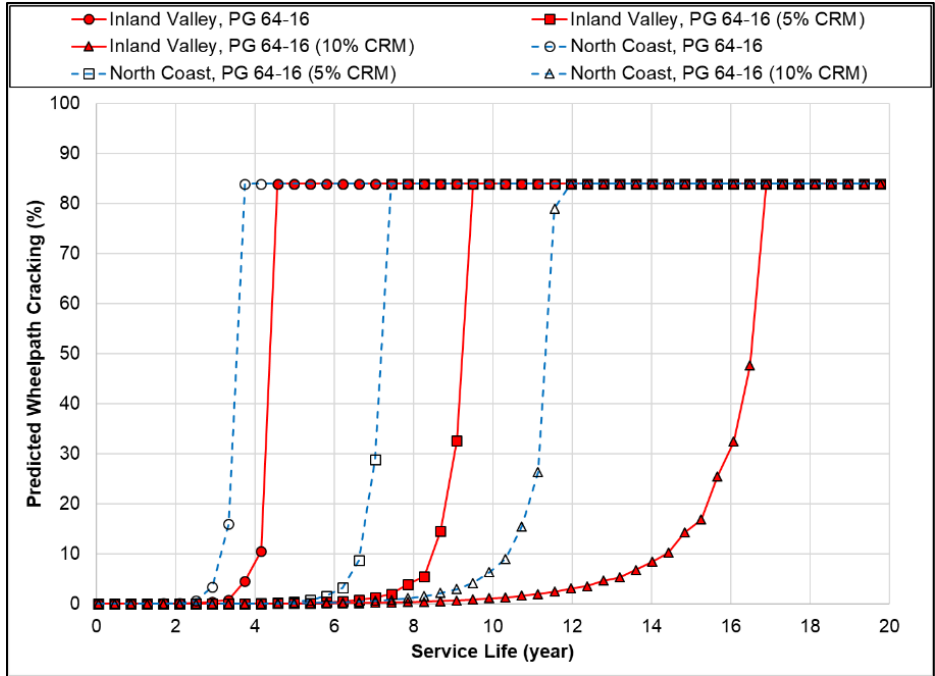
Figure B.13: Asphalt overlay application of Approach-1 Mix A, B, C at 100 mm.
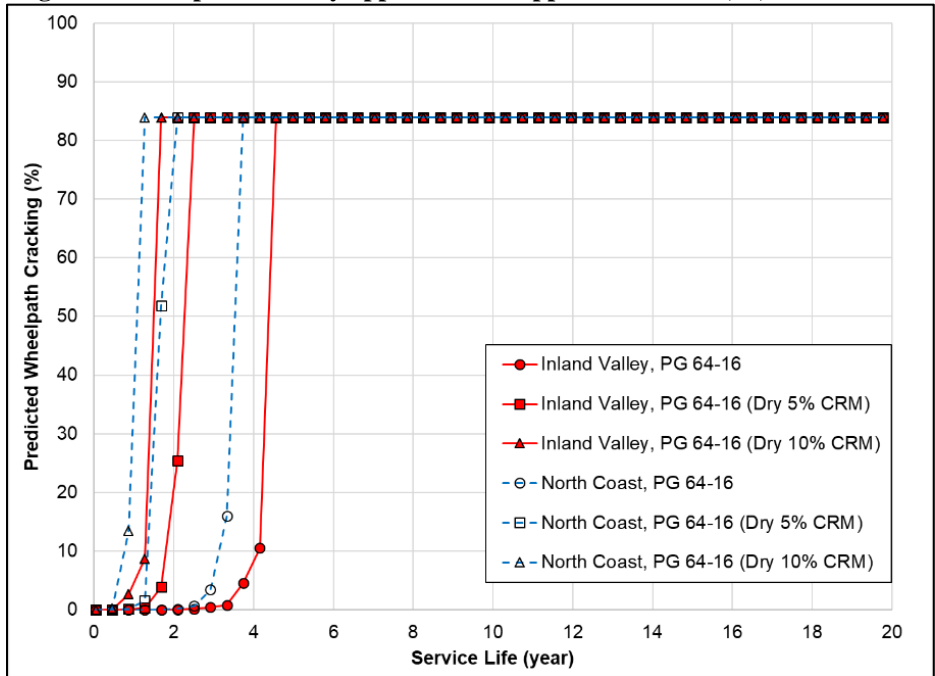
Figure B.14: Asphalt overlay application of Approach-3 Mix A, G, H at 100 mm.
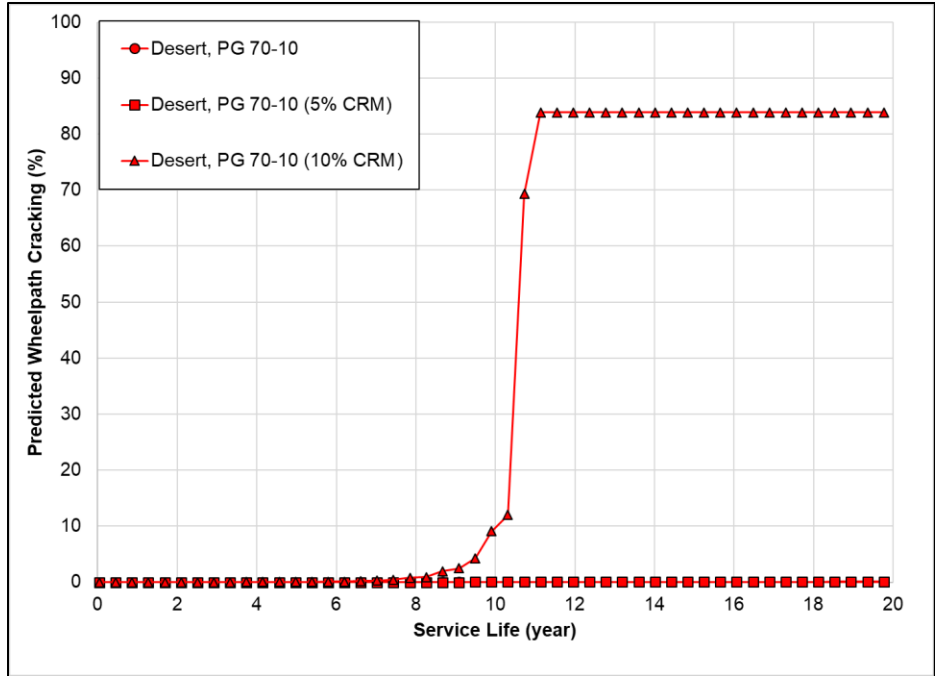
Figure B.15: Asphalt overlay application of Approach-1 Mix D, E, F at 100 mm.
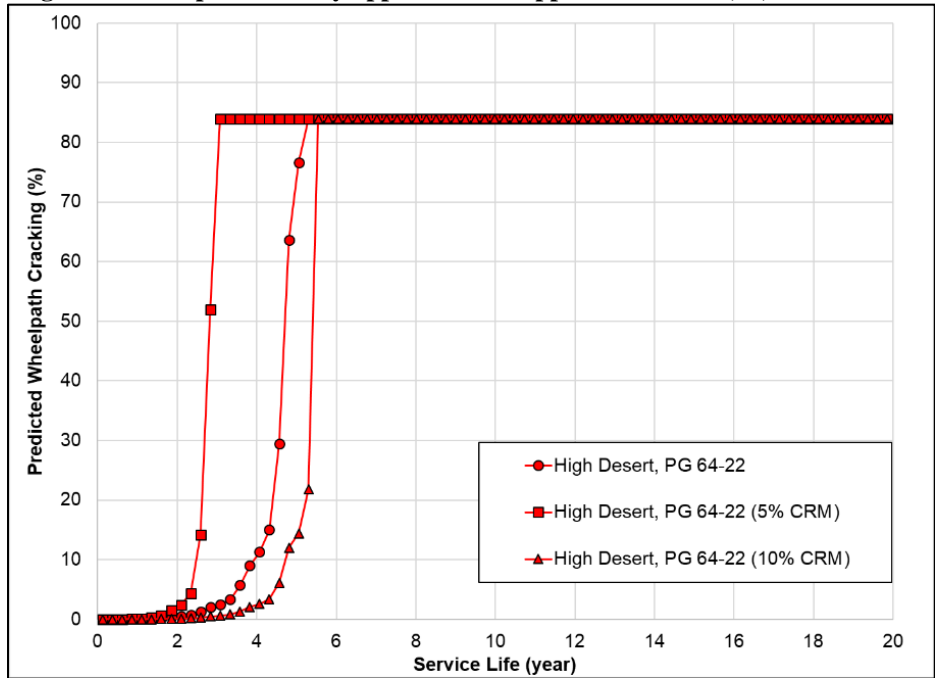
Figure B.16: Asphalt overlay application of Approach-4 Mix J, K, L at 100 mm.

420
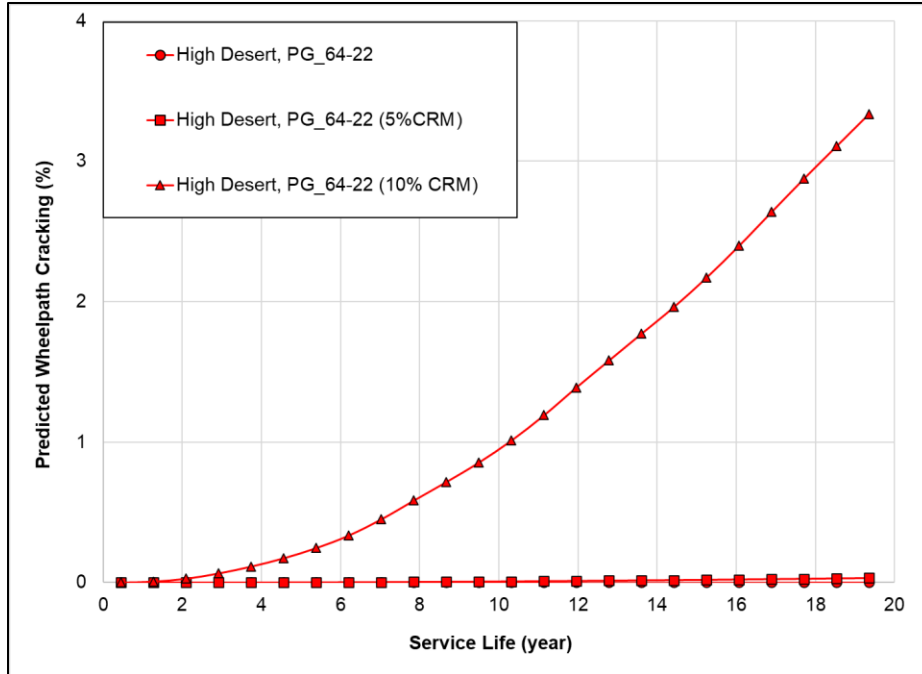
Figure B.17: Asphalt overlay application of Approach-2 Mix S, T, U at 100 mm.
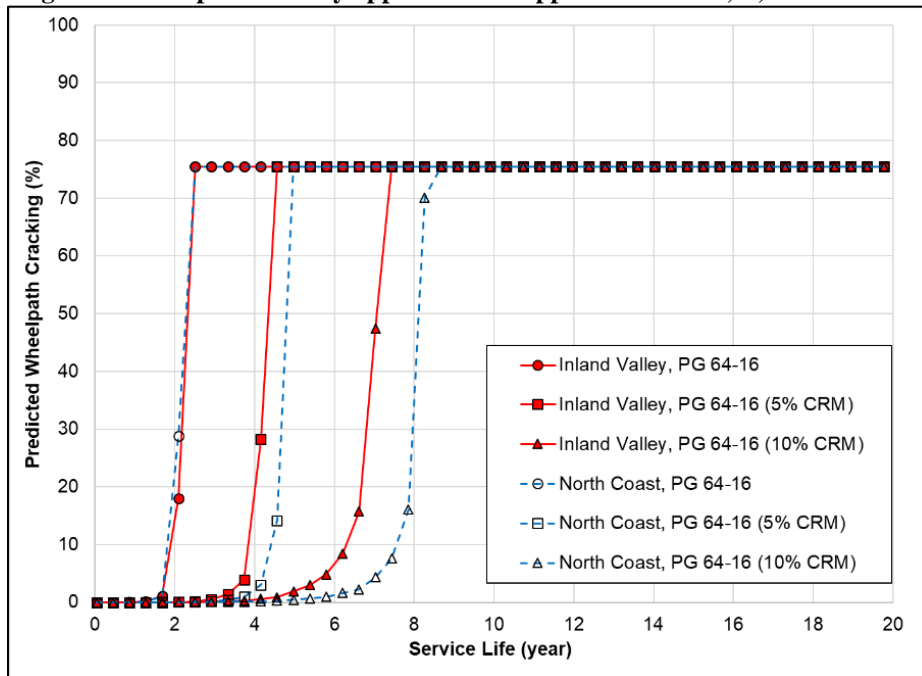
Figure B.18: Asphalt overlay application of Approach-1 Mix A, B, C at 150 mm.
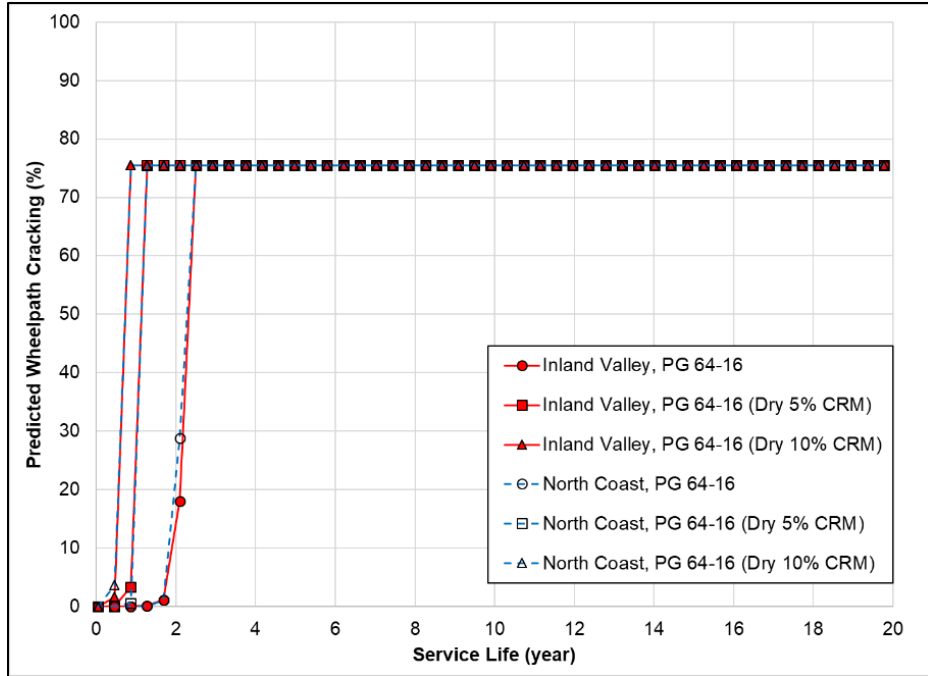
Figure B.19: Asphalt overlay application of Approach-3 Mix A, G, H at 150 mm.
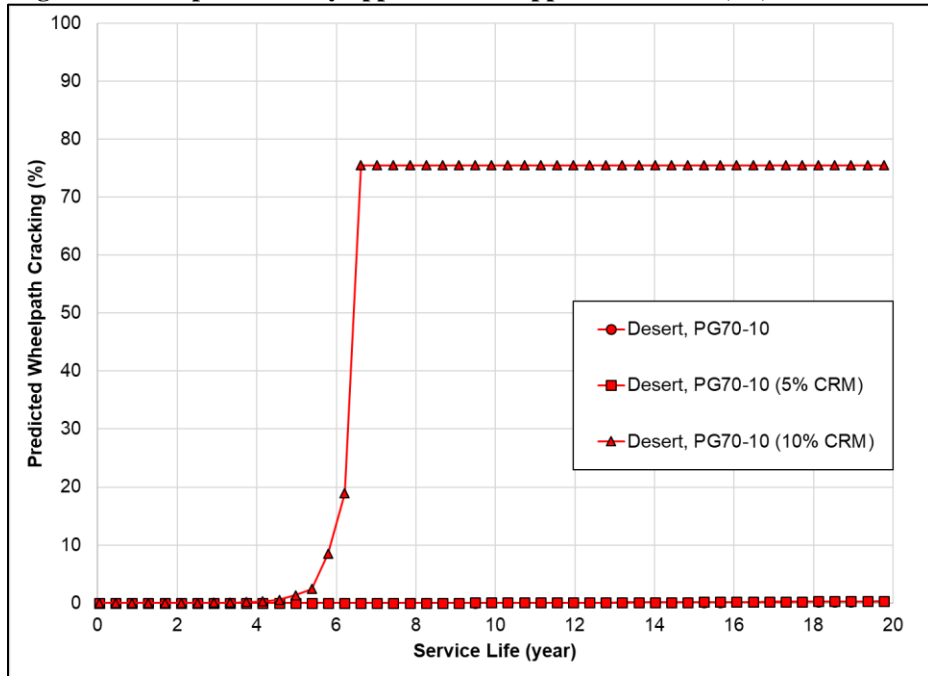
Figure B.20: Asphalt overlay application of Approach-1 Mix D, E, F at 150 mm.
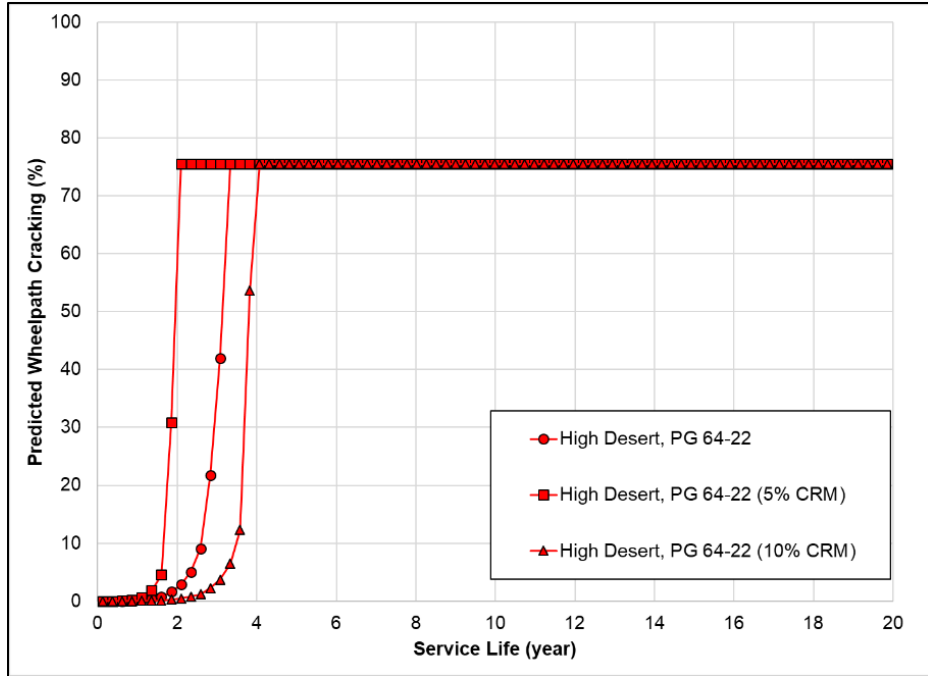
Figure B.21: Asphalt overlay application of Approach-4 Mix J, K, L at 150 mm.
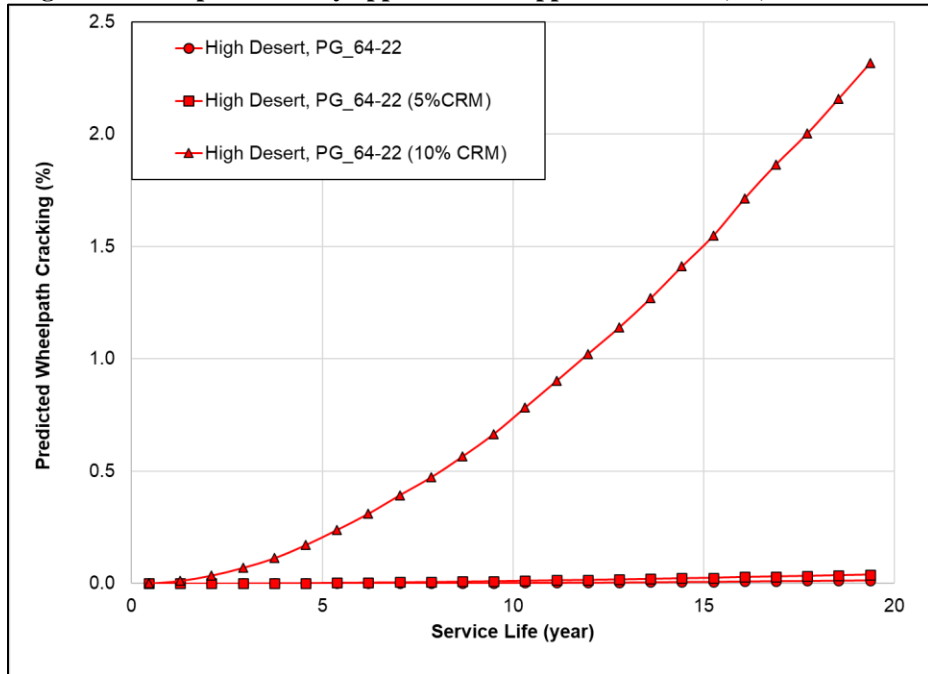
Figure B.22: Asphalt overlay application of Approach-2 Mix S, T, U at 150 mm.
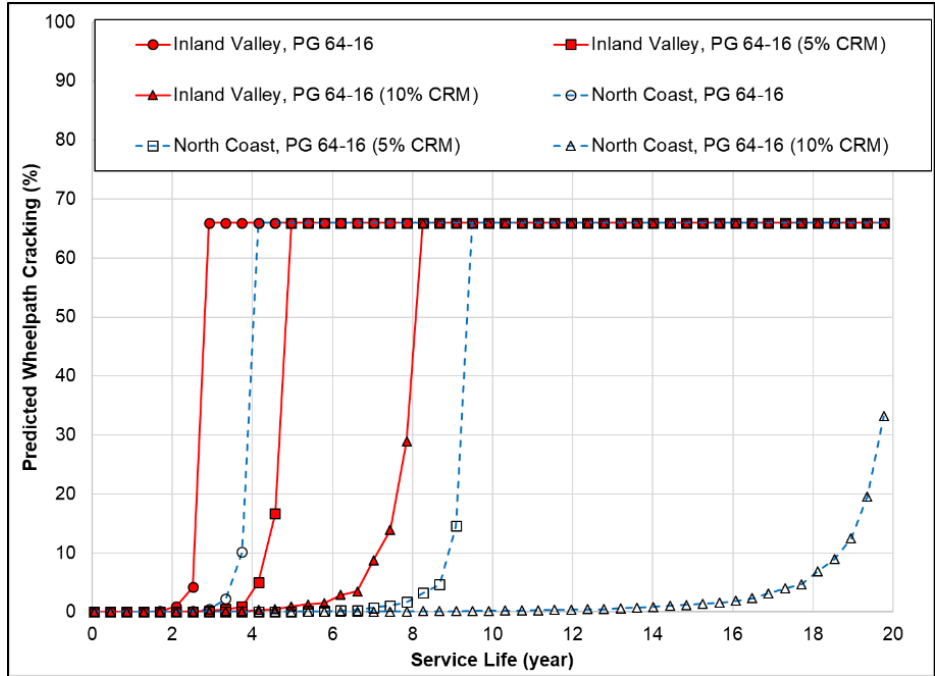
Figure B.23: Asphalt overlay application of Approach-1 Mix A, B, C at 210 mm.
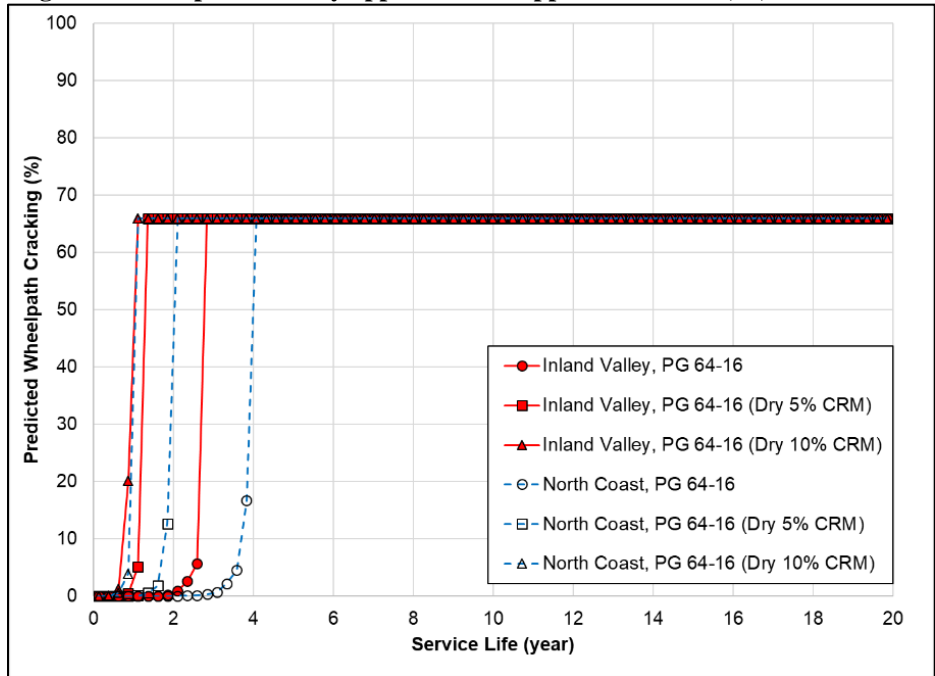
Figure B.24: Asphalt overlay application of Approach-3 Mix A, G, H at 210 mm.
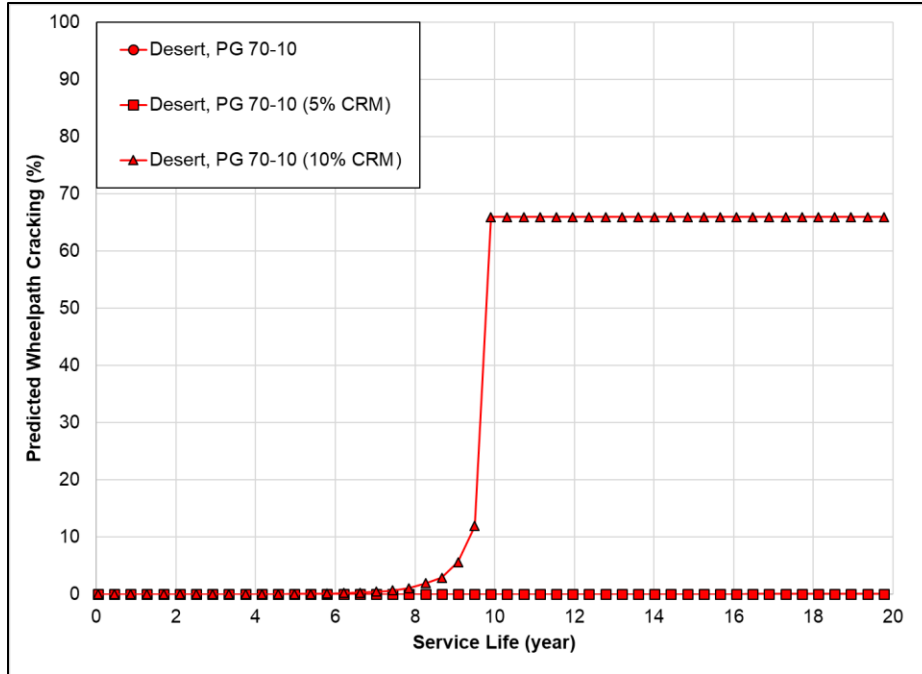
Figure B.25: Asphalt overlay application of Approach-1 Mix D, E, F at 210 mm.
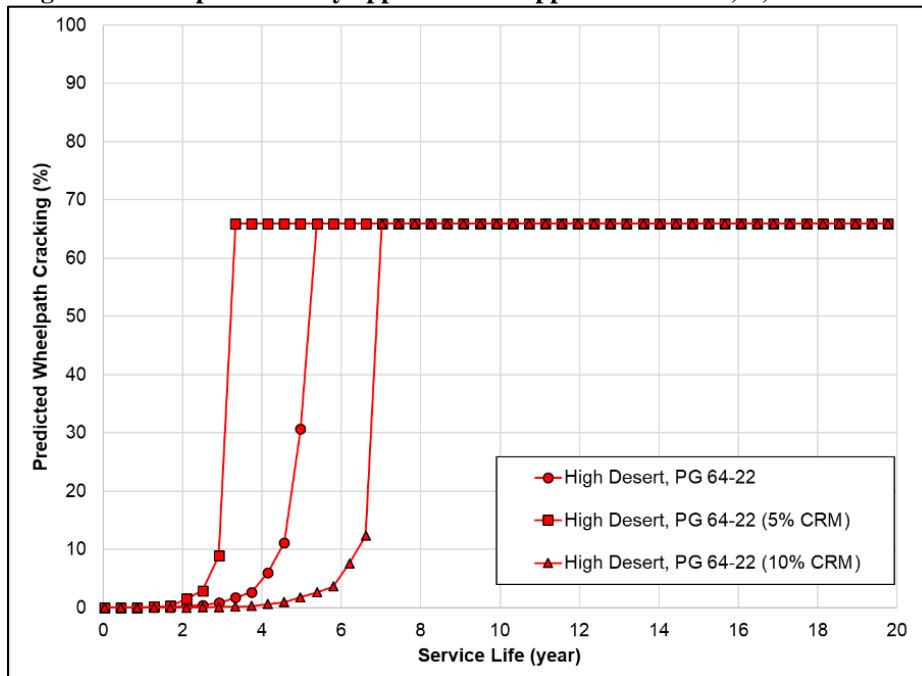
Figure B.26: Asphalt overlay application of Approach-4 Mix J, K, L at 210 mm.

425
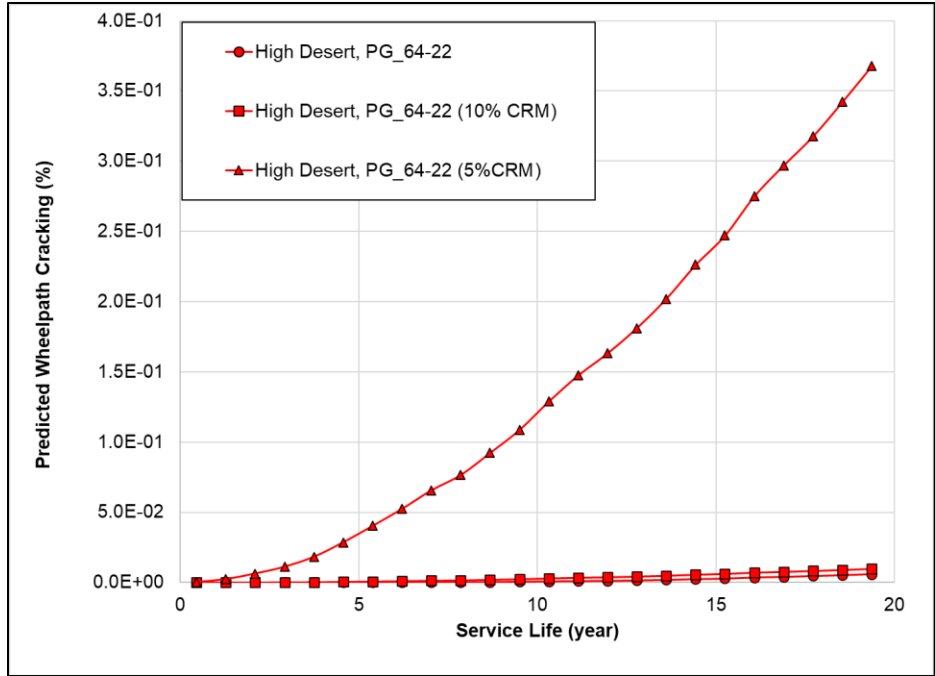
Figure B.27: Asphalt overlay application of Approach-2 Mix S, T, U at 210 mm.
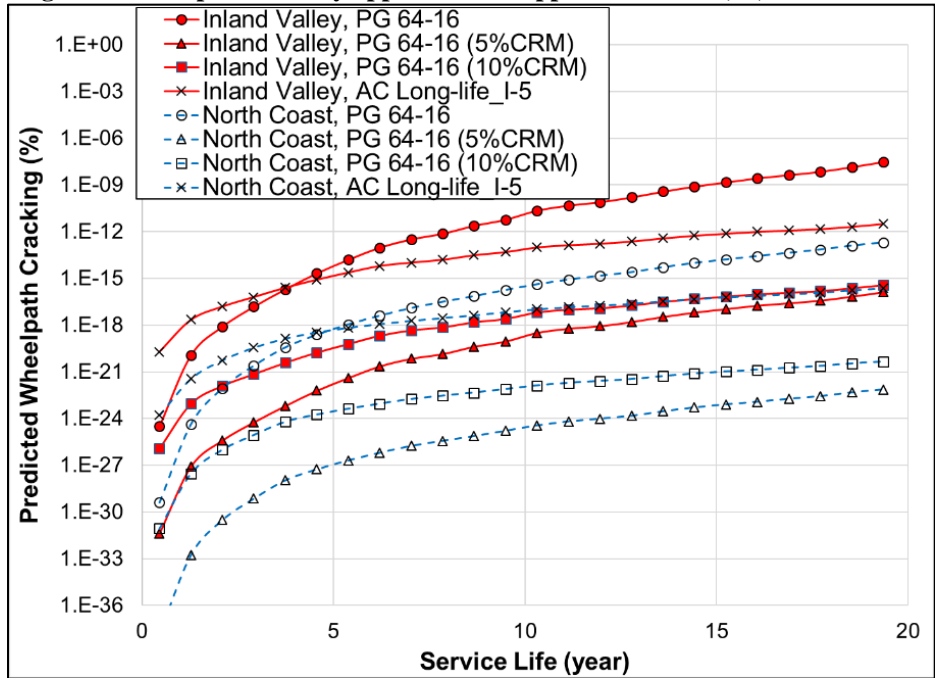
Figure B.28: Thick pavement application of Approach-1 Mix A, B, C, and SAC-5 mixes.
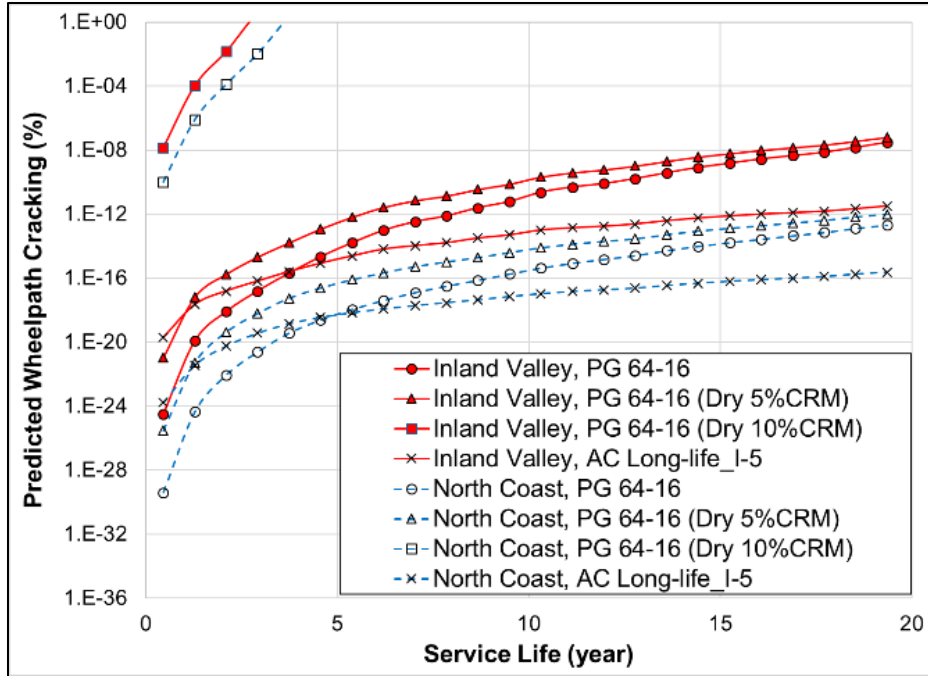
a: Results on the micron-scale
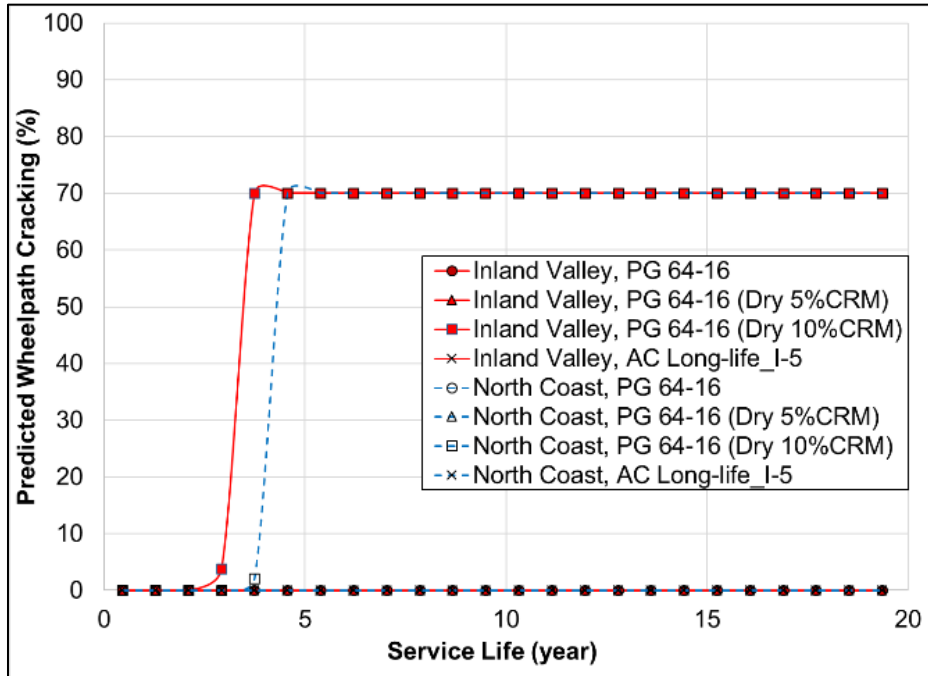
b: Results on the regular-scale

Figure B.29: Thick pavement application of Approach-3 Mix A, G, H, and SAC-5 mixes.
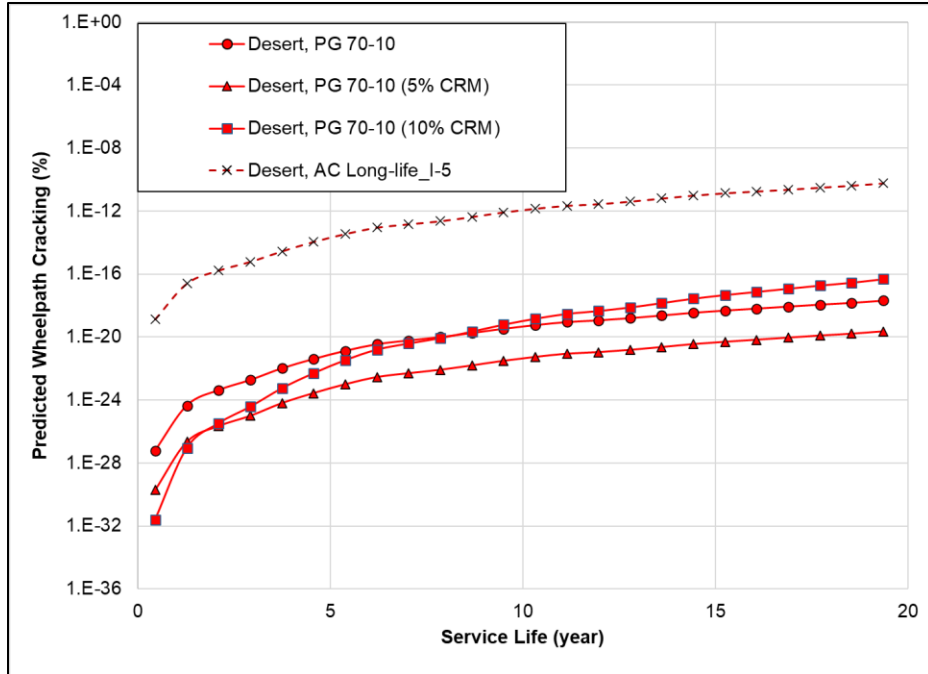
Figure B.30: Thick pavement application of Approach-1 Mix D, E, F, and SAC-5 mixes.
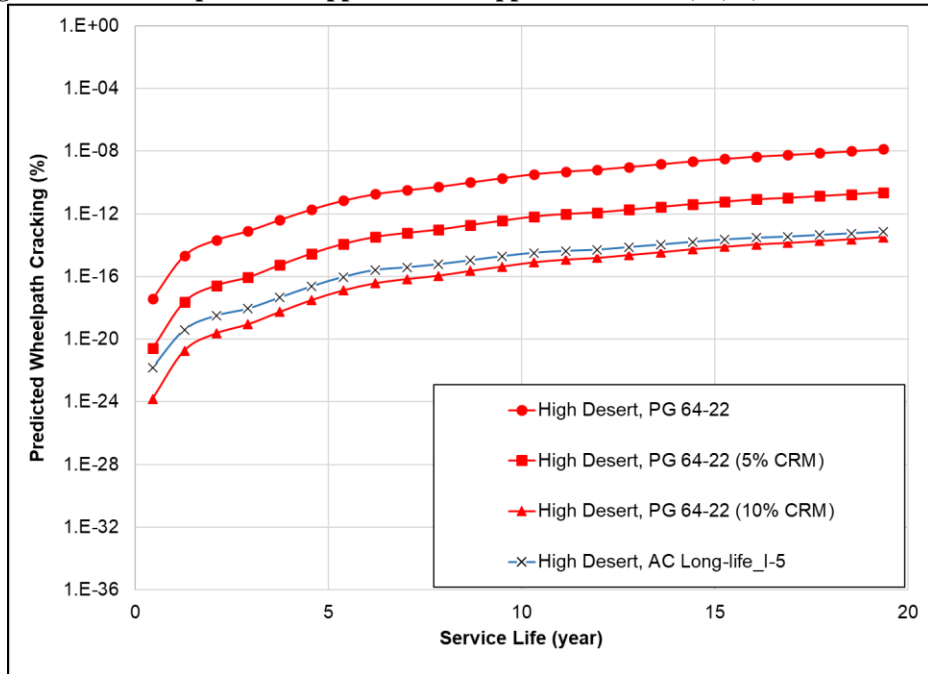
Figure B.31: Thick pavement application of Approach-4 Mix J, K, L, and SAC-5 mixes.

428
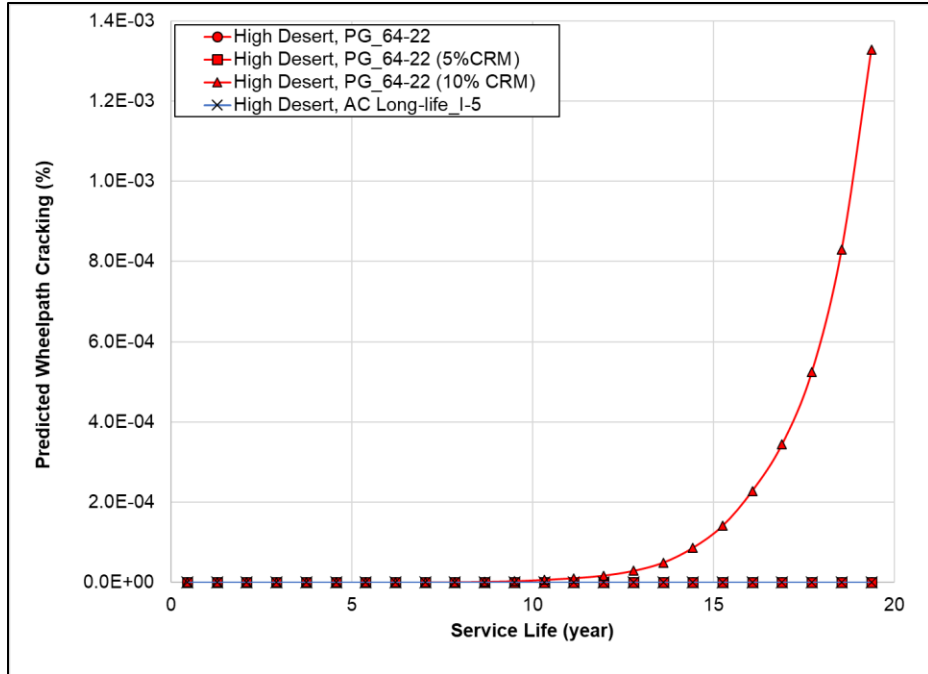
**Figure B.32: Thick pavement application of Approach-2 Mix S, T, U, and SAC-5 mixes.**
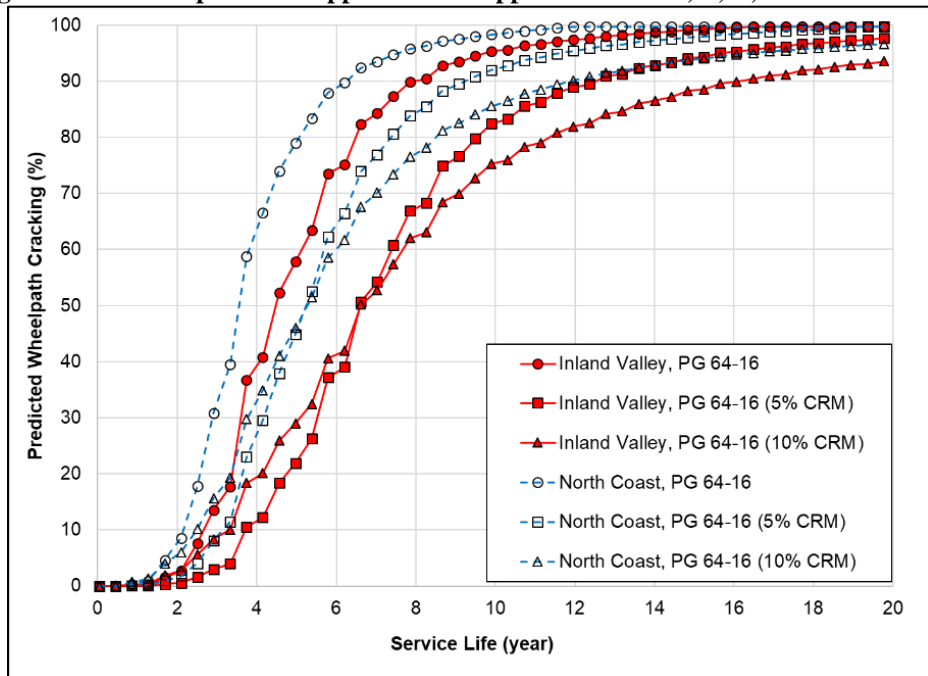
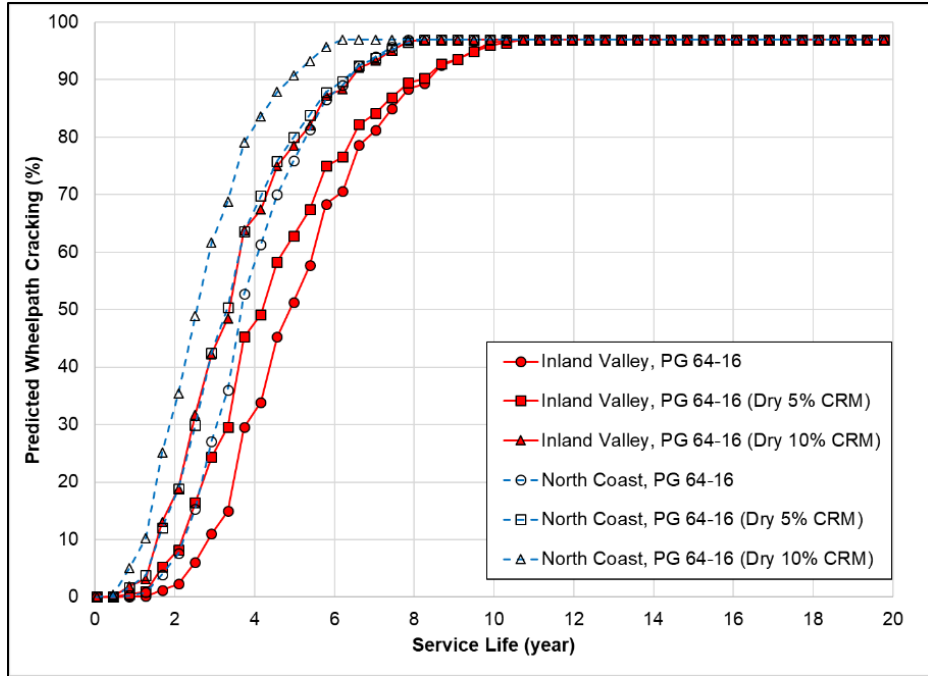**Figure B.33: AC over PCC application of Approach-1 Mix A, B, C at 45 mm.**
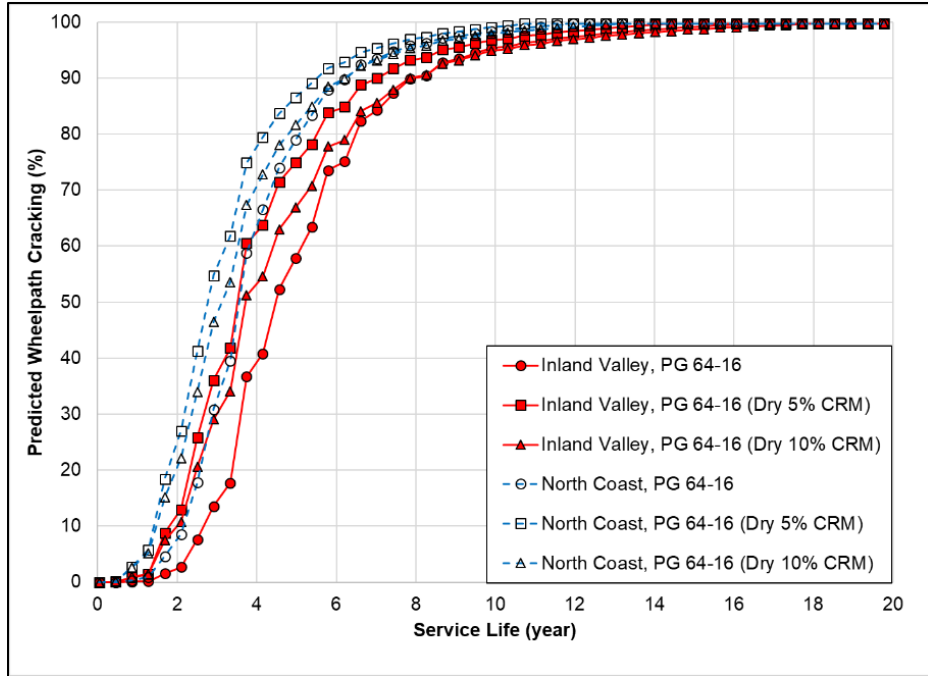
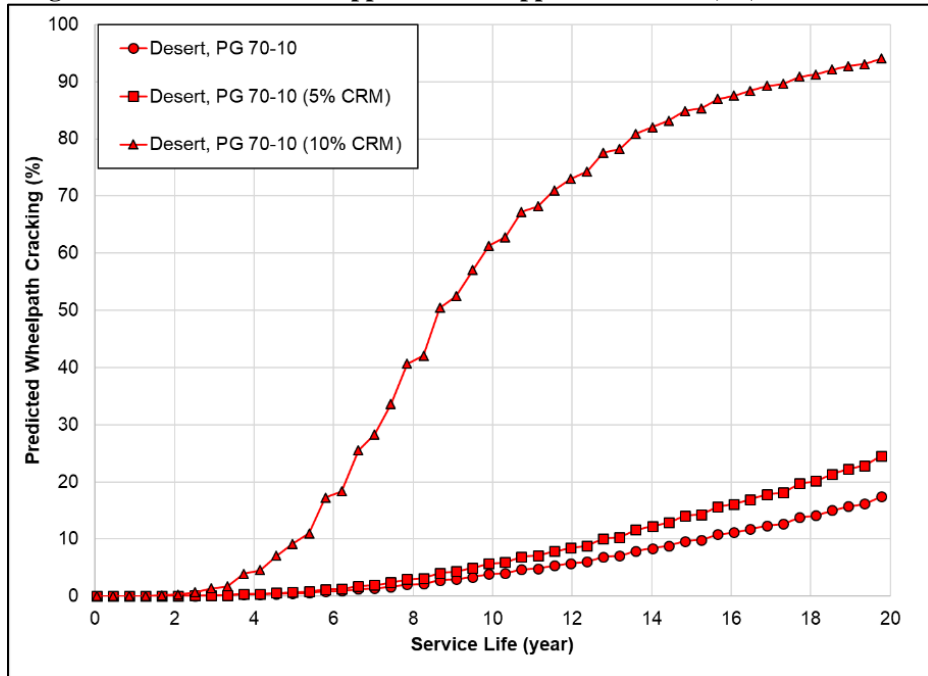**Figure B.34: AC over PCC application of Approach-3 Mix A, G, H at 45 mm.**
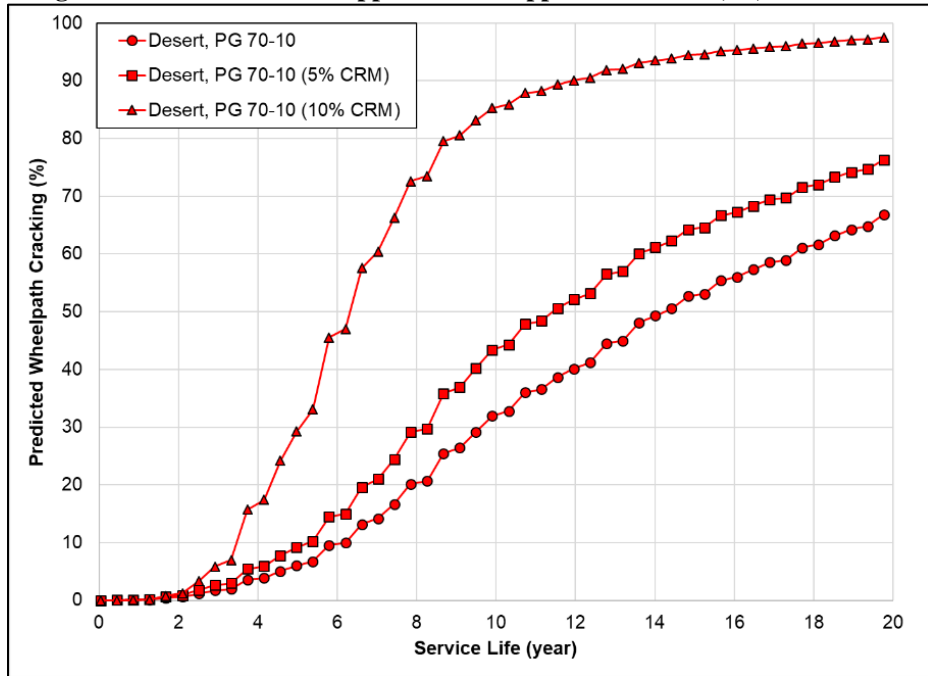
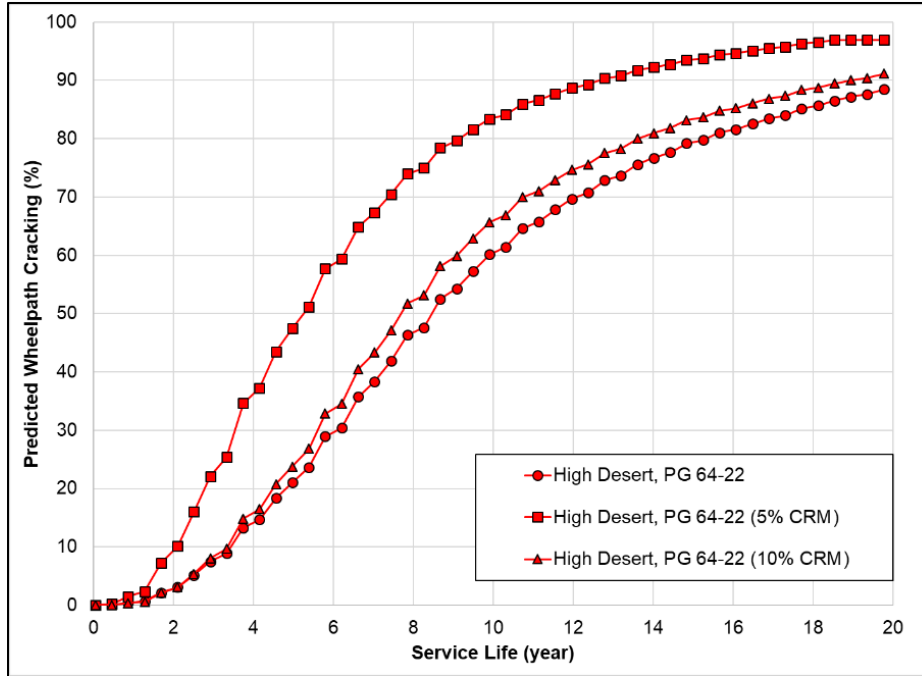**Figure B.35: AC over PCC application of Approach-1 Mix D, E, F at 45 mm.**
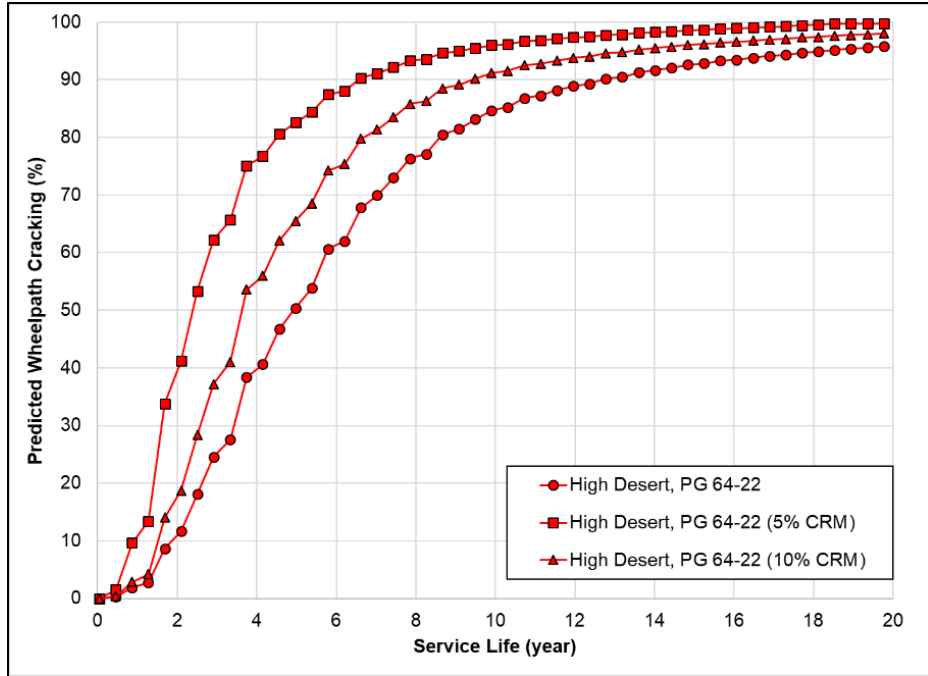
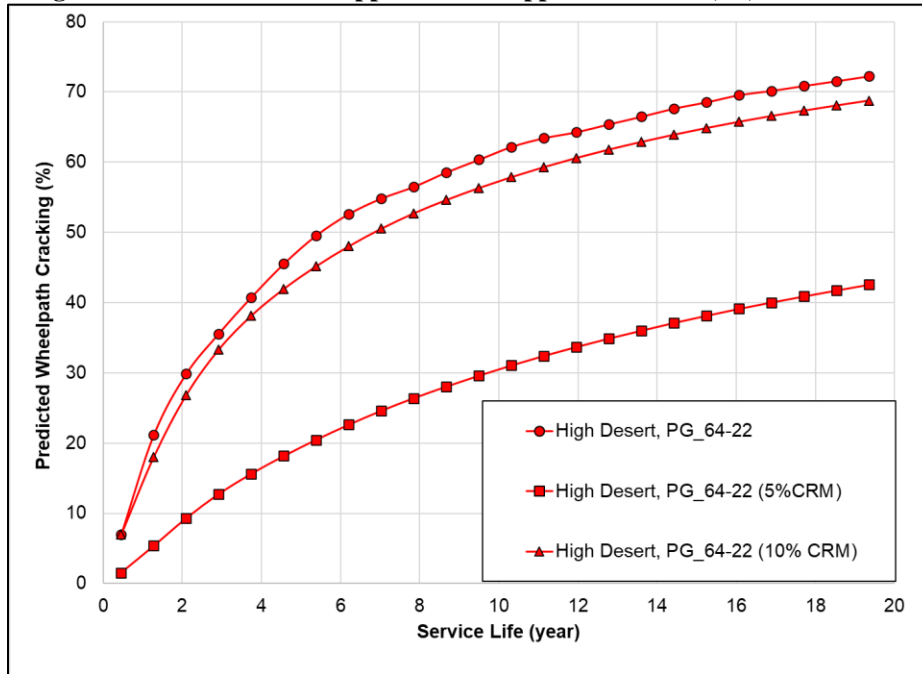**Figure B.36: AC over PCC application of Approach-4 Mix J, K, L at 45 mm.**

Figure B.37: AC over PCC application of Approach-2 Mix S, T, U at 45 mm.

431
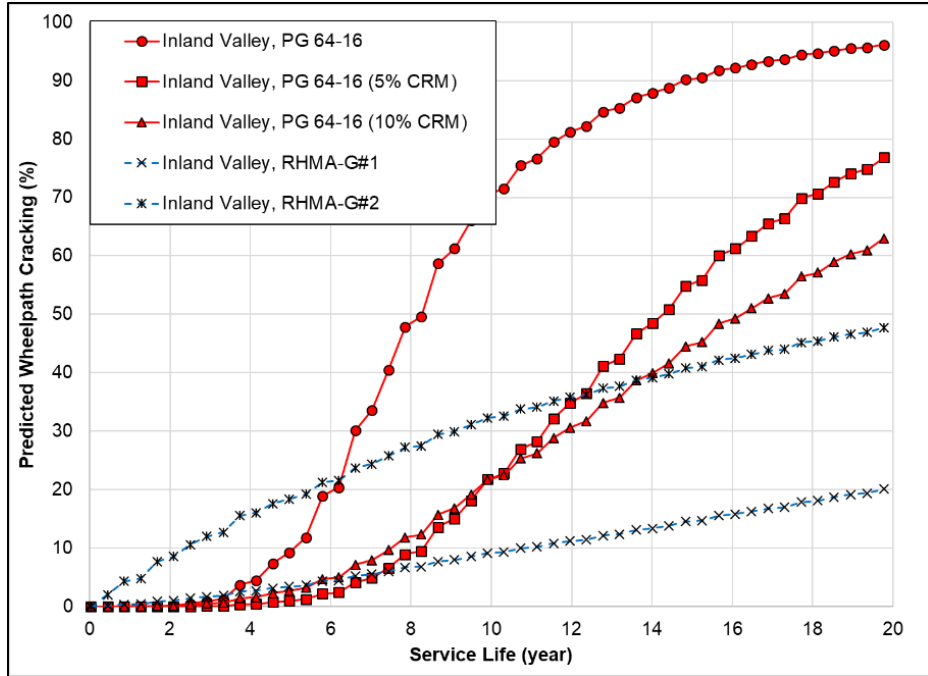
Figure B.38: AC over PCC application of Approach-1 Mix A, B, C, and RHMA-G at 60 mm inland valley.
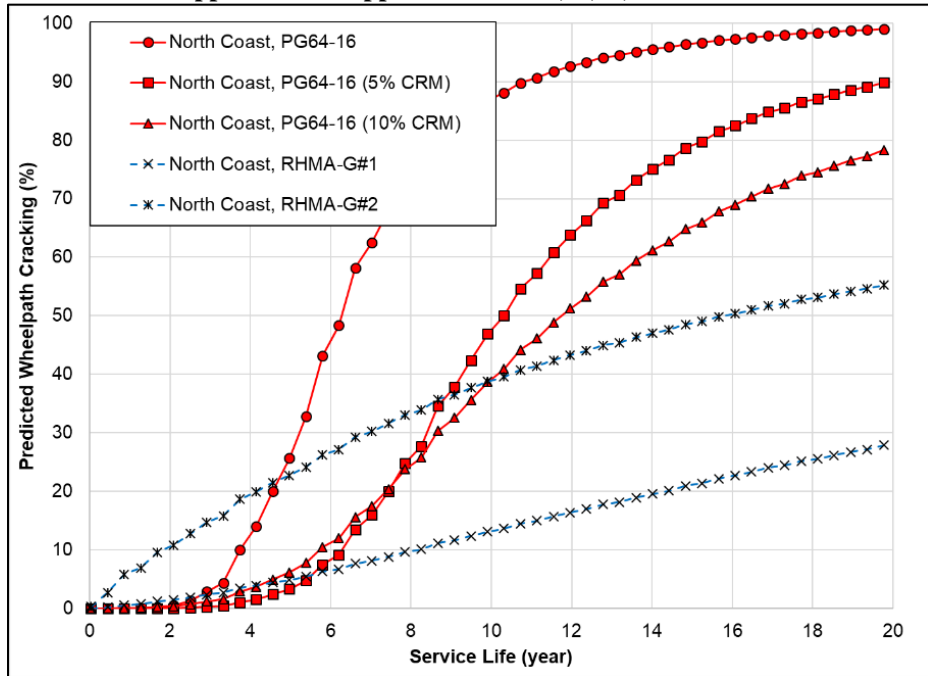
Figure B.39: AC over PCC application of Approach-1 Mix A, B, C, and RHMA-G at 60 mm north coast.
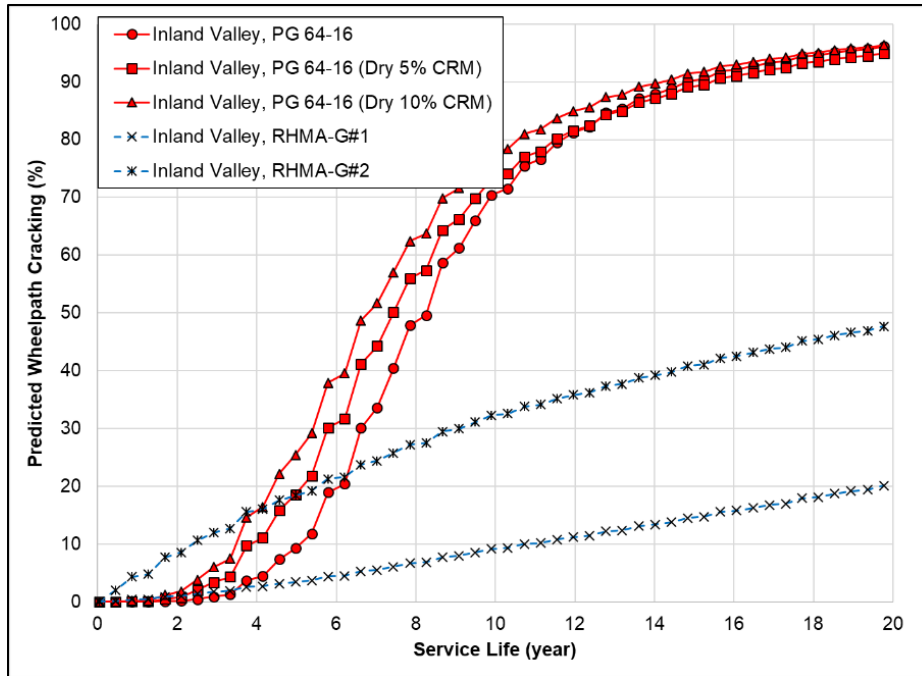
Figure B.40: AC over PCC application of Approach-3 Mix A, G, H, and RHMA-G at 60 mm inland valley.
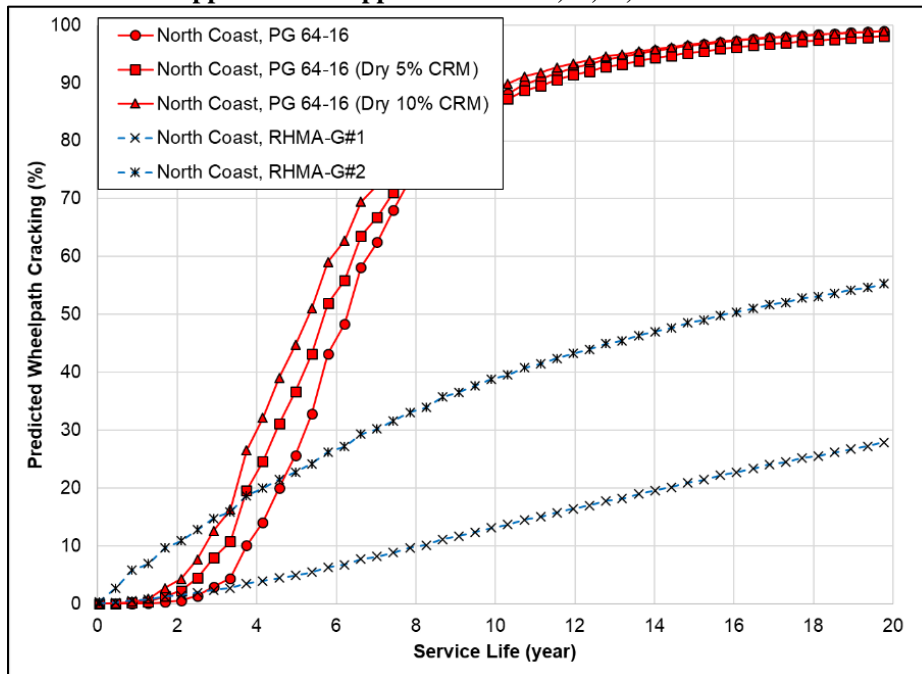
Figure B.41: AC over PCC application of Approach-3 Mix A, G, H, and RHMA-G at 60 mm north coast.
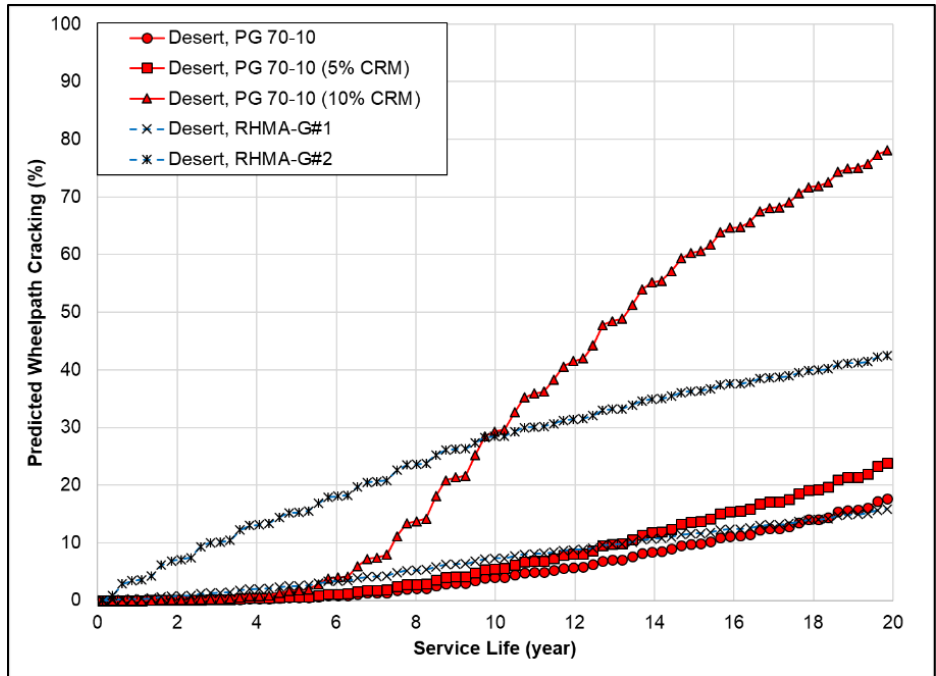
Figure B.42: AC over PCC application of Approach-1 Mix D, E, F, and RHMA-G at 60 mm.
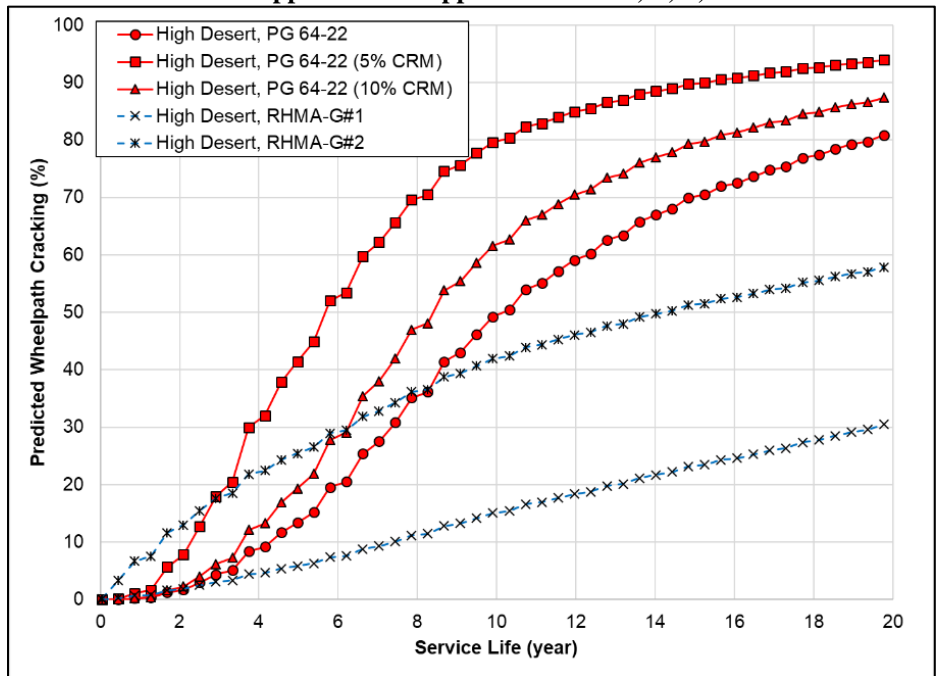
Figure B.43: AC over PCC application of Approach-4 Mix J, K, L, and RHMA-G at 60 mm.
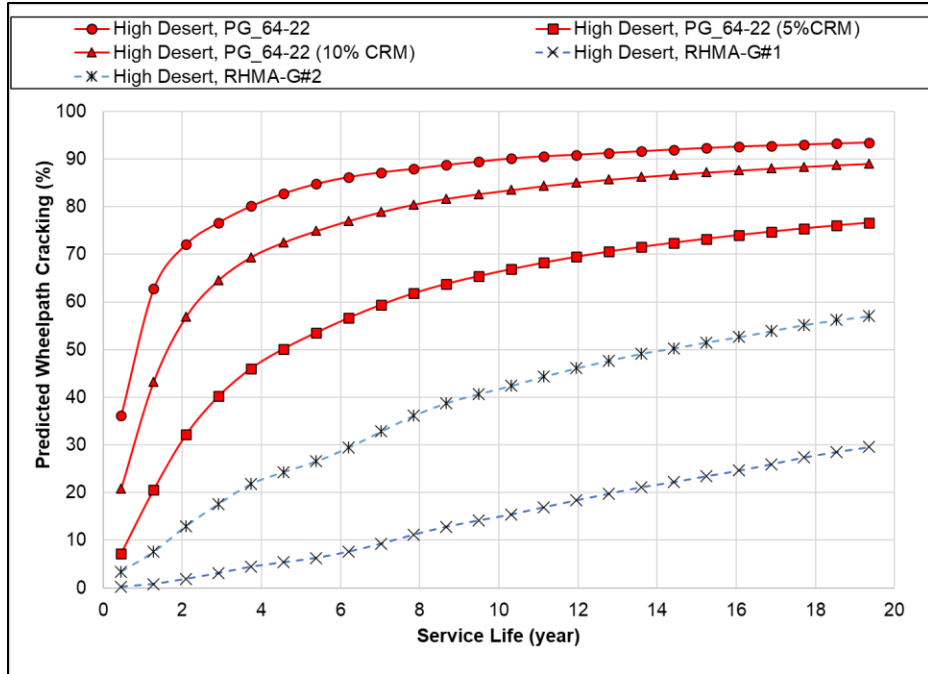
Figure B.44: AC over PCC application of Approach-2 Mix S, T, U, and RHMA-G at 60 mm.
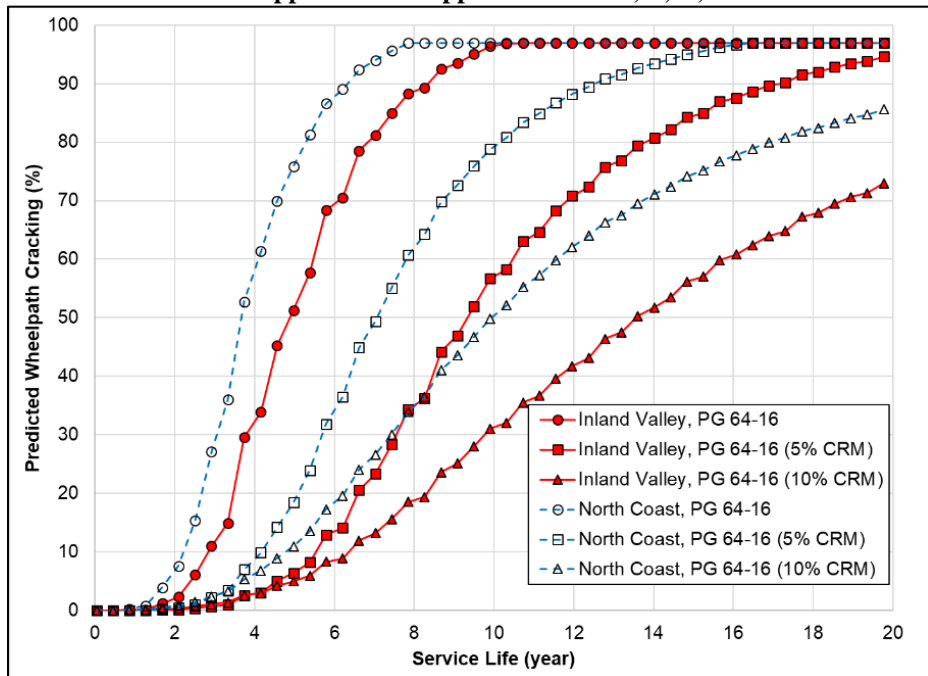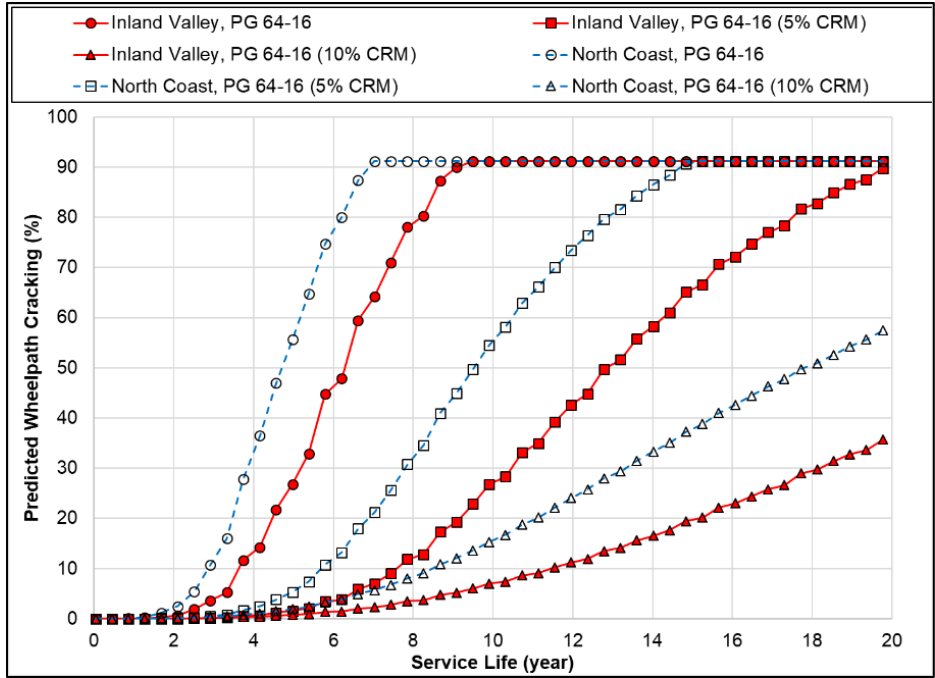

Figure B.45: AC over PCC application of Approach-1 Mix A, B, C at 100 mm.
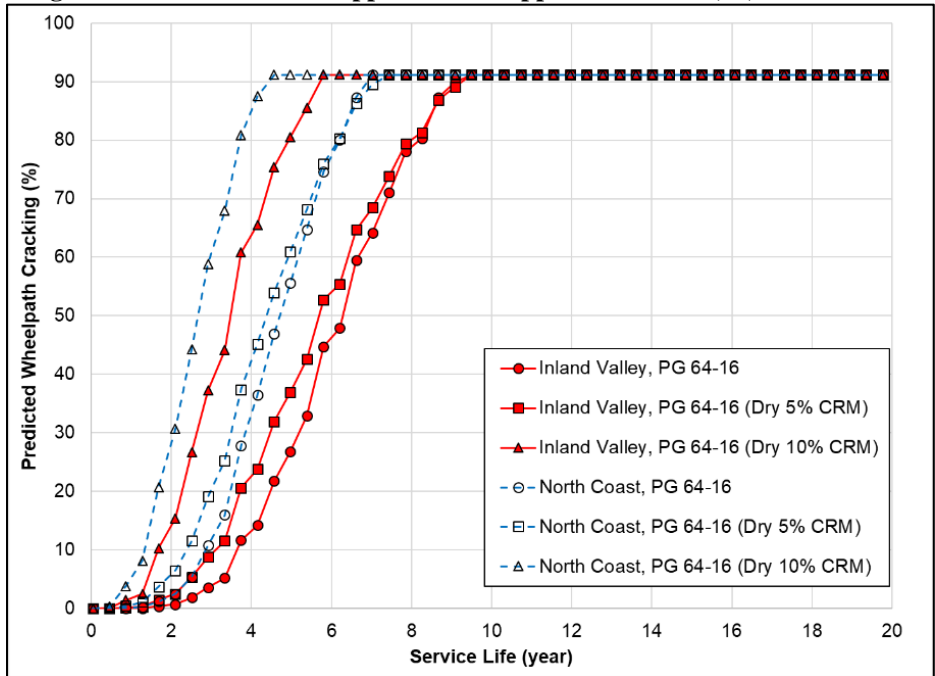
435

Figure B.46: AC over PCC application of Approach-3 Mix A, G, H at 100 mm.

Figure B.47: AC over PCC application of Approach-1 Mix D, E, F at 100 mm.

436

Figure B.48: AC over PCC application of Approach-4 Mix J, K, L at 100 mm.

Figure B.49: AC over PCC application of Approach-2 Mix S, T, U at 100 mm.

437

Figure B.50: AC over PCC application of Approach-1 Mix A, B, C at 150 mm.

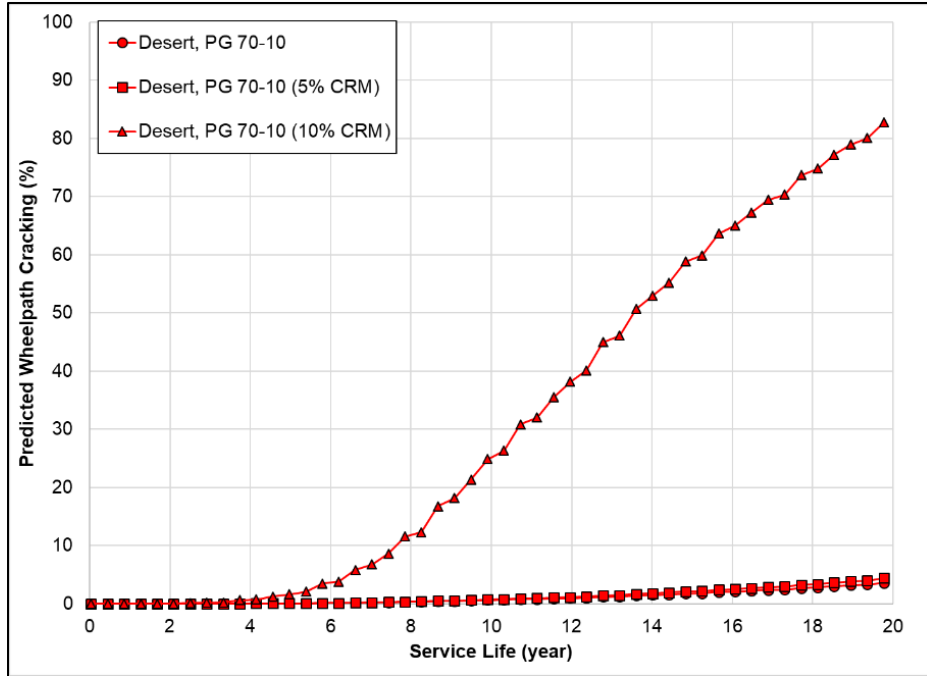**Figure B.51: AC over PCC application of Approach-3 Mix A, G, H at 150 mm.**

438

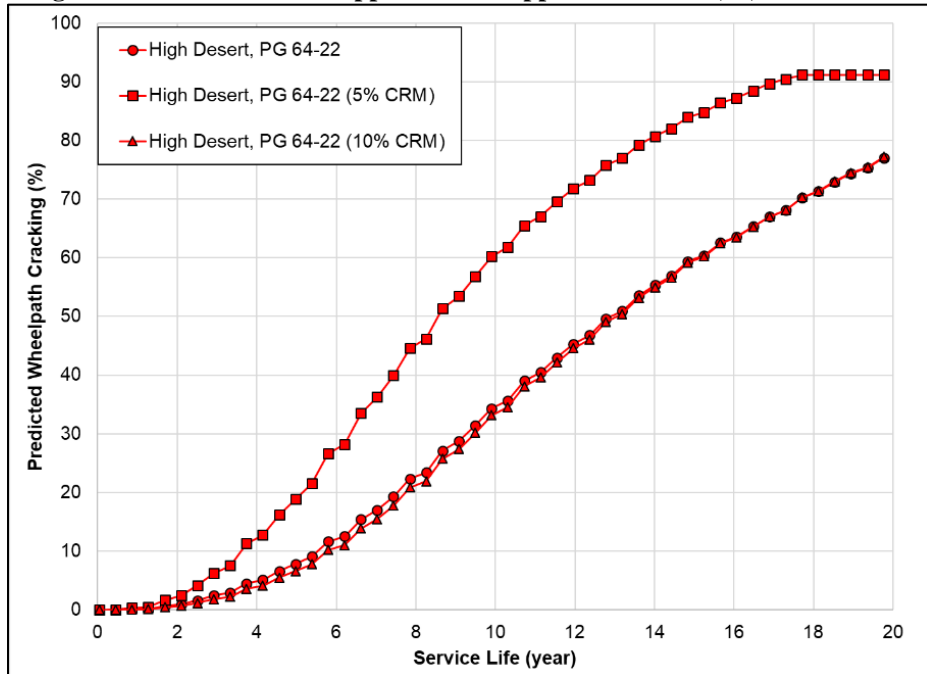**Figure B.52: AC over PCC application of Approach-1 Mix D, E, F at 150 mm.**

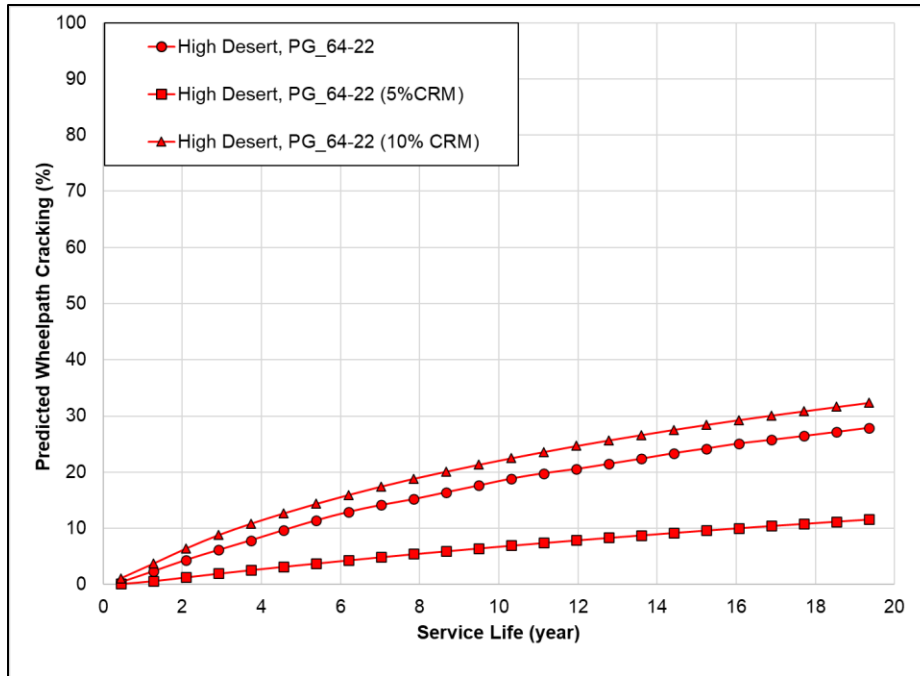**Figure B.53: AC over PCC application of Approach-4 Mix J, K, L at 150 mm.**

439

Figure B.54: AC over PCC application of Approach-2 Mix S, T, U at 150 mm.